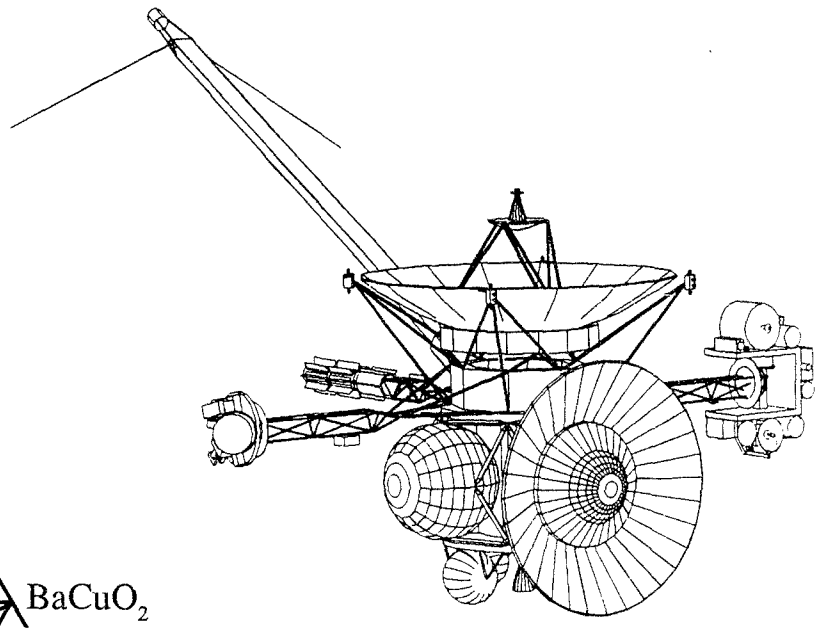
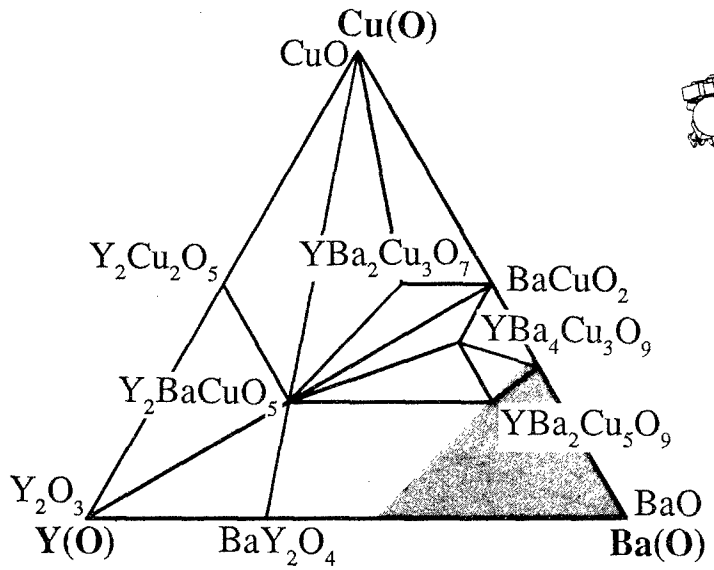
1266

NASA Conference Publication 3100

AMSAHTS '90

Advances in Materials Science and Applications of High Temperature Superconductors





20011109 082

Proceedings of a conference held at
Goddard Space Flight Center
Greenbelt, Maryland
April 2–6, 1990

DISTRIBUTION STATEMENT A
Approved for Public Release
Distribution Unlimited

NIST APL DARPA NASA

Reproduced From Best Available Copy

Cover: The left-hand image shows an equilibrium phase diagram for Y-Ba-Cu-O, projected onto the plane of metallic components for 1 atm oxygen with partial pressure at 910°C (figure courtesy of P. Karen, O. Braaten, H. Fjellvag, and A. Kjekshus, of the Department of Chemistry at the University of Oslo, Norway). The right-hand figure depicts the proposed configuration of the Cassini spacecraft, to be launched by NASA in the late 1990s.

NASA Conference Publication 3100

AMSAHTS '90

Advances in Materials Science and Applications of High Temperature Superconductors

Edited by
Larry H. Bennett
National Institute of Standards and Technology
Gaithersburg, Maryland

Yury Flom
NASA Goddard Space Flight Center
Greenbelt, Maryland

Kishin Moorjani
The Johns Hopkins University
Applied Physics Laboratory
Laurel, Maryland

Proceedings of a conference sponsored by the National Institute of Standards and Technology, The Johns Hopkins University, the National Aeronautics and Space Administration, and the Defense Advanced Research Projects Agency and held at Goddard Space Flight Center
Greenbelt, Maryland
April 2–6, 1990



National Aeronautics and Space Administration

Office of Management

Scientific and Technical Information Division

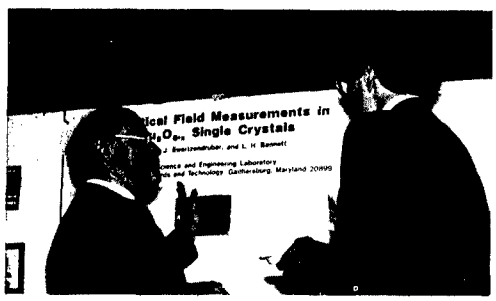
1991




WELCOME




NATIONAL AERONAUTICS AND SPACE ADMINISTRATION U.S.A.


ical Field Measurements in
Single Crystals







FOREWORD

NASA's Goddard Space Flight Center in Greenbelt, Maryland played host to over 200 scientists and engineers from 17 nations who gathered for AMSAHTS '90--Advances in Materials Science and Applications of High-Temperature Superconductors, a 5-day conference in early April of 1990.

AMSAHTS '90 was the second in a series of meetings in the Washington, D.C. area which sought to link theory and experimental efforts with applications efforts in superconductivity near and above liquid-nitrogen temperature. We hoped to provide a forum for interaction between the HTSC research and applications communities and to encourage collaborative and cooperative effort in the field.

The first conference was held at the National Institute of Standards and Technology (NIST) in Gaithersburg, Maryland in October 1988. The objective of that conference was to advance the understanding of high-Tc superconductivity and to discuss practical applications of bulk and thin-film superconductors. A third conference is scheduled for the Fall of 1991 at The Johns Hopkins University Applied PhysicsLaboratory (JHU-APL) in Laurel, Maryland.

The importance of high-Tc technology to NASA's mission cannot be overemphasized. The utilization of superconducting instruments and components in space rests heavily on the progress in understanding the materials science of high-Tc phenomena and on the willingness of the Agency to commit resources to the engineering of high-Tc devices using presently available superconducting materials and knowledge. Much of the success of AMSAHTS '90 was attributable to the broad scope of topics, to the spectrum of expertise of the participants, and also to the active role played by the scientists from NIST and JHU-APL.

The conference began with a keynote address by Professor Bill Little of Stanford University, one of the pioneers of high-Tc superconductivity in the United States. Dr. Little continues to contribute to our understanding, through experimentation, of superconductivity--these days, through high-transition temperature superconductors.

Scientists from the U.S., Germany, Taiwan, France, Australia, Italy, Bulgaria, India and Japan presented their findings in experimental and theoretical superconductivity. The first part of the conference focused on flux creep and pinning, flux flow and flux dynamics, and critical currents. Day 1 finished with a session on fabrication and properties of bulk HTSC.

Thin-film devices and applications were discussed on Day 2. Representatives from NASA, Oak Ridge National Laboratory, and private industry presented results of their work addressing various applications such as microwaves, lasers, satellites, medicine, geophysics and electronics. Other activities on Day 2 included presentations on thermodynamics and chemistry, and a discussion of passive magnetic bearings.

Three sessions of AMSAHTS '90 were devoted to theory--one of HTSC itself, and two of magnetism and experimental techniques. Another two sessions addressed structure and phases of superconducting systems.

On the final day of the conference, the keynote address was presented by Dr. Shoji Tanaka, Director of the International Superconducting Technology Center (ISTEC) in Japan. His remarks highlighted the progress of research in high-Tc superconductors. Also on that day, Government representatives from NASA and the U.S. Navy profiled their respective superconductivity programs.

In all, nearly 50 oral presentations were made during the 5-day meeting. Additionally, there were more than 40 poster presentations (in two scheduled sessions) ranging in scope from theory to application and manufacture.

Panel discussions on flux pinning, thin-film devices, passive magnetic bearings, wires for low-current application, and the relationship between structure and properties drew considerable attention from conference attendees. Summaries of these discussions may be found at the end of this Proceedings.

Dr. Larry H. Bennett, NIST
Dr. Yury Flom, NASA-GSFC
Dr. Kishin Moorjani, JHU-APL

ACKNOWLEDGEMENTS

The editors of this proceedings document wish to thank all of the conference participants for their contributions to this work. Financial support was provided by NASA Headquarters, the National Institute of Standards and Technology (NIST), the Johns Hopkins University Applied Physics Laboratory (JHU/APL), and the Defense Advanced Research Projects Agency (DARPA). Special thanks are extended to NASA's Goddard Space Flight Center for generously sharing its resources--financial, personnel and logistical.

TABLE OF CONTENTS

Foreword iii

Acknowledgements v

FABRICATION AND PROPERTIES

Oxygen Stabilization Induced Enhancement in Superconducting Characteristics of High T_c Oxides 3
M.K. Wu, J.T. Chen & C.Y. Huang

Microstructure and Magnetization of Y-Ba-Cu-O Prepared by Melt Quenching, Partial Melting and Doping 19
H. Hojaji, S. Hu, K.A. Michael, A. Barkatt, A.N. Thorpe & S. Alterescu

Effect of Shock Pressure on the Structure and Superconducting Properties of Y-Ba-Cu-O in Explosively Fabricated Bulk Metal-Matrix Composites 27
L.E. Murr, C.S. Niou & M. Pradhan-Advani

Production of Superconductor/Carbon Bicomponent Fibers 37
S.A. Wise, C.C. Fain & H.D. Leigh

Thermal and Electric Properties of $Nd_{1.85}Ce_{0.15}CuO_{4-y}$ and $Pr_{1.85}Ce_{0.15}CuO_{4-y}$ 43
Z.S. Lim, K.H. Han, S. Lee, Y.H. Jeong, Y.S. Song & Y.W. Park

Ternary and Quarternary Oxides of Bi, Sr and Cu 45
M.T. Casais, P. Millán, I. Rasines & J.A. Campá

Dependence of Transition Temperature on Hole Concentration per CuO_2 Sheet in the Bi-Based Superconductors 55
J. Zhao & M.S. Seehra

Spin Glass Freezing and Superconductivity in $YBa_2 (Cu_{1-x} Fe_x)_3O_7$ Alloys 61
I. Mirebeau, M. Hennion, J. Dianoux, V. Caignaert, T.E. Phillips & K. Moorjani

Thermal Response of Large Area High Temperature Superconducting YBaCuO Infra Red Bolometers 69
A.E. Khalil

Microwave (EPR) Measurements of the Penetration Depth Measurements of High-T_c Superconductors 83
N.S. Dalal, B. Rakvin, T.A. Mahl, A.S. Bhalla & Z.Z. Sheng

Inhomogeneities in Single Crystals of Cuprate Oxide Superconductors 89
K. Moorjani, J. Bohandy, B.F. Kim & F.J. Adrian

The Color of Polarization in Cuprate Superconductors 97
H.A. Hoff, M.S. Osofsky, W.L. Lechter & C.S. Pande

Effect of Doping in the Bi-Sr-Ca-Cu-O Superconductor 107
S.A. Akbar, M.S. Wong, M.J. Botelho, Y.M. Sung, M. Alauddin, C.E. Drummer & M.J. Fair

Stabilization of High T_c Phase in Bismuth Cuprate Superconductor by Lead Doping 113
R.P. Gupta, J.P. Pachauri, W.S. Khokle, K.C. Nagpal & S.K. Date

Structure and Superconducting Properties of $[(Ln_{1-x}Ln^*_x)_{1/2}(Ba_{1-y}Sr_y)_{1/3}Ce_{1/6}]_8Cu_6O_z$ 115
H. Yamauchi, T. Wada, A. Ichinose, Y. Taegashi, T. Kaneko, S. Ikegawa & S. Tanaka

Compatibilities of $YBa_2Cu_3O_{9-\delta}$ Type Phase in Quintenary Systems Y-Ba-Cu-O-X (Impurity) 117
P. Karen, O. Braaten, H. Fjellvåg & A. Kjekshus

Processing Bi-Pb-Sr-Ca-Cu-O Superconductors from Amorphous State 127
C.K. Chiang, W. Wong-Ng, L.P. Cook, S.W. Freiman, N.M. Hwang, M. Vaudin, M.D. Hill, R.D. Shull, A.J. Shapiro, L.J. Swartzendruber & L.H. Bennett

Composite Superconducting Wires Obtained by High-Rate Tinning in Molten Bi-Pb-Sr-Ca-Cu-O System 137
A.D. Grosav, L.A. Konopko & N.I. Leporda

Low Frequency Electrical Noise Across Contacts Between a Normal Conductor and Superconducting Bulk $YBa_2Cu_3O_7$ 145
J. Hall & T.M. Chen

Superconductivity in 2-2-3 System $Y_2Ba_2Cu_2O_{8+\delta}$ 149
H.H. Joshi, G.J. Baldha, R.B. Jotania, S.M. Joshi, H. Mohan, P.B. Pandya, H.N. Pandya & R.G. Kulkarni

Study of the Superconducting Properties of the Bi-Ca-Sr-Cu-O System 155
M.H. Khan, S.M.M.R. Naqvi & S.M. Zia-ul-Haq

Novel Superconducting Phases of TL-Based Compounds 159
I.Z. Kostadinov, M. Mateev, M. Michov, V. Skumriev & E. Tsakin

Synthesis of $Y_1Ba_2Cu_3O_x$ Superconducting Powders by Intermediate Phase Reactions 165
C. Moure, J.F. Fernandez, J. Tartaj, P. Recio & P. Duran

Grain Orientation in High T_c Superconductors by Molten Salt Powder Synthesis 173
S. Gopalakrishnan & W.A. Schulze

Levitation of Superconducting Composites 181
C.K. Chiang, M. Turchinskaya, L.J. Swartzendruber, R.D. Shull & L.H. Bennett

FLUX DYNAMICS

Flux Creep in $Bi_2Sr_2Ca_1Cu_2O_{8+x}$ Single Crystals 189
E. Agostinelli, D. Fiorani, A.M. Testa & J. Tejada

Elliptical Flux Vortices in $YBa_2Cu_3O_7$ 199
H. Hickman, A.J. Dekker & T.M. Chen

Vortex Movement and Magnetization of High T_c Superconductors . . 203
A.L. Roytburd & M.J. Turchinskaya

Flux Flow and Flux Dynamics in High-T_c Superconductors 213
L.H. Bennett, M. Turchinskaya, L.J. Swartzendruber, A. Roytburd, D. Lundy, J. Ritter & D.L. Kaiser

Rigid Levitation, Flux Pinning, Thermal Depinning and Fluctuation in High-T_c Superconductors 230
E.H. Brandt

Comparative Study of Flux Pinning, Creep and Critical Currents Between YBaCuO Crystals With and Without Y_2BaCuO_5 Inclusions 241
M. Murakami, S. Gotoh, H. Fujimoto, N. Koshizuka & S. Tanaka

Lower Critical Field Measurements in $YBa_2Cu_3O_{6+x}$ Single Crystals . 249
D.L. Kaiser, L.J. Swartzendruber, F.W. Gayle & L.H. Bennett

Oxide Superconductors Under Magnetic Field 257
K. Kitazawa

THIN FILMS

Microwave Conductivity of Laser Ablated $YBa_2Cu_3O_{7-\delta}$ Superconducting Films and Its Relation to Microstrip Transmission Line Performance 261
K.B. Bhasin, J.D. Warner, C.M. Chorey, B.T. Ebihara, R.R. Romanofsky, V.O. Heinen, F.A. Miranda & W.L. Gordon

Laser Surface Interaction of High-T_c Superconductors 271
C.H. Chen, M.P. McCann & R.C. Phillips

Perspectives on High Temperature Superconducting Electronics 279
T. Venkatesan

Preparation and Characteristics of Superconducting Cuprate Thin Films: $Nd_{2-x}Ce_xCuO_4$ and Substituted Bi-System 281
H. Adachi, S. Hayashi, K. Setsune, S. Kohiki, Y. Ichikawa & K. Wasa

High-T_c Squid Application in Medicine and Geophysics 291
V.N. Polushkin, S.V. Uchaikin & B.V. Vasiliev

Microstructures and Properties of Superconducting Y-ErBaCuO Thin Films Obtained From Disordered Y-Er-BaF_2Cu Films 297
P. Cikmach, M. Diociaiuti, A. Fontana, C. Giovannella, M. Iannuzzi, C. Lucchini, V. Merlo, R. Messi, L. Paoluzi, L. Scopa & P. Tripodi

Optical and Microwave Detection Using Bi-Sr-Ca-Cu-O Thin Films 307
B.E. Grabow, R.M. Sova, B.G. Boone, K. Moorjani, B.F. Kim, J. Bohandy, F. Adrian & W.J. Green

In-Situ Integrated Processing and Characterization of Thin Films of High Temperature Superconductors, Dielectrics and Semiconductors by MOCVD 317
R. Singh, S. Sinha, N.J. Hsu, R.P.S. Thakur, P. Chou, A. Kumar & J. Narayan

Magnetic Relaxation in the 110 K Superconducting Phase in Bi-Sr-Ca-Cu-O Thin Films 319
A. Tanaka, J. Crain, N. Kamehara & K Niwa

In-Situ Deposition of YBCO High-Tc Superconducting Thin Films by MOCVD and PE-MOCVD 323
J. Zhao, D.W. Noh, C. Chern, Y.Q. Li, P.E. Norris, B. Kear & B. Gallois

An Explanation for the Rise in T_c in the Tl- and Bi-Based High Temperature Superconductors 331
S.M. Bose & P. Longe

Critical Currents and High Temperature Superconductors 333
P. Chaudhari

THEORY

The Superconducting State of the High-Transition Temperature Superconductors: Experimental Basis 337
W.A. Little

Phenomenological Theory of the Normal and Superconductive States of Cu-O and Bi-O Metals 339
C.M. Varma

Charge Transfer Polarisation Wave in High T_c Oxides and Superconductive Pairing 341
B.K. Chakraverty

Correlation of Normal and Superconducting Properties and Unified Approach to the Description of High T_c Oxides 353
V.Z. Kresin & S.A. Wolf

Electronic Structure Fermi Liquid Theory of High T_c Superconductors; Comparison of Predictions with Experiments 365
J. Yu & A.J. Freeman

Incoherent vs. Coherent Behavior in the Normal State of Copper Oxide Superconductors 373
Z. Tesanovic

The Electronic Hamiltonian for Cuprates 375
J.F. Annett, A.K. McMahan & R.M. Martin

The Relation Between Ferroelasticity and Superconductivity 377
A. Molak & R. Mańka

High T_c Superconductors: The Scaling of T_c with the Number of Bound Holes Associated with Charge Transfer Neutralizing the Multivalence Cations 379
G.C. Vezzoli, M.F. Chen & F. Craver

Electron Energy Spectrum and Magnetic Interactions in High T_c Superconductors 385
S.A. Turshevski, A.I. Liechtenstein, V.P. Antropov & V.A. Gubanov

Cuopled Bipolarons and Optical Phonons as a Model for High-T_c Superconductors 389
J. Kasperczyk

XES Studies of Density of States of High Temperature Superconductors 393
G. Jasiolek

Superconductivity in the Sn-Ba-Sr-Y-Cu-O System 395
K.S. Aleksandrov, B.P. Khrustalev, S.N. Krivomazov M.I. Petrov, A.D. Vasilyev & S.A. Zwegintsev

Studies of Local Magnetism and Local Structure in $La_{2-x}Sr_xCuO_4$ . . 397
J.I. Budnick, Z. Tan, M. Filipkowski, C. Niedermayer, H. Gluckler, A. Weidinger & E. Recknagel

Magnetic Correlations in $La_{2-x}Sr_xCuO_4$ from NQR Relaxation and Specific Heat 399
F. Borsa & A. Rigamonti

Magnetism and Superconductivity of Some Tl-Cu Oxides 413
T. Datta, A.M. Hermann & D.U. Gubser

APPLICATIONS

A Technique to Measure the Thermal Diffusivity of High T_c Superconductors 417
C.E. Powers

The Effects of Space Radiation on Thin Films of $YBa_2Cu_3O_{7-x}$ . . . 423
R. Herschitz, A. Bogorad, C. Bowman, S.S. Seehra, A. Mogro-Campero & L.G. Turner

An Instrument for Spatial Conductivity Measurements of High T_c Superconducting (HTSC) Materials 429
T. Van Sant

Plastic Superconductor Bearings Any Size—Any Shape 77 k and up 435
F.G. Reick

Upcoming Planetary Missions and the Applicability of High Temperature Superconductor Bolometers 449
J. Brasunas, V. Kunde, H. Moseley & B. Lakew

The Effect of Temperature Cycling Typical of Low Earth Orbit Satellites on Thin Films of $YBa_2Cu_3O_{7-x}$ 459
A. Mogro-Campero, L.G. Turner, A. Bogorad & R. Herschitz

A YBCO RF-Squid Variable Temperature Susceptometer and Its Applications 464
L. Zhou, J. Qiu, X. Zhang, Z. Tang, Y. Cai & Y. Qian

Static and Dynamical Meissner Force Fields 469
B.R. Weinberger, L. Lynds, J.R. Hull & T.M. Mulcahy

Magnetic Forces in High T_c Superconducting Bearings 471
F.C. Moon

SUPERCONDUCTIVITY PROGRAMS

Progress of Research of High Tc Superconductors 475
S. Tanaka

Prospects and Progress High Tc Superconductivity for Space Applications 477
R.R. Romanofsky and M.M. Sokoloski

US Navy Superconductivity Program 487
D.U. Gubser

PANEL DISCUSSION SUMMARIES

Structure-Property Relationships in High Temperature Superconductors 491
K. Moorjani & A.J. Berlinsky

Thin Films 494
J.C. Brasunas & A. Mogro-Campero

HTSC Wires 496
P. Arsenovic & I. Carlberg

Flux Pinning 498
M. Murakami & L. Swartzendruber

High Temperature Superconducting Bearings 502
F.C. Moon

APPENDIX

List of Attendees 507

Index of Authors 511

SECTION 1:
FABRICATION AND PROPERTIES

OXYGEN STABILIZATION INDUCED ENHANCEMENT IN SUPERCONDUCTING CHARACTERISTICS OF HIGH-T_c OXIDES

M.K. Wu*
Department of Physics and Materials Center
National Tsing-Hua University
Hsingchu, Taiwan, Republic of China

J.T. Chen
Department of Physics
Wayne State University
Detroit, Michigan 48202

C.Y. Huang
Lockheed Missiles and Space Company
Research and Development Division
Palo Alto, California 94304

ABSTRACT

In an attempt to enhance the electrical and mechanical properties of the high-temperature superconducting oxides, we have prepared high-T_c composites composed of the 123 compounds and AgO. The presence of extra oxygen due to the decomposition of AgO at high temperatures is found to stabilize the superconducting 123 phase. Ag is found to serve as a clean flux for grain growth and it precipitates as a pinning center. Consequently, an almost two orders-of-magnitude enhancement in critical current densities has also been observed in these composites. In addition, these composites also show much improvement in workability and shape formulation.

On the other hand, proper oxygen treatment of $Y_5Ba_6Cu_{11}O_y$ was found to possibly stabilize the zero-resistance state near 250 K. I-V, ac susceptibility and electrical resistivity measurements indicate the possible existence of high-temperature zero-resistance state in this compound.

INTRODUCTION

Since the first paper on high-temperature superconductivity reported by Bednorz and Muller [1], several new material systems have been found with their physical properties characterized, and many theoretical models have been proposed. However, no clear understanding of the mechanism responsible for the high-temperature superconductivity has been established. Consequently, there are no science-based guidelines for researchers in the search for new high-T_c materials.

Recently, thermally recycleable zero-resistance states with transition temperatures above 200 K were observed in mixed-phase Y-Ba-Cu-O materials that are treated by a low-temperature oxygenation process and enclosed in an oxygen atmosphere during electrical and magnetic measurements [2]. Although the high-temperature zero-resistance state was verified through careful measurements of the current-voltage characteristics using multiple leads and contact arrangements. Only diamagnetic-like deviations and hysteretic behavior at the same temperature as the resistive transitions were observed in the magnetic measurements.

* On leave from Department of Applied Physics, Columbia University, New York, NY 10027, USA.

At the very early stage of the development of high-temperature superconductivity, we observed several interesting phenomena concerning the processing of superconducting oxides. One example is the preparation of Y-Sr-Cu-O [3] superconducting phase which exists only when the material is processed at temperatures higher than 1300°C, quenched, and then submitted to a controlled oxygenation process. The fabrication of RE123/Ag_2O [4] composites, which were found to exhibit strong pinning effect, also requires stringent processing conditions. Our observations suggested that the phase formation of high-T_c oxides is more favorable in a non-equilibrium state plus a proper oxygenation process. It seems that the presence of a second phase, whether metal or non-metal, and oxide or non-oxide, is useful in enhancing the properties of superconducting phase.

On the other hand, there are problems in achieving technological applications of this new class of materials. One difficulty that stands most squarely in the way of the commercialization of the new high-temperature superconductors is the fabrication of bulk materials with high current densities in high magnetic fields [5, 6]. This implies that highly oriented material [7] is required for most applications.

Other experimental results, such as the evidence for intragrain Josephson junctions [8] and the development of a tail in the resistive transition in the presence of even moderate applied fields, indicate that the phenomenology of the high-T_c oxides is significantly different from that of the classical superconductors.

It also creates serious problems when trying to define the upper critical field and the critical current [9, 10]. Several models have been proposed to explain the broadening of the resistive transition under magnetic fields [9, 11, 12, 13]. However, a clear picture of the phenomenology of the transition is yet to come. In addition, there is also a lack of understanding of such important issues as the effect of oxygen stoichiometry and ordering, boundary effects, and formability.

In order to gain more insight into the above-mentioned observations, we have carried out a series of experiments based on the formation of superconducting oxides through the dispersion of fine metal oxide. In this work, we report the results of: the preparation of single-phase superconducting $YSr_2Cu_3O_{6+y}$ compound by the addition of a small amount of MoO_3; the detailed thermal and microscopic studies of the strong flux pinning RE123/AgO composites; and the magnetic and electron microscopic studies of the $Y_5Ba_6Cu_{11}O_y$ (5-6-11) and Sr-doped 5-6-11 compounds. The results suggest that the observed enhancement in the superconducting properties is likely caused by the stabilization of the superconducting phase (or the oxygen contents) through the introduction of extra oxygen from either the decomposition of the silver oxide (for RE123/AgO composites) or the low-temperature oxygenation process (for 5-6-11).

EXPERIMENTAL

The superconductingY-Ba-Cu-O/Ag_2O composites were prepared by mixing properly prepared Y123 compound of different oxygen concentrations of Ag_2O with weight ratio n. All annealing processes are performed with a constant oxygen flow rate of 20 cc/min. Detailed processing conditions of composites with different superconducting characteristics will be discussed later.

High-T_c YSCO compounds were prepared by mixing appropriate amounts of metal oxides (nominal composition of $YSr_2Cu_{3-x}Mo_xO_{6+y}$ with x in the range of 0.02 to 0.05), pressing it into

pellets, heating it at 950°C for 12 hours, and quenching it to room temperature (RT). The material was then reground, pressed, reheated to 1150°C for 6 hours in O_2, and slowly cooled to RT. High-purity alumina crucibles were used in the sample preparation.

Samples with nominal compositions of $Y_5Ba_6Cu_{11}O_y$ and $Y_5Ba_4Sr_2Cu_{11}O_y$ were synthesized by ceramic techniques from Y_2O_3, $BaCO_3$ and CuO powders. The first step was to repeatedly calcine the unreacted powders at 930°C for 10 hours in either an oxygen atmosphere or in air until a dark black powder and a fine crystalline texture was obtained. The reacted powders were pressed into pellets and sintered at ≅850°C for 2 days (with one intermediate grinding). A last step used a high-pressure vessel filled up to at least 130 bars for the low-temperature oxygenation. Electrical resistivity measurements were made with the conventional 4-probe technique. AC-magnetic moment measurements were made with a home-made magnetic susceptometer. Structural and phase determinations were made by x-ray diffraction. A Cambridge Scanning Electron Micrograph (SEM) equipped with a Kevex EDX system was employed for microstructural study. Thermal studies were carried out using an ULVAC Multi-TAS-7000 thermal analyzer with DTA and TGA capabilities.

RESULTS

A. Electrical and Magnetic Characterization

The temperature dependence of the resistivity of YSCO with a small amount of Mo is shown in Figure 1. The superconducting onset temperature is about 80 K, which is in agreement with that of the magnetic measurement, as shown in the inset of Figure 1. A linear temperature dependence of R before the onset of superconductivity was observed. Based on the magnetic signal, it was estimated that the superconducting phase is about 60 percent in volume. Without the addition of MoO_3, the 80-K superconducting phase does not manifest itself when the samples are prepared at a temperature lower than 1300°C. This indicates that the 80-K phase in the YSCO compound is thermodynamically stable only at higher temperatures. The addition of MoO_3 resulted in the reduction of the reacting temperature.

A typical M-H hysteretic loop of the nY123/Ag_2O (where n=3) composite is plotted in Figure 2. Similar results are also observed in samples with different values for n. The temperature dependence of the residual magnetization increases with decreasing temperature [14, 15]. Such universal behavior was observed for all the composites which show strong pinning.

AC magnetic susceptibility (with a frequency of 37 Hz and a field <2 G) of the mixed-phase Y-Ba-Cu-O (5-6-11) compound is shown in Figure 3. A superconducting transition near 90 K corresponding to the Y123 phase is observed. In addition, a much smaller diamagnetic-like anomaly with the onset near 270 K is also observed, as shown in the inset of Figure 3. Using the 90-K transition as a reference, it is estimated that the volume fraction of the high-temperature signal has an upper limit of 5 percent. Figure 4 is the field-cooled ac susceptibility of two Sr-doped 5-6-11 samples, one of which has been treated in high-pressure oxygen. It is clear that these samples exhibit similar diamagnetic deviation with the onset temperature near 200 K. A hysteretic behavior is also present in the Sr-doped sample.

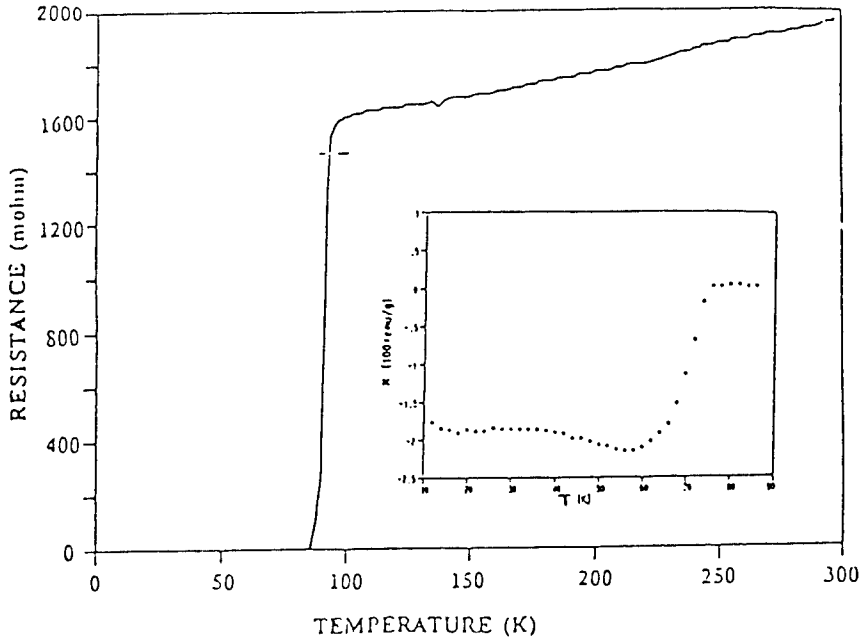


Figure 1. Temperature dependence of resistance of $YSr_2Cu_3O_{6+y}$. Inset: the temperature dependence of the magnetic susceptibility of $YSr_2Cu_3O_{6+y}$.

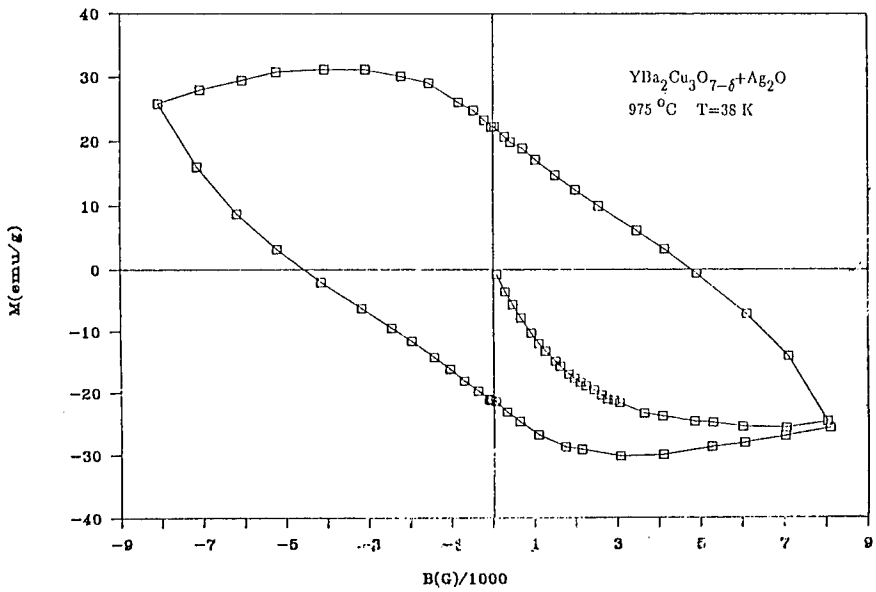


Figure 2. The M-H hysteresis loop of 3Y123/Ag_2O at 38 K.

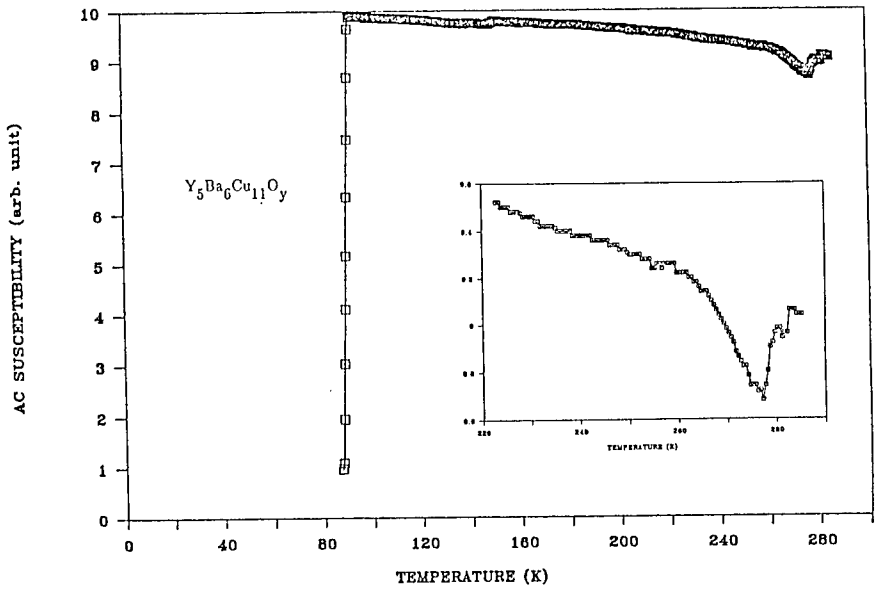


Figure 3. Temperature dependence of ac magnetic susceptibility for $Y_5Ba_4Cu_{11}O_y$.

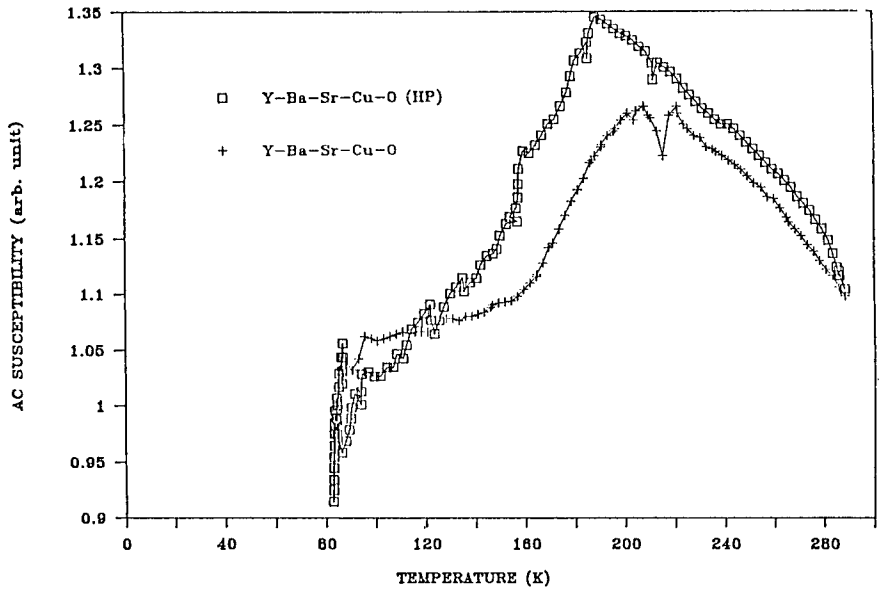


Figure 4. Temperature dependence of ac magnetic susceptibility for $Y_5Ba_4Sr_2Cu_{11}O_y$.

B. Structural Characterizations

The detailed x-ray diffraction pattern of the Y-Sr-Cu-O is shown in Figure 5. A tetragonal structure with lattice constants of a=3.818 A and c=11.555 A was determined using the TREOR program (16). The atomic positions of space group P4/mmm and the isotropic Debye Waller factors listed in Table I were determined with a program based on the stoichiometry of $YSr_2Cu_3O_{6+y}$, where the values of the Debye Waller factors were confined between 0.3 and 4.0 (the corresponding atomic rms displacements are 0.05 A and 0.25 A). The final R factor is 12.6 percent. Atoms O(3) and Cu(1) on the basal plane can be considered relatively unstable due to their large Debye Waller factors. Cu(1) was dragged along by the unstable O(3). The distance between the CuO_2 planes is determined to be 3.305 A, which is smaller than that of the $YBa_2Cu_3O_{6+y}$, which is 3.388 A. It should be noted that a tetragonal phase and an orthorhombic structure for the Y-Sr-Cu-O system [17-20] have been proposed in the literature.

X-ray diffraction patterns of the Ag_2O-added composite show strong c-orientation in the Y123/Ag_2O composites with traces of Ag metal, as shown in Figure 6. The lattice parameters are identical with those of the starting Y123 compound. Figure 7 is the scanning electron micrograph for a 3Y123/Ag_2O composite. EDX has identified the presence of Y123 phase, silver particles, and voids. It shows a microstructure of dispersed silver in the matrix of the Y123 phase. Intergranular silver was observed in some areas and some voids have been filled up by silver, resulting in the reduction of the normal resistivity. More interesting is the observation of large, single crystals in the Ag-dispersed composite. As displayed in Figure 7, the size of the Y123 crystal can be as large as $\cong$ 0.5mm. Similar results are also observed in other composites exhibiting large flux pinning effects.

The high-resolution transmission microscope view of the 5-6-11 sample exhibiting the high-temperature, diamagnetic-like anomaly is shown in Figure 8. While the x-ray diffraction pattern shows the majority of 123 phase, the TEM picture indicates the presence of a glass-like phase. Detailed structural and composition analyses suggest that this glass-like phase may be caused by the intergrowth of the Y123 and Y248 phases.

C. Thermal Characterizations

The heat treatment conditions for the formation of strong pinning RE-123/AgO composites are shown in Table II. In general, the temperatures required are higher than those needed to form the corresponding RE123 compounds, and they do not depend on the weight ratio of RE123 to AgO. It is found that these strong flux pinning RE123/AgO composites form only in a narrow annealing temperature range. The optimum conditions for the formation of strongly pinned superconducting composites can be summarized as: 1) the annealing temperature is $\cong$ 980°C; 2) the cooling rate is $\cong$ 5°C per minute; and 3) there is $\cong$ 20 cc/min. oxygen flow during sintering.

We also observed that in order to obtain better material morphology (i.e., relatively large grains and fine Ag metal dispersion), a particle size ratio of about 5:1 between the Y123 and the Ag_2O powder seems to give the best result.

Figure 9 shows the results of the differential thermal analysis (DTA) and the unreacted Y123, Y123/Ag_2O and Ag_2O, respectively. Data are taken by either heating the samples in air or with a constant oxygen flow. Three reactions are clearly seen in the Ag_2O-added composite. A low-temperature reaction at $\cong$375°C is related to the decomposition of Ag_2O, as clearly seen in

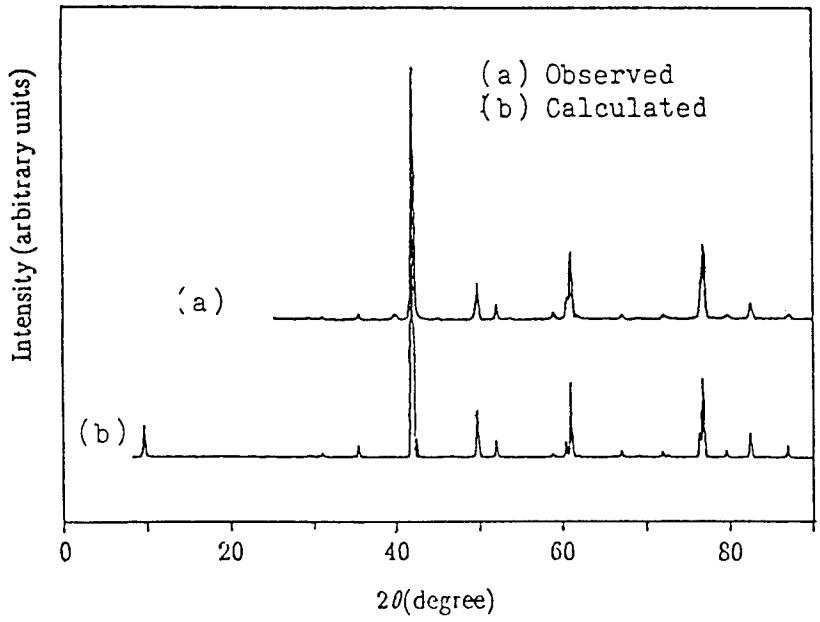


Figure 5. X-ray diffraction pattern of YSCO.

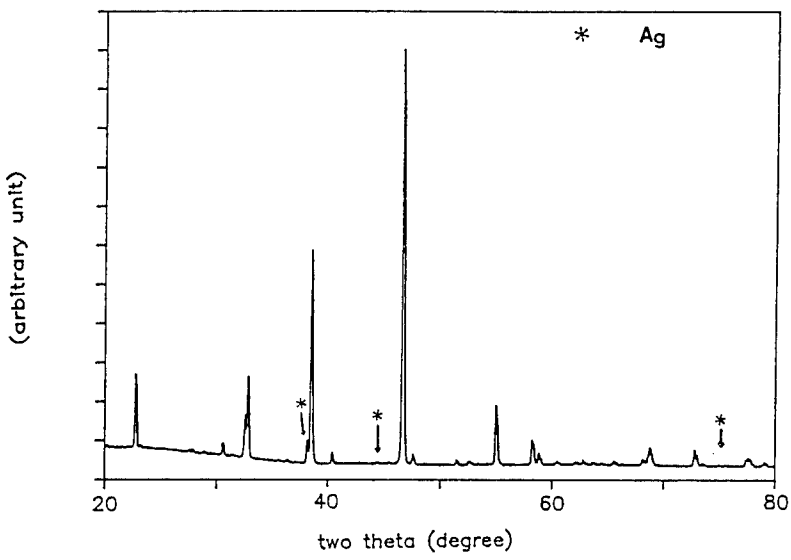


Figure 6. X-ray diffraction pattern of 3Y123/Ag_2O.

TABLE I. Positional parameters and isotropic Debye-Waller factor for the tetragonal structure of $YSr_2Cu_3O_{6+y}$ based on space group P4/mmm and a = 3.818 A, and c = 11.555 A.

Atoms	Wyckoff	x	y	z	B	Occupancy notation
Y	1d	0.5	0.5	0.5	0.3	1
Sr	2h	0.5	0.5	0.197	0.7	1
Cu 1	1a	0	0	0	2.6	1
Cu 2	2g	0	0	0.357	1.3	1
O 1	2f	0	0	0.148	1.1	1
O 2	4i	0	0.5	0.372	4.0	1
O 3	2g	0	0.5	0	4.0	0.6

Table II. Processing Parameters for Y123/Ag_2O Composites

Anneal temp.	$Y_{123}O_x$ x=	Cooling rate	Pinning effect	Grain size	Ag precipitate	Tc* (K)
1000	6.98	5C/min	medium	L	Yes	88
1000	6.72	5C/min	weak	m	Yes	82
1000	6.98	15C/min	weak	m	No	93
980	6.98	3C/min	weak	s	No	93
980	6.98	5C/min	strong	L	Yes	91.3
980	6.72	5C/min	weak	m	Yes	91.3
980	6.98	10C/min	medium	L	No	92.5
980	6.72	10C/min	weak	m	Yes	91.3
980	6.98	20C/min	weak	m	No	92.5
980	6.72	20C/min	weak	m	Yes	91.3

* T_c is the onset of the resistive transition.
+ Oxygen flow rate is 20 cc/min. for all runs.

that of the Ag_2O data. The reaction occurring at ≅ 935°C is identified as the melting of pure silver by comparing the anomaly observed at ≅ 960°C to the Ag_2O DTA result. TGA results of these compounds which were measured at ambient pressure (as displayed in Figure 10) show a prominent oxygen loss at 375°C in the Ag_2O-addition Y123, which corresponds to the dissociation of oxygen in Ag_2O. By correcting the oxygen loss due to the silver-oxide decomposition, the oxygen loss in the Y123 of the composite is found to be about 50 percent lower than that of the pure Y123 for temperatures up to 980°C. The same oxygen losses are also observed in samples reacted in flowing oxygen environments, but their values are only about 25 percent lower in comparison with that of the pure Y123. These results support the suggestion that extra oxygen from Ag_2O serves as an oxygen stabilizer of the superconducting Y123 phase.

DISCUSSIONS

The existence of high-temperature superconducting phase (T_c > 77 K) with tetragonal "123" structure in YSCO is rather unusual, since in the YBCO system high-T_c (> 70 K) phase may be related to the enhancement of the phase stability through the dispersion of fine metallic oxide as usually observed in the oxide dispersion strengthening alloys [21]. It is interesting to note that similar results have been observed in the bismuth- and thallium-based superconductors [22] with the addition of lead oxide. The results of the enhancement in electrical and magnetic properties in the 123/AgO composites, which is to be discussed later, may also come from the same origin.

Several conclusions can be drawn from the results compiled in Table II. These include: 1) superconducting composites with T_c ≅ 90 K are formed independent of the quality of the starting Y123 compounds (i.e., irrelevant to the oxygen contents); 2) samples that exhibit strong pinning are annealed at a temperature higher than the melting temperature of silver metal; and 3) only samples with large grains show strong pinning effect.

We have also observed that superconductivity sustains with the weight ratio of Y123 to Ag_2O up to 2:1. Our observations show that the pinning is independent of the weight ratio n. The superconducting transition temperature, T_c, of the composite remains almost unchanged compared with that of the starting RE-123 compound. The decrease in the normal-state resistivity with the addition of silver oxide suggests a lowering of contact resistances between grains. Nearly identical T_c's suggest that grain interiors experienced little change from the starting RE-123 compounds. One important advantage derived from these RE-123/AgO composites is the reduction of overall contact resistance.

To study in detail the resistive transition of the Y123/Ag_2O composite, we analyzed our data of the RE-123/Ag_2O composites using the model proposed by Tinkham [12]. All of them show that $T_c H^{2/3}$ within our experimental errors. From this result, we estimated that $J_{co}(0)$ $9x10^6$ A/cm^2, which is a reasonable value for the 123 superconductor. A particularly significant result is the unusually large pinning effect in these composites, as evidenced by the still-zero resistance state of several samples at about 80 Kwhile under a magnetic field of 8 T [24].

The sensitivity of the observed pinning effect to the sintering temperature and cooling rate could be due to the change of the interdiffusion rate of silver metal with the superconducting particles, particle surfaces and grain boundaries. The importance of Ag_2O particle size and Y123 grain size suggests the interdiffusion of Ag is, indeed, essential.

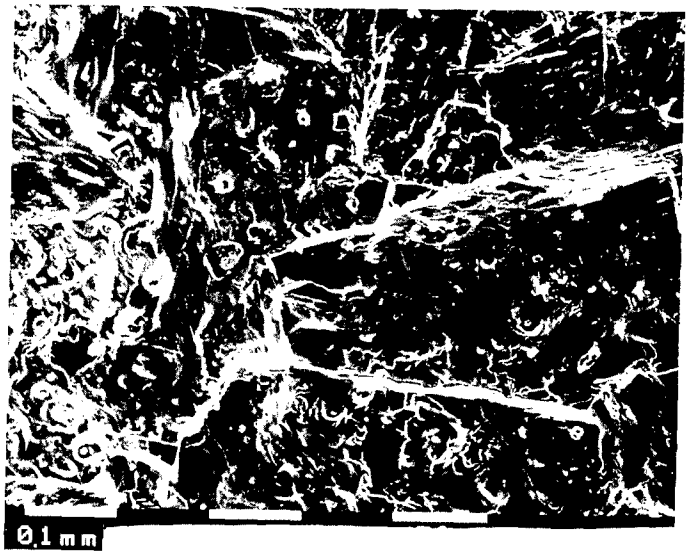


Figure 7. Scanning electron micrograph of 3Y123/Ag_2O.

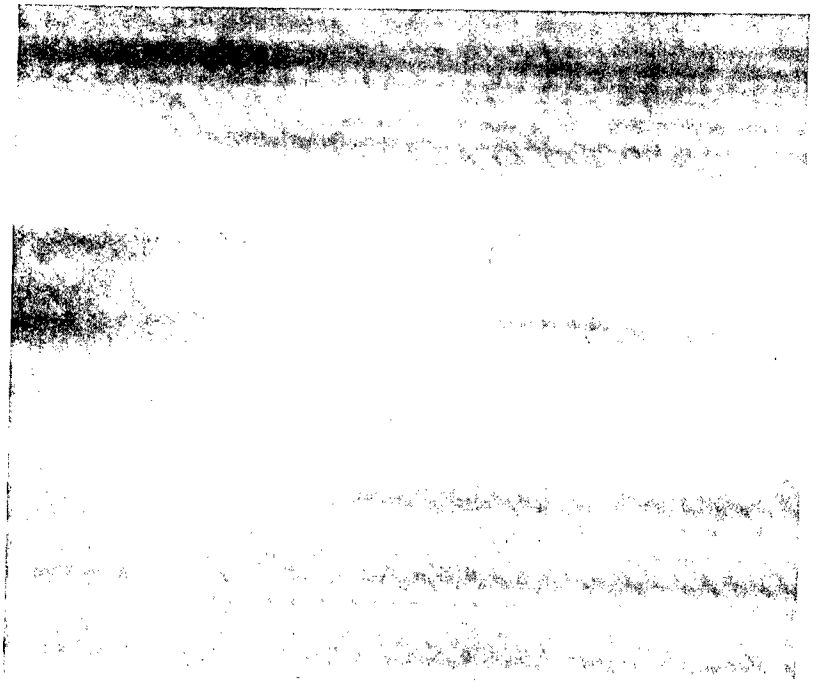


Figure 8. Transmission electron micrograph of $Y_5Ba_4Cu_{11}O_y$.

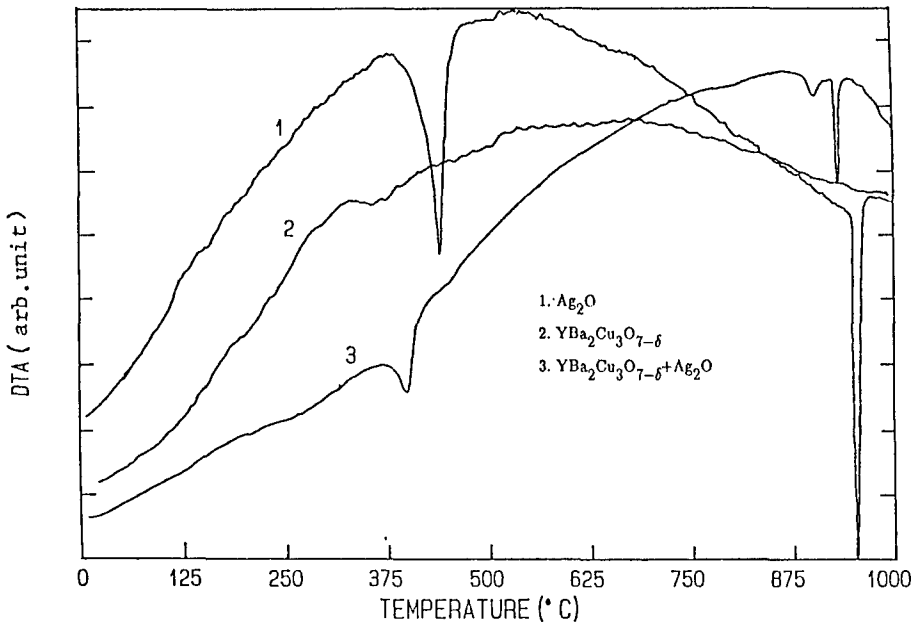


Figure 9. Differential thermal analysis (DTA) of Ag_2O (1), Y123 (2), and Y123/AgO (3). The heating rate is 5°C per minute.

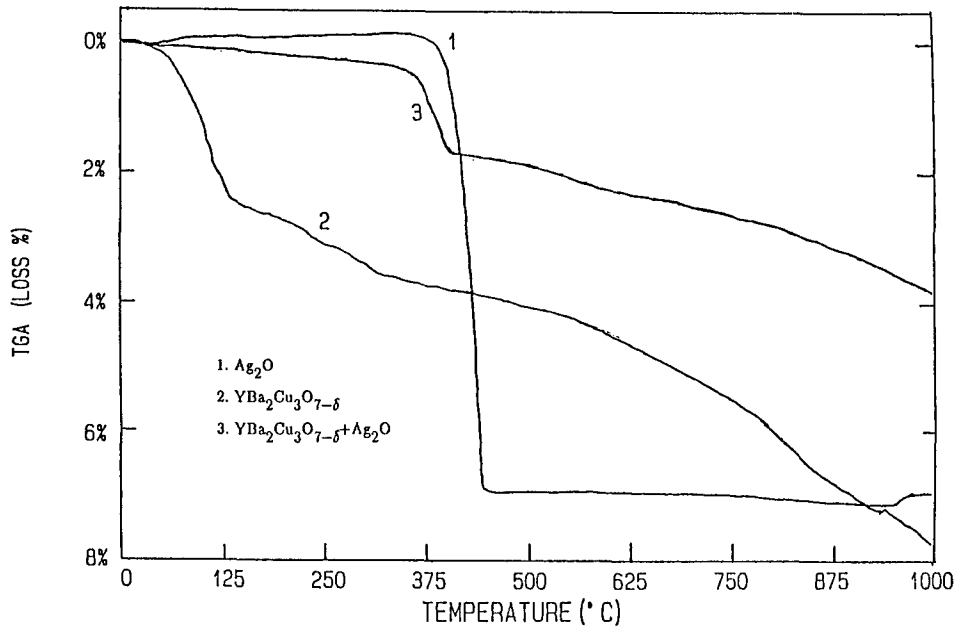


Figure 10. Weight loss of Ag_2O (1), Y123 (2), and Y123/AgO (3) at ambient temperature with a heating rate of 5°C per minute.

The reason for the decrease in melting temperature of the silver metal during the formation of the $Y123/Ag_2O$ composite is not well understood at the present time. It is noted that an opposite result, showing the increase in the liquidus temperature was observed by Chen et al. in their study of the Yb123/Ag metal composite [23]. The 895°C reaction observed may be caused by the reaction of Ag metal with Y123. However, x-ray diffraction studies show that Ag does not permeate the lattice sites of the superconducting oxide. Electron microscopy indicates that Ag metals precipitated on the grain boundaries and filled in some voids [24]. The pinning characteristics of these composites strongly depend on their sample morphologies. The presence of large grains seems to be one of the key factors in the material showing unusual magnetic suspension effects. Another factor is the fine dispersion of silver metal particles in the superconducting grains. It is conceivable that these dispersed silver particles serve as pinning centers which may then be responsible for the strong flux pinning observed.

Many oxygen diffusion studies [25-27] have been carried out in high-T_c oxides. Most of the studies indicated that the in-and-out diffusion of oxygen in the oxides--particularly in 123--is extremely effective. These studies suggest that the out-diffusion is most likely surface-reaction-limited, while the in-diffusion is diffusion-controlled. The diffusion mechanisms are through the defects, which include the oxygen vacancies and the twinnings. In general, several activation energies have been observed corresponding to the out- and in-diffusions (depending on the oxygen concentrations). The higher activation energy for the out-diffusion process suggests that the surface barrier (which can be affected by the grain boundaries and impurities) plays an importat role in controlling the oxygen concentration. If a good oxygen catalyses (or oxygen inert species, such as Ag metal) were used in contact with the oxide, then better stabilization of the phase might be achieved through limiting the oxygen out-diffusion process. This oxygen stabilization process likely may be the reason for the stabilization of 123 phase in the Ag-addition composites. The observation of Y123 phase stabilization in the mixed-phase Y-Ba-Cu-O [28] may also be caused by a similar process attributed to the presence of the insulating 211 phase. The strong oxygen dependence of the Y-Sr-Cu-O [29] system may also be related to this diffusion control step.

Although zero-resistance states under repeated thermal cycles have been observed by one of us (JTC) in the Y-Ba-Cu-O (5-6-11) mixed phase [2], we do not reproduce the same result in this study. On the other hand, diamagnetic-like anomalies are observed in both doped-with-Sr and undoped samples. The relatively small volume percent of the magnetic anomaly may be accountable for the absence of the resistive transitions. However, we do not claim the confirmation of the existence of superconducting phase with transition temperature above 200 K based on our results. More detailed measurements, such as magnetic field dependence, are needed to identify the origin of the observed anomalies.

SUMMARY

We have achieved the preparation of single-phase, high-T_c Y-Sr-Cu-O compound by the addition of a small amount of MoO_3 to the stoichiometry $YSr_2Cu_3O_{6+y}$. The presence of the Mo atom reduces the required reaction temperature to form the high-T_c phase. On the other hand, detailed thermal and microscopic studies of the Ag_2O-added Y123 composites, which exhibit an unusually large pinning characteristic, suggested that silver metal serves as the agent to clean out unwanted nucleation centers, thus allowing the superconducting "123" grains to grow. It is also found that silver particles, in the order of micron, are present dispersively inside grains. It is conceivable that these dispersed silver particles serve as pinning centers for the strong flux

pinning observed. The extra oxygen provided by AgO is believed to enhance the oxygen stability of the superconducting phase, and consequently, the superconducting characteristic of the composites. Based on this study, inclusion of "proper" metal oxides in the formation of high-T_c oxides will enhance the physical properties of the original compound. Diamagnetic-like anomalies were observed in the mixed-phase Y-Ba-(Sr)-Cu-O which have been treated in a low-temperature oxygenation process. Exact origin of the observed anomaly is yet to be determined.

ACKNOWLEDGEMENTS

The authors wish to acknowledge H. Chou, T.L. Kuo, and C.H. Lin of Columbia University; D.C. Ling, M.J. Wang, J.L. Lin, and K.M. Fan of Tsing-Hua University; and K.R. Ma and Dr. S.P. Chang for their contributions. We also thank Dr. H.C. Ku for his support in the thermal analysis work and Dr. L.J. Chen for the TEM work. The work at Tsing-Hua was supported by ROC National Science Council grants NSC79-0208-M007-95.

REFERENCES

1. Bednorz, J.G. and K.A. Muller, 1986, *Z. Phys.*, **B64**, 189.

2. Chen, J.T. et al., 1989, *Mod. Phys. Lett.*, **B3** (November).

3. Wu, M.K. et al., 1988, *Appl. Phys. Lett.*, **52**, 1915.

4. Peter, P.N. et al., 1988, *Appl. Phys. Lett.*, **52**.

5. Dinger, T.R. et al., 1987, *Phys. Rev. Lett.*, **58**, 2687.

6. Chaudhari, P. et al., 1987, *Phys. Rev. Lett.*, **58**, 2684;
   Jin, S. et al., 1988, *Appl. Phys. Lett.*, **52**, 2074.

7. Larbalestier, D. et al., 1987, *J. Appl. Phys.*, **62**, 3308.

8. Esteve, D. et al., 1987, *Europhys. Lett.*, **3**, 1237.

9. Yeshrun, Y. and A.P. Malozemoff, 1988, *Phys. Rev. Lett.*, **60**, 2202.

10. Palstra, T.T. et al., 1988, *Phys. Rev. Lett.*, **61**, 1662.

11. Muller, K.A. et al., 1987, *Phys. Rev. Lett.*, **58**, 1143.

12. Tinkham, M.K., 1988, *Phys. Rev. Lett.*, **61**, 1658.

13. Yeh, N.C. and C.C. Tsuei, 1989, *Phys. Rev.*, **B39**, 9708.

14. Wu, M.K. et al., 1988, Chemistry of High Temperature Superconductor II, ed. by D.L. Nelson and T.F. George, *ACS Symposium Series*, **377**, p. 181.

15. Huang, C.Y. et al., 1988, *Modern Phys. Lett.*, **B2**, 869.

16. Werner, P.E. et al., 1985, *J. Appl. Crystallogr.*, **18**, 367.

17. Mei, Y. et al., 1987, Novel Mechanisms of High Temperature Superconductors, ed. by V. Kresin and S.A. Wolf, p. 1041.

18. Oda, M. et al., 1987, *Jpa. J. Appl. Phys.*, **26**, L804.

19. Zhang, Q.R. et al., 1987, *Solid State Commun.*, **63**, 535.

20. Wu., M.K. et al., 1988, *Phys. Rev.*, **B37**, 9765.

21. Borofka, J.C. et al., 1989, Superalloys, Supercomposites and Superceramics, ed. by J.K. Tien, Academic Press, Inc., 237 pp.

22. Luo, H.L. et al., 1990, Superconductivity and Applications, ed. by Y.H. Kao and H.S. Kwok, Plenum Publishing Co.

23. Chen, H.S. et al., 1989, *Appl. Phys. Lett.*, **55**, 191.

24. Huang, C.Y. et al., 1989, *Mod. Phys. Lett.*, **B3**, 525.

25. Tu, K.N. et al., 1988, *Phys. Rev.*, **B38**, 772.

26. Fueki, K. et al., 1988, *Rev. Solid State Sci.*, **2**, 219.

27. O'Sullivan, E.J.M. and B.P. Chang, 1988, *Appl. Phys. Lett.*, **52**, 1441.

28. Wu, M.K. et al., 1987, *Phys. Rev. Lett.*, **58**, 908.

29. Chien, F.Z. and M.K. Wu, to be published.

MICROSTRUCTURE AND MAGNETIZATION OF Y-Ba-Cu-O PREPARED BY MELT QUENCHING, PARTIAL MELTING AND DOPING

Hamid Hojaji, Shouxiang Hu and Karen A. Michael
Vitreous State Laboratory, The Catholic University of America
Washington, DC 20064

Aaron Barkatt
Department of Chemistry, The Catholic University of America
Washington, DC 20064

Arthur N. Thorpe
Department of Physics, Howard University
Washington, DC 20059

Sidney Alterescu
National Aeronautics and Space Administration
Goddard Space Flight Center
Greenbelt, MD 20770

ABSTRACT

Y-Ba-Cu-O samples prepared by means of a variety of melt-based techniques exhibit high values for their magnetic properties compared with those of samples prepared by solid-state sintering. These techniques include single-stage partial melting as well as melt quenching followed by a second heat treatment stage, and they have been applied to the stoichiometric 123 composition as well as to formulations containing excess yttrium or other dopants. The structure of these melt-based samples is highly aligned, and the magnetization readings exhibit large anisotropy. At 77 K and magnetic field intensities of about 2 kOe, diamagnetic susceptibilities as high as -14×10^{-3} emu/g have been obtained in the cases of melt-quenched samples and remanent magnetization values as high as 10 emu/g for samples prepared by partial melting.

INTRODUCTION

The attainment of high critical current (J_c) values is the key for numerous potential applications of high-T_c superconducting materials.[1] Critical currents of bulk superconducting oxides, such as $YBa_2Cu_3O_z$ with z values close to 7 (often designated 123), prepared by solid-state sintering, are generally low. Much higher values have been obtained using melt-based processing methods such as partial melting,[2-5] melt quenching and subsequent growth at intermediate temperatures,[6] and melt-textured growth using directional solidification.[7] In addition, variations from the exact 123 stoichiometry, based on increasing the proportion of one of its ingredients (in particular, yttrium) or on the introduction of other metal oxides as dopants, have yielded promising results when combined with melt-based preparative methods.[8,9]

SAMPLE PREPARATION

In the study reported here, specimens were prepared using the partial melting and the melt quench techniques. Sample compositions included stoichiometric $YBa_2Cu_3O_z$, yttrium-enriched $Y_xBa_2Cu_3O_z$ with $x > 1$, and doped $YA_{0.1}Ba_2Cu_3O_z$, with the additive A being a rare earth element or niobium. The preparation techniques are described in Refs. 5 and 9. Briefly, sample preparation involved grinding together a mixture of the oxides of Y, Cu and the additive A, whenever introduced, with $BaCO_3$, in the desired proportions. The mixture was subjected to several cycles of calcination and re-grinding. In the cases of samples prepared by partial melting, the oxide mixtures were rapidly heated to a temperature between 1000°C (the decomposition temperature of $YBa_2Cu_3O_z$[10]) and 1200°C, usually between 1030°C and 1100°C, to form a mixture of Y_2BaCuO_5 and a liquid phase[10]. The sample was then cooled down slowly under oxygen to undergo peritectic conversion to $YBa_2Cu_3O_z$ and to ensure that the material was fully oxygenated to maintain the superconducting orthorhombic structure. In cases where melt quenching was employed, the oxide mixtures were first heated to a temperature above 1400°C to yield a mixture of Y_2O_3 and a liquid phase[10], rapidly cooled down to room temperature, and then re-heated at 1030-1100°C and slowly cooled under oxygen as detailed above. The latter procedure permitted control of the growth of the Y_2BaCuO_5 phase as well as of its $YBa_2Cu_3O_z$ product. In the cases of formulations containing excess yttrium or an additive A, the final product contained a second phase based on Y_2BaCuO_5. The substrates used during the heat treatments included platinum, quartz, alumina, and alumina pre-treated with Y-Ba-Cu oxide powder. The latter, in particular, appeared to minimize the extent of sample deterioration due to interaction with the substrate.[9,11-12]

SAMPLE CHARACTERIZATION

The microstructure of the resulting specimens was characterized by means of scanning electron microscopy (SEM). The magnetic susceptibility, chi, was determined using a Faraday balance and the dc magnetization, M, was measured as a function of magnetic field

intensity using a vibrating sample magnetometer. The latter measurements, carried out at field intensities ranging up to 5 kOe, yielded values for the maximum magnetization, M_{max}, obtained at a low field intensity (H_c^*), as well as for the width of the magnetization hysteresis loop,
Delta M = M_+ - M_-. The latter quantity and its relative magnitude Delta M / M_{max} are of great importance because of the inter-relationship between Delta M and the critical current, J_c.[13,14] The results of the magnetic measurements, reported in Table 1, represent values of the magnetic susceptibility and the magnetization obtained at a temperature of 77 K. The magnetic susceptibilities in Table 1 were measured in a field of 2.25 kOe and the remanent magnetization (Delta M) in a field of 2 kOe. The orientation of each sample relative to the magnetic field was optimized prior to each magnetization measurement.

RESULTS AND DISCUSSION

The results in Table 1 cover a range of samples which include materials of stoichiometric 123 composition, materials containing excess yttrium and materials containing rare earth and Nb additives. Some of the samples were prepared by single-stage partial melting (PM), while in other cases this stage was preceded by a melt quenching (MQ) step, as detailed above. In the cases of all the materials included in Table 1, the critical temperature (T_c), based on the onset of the superconducting transition in the magnetic susceptibility measurements, was observed to be (91 +- 2) K.

The microstructure of the various melt-based samples described above, observed in the SEM studies, is generally highly dense and ordered. Unlike sintered samples, which consist of assemblages of poorly aligned small grains,[5] the melt-based samples consistently exhibit the presence of highly aligned regions which are relatively large (of the order of several millimeters). The microstructure of the last sample in Table 1 is shown in Figs. 1a and 1b.

The results shown in Table 1 indicate high values of the magnetic properties can be obtained in the cases of materials prepared using the techniques described above. The maximum magnetization reported here, which ranges up to 8 emu/g, is significantly higher than that of typical materials prepared by solid-state sintering, with values of up to about 2 emu/g.[5] More significantly, the ratio of remanent to maximum magnetization in the melt-based materials is high, ranging about 1 and, in certain cases, even higher. As a result, the remanent magnetization itself is high, reaching values up to 10 emu/g. This indicates that improvements in melt-based processing yield a higher degree of magnetic flux pinning at high fields, which is associated in its turn with higher values of J_c. The magnetization curve of the last sample in Table 1 is shown in Fig. 2. As mentioned above, the magnetization of each sample was measured at different orientations of the sample with respect to the direction of the magnetic field. In general, the magnetization is highly dependent on the orientation of the layered 123 grain structure with respect to the

TABLE 1

Magnetic Properties of Materials Prepared by the Partial Melting and Melt Quench Methods at 77 K

Composition, YxAyBa2CuOz x	A	y	Method	Chi emu/g X1000	Delta M emu/g	Mmax emu/g	Delta M /Mmax	Hc1* Oe
1.0	Tb	0.1	MQ	-14.3	2.0	2.9	0.68	165
1.1			MQ	-12.9	2.4	4.2	0.57	205
1.0			MQ	-11.1	2.5	4.0	0.64	236
1.0			MQ	-11.7	3.1	4.3	0.71	218
1.0	Tb	0.1	MQ	-13.2	3.6	5.3	0.67	196
1.0			MQ	-10.4	3.9	5.7	0.69	237
1.0	Nb	0.1	MQ	-2.2	4.3	6.0	0.72	246
1.0	Ho	0.1	MQ	-1.9	4.4	5.0	0.89	67
1.0	Nb	0.1	MQ		4.8	5.1	0.99	105
1.0			PM		5.0	4.8	1.04	165
1.0	Tb	0.1	PM	-2.1	5.2	3.4	1.52	153
1.1			MQ	-5.9	5.4	3.9	1.38	151
1.0			PM	-3.4	5.7	4.5	1.27	219
1.0			PM	-5.1	7.3	6.1	1.19	281
1.0			PM	-5.1	7.7	8.0	0.97	297
1.0			PM		9.8	7.9	1.24	231



Figure 1. Scanning electron micrographs of a high-magnetization $YBa_2Cu_3O_7$ sample prepared by the partial melting technique.

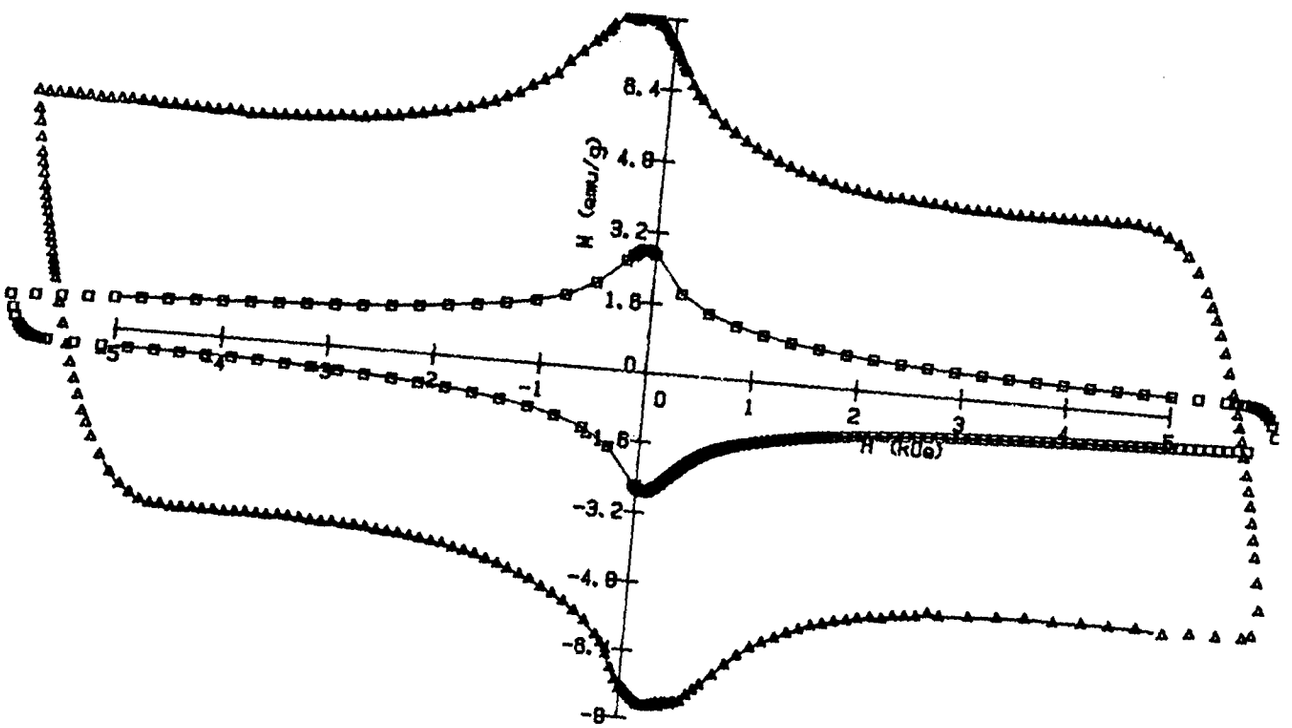


Figure 2. Magnetization hysteresis loop at 77 K for the sample shown in Figure 1. Triangles - field parallel to c axis; squares - field perpendicular to c axis.

applied field. This large anisotropy is reflected in Fig. 2, which shows that the magnetization obtained with the magnetic field perpendicular to the layered structure is much higher than the magnetization obtained when the field is parallel to the 123 layers. These findings are consistent with the notion that the layers are grown in a direction parallel to the ab plane, and that the maximum magnetization is obtained when the applied field is perpendicular to this plane, while the current density is highest parallel to the ab plane.[15] Similar findings were previously reported in magnetization measurements on single crystals.[16]

The formation of more quantitative conclusions on the basis of the data shown in Table 1 is hampered by the irreproducibility among readings obtained with samples prepared using an identical, or near-identical, procedure. This irreproducibility may be due to several factors, including the varying extent of completion of the oxygenation of the samples in the course of the final cooling stage, which is highly dependent on sample dimensions, and the presence of cracks, resulting from the evolution of excessive stresses at grain boundaries during the growth of the 123 phase from the combination of Y_2BaCuO_5 and liquid. The remaining differences in magnetic properties among the various melt-based samples may reflect differences in the extent of mutual alignment among the regions of highly aligned grains, which are shown in Figs. 1a and 1b, in different samples. The degree of domain alignment depends in its turn on the number and size of the domains of parallel 123 crystals and is highly sensitive to the thermal history of each sample.

With these limitations in mind, the data in Table 1 suggest that all three techniques used in the present study (partial melting, melt quenching, use of non-stoichiometric formulations) produce improved magnetic properties compared with those of sintered samples (see above). This may reflect the effectiveness of melt-based techniques and the introduction of dopants, accompanied by slow cooling during the growth of 123 from the melt and its oxygenation, in minimizing the formation of pores, cracks and insulating phases such as $BaCuO_2$[9]. The data obtained so far are not sufficient to determine conclusively which of these techniques could give rise to the highest magnetization. It should be noted, however, that increased magnetization does not appear, in general, to be associated with high diamagnetic susceptibility (see Table 1). The highest values of the diamagnetic susceptibility are encountered in the cases of samples prepared by means of the melt quench technique, but the samples which have the highest susceptibility do not exhibit a very high magnetization. On the other hand, among the samples characterized in the present study, those prepared by partial melting have so far yielded the highest magnetization values, as well as somewhat higher ratios of remanent to maximum magnetization, indicative of highly effective pinning of the magnetic flux.

ACKNOWLEDGEMENT

The authors are very grateful to Dr. A.C. Buechele for his assistance in performing the SEM work. This study was supported by the National Aeronautics and Space Administration under Contract no. NAG 5-1017.

REFERENCES

1. D.U. Gubser, S.A. Wolf and R.J. Soulen, Science, 245, 111-112 (1989).
2. M.E. McHenry, J. McKittrick, S. Sasayama, V. Kwapong, R.C. O'Handley and G. Kalonji, Phys. Rev. B, 37, 623-626 (1988).
3. E. L. Venturini, D.S. Ginley, R.J. Baughman, B. Morosin and J.F. Kwak, in High-Temperature Superconductors, eds. M.B. Brodsky, R.C. Dynes, K. Kitazawa and H.L. Tuller, Mater. Res. Soc. Symp. Proc., Vol. 99, Materials Research Society, Pittsburgh, PA, 1988, pp. 639-642.
4. K. Salama, V. Selvamanickam, L. Gao and K. Sun, Appl. Phys. Lett., 54, 2352-2357 (1989).
5. H. Hojaji, K.A. Michael, A. Barkatt, A.N. Thorpe, M.F. Ware, I.G. Talmy, D.A. Haught and S. Alterescu, J. Mater. Res., 4, 28-32 (1989).
6. M. Murakami, M. Morita and N. Koyama. Jpn. J. Appl. Phys., 28, L1125-L1127 (1989).
7. S. Jin, T.H. Tiefel, R.C. Sherwood, M.E. Davis, R.B. van Dover, G.W. Kammlott, R.A. Fastnacht and H.D. Keith, Appl. Phys. Lett., 52, 2074-2076 (1988).
8. Y. Wadayama, K. Kudo, A. Nagata, K. Ikeda, S. Hanada and O. Izumi, Jpn. J. Appl. Phys., 27, L1441-L1224 (1988).
9. H. Hojaji, A. Barkatt, K.A. Michael, S. Hu, A.N. Thorpe, M.F. Ware, I.G. Talmy, D.A. Haught and S. Alterescu, J. Mater. Res., 5, xxx-xxx (April 1990).
10. M. Murakami, M.Morita, K.Doi, K. Miyamoto and H. Hamada, Jpn. J. Appl. Phys., 28, L399-L401 (1989).
11. W.N. Wang, H.B. Lu, W.J. Lin, P.C. Yao, H.E. Hsu, M.F. Tai and H.C. Ku, Jpn. J. Appl. Phys., 273, L1268-L1270 (1988).
12. K. Yoshiara, K. Kagata, S. Yokoyama, T. Hiroki, H. Higuma, T. Yamazaki and K. Nakahigashi, Jpn. J. Appl. Phys., 27, L1492-L1494 (1988).
13. C.P. Bean, Phys. Rev. Lett., 8, 250-253 (1962).
14. W.A. Feitz, M.R. Beasley, J. Silcox and W.W. Webb, Phys. Rev., 136, A335-A345 (1964).
15. Y. Nakagawa, H. Yamasaki, H. Obara and Y. Kimura, Jpn. J. Appl. Phys., 28, L547-L550 (1989).
16. T.R. Dinger, T.K. Worthington, W.J. Gallagher and R.L. Sandstrom, Phys. Rev. Lett., 58, 2687-2690 (1987).

EFFECT OF SHOCK PRESSURE ON THE STRUCTURE AND SUPERCONDUCTING PROPERTIES OF Y-Ba-Cu-O IN EXPLOSIVELY FABRICATED BULK METAL-MATRIX COMPOSITES.

L. E. Murr, C. S. Niou, and M. Pradhan-Advani

Department of Metallurgical and Materials Engineering
The University of Texas at El Paso
El Paso, Texas 79968-0520 USA

Abstract

Explosively fabricated or shock-wave processed $YBa_2Cu_3O_x$ exhibits a resistance-temperature signature characterized by a semiconducting normal-state behavior and a superconducting transition which is broadened with increasing shock pressure. The relative susceptibility (χ/χ_o) decreases with pressure while characteristic X-ray split-peak broadening is increased. Recovery of superconductivity requires thermal treatment in oxygen at temperatures above 900°C. Transmission electron microscope observations have revealed defect clusters having large, associated strain fields, apparently created by discontinuities in the shock front. A comparison of shock pressure effects with oxygen order-disorder phenomena and radiation (ion, electron, and neutron) effects illustrates the potential for controlling the resistance-temperature signature and the transport supercurrent density through flux pinning microstructures which optimize the explosive fabrication process and the residual superconductor behavior.

Introduction

While it is now well established that copper-oxide-based powder, or virtually any other ceramic superconductor powder, can be consolidated and encapsulated within a metal matrix by explosive consolidation (1-4), the erratic superconductivity following fabrication has posed a major problem for bulk applications of $YBa_2Cu_3O_7$. The nature of this behavior seems to arise from microstructural damage resulting from defects created in the shock front (5,6). Murr, et al. (3,7) have shown that the microtwin density in $YBa_2Cu_3O_7$ increases by an order of magnitude following explosive fabrication of superconducting powder at pressures of 4 to 8 GPa (6).

In this investigation we have examined the effects of shock pressure on the residual superconducting behavior of explosively fabricated bulk composites, principally the resistance versus temperature curve and the effects that heat treatment can have on restoring degraded superconductivity. The effect of shock pressure on residual susceptibility, and the relationship of shock-induced degradation to residual microstructure, especially shock-induced microstructure are also examined.

These features are implicit in systematic peak broadening of

characteristic X-ray spectra or observed directly by transmission electron microscopy. We also examine the implications of these observations in the context of related alterations (and degradation) of superconductivity by a variety of radiation treatments (8-12), elemental substitutions (13), and variations in oxygen content (14).

Experimental Considerations and Results

The details of explosive (shock-wave) fabrication of Y-Ba-Cu-O powder and the shock loading of sintered Y-Ba-Cu-O bulk samples have been given elsewhere (1-3,5,15). Conformal channels milled into a base plate are filled with superconducting Y-Ba-Cu-O powder prepared by a solid-state route described previously (3), and a cover plate is fitted into the channel to contain and pre-compress the powder. The flyer or cladding plate is then explosively welded to the base plate, simultaneously consolidating the powder, bonding it to the channel, and creating a monolithic composite. The accompanying shock wave produces defects which alter the residual superconductivity. The fabricated Y-Ba-Cu-O channel was removed from the metal or alloy monolith, and a four-probe electrode configuration attached using silver paste. The R-T signatures were measured using a standard test current of 10 mA. Coupons of sintered Y-Ba-Cu-O were subjected to a 6 GPa shock pulse (5). The samples were recovered and the resistance versus temperature curve measured as described above.

We have also measured the microwave surface resistance (R_s) for Y-Ba-Cu-O superconducting powder following explosive fabrication and after heat treatment. A resonant microstrip technique was used (16) and compared with a copper reference sample at the same resonant frequency. Figure 1 shows an example of a prototype from which

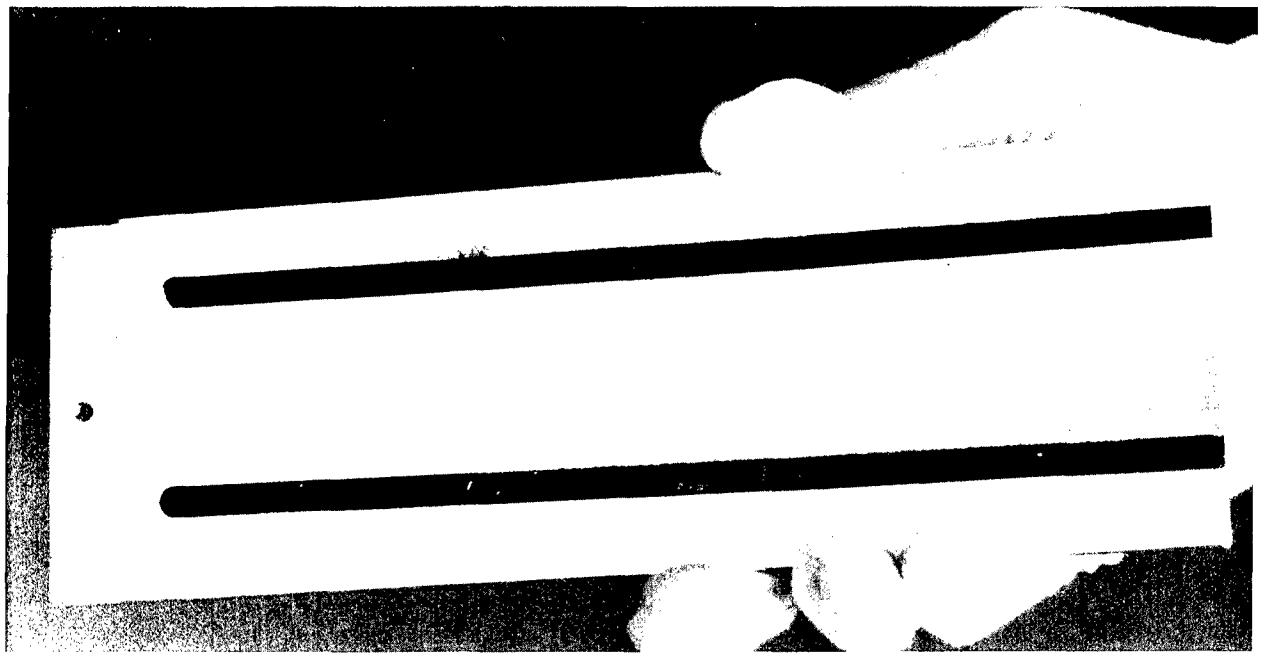


FIG. 1: Example of explosively fabricated, monolithic prototype showing a milled section exposing superconducting channels in A1-6061-T6 tooling plate.

samples have been extracted for R_s measurements, as well as other measurements (including supercurrent density). In the example shown in Fig. 1, the base plate was an aluminum 6061-T6 alloy, the cover plates were silver, and the cladding plate was copper. The copper clad plate and cover plates have been milled away to expose the Y-Ba-Cu-O consolidated powder channel strips.

Figure 2(a) shows the as-fabricated, resonant microwave surface resistance values (R_s) compared with several other experimental measurements at liquid nitrogen temperature (77K). In addition, Fig. 2(a) also shows the annealed R_s value, the bulk d.c. resistance ($R_{d.c.}$) following explosive fabrication, and the annealed, bulk superconductivity (zero resistance) from Fig. 2(b) and (c). The dotted line in Fig. 2(a) corresponds to the bulk resistance at 77K (in liquid nitrogen). It is of interest to note in Fig. 2(a) that while the R_s value for copper increases in the microwave regime in comparison to the bulk, d.c. (zero frequency) regime, the as-fabricated Y-Ba-Cu-O resistance actually decreases ($R_s < R_{d.c.}$). On the other hand, $R_{d.c.}$ (=0) < R_s (=16 mΩ) for the annealed, superconducting Y-Ba-Cu-O (Fig. 2(b)).

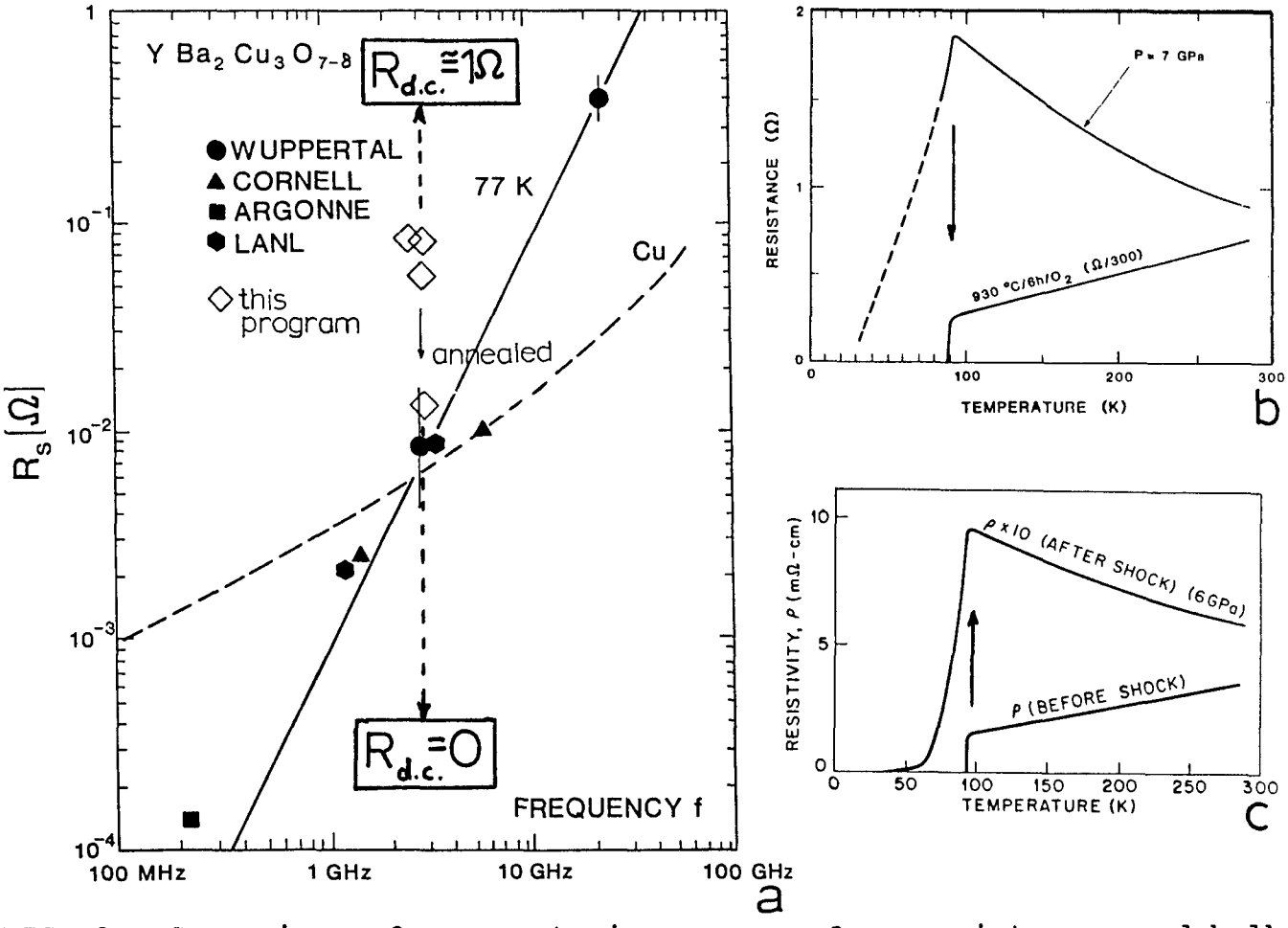


FIG. 2: Comparison of resonant microwave surface resistances and bulk resistance values along with other laboratory data for Y-Ba-Cu-O (a) with shock consolidated and annealed powder (b) and plane-wave shock loaded sintered coupons (c).

We examined the a.c. magnetic susceptibility ($-4\pi\chi$) by regrinding samples of explosively consolidated channel sections extracted from the monolithic composites illustrated in Fig. 1 to the same size and size distribution of the starting powder and pressing these powders into cylindrical pellets having a green density of ~65%. These experimental pellets were then measured along with the starting, unfabricated powder pellets, to obtain relative susceptibility ratios (χ/χ_o); where χ_o is the susceptibility for the unfabricated (unshocked) powder. In addition, portions of the reground powder samples, as well as the unfabricated powders, were examined by X-ray diffraction spectrometry (Cu-Kα radiation), and characteristic, orthorhombic split-peak signatures (corresponding to $2\theta \cong 32^\circ$ and 58°) as discussed previously (4) were compared.

Figure 3 shows for comparison the measured relative susceptibilities and the ratios of X-ray peak broadening (for $\Delta 2\theta \cong 32^\circ$) as a function of shock pressure. It is apparent that there is a consistent and characteristic degradation of diamagnetic shielding (χ/χ_o) with increasing shock pressure. In addition, these results correspond to previous but higher shock pressure research by Morosin, et al. (17), and also correspond to increasing strain energy ($\Delta 2\theta/\Delta 2\theta_o$) consistent with higher densities of shock-induced defects.

We examined the unfabricated powders and sintered Y-Ba-Cu-O as well as the explosively fabricated and shock loaded Y-Ba-Cu-O (Fig. 2(c)) by argon ion milling (at 6keV) of mechanically ground and polished thin sections to produce electron transparent specimens which could be observed in the transmission electron microscope. A Hitachi H-800 analytical STEM was used at 200kV to perform a range of CTEM observations, including high-resolution lattice imaging.

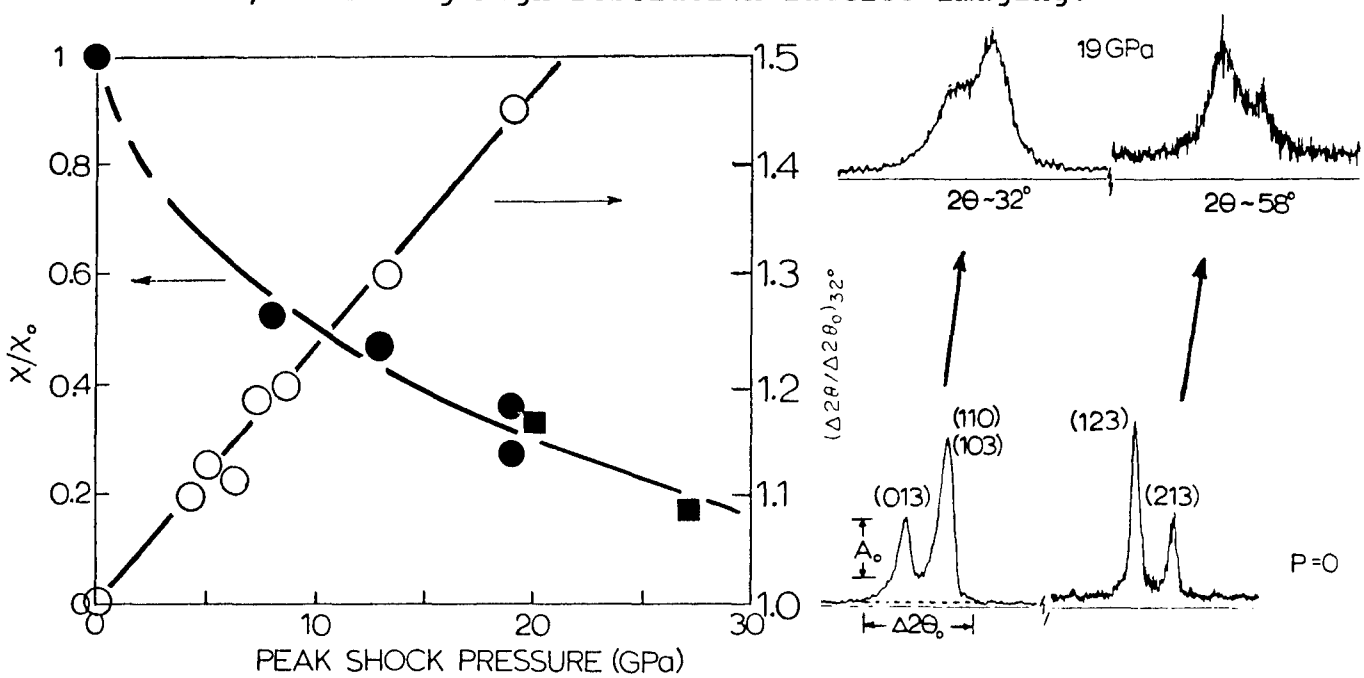


FIG. 3: Relative susceptibility and characteristic orthorhombic X-ray peak broadening ratio versus shock pressure. The data of Morosin, et al. (17) is shown for comparison as solid squares.

Figure 4 illustrates some examples of shock-induced defects which are observed in the explosively fabricated (Fig. 4(a)) as well as the plane-wave shock loaded material (Fig. 2(c)). These defects exhibit significant strain field contrast (Fig. 4(b)) which can phenomenologically account for the significant peak broadening (residual strain broadening) observed in the X-ray diffraction studies illustrated in Fig. 3. Furthermore overlapping strain fields could also phenomenalogically account for the complete lack of a superconducting transition by destroying the phase coherence of the superconducting pair wave function as alluded to in the work of White, et al. (18) where the phase coherence was destroyed by high fluence ion irradiation of $YBa_2Cu_3O_x$ films which produced microstructural damage created by what they described as nuclear-energy loss processes.

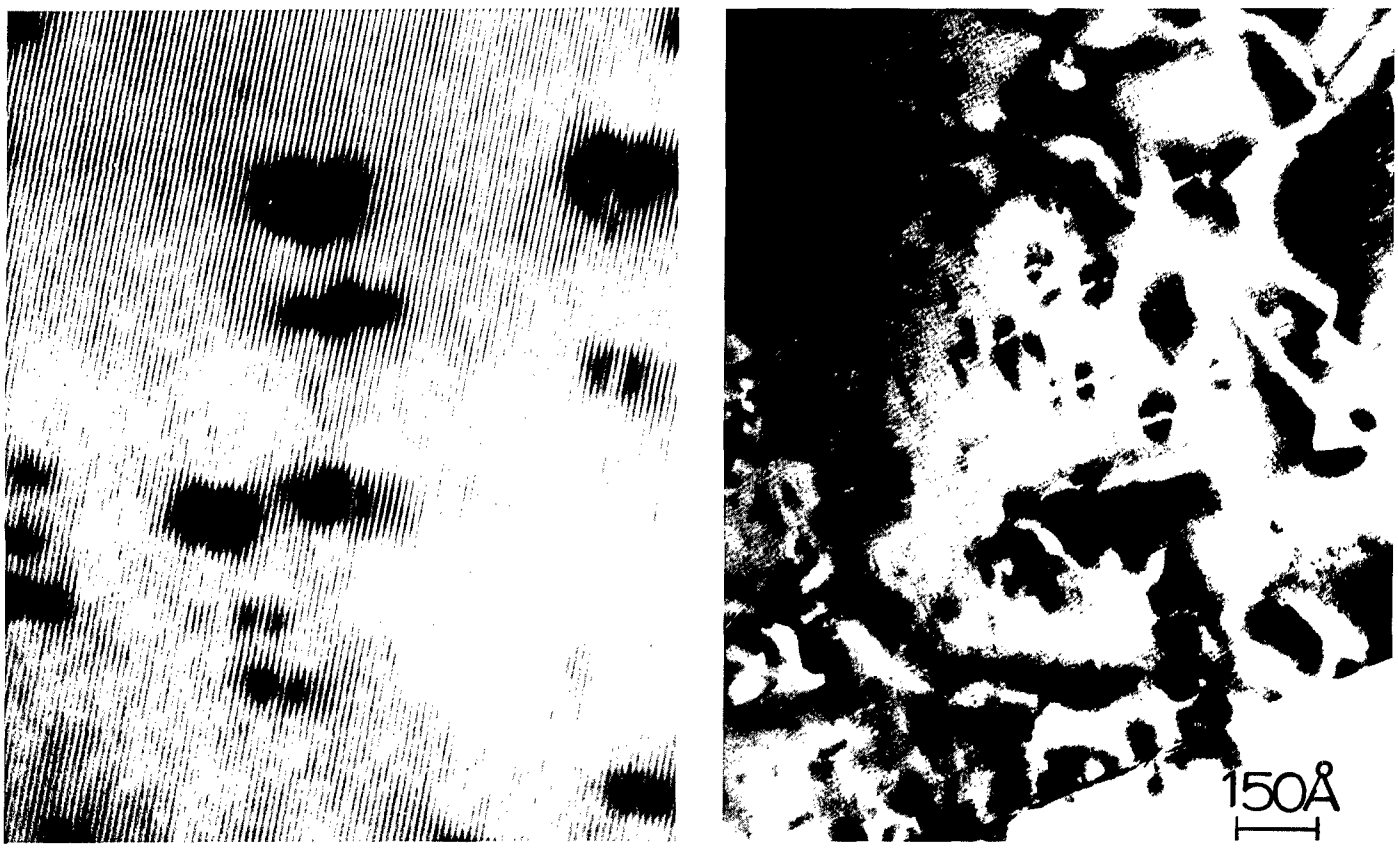
Discussion and Comparison of Shock-Pressure Effects

It is now well established that $YBa_2Cu_3O_{7-\delta}$, either as a thin film or bulk material, is very sensitive to defects, including subsitutional impurities (13), oxygen concentration, (8) (which variously alters the oxygen order-disorder phenomenon, particularly in the context of b-chain Cu-O periodicity (14,19)), and a host of irradiation effects (8-12,18).

These effects are illustrated for comparison with the effect of shock pressure and heat treatment in Fig. 5. An interesting feature about shock or explosive fabrication in contrast to oxygen deficiency or ion or electron irradiation is the fact that the T_c (onset) does not change with pressure or heat treatment. Recent work by van Dover, et al. (12) has indicated that the R-T signature (the transitional broadening) is not changed with neutron irradiation, while significant flux pinning raises the critical current density (as measured from magnetization changes) to a value near 10^6 A/cm^2. A feature observed in Fig. 5 is the rather consistent decrease in T_c (onset) for oxygen deficiency and electron and ion irradiation.

While there have not been any observations of defects in any irradiated samples (except for the early ion damage studies by Clark, et al. (8) which suggested the stimulated growth of an amorphous layer at the grain boundaries in thin films), it is apparent that the defects are different from those observed in Fig. 4. In addition, the effects or radiation may also differ in thin film and bulk materials not dominated by weak-link intergranular connections. It is obvious from Fig. 4 that the shock wave-induced defects are not simple atomic displacements but rather a cluster which resembles a precipitate (6), which is not easily annealed out (Fig. 5(a)). By comparison, the effects of electron and ion irradiation can often be annealed out at temperatures just above room temperature (8,10), suggesting simple displacements, even oxygen displacements from the Cu-O chains may be involved.

It is generally accepted that the ordering of the Cu-O chains is essential for superconductivity in the $YBa_2Cu_3O_7$ (or $YBa_2Cu_3O_x$), especially the so-called chain planes (the basal planes in the unit cell)(14,19,20). In fact, as illustrated schematically in Fig. 6, subtracting only one oxygen from the unit cell of $YBa_2Cu_3O_7$ produces a



(a) (b)

FIG. 4: Defect clusters with associated strain field contrast observed in explosively fabricated and shocked Y-Ba-Cu-O. (a) shows lattice image viewed along the b-chains [010] after explosive fabrication at 7 GPa. (b) Strain-field contrast of defects in plane-wave shock loaded Y-Ba-Cu-O at 6 GPa.

nonsuperconducting, semiconducting (or semi-insulating) material ($YBa_2Cu_3O_6$). Figure 6 also shows the structural variances which can occur for specific oxygen stoichiometries between the superconducting, orthorhombic $YBa_2Cu_3O_7$ and the nonsuperconducting, tetragonal $YBa_2Cu_3O_6$, where the transitional stoichiometries at x = 6.75, 6.5, and 6.25 correspond roughly to the distinctions in the oxygen R-T signatures shown in Fig. 5(b). Figure 7 also elaborates the Cu-O b-chain periodicities which, along with the oxygen order-disorder can account for shifts in the T_c (onset) as well as variations in the normal state resistance (or resistivity)(Fig. 5(b)). The oxygen in the chains (Fig. 7) is the weakest bound of the elemental species in Y-Ba-Cu-O and is easily removed even by thermal treatment (19). Such displacements can also account for the creation of microtwins by systematic displacement of oxygen on the b axis to interstitial locations on the a axis. Indeed there is an increase in microtwin density with explosive processing at lower pressures (4 to 8 GPa)(3) and there is no apparent oxygen loss (5).

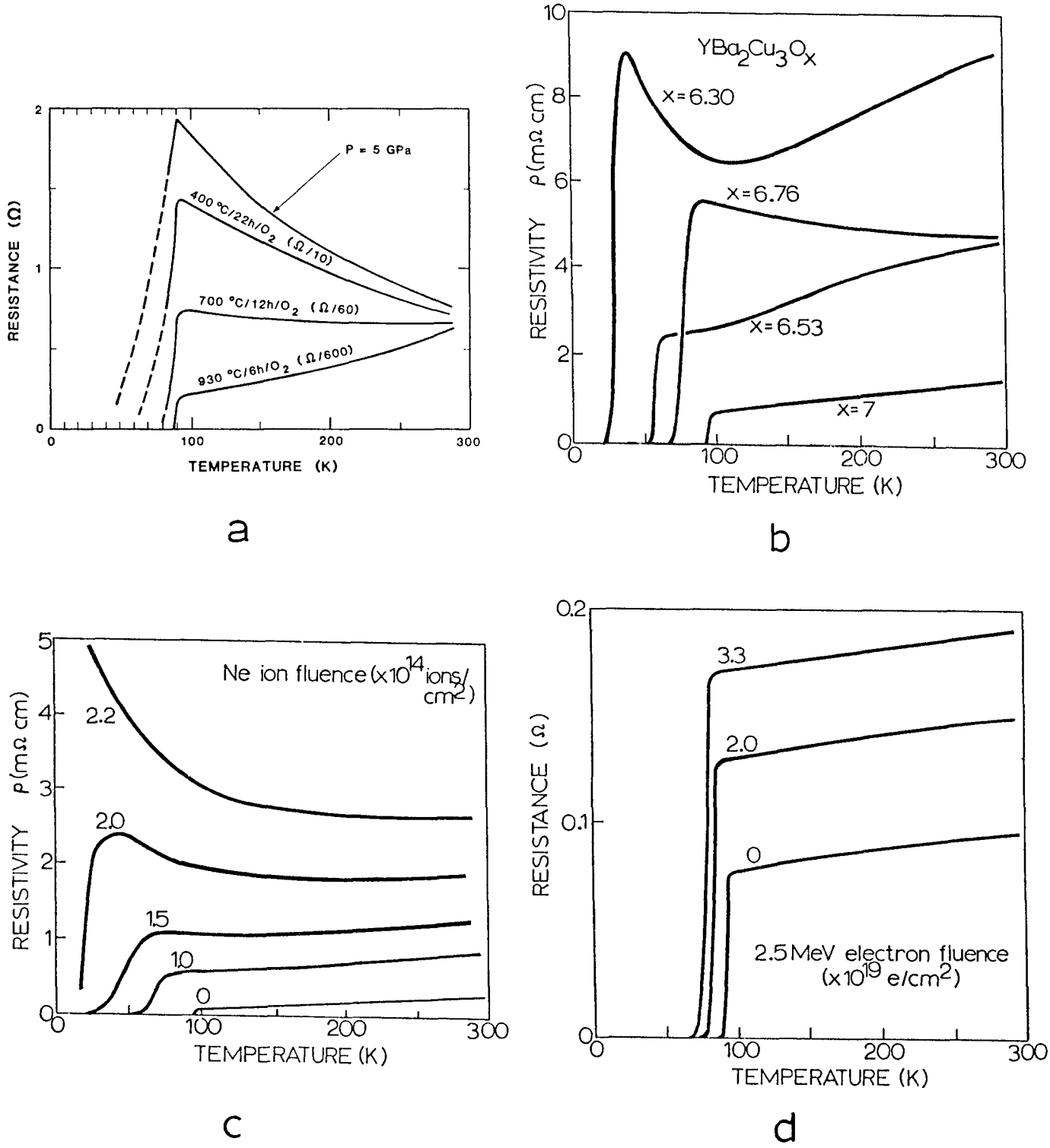


FIG. 5: Comparison of resistance-temperature signatures for shock fabricated and heat treated Y-Ba-Cu-O (a) with those for oxygen (x) deficient (b), ion irradiated (c), and electron irradiated (d) Y-Ba-Cu-O. Data reproduced in (b), (c), and (d) is after references (14), (9), and (10) respectively.

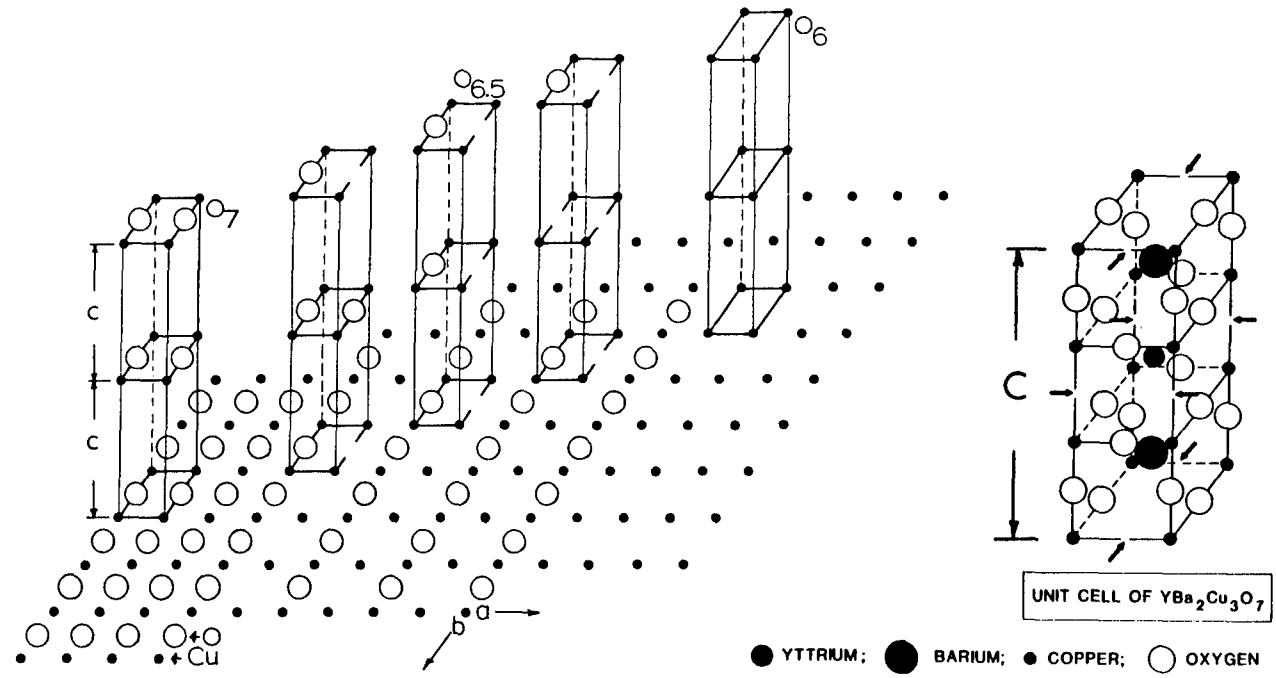


FIG. 6: Basal-plane oxygen (vacancy) order-disorder along b-chains (b-axis) and Cu-O chain periodicity with oxygen content. The double unit cell variances produce variations in b-chain periodicities as shown.

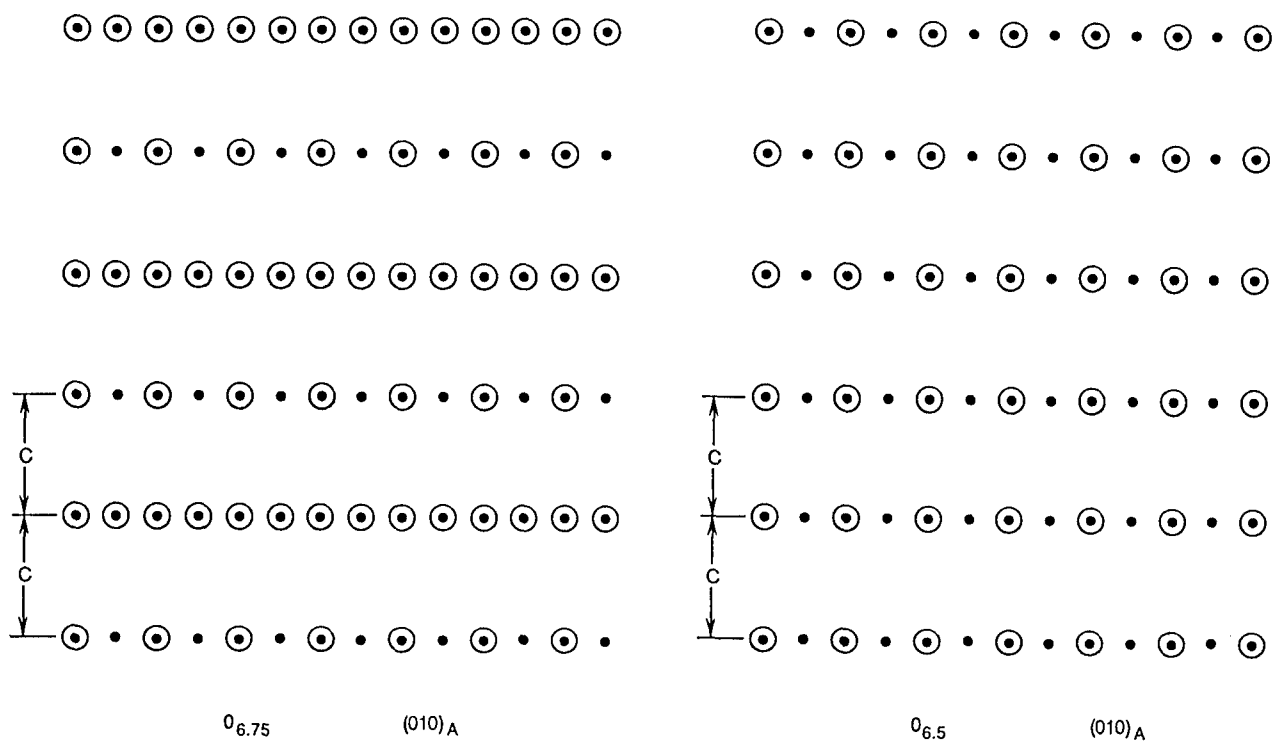


FIG. 7: Schematic views of b-chain periodicities viewed in the b-axis direction (Fig. 6). Solid circles are copper, open circles are oxygen. These views show oxygen vacancy periodicity in the b-chain.

In the context of granularity, macroscopic resistivity is strongly influenced by each grain or microstructural domain which contributes to a partial path across the sample, creating a kind of percolation, with the zero resistance state occurring at or near the percolation threshold (21). However, in bulk superconductors the zero resistance paths can be along the surface, and this phenomena can at least account in principle for the anomalous resistance difference illustrated in Fig. 2(a) which in effect compares the bulk ($R_{d.c.}$) percolation resistance with the surface, microwave resistance (R_s) at constant temperature (77K). This difference may also reflect the relaxation of strain fields or defects near the surface as well.

Conclusions

It is clear from Figs. 5 and 6 that the atomic ordering, and even the ordering of Cu-O chains as suggested in Fig. 7, as well as a variety of crystal defects, have a controlling influence not only on the superconducting transition and the transition temperatures, but also on the normal-state resistance behavior as well. The shape of the R-T curve might therefore be manipulated by a clear understanding of the role that specific defects can play, and their interaction to produce specific resistance-temperature signatures, and flux pinning to accomodate large supercurrent transport densities.

It may be possible to manipulate the microstructure of the starting superconducting powder to optimize the R-T signature as well as the flux pinning properties so that both are enhanced following explosive fabrication. Jin, et al. (22) have in fact recently demonstrated that intragranular flux pinning could be enhanced by fine-scale defects (similar to those shown in Fig. 4) produced by rapid decomposition of the $YB_2Cu_4O_8$ precursor to superconducting Y-Ba-Cu-O. While the shock wave might alter the nature of such defects or create new or additional defects, the residual microstructures might produce a different R-T signature than those shown in Fig. 2(b) and (c) and Fig. 5(a). In effect, it may be possible to take advantage of atomic-scale distortions by tailoring the starting materials microstructures and optimizing the explosive fabrication process by adjusting the shock pressure without compromising the cladding of the metal matrix assembly. This will require a more concerted effort to systematically examine a wide range of microstructures by transmission electron microscopy.

Acknowledgements

This research is supported by the DARPA HTSC Program under Contract ONR-N00014-88-C-0684, and in part by NASA(Goddard)-SBIR Contract NAS5-30504 through Monolithic Superconductors, Inc. We thank Dr. L. H. Schoenlein for his help with some of the electron microscopy analysis and Dr. Wayne Bongianni for his help in measuring the resonant microwave resistances.

References

1. L. E.Murr, A. W. Hare, and N. G. Eror, Nature, 329, 37(1987).
2. L. E. Murr, N. G. Eror, and A. W. Hare, SAMPE J., 24(6), 15(1988).
3. L. E. Murr, T. Monson, J. Javadpour, M. Strasik, U. Sudarsan, N. G. Eror, A. W. Hare, D. G. Brasher, and D. J. Butler, J. Metals, 40(1), 19(1988).
4. L. E. Murr and N. G. Eror, Materials & Manufacturing Processes, 4(2), 177(1989).
5. L. E. Murr, C. S. Niou, S. Jin, T. H. Tiefel, A. C. W. P. James, R. C. Sherwood, and T. Siegrist, Appl. Phys. Lett., 55(15), 1575(1989).
6. L. E. Murr, M. Pradhan-Advani, C. S. Niou, and L. H. Schoenlein, Solid State Comm., in press (1990).
7. L. E. Murr, T. Monson, M. Strasik, U. Sudarsan, N. G. Eror, and A. W. Hare, J. Superconductivity, 1(1), 3(1988).
8. G. J. Clark, A. D. Marwick, R. H. Koch, and R. B. Laibowitz, Appl. Phys. Lett. 51, 139(1987).
9. J. M. Valles, A. E. White, K. T. Short, R. C. Dynes, J. P. Garno, A. F. J. Levi, M. Anzlowar, and K. Baldwin, Phys. Rev. B., 39(16), 11,599(1989).
10. H. Vichery, F. Rullien-Albenque, H. Pascard, M. Konczykowski, R. Kormann, D. Favrot, and G. Collin, Physica C, 159, 697(1989).
11. A. Umezawa, G. W. Crabtree, J. Z. Liu, H. W. Weber, W. K. Kwok, L. H. Nunez, T. J. Moran, and C. H. Sowers, Phys. Rev. B., 36(13), 7151(1987).
12. R. B. van Dover, E. M. Gyorgy, L. F. Schneemeyer, J. W. Mitchell, K. V. Rao, R. Puzniak, and J. V. Waszczak, Nature, 342 55(1989).
13. G. Xiao, F. H. Streitz, A. Garvin, Y. W. Du, and C. L. Chien, Phys. Rev. B, 35, 8782(1987).
14. R. J. Cava, B. Batlogg, L. H. Chen, E. A. Rietman, S. M. Zahurak, and R. Werder, Phys. Rev. B, 36, 5719(1987).
15. L. E. Murr, C. S. Niou, and M. Pradhan-Advani, to be published (1990).
16. J. L. Archer, W. C. Bongianni, and J. H. Collins, J. Appl. Phys., 41(3), 1359(1970).
17. B. Morosin, R. A. Graham, E. L. Venturini, and D. S. Ginley, Proc. 2nd Workshop on Industrial Application Feasibility of Dynamic Composition Technology, Tokyo Institute of Technology, Dec. 1-2, 1988, p. 97.
18. A. E. White, K. T. Short, D. C. Jacobson, J. M. Poate, R. C. Dynes, P. M. Mankiewich, W. J. Kocpol, R. E. Howard, M. Anzlowar, K. W. Baldwin, A. F. J. Levi, J. R. Kwo, T. Hsich, and M. Hong, Phys. Rev. B, 37(7), 3755(1988).
19. G. Van Tendeloo, H. W. Zandbergen, and S. Amelinckx, Sol. St. Comm., 63, 389(1987).
20. T. Siegrist, S. Sunshine, D. W. Murphy, R. J. Cava, and J. M. Zuhurak, Phys. Rev. B, 35, 7137(1987).
21. D. C. Larbalestier, M. Daeumling, P. J. Lee, T. F. Kelly, J. Seuntjens, C. Meingast, X. Cai, J. Mckinnell, R. D. Ray, R. G. Dillenburg, and E. E. Hellstran, Cryogenics, 27, 411(1987).
22. S. Jin, T. H. Tiefel, S. Nakahara, J. E. Graebner, H. M. O'Bryan, R. A. Fastnacht, and G. W. Kammlott, Appl. Phys. Lett., in press (1990).

PRODUCTION OF SUPERCONDUCTOR/CARBON BICOMPONENT FIBERS

S.A.Wise, C.C. Fain, and H.D. Leigh
Dept. of Ceramic Engineering, Clemson University, Clemson, SC

Superconductor/carbon bicomponent fibers have been prepared by filling specially produced C-shaped carbon fibers with a suspension of $YBa_2Cu_3O_{7-x}$ powders. The bicomponent fibers were processed in an inert atmosphere to retain the strength and flexibility of the carbon backbone. However, reactions between the carbon fiber and the oxygen content of the superconductor were observed. In response to this problem, metallic layers were physically evaporated onto the carbon surface, and the fibers were converted to metal oxides, carbides, and nitrides. Superconductor/ceramic bicomponent fibers were then prepared by filling the ceramic fiber with the superconductive suspension and processing in oxidizing atmospheres.

Certain materials are unable to be drawn or spun into fiber form due to their improper melting characteristics or brittleness. However, fibrous samples of such materials are often necessary for the fabrication of intricate shapes and composites. In response to this problem, researchers at Clemson University developed and patented a unique process, referred to as the "piggyback process", to prepare fibrous samples of a variety of non-spinnable ceramics.[1] In this technique, specially produced C-shaped carbon fibers serve as "micromolds" to hold the desired materials prior to sintering. Depending on the sintering atmosphere used, bicomponent or single component fibers result. Alumina, zirconia, silica, and silicon carbide fibers have been produced by this process.

While much has been demonstrated worldwide concerning the $YBa_2Cu_3O_{7-x}$ superconductor, fabrication into unique forms such as fibers and composites has proven quite difficult. Researchers at Clemson University are currently investigating the feasibility of $YBa_2Cu_3O_{7-x}$ fiber production by the piggyback process. Fibrous

superconductor samples would offer the potential advantages of improved flexibility, enhanced critical current density, and unlimited shape formulation through composite development. Multifilamentary composites could be formed using a suitable polymer or metallic matrix, which could be drawn into wires or pultruded into a variety of shapes to meet unique design constraints.

The carbon fibers employed for this research were melt-spun in house from petroleum pitch, oxidized, and carbonized to produce high purity fibers with an approximate web distance of 30 microns. The fibers were attentuated into segments of 1-2 inches. The $YBa_2Cu_3O_{7-x}$ powders were prepared by solid state sintering of Y_2O_3, $BaCO_3$, and CuO and were determined phase pure by X-ray diffraction and a standard four-probe resistivity measurement. An average transition temperature of 90K was obtained.

The carbon fibers were filled with the superconducting material by dipping the fibers into a well-dispersed organic suspension of $YBa_2Cu_3O_{7-x}$ powders and evaporating the solvent. Due to the small web distance of the fibers, careful control of the particle size distribution of the superconducting powders was essential for proper particle packing and improved density of the sintered sample. An optimum distribution consisted of particles between 10 and 0.2 microns.

The filled fibers were subjected to low temperature firings (< 450°C) in air or oxygen to burn out the remaining organics. To retain the carbon backbone, the bicomponent fibers were subsequently heated in an inert atmosphere to 950°C to properly sinter the ceramic. Thermogravimetric analyses showed that a significant amount of oxygen was lost from the superconducting structure during inert atmosphere processing. Although a similar oxygen loss was exhibited from samples processed in oxidizing

atmospheres, the loss was reversible during slow cooling, with the majority of oxygen regained in the temperature range of 700°C-400°C depending on the oxygen partial pressure.[2] As unprotected carbon can withstand up to 450°C in oxidizing atmospheres, a low temperature anneal in flowing oxygen was employed to restore the oxygen content to the superconducting structure. A superconductor/carbon bicomponent fiber is shown in Figure 1.

However, the oxygen released from the $YBa_2Cu_3O_{7-x}$ compound at high temperatures reacted with the unprotected carbon fiber, resulting in the formation of a carbon monoxide atmosphere along the interfacial area. The presence of carbon monoxide served to further reduce the superconductor over time. Due to their unique valency configuration, the copper ions were found to reduce most readily according to the following decomposition reaction[3]:

$$2YBa_2Cu_3O_{7-x} \text{ ---> } Y_2BaCuO_5 + 3BaCO_3 + 6Cu \text{ (metal)}$$

To prevent oxygen loss to the carbon fiber, a variety of potential oxygen diffusion barriers have been examined to determine their effectiveness. The important parameters included oxygen permeability, chemical reactivity, and thermal expansion properties.

A variety of techniques were considered for depositing the thin barrier layers onto the carbon fiber surface. Sol-gel precursors of alumina, zirconia, and barium titanate were used to coat several fiber batches. Although the use of sol-gels allowed for decreased sintering temperature and more homogeneous products, high porosity and large shrinkages resulted, leaving large gaps in the coating for oxygen diffusion.

Metal barrier layers were deposited by sputtering, electroless plating (Enthone Corp), and physical vapor deposition. Sputtering

produced coatings of uniform thicknesses, but the coating was extremely porous and offered little protection against oxygen diffusion. Electroless coatings of nickel and copper were uniformly deposited, but the nickel and copper formed oxides during processing, reacting with the superconductor and also reducing the structure. Physical vapor deposition offered the advantages of more reliable thickness control and unlimited metal selection.

Although easy to deposit onto the fibers, metals exhibit high coefficients of thermal expansion (CTE's). The net CTE for the carbon fiber is 1 x 10^{-6}/°C, while the $YBa_2Cu_3O_{7-x}$ material possesses a net CTE of ~13 x 10^{-6}/°C. This difference in thermal expansion results in shrinkage of the superconductor material away from the fiber (See Figure 2). Metal oxides, carbides, and nitrides typically possess lower CTE values. To produce coatings of these materials, the deposited metals were converted to the desired compound by controlling the sintering atmosphere. Fibers produced to date by this technique include silicon carbide, silicon nitride, nickel carbide, and alumina. The fibers were totally converted to the desired compound, and the C-shape remained intact.

These ceramic fibers can withstand the required sintering temperature for $YBa_2Cu_3O_{7-x}$ in oxidizing atmospheres, eliminating the need for inert atmosphere processing. All oxygen lost during heat-up can be easily regained during slow cooling. Although not as flexible as the carbon backbone, the ceramic fibers do alleviate the thermal expansion mismatch, while providing sufficient strength to protect the superconductor during processing and handling.

Prepared fibers have been analyzed for composition and structure using a Debye-Scherrer camera for small sample X-ray diffraction. Most samples processed without diffusion barriers exhibited the oxygen-deficient tetragonal phase of $YBa_2Cu_3O_{7-x}$.

However, the orthorhombic and tetragonal phases may have coexisted in some samples, preventing the drop in electrical resistivity indicative of superconductivity.[4] Preliminary samples prepared with the diffusion barriers and processed in oxidizing atmospheres have possessed the orthorhombic phase.

Four point probe electrical measurements of the fibers have proven quite difficult. Small microcracks have been discovered by electron microscopy, resulting from the thermal expansion mismatch and improper handling of the fibers after processing. In addition, the fibers produced have proved to be only partially sintered (i.e. ≤50% theoretical density), leading to a drastic decrease in critical current density and potentially prohibiting current flow completely. The low density of the fibers also contributes to their poor mechanical strength. While the feasibility of the piggyback process for $YBa_2Cu_3O_{7-x}$ fiber production has been demonstrated, much work is still necessary to improve the quality of the sintered material if the fibers produced are to be incorporated into useful composites or cables.

Acknowledgements

S.A. Wise was supported by the National Science Foundation.

References

[1] N. Mack, Master's Thesis, Clemson Univ., Clemson, SC, 1987.

[2] Lindemer, Terence B., et.al., "Experimental and Thermodynamic Study of Nonstoichiometry in $YBa_2Cu_3O_{7-x}$," J. Am. Ceram. Soc., **72** (10) 1775-88 (1989)

[3] Bringley, J.F., et.al., "Synthesis and Characterization of $YBa_2(Cu_{1-x}M_x)_3O_{7-\partial}$(M=Co, Ni): Crystal Symmetry, Superconductivity, and the Role of Oxygen," Phys. Rev.B., **38** (4) 2432-8 (1988).

[4] W.Lo, et.al., "Thermodynamic Studies of the Orthorhombic-Tetragonal Transition in $Ba_2YCu_3O_{7-\partial}$," Appl. Phys. Lett., 53 (26) 2710-2 (1988).



Figure 1: Superconductor/carbon bicomponent fiber.



Figure 2: The thermal expansion mismatch between the carbon fiber and the superconductor result in shrinkage of the ceramic away from the mold.

Thermal and electric properties of $Nd_{1.85}Ce_{0.15}CuO_{4-y}$ and $Pr_{1.85}Ce_{0.15}CuO_{4-y}$

Z.S.Lim[a], K.H.Han[b], Sung-Ik Lee[a,b], Yoon H. Jeong[a,b], aPhysics Division, Research Institute of Industrial Science and Technology, Pohang, 790-330, Korea [b]Department of Physics, Pohang Institute of Science and Technology, Pohang, 790-330, Korea; Y.S.Song, Y.W.Park Department of Physics, Seoul National University, Seoul, 151-742, Korea

Electric resistivity, magnetic susceptibility, thermoelectric power, and Hall coefficient of $Nd_{1.85}Ce_{0.15}CuO_{4-y}$ and $Pr_{1.85}Ce_{0.15}CuO_{4-y}$ whose onset temperature of the superconductivity are 24 K and 23 K were measured. Our experimental results show many interesting features. In particular, the Hall coefficients are negative and relatively flat as a function of temperature. However, the temperature dependence of the thermoelectric power (TEP) for these two samples shows the positive sign for both samples in contrast to the previous results. Moreover TEP for both samples remains flat in the normal state below 250 K, but decreases rapidly above 250 K. TEP of only $Pr_{1.85}Ce_{0.15}CuO_{4-y}$ shows a peak near 50 K. Finally onset temperatures of sudden drop of TEP are higher than those of resistance drop.

We also measured the physical properties of these samples produced at different conditions such as different heat treatment temperatures, atmospheres. TEP and resistance measurement show that oxygen deficiency is essential to produce better superconducting samples. Correlation between TEP and superconductivity for these different samples will be discussed.

TERNARY AND QUATERNARY OXIDES OF Bi, Sr AND Cu

M.T. Casais, P. Millán, I. Rasines*, Instituto de Ciencia de Materiales, CSIC
Serrano 113, 28006 Madrid, Spain.

J.A. Campá, Facultad de Ciencias Geológicas, UCM
Ciudad Universitaria, 28040 Madrid, Spain.

Abstract. Among the phases present in the products of thermal treatments of mixtures of analytical grade Bi_2O_3, $Sr(OH)_2.8H_2O$ and CuO, a cubic perovskite, $BiSr_3O_{5.5}$, with 1:1 order at the B-cations sublattice and **a** = 8.493(7) Å has been found. This oxide appears to substitute some Cu for Bi giving rise to materials with lower **a** values. After been grown from mixtures of the same reagents at Bi:Sr:Cu molar ratios (0.7-2.2):(1.0-2.2):1 using techniques of static and revolving crucibles, crystals of four phases have been studied by X-ray diffraction, electron microscopy and electron diffraction, namely the superconducting Raveau oxide, A; a second phase, A_1, very similar to A; and the oxides with Bi:Sr:Cu molar ratios 2:2:1, K; and 4:8:5, G. The conditions (composition, crystallization rate) which lead to A, A_1 or K are established. Each of these phases distinguishes from the two others by its oxygen content, which decreases in the order $A > A_1 > K$.

1. INTRODUCTION

Prior of the discovery[1] of superconductivity in an oxide of Bi, Sr and Cu, several solid phases were known in the two-component regions of the ternary system Bi_2O_3-SrO-CuO. Nevertheless that discovery has created a new interest in ternary and quaternary copper oxides, of which the following phases are at present known.

Oxides of Bi and Cu. Although two compounds of stoichiometries Bi_4CuO_7 and $Bi_2Cu_2O_5$ have been mentioned[2,3], the oxide best characterized[4-7] is tetragonal $CuBi_2O_4$, with unit-cell parameters (Å) **a** = 8.510, **c** = 5.814. The crystal structure of $CuBi_2O_4$ has been simultaneously refined[6,7] in the space groups S.G. P4/ncc (No. 130)[8] and I4 (No. 79)[9], with Cu in a square planar coordination.

Oxides of Sr and Cu. Whereas the existence of two Sr and Cu (II) oxides, Sr_2CuO_3 and $SrCuO_2$, is well established, only the tetragonal oxide $SrCu_2O_2$ of Sr and Cu (I) is known[10], with S.G. $I4_1/amd$ (No. 141)[11], **a** = 5.48, **c** = 9.82, SrO_6 octahedra and Cu in linear two-coordination with oxygen. Sr_2CuO_3 is[12,13] orthorhombic, **a** = 12.684, **b** = 3.9064, **c** = 3.4957, S.G. Immm (No. 71), and includes SrO_7 polyhedra and planar CuO_4 squares; and $CuSrO_2$ is[3,14,15] also orthorhombic, **a** = 3.9136(2), **b** = 16.3313(8), **c** = 3.5730(2), S.G. Cmcm (No. 63). Besides a not too well characterized Sr **cuprate** (III) hydrate[16], $SrCu_2O_4.nH_2O$, a new oxide of Sr and Cu containing some Cu (III) and formulated as $Sr_{14}Cu_{24}O_{41}$, has been recently reported[17,18]. The crystal structure of orthorhombic $Sr_{14}Cu_{24}O_{41}$ is incommensurate and can be described[17] as the result of two interpenetrating structures: one with Sr-(Cu_2O_3 sheets)- Sr layers in an orthorhombic cell with dimensions (Å) of **a** = 11.459(2), **b** = 13.368(5), **c** = 3.931(1), and a second structure with layers of (CuO_2 chains) in a cell having the mentioned **a** and **b** values but with **c** = 2.749(1).

Oxides of Bi and Sr. The first phase described[19,20] in the system Bi_2O_3-SrO is a rhombohedral solid solution with the homogeneity range **s** = 14-26, being **s** the mol percent Sr/(Sr+Bi). This phase, S.G. $R\bar{3}m$ (No. 166), has a rhombohedral primitive unit-cell with **a** = 9.6-9.8 Å and α = 23.8°-23.4°, or a thrice primitive hexagonal cell with **a** = 3.97 Å, **c** = 28.1-28.6 Å. In this oxide, that can be formulated as

$Bi_{2-2x}Sr_xO_{3-2x}$ with **x** = 2**s**/(100+**s**), the metal lattice always seems to remain complete, whereas there is a variable number of vacant positions of the oxygen lattice.

The effect of small SrO additions on the polymorphism of Bi_2O_3 was studied some years later by high temperature X-ray diffraction, and the tentative partial phase diagram in the temperature range 500-900 °C was proposed[21]. This diagram includes the above mentioned rhombohedral phase of variable composition and a solid solution of cubic symmetry. The system Bi_2O_3-SrO has been studied some years ago[22], in the temperature range 620 to 1000 °C by thermal and high-temperature X-ray diffraction analyses. Table I includes the composition, approximate stability regions, crystal system, and unit-cell parameters of the different phases that were found, comprising five solid solutions and three oxides of constant composition, two of which

Table I. Approximate stability regions, symmetry, and unit-cell parameters for oxides[a] of compositions $Bi_{2-2x}Sr_xO_{3-2x}$, according to reference 22.

Oxide	x	T °/C	Symmetry	a/Å	b/Å	c/Å
α_1	0.01-0.12	730-820	C	5.67	-	-
β_1	0.20-0.40	700-900	R	4.0	-	28.7
β_2	0.18-0.43	620-700	R	3.97	-	28.2
Bi_2SrO_4	0.50	620-800	-	-	-	-
γ	0.58-0.64	820-940	T	13.239(2)[b]	-	4.257(1)[b]
γ'	0.58-0.62	900-930	C	4.41[c]	-	-
$Bi_2Sr_2O_5$	0.67	650-950	O	14.293(2)	7.651(2)	6.172(1)
$Bi_2Sr_3O_6$	0.75	810-980	-	-	-	-

C: cubic T: tetragonal R: rhombohedral O: orthorhombic M: monoclinic

[a] excluding four metastable solid solution obtained by annealing α_1 in different conditions

[b] for **x** = 0.615: see ref. 23. [c] for T = 950 °C

have been characterized more recently: Bi_2SrO_4 is[24] monoclinic, S.G. C2/m (No. 12), with **a** = 19.2882(16), **b** = 4.3520(4), **c** = 6.1015(5), β = 94.839(7)°; and $Bi_2Sr_2O_5$ is[25] orthorhombic, S.G. Pmam (No. 51) with the crystallographic constants **a** = 6.1713(6), **b** = 14.3074(15), **c** = 3.8262(4), closely related to those shown in Table I. Some months ago a new oxide of molar ratio Bi:Sr = 1:3 (**x** = 0.857) has been described[26] as crystallizing in the orthorhombic system with **a** = 17.147, **b** = 16.758, **c** = 16.998 Å.

Oxides of Bi, Sr and Cu. The first superconducting material in the system Bi-Sr-Cu-O was described by the group of Raveau[1] and formulated as $Bi_2Sr_2Cu_2O_{7+x}$, with an orthorhombic unit-cell of parameters (Å) **a** = 5.32, **b** = 26.6, **c** = 48.8 and a superconducting transition at 7 K, which was soon confirmed[27]. In a preliminary publication[28] our group reported that mixtures of Bi_2O_3, $SrCO_3$ and CuO in the molar ratios Bi:Sr:Cu = 2:2:2 lead to the oxide $Bi_2Sr_2CuO_{6+x}$, here designed as 221, mixed with small amounts of CuO; and that all the reflexions of the X-ray diffraction patterns of the 221 oxide can be indexed in an orthorhombic unit-cell of parameters (Å) **a** = 5.390(2), **b** = 26.973(8), **c** = 24.69(4). Subsequent diffraction studies (X-ray, electron, neutron) confirmed the composition 221 and propounded the substructures included in Table II.

The actual structure of 221 is a long-period modulated superstructure with different modes that can be observed by electron diffraction and high-resolution electron microscopy. The presence of superstructures was soon established[27] and corroborated later by various authors[32,35,37,26]. Superstructures of the following types

have been described[35]: base-centered monoclinic with parameters (Å) **a** = 5.4, **b** = 27, **c** = 26.9, α = 66.3°; monoclinic with **a** = 5.1, **b** = 27, **c** = 12.6, α = 77.6°; and base-centered orthorhombic with **a** = 5.4, **b** = 22.6, **c** = 24.6.

Table II. Crystal structures proposed for the superconducting oxide of approximate composition $Bi_2Sr_2CuO_{6+x}$

Symmetry	S.G.	a/Å	b/Å	c/Å	(°)	Z	Ref.
T	-	5.381(1)	-	24.65(1)	-	-	29
T	I4/mmm	3.8097(4)	-	24.607(3)	-	2	30
O	Amaa	5.392	5.394	24.537	-	4	31
O	-	10.8	53	24	-	-	32
T	I4/mmm	3.801(3)	-	24.61(9)	-	2	33
O	Amaa	5.362(3)	5.374(1)	24.622(6)	-	-	34
T	-	5.4	-	24.6	-	-	35
M	C2	26.856	5.380	26.908	113.55	4	36
M	-	5.4	26	28	116	-	37

T: tetragonal O: orthorhombic M: monoclinic

Preliminary studies of the authors showed that some other phases appear for compositions Bi, 1.5-2.2; Sr, 1.8-2.2; Cu, 1; and that slight variations in the initial concentration of Bi and Sr favor the appearance of these phases. On the other hand, we observed that the nominal composition 2:2:1 is metastable and changes when heated for a long time. These observations are related to the results of some recent studies[26,38-40]. One of them[26] concludes that three phases coexist at the ideal 221 composition: a superconducting material with the aproximate composition $Bi_{2.125}Sr_{1.875}Cu_{1.031}O_z$ and two oxides, $Bi_{17}Sr_{16}Cu_7O_y$ and $Sr_3Cu_5O_y$, the first of which with parameters **a** = 5.425, **b** = 23.254, **c** = 24.427 Å. The second study[38] points out that nominal 221 is actually a solid solution tolerating a range of Sr deficiency, i.e., $Bi_2Sr_{2-x}CuO_6$ (**x** = 0.1-0.5); that superconducting behaviour is observed for **x** = 0.1-0.25, the solid solution undergoing a metal-to-insulator transition for higher **x** values; and that the stable phase at the 221 composition is a semiconductor designed as the **collapsed** 221 phase. The results of the third study[39] confirm the existence of one oxide with Bi:Sr:Cu ratios of 2:2:1, and a solid-solution phase with (2.2-**x**):(1.8+**x**): 1 ratios, for **x** = 0-0.08. Only this second phase is a superconductor at 9 K and **x** = 0.08. The 2:2:1 compound[39], the **collapsed**[38] 221 phase, and the oxide formulated[26] as $Bi_{17}Sr_{16}Cu_7O_y$ show the same X-ray diffraction pattern, that was indexed[39] with **a** = 23.73(1), **b** = 13.242(6), **c** = 4.081(1) Å. By a combination of electron diffraction and single crystal and powder X-ray diffraction, the phase of composition 221 has been more recently found[40] to have a commensurate lattice with monoclinic symmetry, S.G. C2/m or Cm, **a** = 24.473(2), **b** = 5.4223(5), **c** = 21.959(2) Å and β = 105.40(1)°. In short, it appears that the superconducting oxide thought at the beginning as having the composition 221, is a solid solution with a range of Sr deficiency; and that stoichiometric 221 is not a superconductor. Hence, the structural data shown in Table II correspond to the Sr-deficient solid solution, and stoichiometric 221 is monoclinic, with the X-ray diffraction data[39] indicated. These two phases will be labelled here as A and K respectively.

At least five additional oxides with various Bi:Sr:Cu molar ratios have been described. Two of them, 2:7:2 and 4:9:1, are apparently stabilized by the presence of Li_2CO_3, but do not form without it[39]. Table III includes X-ray diffraction data for these oxides. The cubic oxide which appeared with some impurities from nominal molar ratios 2:4:1 showed[42] the reflexions of a perovskite with 1:1 order at the B-cation sublattice. The authors found later that for Bi:Sr ratios 1:2 and 1:3 a very similar perovskite is formed without copper. This result led them to explore the Sr-rich region of the phase diagram Bi_2O_3-SrO. On the other hand, the authors

Table III. Unit-cell constants for oxides with various Bi:Sr:Cu ratios

Bi:Sr:Cu	Symmetry	a/Å	b/Å	c/Å	Refs.
2 3 2	O	4.888	5.396	24.804	26
4 8 5	O	5.389	24.050	34.035	26
4 8 5	O	5.373(2)	23.966(4)	33.907(6)	41
2 4 1	C	8.480(1)	-	-	42
2 7 2	O	8.769(2)	8.340(2)	7.983(3)	39
4 9 1	T	11.694(3)	-	9.466(4)	39

C: cubic O: orthorhombic T: tetragonal

found that not too long treatments of mixtures with nominal composition 221 at 780–790 °C gave A and small amounts of $Bi_2Sr_2O_5$; that K was obtained with loss of mass after long treatments at 900 °C; and that K, when exposed to the air, becomes A_1, a phase whose X-ray diffraction pattern looks very similar to that of A. These results led them to grow crystals of A, K and A_1 in different conditions. The preliminary results of these experiments are included in this paper.

2. EXPERIMENTAL

Six polycrystalline samples of the compositions indicated in Table IV were prepared by solid-state reactions from mixtures of analytical grade Bi_2O_3 and $SrCO_3$, which were ground and succesively heated in air at 800, 900 and 950 °C in alumina crucibles. After each thermal treatment, which lasted five hours, the samples were weighed, reground and characterized by X-ray diffraction using a SIEMENS Kristalloflex D500.

Table IV. Phases identified in six polycrystalline samples of compositions $Bi_{2-2x}Sr_xO_{3-2x}$

No.	Bi : Sr	x	Phases
1	2.0 3	0.75	J+E(s)
2	3.0 5	0.77	J+E
3	4.0 7	0.78	E+J
4	1.0 2	0.80	E+J(s)
5	1.1 3	0.85	E+J(t)
6	1.0 3	0.86	E

J $Bi_2Sr_3O_6$ E $BiSr_3O_{5.5}$
s small amounts t traces

The crystals were grown from mixtures of 99.9 % Bi_2O_3, $Sr(OH)_2.8H_2O$ and CuO at the molar ratios and conditions shown in Table V. Dense-alumina crucibles were used. Revolving crucibles (60 r.p.m.) with the direction of rotation changing every 10 seconds in a furnace QUASTAR 89 were employed for sample nos. 9–12. Except indicated otherwise (sample nos. 1, 9–11) the samples were preheated at 850 °C for 12 hours, quenched, ground, led to the temperature T (°C), maintained at this temperature for **t** hours as a melt, cooled to 750 °C at $2°Ch^{-1}$, and quenched. A portion of the crystals as grown was pulverized and characterized by X-ray diffraction. The **d**-spacings and relative intensities were measured as indicated elsewhere[43]. The morphological study of the crystals was performed using a JEOL scanning microscope JSM 35-C. For high resolution electron microscopy and electron diffraction, a microscope JEOL JEM-2000 FX was employed. The resistivity measurements were made using a standard four-probe method.

3. RESULTS AND DISCUSSION

Table IV includes the phases identified in six polycrystalline samples of compositions $Bi_{2-2x}Sr_xO_{3-2x}$ ($0.75 \leqslant x \leqslant 0.86$): $Bi_2Sr_3O_6$ and $BiSr_3O_{5.5}$. The oxide with Bi:Sr = 2:3 molar ratio shows the following **d** spacings (Å) with the relative intensities in parentheses: 4.68(10); 4.38(8); 4.23(7); 4.01(10); 3.75(6); 3.14(90); 3.04(100); 2.18(50); 1.81(20); and 1.79(30). The oxygen content for $BiSr_3O_{5.5}$ has been adjusted assuming Bi (V), because the mass changes were followed by weighing before and after each operation and showed that almost the whole Bi (III) oxidized in the course of the thermal treatments. The X-ray powder diffraction pattern for $BiSr_3O_{5.5}$ shows

Table V. Phases identified in crystals grown from mixtures of various Bi:Sr:Cu molar ratios

No.	Bi: Sr: Cu	T/°C	t/h	Phases
1	2.0 2.0 1	890[a]	6	A+A_1(s)
2	2.0 2.0 1	930	6	A
3	2.2 1.8 1	930	6	A_1+A(t)
4	1.8 2.0 1	1000	6	K
5	1.5 2.0 1	1000	6	K
6	1.8 2.2 1	930	6	K+G(s)
7	1.0 1.5 1	1000	6	A_1+G
8	0.7 1.0 1	1000	6	G
9*	2.0 2.0 1	940[b,c]	1	K
10*	2.0 2.0 1	940[d,c]	1	K
11*	2.0 2.0 1	940[c]	1	A_1
12*	2.0 2.0 1	940	1	A+K+A_1

* revolving crucible [a] cooled to R.T.
[b] crystallized at 15 °Ch^{-1} [c] no pretreatment at 850°C
[d] crystallized at 5 °Ch^{-1} (s) small amounts (t) traces
A, Raveau phase; A_1, new phase; K, 221 oxide;
G, $Bi_4Sr_8Cu_5O_{19}$

the reflexions of a cubic perovskite, **a** = $2a_0$ = 8.493(7) Å, with 1:1 order at the B-cations sublattice: $Sr[Sr_{0.5}Bi_{0.5}]O_{2.75}$. This oxide, which appears as not too crystalline, appears to substitute some Cu for Bi giving rise to materials like $Sr[Sr_{0.5}Bi_{0.3}Cu_{0.2}]O_{2.45}$, which was prepared from stoichiometric mixtures of Bi_2O_3, $Sr(OH)_2.8H_2O$ and CuO heated as indicated for the basic compound. The unit-cell parameter of the Cu-containing material is slightly smaller, **a** = 8.465 (14) Å. This could be expected from the different sizes[44] of both cations, 0.76 Å for Bi (V) and 0.73 Å for Cu (II), as well as from the smaller oxygen content of the Cu-containing oxide. This is the phase wich appeared[42] with some impurities from nominal 2:4:1. Apart from this, all the attempts to reproduce the X-ray diffraction pattern reported[26] for $BiSr_3O_z$ were unsuccessful.

All the experiments on crystal growth led to abundant masses of crystals in which the phases included in Table V (A, A_1, K and G) were identified. Three of these, A, K and G, are relatively well known: A, that was present in sample nos. 1, 2 and 12, is the Raveau phase with the unit-cell parameters included in Table II; K is monoclinic[40] 221, which appears as major product after crystallising sample nos. 4, 5, 6, 9 and 10; and G (samples 6-8) is orthorhombic[26,41] $Bi_4Sr_8Cu_5O_{19}$. Crystals of A_1, a new phase closely related to A, are obtained from sample nos 3, 7, and 11. The relation between the X-ray diffraction patterns of both phases is shown in Fig. 1. The morphologies of A and A_1 can only be distinguished by the way of their faces being developed. Crystals of A have planar faces, ordinarily well developed, some of them with edges up to 5 mm long, but forming irregular triangles as Fig. 2 shows. The A_1 phase shows a similar morphology and strong tendencies to be delaminated and to grow by steps. Consequently, voluminous crystals of A_1 cannot easily be grown. When static crucibles are employed, nominal mixtures with Bi:Sr ratio larger than 1 (sample no. 3) lead to A_1 as the major product, whereas stoichiometric 221 gives phase A (sample nos. 1 and 2). The

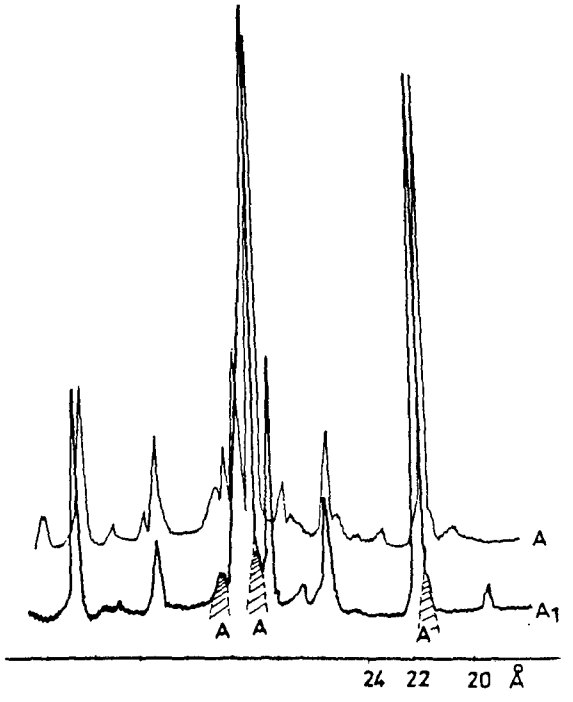


Fig. 1. Comparison of X-ray diffraction patterns of A_1 and A.

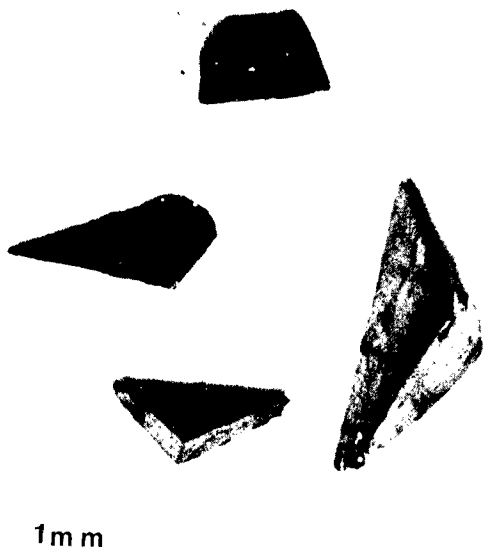


Fig. 2. Optical photomicrograph of the A phase.

presence of traces of A_1 in sample no. 1 can be related with the removal of some oxygen during the 15 days required for lowering from 750 °C to room temperature.

Crystals of phase K are obtained using static crucibles from nominal mixtures with Bi:Sr ratios smaller than 1 (sample nos. 4, 5). For still smaller Bi:Sr ratios, the oxide $Bi_4Sr_8Cu_5O_{19}$ is progressively stabilized (sample nos. 6-8). Crystals of the K oxide show an elongated development and form needle-shaped or fibrous masses including many crystals (Fig. 3).

The results obtained in the experiments with rotating crucibles (sample nos. 9-12) also suggest that the oxygen content increases in the order K < A_1 < A. The rapider crystallization of sample nos. 9 and 10 leads to crystals of K, which is the phase with the smaller oxygen content. For a slower crystallization (sample no. 11), crystals of A_1 result. In the case of pretreated sample no. 12, with smaller oxygen content, the three phases appear at different heigths of the crucible: A, at the bottom; A_1, at the top; and K between A and A_1. This suggests that A has incorporated all the oxygen of the melt at the expense of K, and that the external portion of K has oxidized in contact with air.

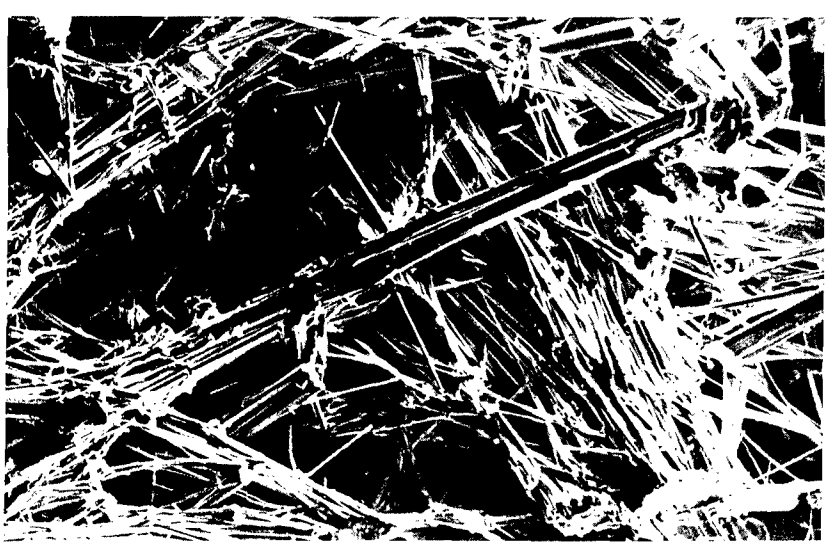


Fig. 3. SEM micrograph showing needle-like crystals of K up to 10 mm long.

Although K crystals obtained in static crucibles (sample nos. 4,5) are grown from mixtures with Bi:Sr ratios smaller than 1, and polycrystalline K is prepared from stoichiometric 221 after long thermal treatments at 900 °C in which some Bi can be lost, K crystals are grown in rotating crucibles at high crystallization rates from stoichiometric 221 mixtures (sample nos. 9-10). This suggests that this composition, 221, is also included in the stability region of the K phase.

In the selected-area diffraction pattern from a crystal of A_1 (sample no. 3), satellites along the **b** axis were observed. Although the (001) planes of A_1 ordinarily present a large number of deformations, modulations of 2.7 nm can be seen in Fig. 4, that represents the high-resolution (HR) lattice image taken with the incidence [001]. The wavy aspect of the (001) planes can also be observed. The high-resolution lattice image of Fig. 5, taken with the incidence [100] from another crystal of A_1

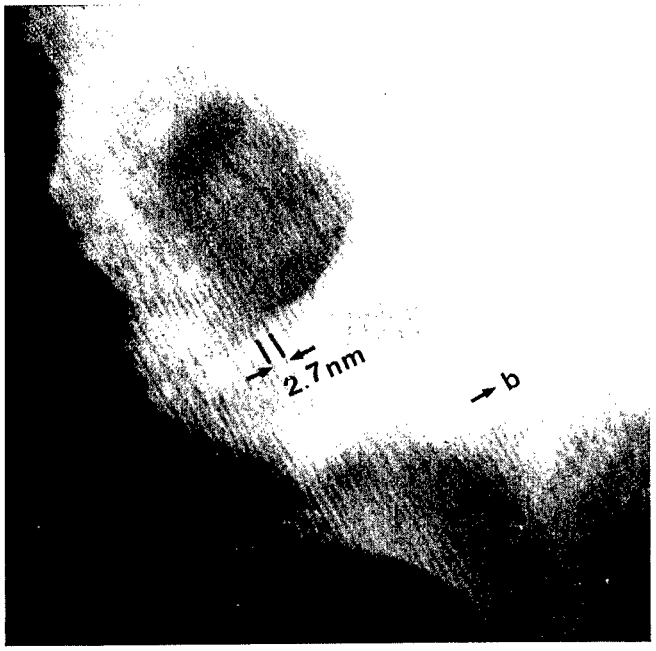


Fig. 4. High-resolution lattice image from A_1 with the incidence [001].

(sample no. 3), contains modulations of 1.2 nm along the **c** axis. And Fig. 6, with the high-resolution lattice image of a different A_1 specimen (sample no. 1) taken with the incidence [100], displays modulations of 11 and 9.5 nm along **b** and **c** axes respectively, the last of which comparable to those of 4x2.4 = 9.6 nm observed in the A phase by depth profile Auger analysis[45]. In short, modulations along **b** and **c** axes observed in the A phase are also evident for A_1.

Figs. 7 and 8 show the selected-area diffraction pattern taken with the incidence [010] from a crystal of the K phase (sample no. 4) and the high-resolution lattice image of the same crystal showing modulations of 2.4 nm along the **c** axis.

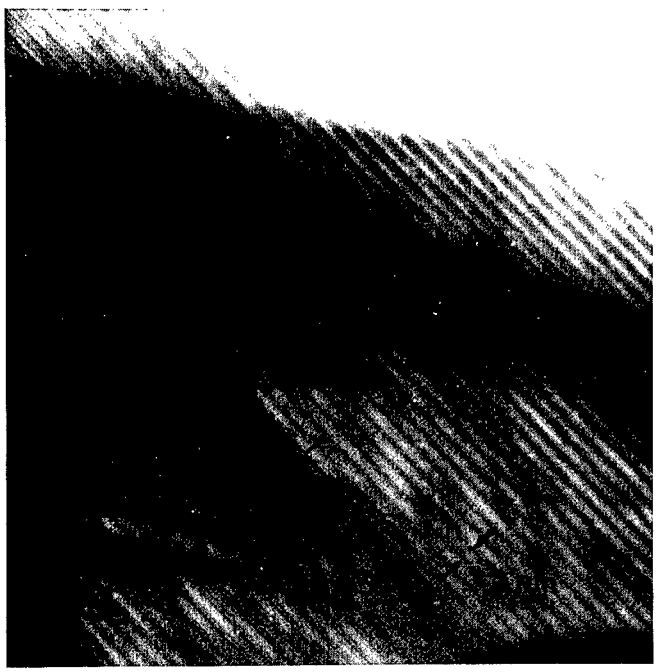


Fig. 5. HR lattice image of A_1 from sample no. 3, taken with the incidence [100].

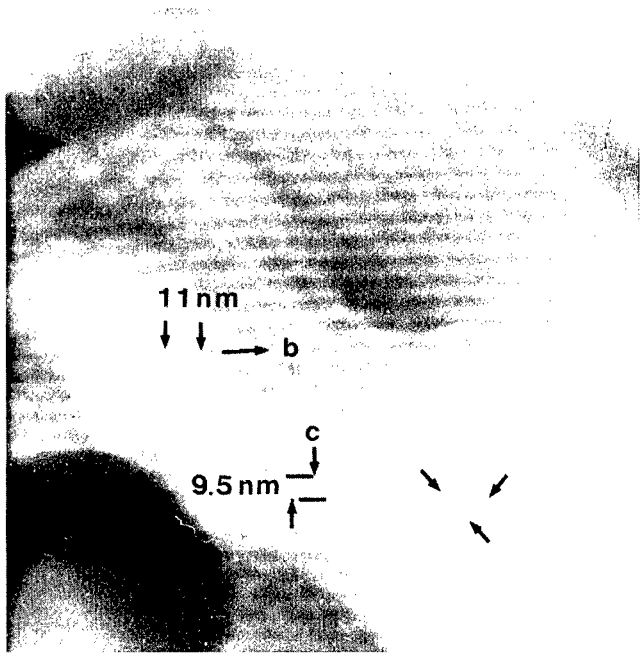


Fig. 6. HR lattice image of A_1 from sample no. 1, taken with the incidence [100].

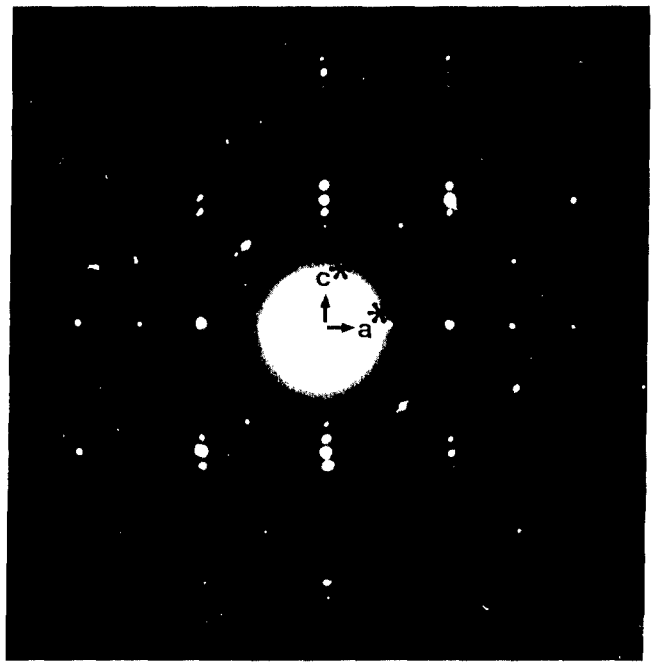


Fig. 7. Selected-area diffraction pattern from a crystal of the K phase.

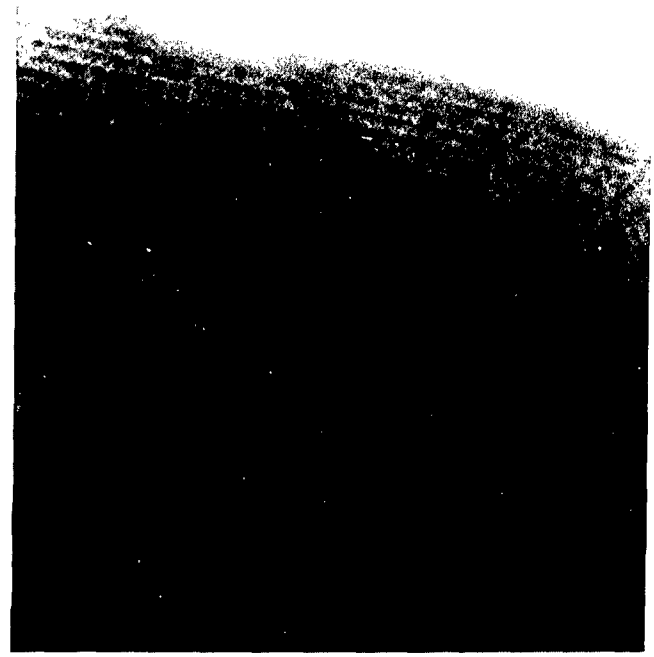


Fig. 8. HR lattice image of phase K taken with the incidence [010].

Acknowledgements. The authors acknowledge the financial aid of the Fundación Domingo Martínez.

4. REFERENCES

1. C. Michel, M. Hervieu, M.M. Borel, A. Grandin, and F. Deslandes, "Superconductivity in the Bi-Sr-Cu-O System", **Z. Phys.** B-Condensed Matter 68 (4), 421-423, 1987.
2. J. Cassedane and C.P. Campelo, "Etude du diagramme d'équilibre Bi_2O_3-CuO" **An. Acad. Brasil. Ci.** 38(1), 35-38, 1966.
3. M. Arjomand and D.J. Machin, "Oxide chemistry. Part II. Ternary oxides containing copper in oxidation states-I, -II, -III, and -IV", **J. Chem. Soc. Dalton Trans.** 1061-1066, 1975.
4. J.-C. Boivin, D. Thomas and G. Tridot, "Determination des phases solides du système oxyde de bismuth-oxyde de cuivre: Domaines de stabilité et étude radiocristallographique", **C.R. Acad. Sc. Paris** 276, Série C, 1105-1107, 1973.
5. Joint Committee on Powder Diffraction (J.C.P.D.) File. Card no. 26-502.
6. J.-C. Boivin, J. Tréhoux and D. Thomas, "Etude structurale de $CuBi_2O_4$", **Bull Soc. fr. Minéral. Cristallogr.** 99, 193-196, 1976.
7. R. Arpe, H. Müller-Buschbaum, "Isolierte quadratisch planare CuO_4^{6-} Polyeder in $CuBi_2O_4$, ein neuer Bautyp zur Formel $Me_2^{3+}M^{2+}O_4$", **Z. anorg. allg. Chem.** 426(1) , 1-6, 1976.
8. The International Union of Crystallography, **International Tables for Crystallography** Volume A, **Space-Group Symmetry**, pp. 440-443, D. Reidel, Dordrecht (Holland) and Boston, MA, 1983.
9. Ref. 8, pp. 326-327.
10. C.L. Teske and H. Müller-Buschbaum, "Zur Kenntnis von $SrCu_2O_2$", **Z. anorg. allg. Chem.** 379(2), 113-121, 1970.
11. Ref. 8, pp. 472-475.
12. C.L. Teske and H. Müller-Buschbaum, "Zur Kenntnis von Sr_2CuO_3", **Z. anorg. allg. Chem.** 371(5-6), 325-332, 1969.

13. J.C.P.D. File. Card no. 34-283.
14. C.L. Teske and H. Müller-Buschbaum, "Zur Kenntnis von Ca_2CuO_3 und $SrCuO_2$", **Z. anorg. allg. Chem.** 379(3), 234-241, 1970.
15. W. Wong-Ng, H.F. McMurdie, B. Paretzkin, C.R. Hubbard and A.L. Dragoo, "Standard X-Ray diffraction patterns of fourteen ceramic phases", **Powder Diff.** 3(2), 114, 1988.
16. R. Scholder and U. Voelskow, "Über Cuprate (III)", **Z. anorg. allg. Chem.** 266(4-5), 256-268, 1951.
17. E.M. McCarron, M.A. Subramanian, J.C. Calabrese and R.L. Harlow, "The incommensurate structure of $(Sr_{14-x}Ca_x)Cu_{24}O_{41}$ $(0 < x \sim 8)$ a superconductor byproduct", **Mat. Res. Bull.** 23(9),1355-1365, 1988.
18. T. Siegrist, L.F. Schneemeyer, S.A. Sunshine, and J.V. Waszczak, "A new layered cuprate structure type, $(A_{1-x}A'_x)_{14}Cu_{24}O_{41}$", **Mat. Res. Bull.** 23(10), 1429-1438, 1988.
19. L.G. Sillén and B. Aurivillius, "Oxide phases with a defect oxygen lattice", **Z. Kristallog.** 101(6), 489-495, 1939.
20. B. Aurivillius. "An X-Ray Investigation of the systems $CaO-Bi_2O_3$, $SrO-Bi_2O_3$ and $BaO-Bi_2O_3-O$. (Mixed oxides with a defect oxygen lattice)", **Arkiv Kem., Mineral Geol.** 16A(17), 1-13, 1943.
21. E.M. Levin and R.S. Roth, "Polymorphism of bismuth sesquioxide. II. Effect of oxide additions on the polymorphism of Bi_2O_3", **J. Res. Nat. Bur. Stand. A. Physics and Chemistry,** 68A(2), 197-206, 1964.
22. R. Guillermo, P. Conflant, J.-C. Boivin and D. Thomas, "Le diagramme des phases solides du système Bi_2O_3-SrO", **Rev. Chim. Minèr.** 15(2), 153-159, 1978.
23. J.C.P.D.S. Card no. 31-1341.
24. W. Wong-Ng, H.F. McMurdie, B. Paretzkin, M.A. Kuchinski and A.L. Dragoo, "Standard X-ray diffraction powder patterns of fourteen ceramic phases", **Powder Diffr.** 3(4) 254, 1988.
25. W. Wong-Ng, H.F. McMurdie, B. Paretzkin, M.A. Kuchinski and A.L. Dragoo,"Standard X-ray diffraction powder patterns of fourteen ceramic phases", **Powder Diffr.** 3(3), 186, 1988.
26. Y. Ikeda, H. Ito, S. Shimomura, Y. Oue, K. Inaba, Z. Hiroi and M. Takano, "Phases and their relations in the Bi-Sr-Cu-O system", **Physica** C 159(182), 93-104, 1989.
27. J. Akimitsu, A. Yamazaki, H. Sawa and H. Fujiki, "Superconductivity in the Bi-Sr-Cu-O system", **Japan. J. Appl. Phys.** 26(12), L2080-L2081, 1987.
28. J. Amador, M.T. Casais, C. Cascales, A. Castro and I. Rasines, "Síntesis y caracterización de nuevos óxidos superconductores del sistema Bi-Ca-Cu-Sr-O", **Rev. R. Acad. Cienc. Ex. Fís. Nat.** 82(3-4), 551-553, 1988.
29. M. Onoda, M. Sera, K. Fukuda, S. Kondoh and M. Sato, "Superconducting and electronic properties of $Bi_{1-x}La_xSrCuO_y$", **Solid St. Commun.** 66(2), 189-193, 1988.
30. J.B. Torrance, Y. Tokura, S.J. LaPlaca, T.C. Huang, R.J. Savoy and A.I. Nazzal, "New class of high T_c structures intergrowth of multiple copper oxide perovskite-like layers with double sheets of BiO", **Solid St. Commun.** 66(7), 703-706, 1988.
31. H.G. von Schnering, L. Walz, M. Schwarz, W. Becker, M. Hartweg, T. Popp, B. Hettich, P. Müller and G. Kämpf. "The crystal structures of the superconducting oxides $Bi_2(Sr_{1-x}Ca_x)_2CuO_{8-\delta}$ and $Bi_2(Sr_{1-y}Ca_y)Cu_2O_{10-\delta}$ with $0 \leq x \leq 0.3$ and $0.16 \leq y \leq 0.33$", **Angew. Chem. Int. Ed. Engl.** 27(4), 574-576, 1988.
32. G. Van Tendeloo, H.W. Zandbergen and S. Amelinckx, "Electron diffraction and high resolution electron microscopic study of the 20 K superconducting phase in the Bi-Sr-Cu-O system", **Solid St. Commun.** 66(9), 927-930, 1988.
33. H. Sawa, H. Fujiki, K. Tomimoto and J. Akimitsu, "Crystal substructure of the Bi-Sr-Cu-O system", **Japan. J. Appl. Phys.** 27(5), L830-L832, 1988.

34. C.C. Torardi, M.A. Subramanian, J.C. Calabrese, J. Gopalakrishnan, E.M. McCarron, K.J. Morrissey, T.R. Askew, R.B. Flippen, U. Chowdhry, and A.W. Sleight, "Structures of the superconducting oxides $Tl_2Ba_2CuO_6$ and $Bi_2Sr_2CuO_6$", **Phys. Rev. B** 38(1), 225-231, 1988.
35. H. Fujiki, M. Sano, K. Tomimoto, H. Sawa, J. Akimitsu and N. Kitamura, "Long period structures in the Bi-Sr-Cu-O system", **Japan. J. Appl. Phys.** 27(6), L1044-L1046, 1988.
36. M. Onoda and M. Sato, "Superlattice structure of superconducting Bi-Sr-Cu-O system", **Solid St. Commun.** 67(8), 799-804, 1988.
37. Y. Matsui, S. Takekawa, S. Horiuchi and A. Umezono, "High-resolution electron microscopy of modulated structure in 20 K superconducting oxide $Bi_2Sr_2CuO_y$", **Japan. J. Appl. Phys.** 27(10), L1873-L1876, 1988.
38. B.C. Chakoumakos, P.S. Ebey, B.C. Sales and E. Sonder, "Characterization and superconducting properties of phases in the Bi-Sr-Cu-O system", **J. Mater. Res.** 4(4), 767-780, 1989.
39. J.A. Saggio, K. Sujata, J. Hahn, S.J. Hwu, K.R. Poeppelmeier and T.O. Mason, "Partial Bi-Sr-Cu-O subsolidus diagram at 800 °C with and without lithium carbonate", **J. Am. Ceram. Soc.** 72(5), 849-853, 1989.
40. R.S. Roth, C.J. Rawn and L.A. Bendersky, "Crystal chemistry of the compound $Sr_2Bi_2CuO_6$", **J. Mater. Res.** 5(1), 46-52, 1990.
41. A. Fuertes, C. Miravitlles, J. González Calbet, M. Vallet-Regi, X. Obradors and J. Rodríguez Carvajal, "The tubular crystal structure of the new phase $Bi_4Sr_8Cu_5O_{19+x}$ related to the superconducting perovskites", **Physica C** 157(3), 525-530, 1989.
42. M.T. Casais, C. Cascales, I. Rasines, J.A. Campá, "Quaternary oxides of Bi, Sr, and Cu", Materials Research Society 1989 Spring Meeting, Final Program and Abstracts, M3.5, 271, MRS, Pittsburg, PA, 1989.
43. J. Amador, C. Cascales, I. Rasines, "Synthesis and characterization of $Ba_2Cu_3PrO_{7-x}$", Materials Research Society Symposium Proceedings, High-temperature superconductors, M.B., Brodsky, R.C. Dynes, K. Kitazawa, H.L. Tuller, eds., 99, 249-252, MRS, Pittsburg, PA, 1988.
44. R.D. Shannon, "Revised effective ionic radii and systematic studies of interatomic distances in halides and chalcogenides", **Acta Crystallog. A** 32(2), 751-767, 1976.
45. J.A. Campá, J. Avila, M.T. Casais, C. Cascales, I. Rasines, J.L. Sacedón, "Irregular oxygen distribution in $Bi_2Sr_2CuO_{6+x}$ crystals", **Physica C**, 162-164, 1223-1224, 1989.

DEPENDENCE OF TRANSITION TEMPERATURE ON HOLE CONCENTRATION PER CuO_2 SHEET IN THE BI-BASED SUPERCONDUCTORS

J. Zhao and M. S. Seehra
Department of Physics, West Virginia University
Morgantown, West Virginia 26506, USA

Abstract

The recently observed variations of the transition temperature T_c with oxygen content in the Bi-based (2212) and (2223) superconductors are analyzed in terms of p^+, the hole concentration per CuO_2 sheet. This analysis shows that in this systems T_c increases with p^+ initially, reaching maxima at $p^+ = 0.2 \sim 0.3$, followed by monotonic decrease of T_c with p^+. The forms of these variations are similar to those observed in the $La_{2-x}Sr_xCuO_4$ and $YBa_2Cu_3O_y$ systems, suggesting that p^+ may be an important variable governing superconductivity in the cuprate superconductors.

Among the cuprate high-T_c superconductors, $La_{2-x}Sr_xCuO_{4-\delta}$ is a prototype since the unit cell of this system contains only a single CuO_2 sheet [1]. The hole concentration or excess valence p^+ on the CuO_2 sheet in an ionic charge lattice represented by $La^{3+}_{2-x}Sr^{2+}_{x}(CuO_2)^{-2+p^+}O^{2-}_{2-\delta}$ is given by $p^+ = x - 2\delta$,

meaning that p^+ can be varied by varying either x or δ [2,3]. With $\delta = 0$, T_c increases from 0 to 38 K as x increases from 0.06 to 0.15, T_c starts to decrease for $x > 0.15$ and superconductivity disappears for $x > 0.27$ [2,3]. This result indicates the existence of two superconducting states: a hole (carrier)-deficient state and hole (carrier)-excess state. For the hole-deficient state, T_c increases with holes concentration whereas for the hole-excess state, T_c decreases as the hole concentration increases.

For the (123) family of superconductors represented by $YBa_2Cu_3O_y$ [4], superconductivity vanishes for stoichiometric composition $y = 6.5$ and for $y > 6.5$, T_c increases with y, reaching 93 K for $y \sim 7.0$. In this system, each unit cell contains two CuO_2 sheets and a CuO chain. The question of where the excess holes resides leading to superconductivity has been studied by Tokura et al [5]. According to their analysis, the excess holes p given by $p = (2y - Q - 6)/3$ is distributed as $p_{sh} = (y - 6.5)/2$, and $p_{ch} = (y - 6.5)$ with $p = (2p_{sh} + p_{ch})/3$. In the above, Q is the total cationic charge (excluding Cu), and p_{sh} and p_{ch} respectively represent the excess holes in the CuO_2 sheets and CuO chain. They further suggested that holes associated with chains, p_{ch}, are localized and merely provide an insulating reservoir of charge whereas p_{sh} is the principal variable governing superconductivity. If p^+ represents hole concentration per CuO_2 sheet, then $p^+ = p_{sh}/2$ for the (123) system. By doping with La and Ca,

Tokura et al. showed that T_c initially increases with p^+ for $p^+ > 0$, reaches maximum of T_c~ 85 K at around $p^+ = 0.2$ and for $p^+ > 0.2$, a decrease of T_c is seen.

The idealized structure of the $Bi_2Sr_2Ca_1Cu_2O_{8+\delta}$ (2212) superconductor is quite similar to that of the (123) compound with Ca, SrO and double BiO layers replacing Y, BaO and CuO chain layers respectively. $Bi_2Sr_2Ca_2Cu_3O_{10+\delta}$ (2223) phase can be formed by inserting one more (CuO_2 + Ca) slab into the (2212) phase. From the structure similarities, one may expect that excess oxygen atoms are residing in the double BiO layer, playing the same role as the excess oxygen in the CuO chains for the (123) superconductor. However, the situation for the Bi (2212) phase is complicated. First of all, the exact location of the excess oxygen atoms in the compound is still unclear. Secondly, there are numerous deviations from the idealized structure and composition in the Bi and Tl superconductor systems, especially in the double Bi(Tl)O layers and the Sr(Ba)O layers. Deviations such as strontium deficiency [6] (Sr:Ca < 2:1 for the (2212) phase) also creates holes on the CuO_2 sheets. Attemp to vary the oxygen content will inevitably alter the structure to some extent. Thirdly, on synthesizing the high T_c (2223) phase, intergrowth with a low T_c phase often occurs in this system which makes quantitative study on a single phase difficult.

A number of studies [7-11] have shown that T_c in the Bi superconductors is sensitive to oxygen stoichiometry. For example, Morris et al [9] observed increase in T_c with the decrease of oxygen content for the (2212) phase. They varied oxygen content by annealing the samples at different oxygen pressures [9]. We used a TGA (Thermogravimetric Analysis) apparatus to heat a $Bi_2Sr_2Ca_1Cu_2O_{8+\delta}$ (2212) sample to < 850°C and subsequently quench the samples in Ar gas [10]. This method is relatively simple. Since the sample treatment was carried out at atmosphere pressure, it is less destructive than other methods and the weight variation can be monitored in-situ with 1 μg sensitivity. By varying the quenching temperature, we were able to affect the oxygen content by different levels and we observed an increase of T_c of 25 K as a result of loss of 0.09 oxygens per formula unit. By the same technique, we studied a Pb-doped Bi superconductor consisting of the (2223) phase with an admixture of the (2212) phase [11]. Here we observed that with loss of oxygen, T_c of the (2212) phase increased from 70 K to 90 K, whereas that of the (2223) phase decreased from 107 to 90 K. These results suggested that the as-prepared Bi (2212) phase is in the hole-excess state whereas the Bi (2223) phase is in the hole-deficient state. For an as-prepared Tl (2223) phase sample, T_c has been observed to decrease with decrease of oxygen content [12,13] whereas for an as-prepared Tl (2201) phase sample [14], T_c increases with decrease of oxygen content.

At first glance, the above findings on the variation of T_c with hole concentration in the (2212) and (2223) phases of the Bi superconductors do not fit into a consistent picture. Furthermore, the T_c's of the Bi (2201), (2212), (2223) and (2234) phases are quite different viz. 10, 85, 110 and 90 K respectively and these results need to be understood. Here we show that when the observed findings of the variation of T_c with oxygen content in the Bi superconductor are analyzed in terms of p^+, the hole concentration per CuO_2 sheet, a consistent picture emerges. In addition, the variation of T_c with p^+ in

Bi and possibly in Tl superconductors is quite similar to that shown in the $La_{2-x}Sr_xCuO_{4-\delta}$ and the $YBa_2Cu_3O_y$ superconductors, providing a consistent picture for the four families of the cuprate superconductors.

The Bi (2223)+(2212) phase sample we prepared is not a simple mixture of two compounds. As mentioned in the previous paragraph, during the formation of the (2223) phase, intergrowth of the (2212) phase occurs. Therefore the double Bi-O layers are often shared by the (2212) and the (2223) phases. If we assume that excess oxygen atoms are residing in the double BiO layers, the amount of the holes provided by the excess oxygen atoms will be shared by two CuO_2 sheets in the (2212) phase case and by three CuO_2 sheets in the (2223) phase case. According to literature [15,16], δ in $Bi_2Sr_2CaCu_2O_{8+\delta}$ varies from 0.15 to 0.6 for the as-prepared (2212) phase sample. With the consideration of the holes created by strontium deficency [6], we assume there is 0.8 holes per formula unit. Then in average, the hole concentration per sheet, p^+, is given by $p^+ = 0.8/n$. This gives $p^+ = 0.4$ and 0.27 for the (2212) and (2223) phases respectively. Using these two values for the as-prepared samples, the variations of T_c with p^+ for the (2212) and (2223) phases based on our data [10,11] are shown in Fig. 1. A different choice of δ shifts p^+ at which the maximum T_c is observed. However general shape of the curve remains the same. Fig. 1 shows that the as-prepared Bi (2223) is in a carrier-deficient state whereas the as-prepared Bi (2212) phase is in a carrier-excess state. This explains the opposite directions of the T_c variation observed in the (2223) and (2212) phases as a result of loss of oxygen [7-11]. According to the above scheme, one may explain that T_c for the (2234) phase with four CuO_2 sheets is lower (90 K) than that for the (2223) phase because of the smaller p^+ value and the low T_c (~ 10 K) for the (2201) phase with one CuO_2 sheet because of the larger p^+ value. In addition, the as-prepared Bi (2234) and (2201) phase samples are expected to belong to carrier-deficient and carreir-excess states respectively if the structure of the double BiO layer and the SrO layers remains the same as that for the (2212) and (2223) phases. We note that Urland and Tietz [15] have reported the variation of T_c with p^+ for the Bi (2212) phase. T_c variation was achieved by varying Sr:Ca ratio and oxygen content. They showed that as p^+ increases from 0.1 to 0.6, T_c first increases from 73 to 80 K, remaining at 80 K for $p^+ = 0.2 \sim 0.4$, then falling for $p^+ > 0.4$. Their results suggest that for a single Bi or Tl phase, the variation of T_c with p^+ may follow the same shape as that in Fig. 1. Recently, similar results have been reported by Yoshizaki et al [17] and Torrance et al [18] respectively in Y doped, and Na and K doped Bi (2212) samples. Maximum T_c's were found at $p^+ = 0.15 \sim 0.25$. In the case of La doped (2201) $Bi_2Sr_{2-x}La_xCuO_{6+\delta}$ compound [19], Groen et al showed that the as-prepared (2201) phase is in a carrier-excess state. Maximum $T_c = 28$ K was observed at $p^+ = 0.3$ and for $p^+ < 0.21$, the sample became non-superconductor.

In the above, we have shown that the variation of T_c with p^+ for the Bi (2212) and (2223) phases may be represented by Fig. 1. Moreover the shape of the curve in Fig. 1 is similar to that for the (123) [5] and $La_{2-x}Sr_xCuO_{4+\delta}$ [2,3] superconductors although the magnitude of p^+ corresponding to the maximum T_c is somewhat different for different families of superconductors. According

to previous experimental results [12,13,14], it is likely that the variation of T_c with p^+ for the Tl-based superconducting phases may follow a pattern similar to that in Fig. 1 with maximum T_c = 125 K. These results suggest that p^+ (excess valence per CuO_2 sheet) may be an important variable for the cuprate superconductors and these results should form the major test for any successful theory of superconductivity.

It is interesting to note that without the hole reservoir, T_c for $La_{2-x}Sr_xCuO_{4-\delta}$ is below 40 K. With CuO chain, double BiO layers and double TlO layers as hole reservoirs, T_c increases to 93 K, 110 K and 125 K respectively. It appears that the key to the differences in T_c is the interaction between the hole reservoir part and the CuO_2 sheets. Bishop et al [20] argued that although superconductivity itself takes place on the CuO_2 sheets, the attractive pairing mechanism is not two-dimensional but may require dynamic coupling of these sheets to the surrounding polarizable environment in order to understand the difference in the T_c's of the four families of superconductors.

Acknowledgements: This research was supported in part by a grant from the Energy Research Center of West Virginia University.

REFERENCES

1. J. G. Bednorz and K. A. Muller, Z. Phys. B66, 189 (1986).
2. J. B. Torrance, Y. Tokura, A. I. Nazzal, A. Bezinge, T. C. Huang, and S. S. P. Parkin, Phys. Rev. Lett. 61, 1127 (1988).
3. H. Takagi, T. Ido, S. Ishibashi, M. Uota, S. Uchida, and Y. Tokura, Phys. Rev. B40, 2254 (1989).
4. M. K. Wu, J. R. Ashburn, C. J. Torng, P. R. Hor, R. L. Meng, L. Gao, Z. J. Huang, Y. Q. Wang, and C. W. Chu, Phys. Rev. Lett., 58, 908 (1987).
5. Y. Tokura, J. B. Torrance, T. C. Huang, and A. I. Nazzal, Phys. Rev. B38, 7156 (1988) .
6. P. Lee, Y. Gao, H. S. Sheu, V. Petricek, R. Restori, P. Coppens, A. Darovskikh, J. C. Phillips, A. W. Sleight, and M. A. Subramanian, Science 244, 62 (1989).
7. J. L. Tallon, R. G. Buckley, P. W. Gilberd, and M. R. Presland, Physica C 158, 247 (1989).
8. T. Ishida, Jpn. J. Appl. Phys. 29, L197 (1989).
9. D. E. Morris, C. T. Hultgren, A. M. Markelz, J. Y. T. Wei, N. G. Asmar, and J. H. Nickel, Phys. Rev. B39, 6612 (1989).
10. J. Zhao and M. S. Seehra, Physica C 159, 639 (1989).
11. J. Zhao, M. Wu, W. Abdul-Razzaq, and M. S. Seehra, Physica C 165, 135 (1990).
12. A. Schilling, H. R. Ott, and F. Hulliger, Physica C 157, 144 (1989).
13. M. R. Presland, R. G. Buckley, J. R. Tallon, R. S. Liu and N. E. Flower, preprint, to appear on Physica C.
14. Y. Shimakawa, Y. Kubo, T. Manako, T. Satoh, S. Iijima, T. Ichihashi and H. Igarashi, Physica C 157, 279 (1989)
15. W. Urland and F. Tietz, Solid State Commun. 69, 995 (1989).

16. J. -M. Tarascon, Y. LePage, P. Barboux, B. G. Bagley, L. H. Greene, M. R. McKinnon, G. W. Hull, M. Giroud, and D. M. Hwang, Phys. Rev. B37, 9382 (1989).
17. R. Yoshizaki, H. Ikeda, Y. Saito and Y. Abe, Physica C 162-164, 67 (1989).
18. J. B. Torrance, A. Bezinge, A. I. Nazzal, and S. S. P. Parkin, Physica C 162-164, 291 (1989).
19. W. A. Groen, D. M. de Leeuw, and G. P. J. Geelen, Physica C 165, 305 (1990)
20. A. R. Bishop, R. L. Martin, K. A. Muller, and Z. Tesanovic, Z. Phys. B76, 17 (1989).

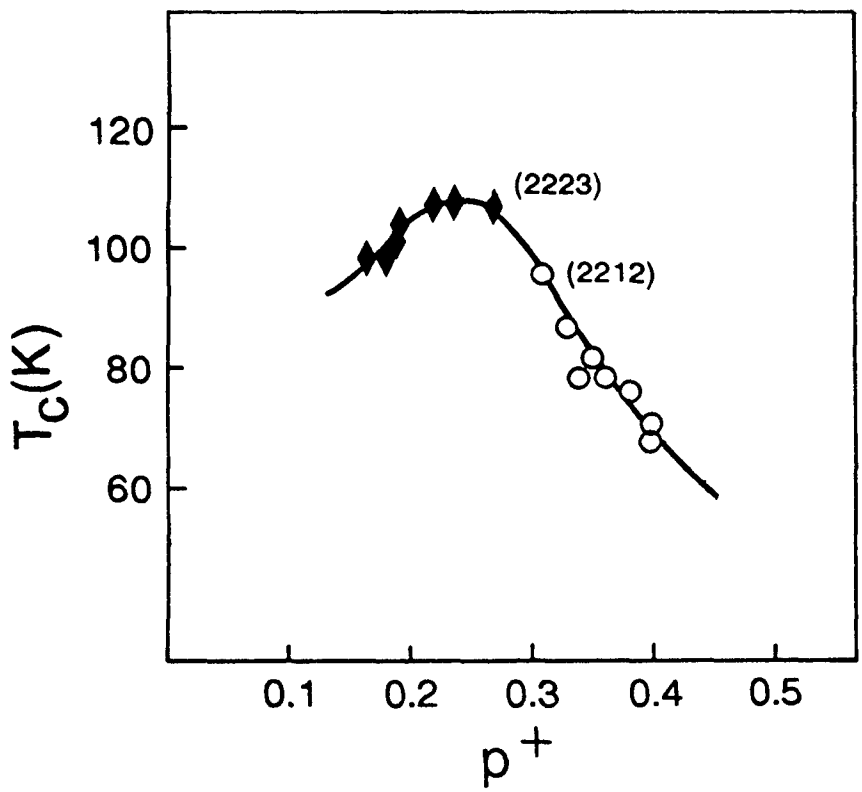


Fig. 1. The variations of T_c's with p^+ for the Bi (2212) and (2223) phases.

SPIN GLASS FREEZING AND SUPERCONDUCTIVITY IN $YBa_2(Cu_{1-x}Fe_x)_3O_7$ ALLOYS

I. Mirebeau, M. Hennion - *Laboratoire Léon Brillouin (CEA-CNRS) CEN-Saclay, 91191 Gif-sur-Yvette Cedex, France*

J. Dianoux, *Institut Laue Langevin 156X Centre de Tri, 38042 Grenoble Cedex, France*

V. Caignaert, *Laboratoire CRISMAT I.S.M., Université de Caen, 14032 Caen, France*

T.E. Phillips, K. Moorjani, *Applied Physics Laboratory, The John Hopkins University, Laurel, Maryland 20707, USA*

We have studied the dynamics of the iron spins in superconducting $YBa_2(Cu_{0.94}Fe_{0.06})_3O_7$ by neutron time-of-flight measurements. Two samples were investigated with slightly different characteristics, as shown by resistivity and neutron diffraction measurements. The same dynamical anomalies are observed by neutrons in both samples. Differences appear qualitative but not quantitative. In the whole temperature range, the q-dependence of the magnetic intensity mainly reflects the magnetic form factor of iron which shows that the iron spins are almost uncorrelated. The elastic and quasielastic intensities strongly vary with temperature. A spin glass like freezing is revealed at low temperature by a sharp decrease of the quasielastic intensity, an increase of the "elastic" or resolution limited intensity and a minimum in the quasielastic width. The freezing temperature (T_f = 18 K) corresponds to that already determined by a magnetic splitting in Mössbauer experiments. Above T_f, the relaxation of the iron spins in the paramagnetic state is modified by the occurence of superconductivity. We observe an increase of the quasielastic intensity and of the quasielastic width at the superconducting transition.

In the superconducting ceramics $YBa_2(Cu_{1-x}Fe_x)_3O_7$ the substitution of iron for copper leads to a rather slow decrease of the superconducting temperature T_c [1]. Electron microscopy [2], neutron diffraction[2] and Mössbauer experiments [3] show that the Fe atoms mainly substitute on the Cu_1 sites in agreement with energy considerations for the thermal equilibrium state. Moreover, Mössbauer experiments show the occurence of a Zeeman splitting in the spectra, indicating a freezing process of the Fe spins below some temperature T_f (fig.1). Interestingly enough, the spin freezing does not suppress the superconductivity. The nature of the correlations between the Fe atoms below T_f (ferromagnetic, antiferromagnetic or uncorrelated) has been controversial due to the strong difficulties in analysing the Mössbauer spectra. Therefore, this system provides a very interesting opportunity to investigate the interplay between magnetism and superconductivity by neutron scattering measurements.

We have performed inelastic neutron scattering measurements in order to study (i) the relaxation of the iron spin-above T_f (is it modified by the occurence of the superconducting state ?) (ii) the characteristics of the

freezing itself, with a typical time window ($\sim 10^{-11}$ s)comparable to that of the Mössbauer probe. The concentration $x = 0.06$ is particularly suitable for this study since T_c and T_f are rather far from each other ($T_c \sim 65$ to 80 K, see Fig.1), $T_f \sim 18$ K . The time of flight measurements, performed with an excellent resolution, yield new and original informations. At low temperature, a spin-glass like freezing is clearly evidenced, which has all the characteristics previously observed in usual metallic spin glasses. At higher temperature, the enhancement of the quasielastic intensity and of the quasielastic width which occurs near the superconducting transition strongly suggests a coupling between the iron and the copper spin dynamics. These experiments extend those previously reported[4] where only the spin glass freezing was clearly apparent. A short report of the present ones has been given in reference 5.

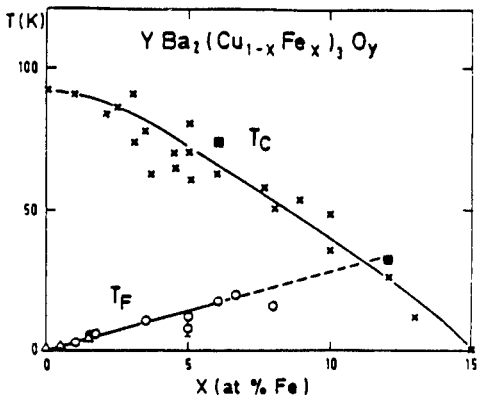


Fig.1. Typical superconducting temperatures T_c (x) and freezing temperatures T_f in the $YBa_2(Cu_{1-x}Fe_x)_3O_7$ as measured from various authors[1,3]. T_f is determined from Mössbauer (o) or NQR (Δ) measurements. (■) T_c values of our own samples.

1. SAMPLE PREPARATION AND CHARACTERIZATION

We compare here two samples of the same nominal concentration but with slightly different characteristics. These two samples of $YBa_2(Cu_{1-x}Fe_x)_3O_y$ with $x = 0.06$, $y \sim 7$, called samples a and b, were prepared respectively at B. Raveau Laboratory (Caen, France) and at Johns Hopkins Applied Phys. Lab. (Laurel,MD, USA). The procedure of preparation was basically the same in both cases. Appropriate amounts of Y_2O_3, $BaCO_3$, CuO and Fe_2O_3 in fine mesh powders were ground, pressed and heated at 950°C for 50 hours and then cooled over 15 hours in a constant O_2 flux. This procedure was repeated several times. After the final firing the samples were stored in a dry atmosphere. The samples used for neutron measurements were shaped in cylinders of 12mm diameter and 5cm length.

As shown in Fig.2, the neutron diffraction patterns correspond to a mean tetragonal phase, but small orthorhombic domains might be present as shown previously by electron microscopy[2]. The lattice constants, determined from the peak positions by a Rietveldt refinement are the same in the two samples. Small differences in the peak intensities can be related either to slightly different occupancies at the oxygen and Fe sites or to preferential grain orientations. In sample a, all the observable Bragg peaks belong to the structure whereas in sample b small peaks of impurities ($BaCuO_2$ mainly) are clearly visible between the main Bragg peaks.

Resistivity measurement (Fig.3) shows for sample a an onset of the superconducting transition at $T_c = 78$ K. In sample b, the resistivity clearly shows a slight maximum versus temperature, then a decrease below 63 K. This maximum in the resistivity curve is enhanced in the more concentrated samples and suggests that this second sample is rather close to a semiconducting behavior. Most probably, in sample a, all the Fe atoms occupy the Cu^{I} sites (Cu-O chains) while in sample b, a small fraction of iron might occupy the Cu^{II}

sites (Cu-O planes) which are mainly responsible for superconductivity. We note that some some substitution of Fe on the planar sites has been already achieved[2,6], depending on the heat treatment, but seems to be rather difficult to obtain. Extended neutron and X-rays measurements on our two samples are being performed in order to clear this point.

Magnetization measurements indicated a diamagnetic volume of about 36% at low temperature and a superconducting transition in rather good aggrement with the previous determinations ($T_c \sim 74$ K in sample a).

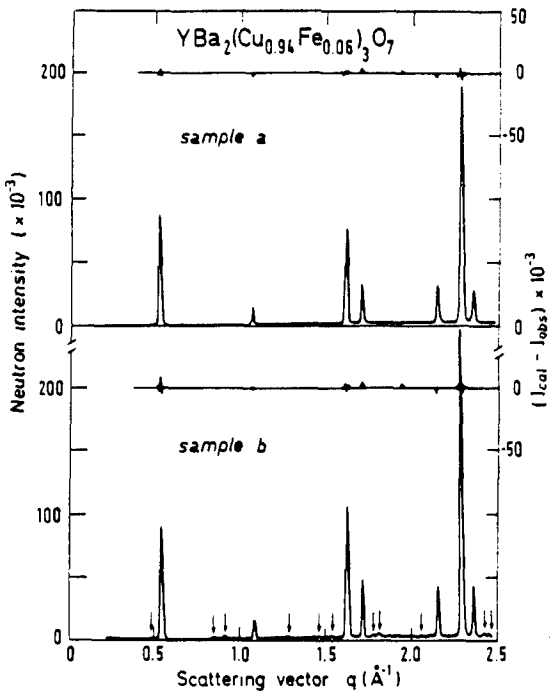


Fig.2. Neutron diffraction patterns in the two $YBa_2(Cu_{0.94}Fe_{0.06})_3O_7$ samples at 300 K. In 2b the arrows indicate impurity peaks (of $BaCuO_2$ mainly). Rietveldt refinements are also plotted.

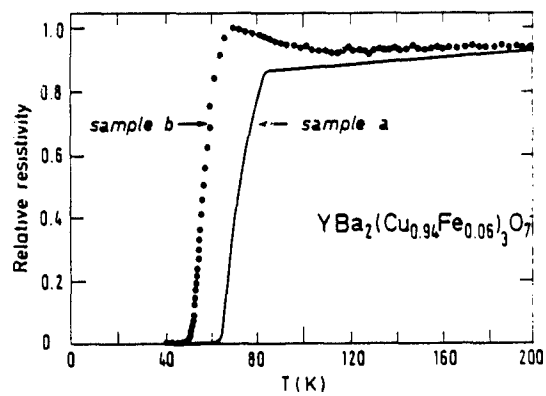


Fig.3. Relative resistance as a function of temperature in the two x=0.06 samples.

2. TIME OF FLIGHT NEUTRON MEASUREMENTS

The Time of Flight (TOF) neutron scattering measurements were performed on the spectrometer IN6 of the high neutron flux source of ILL (Grenoble). In these experiments a monokinetic neutron pulse, corresponding to an incident neutron wavelength λ of 5 Å was selected by a "chopper" disk. The neutrons scattered by the sample were registered as a function of their time of arrival in each of the 336 counters which were positioned at selected angles θ between the Bragg peak positions. The range of the scattering vector q ($q = \frac{4\pi \sin\theta}{\lambda}$ where 2θ is the scattering angle) was $0.1 < q < 2.1$ Å^{-1}, a range which roughly corresponds to the one covered in the diffraction patterns of Fig.2. Due to the high neutron flux source and to the use of a triple graphite monochromator, very good statistics could be achieved with a rather short counting time of about 4 hours at each temperature. The energy resolution of the spectrometer of 80 μeV corresponds to a typical time window of 10^{-11}s. The temperature was varied from 300 K to 1.8 K using a helium cryostat.

In a typical TOF spectrum, measured for a given value of the scattering angle 2θ, the neutron intensity is plotted as a function of time, or equivalently as a function of the energy transfer ω between the neutrons and the sample.

In pure $YBa_2Cu_3O_7$, a TOF spectrum consists of an elastic signal of nuclear origin and of an inelastic one due to the phonons. When the temperature decreases, the elastic intensity slightly increases due to the Debye Waller effects, whereas the phonon contribution decreases. In the substituted samples, the elastic intensity may have also a magnetic contribution and we observe in addition a quasielastic signal due to the relaxation of the iron spins. Focusing on the quasielastic region, we report in Fig.4 a typical TOF spectrum for the x = 0.06 sample as measured at the temperature of 10 K for a q value of 0.7 $Å^{-1}$.

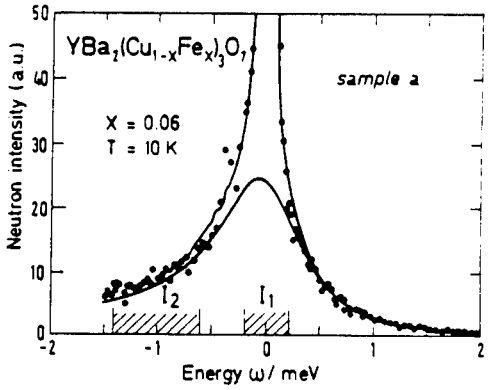


Fig.4. Typical time of flight spectrum measured at 10 K for a q-value of 0.7 $Å^{-1}$ in the sample a. The domain of energy integration corresponding to the intensities I_1 and I_2 (see text) are shown by dashed areas. The solid lines are fits to the data according to equation (1)

In fig.5a, we have plotted the temperature dependence of the intensities I_1 and I_2, measured at q = 0.7 $Å^{-1}$ and corrected for background. I_1 corresponds to an integration of the TOF spectrum within the elastic window, in the energy range (-0.2, 0.2) meV, and possesses an elastic and a quasielastic contribution. I_2 is the intensity integrated just aside the elastic signal, in a purely inelastic energy range (-1.4, -0.6) meV where the phonon contribution is small.We notice that both I_1 and I_2 present anomalies at the freezing and at the superconducting transitions. A very similar behavior is observed for the other sample b (Fig.5b). However, in the second sample which is clearly less homogeneous,as shown by the neutron diffraction and resistivity measurements, we note that although the freezing transition is still very well defined, the anomalies which occured in the T_c region are much more smeared.

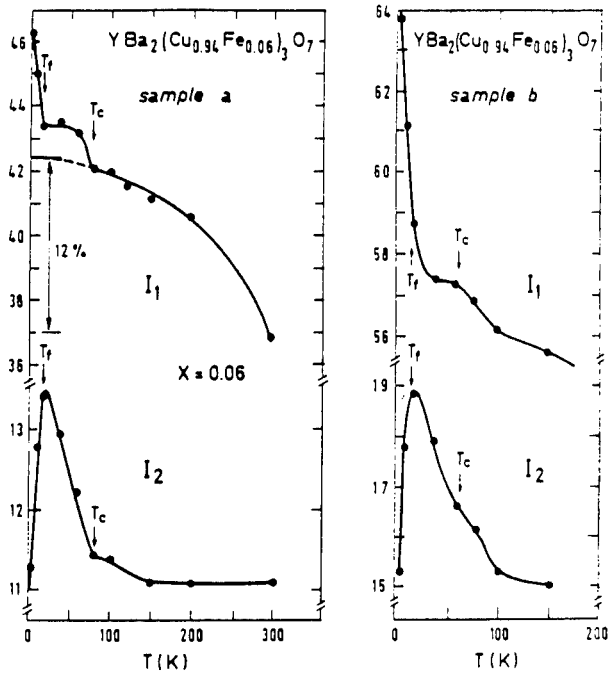


Fig.5. Intensities I_1 and I_2 versus temperature measured at q ~ 0.7 $Å^{-1}$ for the two samples a and b. The solid lines are a guide to the eye.

The corrected spectra were fitted by the sum of a delta function of norm $c_1(q)$ and of a quasielastic scattering function $S(q,\omega)$ convoluted with experimental resolution. Assuming a lorentzian shape for the relaxation process, and a Bose statistics for the magnetic excitations, it may be written :

$$S(q,\omega) = c_2 \frac{\hbar\omega/kT}{e^{\hbar\omega/kT} - 1} \times \frac{\Gamma}{\Gamma^2 + (\hbar\omega)^2} \times \frac{1}{\pi} \qquad (1)$$

where c_2 and Γ are respectively the norm and the width of the quasielastic signal. c_2 is equal to $kT\, f^2(q)\, \chi(q)$ where $f(q)$ is the magnetic form factor of iron and $\chi(q)$ the static suceptibility. The fits were performed in an energy range (-1.5, 2) meV where the phonon contribution was small and could be adjusted at each temperature as an energy-independent background.

a) q-Dependence of the Intensities

As shown in Fig. 6, the quasielastic intensity $c_2(q)$ mainly reflects the variation of $f^2(q)$ ($f(q) \simeq e^{-0.06\, q^2}$ in the measured q-range), which shows that the Fe spins are almost uncorrelated. Slight enhancements around the Bragg peak positions suggest some short range ferromagnetic correlations. The quasielastic width Γ remains q-independent up to $q = 1.5$ Å^{-1} and increases beyond. The q-dependence of c_2 and Γ remains the same in all the measured temperature range.

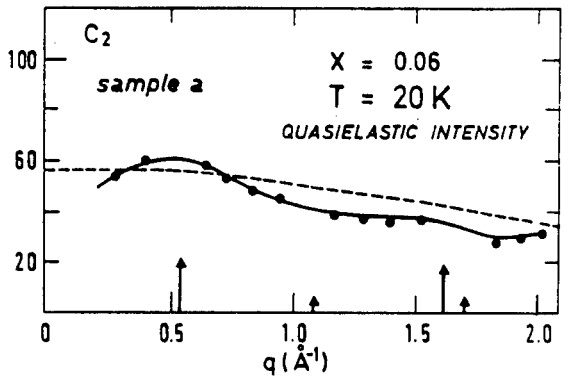


Fig.6. Quasi-elastic intensity $c_2(q)$ measured at 20 K in sample a. The dashed line is proportional to the magnetic iron form factor $f^2(q)$. The solid lines are a guide to the eye. The arrows indicate the Bragg peak positions.

The elastic intensity $c_1(q)$ is shown in Fig.7 for the sample a at several temperatures. In this very clean sample we clearly observe a large modulation of the intensity between the Bragg peaks which correspond to short range ordering effects. In order to analyse these effects quantitatively, experiments on a single crystal would be necessary. We note that this modulation is unlikely due to some ordering between the iron atoms since the rather small difference between the coherent scattering lengths of the Cu and Fe atoms induces a very low contrast. Most probably it reflects the existence of short range ordering effects between the oxygens which could be either intrinsic or induced by the iron substitution. In the other sample b, the presence of many small peaks of impurities prevents the observation of modulations of the elastic intensity.

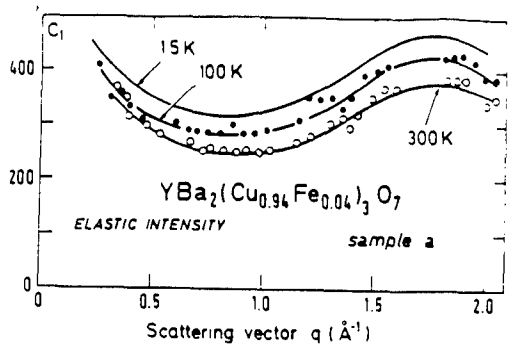


Fig.7. Elastic intensity $c_1(q)$ measured in sample a at several temperatures. The solid lines are a guide to the eye.

b. Temperature Dependence of the Intensities

The parameters c_1, c_2 and Γ are plotted versus temperature in Fig. 8 for the sample a. We consider successively the high temperature regime (around and above T_c), and the low temperature one (around T_f).

In the first regime, which corresponds to a paramagnetic state, the elastic intensity c_1 smoothly increases with decreasing temperature, showing no anomaly at T_c. This increase probably reflects the decrease of the Debye Waller factor, being similar to the behavior observed in $YBa_2Cu_3O_7$. The quasielastic intensity c_2 is almost temperature independent at high temperature, which shows that the susceptibility follows a Curie Law ($\chi \propto 1/T$) ; it increases slightly when approaching T_c from above and shows a stronger increase below T_c. This anomaly at T_c was more apparent in the intensities I_1 and I_2 obtained by integration. The quasielastic width Γ shows an intricate temperature dependence. It decreases between 300 K and 200 K then further increases and exhibits a change of slope at T_c.

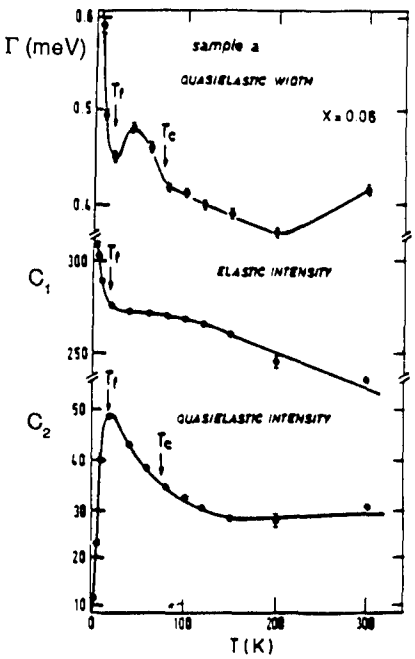


Fig.8. Elastic intensity c_1, quasi-elastic intensity c_2 and quasi-elastic width Γ (meV) measured at $q \sim 0.7$ Å in the sample (a), versus temperature.

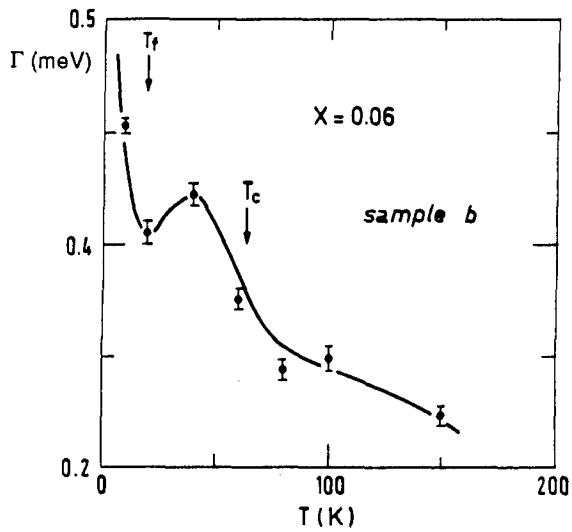


Fig.9. Quasielastic width Γ (meV) measured in sample b versus temperature.

In the low temperature regime, we observe the usual characteristics of a spin glass freezing, as previously reported in metallic spin glasses[7] and in a x=0.12 sample[4] , namely a sharp increase of the elastic intensity c_1, and a decrease of the quasielastic intensity c_2. Moreover, we can ascertain that around T_f, the linewidth Γ exhibits a minimum, as previously suggested from measurements at x=0.12.[4] The existence of this minimum was already suggested in archetypal spin glasses AuFe and CuMn[7]. It has been recently confirmed by us in another metallic spin glass a-FeMn . All the features observed at low temperature can be understood on the basis of spin clusters. The freezing of clusters of coupled spins yields a progressive transfer from the quasielastic signal to the resolution limited "elastic" one. The decrease of Γ when the temperature approaches T_f from above corresponds to an increase of the typical relaxation time within the clusters ($\Gamma \sim 1/\tau$). Its further increase is more surprising : it reveals a change in the distribution of the relaxation times which could be understood within the fractal cluster model of Malozemov and Barbara[8] as suggested in reference 4.

The above results represent a considerable improvement of our first measurements, due to the very high statistics which could be achieved in the ILL reactor. The spin glass freezing which occurs at low temperature is now clearly ascertained. The occurence of a spin glass state with almost uncorrelated spins does not destroy the superconductivity. The new result is that the neutron probe provides evidence for a change in the relaxation of iron spins at the superconducting transition. It appears in the quasielastic signal but not in the elastic one. This last event was first suspected from our preliminary measurements[4] but it is clearly ruled out in these more complete and accurate data.

The most surprising result remains the temperature dependence of Γ above and around the superconducting temperature T_c . As shown in Fig.9, this interesting behavior is also observed in the second sample b which contains some impurities and has a lower T_c value. In an attempt to analyse $\Gamma(T)$, above and around T_c, we recall that in a metal, the spin relaxation time τ, ($\Gamma \sim 1/\tau$) is mainly controlled by the electron density of states at the Fermi level. In superconducting metals, for non-interacting spins one could expect that Γ would decrease linearly with T at high temperature, following a Korringa process ($\Gamma \propto T$), and would show a much stronger decrease below T_c, corresponding to the disappearance of possible relaxation processes (those involving an energy transfer smaller than the superconducting gap). Just below T_c, where the gap is small compared to the energy transfers between the spins and the electrons, one could expect a small bump in Γ, revealing the singularity of the electron density of states which diverges at the gap edge in BCS theory[9].

Actually, as shown by NMR experiments[10] mainly, the relaxation time of the Cu nuclear spins is very different from that expected in a usual superconductor. First of all, it never follows a Korringa process above T_c, which seems to characterize the so called "normal" state of these new superconductors. Secondly, the small bump of Γ expected just below T_c is observed in some NMR experiments on the oxygen and on the Cu^I sites but not on the Cu^{II} sites of $YBa_2Cu_3O_7$. However, the strong expected decrease of Γ below T_c

is observed by NMR on the Cu^{II} sites as well, and was also observed by neutrons in recent studies of excitation between crystalline field levels[11]. In our case, the relaxation of the iron spins which substitute for the copper is very different and calls for another explanation.

References

1. K. Moorjani et al. J. Appl. Phys. **63**, 4161, 1988 ;
   B. Ullman et al., Physica C **153-155**, 872, 1988.
2. P. Bordet et al. Solid State Comm. **66**, 435, 1988 ;
   G. Roth et al., Z. Phys. B **71**, 43, 1988.
3. Z.Q. Diu et al. J. Mag. Mat. Mat. **69**, 221, 1987 ;
   P. Imbert, G. Jehanno, J. Physique **49**, 7, 1988 ;
   P. Dalmas de Reotier et al., Proceedings of the ICM Conf. Paris 1988, J. Phys. Coll. 1989.
   T. Tamaki et al., Solid. State Comm. **65**, 43, 1988.
4. I. Mirebeau et al., Europhys. Lett. **9**, 181, 1989 and J. Appl. Phys. 90 ;
   M. Hennion et al., Physica C **159**, 124, 1989.
5. I. Mirebeau et al., Proceedings of the MMM Conference 1989, to be published in J. Appl. Phys. 1990
6. T.J. Kistenmacher, Phys. Rev. B **38**, 8862, 1988 ;
   Z.Q. Qiu, Y.W. Du, H. Tang, J.C. Walker, Proceedings of the MMM Conf., Boston 1989, to appear in J. Appl. Phys. 1990.
7. A.P. Murani, J. Phys. (Paris) Coll. **39**, 1517, 1978 ; Proceedings of the Conference on Inelastic Neutron Scattering, Vienna vol.2, 213, 1977
8. A.P. Malozemov, B. Barbara, J. Appl. Phys. **57**, 3140, 1985
9. L.C. Hebel, C.P. Slichter, Phys. Rev. **113**, 1504, 1959.
10. M. Mali et al., Phys. Lett. A, **112**, 1987 ;
    Y. Kitaoka et al., Proceedings ofthe ICCF6 Conference, July, 1988, Frankfurt ;
    P.C. Hammel et al., Phys. Rev. Lett. **63**, 1992, 1989.
11. R. Fiele et al., Phys. Rev. Lett.**47**, 610, 1981 ; U. Walker et al., Phys. Rev. B **36**, 8899, 1987 ; Physica C **153-155**, 1988

THERMAL RESPONSE OF LARGE AREA HIGH TEMPERATURE SUPERCONDUCTING YBaCuO INFRA RED BOLOMETERS

Ali E. Khalil*

GE Astrospace Division, Princeton NJ 08543

Abstract:

Thermal analysis of large area high temperature superconducting infra red detector operating in the equilibrium mode (bolometer) is performed. The spatial spread of the heat pulse as a result of the initial thermal excitations due to the incident radiation is modeled using heat conduction. An expression for the temperature coefficient $\beta=1/R(dR/dT)$ in terms of the thermal conductance of the insulating substrate and the thermal time constant of the detector were derived. In addition, the thermal responsivity and the thermal cross talk between different elements of the array as a function of the angular frequency and the spatial modulation frequency of the incident radiation were examined. The results of this theoretical modeling were compared with recent measurements on YBaCuO thin film using YAG laser with clear excellent agreement between theory and experiment. This analysis can be critical for future design and applications of large area focal plane arrays as broad band optical detectors made of granular thin films high temperature superconductors YBaCuO.

* Paper to be submitted to Applied Physics Letters and NASA workshop on HTC applications.

INTRODUCTION

Recent reports of optical interactions of high temperature superconducting (HTS) thin film YBaCuO have demonstrated equilibrium[1] (bolometric) and non-equilibrium[2] (quasi particle excitations) responses. These results have very promising applications for broad band optical detectors from ultraviolet to near infrared. A thin film high temperature superconducting transition edge bolometer can potentially have much better sensitivity for wavelengths greater than 20μm. In addition, utilizing high temperature superconducting thin film technology can lead to the state of the art thermal detectors operating at the theoretical noise limit. A proper choice of the detector backing can result in a flat spectral response at near perfect effeciency for wavelengths out to 250 μm. At these longer wavelengths where detector operations are mostly needed the bolometer area required for efficient coupling to an optical signal increases with the wave length. In addition, the bolometer thickness must also increase with wavelength for good optical efficiency. In general a careful design can provide a control over the thermal conductance between the thin film and the insulating substrate. A wide spectrum of values ranging from 0.005 μW/K to 1000 μW/K can be achieved in order to suit the background noise and or the detector speed requirements[3], while the film thickness can be adjusted to provide absorption over a wide range of wavelengths.

A superconducting transition edge bolometer is a thermistor consisting of a thin film superconducting YBaCuO evaporated into a suitable thermally isolated substrate. The operating temperature of the bolometer is maintained close to the midpoint of the superconducting transition region where the resistance R has a maximum dynamic range. Measurements on the electrical response of YBaCuO thin films to a fast optical laser pulses (100 Ps long) was recently reported[4]. It was found that although the magnitude of the signal corresponds to radiation heating, nonequilibrium energy transport have played a part in distributing the heat through the thickness of the film. Several models have been proposed to explain the experimental observations on optical excitations of the oxide superconductors however, complete understanding of this phenomena remains far from being clear[5].

In this article the performance of a thermal imaging system utilizing HTS thin film detector arrays and using the heat transport mechanism is examined. One of the key aspects of the performance of such system is the thermal response of the array to the incident radiation. These calculations require solving the heat conduction equation in the high temperature superconducting material (HTS) subject to the appropriate boundary conditions. An important feature of the thermal

response is the lateral heat conduction which may tend to degrade the performance of the material by introducing cross coupling decreasing the signal to noise ratio. This problem may be particularly severe in a spread sheet configuration. However, a system of linear arrays with discrete detector elements and separate readout for each element will tend to eleviate the thermal spreading problem.

In order to simplify the modeling and numerical calculations it is useful to consider the case of a uniform illumination (heating) of the detector material. An array of detectors without adequate thermal isolation between different elements will experience severe thermal spreading. These effects will be accounted for using heat diffusion modeling in the later part of this article. The analysis does not include non-equilibrium behavior of the superconductor and only operations at the equilibrium conditions where thermal phonons are totally decoupled from the charged particle carriers are modeled.

Consider a thin film YBaCuO superconducting bolometer of the geometry defined in Fig.1 with volume specific heat C, thermal conductivity K, mass density γ , and thickness b. The film is at ambient temperature T(r,t) coupled to a heat sink (thermal insulator) of thickness c and temperature T_0 through a thermal conductance G. The thermal equilibrium of the entire system (the film + substrate) can be derived on the basis of the first principles. In the normal mode of operation energy is added to the system by incident photon flux of power density P_i and scene temperature $T_s(r)$ causing the system temperature to rise by an amount ΔT above the ambient. When thermal equilibrium is established the thermal response will depend on the temperature gradient $\Delta T/c$ across the insulator layer. This temperature gradient will cause heat flow per unit area of the thin film surface to the insulating substrate at a rate given by $K\,\Delta T/c$. In the steady state the amount of heat escaping to the insulator is balanced by the rate of heat conduction through the film, the radiation input flux, and the rate of energy loss per unit area out of the insulator to the surrounding, in this case the energy rate equation can be written as,

$$-\Delta TK/c = b\gamma C\delta\Delta T/\delta t + F_0 - P_i b \qquad (1)$$

F_0 is the heat conduction loss through the insulator, we assume a blackbody radiation model where this quantity is given by $(4e\sigma T_0^3)\Delta T$. σ is the Boltzman's constant and e is the emissivity of the insulating layer. Equation (1) describes the system response to the initial external perturbation with a thermal time constant t_h and a temperature rise ΔT given by,

$$t_h = bC\gamma/(4e\sigma T_0^3 + K/c) \qquad (2)$$

$$\Delta T = (P_i t_h/C\gamma)(1-\exp(-t/t_h)) \qquad (3)$$

ΔT is the increase in the detector temperature above the ambient due to a uniform illumination with a source of power density P_i. This temperature rise will saturate reaching a terminal value $P_i t_h/C\gamma$ at the complete phase transition where the superconducting thin film is totally switched to the normal state. For normal bolometer operation the superconducting resistive element of the thermometer is always operated at the midpoint of the transition region for maximum dynamic gain (dR/dT is maximum). In this case the temperature coefficient $\beta = 1/R(dR/dT)$ in conventional bolometer theory can be identified as the inverse of the half-width ΔT of the superconducting transition and,

$$\beta \simeq (G\gamma/P_i)(1-\exp(-t/t_h))^{-1} \qquad (4)$$

where $G=C/t_h$ is the thermal conductance between the film and the insulating layer. A superior bolometer performance requires β to be as large as possible[6]. These criteria can only be satisfied within the dynamic operating regime of the bolometer defined by equation (4). On a very short time scale immediately following the initial thermal disturbance and for small values of $t<<t_h$ the temperature coefficient of the detector β is proportional to $1/t$ and consequently has a very large value (see Fig.2) which corresponds to optimum operating conditions of a thermal bolometer. However, for later times $t>>t_h$, β is inversly proportional to the detector substrate thickness b and within this dynamic range a thiner detector substrate is preferable to improve the detector responsivity. These conclusions were recently confirmed where measurement on β for thin film HTS reported values much higher than those of low temperature superconductors[6].

Another important factor affecting the detector performance is the thermal coupling and the heat dissipation through the insulating substrate. In the special case when $T_o^3 c<<K/4e\sigma$, the thermal time constant t_h is proportional to $bc(\gamma C/K)$, a maximum value of β will be reached when t_h is as small as possible. Since, the ratio $(\gamma C/K)$ is fixed by the choice of the superconducting film material the product (bc) should be minimal and the design of a large area array requires in principle that the detector thickness b and the substrate thickness c to be small for optimum thermal response.

In order to check the validity of our analysis a comparison between the theoretical predictions of equation (3) and recent experimental measurement reported in Ref.3 was performed. In the experiment described above a Nd:YAG laser was used as infrared source with pulses of 1.06 μm wavelength and $\simeq$150psec long to illuminate a superconducting YBaCuO granular film of thickness 0.7μm. The authors observed that the voltage rise following laser excitation of the thin film was consistent with a bolometric (thermal) response. This was evident from the dependence of the voltage rise on the laser fluence. We have calculated that dependence using equation (3) together with R aganist T data provided in ref3. We have also used other parameters provided by the same reference for the film thickness, pulse duration,thermal conductivity, density and bias current of the thin film. Results of these calculations together with the measurements of reference3 are shown in fig.5 where clear agreement are evident.

In the above analysis an expression for the temperature coefficient of HTS bolometer when its dynamical behavior is governed by thermal balance of the system was derived. It was found that the temperature coefficient strongly depends on the geometry of the film and the insulating substrate. In addition, due to the rapid transition from superconducting to the normal state of the material very large values of β can be achieved when the thermal time constant is adjusted to acquire small values.

Thermal Responsivity

A thermal imaging system utilizing discrete HTS thin film detector arrays with solid state readout (CCD or CID) can be constructed. An accurate prediction of the performance of the detector array requires full thermal diffusion analysis with appropriate boundary conditions. Consider one element in the detector array with the configuration shown in Fig (1) and assuming the cross section area A of the thin film is normal to the Z-axis. In the case of a uniform illumination of the detector surface the diffusion equation can be written as,

$$1/k\Delta T-\delta T/\delta t=0 \qquad (5)$$

Δ stands for three-dimensional Laplacians operator

with the boundary conditions,

$$K\delta T/\delta Z= -I_i T \qquad Z=0 \qquad (6)$$

$$K\delta T/\delta Z= I_o T \qquad Z=-b \qquad (7)$$

I_i and I_o are the radiative heat flow at the front and back electrode boundaries, $k=K/C\gamma$ is the thermal diffusity of the substrate. Integrating the Fourier transform of equation (5) over the Z-axis and applying the appropriate boundary conditions (6) and (7) we have,

$$q^2T_a(s,\Omega)=1/Kb\{I_oT(s,\Omega,-b)+I_iT(s,\Omega,0)\} \qquad (8)$$

and $$q^2=s^2_x+s^2_y+i\Omega/K$$
$$i=(-1)^{1/2}$$

T_a is the mean temperature change inside the film and is given by

$$T_a=1/b\int_{-b}^{o}T(x,y,z,t)dz$$

the thermal responsivity function of the detector is defined as

$$R_t=T_a(s,\Omega)/I_iT(s,\Omega,0)$$
$$=1/q^2Kb[1+ I_oT(s,\Omega,-b)/I_iT(s,\Omega,0)] \qquad (9)$$

for a very thin detector of few microns thick the diffusion length of the heat pulse in the Z-direction is much larger than the wafer thickness and $|qb|<<1$, $T(s,\Omega,-b)\approx T(s,\Omega,0)$, in this case equation (9) reduces to,

$$|R_t|=(1+e_o/ei)/Kb(1+\Omega^2/s^2K^2) \qquad (10)$$

e_i and e_o are the respective emissivities at the front and back surfaces of the film. Equation (10) is plotted in fig (3) as a function of the variable $(s/\Omega^{1/2})$ where s is the spatial modulation frequency and Ω is the angular frequency of the incoming radiation. Two graphs were plotted for two different values of the thermal diffusivity k. Inspection of this figure reveals that for the superconducting material with its characteristic diffusivity value, higher chopping frequency results in higher spatial frequency to produce the same thermal response while quadrupling the chopping frequency will require doubling the spatial frequency.

The response of the HTS detector will ultimately be determined by trading off the electrical-thermal gain bandwidth and the noise

bandwidth. The bandwidth limits are determined by the thermal time constant t_h and by the electrical time constant t_e, generally $t_h >> t_e$ and the rise time of the signal will be affected by the thermal coupling between the film and the insulator substrate. A current will appear in the HTS material only in response to temperature variations which produces a resistive load in the superconducting element. The temperature variations of the incident radiation flux can be achieved by different types of modulation schemes. Depending on the particular application, chopper modulation of a stationary source can be established. In outer space applications since, a linear or constant velocity scan is necessary when a large field of view is to be covered by a linear array the satellite motion will induce the temperature variation of the covered scene. In most of these applications and due to the large dynamic gain of HTS material (β is large) thermal crosstalk between different elements may degrade the detector response by decreasing the signal to noise ratio.

To address the problem of the thermal cross talk between different detector elements we assume a monolithic HTS detector array with a row of square elements of dimensions 2a and CCd or CID readout electronics. We define the thermal spread function of two detector elements to be given by,

$$W_s = |R_1/R_2| \qquad (11)$$

W_s describes the noise effects of the element 1 which is adjacent to element 2 in the array due to the same input pulse and R_i is proportional to the voltage response of an element i to the thermal excitations, this function is defined as,

$$R_i = 1(/2\pi)^2 \int d^2k T_a(k,\Omega) S_i(k) \qquad (12)$$

and

$$S_i(k) = (\sin k_x a/k_x a)\ (\sin k_y a/k_y a)\ \exp(ik_x x_o + ik_y y_o)$$

$S_i(k)$ is the spatial transform function of a detector element i centered at (x_o, y_o), the element electrode is defined to have a uniform thermal response in the electrode area and zero outside this area. The thermal spread function of equation (11) was calculated for different spacings between the elements. The results are plotted in Fig.4 as a function of the parameter $a(\Omega/k)^{1/2}$. These curves reveal that the thermal cross talk decreases rapidly with increasing the spacing between elements in the array while decreasing the thermal diffusivity of the material may improve the overall array performance. It is important to realize that If phase sensitive detection is employed then W_s has to be multiplied by cosine the phase

difference between the signals from two adjacent elements.

In this article a theoretical model was developed to describe thermal excitations of large area high temperature superconducting thin film bolometers. As a result of this analysis it was found that large values of β (temperature coef.) can be achieved and for optimum array performance a superconducting thin film is preferable in constructing array configurations to thick films. Although the results of the second part of the analysis are generic in nature and applicable to any focal plane array configuration it shows that thermal cross talk can be minimized by increasing the element spacing in the array or increasing the spatial chopping frequency of the incoming radiation. The results of these calculations together with recent measurements on laser excitations of thin film agree reasonably well. This modeling can be utilized in future design of hyprid focal plane array IR detectors using HTC technology.

REFERENCES

1) P.L. Richards et al, Appl.Phys.Lett.54, 283(1989).
2) M. Leung et al, Appl.Phys.Lett.51, 2046(1987).
3) C. Johnson et al, SPIE 172, 178(1979).
4) W.R. Donaldson et al, "Interactions of Picosecond Optical Pulses With High-Tc superconducting Films" submitted to Appl.Phys.Letters, February 23, 1989.
5) U. Strom et al, IEEE Trans.Mag. 25, 1315(1989).
6) J.C. Brasunas et al, "Construction and Performance of a Thin-Film Transition Edge, Hightemperature Superconductor Composite Bolometer", Laboratory For Extraterrestrial Physics, NASA GSFC, March, 1989.

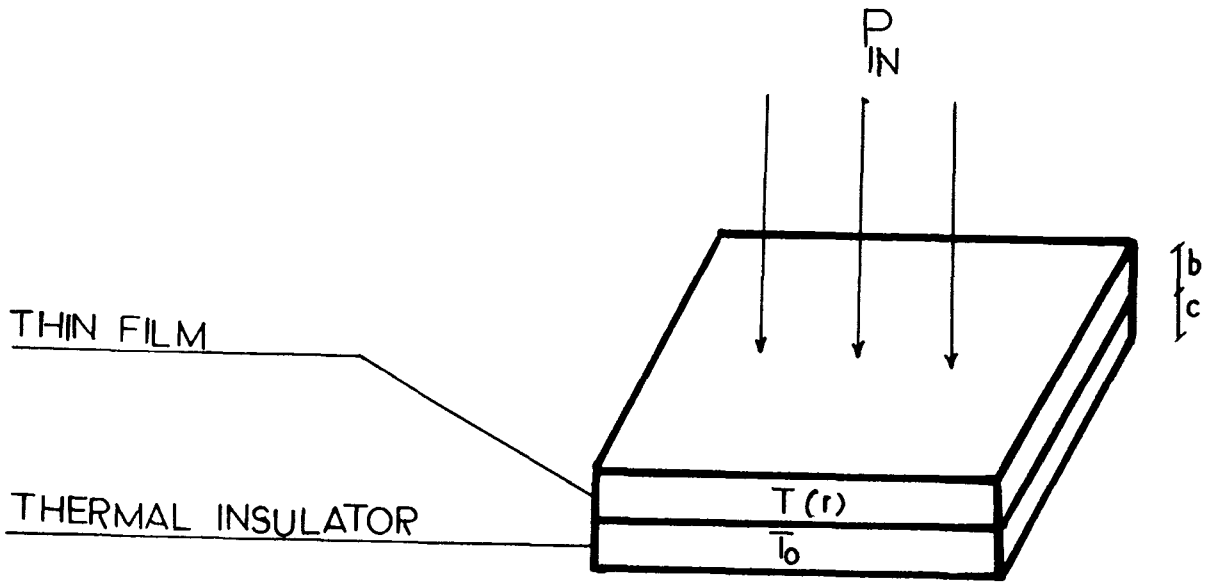


Figure 1: Detector-insulator configuration.

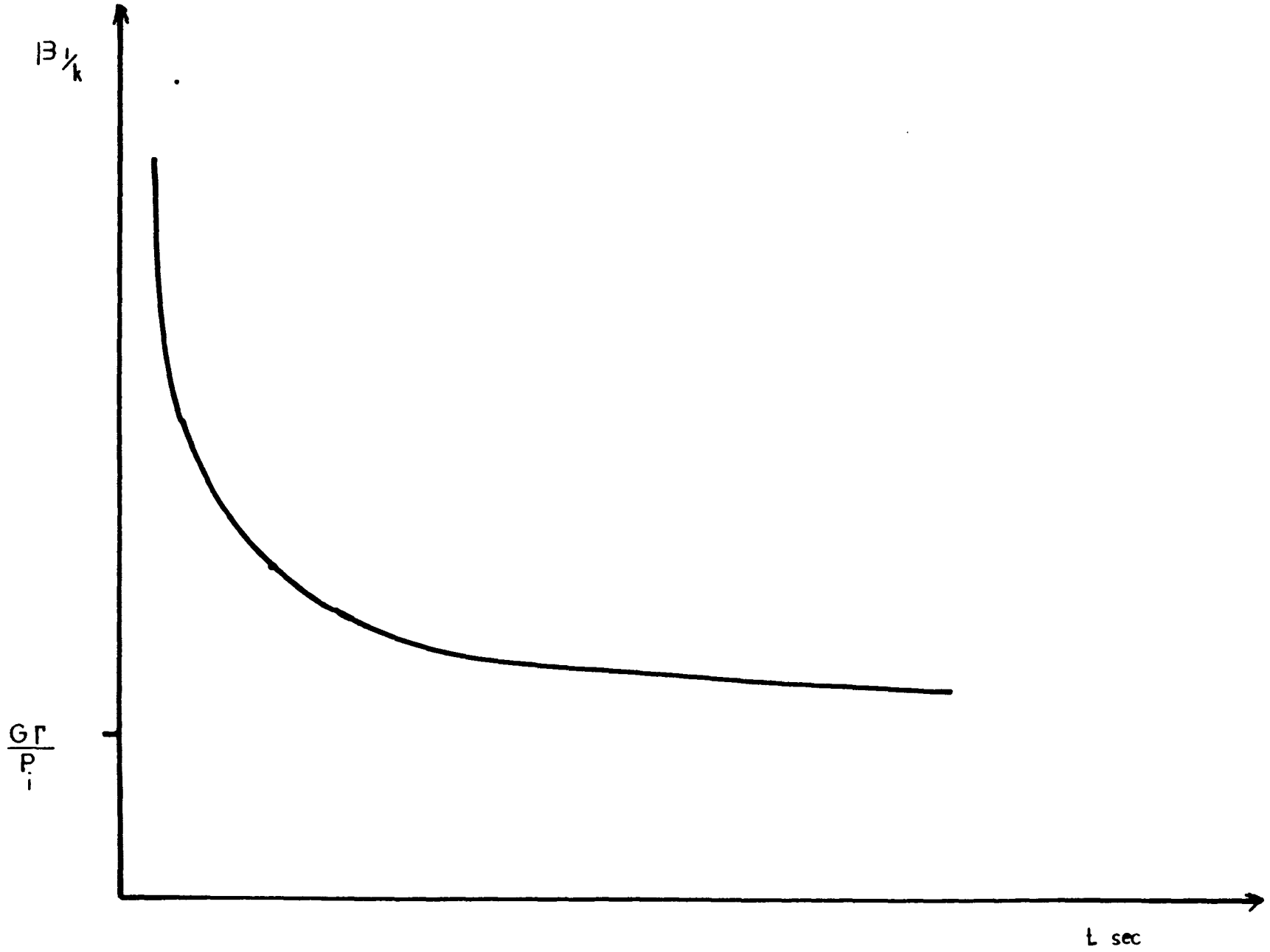


Figure 2: Temperature coefficient β as a function of time.

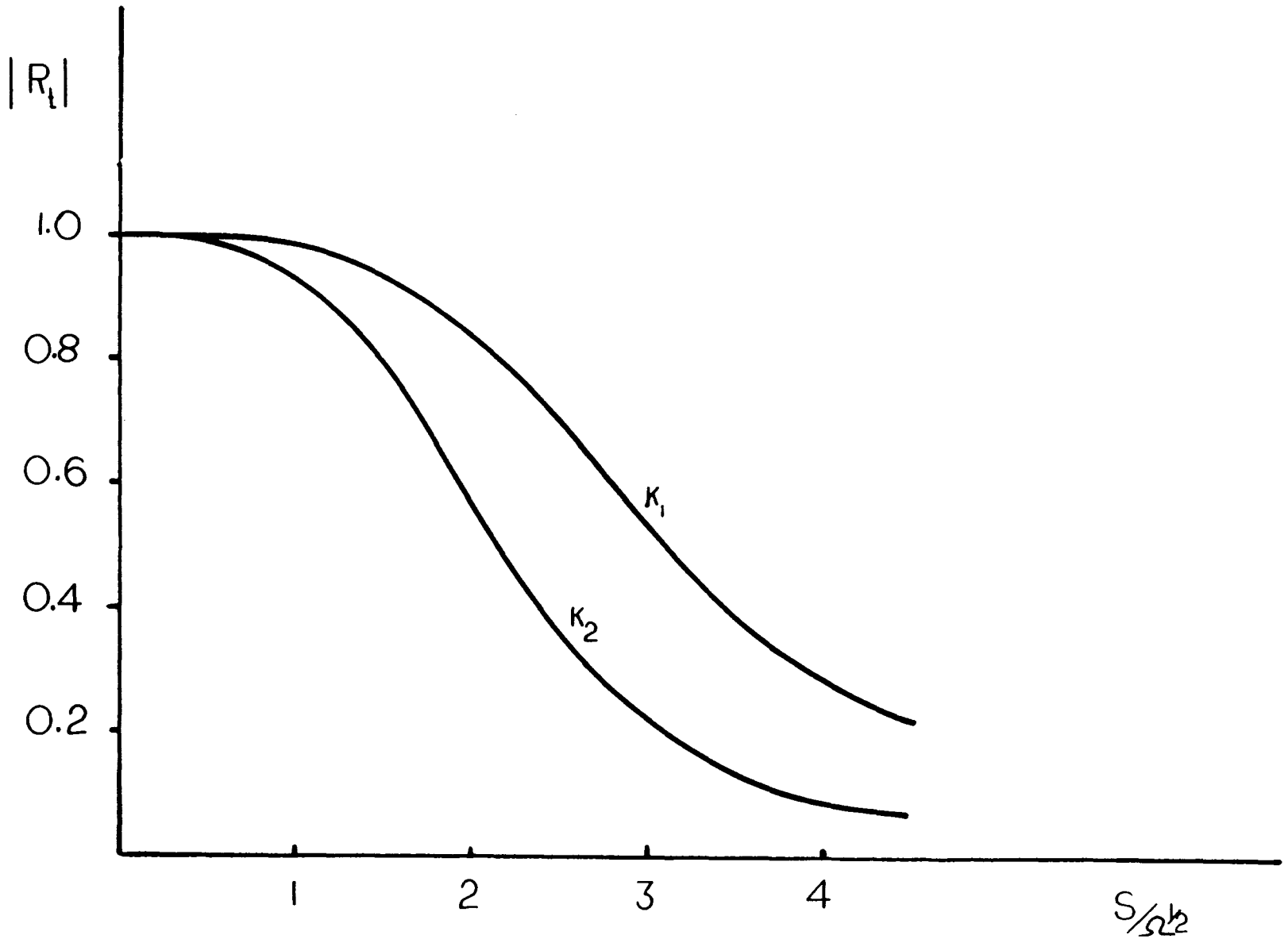


Figure 3: Thermal responsivity as a function of $S/\Omega^{1/2}$ and different values of thermal conductivities. $K_2/K_1=4$.

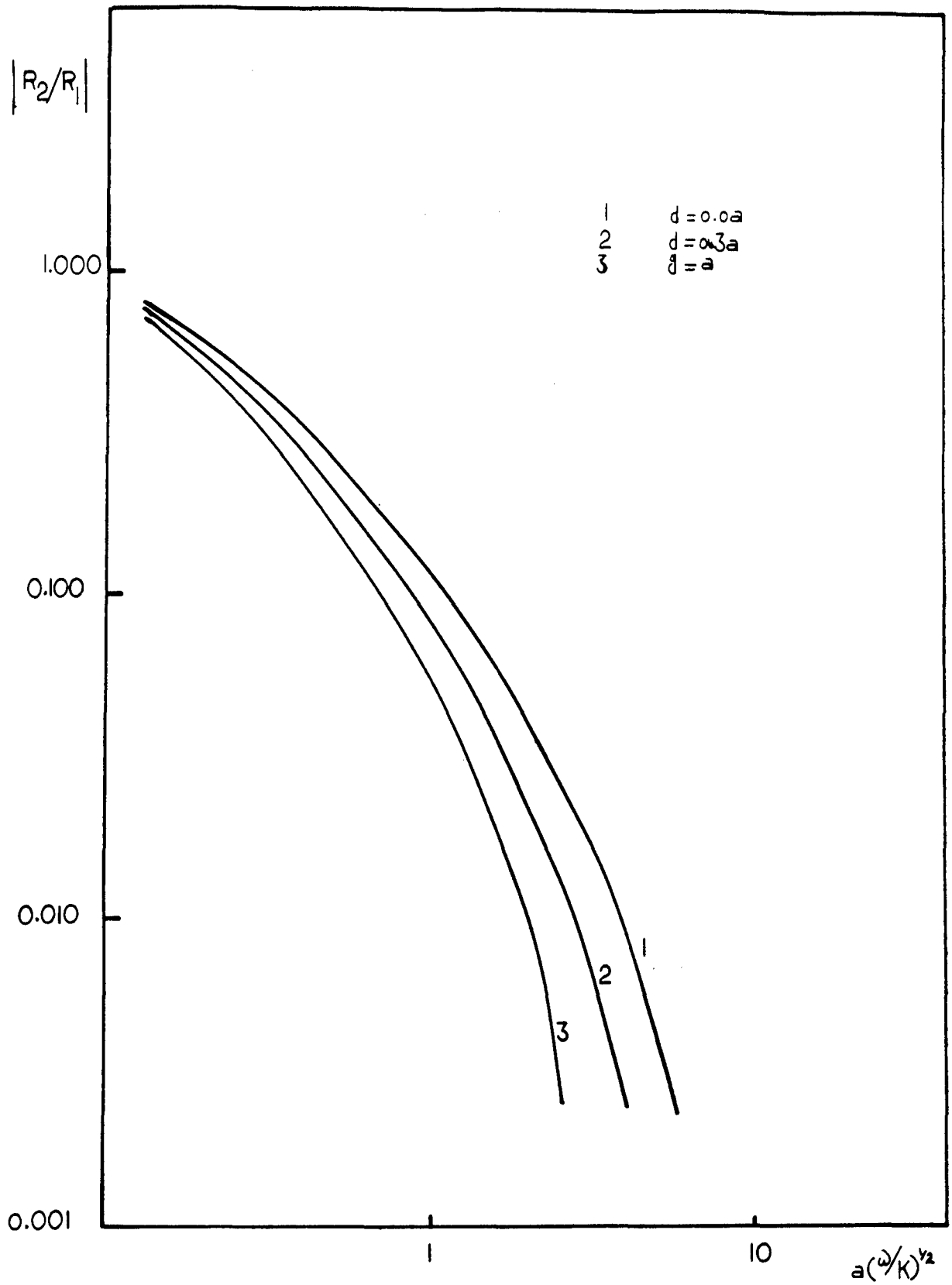


Figure 4: Variation of thermal spread function with $a(\Omega/K)^{1/2}$ for three different values of spacing between elements d.

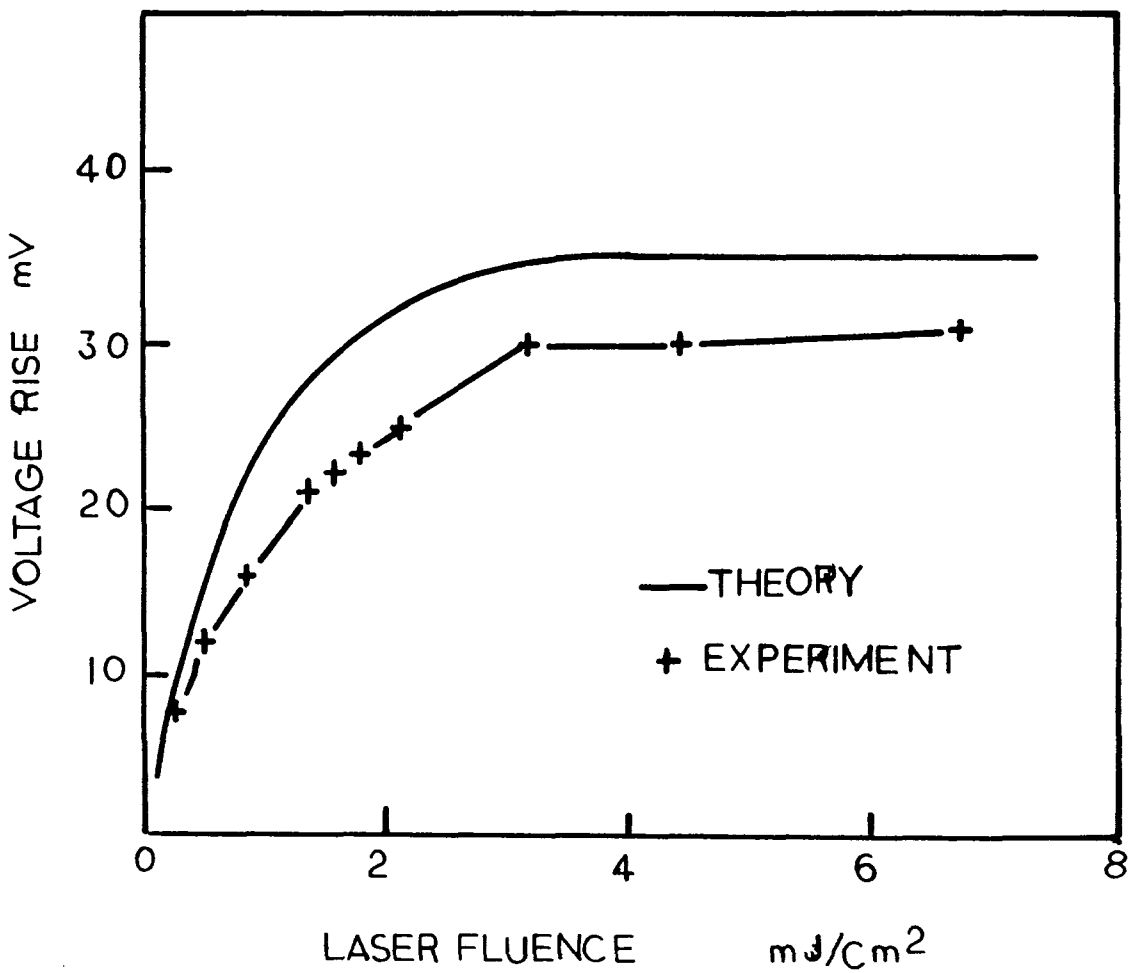


Figure 5: Comparison between experimental measurements of Ref.3 and theoretical calculations of our model. Different parameters were taken from Ref.3.

MICROWAVE (EPR) MEASUREMENTS OF THE PENETRATION DEPTH MEASUREMENTS OF HIGH-T_c SUPERCONDUCTORS

N.S.DALAL*, B.RAKVIN[a)], T.A.MAHL, A.S.BHALLA[b)], AND Z.Z.SHENG[c)]

Department of Chemistry, West Virginia University
Morgantown WV 26506-6045

Abstract Electron Paramagnetic Resonance (EPR) has been found to be a quick and easily accessible method for measuring the London penetration depth, λ, for the high-T_c superconductors. The method utilizes the broadening of the EPR signal of a spin-probe compound adsorbed to the surface of the superconductor. The broadening of the EPR signal is due to the formation of the magnetic flux lattice below T_c and is measured as the second moment, $\langle\Delta H^2\rangle$. $\langle\Delta H^2\rangle$ is fitted to the Brandt equation for a simple triangular lattice: $\langle\Delta H^2\rangle = 0.00371\lambda_0[1-(T/T_c)^4]^{-1/2}$. This method yields λ_0 = 2700 ± 100 Å with a T_c of 84 K for $Bi_2Sr_2CaCu_2O_x$ and 2520 ± 100 Å with a T_c of 119 K for $Tl_2Ba_2Ca_2Cu_3O_x$. The precision of ±100 Å or better compares well with those of the more traditional techniques of μ^+SR, neutron diffraction, and magnetic susceptibility.

INTRODUCTION

Currently several methods are in use for the measurement of λ, such as muon spin resonance (μ^+SR)[1,2], d.c. susceptibility[3,4], neutron scattering[5], and NMR[6,7]. However, each of these methods has some shortcomings[1-6]. For example, muon spin resonance measures λ via line broadening as a result of the flux penetration. However, one must estimate the contribution from relaxation broadening, which appears hard to do[1,2]. Neutron scattering needs access to a high (neutron) flux reactor and studies the bulk properties of a sample[5].

Susceptibility measurements require an estimation of the lower critical field H_{c1} , since λ is measured via $H_{c1} = \phi_0/(\lambda_0^2)$ [3,4,8]. However, H_{c1} is hard to measure for these materials[9].

To our knowledge, there is only one, rather recent report[10] on the use of EPR spectroscopy for the measurement of λ. However, the measurements were only made on $YBa_2Cu_3O_{7-x}$, and over a small temperature range ($\approx 15^\circ$) below T_c while measurements at lower temperatures were particularly desirable[10]. The present work has improved the methodology by making more detailed measurements over a wider range of temperatures, analyzing the data with a more accurate theoretical model[11], and applying it to two new lattices.

PRINCIPLE OF THE EPR METHODOLOGY FOR MEASURING λ

The principle of the EPR methodology is similar to that proposed by Pincus et al.[7] in 1964 for NMR for the Type-II superconductors. The linewidth of the NMR signal is increased by the inhomogeneous magnetic fields created by the emergence of a magnetic flux lattice below T_c, when the external field H_0 satisfies the condition $H_{c1} < H_0 < H_{c2}$. The same type of inhomogeneous broadening is expected to influence the EPR line since the flux lattice should be field independent within the magnetic field range described. Thus the EPR method is based on the measurement of the linewidths or second moment of the EPR line of a paramagnetic probe adsorbed on the surface of a Type-II superconductor. In the absence of detailed knowledge of the flux lattice in these high-T_c superconductors, we shall assume a simple model of a perfect triangular lattice for a Type-II superconductor[11].

Brandt[11] recently reported for Type-II superconductors the formula for the second moment data in the case of a perfect triangular lattice as:

$$\langle \Delta H^2 \rangle = 0.00371 \Phi_0^2 / \lambda^4 \quad (1)$$

$$\lambda = \frac{\lambda_0}{[1-(T/T_c)^4]^{1/2}} \quad (2)$$

where Φ_0 is the flux quantum and λ_0 is the penetration depth at T = 0. The temperature dependence of λ is assumed to be described with the standard two-fluid form[12] (eq. 2).

EXPERIMENTAL

The paramagnetic probe used for the measurements was the stable free radical Diphenylpicrylhydrazyl (DPPH). The DPPH was dissolved in acetone to $\approx 10^{-2}$ M concentration. A few milligram sample of the superconductor was then immersed in the ($\approx 10^{-2}$M) DPPH solution and then dried in air. The EPR measurements were made using a Bruker ER 200D EPR spectrometer, operating in th X-band (9.5 GHz). The temperature was controlled to ±0.1 K using an Oxford Instrument model DRC1 temperature controller. All measurements were performed with magnetic field modulation amplitudes in the range of 0.8 - 4 Oe at a frequency of 100 kHz. The microwave power was kept low (~1mW) to minimize power saturation and broadening of the DPPH EPR signal. The superconductors, $Tl_2Ba_2Ca_2Cu_3O_x$ and $Bi_2Sr_2CaCu_2O_x$ were studied.

RESULTS

Typical EPR spectra for the DPPH radical[13,14] adsorbed on both the $Tl_2Ba_2Ca_2Cu_3O_x$ (T_c = 119K) and the $Bi_2Sr_2CaCu_2O_x$ (T_c= 82K) superconductors are shown in Figure 1. As can be seen, the signal broadens rapidly for temperatures less than T_c for each sample. The spectra showed no significant broadening above T_c. The second

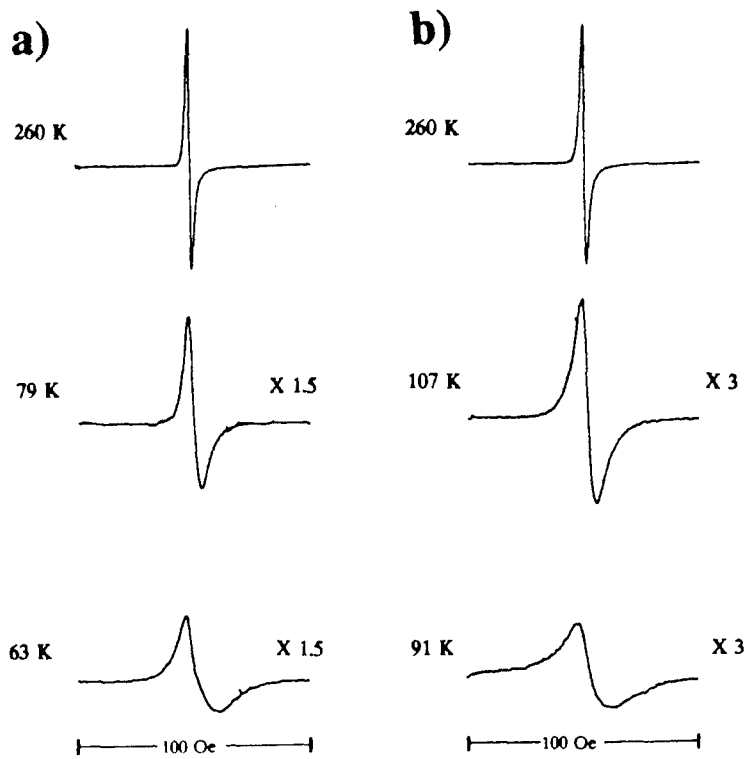


Figure 1. The EPR signals of DPPH adsorbed on (a) $Bi_2Sr_2CaCu_2O_x$ and (b) $Tl_2Ba_2Ca_2Cu_3O_x$ at the indicated temperatures.

moments of the EPR signals were calculated using the equations described by Poole[14]. The second moment values from the experimental results are shown as symbols in Figure 2a and 2b for $Bi_2Sr_2CaCu_2O_x$ and $Tl_2Ba_2Ca_2Cu_3O_x$ respectively.

The best fitting curves that were obtained are with the parameters λ_0 = 2520 Å and T_c = 119 K for $Tl_2Ba_2Ca_2Cu_3O_x$ and λ_0 = 2700 Å and T_c = 84 K for $Bi_2Sr_2CaCu_2O_x$ as can be seen by the solid lines in Figure 2. The dashed lines in the figures indicate plots for λ_0 differing by ± 100 Å demonstrating the precision of the fitting procedure. It can be seen that all of the experimental data points lie within these lines indicating that this method can yield λ_0 well within an precision of ±100 Å.

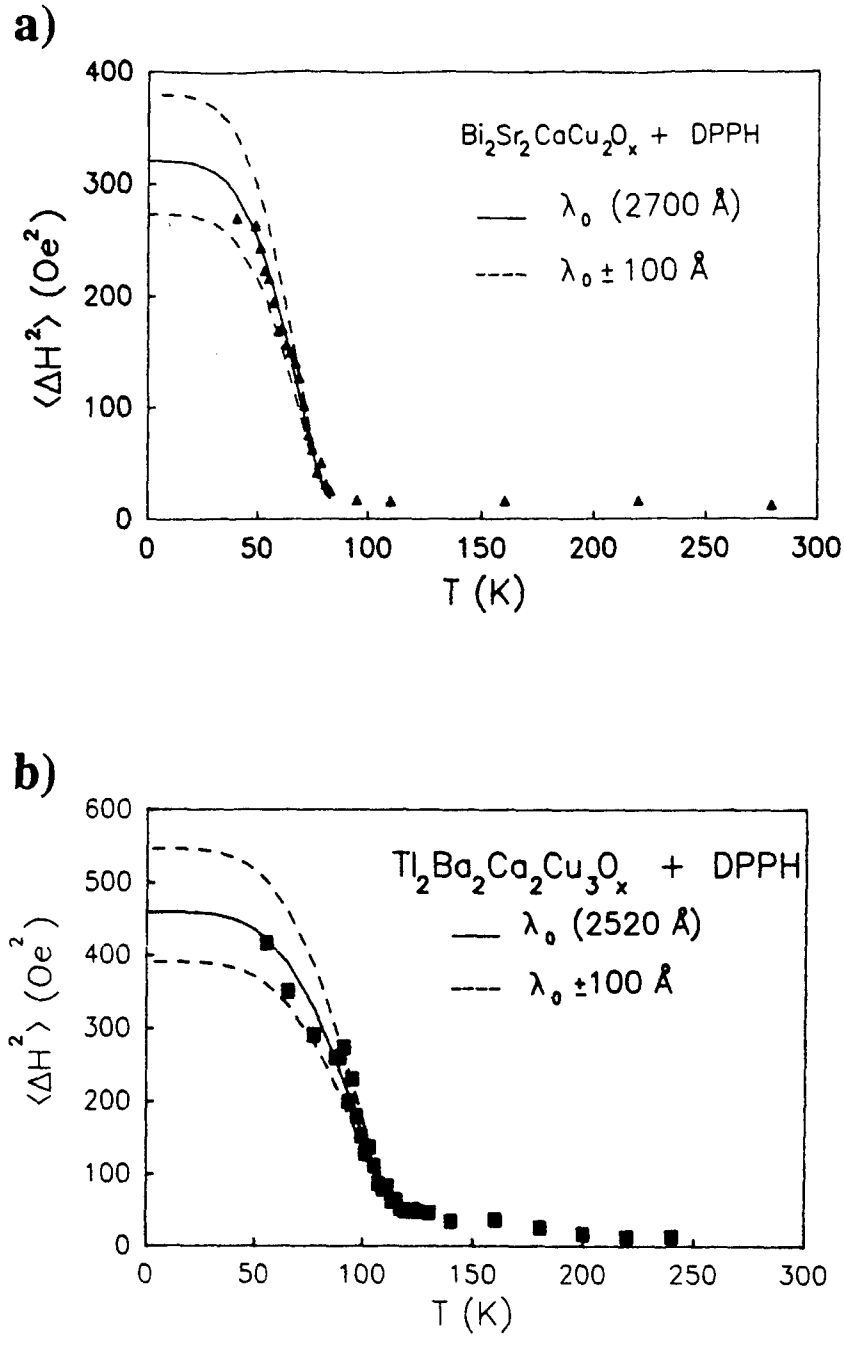


Figure 2 The second moment, $\langle \Delta H^2 \rangle$, vs. temperature for DPPH adsorbed on (a) $Bi_2Sr_2CaCu_2O_x$ and (b) $Tl_2Ba_2Ca_2Cu_3O_x$. The curves are fits to equations (1) and (2) in the text.

Accurate measurements of λ_0 for these samples by the established methods of μ^+SR and polarized neutron scattering are not available. However, the $Bi_2Sr_2CaCu_2O_x$ result of λ_0 = 2700 Å is in the range of values of 1585 Å and 3650 Å determined from critical field measurements for the related compound $Bi_4Ca_3Sr_3Cu_4O_{16}$[8]. There are to this point no literature values for the $Tl_2Ba_2Ca_2Cu_3O_x$.

REFERENCES

* Address correspondence to this author.

a) Permanent address: Ruder Boskovic Institute, University of Zagreb, POB. 1016, 41001 Zagreb, Croatia, Yugoslavia.

b) Permanent address: Materials Research Laboratory, Pennsylvania State University, University Park, Pa 16802.

c) Permament address: Physics Department, University of Arkansas, Fayetteville, AK 72701.

1. D.R.Harshman, G.Aeppli, E.J.Ansaldo, B.Batlogg, J.H.Brewer, J.F.Carolan, R.J.Cava, M.Celio, A.C.D.Chakler, W.N.Hardy, S.R.Kreitzman, G.M.Luke, D.R.Noakes, M.Senba, Phys. Rev. B 36, 2386 (1987).
2. D.R.Harshman, L.F.Schneemeyer, J.V.Waszczak, G.Aeppli, R.J.Cava, B.Batlog, L.W.Rupp, E.J.Ansaldo, D.L.Williams, Phys. Rev. B 39, 851 (1989).
3. L.Krusin-Elbaum, L.R.Greene, F.Holtzberg, A.P.Malozemoff, Y.Yeshurun, Phys. Rev. Lett. 62, 217 (1989).
4. L.Krusin-Elbaum, A.P.Malozemoff, Y.Yeshurun, D.C.Cronemeyer, F.Holtzberg, Phys. Rev. B 39, 2936 (1989).
5. R.Felici, J.Penfold, R.C.Ward, E.Olsi, C.Matacotta, Nature, 329, 523 (1987).
6. H.Niki, S.Tomiyoshi, H.Hentona, M.Omori, T.Kajitani, R.Igei, Solid State Commun., 69, 547 (1989).
7. P.Pincus, A.C.Gossard, V.Jaccarino, J.H.Wernick, Phys Lett. 13, 21 (1964).
8. M.G.Alexander, Phys.Rev. B 38, 9194 (1988).
9. Y.Isikawa, K.Mori, K.Kobayashi, and K.Sato, Japanese J. Appl. Phys., 26, 1535 (1987).87).
10. B.Rakvin, M.Pozek, A.Dulcic, Solid State Commun. in press (1989).
11. E.H.Brandt, Phys. Rev. B 37, 2349 (1988).
12. R.P.Huebener, Magnetic Flux Structures in Superconductors, Springer-Verlag, New York, Chap. 2 (1979).
13. C.S.Singer, E.G.Spencer, J. Chem. Phys. 21, 939 (1953).
14. C.P.Poole Jr., Electron Spin Resonance, Interscience Publishers, New York, 791 (1967).

Inhomogeneities in Single Crystals of Cuprate Oxide Superconductors

K. Moorjani, J. Bohandy, B. F. Kim and F. J. Adrian
The Johns Hopkins University
Applied Physics Laboratory
Laurel, Maryland 20723

Abstract

The next stage in the evolution of experimental research on the high temperature superconductors will require high quality single crystals and epitaxially grown crystalline films. However, inhomogeneities and other defects are not uncommon in single crystals of cuprate oxide superconductors, so a corollary requirement will be reliable methods for judging the quality of these materials. The application of magnetically modulated resistance methods in this task will be briefly described and illustrated in this paper.

Significant and, equally important, reproducible experimental results on single crystalline samples of the cuprate oxide superconductors are now being reported. Less progress has been made on methods for assessing the quality of these samples. Ideally, such methods must be capable of probing the entire sample, a difficult requirement given that the optical opacity of these materials rules out most spectroscopic approaches. The methods that do satisfy this requirement have various drawbacks, as, for example, X-ray and neutron diffraction methods are tedious and lack the sensitivity required to detect small regions of inhomogeneity, while specific heat and other thermodynamic measurements are hard to interpret because of the limited theoretical understanding of the cuprate oxide superconductors.

Given the foregoing difficulties, the magnetically modulated resistance (MMR) methods, developed by us over the past three years and found to be ideal tools for detection of intrinsic and weak link superconductivity in both conventional and high-T_c superconductors, should play an important role in assessing the quality of crystalline superconductors. The details of the experimental implementation of the methods as well as results on powders, bulk sintered samples, thin films and single crystals have been described in detail in previous publications,[1-9] and here we will only briefly discuss the advantages of the MMR technique in revealing inhomogeneities in single crystals and thin films of high temperature superconductors. These inhomogeneities can arise from structural and chemical disorder in samples either due to inhomogeneous doping (e.g., replacement of La by Sr in La-Sr-Cu-O single crystals) or incomplete oxygenation (e.g., in Y-Ba-Cu-O single crystals) and/or the presence of defects, grain boundaries etc. (e.g., in thin film samples). The effect of these inhomogeneities is revealed in the MMR data as the presence of multiple superconducting phases and/or weak links where Josephson tunnelling, flux trapping or both can occur. As such, MMR methods are excellent tools for judging the quality of superconducting samples.

The basis of the MMR techniques lies in the magnetic field dependence of the superconducting transition as seen in the resistance measurements either at zero or any convenient frequency, ω. Consequently, with a small dc magnetic field H_o, is applied along with a modulation field, $H_m \sin \omega_m t$ ($H_m < H_o$), varying at frequency ω_m, the resistance R(T,H) can be written as,

$$R(T,H) = R(T,H_0) + \frac{\partial R}{\partial H} H_m \sin \omega_m t,$$

and a measured response is detected at the modulation frequency, ω_m, only if R is magnetic field dependent. Unlike superconducting transitions, most resistance-changing phase transitions are virtually independent of magnetic field so the former are unequivocally detected by this method. In the vicinity of the transition temperature, T_c, where the resistance drops precipitously, the response is then proportional to $(\partial R/\partial H)_{T_c} = (\partial R/\partial T)_{T_c}(\partial T_c/\partial H)$ so that for a superconducting transition $(\partial T_c/\partial H \neq 0)$ one obtains a peak located at T_c and approximately proportional to $(\partial R/\partial T)$. Such a peak response has been observed in every superconducting sample of low and high T_c material examined to date[10] in the magnetically modulated electrical resistance (MAMER) configuration implemented at $\omega = 0$ and the magnetically modulated microwave absorption (MAMMA) carried out at microwave frequencies ($\omega = 9.3$ GHz). An example of MAMER in this film of the conventional superconductor niobium nitride is shown in Fig. 1.

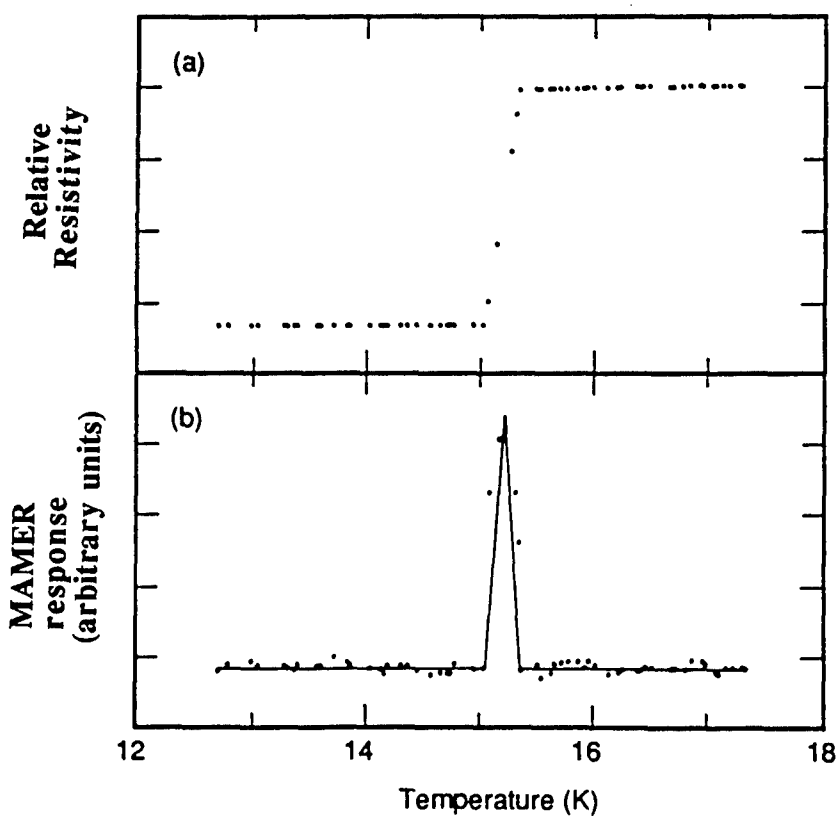


Fig. 1: The dc resistance (top) and the magnetically modulated electrical resistance (bottom) of NbN film as a function of temperature. The lines in the bottom figure are a guide to the eye.

Similarly, an example of MAMMA in a melt-processed, melt growth sample of $YBa_2Cu_3O_7$ is shown in Fig. 2.

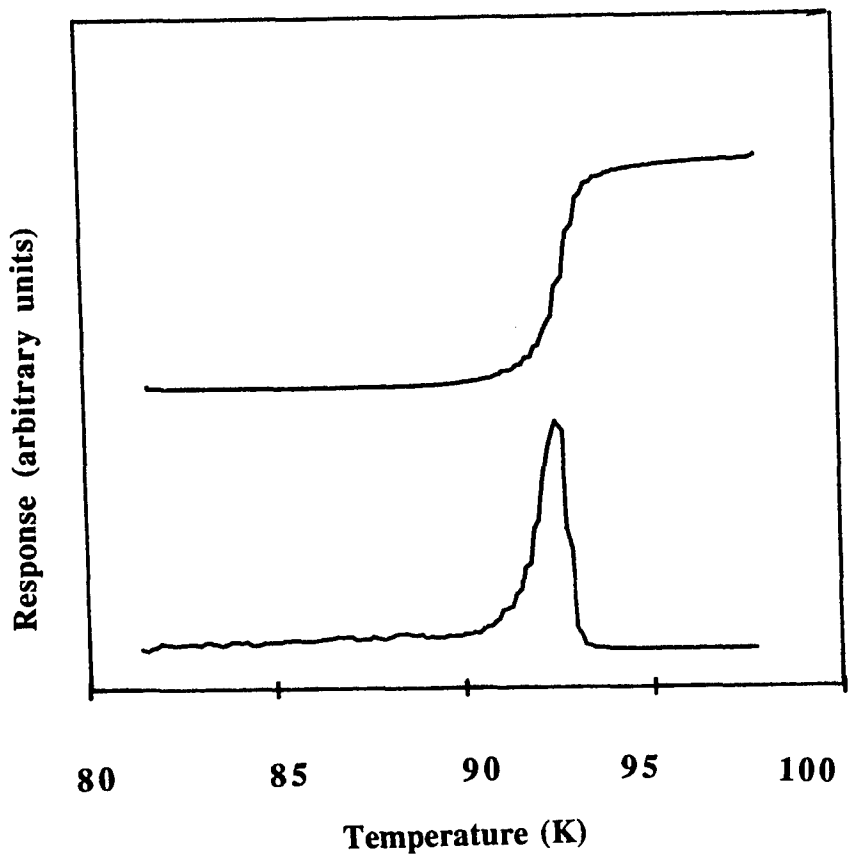


Fig. 2: Microwave absorption (top) and magnetically modulated microwave absorption (bottom) of a melt-processed, melt-growth $YBa_2Cu_3O_7$ sample.

The MMR methods become particularly useful for judging the quality of superconducting samples containing inhomogeneities in the form of multiple superconducting phases and/or weak links, that is, superconducting regions separated by non-superconducting phases. As shown elsewhere[6,11] the MAMMA and MAMER responses due to these weak links appear at temperatures below T_c and often can be distinguished from the intrinsic responses which indicate the superconducting transition itself on the basis of dependence on magnetic field, sample current, etc. In other cases the intrinsic and weak link responses can be distinguished by the aforementioned fact that only the intrinsic response is appropriately proportional to (dR/dT), which quantity can be calculated from the R vs. T curves for comparison with the MAMMA or MAMER response. Multiple superconducting phases, with T_c's less than 2 K apart, can be easily resolved as seen in Fig. 3 for a single crystal of $YBa_2Cu_3O_7$. SQUID measurements on the same sample do not resolve these two phases located at 88 K and 86.5 K but only show a diamagnetic susceptibility– that drops over a temperature spread of 3 K. As the higher T_c is only 88 K, the existence of two superconducting phases is likely to be related to incomplete oxygenation or the presence of impurities. Pure fully oxygenated samples of $YBa_2Cu_3O_7$ indeed give a single sharp peak located near 93 K as is the case for the sample shown in Fig. 2.

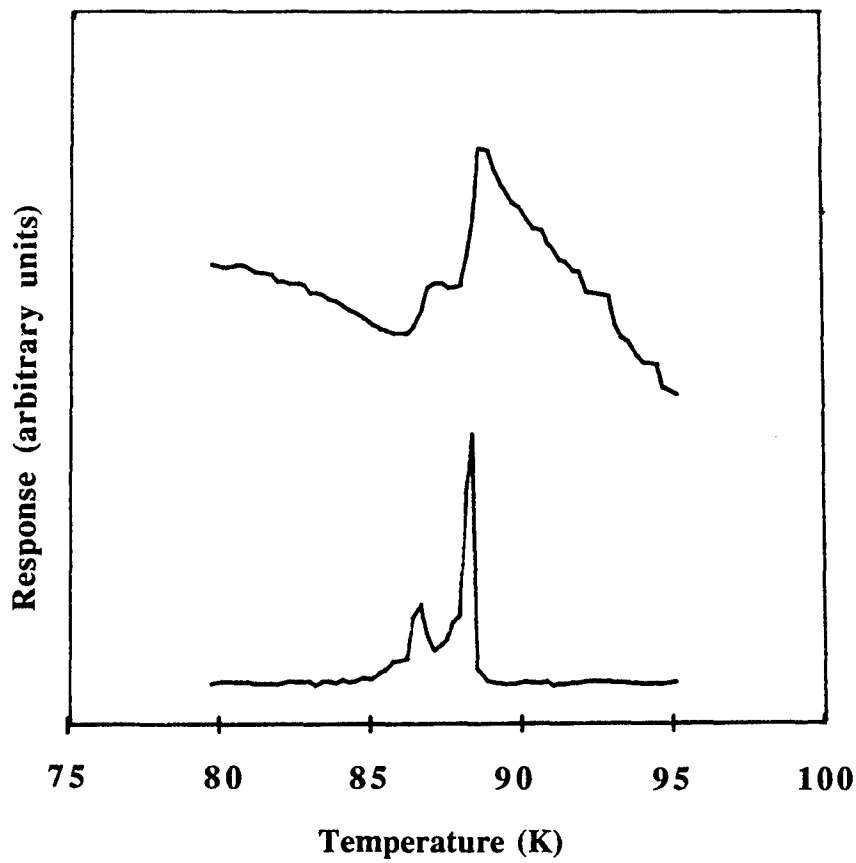


Fig. 3: Microwave absorption (top) and magnetically modulated microwave absorption (bottom) vs. temperature in a twinned single crystal of $YBa_2Cu_3O_7$.

Another example of inhomogeneity and multiple super–conducting phases is shown in Fig. 4 for a single crystal of $La_{1.88}Sr_{0.12}CuO_4$. One piece of this crystal reported on elsewhere showed a sharp drop in dc resistivity at 33 K and a broadened Meissner transition.[12] As shown in Fig. 4a, however, dc resistance measurements on the piece used here indicate a relatively sharp superconducting transition centered at a lower temperature (T_c = 29.5 K). Although there is little or no indication of multiple phases in the dc resistance measurement, the multiphasic character of the sample is clearly revealed by the presence of several closely spaced peaks in the corresponding MAMER response, also shown in Fig. 3a. The microwave resistance vs temperature, shown in Fig. 4b, shows a considerably broader superconducting transition centered at 27.9 K, while the MAMMA response shown in Fig. 4b clearly shows the presence of several different phases whose superconducting transition temperatures are spread over about 5 K.

Clearly there are significant differences between these two pieces of the same crystal of the same nominal composition. It remains to be determined whether the difference is due to inhomogeneities in Sr doping or loss of oxygen in that part of the crystal with the lower T_c. In the latter case the difference in oxygen content could have been produced during growth and/or annealing of the crystal or, alternatively, it could have taken place during the time that elapsed between the growth of the crystal and our examination of it. In any event this result highlights the need for examination of individual pieces of crystalline samples at the time they are used.

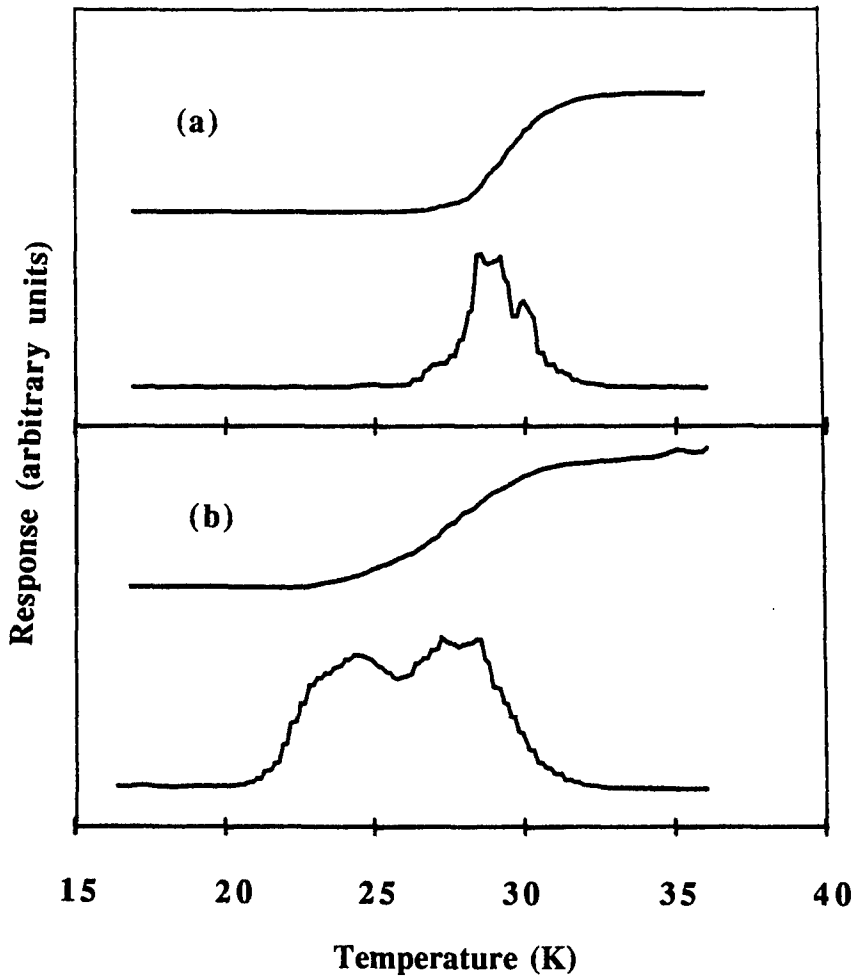


Fig. 4: (a) Electrical resistance (top) and magnetically modulated resistance (bottom) vs. temperature in a $(La_{0.94}Sr_{0.6})_2CuO_4$ single crystal.

(b) Microwave absorption (top) and magnetically modulated microwave absorption (bottom) vs. temperature in the same sample.

The difference between the dc and microwave measurements is readily understood, and shows the complementary nature of these measurements in examining all regions of the sample. The dc resistance and MAMER reflect the best superconducting path through the sample, and thus should, and does, yield the narrowest transition and highest T_c. The microwave resistance and MAMMA measurements, on the other hand, provide information about all regions of the sample penetrated by the microwaves. In the case of a single crystal sample this is primarily the surface regions as the skin depth at microwave frequencies is small compared to the crystal dimensions. In the present case the superconducting properties of these surface regions are considerably worse, particularly as regards the presence of multiple phases, than is the best superconducting path through the sample. Accordingly, microwave measurements will be especially important for examining specimens to be used in experiments involving the crystal surface.

ACKNOWLEDGMENT

We are very pleased to acknowledge and thank our colleagues for providing a number of samples for our investigations. The NbN film was kindly furnished by Dr. H. Cukauskas of the Naval Research Laboratory, Washington, DC. The single crystals of $YBa_2Cu_3O_7$ were grown by Dr. D. Kaiser and kindly provided to us by Dr. L. H. Bennett,

both of the National Institute of Science and Technology, Gaithersburg, Maryland. The single crystal of $La_{1.88}Sr_{0.12}CuO_4$ was grown at the Institute of Organic Syntheses, Yamanashi University, Kofu, by Profs. I. Tanaka and H. Kojima and was kindly sent to us by Prof. K. Kitazawa of the University of Tokyo. The bulk melt-processed, melt-growth sample of $YBa_2Cu_3O_7$ was grown by Dr. K. Sawano of the Nippon Steel Corporation. This work was supported by the Department of Navy, Space and Naval Warfare Systems Command, under Contract No. N00039-89-C-5031.

REFERENCES

1. K. Moorjani, B. F. Kim, J. Bohandy and F. J. Adrian, "Investigation of High Temperature Superconductivity by the Magnetically Modulated Microwave Absorption Method," Rev. Sol. State Sci. **2**, 263 (1988.)

2. J. Bohandy, T. E. Phillips, F. J. Adrian, K. Moorjani and B. F. Kim, "Detection of Superconducting Transitions by Magnetically Modulated Electrical Resistance," Mod. Phys. Lett. B, **3**, 933 (1989).

3. B. F. Kim, J. Bohandy, K. Moorjani and F. J. Adrian, "A Novel Microwave Technique for Detection of Superconductivity," J. Appl. Phys. **63**, 2029 (1988).

4. K. Moorjani, J. Bohandy, F. J. Adrian, B. F. Kim, R. D. Shull, C. K. Chiang, L. J. Swartzendruber and L. H. Bennett, "Superconductivity in Bulk and Thin Films of $La_{1.85}Sr_{0.15}CuO_{4-\delta}$ and $Ba_2YCu_3O_{7-\delta}$," Phys. Rev. B **36**, 4036 (1987).

5. J. Bohandy, B. F. Kim, F. J. Adrian and K. Moorjani, "Particle-size and Temperature Dependence of Microwave Noise in Superconducting $YBa_2Cu_3O_{7-y}$: Evidence for Random Josephson Junctions," Phys.. Rev. B **39**, 2733 (1989).

6. B. F. Kim, J. Bohandy, T. E. Phillips, F. J. Adrian and K. Moorjani, "Detection of Weak Link Superconductivity by Magnetically Modulated Electrical Resistance," Physica C **161**, 76 (1989).

7. F. J. Adrian, J. Bohandy, B. F. Kim and K. Moorjani, J. S. Wallace, R. D. Shull, L. J. Swartzendruber and L. H. Bennett, "Magnetic Field Dependence of the Superconductivity in Bi-Sr-Ca-Cu-O Superconductors," Physica C **156**, 184 (1988).

8. B. F. Kim, J. Bohandy, T. E. Phillips, W. J. Green, E. Agostinelli, F. J. Adrian, K. Moorjani, L. J. Swartzendruber, R. D. Shull, L. H. Bennett and J. S. Wallace, "Superconducting Thin Films of Bi-Sr-Ca-Cu-O Obtained by Laser Ablation Processing," Appl. Phys. Lett. **53**, 321 (1988).

9. L. H. Bennett, D. Kaiser, L. J. Swartzendruber, J. Bohandy, B. F. Kim, F. J. Adrian and K. Moorjani, "SQUID and MAMMA Observations of the Superconducting Transition in Single Crystals of $YBa_2Cu_3O_{7-x}$,"J. Appl Phys., **67**, 5044 (1990).

10. See for example, the recent review article, "Modulation Techniques for Studying Superconductors by K. Moorjani, B. F. Kim, J. Bohandy and F. J. Adrian, to be published in the Proc. of Intl. Conf. on Superconductivity in Bangalore, India, January 10-14, 1990.

11. K. Moorjani, J. Bohandy, B. F. Kim and F. J. Adrian, "On Distinguishing Intrinsic and Weak-link Responses in Magnetically-Modulated Dissipation in High T_c Superconductors," Solid State Commun., 74, 497 (1990).

12. G. Shirane et al., "Temperature Dependence of the Magnetic Excitations in $La_{1.85}Sr_{0.15}CuO_4$ (T_c = 33 K)," Phys. Rev. Letters, 63, 330 (1989).

THE COLOR OF POLARIZATION IN CUPRATE SUPERCONDUCTORS

H.A. Hoff, M.S. Osofsky, W.L. Lechter*, and C.S. Pande
Naval Research Laboratory
Washington, D.C. 20375
*Sachs-Freeman Associates
Landover, Maryland 20875.

A technique for the identification of individual anisotropic grains in a heterogeneous and opaque material involves the observation of grain color in reflected light through crossed polarizers (color of polarization). Such colors are generally characteristic of particular phases. When grains of many members of the class of hole-carrier cuprate superconductors are so viewed at room temperature with a 'daylight' source, a characteristic color of polarization is observed. We have studied this color in many of these cuprate superconductors and found a strong correlation between color and the existence of superconductivity. We have also examined two members of the electron cuprate superconductors and found that they possess the same color of polarization as the hole-carrier cuprate superconductors so far examined. The commonality of the characteristic color regardless of charge carrier indicates that the presence of this color is independent of carrier type. The correlation of this color with the existence of superconductivity in the cuprate superconductors suggests that the origin of the color relates to the origin of superconductivity.

Using photometric techniques, we have quantified the color of polarization in the superconductors $ErBa_2Cu_3O_7$ and $Bi_2Sr_2CaCu_2O_8$. Reflectivity measurements have been made with a tungsten-halogen light source (3400 K color temperature) on a series of $ErBa_2Cu_3O_{7-x}$ samples, where $0.1 \leq x \leq 0.7$, so as to include both tetragonal insulators and orthorhombic superconductors. Using a simple model, the data have been iteratively fitted with smooth curves to represent the spectra for visible wavelengths. From these curves, we have calculated the coordinates on a chromaticity diagram. The colors compare well with those observed visually. The fits are consistent with ellipsometry and transmissivity results and are compared with the absorption characteristics of Cu^{2+} and Cu^{3+}. We have shown that the structure observed by ellipsometry at ~2.1 eV is apparently a combination of an absorption band in the CuO_2 planes and an extension of the free-carrier distribution into the visible. A second absorption band, also in these planes, appears to shift to higher energy with increasing oxygen concentration in $ErBa_2Cu_3O_{6-7}$ and is present in $Bi_2Sr_2CaCu_2O_8$. This band subtracts blue from the white light reflected, thereby contributing the yellow component of the characteristic golden color of the cuprate superconductors. Both absorption bands are apparently of 3d x^2-y^2 type.

1. INTRODUCTION

The processing of single crystals, polycrystalline bulk, or thin films to produce electronic devices quickly and efficiently out of the copper oxide, high-transition temperature (T_c) superconductors can be assisted by microscopic examination. The differentiation at room temperature of the $YBa_2Cu_3O_7$-type superconducting phase on a crystal-by-crystal basis can benefit from the optical observation of twinning in the orthorhombic superconductors (1). But the presence of untwinned grains or areas of grains and the production of untwinned (1) or detwinned material (2) makes phase identification more difficult. Optical examination of both hole-carrier (3) and electron (4,5) cuprate superconductors has led to the discovery that, generally, these materials have the same characteristic color when viewed through crossed polarizers (polarization color).

Many opaque, anisotropic materials, with unique structures and compositions, have their own characteristic polarization color (6). However, if the structure or composition is changed, the polarization color generally changes or disappears. For the various cuprate superconductors, from, e.g., $Nd_{1.85}Ce_{0.15}CuO_{4-x}$ (T_c ~ 23 K) to $Tl_2Ba_2Ca_2Cu_3O_{10}$ (T_c ~ 125 K), regardless of changes in structure or

composition, as long as the material contains CuO_2 planes and is superconducting, the same brownish yellow (golden) polarization color is observed.

If the concentration of free-carriers (produced by doping the precursors) is reduced to produce an insulator either by changing the copper, oxygen or cation dopant concentration, the golden color also disappears (3). The change in color from golden to colorless (precursor) occurs for $YBa_2Cu_3O_7$-type materials (3) and for other cuprate superconductors (3,7).

With the sequence of polarization colors well studied and applicable to hole-carrier cuprate superconductors, and perhaps to negative carrier type, it is important to determine the likely band shifts taking place throughout the visible energy range in the Cu^{2+} 3d x^2-y^2 orbitals that combine with the oxygen 2p to construct the CuO_2 planes. We present here a more in depth examination of reflectivity data taken on representative individual grains of $ErBa_2Cu_3O_7$ and $Bi_2Sr_2CaCu_2O_8$ and propose a simple model in an effort to understand the color changes that correlate with superconductivity.

2. MODEL

In order to consider correlating the characteristic golden polarization color to absorption bands or reflection due to free carriers, it is necessary to show directly or by process of elimination that only such phenomena can account for the color. Table 1 contains a list of phenomena including structural ones that have been eliminated as possible origins for the golden color or its coupling with superconductivity. (The structural effect, or lack, of buckling of the CuO_2 planes has not been considered.) Generally, from Table 1 by process of elimination, only a combination of phenomena in a relatively specific arrangement is likely to result in both superconductivity and the golden color. Structurally then, the color originates from the two-dimensional CuO_2 planes by absorption and/or reflectance only. Apparently, the varying indices of refraction play no part in the production of color.

Because the superconductor to insulator sequence of polarization colors is, so far, reproducible for doping by alkaline earth cation, oxygen, or replacement of Cu, determining the various copper-oxygen colors and possible copper-oxygen absorption bands that may produce these colors can be aided by noting the colors of similar Cu oxide materials. Table 2 contains a list of impurity phases observed in various cuprate systems which contain superconductors.

The colors observed for various copper oxide containing phases (Table 2) suggests that absorption bands may exist in the visible. Note that the color of polarization of Bi_2CuO_4 is red. Absorption bands in the blue and green (or a large band across both) could produce this color. CuO is blue which may be due to absorption bands in the red-green. The R_2BaCuO_5 (2-1-1) phase has a green color which may be due to the presence of both an absorption band in the red and one in the blue. For those phases with Cu^{2+} present, absorption bands in the blue, green and red in various combinations would account for the colors and indicate that Cu^{2+} can disperse throughout the visible. A variety of colors, changing probably with orientation, for a given phase may have an origin in both birefringence and differential absorption.

As the origin of the characteristic color is a two dimensional structure within the various cuprate superconductors, spectroscopic data on various two-dimensional Cu^{2+} and perhaps Cu^{3+} complexes in aqueous solution are expected to indicate likely absorption bands contributing to the color and the color changes from precursor to superconductor. Table 3 contains absorption band parameters for Cu^{2+} and Cu^{3+} in the visible (700-400 nm, 1.77-3.10 eV, 14300-25000 cm^{-1}) to near visible range. To produce a yellow color by absorption, there need only be an absorption band in the blue range (white minus blue produces yellow). The golden color is in part due to yellow (4). The absorption bands included in Table 3 from Cu^{3+} are in the violet, which suggests that the presence of the yellow component may be due to charge transfer. For absorption bands to account for the color in Bi_2CuO_4 (red), either a large band extending across the blue-green range or two bands, one in the blue and one in the green, are needed. The necessity of a blue absorption band contributing to produce the green color of the 2-1-1 phase has also

Table 1 Origin of the Copper Oxide Superconductor Color of Polarization

Possibility	Comment
Water contamination (surface contamination)	color seen in unpolished thin films of $RBa_2Cu_3O_7$, freshly broken single crystals, and in $Bi_2Sr_2CaCu_2O_8$ which is not readily affected by water. Auger electron spectroscopy of such surfaces has shown only slight carbon contamination. Freshly fractured and ion milled surfaces show the color.
Instrument characteristics	color seen in reflection with other types of polarizing microscopes, as long as a 'daylight' source is used and polarizers are crossed.
Grain size effect	color seen in thin films (~1μm) to crystals 3 mm x 1 mm.
Depth of penetration	reflectivity measurements on progressively thicker films of $RBa_2Cu_3O_7$ have shown the light penetration depth to be on the order of several hundred nanometers. Even if the first few atomic layers are not superconducting, much of the reflected light seen is coming from greater depth.
Three dimensional structure	color not seen in ordinary illumination (bright field) nor in total reflectance measurements.
Presence of copper oxide alone	CuO (tenorite) has a blue color of polarization.
Perovskite structure	color not seen in $BaTiO_3$ or in $RBa_2Cu_3O_6$.
Copper oxide chains	color seen in $Bi_2Sr_2CaCu_2O_8$ and $Tl_2Ba_2Ca_2Cu_3O_{10}$ which have no long range chains.
CuO_2 planes	color not seen in $RBa_2Cu_3O_6$, which has CuO_2 planes.
Orthorhombic structure	color seen in tetragonal $Tl_2Ba_2Ca_2Cu_3O_{10}$ and not in La_2CuO_4 which is orthorhombic and blue(purple).
Presence of rare earth	$Bi_2Sr_2CaCu_2O_8$ and $Tl_2Ba_2Ca_2Cu_3O_{10}$ do not contain them.
Presence of an alkaline earth	$RBa_2Cu_3O_6$ contains an alkali earth and is not a superconductor. $Nd_{1.85}Ce_{0.15}CuO_4$ does not contain an alkaline earth.
Apical oxygen	absent in $Nd_{1.85}Ce_{0.15}CuO_4$.
Electron holes	$Nd_{1.85}Ce_{0.15}CuO_4$ is an electron superconductor.
Cu^{1+} state	Cu_2O, when a distorted cubic due to impurities, is red.
Cu^{2+} state	Bi_2CuO_4 is red, Er_2BaCuO_5 is green and CuO is blue.
Cu^{3+} state	unlikely in $Nd_{1.85}Ce_{0.15}CuO_4$ or $Pr_{1.85}Ce_{0.15}CuO_4$.

Table 2 Colors Through Crossed Polarizers of Impurity Phases in Superconductor Materials

Material	Color
Cu_2O	red
CuO	blue
Bi_2O_3	orange-yellow
Pb_3O_4	orange
Ba cuprate	remains dark as stage is rotated
Bi_2CuO_4	red
R_2BaCuO_5	green
Sr_2CuO_3	white-purple-aqua blue
$(Sr,Ca)_2CuO_3$	white-purple-aqua blue
Ca_2CuO_3	pale yellow-white
$(Ca,Sr)_2CuO_3$	pale yellow-white
Bi-Sr-Ca-O	colorless

been suggested. The presence of an absorption band in the blue range may occur for Cu^{2+}.

Table 3 Near Visible Absorption Band Parameters for Cu^{2+} and Cu^{3+} in Complexes (8,9)

Complex	Geometry	Extinction Coefficient $M^{-1}cm^{-1}$	Peak Centroid cm^{-1}	Half Width Half Maximum cm^{-1}	
$(NO_3)_2$	square planar	12.85	12630	1979	
$(NO_3)(NH_3)$	square planar	93.00	15670	2271	
$(NH_3)_4$	square planar	54.00	16900	2542	
$(HIO_6)_2$	square planar	90.28	23750	2878	(Cu^{3+})
$(H_2TeO_6)_2$	square planar	73.68	24880	4101	(Cu^{3+})

For any phase that is semiconducting or metallic, an increase in overall reflectivity may occur due to the presence of free carriers. But the presence of free carriers alone is not responsible for the golden color or

superconductivity. The metallic $La_5SrCu_6O_{15}$ material is anisotropic, white (3) and not superconducting. A relatively uniform distribution of free carriers throughout the visible can reflect white.

We have found by optical inspection of tetragonal $ErBa_2Cu_3O_6$ (colorless) single crystals (~0.5 mm x ~0.5 mm) and very thin, on the order of ~1 μm, that in ordinary reflected light the crystals are opaque. When viewed through crossed polarizers at maximum brightness, they are sufficiently transparent to allow the surface beneath to be seen. Apparently, as the $ErBa_2Cu_3O_6$ phase is undoped, either the production of absorption bands or the presence of free carriers limits the depth of penetration of polarized light. From previous reflectivity (10) and ellipsometry (11), the free carrier distribution is limited primarily to the infrared, with some extension into the visible. For reflectivity measurements on $YBa_2Cu_3O_7$-type superconductors and other cuprate superconductors, a continuously increasing reflectivity from approximately the yellow (~2.1 eV, ~580 nm) into the infrared is expected.

The spectroscopic measurements made on various copper complexes are obtained in transmission. Since the optical density measurements (transmissivity) on $YBa_2Cu_3O_7$-type superconductors (10) have the same structural features as obtained in reflectivity measurements (4,10), it is reasonable to assume that at least across the visible range structures in reflected spectra (through crossed polarizers) are the same, except for intensity, as those in transmitted spectra (through crossed polarizers). The reflectivity (R), then, can be described in the same way as optical density with $R = I/I_o$:

$$R = 10^{-c\varepsilon}, \tag{1}$$

where c is the molar concentration of the two-dimensional (or less) color producing structure and ε is the extinction coefficient. The reflectance (I) through crossed polarizers for each grain measured is normalized to the white reflectance (I_o) spectrum of a powdered Si oxide standard (4).

In general any absorption band can be approximated with a gaussian function. The gaussian expression we have chosen to use is as follows:

$$\varepsilon = \varepsilon_{Max} e^{-(\nu-\nu_{Max})^2/\theta^2}, \tag{2}$$

where ε_{Max} is the extinction coefficient, ν_{Max} is the centroid position and θ is the half width at half maximum in wavenumbers for a particular absorption band. In all the colors exhibited by the various cuprates (Table 2), a minimum of two absorption bands are needed, generally. In addition, the presence of free-carriers is expected to increase reflectivity. If each of these components occurs, the complete expression for the extinction coefficient is as follows:

$$\varepsilon = \varepsilon_{Max1} e^{-(\nu-\nu_{Max1})^2/\theta_1^2} + \varepsilon_{Max2} e^{-(\nu-\nu_{Max2})^2/\theta_2^2} - \varepsilon_{Max3} e^{-(\nu-\nu_{Max3})^2/\theta_3^2}. \tag{3}$$

Since the individual ε_{Maxi} are not known, a combined factor of $\varepsilon_{Maxi}c$ is obtained and referred to as an extinction/reflection coefficient. Iterative fitting is accomplished by applying first a single gaussian function, then two and finally three, if required, to conform to the structures apparent in the data.

3. EXPERIMENTAL

The preparation of $ErBa_2Cu_3O_{6+x}$ and $ErBa_2Cu_3O_{7-x}$, examined by reflectivity (4), the $Bi_2Sr_2CaCu_2O_8$ (BiSCCO, T_c ~ 85 K, R_0 ~ 75 K), $Tl_2Ba_2Ca_2Cu_3O_{10}$ (T_c ~ 120 K) and $Nd_{1.85}Ce_{0.15}CuO_{4-x}$ (T_c ~ 23 K) samples has been described (3,4). The same microscope-monochromator arrangement for the reflectivity measurements (4) has been used to measure reflectivity on BiSCCO, $Tl_2Ba_2Ca_2Cu_3O_{10}$ (T_c ~ 120 K) and $Nd_{1.85}Ce_{0.15}CuO_{4-x}$ (T_c ~ 23 K). Preliminary reflectivity data have been taken on a few representative

grains per sample. Representative spectra are plotted and iteratively fitted with smooth curves. The reflectivity data are considered as preliminary because the light levels involved are close to the lower detection limit which may increase error.

4. RESULTS

Representative reflectivity spectra for BiSCCO and for $ErBa_2Cu_3O_{6-7}$ versus oxygen concentration are shown in Figure 1.

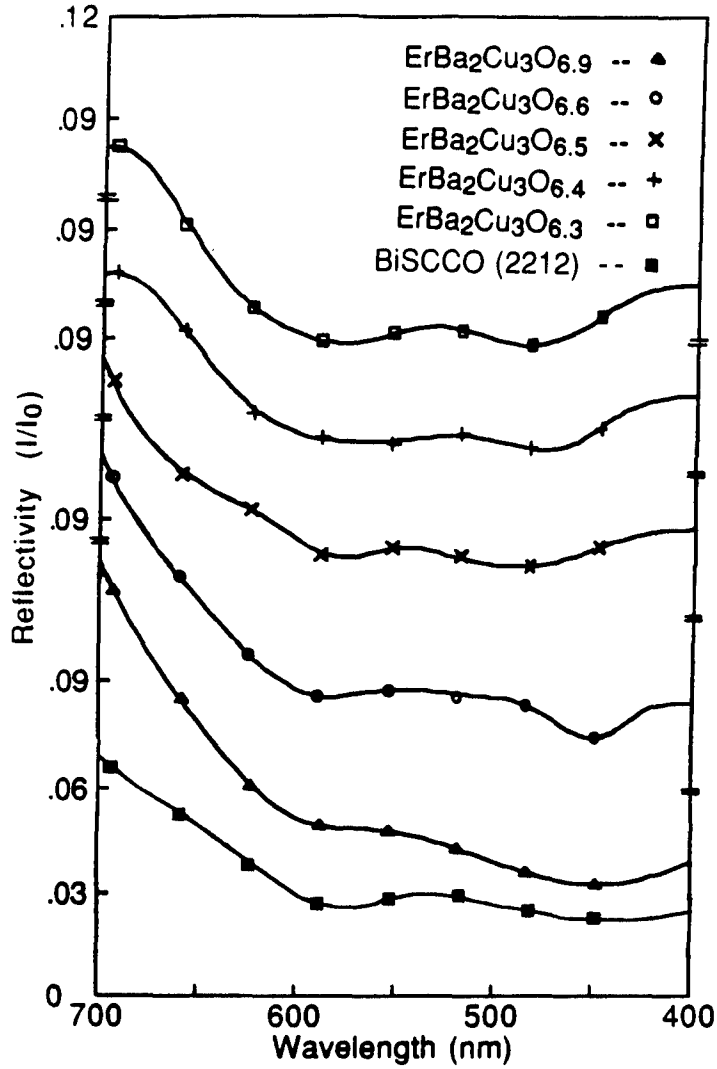


Figure 1 Reflectivity spectra for $ErBa_2Cu_3O_{6.3}$, $ErBa_2Cu_3O_{6.4}$, $ErBa_2Cu_3O_{6.5}$, $ErBa_2Cu_3O_{6.6}$, $ErBa_2Cu_3O_{6.65}$ and $ErBa_2Cu_3O_{6.9}$ (identical spectra, only one plotted), and $Bi_2Sr_2CaCu_2O_8$. The smooth curves plotted through the data have been iteratively fitted.

The preliminary reflectivity data from $Tl_2Ba_2Ca_2Cu_3O_{10}$ and $Nd_{1.85}Ce_{0.15}CuO_{4-x}$ show structures similar to those in Figure 1, but some portion of the spectra may be due to impurities because the aperture size is much larger than that of the individual grains in these samples.

Each data set has been fit successively and alternately with one, two or three gaussian functions to confirm that only the use of three gaussians can conform to the structures apparent in the spectra. The resulting parameters are listed in Table 4. The chromaticity coordinates have been calculated for each spectrum using the smooth curves of the iterative fits. These have been plotted on a chromaticity diagram in which

the color (hue) fields are delineated. In general, the resulting colors agree well with those observed visually and recorded on film (3). Only the data obtained on the $ErBa_2Cu_3O_{6.5}$ grains is on the border between the orange-red (brown) field and the yellow-orange (golden) field suggesting the presence of both orthorhombic and tetragonal material within the grains.

Table 4 Fitting Parameters for Reflectivity on Cuprate Phases

Phase	Absorb (-) Reflect (+)	Extinction/ Reflection Coefficient	Peak Centroid cm^{-1}	Half Width Half Maximum cm^{-1}	T_c
$ErBa_2Cu_3O_{6.3}$	+	0.27	14400	1100	---
(Blue/Purple)	-	0.19	17200	1400	
(940°C)	-	0.205	20650	1900	
$ErBa_2Cu_3O_{6.4}$	+	0.35	14500	1500	---
(Brown)	-	0.165	16800	3600	
(800°C)	-	0.14	21200	1500	
$ErBa_2Cu_3O_{6.5}$	+	240	0	5600	~50 K
(Golden)	-	0.12	17200	800	
(710°C)	-	0.16	20400	2200	
$ErBa_2Cu_3O_{6.6}$	+	15.7	0	7600	~63 K
(Golden)	-	0.095	16800	1000	
(610°C)	-	0.14	22200	1100	
$ErBa_2Cu_3O_{6.65}$	+	12.8	0	7800	~85 K
(Golden)	-	0.072	16700	1100	
(500°C)	-	0.15	22300	3000	
$ErBa_2Cu_3O_{6.9}$	+	12.8	0	7800	~95 K
(Golden)	-	0.072	16700	1100	
(25°C)	-	0.15	22300	3000	
$Bi_2Sr_2CaCu_2O_8$	+	5.7	0	8600	~85 K
(Golden)	-	0.15	17100	1100	
	-	0.10	22300	3000	

5. DISCUSSION

The estimated percent error based on reproducibility for reflectivity is approximately 5 % overall, with a lower value for reflectivity above 9 %. The increased error below $R \approx 0.09$ is assumed to be due to light levels at or just above the lower limit for the detector. Generally, for so few points (eight) per spectrum only a single gaussian (three variables) would be warranted. However, for the most part, there has been structural reproducibility between grains of the same sample and between samples which suggests that the fluctuations across the spectra are not random. A two-gaussian function (one for absorption at high energies and one for reflection at low energies) cannot account for the structure at ~590 nm (~2.1 eV) between them. At the high-energy end (violet range) for the superconductors $ErBa_2Cu_3O_{6.9}$ and $Bi_2Sr_2CaCu_2O_8$, the absorption band may extend further into the ultraviolet. See Figure 1.

Figure 2 is a plot of the centroid shifts relative to the centroid of the two end-point superconductors $ErBa_2Cu_3O_{6.9}$ and $Bi_2Sr_2CaCu_2O_8$ for the absorption band at the high-energy end of the visible range. Although there appears to be a systematic shift in this band with increasing oxygen content which

compares with a similar shift observed by ellipsometry (12), the measurement on $ErBa_2Cu_3O_{6.5}$ is an exception. If the shift is confirmed by forthcoming measurements using a more sensitive photomultiplier (detector) and a xenon 'daylight' source on homogeneous materials, then the likely position of the band for $ErBa_2Cu_3O_{6.0}$ is at ~19000 cm^{-1} (~520 nm, ~2.4 eV). This amounts to a shift of 0.4 eV from ~2.4 eV to ~2.8 eV, whereas ellipsometric results found a shift from ~2.6 eV to ~2.8 eV (12), with increasing oxygen. This band also appears to widen with increasing oxygen, see Table 4. The shift of the band to higher energy, near those of Cu^{3+} (see Table 3) suggests a charge-transfer band, although the apparent location in the blue range, instead of violet, may indicate a Cu^{2+} band that is only partially of a charge-transfer nature. The presence of this 3d x^2-y^2 band in the reflectivity and its necessity for the production of the golden color of the electron superconductors tends to preclude it being solely a Cu^{2+} to Cu^{3+} charge-transfer band. The band is independent of the type of charge transferred and apparently energy symmetric ($Cu^{1+} \leftrightarrow Cu^{2+} \leftrightarrow Cu^{3+}$).

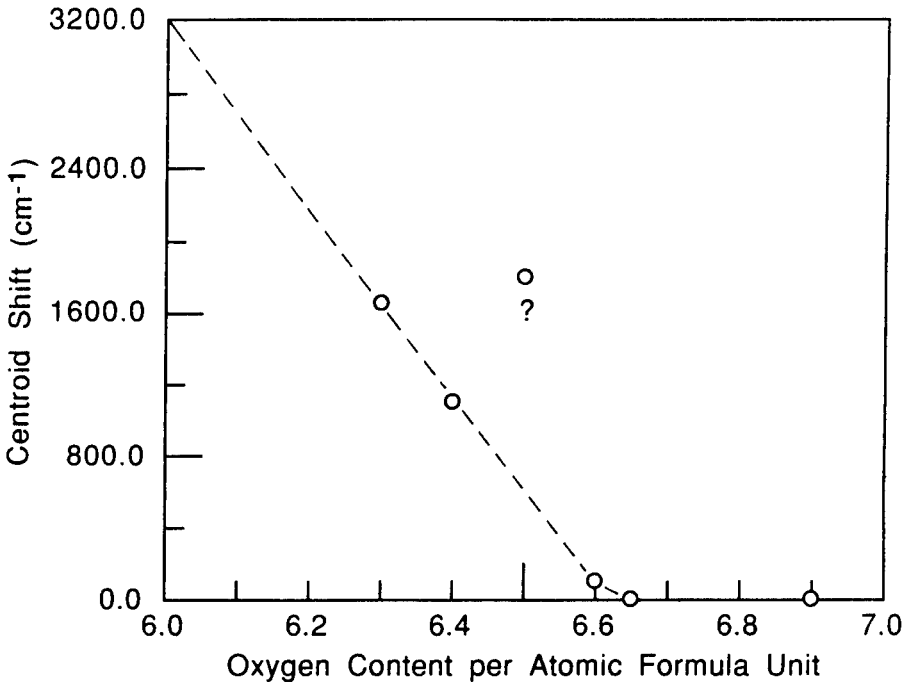


Figure 2 Plot of the centroid shifts for the absorption band at the high-energy end obtained from the iterative fits to the reflectivity data on the $ErBa_2Cu_3O_{6-7}$ samples. The position of the centroid for the two end-point superconductors $ErBa_2Cu_3O_{6.9}$ and $Bi_2Sr_2CaCu_2O_8$ is taken as zero.

Previous reflectivity (10) and ellipsometry (11,12) have reported a structure at ~2.1 eV that appears to vary with oxygen concentration in $ErBa_2Cu_3O_{7-x}$ and may be affected by out-of-plane oxygen (11). It also occurs in BiSCCO, see Figure 1. From the parameters listed in Table 4, there is an absorption band centered at ~2.1 eV (17000±200 cm^{-1}, with half width at half maximum of 2500±900 cm^{-1}), which does not shift with changes in the oxygen concentration, but decreases in apparent intensity (decrease in extinction/reflection coefficient) as the free carrier concentration increases. The location and width of this band corresponds with a band observed for the molecular complex $Cu(NH_3)_4$, $(H_2O)_2^{2+}$ (8), see Table 3, in the plane between Cu^{2+} and NH_3^{1-}. As it is a Cu^{2+} 3d x^2-y^2 band in $Cu(NH_3)_4$, $(H_2O)_2^{2+}$, it is presumed to be so in the cuprate CuO_2 planes between Cu^{2+} and oxygen. Variations in the structure may be due in part to the extension of the free-carrier distribution into the visible and to the systematic intensity decrease (decreased extinction/reflection coefficient, see Table 4) of the band with increasing oxygen content.

With regards to the three structures observed across the visible, we note that ellipsometry measurements (in the superconducting and normal state) at 7 K and 300 K (12) show no significant shifts in any of the three structures indicating that the golden color remains below T_c.

6. CONCLUSIONS

Using a simple model based on gaussian functions to represent absorption bands and reflectivity by free carriers preferentially distributed primarily in the infrared, we have iteratively fitted reflectivity data for $ErBa_2Cu_3O_{6.9}$ and $Bi_2Sr_2CaCu_2O_8$ superconductors. By comparing these fits to those obtained from $ErBa_2Cu_3O_{6.7}$ and to known bands for Cu^{2+} and Cu^{3+}, we have shown that the structure observed with ellipsometry at ~2.1 eV is apparently due to an absorption band in the CuO_2 planes, which decreases in intensity with increasing oxygen concentration, and the extension of the free-carrier distribution into the visible. A second absorption band, also in these planes, appears to shift to higher energy with increasing oxygen concentration in $ErBa_2Cu_3O_{6.7}$ and is present in $Bi_2Sr_2CaCu_2O_8$. This band subtracts blue from the white light reflected, thereby contributing the yellow component of the golden color characteristic of both electron and hole-carrier cuprate superconductors. Both bands are apparently of 3d x^2-y^2 type. The colors calculated from the iterative fits to the reflectivity data generally correspond with the colors observed visually and recorded on film using a 'daylight' source.

7. ACKNOWLEDGMENTS

We wish to acknowledge the Office of Naval Research (ONR), the Office of Naval Technology (ONT), the Strategic Defense Initiative Organization, Office of Innovative Science and Technology (SDIO/IST), the Defense Advanced Research Project Agency (DARPA), and the Nuclear Defense Agency (DNA) for sponsoring this work.

8. REFERENCES

1. H.A. Hoff and C.S. Pande, "Twins in High T_c Superconductors," Studies of High Temperature Superconductors, ed. A.V. Narlikar, vol. 3, 333-368, Nova Science Publishers, Inc.: Commack, NY 1989).

2. D.L. Kaiser, F.W. Gayle, R.S. Roth, and L.J. Swartzdruber, "Thermomechanical Detwinning of Superconducting $YBa_2Cu_3O_{7-x}$ Single Crystals," J. Mater. Res. 4, 745-747 (1989).

3. H.A. Hoff, M. Rubinstein, M.S. Osofsky, A.K. Singh, L.E. Richards, W.L. Lechter, L.E. Toth, B.N. Das, and C.S. Pande, "Color Indicator of Cuprate Superconductivity Observed by Polarized Light Microscopy," J. Superconduct. 2, 351-359 (1989).

4. H.A. Hoff, M.S. Osofsky, W.L. Lechter, L.E. Toth, M. Rubinstein, T.A. Vanderah, B.N. Das, L.E. Richards, R.J. Soulen, Jr., S.A. Wolf, and C.S. Pande, "The Color of Polarization in High Temperature Superconductors," Physica C 162-164, 1115-1116 (1989).

5. K.T. Mulville, N.G. Wimer, H.A. Hoff, L.E. Richards, and V.M. Browning, "Microstructure and Optical microscopy of Pr Containing Cuprates," High Temperature Superconducting Compounds: Processing & Related Properties, eds. S.H. Whang and A. DasGupta, vol. 2, in press, The Minerals, Metals & Materials Society: Warrendale, PA (1990).

6. W. Uytenbogaardt and E.A.J. Burke, Tables for Microscopic Identification of Ore Minerals, Elsevier Publishing, Inc.: Amsterdam (1971).

7. H.A. Hoff, W.L. Lechter, M.S. Osofsky, and G.A. Candela, "Microanalysis of Cuprate Superconductors Using the Color of Polarization," High-Temperature Superconductors: Fundamental Properties and Novel Materials Processing, eds. J. Narayan, L.F. Schneemeyer, P.W. Chu, and D.K. Christen, vol. 169, in press, Materials Research Society: Pittsburgh, PA (1990).

8. J.Bjerrum, C.J. Ballhausen and C.K. Jorgensen, "Studies on Absorption Spectra I. Results of Calculations on the Spectra and Configuration of Copper (II) Ions," Acta Chem. Scand. 8, 1275-1289 (1954).

9. A. Balikungeri and M. Pelletier, "Electronic Spectra of Bis (dihydrogen tellurato) and Bis (hydrogen periodato) Complexes of Copper (III), Silver (III) and Gold (III), Inorg. Chim. Acta 29,, 141-148 (1978).

10. H. Schmid, J.P. Rivera, M. Clin, A. Williams, and E. Burkhardt, "Bireflectance, Absorption and Transmission Dichroism of Single Domains, and Bireflectance of Layered Polydomains of Normal State $YBa_2Cu_3O_{7-x}$ in the Visible," Physica C 153-155, 1748-1751 (1988).

11. M.K. Kelly, P. Barboux, J.M. Tarascon, and D.E. Aspnes, "Optical Properties of Copper-Oxygen Planes in Superconducting Oxides and Related Materials," Phys. Rev. B 40, 6797-6805 (1988).

12. M. Garriga, J. Humlicek, M. Cardona, and E. Schönherr, "Effects of Oxygen Deficiency on the Optical Spectra of $YBa_2Cu_3O_{7-x}$," Solid State Commun. 66, 1231-1235 (1988).

EFFECT OF DOPING IN THE Bi-Sr-Ca-Cu-O SUPERCONDUCTOR

S. A. Akbar, M. S. Wong, M. J. Botelho, and Y. M. Sung
Department of Materials Science and Engineering
The Ohio State University
Columbus, OH 43210

and

M. Alauddin, C. E. Drummer, and M. J. Fair
Department of Chemistry
Wagner College
Staten Island, NY 10301

Abstract

The results of the effect of doping on the superconducting transition in the Bi-Sr-Ca-Cu-O system are reported. Samples were prepared under identical conditions with varying types (Pb, Sb, Sn, Nb) and amounts of dopants. All samples consisted of multiple phases, and showed stable and reproducible superconducting transitions. Stabilization of the well known 110 K phase depends on both the type and amount of dopant. No trace of superconducting phase of 150 K and above was observed.

I. Introduction

Superconductivity in the Bi-Sr-Ca-Cu-O system was originally reported by Michel et al. [1] and later by Maeda et al. [2] and Chu et al. [3]. There exists three distinct superconducting phases [1-7] in this system, the orthorhombic unit cell structures of which differ [8] in the number of Cu-O planes (n). The nominal compositions of these phases are: (i) $Bi_2Sr_2CuO_4$ (n=1, T_c < 20K; 2201 phase), (ii) $Bi_2Sr_2CaCu_2O_y$ (n=2, T_c = 85K; 2212 phase) and (iii) $Bi_2Sr_2Ca_2Cu_3O_y$ (n=3, T_c =110K; 2223 phase). It has been quite difficult to synthesize the 110K phase, the formation of which has been reported to be enhanced by Pb doping [9-16].

Recently, Hongbao et al. [17-19] reported even higher transition temperatures (as high as 164K) in the Bi-Pb-Sb-Sr-Ca-Cu-O system. They, however, reported significant instability of the high-temperature superconducting phase. Their data show large drops in T_c values after the samples are circled from liquid nitrogen to room temperature in air. This prompted us to do a systematic study of the effect of doping on superconductivity in these systems, and the results are communicated in this paper. Since our objective was to investigate the effect of doping, all the samples in this study were prepared under the same processing condition. The effect of variation in processing conditions is under investigation and will be reported in a future communication.

II. Experimental

The samples were prepared by the standard solid state reaction route by mixing Bi_2O_3, PbO, Sb_2O_3 (Sb_2S_3 for sample #12), SnO (for #13), Nb_2O_5 (for #14), $SrCO_3$, $CaCO_3$, and CuO in stoichiometric ratios. All of the starting materials were dried in oven at 160 °C for an hour and stored in desicator prior to weighing. This is clearly preferable to weighing the raw materials "as is" since a recent report (20) indicates that many oxides contain variable amount of hydroxides which may affect the composition of the final product. The mixtures were calcined at 820 °C for 12 hrs. After grinding and

pressing into disk-shaped pellets, the samples were then sintered in air at 860 °C for 60 hrs. followed by a fast cool (10 °C/min.). The nominal compositions of the samples prepared are given in Table I.

Table I: Summary of properties of the samples investigated

No.	Composition*	Processing Conditions	$T_{c,zero}$ (K)
1	2-0-0-0-0-2-2-3-y-0	calcined at 820 °C for 12 hrs. and sintered at 860 °C for 60 hrs.	80
2	1.7-.25-.05-0-0-2-2-3-y-0	"	94
3	1.7-.2-.1-0-0-2-2-3-y-0	"	107
4	1.7-.15-.15-0-0-2-2-3-y-0	"	100
5	1.6-.3-.1-0-0-2-2-3-y-0	"	106
6	1.7-.2-.1-0-0-2-2-3.4-y-0	"	95
7	1.6-.2-.2-0-0-2-2-3-y-0	"	82
8	1.7-.2-.1-0-0-2-2-2.6-y-0	"	<70
9	1.5-.4-.1-0-0-2-2-3-y-0	"	99
10	1.5-.5-0-0-0-2-2-3-y-0	"	90
11	1.7-.3-0-0-0-2-2-3-y-0	"	<70
12	1.7-.2-.1-0-0-2-2-3-y-z	"	81
13	1.7-0-.1-0-.2-2-2-3.6-y-0	"	72
14	1.5-.2-.1-.2-0-2-2-3-y-0	"	107

*Numbers represent p, q, r, s, u, v, w and x in $Bi_pPb_qSb_rNb_sSn_uSr_vCa_wCu_xO_yS_z$

Resistance vs. temperature measurements were performed by the standard four-probe ac method with a PAR lock-in amplifier. The X-ray powder diffraction (XRD) patterns were taken on a Philips diffractometer at room temperature. The microstructural pictures were taken on an ISI-SX-40 scanning electron microscope (SEM). The ac magnetic susceptibility measurements were performed using a recently developed system by Xenikos et al. (21). This system detects the variation in the inductance of a coil which is induced when the sample changes its magnetic behavior. This variation causes change in the resonant frequency of the coil which corresponds to a change in the output voltage. The data is therefore conveniently represented in terms of detector output voltage as a function of temperature.

III. Results and Discussions

Most of our samples, with the exception of a few, exhibited superconductivity. The pure 2223-sample (#1) showed a very broad transition (Fig.1a) with a low T_c (~80 K). The doped samples, on the other hand, showed sharp transition with higher T_c ~107 K (a plot is shown in Fig.1b for sample #3). The T_c values reported in this paper represent the temperatures at which the resistance of the samples

goes to zero. It is interesting to note that none of our samples showed significant hysteresis in R vs. T behavior with temperature cycles as reported by Hongbao et al. [18,19]. This indicates that we were able to make rather stable and reproducible samples. We were, however, unable to make any sample showing T_c values as high as reported by Hongbao et al. We prepared one sample (#12) with similar nominal

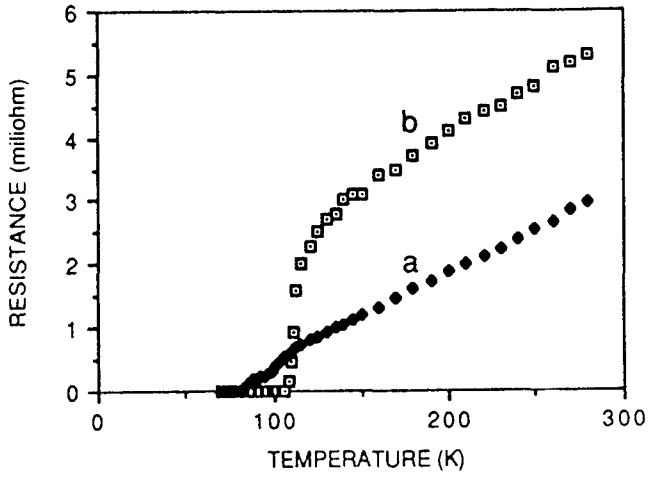


Fig.1 Resistance vs. temperature of sample #1 (a) and sample #3 (b).

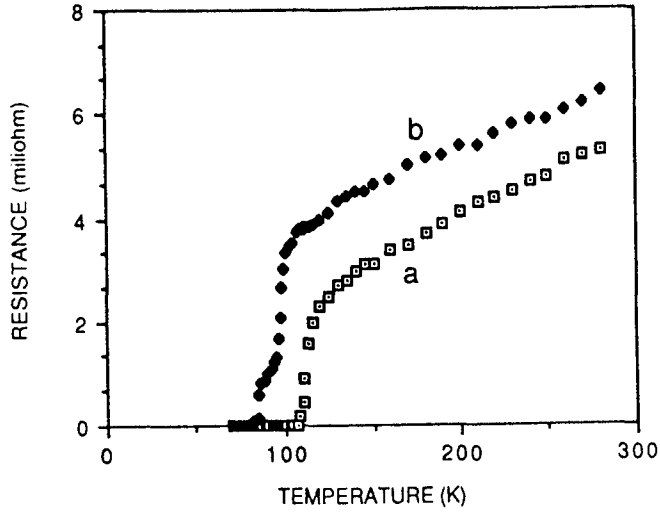


Fig.2 Resistance vs. temperature of sample #3 (a) and sample #12 (b)

composition as that of sample #2, but with different oxygen stoichiometry (Sb_2S_3 was used instead of Sb_2O_3). And our data (Fig.2a; #3 and Fig.2b; #12) indicates that the use of sulfide dopants instead of oxides is detrimental to superconductivity in this system. Also a Sn-doped sample shows a lower T_c than a corresponding Pb-doped sample (Fig.3). On the other hand, both Nb and Pb doping seem to stabilize the well known 110 K phase (Fig.4). The superconducting transitions in our samples were also confirmed by the ac magnetic susceptibility measurements. Figure 5 shows susceptibility data for samples #1(a) and #3(b).

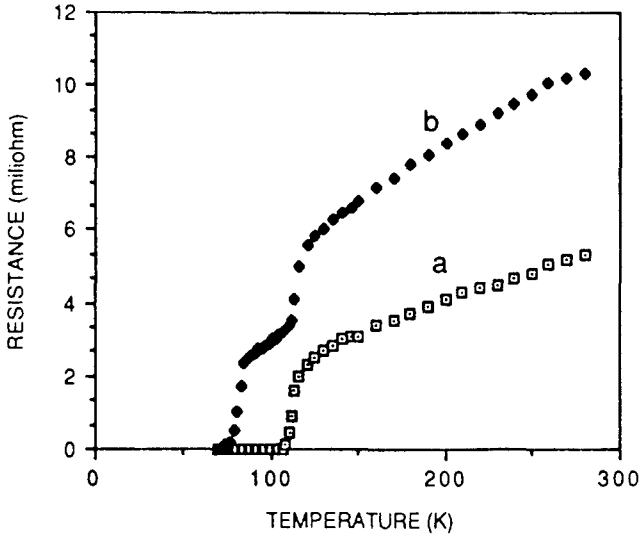


Fig.3 Resistance vs. temperature of sample #3 (a) and sample #13 (b).

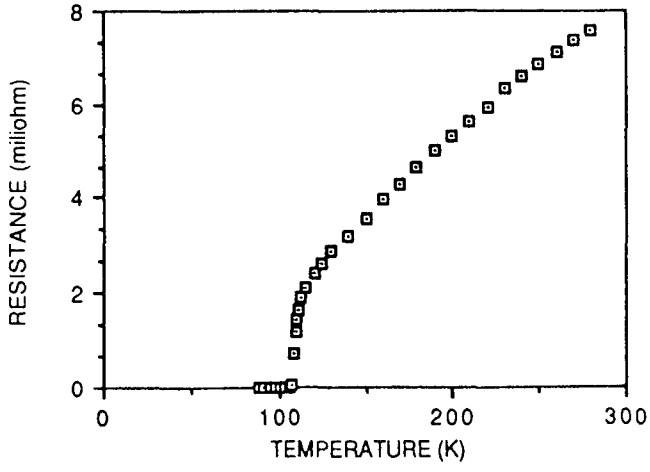


Fig.4 Resistance vs. temperature of a Pb and Nb-doped sample (#14)

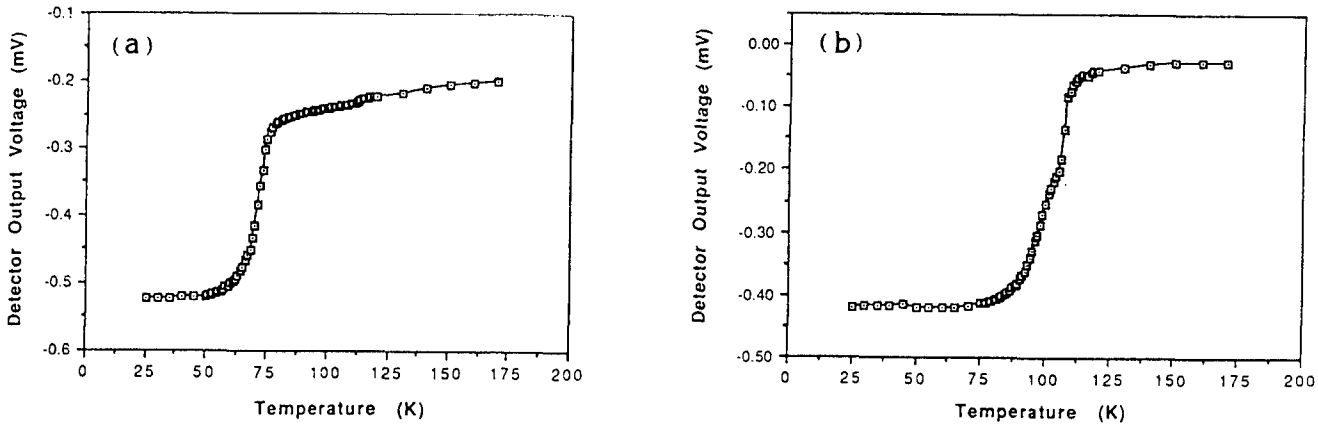


Fig.5 The ac magnetic susceptibility data of samples #1 (a) and #3 (b). The zero of the voltage scale is arbitrary.

The X-ray diffraction data of samples #1, 2, 3 and 4 are shown in Fig.6, which compare very well with those reported in the literature. It is quite evident that our samples constituted mostly of 2223 and 2212 phases and some 2201 phase. It is also interesting to note that as the amount of Sb

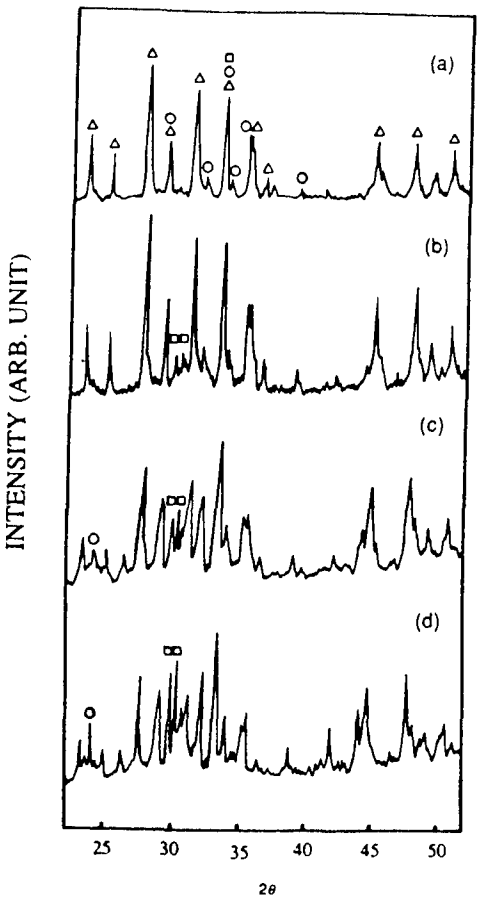


Fig.6 X-ray diffraction of samples #1 (a), #2 (b), #3 (c) and #4 (d). □ 2201, △ 2212 and ○ 2223.

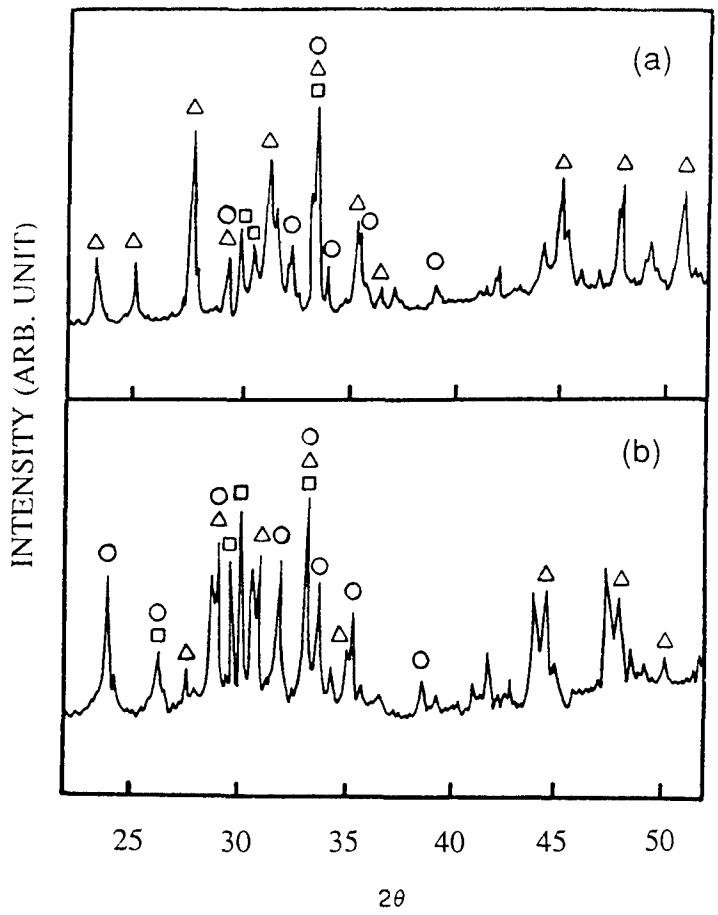


Fig.7 X-ray diffraction of samples #13 (a) and #14 (b).

increases from sample #1 to #2 to #3 to #4, two diffraction peaks around 30° become more and more dominant. The XRD patterns of the Sn and Nb-doped samples (Fig.7) indicate that they are also multiphase, consisting of mostly 2223 and 2212 peaks.

Figure 8 shows SEM micrographs of sample #3 (a: as prepared surface, b: fractured surface) revealing plate-like grains, a characteristic of all the samples including the Sn and Nb-doped samples. None of the micrographs of our samples showed any indication of thin filaments which were claimed to be responsible for superconductivity above 150K in the work of Hongbao et al. [19].

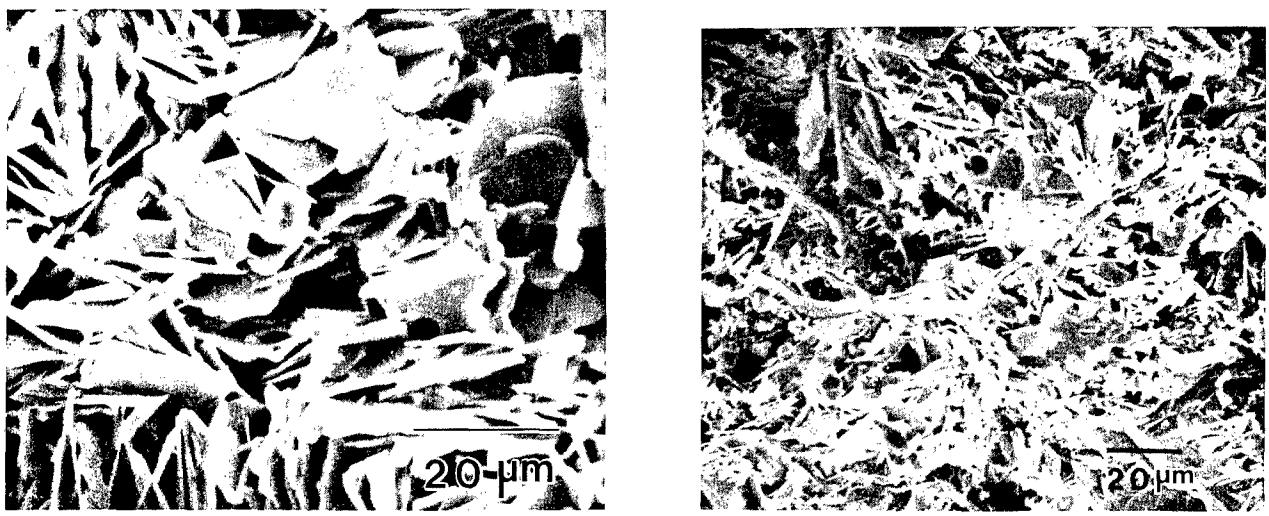


Fig.8 SEM micrograph of sample #3 (a: as prepared surface, b: fractured surface).

This study was not able to reproduce any of the superconducting phase above 150 K as reported by Hongbao et al. [19] in the Bi-Pb-Sb-Sr-Ca-Cu-O system. In the composition range of Pb and Sb doping we studied, the optimum nominal composition for the well known 110 K phase is that of sample #3. Doping the material with both Pb and Nb seem to stabilize the 110 K phase. Based on the XRD and SEM data, it is not possible to highlight any particularly distinguishing features of the Sn and Nb-doped samples from their Pb-doped counterpart.

IV. References

1. C. Michel, M. Herrien, M. M. Borel, A. Grandin, F. Deslandes, J. Provost and B. Raveau, Z. Phys., **B68**, 421 (1987).

2. M. Maeda, Y. Tanaka, M. Fukutomi and T. Asano, Jpn J. Appl. Phys. Lett., **27**, L209 (1988).

3. C. W. Chu, J. Bechtold, L. Gao, P. H. Hor, Z. J. Huang, R. L. Meng, Y. Y. Sun, Y. Q. Wang and Y. Y. Xue, Phys. Rev. Lett., **60**, 941 (1988).

4. S. S. P. Parkin, V. Y. Lee, A. I. Nazzal, R. Savoy, R. Beyers and S. J. Laplaca, Phys. Rev. Lett., **61**, 750 (1988).

5. M. A. Subramanian, C. C. Torardi, J. C. Calabrese, J. Gopalakrishnan, K. J. Morrissey, T. R. Askew, R. B. Flippen, U. Chowdhury and A. W. Sleight, Science, **239**, 1015 (1988).

6. H. W. Zandbergen, Y. K. Huang, M. J. V. Menken, J. N. Li, K. Kadowaki, A. A. Menovsky, G. Van Tendeloo and S. Amelincky, Nature, **333**, 620 (1988).

7. R. M. Hazen, C. T. Prewitt, R. G. Angel, N. L. Roy, L. W. Finger, C. G. Hadidiacos, D. R. Veblen, P. J. Heaney, P. H. Hor, R. L. Meng, Y. Y. Sun, Y. Q. Wang, Y. Y. Xua, Z. J. Huang, L. Gao, J. Bechtold and C. W. Chu, Phys. Rev. Lett., **60**, 1174 (1988).

8. D. Shi, M. Tang, K. Vandervoort and H. Claus, Phys. Rev. **B39**, 9091 (1989).

9. U. Balachandran, D. Shi, D. I. Dos Santos, S. W. Graham, M. A. Patel, B. Tani, K. Vandervoort, H. Claus and R. B. Poeppel, Physica C **156**, 649 (1988).

10. T. Kanai, T. Kumagai, A. Soeta, T. Suzuki, K. Aiharaa, T. Kamo and S. Matsuda, Jpn. J. Appl. Phys., **27**, L1435 (1988).

11. T. Hatano, K. Aota, S. Ikeda, K. Nakamura and K. Ogawa, Jpn. J. Appl. Phys., **27**, L2055 (1988).

12. T. Komatsu, R. Sato, K. Matusita and Y. Yamashita, Appl. Phys. Lett., **54**, 1170 (1989).

13. S. M. Green, C. Jiang, Y. Mei, H. L. Luo and C. Politis, Phys. Rev, **B38**, 5016 (1988).

14. S. M. Green, Y. Mei, A. E. Manzi, H. L. Luo, R. Ramesh and G. Thomas, J. Appl. Phys., **66**, 728 (1989).

15. Y. Mei, S. M. Green, C. Jiang and H. L. Luo, J. Appl. Phys., **66**, 1777 (1989).

16. D. Shi, M. S. Boley, J. G. Chen, M. Xu, K. Vandervoort, Y. X. Liao, A. Zangvil, J. Akujieze and C. Segre, Appl. Phys. Lett., **55**, 699 (1989).

17. L. Hongbao, Z. Xiaonxong, C. Yaogu, Z. Guien, R. Yaozhong, C. Zhaojia and Z. Yuheng, Physica C, **156**, 804 (1988).

18. L. Hongbao, C. Liezhao, Z. Ling, M. Zhiqiang, Z. Weijie, L. Xiaoxian, Y. Zhidong, X. Bai, M. Xianglei, Z. Guein, R. Yaozhong, C. Zhaojia, and Z. Yuheng, Solid State Commun., **69**, 867 (1989).

19. L. Hongbao, C. Liezhao, M. Zhiqiang, Z. Ling, Z. Weijie, L. Jiang, X. Bai, M. Xianglei, L. Biyou, R. Yaozhong, C. Zhaojia and Z. Yuheng, preprint.

20. C. E. Hamrin, Jr., W. D. Arnett, R. J. DeAngelis, X. X. Ding and W. D. Ehmann, Solid State Commun., **69**, 1063 (1989).

21. D. G. Xenikos and T. R. Lemberger, Rev. Sci. Instrum., **60**, 831 (1989).

STABILIZATION OF HIGH Tc PHASE IN BISMUTH CUPRATE SUPERCONDUCTOR BY LEAD DOPING

Ram. P. Gupta, J.P. Pachauri, and W.S. Khokle
Semiconductor Devices Area
Central Electronics Engineering Research Institute
Pilani 333031 Rajasthan-INDIA

K.C. Nagpal
National Physical Laboratory, New Dehli-INDIA

S.K. Date
National Chemical Laboratory, Poona-INDIA

ABSTRACT

It has widely been ascertained that doping of lead in Bi:Sr:Ca:Cu:0 systems promotes the growth of high Tc (110 K) phase, improves critical current density, and lowers processing temperature. A systematic investigation is undertaken in the present study to determine optimum lead content and processing conditions to achieve these.

A large number of samples with cationic compositions of $Bi_{2-x}Pb_xSr_2Ca_2Cu_3$ (x=0.2 to 2.0) were prepared by conventional solid-state reaction technique. Samples of all compositions were annealed together at a temperature and characterized through resistance-temperature (R-T) measurements and X-ray diffraction (XRD) to determine the zero resistance temperature, Tc(0) and to identify presence of phases, respectively. The annealing temperature was varied between 790°C and 880°C to optimize processing parameters.

For x value between 0.3 to 0.8, Tc(0) above 110 K is obtained when the samples were annealed at a temperature in the range of 855°C to 870°C for 40 hours. The best samples showed Tc(0)=113 K and critical current density of about $200A/cm^2$. An optimum process yielded a large volume fraction of high Tc phase as determined from intensity peaks in XRD spectra. These results were supported through magnetic susceptibility measurements on samples having high Tc(0) values. The samples showed no change in R-T characteristics on repeated thermal cycling between 77 K and 300 K, even after a few weeks of their preparation.

In brief, we report an optimum process and composition of leaded bismuth cuprate superconductor which yields nearly a high Tc single phase with highly stable superconducting properties.

STRUCTURE AND SUPERCONDUCTING PROPERTIES OF $[(Ln_{1-x}Ln^*_x)_{1/2}(Ba_{1-y}Sr_y)_{1/3}Ce_{1/6}]_8Cu_6O_z$

H. Yamauchi, T. Wada, A. Ichinose, Y. Taegashi, T. Kaneko,
S. Ikegawa, and S. Tanaka

Superconductivity Research Laboratory
International Superconductivity Technology Center
10-13 Shinonome 1-Chome, Koto-ku
Tokyo 135, Japan

ABSTRACT

A variety of new oxide superconductors that can be represented by the formula, $[(Ln_{1-x}Ln^*_x)_{1/2}(Ba_{1-y}Sr_y)_{1/3}Ce_{1/6}]_8Cu_6O_z$ (Ln, Ln* = lanthanide elements), have been prepared. The crystallographic structures of the oxides were all tetragonal and of the $(Ln^+,Ce)_4(Ln^+,Ba)_4Cu_6O_z$ (Ln^+ = Nd, Sm or Eu) type which had been previously discovered by Akimitsu et al. As the Sr content, y, increased when Ln=Ln*=Nd, the oxygen content, z, monotonically increased and the superconducting transition temperature, T_c, varied exhibiting a maximum. When z was controlled directly by means of high oxygen pressure sintering techniques, T_c was changed accordingly. T_c's of samples with different combinations of Ln and Ln* and different values of x and y were found to depend on the magnitude of the bond valence sum for a Cu atom located in the bottom plane of the $Cu-O_5$ pyramid. Transport and magnetization measurements were carried out to investigate the magnetic field dependence of superconducting properties and to determine the phenomenological parameters. The Hall coefficients were positive below room temperature and varied yielding a maximum with respect to temperature.

COMPATIBILITIES OF $YBa_2Cu_3O_{9-\delta}$ TYPE PHASE IN QUINTENARY SYSTEMS Y—Ba—Cu—O—X (IMPURITY)

P. Karen, O. Braaten, H. Fjellvåg and A. Kjekshus
Department of Chemistry, University of Oslo, Blindern, N-0315 Oslo 3, Norway

Isothermal phase diagrams at various oxygen pressures are investigated by powder diffraction and chemical analytical methods. The components, Y, Ba, Cu, and O, (specifically O_2, O^{2-} and O_2^{2-}) are treated, together with C (specifically CO_2 and CO_3^{2-}), alkaline metals, Mg, alkaline earths, Sc, 3-d and 4-f elements. Effects of the substitutions at the structural sites of $YBa_2Cu_3O_{9-\delta}$ on T_c are discussed with respect to changes in crystallochemical characteristics of the substituted phase and to the nature of the substituents.

1. INTRODUCTION

Electrical transport properties of the oxidic high-Tc superconductors are significantly affected by the presence of minor amounts of various elements added inadvertently as impurities, e.g., from the chemical environment during manufacturing. $YBa_2Cu_3O_{9-\delta}$ tends to lose its superconductivity upon (partial) substitution of any of the four elemental components. Most of the substituents, and particularly Pr (for Y) [1], La (for Ba) [2,3], Fe, Co, Ni and Zn (for Cu) [4], alter some of the prerequisites of superconductivity, such as mixed valency state in the Cu—O network or a structural distortion of the network [5,6].

Although various pseudo-ternary equilibrium chemical phase diagrams of the Y(O)—Ba(O)—Cu(O) system have been proposed [7-11], no consensus has been reached to date, partly due to inconsistent equilibrium conditions. Even less information is available [12,13] about the phase compatibilities in the appropriate quaternary phase diagram (including oxygen and implying redox relations). Virtually no information exists about any quintenary phase diagrams (including one additional element). Due to the complexity of such systems, also this presentation is limited to more or less close surroundings of the $YBa_2Cu_3O_{9-\delta}$ type phase (123) in the appropriate pseudo-quaternary or pseudo-pseudo-ternary diagrams.

2. EXPERIMENTAL

Samples were prepared by liquid mixing in citrate gels using basic copper carbonate, barium carbonate and yttrium oxide. Additional metal oxides were introduced into the gels in a water soluble (complexed) form. The incinerated gels were fired repeatedly in purified oxygen, with intermittent rehomogenizations followed by a 16 h equilibration at 340 °C. Low O_2 pressures above the samples were maintained (when neccessary) by means of Cu_2O/CuO, Cu/Cu_2O or Ni/NiO getters in closed systems at variable temperatures. The degree of (de)oxidation was determined iodometrically. Gravimetrical analyses by reduction in pure H_2 at 1000 °C were also performed. The carbon was determined coulometrically as CO_2 released from the sample at 1100 °C in oxygen. The equilibria of the reactions with O_2 and CO_2 were investigated by a thermogravimetric analysis (TGA). Powder X-ray diffraction data (PXD) were collected using Guinier-Hägg cameras. Powder neutron diffraction data (PND) were collected with a two-axis diffractometer at 8-300 K. Structural parameters were refined according to the Rietveld method. Magnetic susceptibility was measured using a SQUID magnetometer at 4-300 K in a 10-30 G magnetic field. T_c is evaluated as the point with 0.5 % of the remaining Meissner effect upon increasing temperature conditions.

3. THE PHASE SYSTEMS

3.1. The System Y-Ba-Cu-O

Due to the variable valency of copper, a true quaternary system should be considered, including also redox interphase relations. Although the redox reactions (decompositions) of the particular phases

occur at generally different partial pressures of oxygen, for practical reasons only some isobaric phase diagrams are reported here. As another experiment–related constraint, the corner adjacent to the highly reactive BaO is omitted from consideration in the phase diagrams.

At *high oxygen partial pressures*, Cu^{III} (formally) compounds may be stabilized. $YCuO_3$ and $BaCuO_{2.5}$, are formed under $\sim$ 300 atm O_2 pressure and reported [15,16] to be stable up to some 600 °C. At higher temperatures, the highest attainable copper valency decreases. At 910 °C, the ambient pressure phases, *viz.*, $Y_2Cu_2O_5$ and $BaCuO_{2+\nu}$, together with Y_2BaCuO_5 (211), are apparently stable even at high oxygen pressures. In principle, the 123 phase is preserved as well [10,17,18]. At such conditions, though, in some reports [19,20], it is proposed to accommodate additional oxygen as peroxygroups. Two other phases occur, which are closely structurally related to 123, *viz.*, $Y_2Ba_4Cu_7O_{\sim 15}$ (247), stable between 7 and 20 atm O_2 at 910 °C, and $YBa_2Cu_4O_{\sim 8}$ (124), stable above $\sim$20 atm O_2 at 910 °C [21].

For *1 atm O_2 pressure*, the phase diagram at 910 °C is shown in Fig. 1A. A portion of the diagram is already above the solidus line, and $YBa_2Cu_3O_{9-\delta}$ melts incongruently at $\sim$ 960 °C [22]. Below 830 °C, the 124 phase is stable also at the 1 atm oxygen pressure, see Fig. 1B. This is connected apparently with the increased stability of Cu^{II} at lower temperatures, which preserves the double–square structural chains of copper and oxygen atoms. At 800 °C, no formation of 123 is observed upon prolonged annealing of 124 (>200 h, and rehomogenizations). Neither the parallel extended annealing of 123 provides indices for decomposition of 123 into the neighbouring phases, *viz.*, 124, 211 and $BaCuO_{2+\nu}$.

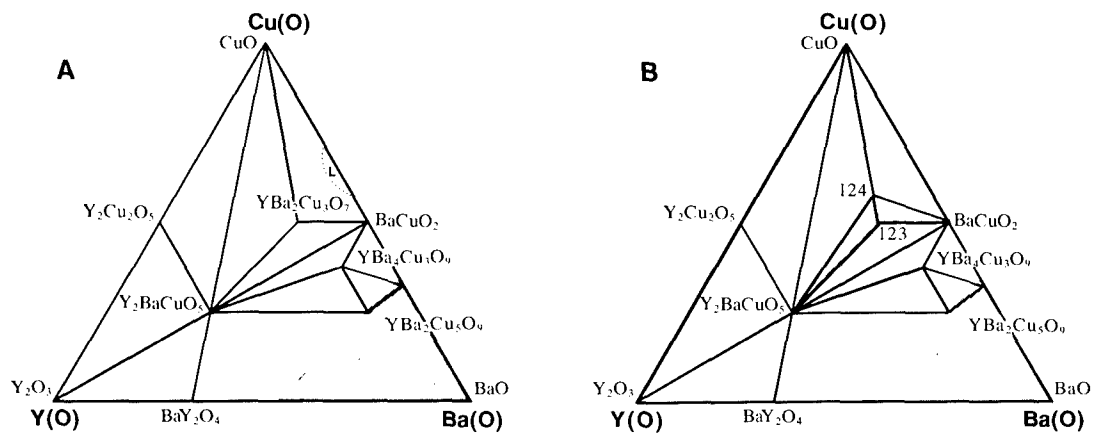


Figure 1. Equilibrium phase diagram Y—Ba—Cu—O, projected onto the plane of metallic components for 1 atm oxygen partial pressure at 910 °C (A) and 800 °C (B). BaO–rich phases omitted.

Low oxygen partial pressures at high temperatures lead to decomposition of the copper–rich, Cu^{II} containing phases, particularly those which cannot accommodate substantial amounts of Cu^{I} in their structures, like 124 or $BaCuO_{2+\nu}$. The 124 phase becomes unstable even at temperatures below 830 °C, and its rapid decomposition into CuO and 123 is observed at, e.g., 800 °C for $\sim 1.3 \cdot 10^{-3}$ atm O_2, above Cu_2O/CuO. In addition, some of the Ba–rich quaternary oxides become less stable at these conditions, e.g., $YBa_4Cu_3O_{\sim 8}$ (143) decomposes into $BaCuO_{2+\nu}$, Y_2BaCuO_5 and a more Ba–rich quaternary oxide. The 123 phase decomposes into the Cu^{II} containing, however, Cu–poor and very stable phase Y_2BaCuO_5, and into $BaCu_2O_2$ and a Ba–rich quaternary oxide, e.g., at 850 °C and $4 \cdot 10^{-4}$ atm O_2 [12].

At even lower oxygen pressures, the $Y_2Cu_2O_5$ phase is also reduced, *viz.*, into $YCuO_2$. If the oxygen pressure is further lowered, e.g., to $2.4 \cdot 10^{-14}$ atm, above the Ni/NiO system at 820 °C, all the Cu containing phases decompose into metallic Cu and oxides from the pseudo–binary section

Y—Ba—O, see Fig. 2.

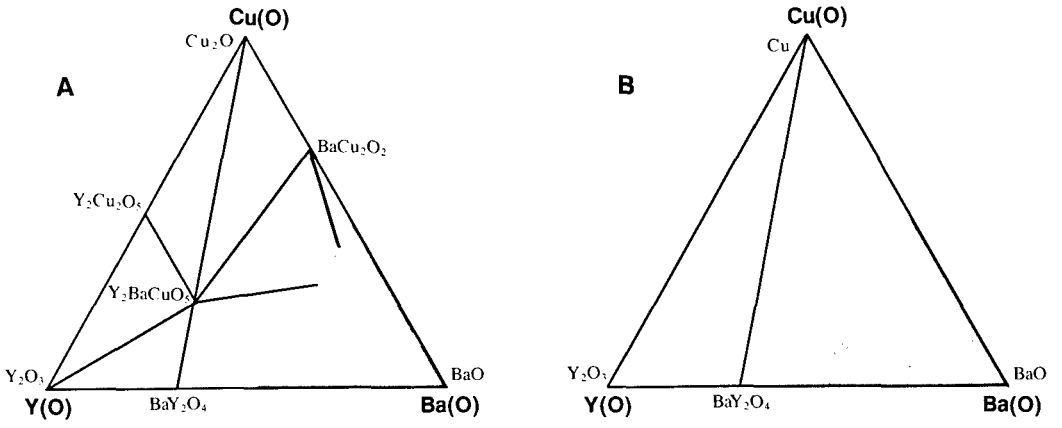


Figure 2. Equilibrium phase diagram Y—Ba—Cu—O, projected onto the plane of metallic components at 820 °C for low oxygen partial pressures, *viz.*, $2.5 \cdot 10^{-9}$ atm above Cu/Cu_2O (A) and $2.4 \cdot 10^{-14}$ atm above Ni/NiO (B). BaO-rich phases omitted.

3.2. The Y—Ba—Cu—O—□ System

With an exception of the Y_2BaCuO_5 phase, all the other quaternary phases contain mixed-valent Cu. This is related to the presence of oxygen vacancies in their structures, and the phases therefore have a homogeneity range with respect to the oxygen content, see Table I.

Table I. Oxygen content, unit cell parameters and volume for some oxidized and reduced (the latter above Cu/Cu_2O or Cu_2O/CuO), mixed-valent Y—Ba—Cu—O phases.

formula	t (°C)	p_{O_2} (atm)	x	a (Å)	b (Å)	c (Å)	V (Å^3)
$YBa_2Cu_4O_x$	340	1.0	7.99(2)	3.8427(10)	3.8704(6)	27.250(5)	405.3(1)
$YBa_2Cu_3O_x$	340	1.0	6.96(2)	3.8187(3)	3.8859(3)	11.6795(11)	173.32(2)
	800	$> 10^{-3}$	6.18(3)	3.8599(2)	—	11.8061(9)	175.90(2)
	800	$> 10^{-9}$	6.00(5)	3.8583(1)	—	11.8253(8)	176.03(2)
$BaCuO_x$	340	1.0	2.09(1)	18.303(6)	—	—	6132(6)
	800	$> 10^{-3}$	2.00(2)	18.293(4)	—	—	6121(4)
	800	$> 10^{-9}$	1.98(2)	18.288(4)	—	—	6116(4)
$YBa_4Cu_3O_x$	340	1.0	9.21(2)	8.102(2)	—	—	531.8(4)

Formally, the deoxidation process may be treated as a pseudochemical equilibrium between the gas phase and the vacancies in the solid. Unlike the true chemical equilibrium, the composition of the individual solid phase also varies, and the equilibrium should be expressed in a three dimensional space. In Fig 3, such equilibrium is exemplified [14] by $YBa_2Cu_3O_{9-\delta}$.

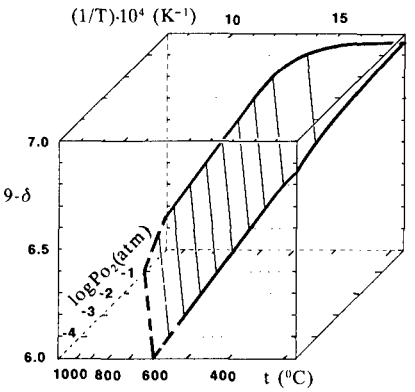


Figure 3. Pseudochemical equilibrium diagram between $YBa_2Cu_3O_{9-\delta}$ and oxygen as a function of partial pressure (p_{O_2}), temperature (T, t) and composition ($9 - \delta$) as obtained by TGA.

3.3. The Y—Ba—Cu—O—C System

This system is of considerable importance, since carbon (particularly CO_2) is a component of various chemical environments and specifically, some common oxide–preparation routes involve carbon compounds which ultimately become carbonates. Specifically, the Y(O)—Ba(O)—Cu(O)—CO_2 system and a high temperature reaction of CO_2 with $YBa_2Cu_3O_{9-\delta}$ are shown here as important examples.

Ba forms an extremely stable carbonate, due to its high electropositivity and the relatively large ionic size. It is, therefore, not surprising that carbonate anions may be stabilized as oxidecarbonates in the Ba rich regions of the oxidic phase systems. Considering the *Y(O)—Ba(O)—Cu(O)—CO_2 system*, the oxidecarbonate stability may prove to be particularly significant if barium carbonate appears as a starting material or as a reaction intermediate. Examples of such phase diagrams are shown in Fig. 4.

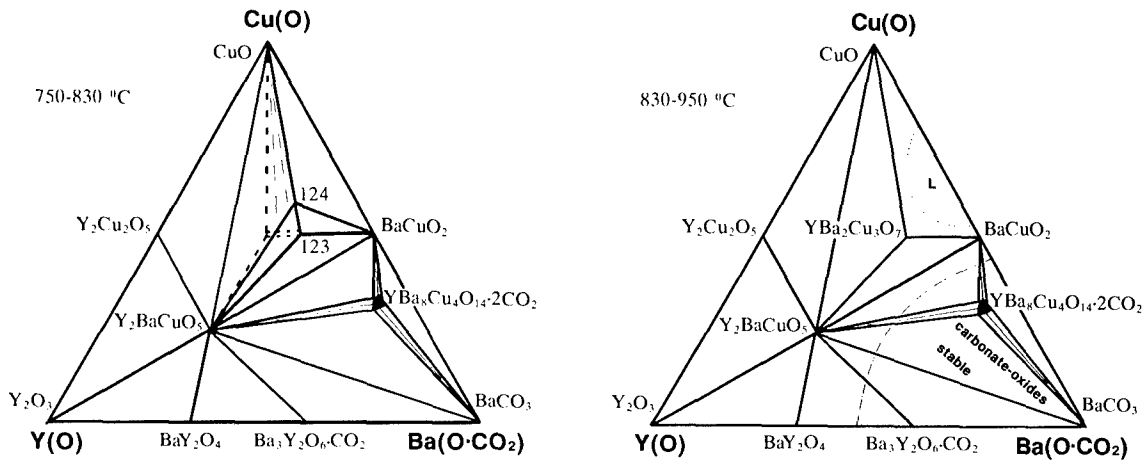


Figure 4. Phase diagrams of the Y(O)—Ba(O)—Cu(O)—CO_2 system at various temperatures as seen after equilibrium firing of carbonate–containing starting materials in 1 atm O_2 ($\leq$ 5 ppm CO_2). Metastable phases are marked by dashed lines. An above–solidus region is marked by dotted lines for $\sim$ 950 °C.

Oxidic materials may be obtained from carbonate precursors in O_2 at relatively low temperatures, say above 750 °C, if a liquid–mixing technique is used and the composition of the oxide phase is not too rich in BaO. Thus, between $\sim$ 750 and 830 °C, the 123 phase is still formed, however, with unusual structural characteristics. Its crystal structure is tetragonal with a = 3.8738(3) Å and c = 11.612(4) Å, but the diffraction pattern shows apparent signs of structural disorder. The enhanced unit cell parameter a and the contracted parameter c may indicate substitution by carbonate or peroxyanions into the Cu—O chains. The carbon analyses and the H_2–reduction gravimetrical analyses of independent samples indicate a presence of 0.1 to 0.2 CO_2 per formula unit, while no enhanced oxygen content is indicated by iodometry. The possibility of a corresponding presence of up to $\sim$ 7 wt.% of $BaCO_3$ in the samples is not substantiated by PXD. For parallel samples of 124, less than 0.02(1) CO_2 (per 124) is found. The oxidecarbonate stabilization up to an approximate formula $YBa_2Cu_3O_{6.8}(CO_3)_{0.2}$ is therefore feasible. It is remarkable that an extended ability of the Ba–site to accommodate smaller substituents is shown by this phase. Actually, up to approximately 1/3 of Ba may be statistically replaced by Y. During repeated firings, this substituted phase decomposes much faster than the parent (oxidecarbonate) phase, indicating that the random Y/Ba distribution is a remnant of the atomic–level mixing in the citrate precursor, rather than representing any real thermodynamic stability.

More defined oxidecarbonates are formed in the region closer to the Ba corner. In the literature, they are often misinterpreted as true oxides. Up to 950 °C, a 184 phase is formed,

$Y_{1+x}Ba_8Cu_{4+z}(CO_3)_2O_{10+\eta}$, having both cationic and anionic vacant, perovskite based structure, the rough features of which are outlined in [23,24]. Its range of homogeneity with respect to the metal content extends to $x = 0.3$ or $z = 0.5$. The content of the anionic component may be varied in a similar way as with the 123 compound, i.e., in a gas–vacancy equilibrium. The oxygen saturated 184 phase has $\eta = 2.08(2)$. Deoxidation at 800 °C above the Cu/Cu_2O system leads to $\eta = 1.05(2)$. If the additional metal atoms ($x > 0, z > 0$) are introduced into the vacant cationic sites, η increases proportionally. None of the purely oxidic phases reported by De Leeuw et al. [25] in the vicinity of the 184 composition are formed in oxygen (< 5 ppm CO_2) from carbonaceous starting materials below 950 °C. Of these phases, 143 and 152 are readily formed at 1000 °C, whereas formation of the other two reported phases, 385 and Ba_2CuO_3, was not observed after 4 times firing in oxygen for 20 h. In the subsolidus region (< 1000°C), the 184 phase starts to decompose slowly and incompletely above 950 °C, under formation of phases having distorted and disordered, 143 and 152–related structures, besides yet unidentified intermediates.

Another oxidecarbonate is formed in the Y—Ba—O pseudo–binary section. The phase earlier named $Y_2Ba_2O_5$, which always was found in multi–phase mixtures, was shown [25] to be an oxidecarbonate. Its actual composition is $Y_2Ba_3O_6 \cdot \sim 0.6CO_2$, and it has a tetragonal crystal structure (currently being solved from PXD and PND data) with $a = 4.3861(5)$ Å and $c = 23.719(4)$ Å which is reminiscent of that of $Sr_3Ti_2O_7$ [26]. The oxidecarbonate decomposes abruptly at 980 °C in "pure" oxygen (<5 ppm CO_2). Another apparent analogue of the Sr, Ti oxides [26] is $Y_3Ba_4O_7 \cdot CO_2$ which is formed above 1000 °C [25]. Obviously, an array of oxidecarbonates exists here with increasing BaO content and increasing decomposition temperature.

If the CO_2 content in the atmosphere during firing is increased, both the oxidecarbonates and the pure oxides are subject to a more complete reaction with CO_2. This carbonatization transfers all the present barium into $BaCO_3$. The other reaction products may be variable, as exemplified by the *reaction of* $YBa_2Cu_3O_{9-\delta}$ *with* CO_2 in Fig. 5. Namely, below 730 °C, only binary oxides occur in the reaction products besides barium carbonate, whereas $Y_2Cu_2O_5$ is formed [14] at higher temperatures.

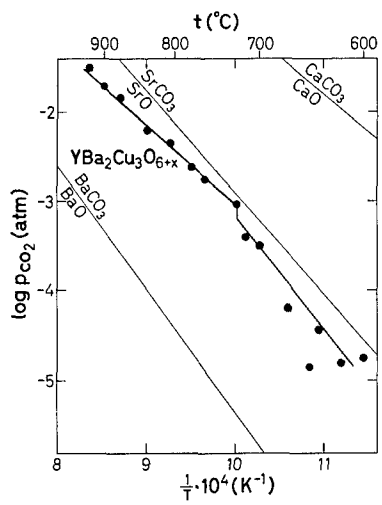


Figure 5. $YBa_2Cu_3O_{9-\delta}$ stability with respect to carbonatization in O_2/CO_2 atmospheres at ambient pressure. The equilibrium state is tentatively indicated by the solid line and the shaded strip. Thinner lines depict calculated data for alkaline earths.

The equilibrium in Fig. 5 illustrates that the average basicity of the 123 oxide at high temperatures may be compared with that of SrO. For any judgement about the stability of 123 in a reaction atmosphere, it may be of importance that the reaction of 123 with a dry, CO_2–containing gas is not effectively stopped by the kinetics until a temperature below 400 °C is reached.

3.4. The Systems RE—Y—Ba—Cu—O, RE = Rare Earth Element

Introduction of another RE into the Y—Ba—Cu—O system leads in many cases to formation of a solid solution due to the chemical similarity of the rare earths. Ce, Tb and pairs of the dimensionally very different RE's are examples of breaking this rule. Though some of these phases have very interesting superconducting properties, they fall outside the titled scope of this paper.

Many of the RE elements may, at least partially, be accommodated at the Y–site and some even at the Ba–site of $YBa_2Cu_3O_{9-\delta}$ as well as of neighbouring phases in the phase diagram. In

$YBa_2Cu_3O_{9-\delta}$, yttrium may be fully replaced by the rare earths Yb–to–Dy and Gd, Eu and Sm. According to equilibrium samples fired at 910 °C, and oxygen saturated at 340 °C, Lu and Tb replace Y up to 1/3. For Nd, Pr and La, an occupational equilibrium between the Y and Ba sites exists, which means that the Ba site may accommodate large rare earths. For the smallest of these, Nd, the equilibrium favours occupation of the Y–site, whereas the Ba–site is preferred in the case of La. No substitution solely for Y may be reached using Nd and larger rare earths, neither may any substitution solely for Ba be obtained for Pr and smaller rare earths. If the former is attempted, the $BaCuO_{2+\nu}$ impurity phase binds the simultaneously replaced Ba. If the latter is attempted, an Y_2BaCuO_5–type phase binds the simultaneously replaced Y and emerges together with CuO. Only La is large enough not to attack the Y–site unless it is present at the Ba–site in a concentration higher than 35%. In which case, Y is substituted by La as well and emerges as $Y_2Cu_2O_5$. In Fig. 6., these situations are shown in tetrahedral diagrams. Cerium does neither substitute Y nor Ba by more than a few %. The excess Ce is bound into both $BaCeO_3$ and $(Ba,Ce,Y)_2CuO_4$ (T^*–type [27]) phases, emerging together with $BaCuO_2$ as impurities to 123.

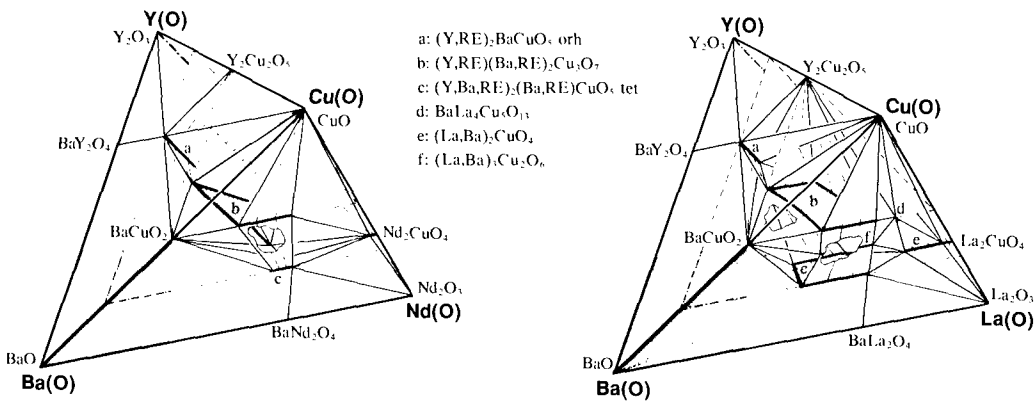


Figure 6. Pseudo–quaternary tetrahedral phase diagrams of RE—Y—Ba—Cu—O system for RE = Nd and La, for samples fired at 910°C and oxygen saturated at 340°C. Floors at 25 and 50 pseudoatom–% Cu are drawn as nontransparent and marked by broken line. The $(Y,RE)(Ba,RE)_2Cu_3O_{9-\delta}$ solid solution regions in the pseudo–pseudo–ternary cut are dotted. BaO–rich phases omitted (dashed region).

As may be apparent in Fig. 6, the Y_2BaCuO_5 phase has a higher accommodative ability for smaller RE's than does the 123 phase. On the other hand, already for Nd and larger RE's, another structure type is adopted for the 211 phase. Extended regions of solid solubility are found in the pseudo–binary systems between phases Y_2BaCuO_5 and Nd_2BaCuO_5 type e.g., the mutual solid solubility Nd/Y is respectively 85 and 5 mole–%. The corresponding values for the La/Y pair are respectively ~30 and ~10 mole–%. The Nd_2BaCuO_5 type structure may moreover accommodate some Ba at the RE–sites, *viz.*, 0–15 % for RE = Nd and 4–65 % for RE = Nd and La.

A substitution of Ba by the larger RE's (Nd to La) in the $BaCuO_{2+\nu}$ phase is obviously possible as indicated by a decrease in its unit cell volume in some investigated systems. However, no exact data are available and the solid solutions are not shown in Fig. 6.

Specifically for La, a close neighbouring phase occurs to the $(Y,La)(Ba,La)_2Cu_3O_{9-\delta}$ frontier of the solid solution area in the phase diagram. This phase, $(La,Ba)_3Cu_2O_x$, has a region of homogeneity around the La/Ba ratio 1/1. Probably, the phase has also a small solid solubility region towards Y.

3.5. The Systems Ca/Sr—Y—Ba—Cu—O

Due to considerable differences in size between the Ca, Sr and Ba ions, different structures are frequently adopted with the same nominal composition. For the same reason, only limited regions

of solid Sr/Ba miscibility are observed in the particular phases here under consideration. No indications were found for any Ca/Ba miscibility and the Sr/Y substitution limit is close to zero. On the other hand, by size considerations, the aliovalent Ca/Y substitution is feasible. However, the process only occurs in oxygen-defect phases, like $YBa_2Cu_3O_{9-\delta}$, where Ca may substitute for Y up to 25 %. The Sr substitution in $YBa_2Cu_3O_{9-\delta}$ is exemplified here more particularly. Replacement up to 35 % is reached. Above this limit, Y_2BaCuO_5 and $Sr_{14}Cu_{24}O_{41}$ [29] emerge as impurity phases. If substitution of Sr for Y is attempted, virtually no replacement, $(4 \pm 4)\%$, is achieved; a portion of Ba is substituted instead, and $BaCuO_2$ appears as impurity. This situation is shown in Fig. 7.

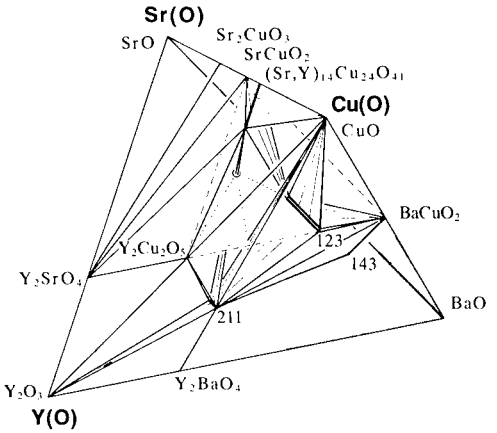


Figure 7. Pseudo-quaternary tetrahedral phase diagram of the Sr—Y—Ba—Cu—O system, for samples fired at 910°C and oxygen saturated at 340°C. A non-transparent floor at 50 pseudoatom-% Cu is marked by a broken line. BaO-rich phases omitted (dashed region).

3.6. Substitution for Ba and Y in $YBa_2Cu_3O_{9-\delta}$ by Alkali Metals

Contrary to some reports, a rather limited substitution by alkali metals into $YBa_2Cu_3O_{9-\delta}$ is found, although various precautions were taken to prevent evaporation of the alkali metal peroxides which are readily formed in the system, *viz.* by using closed system, reducing atmosphere or vapour saturation from additional peroxide. At 850 °C, no more than $\sim$ 8 % of Ba is replaced by Na, with possibly up to 4 % of Y being replaced simultaneously. No substitution of Ba with elements similar in size, K-to-Cs, was accomplished for levels above 10 %.

3.7. Substitution for Cu in $YBa_2Cu_3O_{9-\delta}$ by Li, Mg and 3-d Elements

The affinity of these substituents for the Cu-sites follows the common trends of chemical similarity, as defined by, e.g., electronic configuration, coordination and ionic size. The substitutions preserve the formal high oxidation state of Cu, and the substituents themselves adopt high valency states, *e.g.*, Fe^{III}, Co^{III}, $Ni^{>II}$, which in turn is reflected in the oxygen content per formula unit, $9 - \delta$. The compositional limits, obtained by mass-balances from PXD quantitative analyses, are listed in Table II, together with (identified) phases in equilibrium at the substitution limit [4].

Table II. Qualitative phase composition at the limits of solid solubility for Li, Mg and first row transition metal (M) substitution in $YBa_2(Cu_{1-z}M_z)_3O_{9-\delta}$ for firings at 910 °C and oxidation at 340 °C.

M	Y_2BaCuO_5	$BaCuO_{2+\nu}$	other observed phases	$z_{max.}$	$(9-\delta)_{z_{max}}$
Li	+	+	$BaCO_3$, Li_2CO_3	0.04(1)	6.90
Mg	+	+	MgO	0.04(1)	6.88
Sc	+	−	$BaSc_2O_4$	0.01(1)	6.96
Ti	+	−	[a] barium titanates	0.00(2)	6.96
V	+	−	$Ba_3V_2O_8$	0.00(4)	6.96
Cr	+	−	$BaCrO_4$	0.02(1)	6.96
Mn	+	−	$Ba_3Mn_2O_8$	0.00(3)	6.96
Fe	−	+[b]	[c] $BaFeO_3$ + ?	0.22(1)	7.17
Co	−	−	?	0.30(5)	7.23
Ni	+[d]	+[d]	NiO	0.08(1)	6.98
Zn	+[d]	+[d]	−	0.09(1)	6.90

[a] Ba_2TiO_3, $BaTi_2O_5$, $BaTi_4O_9$. [b] Fe/Cu substitution occurs; $Ba(Cu_{1/3}Fe_{2/3})O_{2+\nu}$, from a = 1842.4(4) pm by molar volume difference, $\mathcal{V}_{FeO_x} - \mathcal{V}_{CuO_x}$, [c] a = 408.4(3) pm. [d] Ni/Cu, Zn/Cu substitution.

4. SUPERCONDUCTING PROPERTIES OF SUBSTITUTED $YBa_2Cu_3O_{9-\delta}$

4.1. Y–substituted $YBa_2Cu_3O_{9-\delta}$

Substitutions for Y which do not change the charge balance in the compound, do not affect the superconducting properties. This is valid particularly for substitutions by trivalent rare earths [30] of the type $(Y_{1-x}M_x)Ba_2Cu_3O_{9-\delta}$. However, a decrease in T_c, $(\partial T_c/\partial x)_{x\to 0} = -200$ K, is observed if Pr is partially introduced into the Y–site (and necessarily into a small portion of Ba simultaneously, see 3.4.). This may be explained by an electron injection of the Cu—O net from the *mixed valent* $Pr^{>III}$ which generally may act as a sort of charge buffer during the pairing process. Remarkably, Tb, if substituted for Y, behaves in conformity with the valency III and no decrease in T_c is observed. If a lower valent element is substituted for Y, like Ca, the oxygen content is decreased and a decrease in T_c is observed, with derivative $(\partial T_c/\partial x) = -50$ K.

4.2. Ba–substituted $YBa_2Cu_3O_{9-\delta}$

Of the few elements which may substitute solely according to the $Y(Ba_{1-y}M_y)_2Cu_3O_{9-\delta}$ formula, i.e., without simultaneously entering the Y–site, both La and Sr cause a decrease in T_c, with $(\Delta T_c/\Delta y)_{y=0,0.2} \approx -250$ K for M = La (non-linear) and $(\partial T_c/\partial y)_{y\in 0,0.3} = -20(2)$ K for M = Sr, in oxygen saturated samples [6,29,30]. The results for La substituted samples [6] are shown in Fig 8.

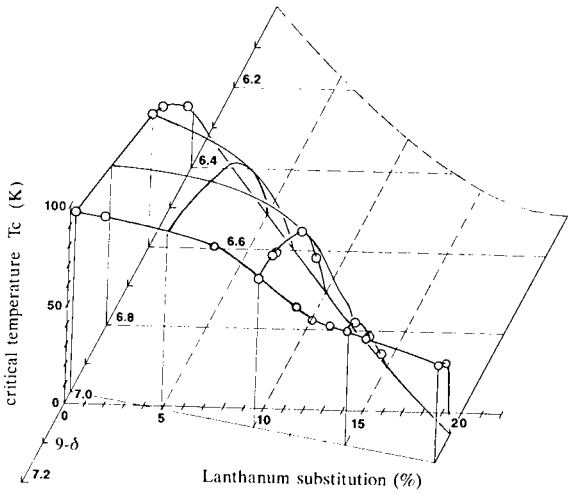


Figure 8. T_c (in K) for $Y(Ba_{1-y}La_y)_2Cu_3O_{9-\delta}$ as a function of oxygen content $9-\delta$ and of the La for Ba substitution in at–%.

T_c of $Y(Ba_{1-y}La_y)_2Cu_3O_{9-\delta}$ increases with increasing oxygen content up to the lower limit of δ, where the Cu valency reaches ~2.30. This happens irrespectively whether or not the oxygen content exceeds $9-\delta = 7$. T_c decreases nonlinearly with increasing La/Ba substitution. The nonlinearity is assumed [6] to be a consequence of a redistribution of oxygens in the Cu—O chains, leading to a transition from the orthorhombic to tetragonal crystal structure. As a consequence of both Sr and La substitutions, an anisotropic compression of the structure takes place along the *c* axis. The degree of compression correlates with the decrease of T_c, as long as the Cu valency is kept constant (i.e., the formal average concentration of hole carriers is constant).

4.3. Cu–substituted $YBa_2Cu_3O_{9-\delta}$

Generally, upon any substitution for Cu in $YBa_2(Cu_{1-z}M_z)_3O_{9-\delta}$, a decrease in T_c is observed. Phenomenologically, the substituents may be divided into three groups according to their effect on T_c:

($\mathcal{A}$) Substituents causing an initially rapid decrease of T_c. Zn and Mg may serve here as examples, with $(\partial T_c/\partial z)_{z=0.005} \cong -1200$ K.

($\mathcal{B}$) Substituents causing a tilde–shaped ($\sim$) decrease of T_c, with an induction period and an intermediate value of the substitutional derivative at the maximal decrease. Fe and Co with maximum $(\partial T_c/\partial z) \cong -800$ K at the inflexion point ($z \cong 0.05$) exemplify this case.

($\mathcal{C}$) Substituents with an almost linear decrease of T_c and with low substitutional derivative. As examples, Ni with $(\partial T_c/\partial z)_{z=0.005} \cong -400$ K and Li with $(\partial T_c/\partial z)_{z=0.03} \cong -200$ K.

4.4. Correlation of T_c with Structural Characteristics

Any correlation between the observed differences in behaviour of the substituted phases and the fundamental properties of the solid are of obvious interest in order to abstract the preconditions of the high-T_c superconductivity and to test the theoretical hypotheses. Generally, T_c should be correlated to variables in terms of electronic wave functions represented in the band structure of the solid. However, since these primary variables are not accessible for comparison, a correlation is sought to the derived properties, e.g., crystallochemical variables, like Cu coordination, Cu—O bond distances, short range order of the oxygen vacancies, and roughly also to the unit cell metric. Naturally, the important transport properties, like the concentration of charge carriers, should be considered as well.

To discuss the suppression of T_c in connection with structural changes, two principal structural distortions may be introduced, which both have been used in formulating phenomenological rules on occurence of superconductivity in the 123 phase:

(1) The *orthorhombic distortion*, $D_{b/a} = (b/a) - 1$, which to some extent may serve as a gauge for the continuity of the Cu—O chains;

(2) The *tetragonal deformation*, $D_{c/ab} = [2c/3(a+b)] - 1$, which narrows the band at the Fermi level, or, in a ligand field model, forms a more solitary, partially filled orbital.

An overview showing T_c and the tetragonal deformation for the particular substituents in $YBa_2Cu_3O_{9-\delta}$ is given in Fig. 9.

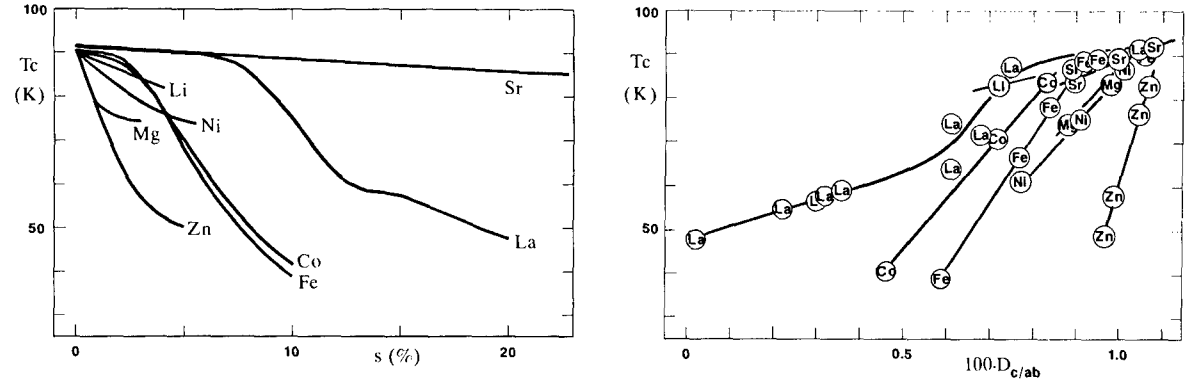


Figure 9. T_c of substituted, oxygen-saturated $YBa_2Cu_3O_{9-\delta}$ (substitution s in %) and the tetragonal deformation $D_{c/ab} = [2c/3(a+b)] - 1$.

No change in T_c is observed upon varying the effective size of an equivalent atom at the Y-site (substitution by RE), which separates the Cu—O slabs in the structure. A contraction of the Cu—O slabs upon substitution of the large Ba by the smaller Sr atom is accompanied by a mild suppression of T_c, whereas the La/Ba substitution decreases T_c more strongly. A significant decrease in T_c is observed with substitutions for Cu. Of these, the most effective suppressors of T_c, *viz.*, Zn and Mg do not decrease the orthorhombic distortion of the structure. The Fe and Co substituents, which rapidly induce the tetragonal structure (by PXD), are rather mild suppressors of T_c, and superconductivity is maintained in the tetragonal phase over a wide substitutional range. However, a possible effect of the short range vacancy ordering in the twinned orthorhombic nanodomains [31] may be considered, which would preserve a certain length of the Cu—O chains even within the apparent tetragonal symmetry. The substitution by Li appears to suppress T_c the least, though a significant decrease in the orthorhombic distortion is observed.

On the other hand, a decrease in the tetragonal deformation is always accompanied by a decrease of T_c for all substitutions, see Fig. 9. If the substituents are correlated to T_c according to the extent of the tetragonal deformation, Sr, La and Li emerge in one group with Fe and Co (which substitute for Cu in the chains) in another group. The strongest suppression of T_c is provided by

Ni, Mg and Zn, which replace the Cu atoms having square–pyramidal coordination. Zn acts most effectively, possibly by introducing a portion of the d^{10} state at the Cu–site, thereby decreasing the hole concentration.

The experiments on substitution seem to support the view that the Cu—O pyramidal sheets are crucial for the superconductivity in cuprates, where they apparently serve as pairing centres. As such, they are very sensitive to any alteration of the local electronic structure and to deformations which would degenerate the Cu $(3d_{x^2-y^2})$—O $(2p_{x,y})$ orbitals participating in the band at the Fermi level. The Cu—O chains, serving then as charge reservoirs, are less capable of destroying superconductivity. A rather massive alteration of the local electronic structure, a large charge deficit or a considerable structural disorder must be introduced in the chains in order to suppress the superconductivity.

Acknowledgement This work has received financial support from the Norwegian Council for Science and Humanities (NAVF). The assistence of Cand. mag. Rita Glenne and Cand. scient. Per H. Andresen in some experiments is gratefully acknowledged.

References

1. Karen, P., Braaten, O., Fjellvåg, H. and Kjekshus, A. *Acta Chem. Scand.* **44** (1990) (submitted).
2. Andresen, A. F., Fjellvåg, H., Karen, P. and Kjekshus, A. *Z. Cryst. 185* (1988) A2.
3. Karen, P., Fjellvåg, H., Kjekshus, A. and Andresen, A. F. *J. Solid State Chem.* (submitted).
4. Karen, P., Andresen, P. H., Fjellvåg, H. and Kjekshus, A. *Acta Chem. Scand.* **44** (1990) (submitted).
5. Fjellvåg, H., Karen, P., Kjekshus, A. and Andresen, A. F. *Physica C (Amsterdam)* **162–164** (1989) 49.
6. Karen, P., Fjellvåg, H. and Kjekshus, A. *Supercond. Sci. Technol.* **3** (1990) (submitted).
7. Frase, C. G. , Liniger, E. G. and Clarke, D. R. *J. Amer. Ceram. Soc.* **70**[9] (1987) C–204.
8. Roth, R. S., Davis, K. L. and Dennis, J. R. *Adv. Ceram. Mat.* **2**[3B] (1987) 303.
9. Wang, G., Hwu, S.–J., Song, S. N. , Ketterson, J. B. , Marks, L. D. , Poeppelmeier, R. and Mason, T. O. *Adv. Ceram. Mat.* **2**[3B] (1987) 313.
10. Fjellvåg, H., Karen, P. and Kjekshus, A. *Acta Chem. Scand. A* **41** (1987) 283.
11. DeLeeuw, D. M., Mutsaers, C. A. H. A. , Geelen, G. P. J. , Smoorenburg, H. C. A. and Langereis, C. *Physica C (Amsterdam)* **152** (1988) 508.
12. Ahn, B. T., Lee, V. Y., Beyers, R., Gür, T. M. and Huggins R. A. *Physica C (Amsterdam)* **162–164** (1989) 883.
13. Borowiec, K. and Kolbrecka, K. *Jpn. J. Appl. Phys.* **28** (1989) L1963.
14. Fjellvåg, H., Karen, P., Kjekshus, A., Kofstad, P. and Norby, T. *Acta Chem. Scand. A* **42** (1988) 178.
15. Arjomand, M. and Machin, D. J. *J. Chem. Soc. Dalton Trans.* **1975** 1061.
16. Webb, A. W., Skelton, E. F., Qadri S. B., Carpenter E. R., Osofsky, M. S., Jr., Soulen, R. J. and Le Tourneau, V. *Physica C (Amsterdam)* **162–164** (1989) 899.
17. Karpinski, J. and Kaldis, E. *Nature* **332** (1988) 242.
18. Sato, M., Konaka, T. and Sankawa, I. *Jpn. J. Appl. Phys.* **27** (1988) L1047.
19. Dai, Y., Manthiram, A., Campion, A. and Goodenough, J. B. *Phys. Rev. B: Condens. Matter* **38** (1988) 5091.
20. Rao, C. N. R. , Ganguly, P., Hedge, M. S. and Sarma, D. D. *J. Amer. Chem. Soc.* **109** (1987) 6893.
21. Karpinski, J., Rusiecki, S., Bucher, B., Kaldis, E. and Jilek, E. *Physica C (Amsterdam)* **161** (1989) 618.
22. Nevřiva, M., Pollert, E., Šesták, J. and Tříska, A. *Thermochimica Acta* **127** (1988) 395.
23. Fjellvåg, H., Karen, P., Kjekshus, A. and Grepstad, J. K. *Acta Chem. Scand. A* **42** (1988) 171.
24. Osamura, K. and Zhang, W. *Jpn. J. Appl. Phys.* **26** (1987) L2094.
25. De Leeuw, D. M., Mutsaers, C. A. H. A., Langereis, C., Smoorenburg, H. C. A. and Rommers, P. J. *Physica C (Amsterdam)* **152** (1988) 39.
26. Ruddlesden, S. N. and Popper, P. *Acta Crystallogr.* **11** (1958) 54.
27. Tokura, Y., Takagi, H., Uchida, S. *Nature* **337** (1989) 345.
28. McCarron, E. M. , Subramanian, M. A. , Calabrese, J. C. and Harlow, R. L. *Mater. Res. Bull.* **23** (1988) 1355.
29. Fjellvåg, H., Karen, P., Kjekshus, A. and Andresen, A. F. *Physica C (Amsterdam)* **162–164** (1989) 49.
30. Karen, P., Fjellvåg, H., Kjekshus, A. and Andresen A. F. *J. Solid State Chem.* (submitted).
31. Hiroi, Z., Takano, M., Takeda, Y., Kanno, R., and Bando, Y. *Jpn. J. Appl. Phys., Part 2* **27** (1988) L580.

PROCESSING Bi-Pb-Sr-Ca-Cu-O SUPERCONDUCTORS FROM AMORPHOUS STATE

C. K. Chiang, W. Wong-Ng, L. P. Cook, S. W. Freiman,
N. M. Hwang, M. Vaudin and M. D. Hill

Ceramics Division
National Institute of Standards and Technology
Gaithersburg, MD 20899

R. D. Shull, A. J. Shapiro, L. J. Swartzendruber, and L. H. Bennett

Metallurgy Division
National Institute of Standards and Technology
Gaithersburg, MD 20899

ABSTRACT

The bismuth-based high-Tc superconductors can be processed via an amorphous Bi-Pb-Sr-Ca-Cu oxide. The amorphous oxides were prepared by melting the constituent powders in an alumina crucible at 1200°C in air followed by pouring the liquid onto an aluminum plate, and rapidly pressing with a second plate. In the amorphous state, no crystalline phase was identified in the powder X-ray diffraction pattern of the quenched materials. After heat treatment at high temperature the amorphous materials crystallized into a glass-ceramic containing a large fraction of the $Bi_2Sr_2Ca_2Cu_3O_x$ phase (T_C=110K). The processing method, crystallization, and results of dc electrical resistivity and ac magnetic susceptibility measurements are discussed.

1. INTRODUCTION

The Bi-based system of high T_C superconductors can be prepared by forming an amorphous oxide followed by heat treatment [1-7]. The amorphous state of the oxides, also known as glasses, are defined by an amorphous x-ray diffraction pattern (Figure 1). Preparation of high T_C superconductors using the glass technology has many technological advantages such as homogeneity, fine-grained microstructure, reduced segregation, and extended solid solubility. The glass can be molded into various shapes, or used as a thick film coating. To exploit these

advantages, it is important to provide an understanding of the microstructure and phase formation in the complicated processing of these superconductors. A particular goal is to maximize the formation of the high-temperature ($T_C > 100K$) phase.

Three starting compositions: 1) $Bi_1.5Pb0.5Sr_1.25Ca_1.75Cu_2O_x$ (G1), 2) $Bi_2PbSr_2Ca_2Cu_4O_x$ (G2), 3) $Bi_{1.84}Pb_{0.34}Sr_{1.91}Ca_{2.03}Cu_{3.06}O_x$ (G3) were studied. The compositions with addition of Pb were selected to promote the formation of the $Bi_2Sr_2Ca_2Cu_3O_x$ phase [7-9]. The formation of the crystalline phases depends on the temperature, atmosphere and length of the heat treatment time. We have performed an extensive heat treatment study to identify those crystalline phases [8,9]. It is found that the phase formation is very complicated and very sensitive to the starting composition.

In this paper, we show that a Bi-based high T_c superconductor can be processed from a amorphous state. Both superconducting and non-superconducting oxide phases are crystallized through subsequent heat treatments. After heat-treatment, the superconductor contains a large fraction of the $Bi_2Sr_2Ca_2Cu_3O_x$ phase.

2. EXPERIMENTAL

Amorphous oxides were prepared from as-received analytical grade powders of Bi_2O_3, PbO, $SrCO_3$, $CaCO_3$, and CuO. The stoichiometric oxide powders were well mixed with mortar and pestle. The powder was first calcined at 800°C for 20 hours. The calcined powder was heated to 1200°C in alumina crucibles to form a liquid. The viscous liquid was held at 1200°C for about 10 minutes and stirred occasionally. The liquid was quenched to room temperature onto one aluminum plate and rapidly pressed with another plate to in order to preserve the amorphous state.

1Differential thermal analysis (DTA) was carried out on the amorphous oxides in order to determine the temperatures at which crystallization would occur. The DTA traces were obtained using a commercial system equipped with a computer [9]. Powdered samples were placed in an alumina sample holder and measured in air.

The heat treatment of the samples was guided by DTA, DSC, and on-line resistivity measurements. The heat-treatment temperature varied from 400°C to 900°C. The length of heat treatment ranged from 30 minutes to 15 days. The heat treatments were carried out in air, as well as in controlled atmospheres of nitrogen, an oxygen-nitrogen mixture, and oxygen [8,9]. The electrical resistivity of the oxide was used to monitor the change of the electrical properties of the oxide (Figure 2). In this experiment, the resistivity of a sample with four-leads attached was measured at room temperature after annealing at fixed temperature for one hour. The measurement was repeated from room temperature to 850°C using the same sample.

X-ray powder diffraction patterns were used to identify the crystalline oxide phases formed after a heat treatment. The pattern was measured on powdered samples at room temperature with $CuK\alpha_1$ radiation. Sample preparation followed the methods described by McMurdie [10].

Electrical resistivity and ac magnetic susceptibility were measured as a function of temperature from 295K to 20K. Alternating-current magnetic susceptibility was measured using a computerized ac magnetometer with applied ac voltage at 1.68 kHz and ac field at 0.5 gauss. The electrical resistivity was measured using a standard four-probe dc technique. Bar-like samples of 1.5mm x 1.5mm x 8mm were used. Currents from 0.01μA to 10 mA were used for the resistivity measurements.

3. RESULTS AND DISCUSSION

a. Amorphous State of Bi-Pb-Sr-Ca-Cu Oxide:

The amorphous state is characterized by an amorphous x-ray diffraction pattern as shown in Figure 1. The pattern has two broad scattering bands ($2\Theta=29°$) and no sharp crystalline peaks above the amorphous curve. In Figure 1, the small peak at $2\Theta\simeq44°$ is a residual crystalline oxide. The material remained amorphous as long as the temperature never rose above the glass transition temperature, Tg, where the material changes from an amorphous to a crystalline state (Figure 2). The T_g of the glasses determined from the data of DTA and DSC data is in the range from 400°C to 450°C.

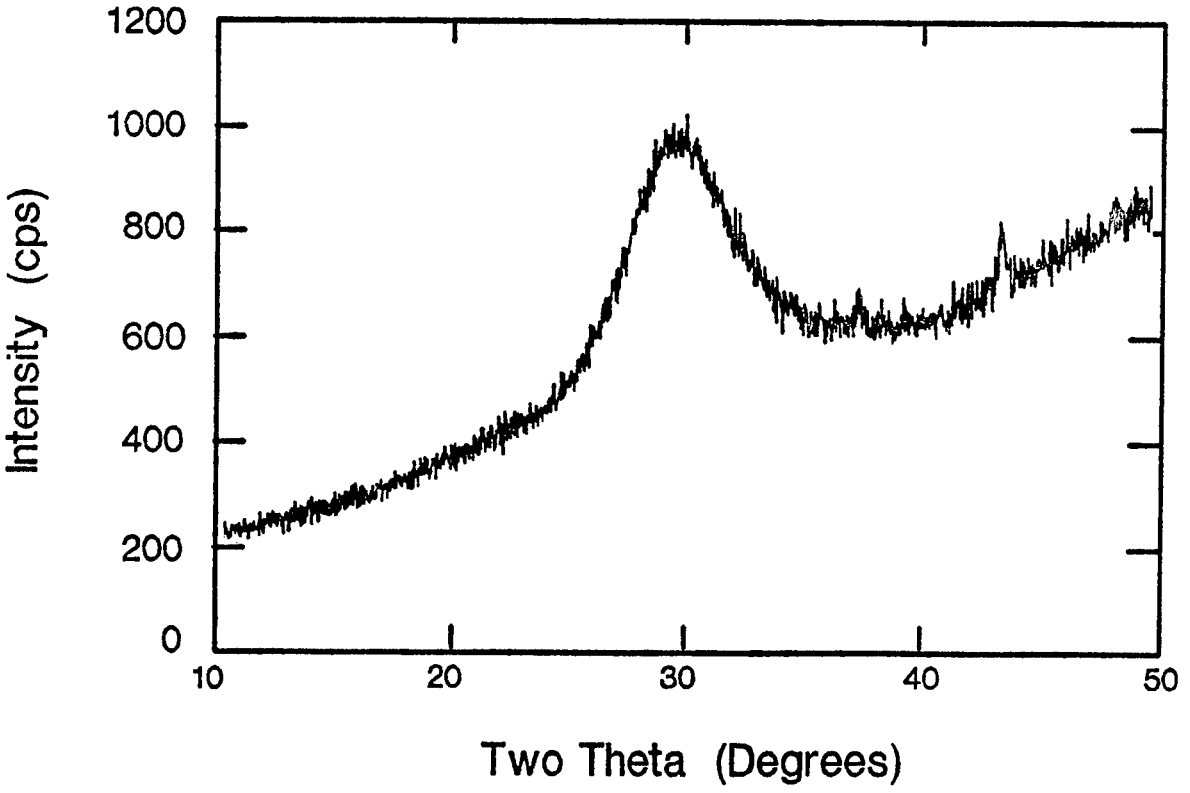


Figure 1. The x-ray powder patterns of the as-quenched Bi-Pb-Sr-Ca-Cu-O oxide (G3).

The microanalysis of the amorphous oxide with a scanning electron microscopy showed that the composition of the sample was uniform. The compositional analysis was done across the thickness, approximately 400 um, of an as-quenched amorphous oxide, using a 6 um diameter beam. Further analysis of the SEM data with a crushed sample having particles less than $\approx 0.1\mu m$ indicated that the amorphous sample is locally heterogeneous.

The amorphous oxide showed no evidence of superconductivity based on electrical resistivity and ac susceptibility measurements from room temperature to 20K.

b. Crystallization Processes:

Crystallization occurs when the amorphous Bi-Pb-Sr-Ca-Cu oxides are heated above the glass transition temperature. Details of the x-ray characterization of the crystallization process are reported elsewhere.[8,9]

The crystallization process for the three compositions can be divided into two temperature ranges based on the thermal analysis data. The DTA curve for the glass G2 is illustrated in Figure 2. In the temperature range from 400°C to 700°C, DTA traces of the glasses reveal many exothermal peaks. These peaks are associated with the thermal energy released while forming crystalline phases of CaO, Cu_2O, $CaPbO_{3-x}$, Ca_2CuO_3, $SrCO_3$, Ca_2PbO_4, and $(Bi,Pb)_{2.2+y}Sr_{1.8-y}Cu_{1+y}O_x$. These oxides are not desirable high T_C superconducting phases.

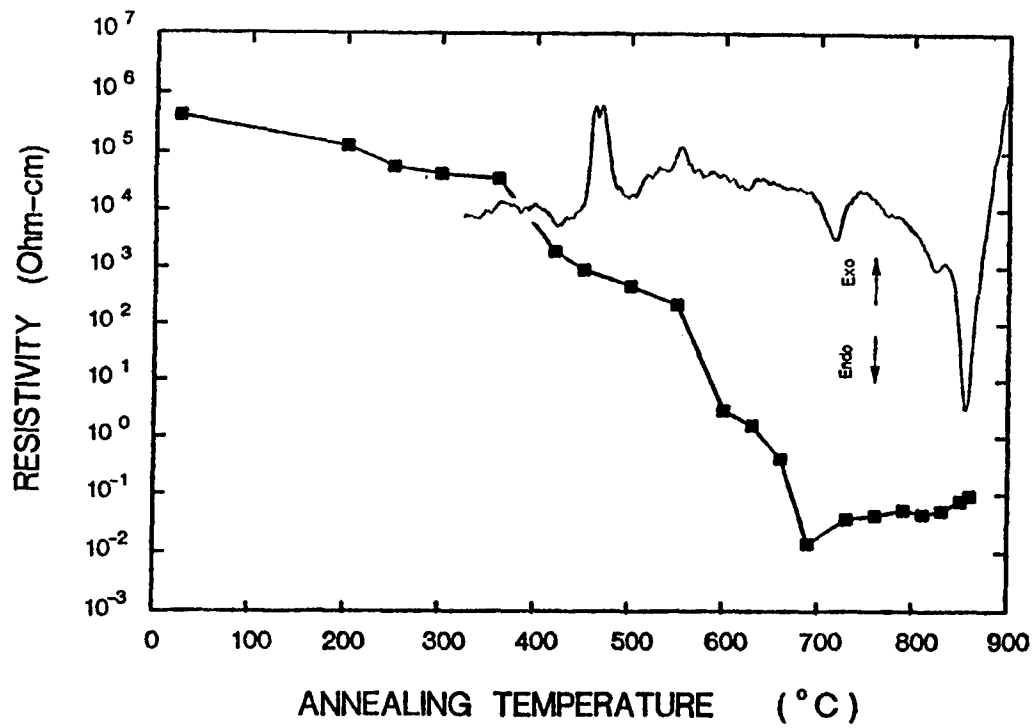


Figure 2. The room temperature resistivity as a function of annealing temperature, and DSC trace of as the Bi-Pb-Sr-Ca-Cu oxide, G2.

In the temperature range from 700°C to 900°C, several melting peaks (endothermic peaks) were observed in DTA traces. The crystalline phases found in this temperature range are$(Bi,Pb)_{2.2+y}Sr_{1.8-y}Cu_{1+y}O_x$, Ca_2PbO_4, and CuO, $Bi_2Sr_2CaCu_2O_x$, and $Bi_2Sr_2Ca_2Cu_3O_x$. The last two oxides are the superconducting phases whose critical temperatures are 80K and 110K, respectively. The endothermic peaks associated with forming these phases suggest that the formation of the superconducting phases is probably a product of a chemical reaction.

To obtain a superconducting phase, the heat treatment temperature for the amorphous Bi-Pb-Sr-Ca-Cu oxide are listed in Table 1. Note that starting with compositions G1 and G2, the major phase is $Bi_2Sr_2CaCu_2O_x$. After prolonged annealing at 850°C, the composition develops a nominal amount (less than 10%) of the $Bi_2Sr_2Ca_2Cu_3O_x$ phase. However, starting from the composition G3, both $Bi_2Sr_2CaCu_2O_x$ and $Bi_2Sr_2Ca_2Cu_3O_x$ can be obtained. The fraction of the $Bi_2Sr_2Ca_2Cu_3O_x$ phase increased with annealing time.

c. Electrical and Magnetic Properties:

The room temperature electrical resistivities of the amorphous oxides are very high, and vary according to the quench conditions.

TABLE I

Temperature Range for Forming Superconducting Phases

	Resulting Phases	
Material	$Bi_2Sr_2CaCu_2O_x$ (T_c=80K)	$Bi_2Sr_2Ca_2Cu_3O_x$ (T_c=110K)
$Bi_{1.5}Pb_{0.5}Sr_{1.25}Ca_{1.75}Cu_2O_x$	750°C-850°C	-----
$Bi_2PbSr_2Ca_2Cu_4O_x$	750°C-850°C	-----
$Bi_{1.84}Pb_{0.34}Sr_{1.91}Ca_{2.03}Cu_{3.06}O_x$	500°C-860°C	840°C-850°C

Figure 2 shows the decrease of the room temperature resistivity as a function of the heat treating temperature. A DTA curve was superimposed on the figure for comparison. In the vicinity of 410°C, a glass transition was observed electrically. Two step-like decreases of the electrical resistivity were observed at 550°C and 700°C which can be correlated to the DTA peaks and phase formation at same temperature range. Each phase formation or transition appears to result in the decrease of resistivity over one order in magnitude. After heat treatment at 850°C, the total decrease of the room temperature resistivity is nearly 8 orders of magnitude. The resistivity of the sample is at minimum at 750°C-780°C. But neither the sample with the minimum resistivity nor the sample after a on-line heating run show any superconductivity when measured down to 40K electrically.

Both DTA and the electrical monitoring studies reveal that the crystallization of the high T_C superconducting phases from the amorphous phase require proper temperature control and long annealing time. For single step processing in air, the most suitable conditions to form the $Bi_2Sr_2Ca_2Cu_3O_x$ phase is 72 hours at 850°C.

The x-ray diffraction patterns of the samples annealed for 72 hours at 850°C are shown in Figure 3 and 4. The detailed identification of these patterns were reported previously [8,9]. As far as high T_C superconducting phase is concern, the sample G1 and G2 are very similar. However, the peaks associated with the $Bi_2Sr_2Ca_2Cu_3O_x$ phase ($2\Theta=4.8°$ and $2\Theta=24°$) are significantly larger for the sample G3.

Figure 5 shows the electrical resistivity as function of temperature for the sample G1 after annealing at 850°C for 120 hour in air. The solid line in Figure 5 is the first derivative of the resistivity against temperature (dR/dT). A peak in the dR/dT reflects the sharp decrease of resistivity which can be interpreted as a phase transition if part of the sample is superconducting. A large peak at 80K agrees with the large superconducting phase and a small peak at 110K is consistent with the small amount (less the 5%) of non-continuous $Bi_2Sr_2Ca_2Cu_3O_x$ phase.

Figure 6 shows the electrical resistivity as function of temperature for the annealed sample G3 whose x-ray pattern is shown in Figure 4. The zero resistivity near 100K indicates that $Bi_2Sr_2Ca_2Cu_3O_x$ is continuous throughout the sample. The ac susceptibility of the annealed G3, shown in Figure 7, indicates that the fraction of the sample that is superconducting at 110K is about 50%, i.e. 50% of the annealed material is the $Bi_2Sr_2Ca_2Cu_3O_x$ phase.

In conclusion, we processed the Bi-based high T_c superconductors from the amorphous state. The glasses transform into polycrystalline ceramics upon heat treatment at high temperatures. Heat treatments below 700°C produces various non-superconducting oxides. Heat treatments between 750°C and 850°C produce the superconducting $Bi_2Sr_2CaCu_2O_x$ and $Bi_2Sr_2Ca_2Cu_3O_x$ phases. The former phase formed easily from all three composition with short heat treatment times. The latter phase can be formed only in the composition G3 and after prolonged heat treatment.

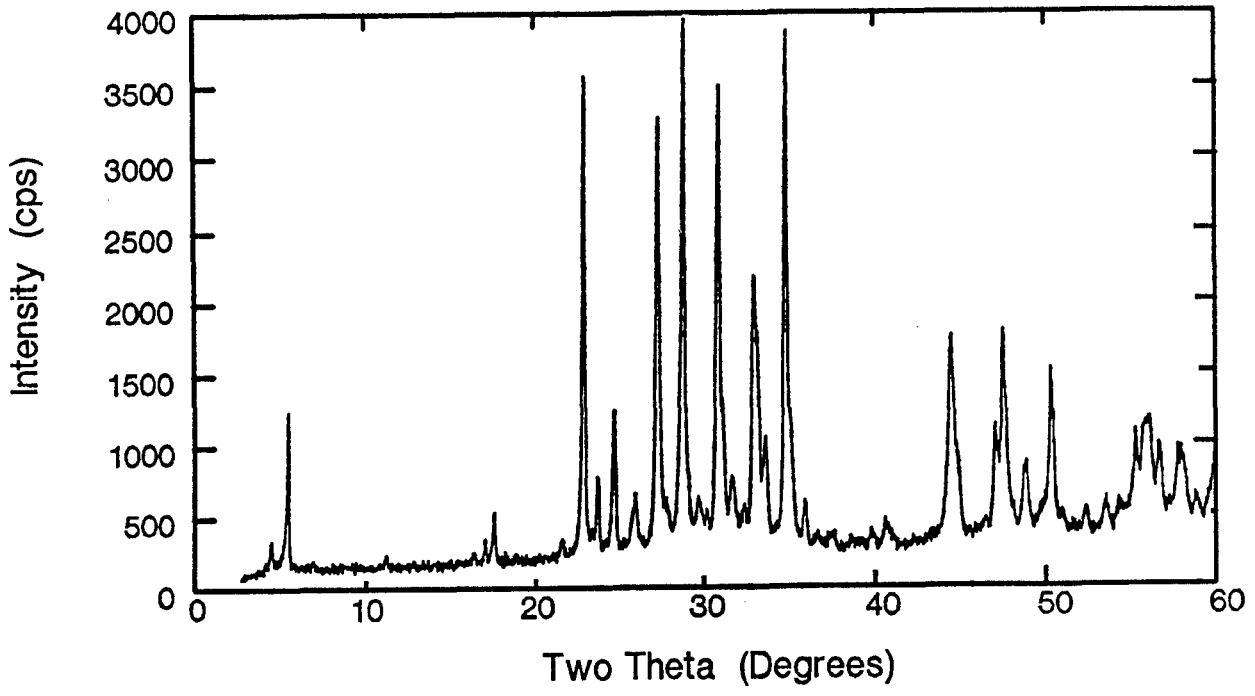


Figure 3. X-ray powder diffraction pattern of the Bi-Pb-Sr-Ca-Cu oxide, G2, after annealing at 850°C for 71 hours in air.

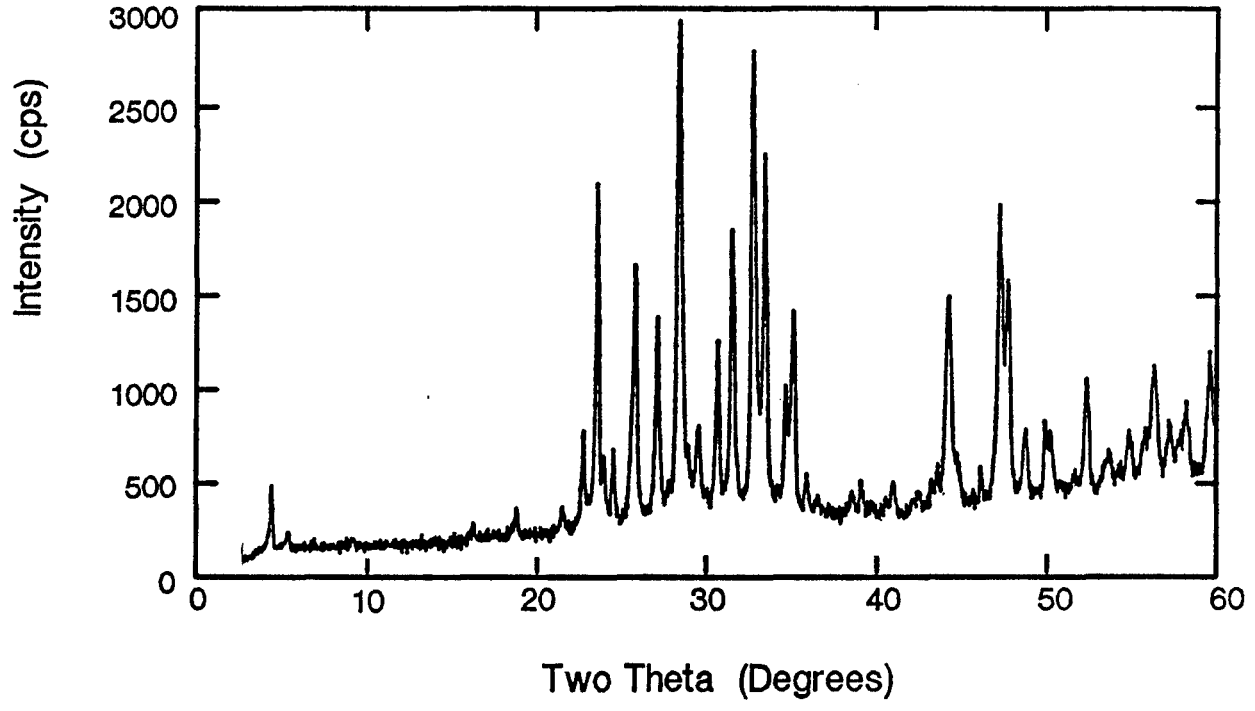


Figure 4. X-ray powder diffraction pattern of the Bi-Pb-Sr-Ca-Cu oxide, G3, after annealing at 850°C for 76 hours in air.

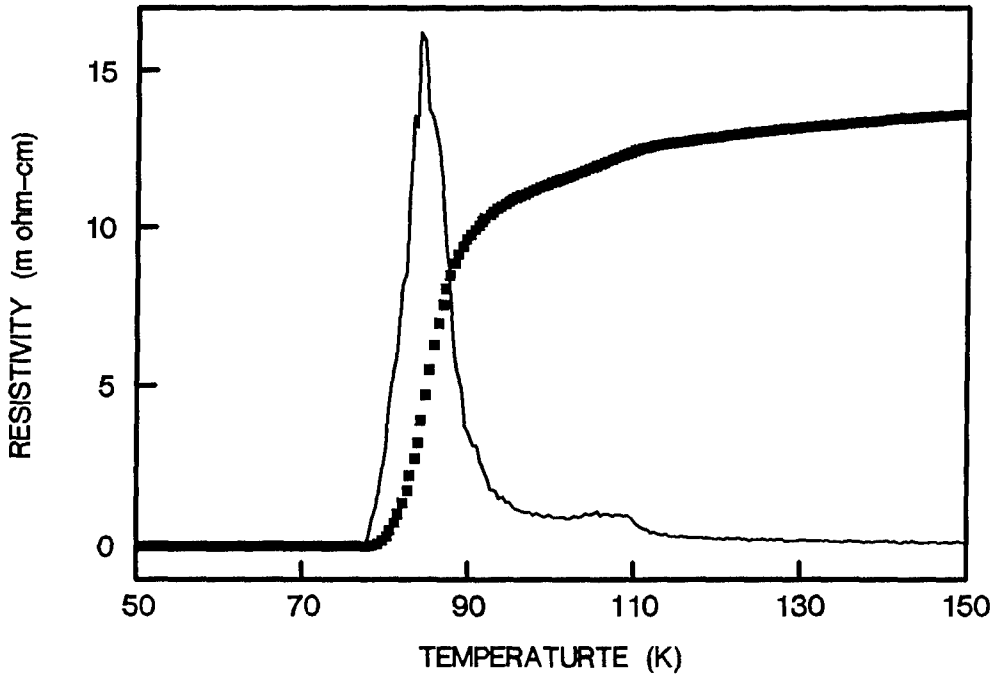


Figure 5. The resistivity of the Bi-Pb-Sr-Ca-Cu oxide, G1, as a function of temperature (heat treated at 850°C for 120 hours in air). The solid curve is the dR/dT to show the transition temperature.

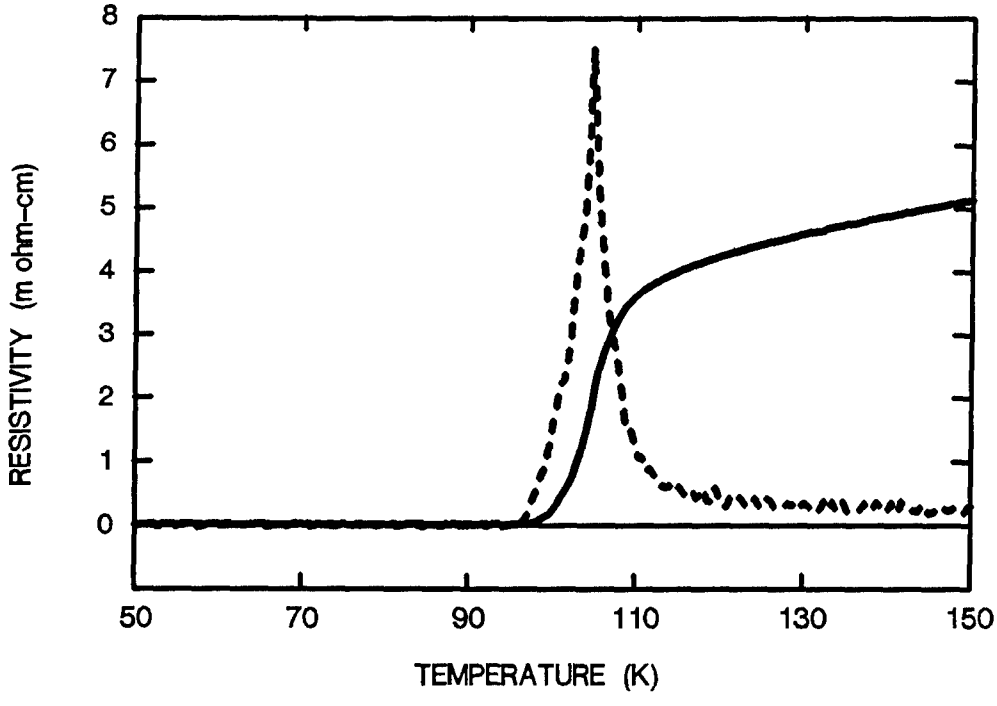


Figure 6 The resistivity of the Bi-Pb-Sr-Ca-Cu oxide, G3, as a function of temperature (heat treated at 850°C for 76 hours in air). The dashed curve is the dR/dT to show the transition temperature.

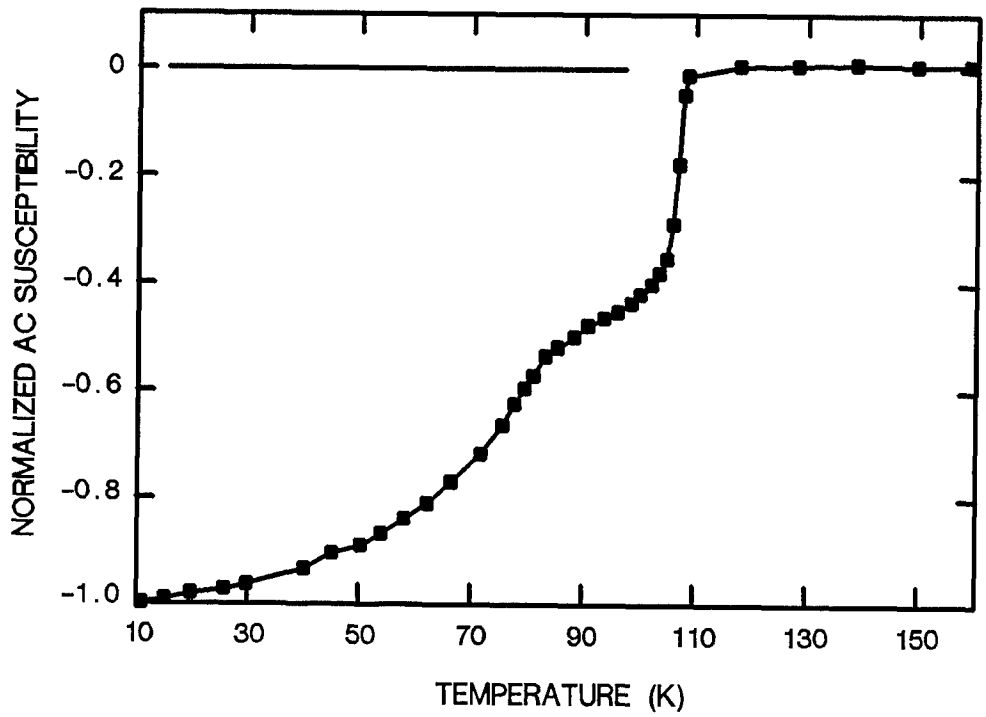


Figure 7. The ac susceptibility of the Bi-Pb-Sr-Ca-Cu oxide, G3, as a function of temperature (heat treated at 850°C for 76 hours in air).

ACKNOWLEDGEMENT

We like to acknowledge D. Kauffman for assistance in melting the glasses and R. Drew and D. Mathews for measuring the ac susceptibility.

REFERENCES

1. T.Komatsu, K.Imai, R.Sato, Jap. J. Appl. Phys., 27, L533, (1988).

2. T.Komatsu, R.Sato, and K.Imai, Jap. J. Appl. Phys., 27, L550, (1988).

3. F.H.Garzon, J.G.Beery, and I.D.Raistrick, Appl. Phys. Lett., 53, 805, (1988).

4. H. Zheng and J.D.Mackenzie, Phys. Rev., B38, 7166, (1988).

5. D.G.Hinks, L.Soderholm, D.W.Capone II, B.Dabrowski, A.W.Mitchell, D.Shi, 53, 423, (1988).

7. C. K. Chiang, S. W. Freiman, W. Wong-Ng, L. P. Cook, R. D. Shull and J. Shapiro,

Physica, C162-164, 901, (1989).

8. Winnie Wong-Ng, C. K. Chiang, S. W. Freiman, L. P. Cook, N. M. Hwang, and M. D. Hill, "High Temperarature Superconductors: Fundamental Properties and Novel Materials Processing", Mat. Res. Soc. Proc., 169, (1990).

9. W. Wong-Ng, C. K. Chiang, S. W. Freiman, L. P. Cook, N. M. Hwang, and M. D. Hill, Proc. First International Ceramic Science and Technology Congress, Anahem, CA., (Oct. 1990).

10. H.F.McMurdie, M.C.Morris, E.H.Evens, B.Paretzkin, W.Wong-Ng and C.R.Hubbard, Powder Diff., 1, 40, (1986)

COMPOSITE SUPERCONDUCTING WIRES OBTAINED BY HIGH-RATE TINNING IN MOLTEN Bi-Pb-Sr-Ca-Cu-O SYSTEM

A.D. Grosav, L.A. Konopko, N.I. Leporda
Institute of Applied Physics, Kishinev, 277028, USSR

ABSTRACT

Long lengths of metal-superconductor composites have been prepared by passing a copper wire through the bismuth-based molten oxide system at a constant speed. The key to successful composite preparation is the high pulling speed involved, which permits minimization of the severe interaction between the unbuffered metal surface and the oxide melt. Depending on the temperature of the melt and the pulling speed, a coating with different thickness and microstructure appeared. The nonannealed thick coatings contained a $Bi_2(Sr,Ca)_2Cu_1O_6$ phase as a major component. After relatively short time annealing at 800°C, both resistivity and initial magnetization-versus-temperature measurements show superconducting transitions beginning in the 110-115 K region. The effects of annealing and composition on obtained results are discussed.

INTRODUCTION

Bi-Sr-Ca-Cu oxide is one of the most promising high-T_c superconductors currently under investigation. Both stoichiometry and dopant impurities affect the electrical and magnetic properties to the point that Bi-Sr-Ca-Cu-O system can be either a near-insulator or a superconductor, whose transition temperature is well above 77 K. Partial substitution of Pb for Bi has been reported to be effective in obtaining zero-resistance temperatures, T_c^{off}, up to 112 K (1). A potential, low-cost alternative to classical Y-Ba-Cu oxide, Bi-Pb-Sr-Ca-Cu-O has many advantages--among them, a lower melting temperature. The latter is very important from a practical point of view.

The introduction of bismuth-oxide-based compounds into the superconducting industry requires the fabrication of the brittle materials into wires and tapes. Several groups have been able to obtain very good quality Pb-free Bi-Sr-Ca-Cu-O fibers with resistive transition comparable to those of $Bi_2Sr_2Ca_1Cu_2O_8$ bulk samples and with high critical current densities. The chosen preparation techniques having included a laser-heated pedestal growth method (2) and a micro-Czochralski method (3). However, it is highly desirable to be able to incorporate these oxides into the existent technology of metal-superconductor composites. The main obstacle to overcome in order to attain this goal is the choice of the proper metal for high-T_c composite fabrication. A number of studies have recently been made on the preparation of Bi-Pb-Sr-Ca-Cu-O superconducting composite wires and tapes by a standard sheathing method (4, 5). This processing technique involves a long annealing step (more than 8 hours) at high temperatures (typically reaching 850°C), which makes the sheathing method incompatible with most low-cost metals and alloys, and up until now, required for its utilization only high-cost, noble metals--usually silver.

Our basic aim was to produce long high-T_c superconducting composite wires with low-cost components in as simple a way as possible to facilitate useful applications in the future, which explains our choice of depositing Bi-Pb-Sr-Ca-Cu-O layers directly on copper wires by passing the wires through a bismuth-based molten oxide system. This deposition procedure is similar in a way to a tinning technique employed for the fabrication of metallic superconducting wires such as Nb_3Sn (6). Copper is a relatively inexpensive metal and is commonly used as a ductile matrix in various

composites. We report encouraging results (7) on Pb-free $Bi_1Sr_1Ca_1Cu_2O_x$ wires with unbuffered copper core (T_c^{off}=40-50 K). However, copper has proven to be an intractible core material due to the inevitable dissolution and diffusion of Cu into the envelope during the coating and annealing procedures. On the other hand, the communication about superconducting Pb-doped Bi-Sr-Ca-Cu-O glass ceramics (T_c^{off}=100 K) (8) having Cu content of higher-than-ideal composition (9, see also 10) gave some hope that Cu wires could be used in the case when the source of melt has a stoichiometrical chemical formula of $(Bi,Pb)_2Sr_2Ca_2Cu_3O_x$.

EXPERIMENTAL PROCEDURE

Commercial powders of Bi_2O_3, PbO, $SrCO_3$, $CaCO_3$ and CuO were mixed at the nominal cation ratio Bi:Pb:Sr:Ca:Cu=1.5:0.5:2:2:3, then ground and calcined at 800°C for 24 hours. The product was reground and then cold-pressed under 8 kBar into a rod (8 mm diameter, 16 mm long). After sintering at 860°C for 150 hours in air, the rod was held at 800°C for 24 hours and subsequently air cooled to room temperature. The zero-resistivity transition temperature of the ceramic rod was around 70 K. Available polycrystalline copper wires with diameters from 100 to 400 μm and lengths from 0.5 to 1 m were used for preparing metal-superconductor composites in this study.

The ceramic rod was vertically suspended and was heated above 900°C in order to form a small molten zone ($\leq$ 100 mm^3) at the bottom part. A copper wire, moving at a constant speed, was passed through the narrow molten zone. The copper wire was not intentionally heated. In a molten state, the Bi-based oxide system is a viscous liquid and it has a strongly pronounced ability to spread on copper wire surfaces. LeBeau et al. (11) reported that the Bi-Sr-Ca-Cu-O melt showed a favourable viscosity-temperature profile for practical shaping during solidification. Although in our case, the melt temperature was not directly measured, it is believed to be above 900°C and below 1000°C. Moreover, the real melt temperature was found to vary with the diameter of the copper wire and the speed of its pass. The pass speed of the copper wire has been chosen as a compromise between an adhesion of the melt and a short residence time of the wire in the liquid zone. The residence time was estimated by dividing the measured width of the molten zone by the value of pulling speed (~5-15 cm/s). Residence times thus calculated were less than 0.1 s. Because of a very short time during which the wire surface and the melt are in direct contact, they seem to contact without disastrous effects in the coating composition due to copper dissolution and diffusion--at least for thick coatings. The realization of the given method of high-rate tinning using a simple laboratory-manufactured technique allowed us to make the long, cylindrical composite wires consisting of the copper in a dense envelope with uniform (to the unaided eye) thickness. Solidified coating thicknesses (h) were typically from 5 to 50 μm.

The microstructures of the coatings were examined by optical and scanning electron microscopes. Most of the electrical and magnetic measurements have been performed with wires having textured coatings (see below). Resistance-versus-temperature curves of the composite wires were measured using a standard DC four-terminal method. Voltage and current probes were attached to the coating surface with silver paste. The sample was 20 mm long and the distance between voltage contacts was about 5 mm. Comparison of 2- and 4-probe resistivities demonstrated ~10 Ω contact resistances. Magnetization measurements were performed using a SQUID magnetometer.

RESULTS AND DISCUSSION

The morphology and electrical properties of the envelopes appear to be highly dependent upon thickness and the parameters of the coating procedure (molten zone temperature, pulling speed, copper wire diameter), perhaps resulting from different solidification rates. The composite wires

with thin cores obtained at the highest possible pulling speeds have a smooth coating surface characteristic for amorphous materials (Figure 1) and good flexibility. For example, composite wire with h≅10μm (h/d≅0.05) sustained bending on a 30-mm-diameter bobbin (Figure 2) without breaking. The thicker coatings are composed of densely connected crystallites that are very often overlapping each other. Figure 3 shows a scanning electron micrograph (SEM) of a surface of the coating with a 25-μm thickness and an average crystallite size of several tens of microns. The majority of crystallites are oriented with their basal planes almost parallel to the core axis. It was observed that the size and degree of alignment of the crystallites decreases with pulling speed and distance from the outer coating surface.

As a rule, the thicker the coating, the smaller its resistivity. However, all of the coatings possessed nonmetallic properties. According to X-ray diffraction (XRD) studies, the nonannealed coatings contained a $Bi_2(Sr,Ca)_2Cu_1O_6$ phase,* as a major component, and exhibited 0-1-1 texture. Some of the X-ray peaks belong to CuO and Cu_2O. The average composition of the coatings was found to deviate from the starting nominal composition, becoming Cu-rich and (Bi,Pb)-deficient. Nevertheless, sometimes only several minutes in a post-annealing treatment were necessary to obtain a coating with metallic resistivity.

The pieces of composite wire about 50 mm long were annealed in a tube furnace in air at temperatures from 500°C to 800°C. The furnace was heated to the annealing temperature and wires were inserted into the furnace. After the desired annealing time, the wires were quenched to room temperature by removing them from the furnace as fast as possible. Sufficiently high annealing temperature was found to be a decisive factor in obtaining superconductivity; the wires annealed at temperatures below 750°C remained semiconducting.

Figure 4 shows the temperature dependencies of resistance and its derivative, dR/dT, for the composite wire annealed at 800°C for 40 minutes. The outer wire diameter and the thickness of the coating were about 450 and 30 μm, respectively. The midpoint of the transition is designated as T_c^{mid} and in present work, corresponds to the point where the curve dR/dT versus T has a maximum. Offset (T_c^{off}) and onset (T_c^{on}) of the transition are defined as the temperatures corresponding to the achievement of zero resistance, R(I=10 μ Å)=0, and to the deviation from linear of the dR/dT - T plot. In the case of the sample that was annealed for 40 minutes, T_c^{on}, T_c^{mid} and T_c^{off} are 110.0, 75.5, and 69.5 K, respectively.

Figure 5 shows changes in T_c^{off}, T_c^{mid} and T_c^{on} with annealing time, t, for composite wires annealed at 800°C. One can see that relatively high critical temperatures can be easily attained for short annealing times (less than 40 minutes). The value of T_c^{off} (t=10 minutes)=62.5 K, which is higher than we have previously reported (7). T_c^{off} = 45 K for annealing at 800°C for 10 minutes, using Pb-free Bi-Sr-Ca-Cu-O composite wire with copper core, indicating that Pb doping strongly contributes to increasing the volume fraction of the superconducting phase, even for a relatively rapid thermal annealing. The critical temperatures are observed to gradually increase with time (Figure 5), however, when the duration of annealing is beyond 60 minutes, T_c^{off} begins to quickly decrease (not shown here), making the superconducting transitions broader due to the diffusional effects. Besides

* Sometimes the X-ray peaks of the thick coatings may be assigned as a mixture of two tetragonal crystalline lattices with a≅5.36 Å, c≅24.40 Å; and a≅5.60 Å, c≅25.86 Å, where the former lattice corresponds to the "pure" $Bi_2Sr_2Cu_1O_6$ phase. We think that both phases are crystallized together due to a stacking disorder caused by a compositional fluctuation in the melt around the moving copper wire.

that, during long annealing, microcracks are introduced in the coating. These results indicate that there may be a clearly optimum annealing time.

Magnetization-versus-temperature curves of the composite wire annealed at 800°C for 20 minutes are shown in Figure 6. Both the zero-field-cooled (ZFC) and field-cooled (FC) magnetizations were obtained with the magnetic field parallel to the core axis. Because of the small coating volume, a fairly large magnetic field (H=65 G) was required to obtain a good signal-to-noise ratio. The ZFC data revealed diamagnetization below 110 K. This result is consistent with that of resistance measurements (Figure 5).

Magnetization measurements and studies on the annealing process by X-ray diffraction analyses indicate that the $Bi_2(Sr,Ca)_2Cu_1O_6$ phase formed during coating solidification is converted to the $Bi_2Sr_2Ca_1Cu_2O_8$ phase ($a \cong 5.4$ Å, $c \cong 30.6$ Å) during the annealing at 800°C. After 40 minutes, no peaks corresponding to the $Bi_2(Sr,Ca)_2Cu_1O_6$ phase were observed in the X-ray diffraction scans, although the coating did contain large amounts of CuO and (Bi,Pb)-free (Sr,Ca)-Cu-O compounds. At the same time, the broad tail in ZFC magnetization above 85 K suggests the presence of the $Bi_2Sr_2Ca_2Cu_3O_{10}$ phase as well. Note that since the annealing was carried out at 800°C, only a very small amount of $Bi_2Sr_2Ca_2Cu_3O_{10}$ phase can be formed (12).

The surface of 800°C-annealed coatings (Figure 7) is covered with granular particles of several microns of average diameter, and the original crystallite surfaces became roughened. It seems that after rapid cooling from the melt, (Sr-Ca)-Cu-O was in the glassy state, and that it became crystalline when the sample was annealed. The SEM observations, however, clarified within their degree of resolution that no apparent change occurred in the bulk part of the coatings by annealing at 800°C. Further details are under investigation.

CONCLUSION

In summary, we have shown that composite wires with ductile cores can be obtained by passing a copper wire through the molten Bi-Pb-Sr-Ca-Cu-O system at a high speed. Depending on the pulling speed and the viscosity of the melt, a different coating microstructure with different crystallite sizes appeared. After isothermal annealing at 800°C in air for 20-40 minutes, composite wires with textured coatings exhibited superconductivity onsets above 100 K and zero resistance in the range of 65-70 K. We expect that some improvements in superconductivity properties may be possible by optimizing the annealing conditions in air, or by conducting the heat treatment in a vacuum-sealed system or under low oxygen pressures, where the melting temperature is lowered and, respectively, superconducting phase formation is enhanced (13, 14). This appears to be especially important for the composites.

According to preliminary energy-dispersive X-ray analyses, the coating composition shifts from the starting nominal composition, becoming Cu-rich and (Bi,Pb)-deficient. Considering the origin of core materials and the high evaporation rates of Bi and Pb from the molten zone during coating procedures, these results are reasonable. Taking the latter into account (i.e., the reduction of the Bi and Pb contents in the solid-state coating), the pieces of as-prepared composite were coated thickly with molten binary alloy (Bi:Pb=1.5:0.5), and later annealed with the same heat treatment used for the wires as described above. For composite wires coated with Bi-Pb alloy, the values of T_c^{on} were gathered in the region of 77 K (Figure 8 presents one of the resistance measurements), which is almost 10 K higher than the maximum T_c^{on} for the (Bi,Pb)-poor coatings (Figure 4). Therefore, though the conditions for the coating and annealing processes have not been optimized yet, one may assume that



Figure 1. Scanning electron micrograph of the 200-μm-diameter metal wire after it had been rapidly coated with the molten Bi-Pb-Sr-Ca-Cu-O oxide. It can be seen that the thin coating is dense and has a fairly smooth surface. The bar represents 100 μm.

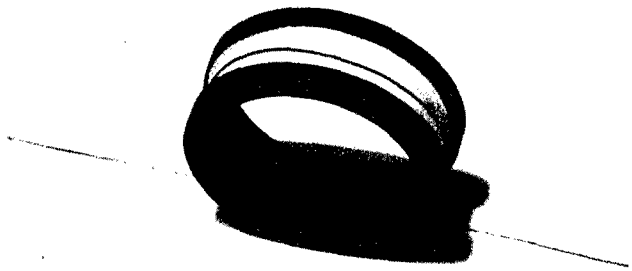


Figure 2. Bi-Pb-Sr-Ca-Cu-O composite wire of the type illustrated in Figure 1 bent on a 30-mm-diameter bobbin.



Figure 3. Scanning electron micrograph showing surface of as-prepared Bi-Pb-Sr-Ca-Cu-O composite wire with 25- μm coating thickness and 400-μm core diameter. The bar represents 200 μm.

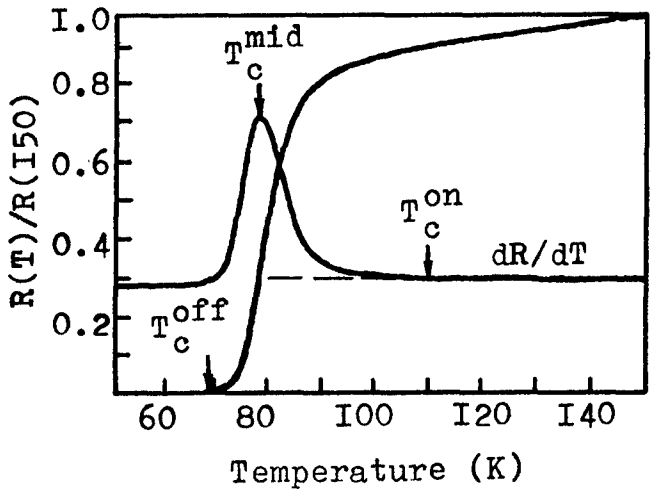


Figure 4. Temperature dependences of the relative resistivity, R(T)/R (150), and derivative of the resistance, dR/dT, for composite wire annealed at 800°C for 40 minutes.

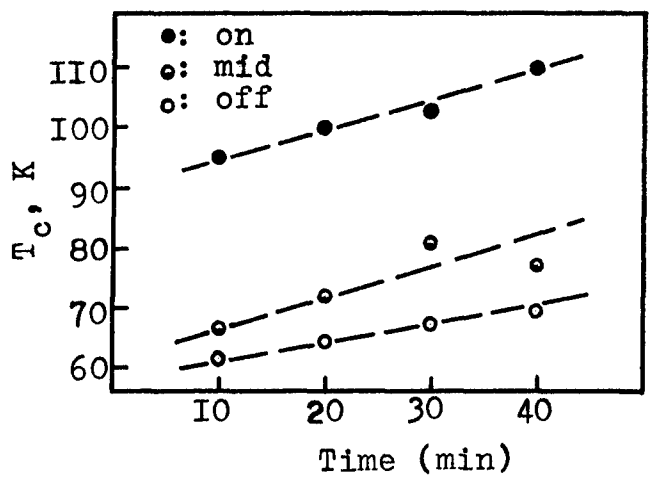


Figure 5. Changes in T_c^{off}, T_c^{mid}, and T_c^{on} with annealing time for composite wires annealed at 800°C.

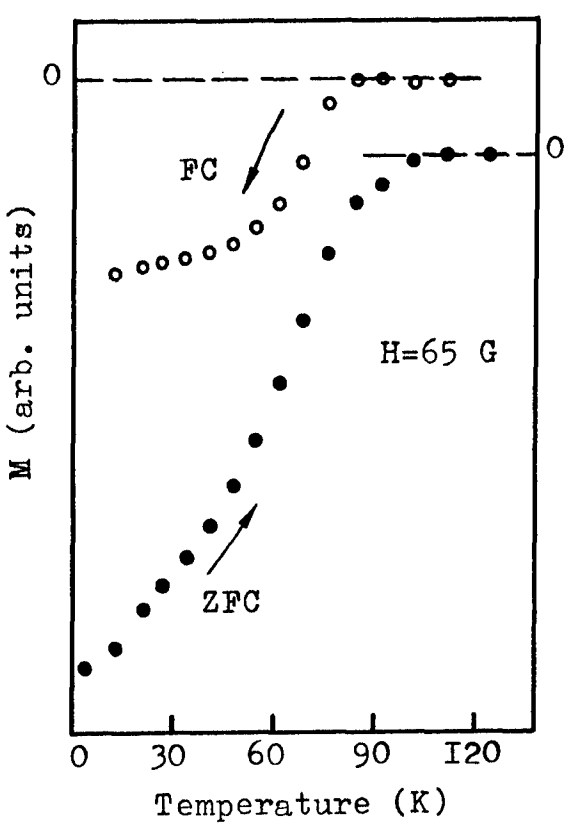


Figure 6. The dc magnetization as a function of the temperature for the composite wire annealed at 800°C for 20 minutes in air.



Figure 7. Scanning electron micrograph of the composite wire annealed at 800°C for 30 minutes. The bar represents 200 μm.

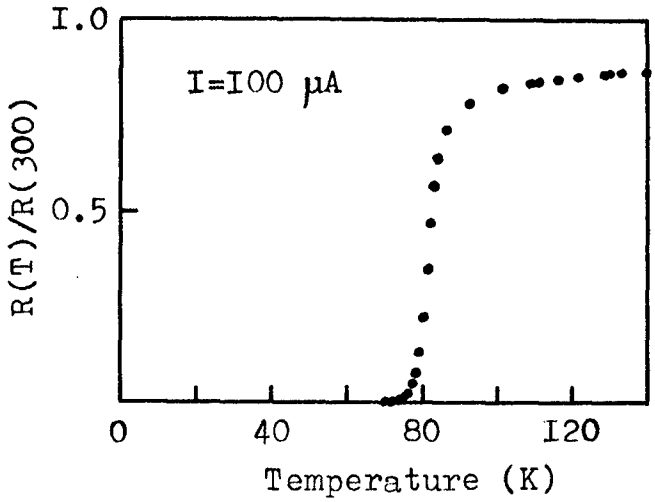


Figure 8. Superconducting transition curve of a Bi-Pb-Sr-Ca-Cu-O composite wire heat-treated with coated Bi-Pb alloy.

for the fabrication of composite wires with improved superconducting properties (especially to obtain the $Bi_2Sr_2Ca_2Cu_3O_{10}$ phase in appreciable proportion), it is necessary to use starting material with a nonstoichiometric composition having an excess of Bi and Pb, a lack of Cu, and probably, the addition of Ca.

ACKNOWLEDGMENTS

The authors would like to acknowledge D.V. Gitsu, F.M. Muntianu and V.G. Kantser for continuous encouragement and helpful discussions. We also wish to thank G.I. Panaitov for taking the magnetization measurements, and A.I. Socolovsky, Y.G. Soltanovsky, G.F. Volodina and M.I. Onu for technical assistance.

REFERENCES

1. Togano, K. H. Kumakura, and D.R. Dietderich, 1989, "Critical currents and magnetic properties of Bi- and Tl-based new high T_c superconductors," Cryogenics, **29**, 3A, pp. 286-290.

2. Feigelson, R.S., D. Gazit, D.K. Fork, and T.N. Geballe, 1988, "Superconducting Bi-Ca-Sr-Cu-O fibers grown by the laser-heated pedestal growth method," Science, **240**, pp. 1642-1645.

3. Kurosaka, A., M. Aoyagi, H. Tominaga, O. Fukuda, and H. Osanai, 1989, "Superconducting Bi-Sr-Ca-Cu-O crystalline fibers prepared by the micro-Czochralski method," Applied Phys. Lett., **55**, 4, pp. 390-392.

4. Sekine, H., K. Ogawa, K. Inoue, H. Maeda, and K. Numata, 1989, "Metallurgical studies and optimization of critical current density in Bi-(Pb)-Sr-Ca-Cu-O superconductors," Jap. J. Appl. Phys., **28**, 7, pp. 1185-1188.

5. Hikata, T., T. Nishikawa, H. Mukai, K. Sato, and H. Hitotsuyanogi, 1989, "Electromagnetic properties and morphology of Ag-sheathed Bi-Pb-Sr-Ca-Cu-O superconducting wires," Jap. J. Appl. Phys., **28**, 7, pp. L1204-L1206.

6. Savitsky, E.M., 1981, "Phisico-himicheskie osnovy poluchenya sverhprovodyaschih materialov," Metallurgia, Moscow, pp. 193-218 (in Russian).

7. Grozav, A.D., L.A. Konopko, and N.I. Leporda, 1989, "Superconducting composite wires prepared by high-rate tinning in molten Bi-Sr-Ca-Ca-Cu-O system," Pis ma Zh. Techn. Fiz. *(Sov. Techn. Phys. Lett.)* **15**, 19, pp. 1-5.

8. Komatsu, T., R. Sato, K. Imai, K. Matusita, and T. Ymashita, 1989, "High-T_c superconducting glass ceramics based on the Bi-Ca-Sr-Cu-O system," IEEE Trans. Magn., **25**, 2, pp. 2150-2153.

9. Statt, B.W., Z. Wang, M.J.G. Lee, J.V. Yakhmi, P.C. deCamargo, J.F. Major, and J.W. Rutter, 1988, "Stabilizing the high-T_c superconductor $Bi_2Sr_2Ca_2Cu_3O_{10+x}$ by Pb substitution," Physica C, **156**, 2, pp. 251-253.

10. Zhu, W., M.M. Miller, P.A. Metcalf, and H. Sato, 1989, "Preparation of superconducting films of Bi-Sr-Ca-Cu oxides by in-situ melting, " II. Materials Letters, **8**, 9, pp. 340-342.

11. LeBeau, S.E., J. Righi, J.E. Ostenson, S.C. Sanders, and D.K. Finnemore, 1989, "Preparation of superconducting Bi-Sr-Ca-Cu-O fibers," Appl. Phys. Lett., **55**, 3, pp. 292-294.

12. Nishi, Y., S. Moriya, and T. Manabe, 1989, "Effect of annealing on T_c of liquid-quenched $Bi_{0.7}Pb_{0.3}SrCaCu_{1.8}O$," J. Appl. Phys., **65**, 6, pp. 2389-2391.

13. Oka, Y., N. Yamomoto, A. Yuba, H. Kitaguchi, and J. Takada, 1988, "Crystal phases of $BiSrCaCu_2O_x$ heat treated in a vacuum-sealed system," Jap. J. Appl. Phys., **27**, 8. pp. L1429-L1431.

14. Endo, U., S. Koyama, and T. Kawai, "Preparation of the high-T_c phase of Bi-Sr-Ca-Cu-O superconductor," Jap. J. Appl. Phys., **27**, 8, pp. L1476-L1479.

LOW FREQUENCY ELECTRICAL NOISE ACROSS CONTACTS BETWEEN A NORMAL CONDUCTOR AND SUPERCONDUCTING BULK $YBa_2Cu_3O_7$

J. Hall and T.M. Chen

Noise and Reliability Research Lab, Electrical Engineering Department
University of South Florida, Tampa, Florida 33620

Abstract– Virtually every practical device that makes use of the new ceramic superconductors will need normal conductor to superconductor contacts. The current-voltage and electrical noise characteristics of these contacts could become important design considerations. This paper presents I–V and low frequency electrical noise measurements on contacts between a normal conductor and superconducting polycrystalline $YBa_2Cu_3O_7$. For small current densities, current through the contacts was found to be proportional to $V^{1.7}$. The voltage spectral density, $S_V(f)$, very closely followed an empirical relationship given by, $S_V(f) = C(V_cR_c)^2/f$, where V_c is the DC voltage across the contact, R_c is the contact resistance, f is frequency, and C is a constant found to be $2 \times 10^{-10}/\Omega^2$ at 78° K. This relationship was found to be independent of contact area, contact geometry, sample fabrication technique, and sample density.

INTRODUCTION

In the past few years the discovery of new high-transition temperature (high-T_c) superconductors has led to an abundance of research on the fundamental properties of these materials. For practical devices to be constructed from these materials the electrical contacts to the superconductor need to be investigated. Several researchers have investigated the theoretical[1,2] and experimental[3,4,5] characteristics of normal metal to low-temperature superconductors. The normal metal to bulk superconducting $YBa_2Cu_3O_7$ contact is of particular importance because the material is not a traditional metal. One method of investigation is the current–voltage (I–V) characteristics of the contact. This information is needed for device work if the contact resistance is not a constant. Another important tool in investigating materials and junctions is noise measurement. Noise measurements can be used to define the minimum sensitivity of a device as well as illuminate physical processes occurring in a material or junction. The Noise and Reliability Research Laboratory at the University of South Florida has been investigating the noise characteristics in $YBa_2Cu_3O_7$ superconductors since these materials were discovered.

In this paper, we investigate the current–voltage and noise characteristics of the normal–superconductor (N–S) contacts at liquid nitrogen (LN_2) temperatures for several contacts of different geometries and contact resistances. The noise experiments lead to an important empirical formula for predicting the noise voltage in an N–S contact.

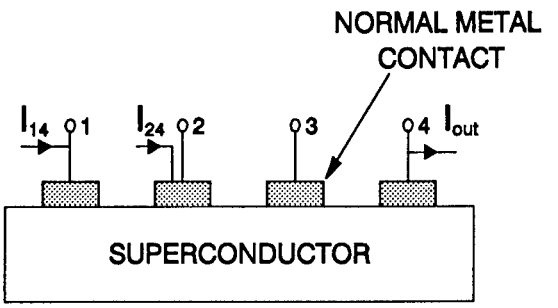


Figure 1: Typical sample contact configuration for normal metal (Ag) to superconductor (bulk $YBa_2Cu_3O_7$) junction.

EXPERIMENTAL METHODS

For this experiment, the $YBa_2Cu_3O_7$ bulk samples used were of three different densities (4.44, 4.46, and 5.02 g/cm^3) and two different fabrication techniques: oxalate precipitation (OP) and solid–state reaction (SSR). All the samples had transition temperatures around 90K and were verified to be deep within the superconducting region at the experimental temperatures (78K).

Each sample consisted of at least four contacts with a typical contact configuration show in figure 1. The contacts made to these samples were made in the following manner. The bulk $YBa_2Cu_3O_7$ surface was sanded with very fine grain sandpaper to remove any of the exposed surface which may have oxidized. It was then ultrasonically cleaned for two minutes in a 100% ethyl

Table 1: Parameters for the 5 different contacts used in this investigation.

Samp no.	Samp name	Dens g/cm^3	Area mm^2	Contact shape	Contact no.	Max Res (Ω)
1	Trak	4.46	15	Rect	1	1.1
2	Trak	4.46	15	Rect	2	0.65
3	Trak	4.46	15	Rect	4	2.5
4	Fsu25	5.07	12	Semicr	1	0.91
5	Fsu26	4.44	7	Circ	2	1.6

alcohol bath. The contact mask was then fastened to the sample and it was then sputtered with a 300 nm layer of gold–palladium (AuPd). The AuPd pads were then covered with silver epoxy and silver coated wires were pressed into the epoxy. The epoxy was cured at 180°C for 1 hour. These contacts usually yielded a contact resistance between 0.5–2.5Ω for a 0.25 cm^2 area contact. Table 1 shows the various parameters for the sample contacts used.

The samples were then wired and connected to the measurement equipment. Each sample was suspended about 1 inch above the LN_2 level in a 3-liter MVE dewar. The temperature at this level was 78K and was found to remain constant for at least 12 hours. The sample was first connected to verify superconductivity in the region to be measured. Refering to figure 1, the current was passed from 1 through 4 and the voltage was checked across contacts 2 and 3 for zero resistance. After superconductivity was verified, the current is passed from 2 to 4 and the voltage is measured across contacts 2 and 3. Since the bulk material in that region was already found to have no resistance or noise, any resistance or noise generated must come from the junction between the normal metal at contact 2 (now current carrying) and the superconducting $YBa_2Cu_3O_7$. The sample contact was then subjected to I–V measurements. The contacts were connected to a Keithley Constant Current Source with a Keithley Nanovoltmeter for reading the contact voltage (V_c). The measurement equipment was controlled by a PC-compatible computer with software written for this experiment. The noise measurement system was constructed as shown in figure 2. The system consisted of a DC biasing circuit consisting of 2–12V gel cells connected in parallel and various wirewound resistors for selecting different bias currents through the sample contact. The current flowing in the system was measured by reading the voltage across V_s and dividing by R_{control}.

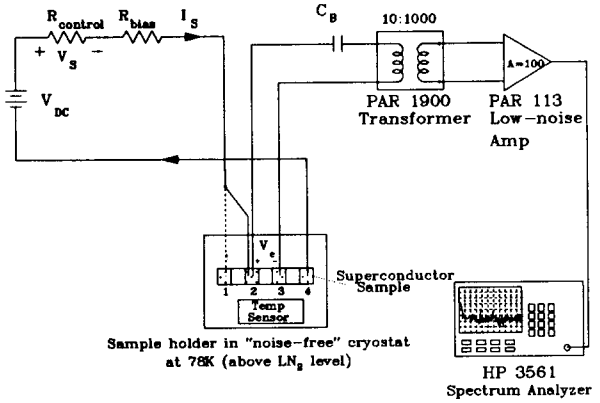


Figure 2: Experimental apparatus for contact noise measurements.

The R_{bias} resistor was used to adjust the biasing current in the system. The current was passed through contact 2 to contact 4. The blocking capacitor, C_B, was used to block DC current from magnetizing PAR-1900 transformer. The PAR-1900 transformer was connected from the 10:1000 turns ratio giving a gain of 100 through the transformer. It was connected to a PAR-113 Low–noise Amplifier with the gain set at 100. This combination of the transformer and amplifier gave an overall gain of 10 000. The HP 3561 Spectrum Analyzer was used to collect the noise traces. The traces were collected in the low-frequency region of 1–51 Hz with 25 averages per trace to yield more than sufficient resolution.

Excess noise checks were made at various stages of the experiment to assure that the noise measured was coming from the N–S contact and not an element of the measurement system. Also the silver epoxy was tested and showed no excess noise.

RESULTS AND DISCUSSION

I. Current–voltage experiments

The results obtained for the I–V relationship of these contacts were a little surprising. These contacts showed a decreasing resistance as the voltage across the contact increased. This same effect was observed by Van Schevicoven and De Waele [6] for bulk point contacts between a normal metal and high-T_c superconductor. Moreland, et al[7], also found similar results in break junctions in a bulk $YBa_2Cu_3O_7$ sample. Figure 3 shows a typical I–V curve for the bulk contacts used in this investigation. The figure shows the parabolic nature of the curve as well as the symmetry in both the positive and negative voltage regimes. The parabolic shape of the curve was common for all the contacts investigated and led to an

Reproduced From
Best Available Copy

Table 2: Experimental results of current–voltage measurements.

Sample number	A	λ	Zero-bias Res. (Ω)
1	9.57	1.68	1.1
2	13.8	1.76	0.65
3	3.47	1.66	2.5
5	3.34	1.57	1.6

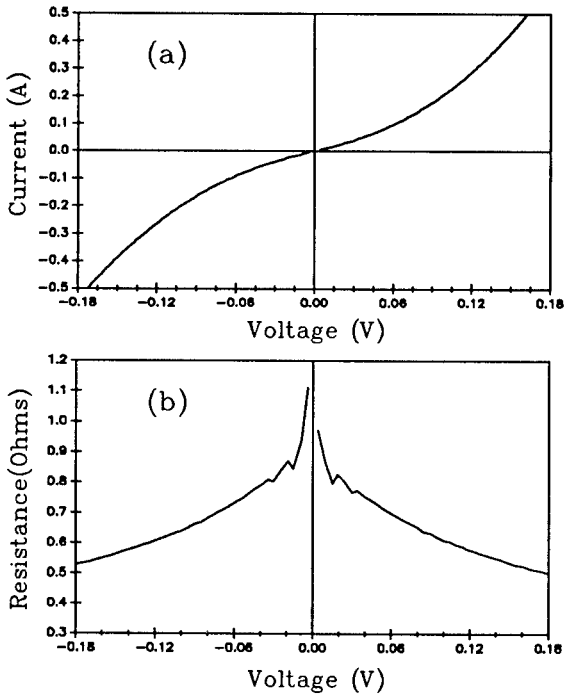


Figure 3: Typical electrical characteristics of a normal metal–superconducting $YBa_2Cu_3O_7$ contact; (a) Current–Voltage graph; (b) Resistance–Voltage graph.

empirical formula

$$I = AV_c^{\lambda} \tag{1}$$

where I is the current flowing through the contact, V_c is the voltage across the contact, A is a constant related to the resistance of the sample, and λ is a power factor which is around 1.7 for the samples tested. Table 2 gives the A and λ values for the various contacts used in this investigation. Van Schevicoven and De Waele attribute this parabolic behavior to normal electron tunneling between the normal metal contact to high–T_c superconductor.

II. Noise experiments

The noise measurements were taken over a 0.1 to 30 mV bias voltage range for the five contact samples. The noise traces were dumped from the HP 3561 into a lab computer where they were analyzed using a least-squares line fitting method to determine the slope as a function of frequency. All the noise traces were "$1/f$ noise" where "$1/f$ noise" is defined as noise proportional to $1/f^{\alpha}$ where α ranges between 0.8 and 1.2. After this data was analyzed, the value of each trace at 10 Hz was recorded and compared to the bias voltage, current, resistance, and other parameters. All the experimental noise current spectral densities were found to follow an empirical formula. Figure 4 shows the plot of the noise current spectral density ($S_I(f)$ or $S_V(f)/R_c^2$) vs. the contact voltage (V_c) for the five sample contacts used. The log $S_I(f)$ vs log V_c forms a straight line for which all the data collected lies in close proximity. The empirical formulas for the noise voltage spectral density and the noise current spectral density, respectively, are

Table 3: Contact noise measurement results for the equation $S_V(f) = CV^{\beta}R^2/f$.

Sample number	Zero-bias Res (Ω)	C ($1/\Omega^2$)	β for V^{β}
1	1.1	2.1×10^{-10}	1.90
2	0.65	3.3×10^{-10}	2.06
3	2.5	2.1×10^{-10}	1.98
4	0.91	1.6×10^{-10}	1.90
5	1.6	7.8×10^{-11}	1.98
Empirical formula	—	2.0×10^{-10}	2.00

$$S_V(f) = \frac{C(V_cR_c)^2}{f} \tag{2}$$

$$S_I(f) = \frac{CV_c^2}{f} \tag{3}$$

where C is an empirical constant found to be approximately $2 \times 10^{-10}/\Omega^2$, V_c is the contact voltage, R_c is the contact resistance, and f is the frequency. Table 3 shows the experimental values of C for the various contacts. The noise which was measured in the contacts was very different from the results found in bulk $YBa_2Cu_3O_7$ which has been reported by several experimenters[8,9,10]. The implications of this empirical equation are that the noise voltage spectral density can be predicted by measuring the contact resistance which may be of great advantage when practical devices are to be fabricated from high–T_c materials.

CONCLUSIONS

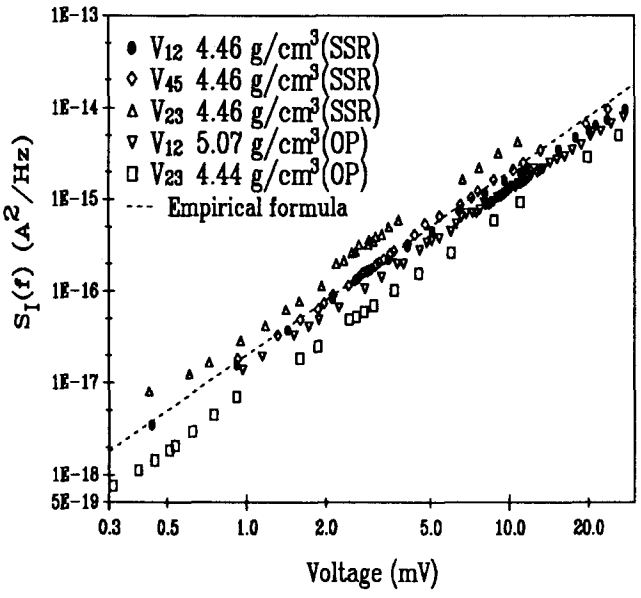


Figure 4: Graph of noise current spectral density ($S_I(f)$ or $S_V(f)/R^2$) for normal metal–superconducting $YBa_2Cu_3O_7$ contacts. The dotted line shows the empirical formula obtained from the data.

Five normal metal–superconducting $YBa_2Cu_3O_7$ sample contacts were thoroughly studied for their current–voltage and noise characteristics. The I–V measurements led to an empirical formula, $I = AV^\lambda$, to describe the parabolic relationship between I and V. The noise measurements yielded an empirical equation of the form, $S_V(f) = C(V_cR_c)^2/f$, which describes the noise voltage spectral density for a contact with resistance, R_c, and voltage, V_c.

The N–S contact characteristics are very important and need to be thoroughly understood for any practical device made from superconducting $YBa_2Cu_3O_7$. The noise limits the sensitivity of any device and since the superconductor itself yields no measurable noise in the superconducting region, the normal metal contact noise would most likely be the source of excess noise in such a device.

This work was partially supported by DARPA Superconductivity Grant No. MDA 972-88-J-1006. The authors wish to thank Dr. H. Hickman and Dr. A.J. Dekker for their help in preparing and performing the experiments presented in this manuscript.

REFERENCES

1. V.A. Khlus, "Current and voltage fluctuations in microjunctions between normal metals and superconductors," Sov Phys JETP, **66**, 1243, (1987).

2. W.L. McMillan, "Theory of Superconductor–Normal-metal Interfaces," Phys Review, **175**, 559, (1968).

3. G.E. Blonder, M. Tinkham, T.M. Klapwijk, "Transition from metallic to tunneling regimes in superconducting microconstrictions: Excess current, charge imbalance, and supercurrent conversion," Phys Rev B, **25**, 4515, (1968).

4. F. Bedard, H. Meissner, "Measurements of Contact Resistance between Normal and Superconducting Metals," Phys Review, **101**, 26, (1956).

5. T.Y. Hsiang, J. Clarke, "Boundary resistance of the superconducting-normal interface," Phys Rev B, **21**, 945, (1980).

6. H.J. Van Schevicoven, A.Th.A.M. De Waele, "Tunneling Characteristics of Point Contacts with High–T_c Material," Physica C, **164**, 1055, (1989).

7. J. Moreland, et al, "Break-junction tunneling measurements of the high-T_c superconductor $YBa_2Cu_3O_7$," Phys Rev B, **35**, 8856, (1987).

8. H. Hickman, T.M. Chen, W.J. Wallace, S.T. Liu, "Low Frequency Electrical Noise in Bulk $YBa_2Cu_3O_7$," Proceedings of the 1989 SOUTHEASTCON, **3**, 1057, (1989).

9. B.W. Ricketts, R. Driver, H.K. Welsh, "Low Frequency Excess Noise in Bulk $YBa_2Cu_3O_7$ Samples," Sol St Comm, **67**, 133, (1988).

10. J.A. Testa, et al, "$1/f$–noise–power measurements of copper oxide superconductors in the normal and superconducting states," Phys Rev B, **38**, 2922, (1988).

Reproduced From
Best Available Copy

SUPERCONDUCTIVITY IN 2-2-3 SYSTEM $Y_2Ba_2Cu_2O_{8+\delta}$

H.H. JOSHI, G.J. BALDHA,, R.B. JOTANIA, S.M. JOSHI, H. MOHAN,
P.B. PANDYA, H.N. PANDYA and R.G. KULKARNI

Department of Physics, Saurashtra University
RAJKOT-360 005, INDIA

We have synthesized a new high-Tc 2-2-3 superconductor $Y_2Ba_2Cu_3O_{8+\delta}$ by a special preparation technique and characterized it by ac-susceptibility measurements. Diamagnetism and Meissner effect sets in at low fields and superconducting transition onsets at 90 K. The systematic investigation of the real and imaginary components of ac-susceptibility as a function of temperature and applied ac magnetic field reveals that the magnetic behaviour is that of granular-type superconductor.

INTRODUCTION

In general, in the high-Tc granular bulk superconductors it is necessary to distinguish between the superconducting properties of unconnected "grains" and the "bulk" of grains connected through Josephson junctions. AC susceptibility measurements as a function of temperature and magnetic field allow observation of this double behaviour.

No attempt has been made to synthesize and observe superconductivity in 2-2-3 type systems except for our most recent communication (1) of superconductivity in a new 2-2-3 type system $Y_2Ba_{1.5}Ca_{0.5}Cu_3O_{8+\delta}$ by ac-susceptibility and resistivity measurements. In this paper, we report the synthesis and the characterization of another new 2-2-3 superconductor $Y_2Ba_2Cu_3O_{8+\delta}$. Superconductivity in $Y_2Ba_2Cu_3O_{8+\delta}$ (2-2-3) was identified by the systematic measurements of the real and imaginary (lossy) components of ac-susceptibility as a function of temperature and applied ac field.

EXPERIMENTAL

Samples of nominal composition $Y_2Ba_2Cu_3O_{8+\delta}$ were prepared from the appropriate amounts of the finely ground mixed Y_2O_3, $BaCO_3$ and CuO (all 99.9% purity). The mixed powders were pressed into pellets of 1-cm diameter and .2-cm thickness under a pressure of 25 KPSi. We have devised a special technique of sample preparation known as rapid thermal processing (RTP) treatment which is described in detail elsewhere (2). According to this technique 2-2-3 pellets were introduced in a preheated furnace at 950°C and fired for two hours in closed condition. Then the top of the furnace was opened to air for half an hour at 950°C and the samples were rapidly cooled to room temperature. The cooled samples were recycled once more as above. Thus, 2-2-3 samples require two-step processing.

X-ray diffraction data were obtained at room temperature using a Philips PW1820 powder diffractometer with FeKα radiation. X-ray diffraction (Fig. 2) showed single phase for 2-2-3 samples. The real (X') and imaginary (X") components of the ac-susceptibility of a sintered $Y_2Ba_2Cu_3O_{8+\delta}$ were measured as a function of temperature (4.2K to 128K) for different ac field amplitudes (24A/m to 2400A/m or 0.3 Oe

to 30 Oe) at a frequency of 100Hz. In these measurements the samples were first zero-field cooled to liquid helium temperature and then measured in applied ac fields during the warming run.

RESULTS AND DISCUSSION

All observed X-ray powder diffraction peaks of $Y_2Ba_2Cu_3O_{8+\delta}$ can be accounted for by an orthorhombic unit cell of a=4.0314 (11) Å, B=3.7202 (8) Å and c=13.338 (5) Å crystallographically. The observed X-ray diffraction pattern of this new superconducting compound is compared with the corresponding computer X-ray diffraction spectra obtained employing the refined unit cell constants and the atomic fractional coordinates assuming space group symmetry Pmmm. A very good agreement is found between the observed and computed X-ray spectra confirming that the atomic arrangement is of a simple perovskite-type belonging to the orthorhombic Pmmm space group. From a comparison of lattice parameters of 1-2-3 (3.4) with the present 2-2-3, it is evident that a and c parameters have respectively increased by 0.21 Å and 1.68 Å. Moreover, the unit cell volume of 1-2-3 is 173.7 $Å^3$ (3.4) and that of 2-2-3 is 200.2 $Å^3$. These observations indicate that the excess "Y" in 2-2-3 is responsible for the expansion of the unit cell and possibly additional "Y" is located along the c axis. The temperature dependence of both the real (X') and imaginary (X") of the ac-susceptibility data measured at 100Hz and in applied ac fields 0.3 Oe, 3.0 Oe and 30.0 Oe is shown in Fig. 2. As observed from X'(T) data in Fig. 2, the sample $Y_2Ba_2Cu_3O_{8+\delta}$ exhibits diamagnetism and Meissner effect at low field 0.3 Oe, and the onset of superconducting transition starts at 90K. For a perfect superconducting state, at the lowest applied field and at low temperatures, X' and X" should attain values of -1 and 0, respectively, implying complete diamagnetic shielding and the absence of any losses due to the trapped flux.

In the present case, at 0.3 Oe (low field) and at 4.2K (low temperature), X' and X" achieve values of -0.92 and 0.007, respectively, implying 92% diamagnetic shielding and slight imperfect diamagnetism below Tc. With increasing temperature at 0.3 Oe, X' changes from -0.92 below Tc to a small positive value above Tc, while the imaginary part, X" , peaks at Tc and is practically zero above and below Tc. Both X' (T) and X" (T) are sensitive to the ac-applied fields and thus can give significant insight into the role of microstructure on the superconducting properties of these new high-Tc oxide sintered materials.

It is evident from Fig. 1 that as the ac-applied field is increased to 240 A/m (eOe), X' reduces to 85% diamagnetic shielding, while the X" exhibits a slight peak at Tc in addition to a major broadened peak at about 40K. These features indicate two contributions to the susceptibility of the material; one very sensitive to measuring field and the other, relatively insensitive to field (5,6). On the other hand, for moderate fields like 0.3 Oe (Fig. 1), the two contributions to the susceptibility are not separable or it is sufficient to supress one of the contributions near Tc at this field. These observations suggest that the investigation of the magnetic field dependence of ac susceptibility is a particularly useful method for separating the two contributions. Further increase in ac-applied field to 2400 A/m (30 Oe), X' reduces to 45% diamagnetic shielding and X" again shows a peak near Tc along with very broad indication of peak. Also note that the lossy component X" which should ideally be zero for the superconducting state is rather large and positive at liquid helium temperature at fields above 3 Oe. This is unusual if the

material was indeed a bulk superconductor. These observations indicate that a significant amount of flux indeed penetrates through the system even at low fields, and that in fields above 30 Oe, one essentially is looking at the intra-granular superconducting properties. The "two-stage" ac-susceptibility behaviour can be explained as arising from two contributions to the susceptibility; one of which is intrinsic to the superconducting grains, and the other originating from the network that links the grains weakly.

In conclusion, we have prepared and identified a new high-Tc superconductor $Y_2Ba_2Cu_3O_{8+\delta}$ (2-2-3) by ac-susceptibility measurements. The systematic investigation of the real and imaginary components of ac-susceptibility as a function of temperature, applied field and frequency reveals that the magnetic behaviour is that of a granular-type superconductor in which "strongly" superconducting grains are coupled via weak superconducting links.

ACKNOWLEDGEMENTS

The authors are thankful to Prof. K.V. Rao, Department of Solid State Physics, Royal Institute of Technology, Stockholm, Sweden, for extending experimental facilities. This work was financially supported by University Grants Commission, New Dehli.

REFERENCES

1. KULKARNI, R.G., G.J. BALDHA, H. MOHAN, R.B. JOTANIA, and H.H. JOSHI, "New High-Tc 2-2-3 type Superconductor $Y_2Ba_{1.5}Ca_{0.5}Cu_3O_{8+\delta}$," Solid State Commun. (in press), 1990.

2. KULKARNI, R.G., "Synthesis and Crystal structure of the High-Tc Superconductor $Y_2Ba_{1.5}Ca_{0.5}Cu_3O_{8+\delta}$," J. Master. Sci., 1990.

3. CAVA, R.J., B. BATLOGG, R.B. VAN DOVER, D.W. MURPHY, S. SUNSHINE, T. SIEGRIST, J.P. RAMEIKA, E.A. REIRMAN, S. ZAHURAK, and G.P. SPINOSA, Phy. Rev. Lett., 58, 1676 (1987).

4. TARASCON, J.M., W.R. McKINNON, L.H. GREENE, G.W. HULL, and E.M. VOGEL, Phy. Rev., B36, 226 (1987).

5. GOLDFARB, R.B., A.F. CLARK, A.I. BRAGINSKI, and A.J. PANSON, Cryogenics, 27, 475 (1987).

6. CHEN, C.X., J. NOFUES, N. KARPE, and K.V. RAO, Kexue Tongbao, 33, 560 (1988).

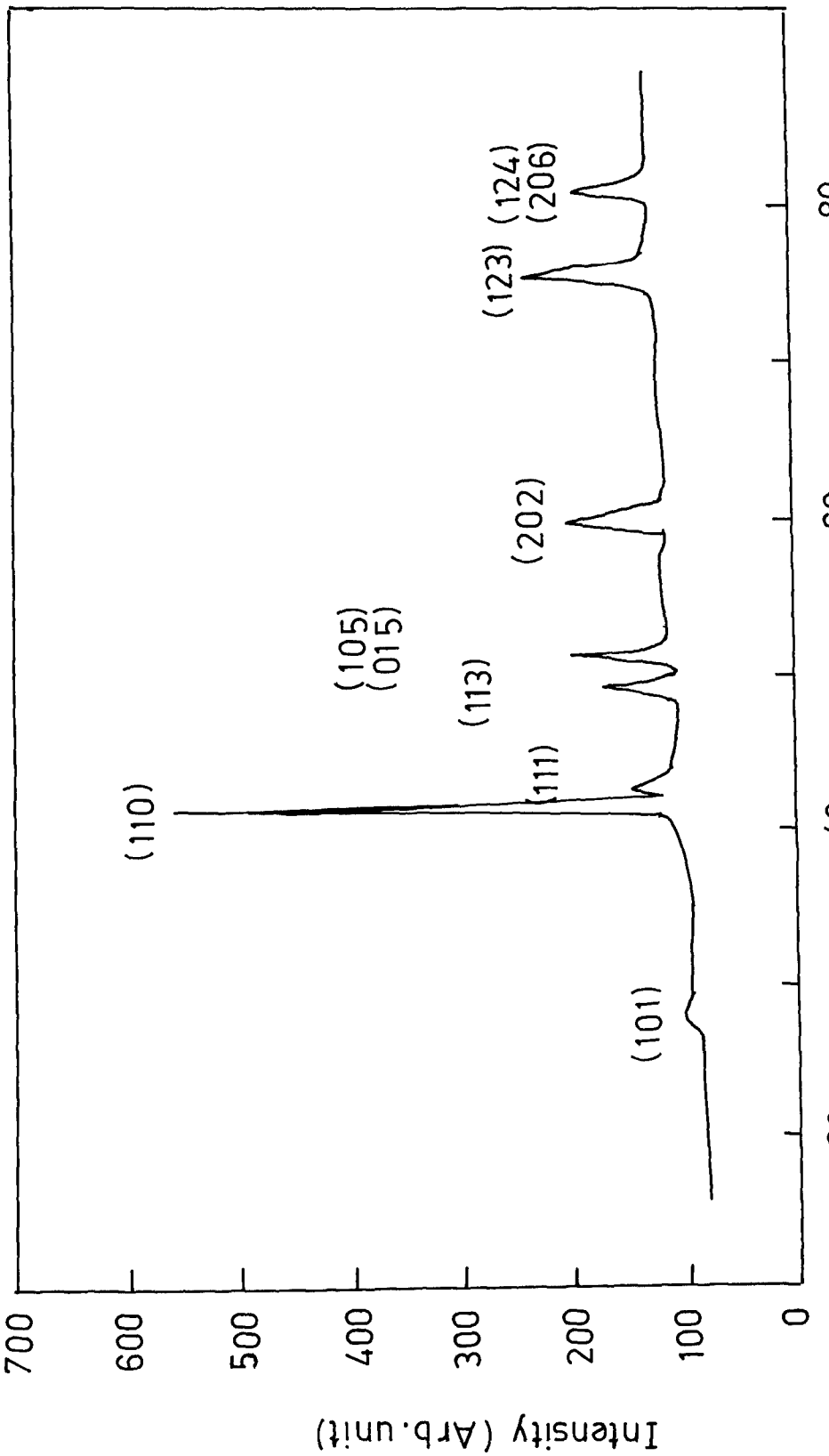
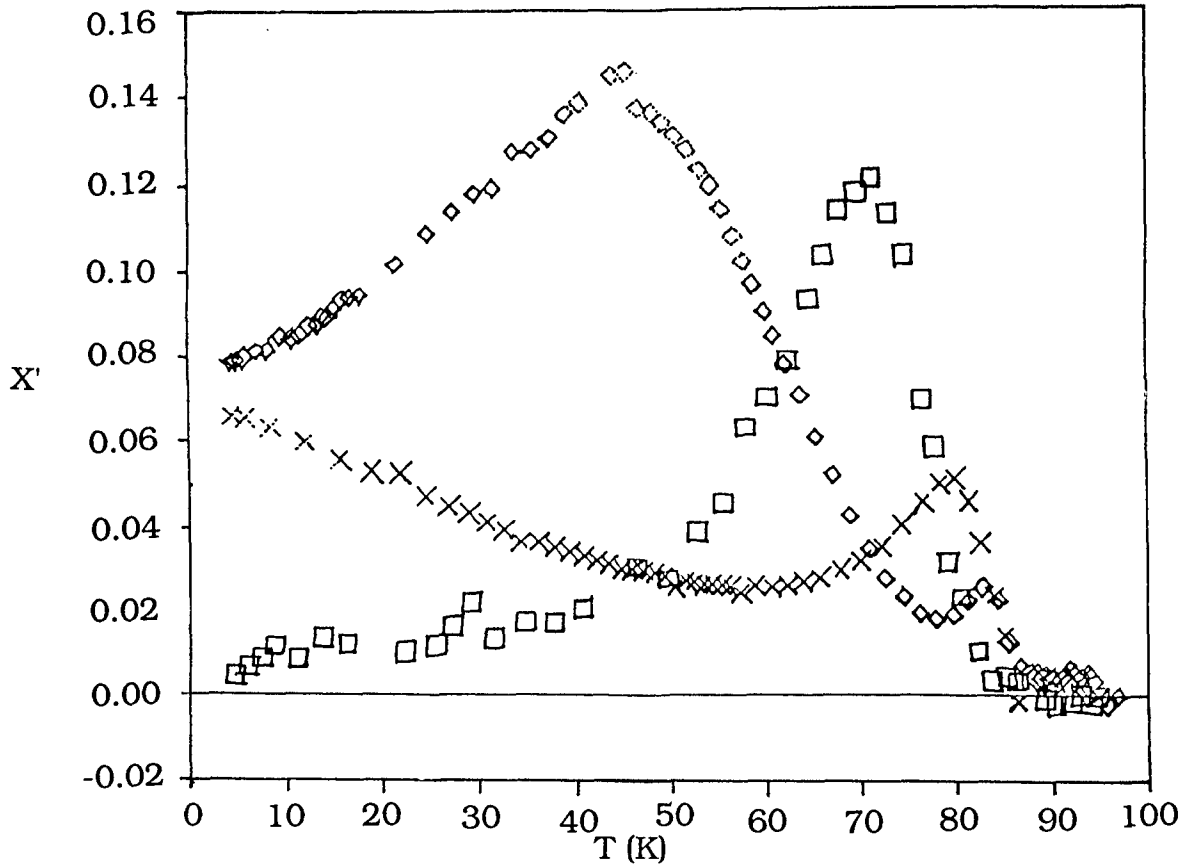


Figure 1. X-ray data for $Y_2Ba_2Cu_3O_{8+\delta}$.



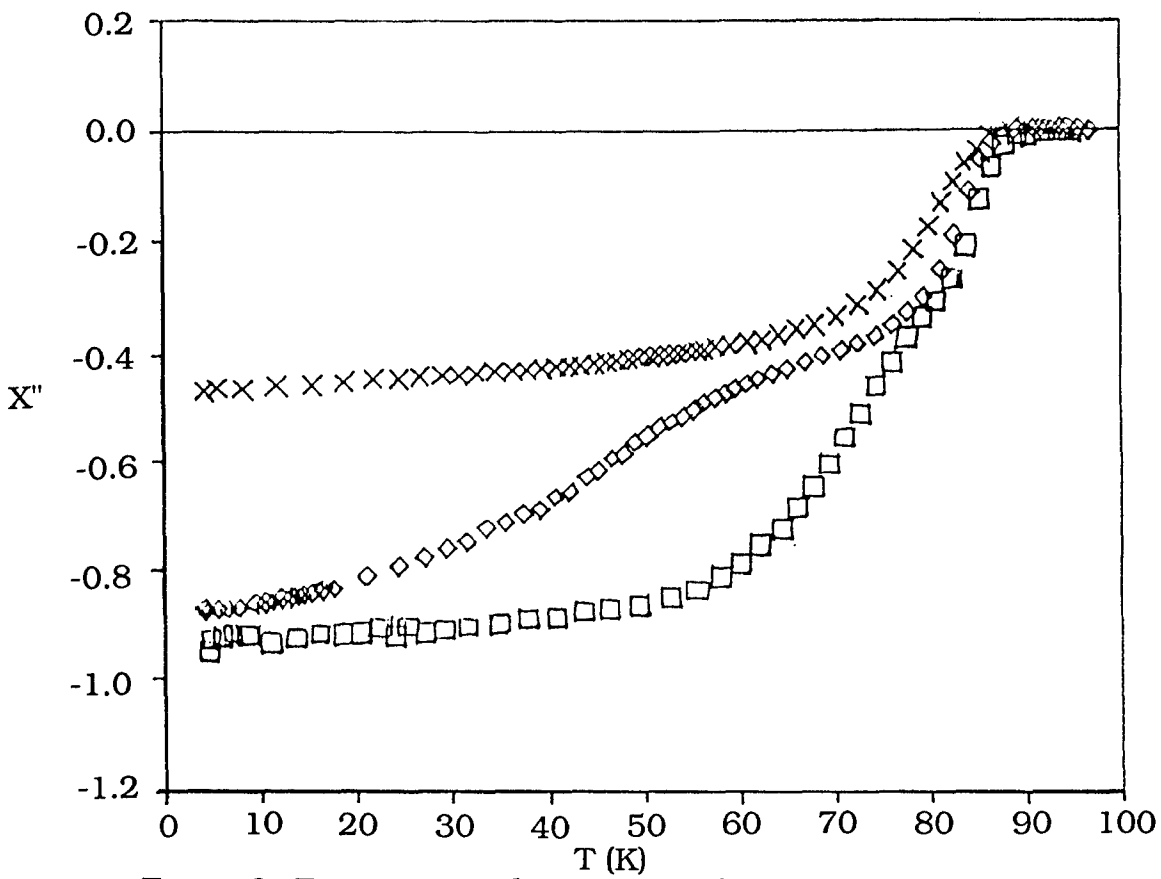


Figure 2. Temperature dependence of the real (X') and imaginary (X'') components of the ac-susceptibility of $Y_2Ba_2Ca_3O_{8+\delta}$ at 24 A/m (□); 240 A/m (◇); and 2400 A/m (X).

STUDY OF THE SUPERCONDUCTING PROPERTIES OF THE Bi-Ca-Sr-Cu-O SYSTEM

Musheer H. Khan, S.M.M.R. Naqvi, and S.M. Zia-ul-Haq
Solid State Research Laboratory, Department of Physics
University of Karachi
Karachi, Pakistan

ABSTRACT

We have studied the electrical properties of unquenched and rapidly quenched bulk samples of granular $Bi_2Ca_1Sr_2Cu_2O_x$ system. Electrical resistivity measurements show the superconducting transition temperature (R=0) at 72 K, 80 K, and 90.5 K. X-ray crystallographic studies showed that most of the samples were of single phase.

1. INTRODUCTION

High-temperature superconductivity in the Bi-Ca-Sr-Cu-O system has been observed and has attracted considerable attention in the year 1988 (Maeda et al., 1988; Rao, 1988; Hazen et al., 1988; Tarascon et al., 1988; and Rao et al., 1988). Furthermore, the X-ray diffraction studies have also been carried out by many researchers (Bordet et al., 1988; Takayama et al., 1988, and Syono et al., 1988) with the objective of identifying and characterizing the superconducting phase.

The 80 K superconductivity phase has been identified to have a composition of $Bi_2Ca_1Sr_2Cu_2O_x$ while 110 K phase as reported in the literature has a possible composition of $Bi_2Ca_2Sr_2Cu_3O_y$ system (Zandenbergen et al., 1988). It has become clear that this class of materials encompasses several distinct superconducting phases and that the physical properties measured depend greatly not only on the elemental composition, but also on the details of the preparation method. Present work reports the preparation of two batches of superconducting samples (quenched and unquenched) and the measurement of their electrical resistivity and X-ray diffraction to understand the effect of oxygen stoichiometry on T_c of the Bi-Ca-Sr-Cu-O system.

2. EXPERIMENT

Bulk samples with the 2:1:2:2 composition have been prepared by solid-state reaction of Bi_2O_3, CuO, $SrCO_3$ and $CaCO_3$ powders. The method of synthesis consisted of reacting together Bi_2O_3 and a base matrix of $CaSr_2Cu_2O_5$. The matrix was first made by thoroughly mixing appropriate amounts of $CaCO_3$, $SrCO_3$ and CuO by heating in an alumina boat at 800°C to 900°C with intermittent grinding. The reacted powder was cooled, ground well and made into pellets, and was heated for a couple of hours.

One batch of pellets was slowly removed from the furnace and cooled to room temperature (unquenched), while another batch was pulled out of the furnace and immediately quenched by immersion in liquid nitrogen. Pellets were cut in the shape of a parallelepiped for the electrical resistivity measurements. Contacts were made with the help of silver paste to the surface of the sample. Resistivity temperature and current-voltage data were measured by a conventional

four-probe method. The experimental parametric details of the measuring techniques have already been reported in our previous work (Naqvi et al., 1989a, 1989b).

3. RESULTS AND DISCUSSION

Resistivity-versus-temperature curves for typical unquenched and rapidly quenched specimens are shown in Figures A and B. The resistivity of the unquenched sample, curve C-I from Batch 1 shows metallic temperature behavior down to the superconducting onset which begins at 90 K, while zero resistance T_c is observed at 72 K. It is worthwhile to mention here that from Batch 1, most of the unquenched samples showed a zero resistance around 72-75 K. Shown in curve C-I of Figure A is the typical behavior of one of the representative samples belonging to Batch 1. These measurements have been done at a current density of 15 mA/mm^2. It was observed that the T_c of the sample did not degrade at all with the increase of current density. This is indicative of the fact that the sample can endure current density variations. The transition width in the sample is found to be around 18 K.

The resistivity of the rapidly quenched sample from Batch 2, shown in Figure B, curve II showed improved metallic behaviour above the superconducting onset around 105 K while zero resistance was found at 90.5 K. None of the samples showed any evidence of a second onset at 105-110 K as reported in the literature (Shi et al., 1988) for samples deviating from the 2:1:2:2 composition. Some of our rapidly quenched samples were found to slowly relax to the behaviour of unquenched material over a period of some days if exposed to the atmosphere at ambient temperatures. The resistivity curve for a sample similar to curve II but exposed to the atmosphere for 15 days is shown in curve III. It has been suggested that the improved behaviour of quenched material is caused by an oxygen deficiency (Tallon et al., 1988) and this decay could then result from the uptake of atmospheric oxygen. This behaviour is in fine agreement with the work reported by King et al., 1989. This behaviour is not clear but the technological implications of this decay clearly indicate the need for a detailed study of the quenching mechanism. The specimens of samples of Batches 1 and 2 were examined by an X-ray diffractometer after crushing. The crystal structure was found to be orthorhombic (Bordet et al., 1988). X-ray crystallographic studies showed that most of the samples were of single phase.

4. CONCLUSIONS

It is established that in using a matrix method it is possible to prepare the pure superconductivity phase in the Bi-Ca-Sr-Cu-O system starting from stoichiometric ratios (2122) of the constituent oxides. Besides this, superconducting phase (2122) can also be prepared from quenching and slow cooling (unquenched).

ACKNOWLEDGEMENTS

We are grateful to Professor S.A. Hussain, Director of the Institute of Pure and Applied Physics, University of Karachi, and to Dr. Y. Khan of Institut fur Werkstoffe der Electrotechnik, Ruhr Universitat, Bochum, West Germany, for providing the experimental facilities. Financial assistance from the National Scientific Research and Development Board (N.S.R.D.) and the Dean of the Faculty of Science, University of Karachi for this work is greatly acknowledged. One of us (M.H. Khan) is grateful to ICTP Trieste, Italy, for providing facilities in the Adriatico Laboratory.

Bordet, P., J.J. Cappone, C. Challout, J. Chenavas, A.W. Hewat, E.A. Hewat, J.L. Hodeau, M. Marezio, J.L. Thalence, and D. Tranqui, 1988, *Interlaken Conference, Physica C.*, pp. 153-155.

Hazen, R.M., C.T. Prewitt, R.J. Ange, N.I. Ross, N.L. Ross, L.W. Finger, C.G. Hadidiacos, D.R. Veblen, P.J. Heaney, Z. Huang, L. Gao, J. Bechtold, and C.W. Chu, 1988, *Phys. Rev. Lett.*, 60, p. 1174.

King, P., D.S. Misra, and W.B. Roys, 1989, *Supercond. Sci. Technol.*, 1, pp. 227-231.

Maeda, H., Y. Tanaka, M. Fukutomi, and T. Asano, 1988, *Jpn. J. Appl. Phys. Lett.*, 27, p. L-209.

Naqvi, S.M.M.R., F. Ahmad, J. Alam, and S. Ahmad, 1989, *Indt. Jour. of Mod. Phy. B.*, 3, 3, pp. 441-444.

Naqvi, S.M.M.R., J. Alam, F. Ahmad, and M.H. Khan, 1989, *Int. Jour. of Mod. Phy. B*, 3, 8, pp. 661-664.

Rao, C.N.R., ed., 1988, Chemistry of oxide superconductors, Blackwell, Oxford, U.K.

Rao, C.N.R., R.A. Mohan Ram, L. Ganapathi, and R. Vijayaraghavan, 1988, *Pramana J. Phys.*, 30, 5, p. L-495.

Shi, D., M. Blank, M. Patel, D.G. Hinks, and A. Mitchell, 1988, *Physica C*, 156, pp. 822-826.

Syono, Y., K. Hiraga, N. Kobayashi, M. Kikuchi, K. Kusaba, T. Kajitani, D. Shindo, S. Hosoya, A. Tokiwa, S. Terada, Y. Muto, 1988, *Jpn. J. Appl. Phys.*, 27, p. L-569.

Tallon, J.L., R.G. Buckley, P.W. Gilberd, M.R. Presland, I.W.M. Brown, M.E. Bowden, L.A. Christion, and R. Goguel, 1988, *Nature*, 333, p. 153.

Takayama-Muromachi, E., Y. Uchida, A. Ono, F. Izumi, M. Onoda, Y. Matsui, K. Kosuda, S. Takekawa, and K. Kato, 1988, to appear in *Jpn. J. Appl. Phys.*, 27.

Tarascon, J.M., Y. Le Page, P. Barboux, B.G. Bagley, L.H. Greene, W.R. McKinnon, G.W. Hull, M. Giroudi, and D.M. Hwang, 1988, *Phy. Rev. B*, 37, p. 9382.

Zandbergen, H.W., Y.K. Huang, M.J.V. Menken, J.N. Li, K. Kadowaki, A.A. Menovsky, G. Tendelloo, X.S. Amelinck, 1988, *Solid State Commun.*, 66, p. 297.

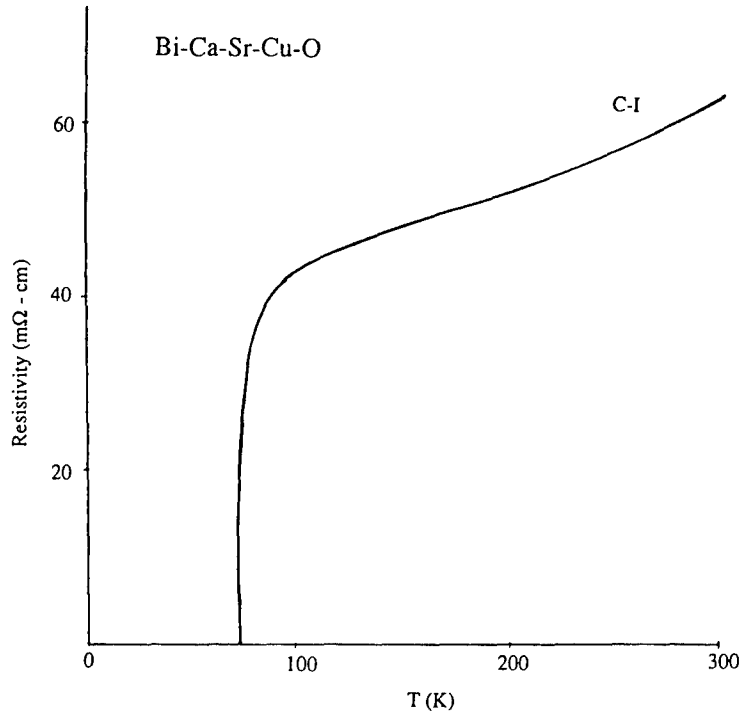


Figure A. The temperature-dependent resistivity of the unquenched sample.

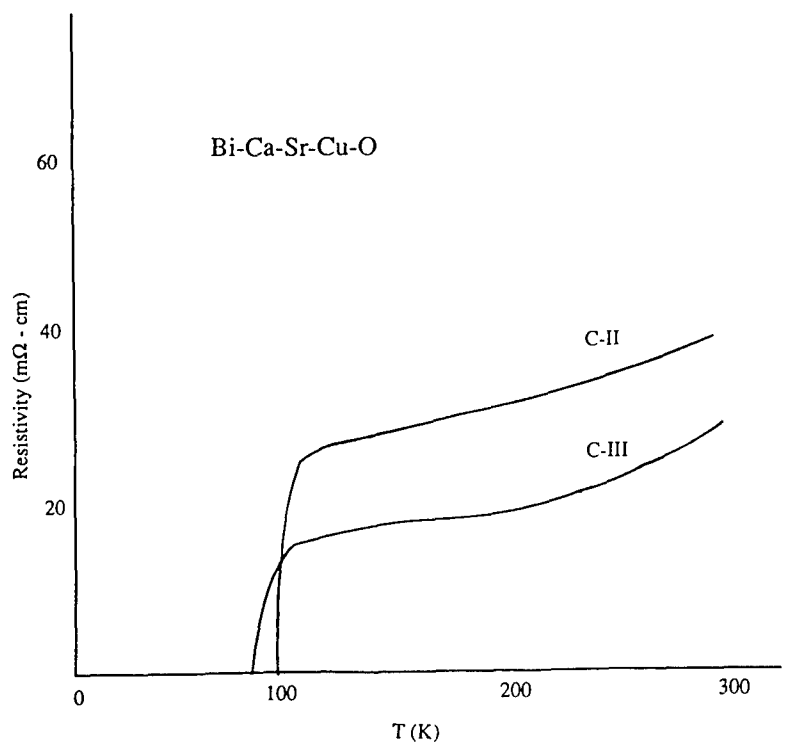


Figure B. The temperature-dependent resistivity of the quenched sample; curve II showing the $T_{co} = 90.5$ K.

NOVEL SUPERCONDUCTING PHASES OF TL-BASED COMPOUNDS

I.Z.Kostadinov, M.Mateev, M.Michov, V.Skumriev and E.Tsakin

Faculty of Physics, Sofia University, 1126 Sofia, BULGARIA

1. Introduction

The interest in novel superconducting compounds has been attracted, recently, by the Pb-containing High Temperature Superconductors (HTS) [1-5]. The larger part of work has been done on Bi-Pb type HTS [6,7]. The Tl-based HTS, howeever, are also of considerable importance because of their highest critical parameters (T_c, H_c) [8,9]. Due to the dangerous properties of Tl the research in this area is progressing more slowly. The list of the stable phases of Tl-Ba-Ca-Cu-O HTS is still incomplete. The Tl-Pb HTS were studied mostly in the compound Tl-Pb-Sr-Ca-Cu-O [10] and less in the family Tl-Pb-Sb-Ca-Ba-Cu-O [11]. The substitution of Tl with Pb is intended to stabilize some phases with high T_c. We found phases with T_c = 82, 90, 102 and 121 K. Here we report the measurements of the $I_c(T)$ of the 102 K phase. We also discuss briefly the influence of the composition on the lattice parameters and the a.c. susceptibility relation to the grain size and microstructure.

2. Experimental

The nitrates solution of the metals Tl, Pb, Sb, Ba, Ca, Cu of starting composition $Tl_{0.75}Pb_{0.2}Sb_{0.05}Ca_2Ba_3Cu_4$ was dried and decomposed at 780°C. Pellets were prepared under 1-2 kbars pressure and annealed at different temperatures from 820°C to 915°C. The highest critical temperature phase was found to be the 121 K. It was prepared by a 3 min annealing at 891°C in oxigen atmosphere. The lattice parameters of this tetragonal phase are a = b = 3.84 Å and c = 31.96 Å. The average composition of the pellets of this type found by SEM analysis was $(Tl, Pb)_1 - Ca_2 - Ba_{4.1} - Cu_{5.6} - O$, the Tl-Pb ratio being 4.4. We should mention here that a slight change in the composition lead to different c-parameter of the tetragonal elementary cell. For example the composition $(Tl + Pb)_1 - Ca_{2.8} - Ba_{2.8} - Cu_{4.4} - O$ with the ratio Tl:Pb equal to 3.17 has a cell length of 32 Å. The X-ray powder diffraction pattern is practically the same as the one of the first mentioned compound but the peak at low angles being quite well pronounced is slightly displaced. We mention here

this observation in order to illustrate the similarity of the Tl-Pb system to solid solutions compounds.

We turn next to another phase with lower T_c = 102 K but the same starting composition prepared by annealing first at 820°C for 3 min in oxigen atmosphere. After quenching and grinding the pellet was annealed for 6 min at 915°C. The result was an remarkably homogeneous sample with sharp transition at T_c = 102 K. This phase was studied by SEM and in the μm range it has the microstructure shown on Fig. 1.



Fig. 1.
SEM microstructure of the 102 K ceramic sample. Large voids are seen and crystals are absent

This crystals free structure is closely related to the a.c. susceptibility of the sample measured at different magnetic fields.

3. A.C.Susceptibility

The real χ' and imaginary χ'' parts of the magnetic susceptibility were measured simultaneously at different temperatures upon warming. The a.c. field amplitude was between 24 A/m and 800 A/m, the frequency being 10 Hz.

The sample was in the form of a prism (2 × 4 × 10 mm). In order to minimize the demagnetization effect, the a.c. field was chosen to be parallel to the length of the sample. Corrections for the demagnetization were performed [12]. On Fig. 2a and Fig. 2b the temperature dependence of the susceptibility χ' and χ'' are presented.

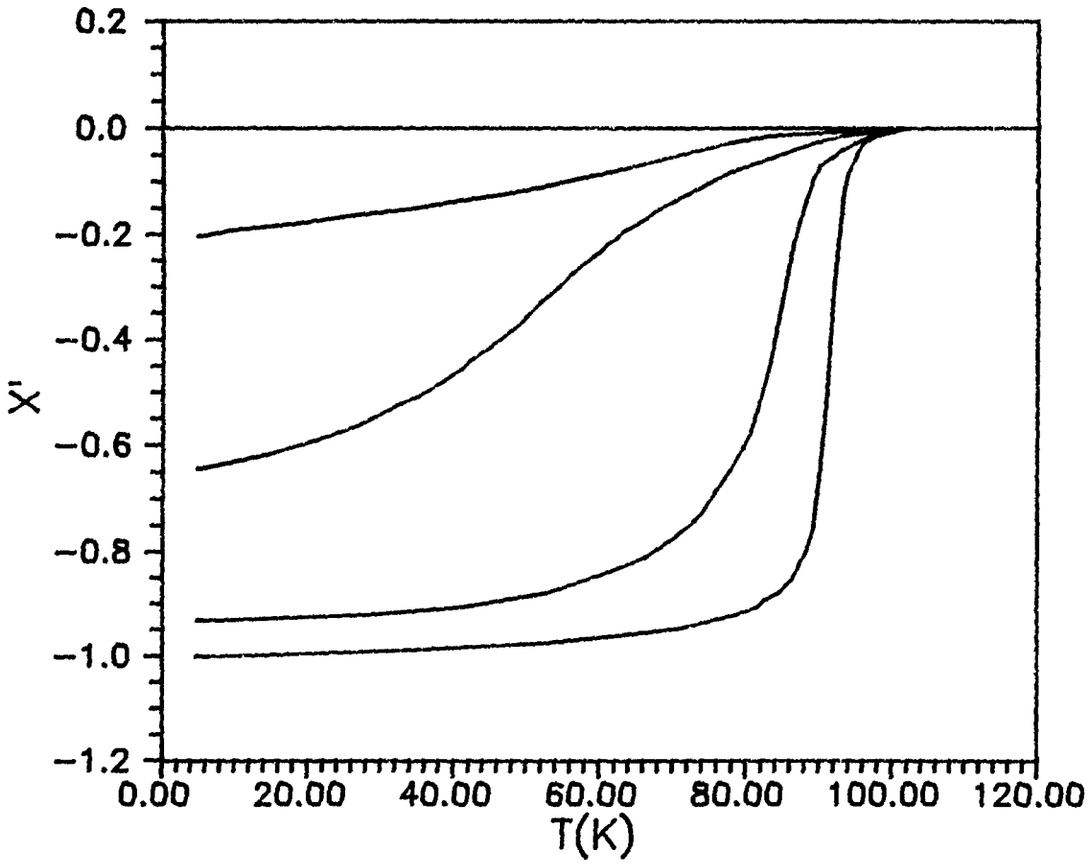


Fig. 2a.
Temperature dependence of χ' measured at fields 24 A/m - curve *a*; 240 A/m - curve *b*; 2400 A/m - curve *c* and 8000 A/m - curve *d*

The complete diamagnetic shielding is demonstrated by the value -1 of χ' (or $\chi'' = 0$) below 60 K at low magnetic fields. At higher fields, however, the situation is entirely different.

The χ'(T) curves are well above the low field one with complete absence of common part. Two stage behaviour in χ' is not seen also, in contrast with the typical ceramic HTS like *YBaCuO*.

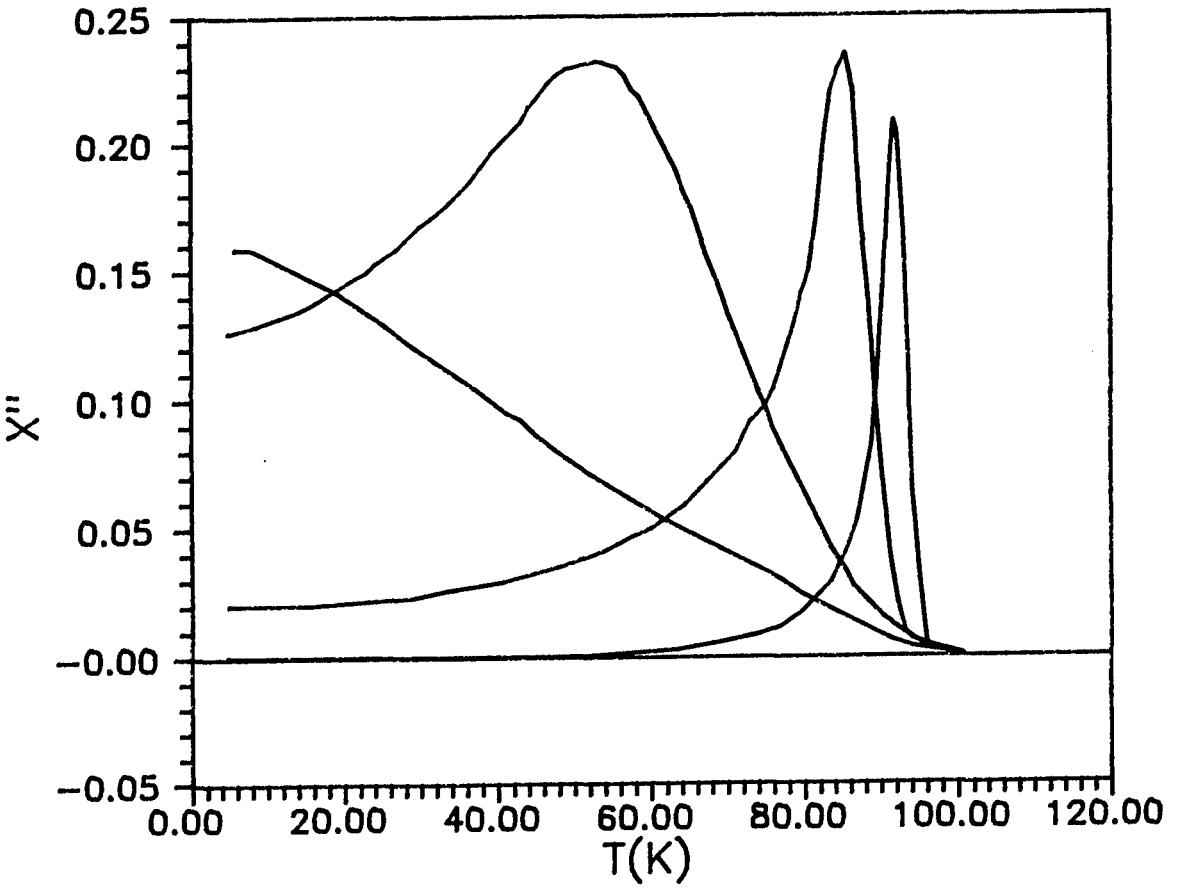


Fig. 2b.

Temperature dependence of χ'' measured at the same fields as χ' (Fig. 2a)

The second peak in χ'' is also absent in agreement with the χ'(T) dependence. The maximum value of χ'' (in fields between about 24 A/m and about 2400 A/m), at which the magnetic field penetrates completely the coupling matrix is in agreement with the larger part of the data reported for ceramic samples [13]. It is worth mentioning that strong field dependence of the χ'' maximum suggesting usually Josephson type grains coupling was not observed, at least in the fields range of measurement. In principle, the observed behaviour can happen in the case when the contributions to the susceptibility of the grains and the coupling matrix are not well temperature-separated. To our knowledge this situation is not valid in our case.

The a.c. susceptibility data were used recently by several authors to estimate the transport critical current. Based on Kim's critical state model a method for determining the temperature dependence of the intergranular critical current has been developped by Chen et al.[12]. Using this method and neglecting the volume fraction of the grains the temperature dependence of the transport critical current $I_c(T)$ has been reconstructed of Fig. 3 from the measured

susceptibilities.

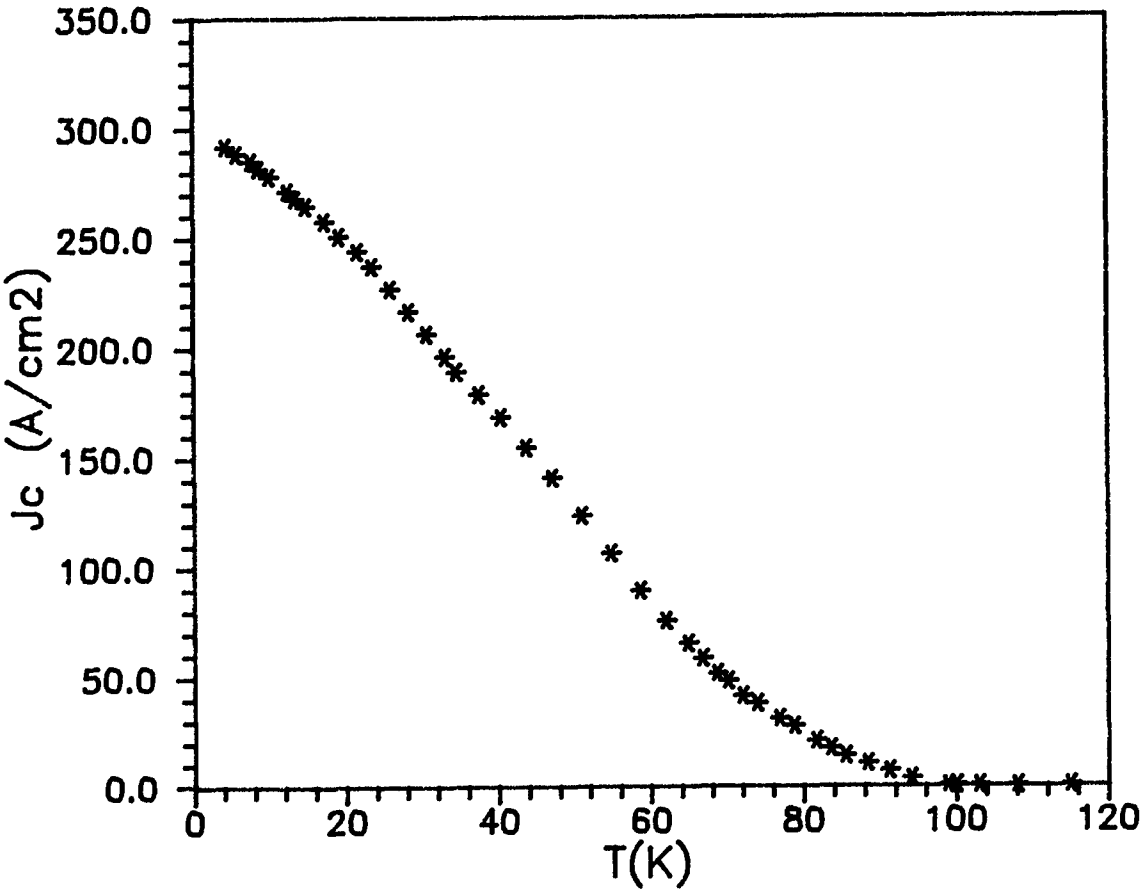


Fig. 3.
Critical current temperature dependence of the 102 K phase.

4. Results

In conclusion we briefly enumerate the results reported here. First we mention the observed variety of phases of the superconducting compound *Tl–Pb–Sb–Ca–Ba–Cu–O*. Among them we concentrated our affention here on the 102 K phase, which being homogeneous appears to have monocrystalline-like microstructure, complete diamagnetic shielding and specifie behaviour of the complex susceptibility (Fig. 2 a,b). Finaly, we mention the reconstruction of the critical current temperature dependence $I_c(T)$ shown on Fig. 3 from the measured susceptibilities.

REFERENCES

1. S.M.Green, C.Jiang, Y.Mei, H.L.Luo, and C.Politis, Phys. Rev. B, 38 (1988) 5016.
2. S.Koyama, U.Endo, and T.Kawai, Jpn. J. Appl. Phys., 27 (1988) L1861.
3. U.Endo, S.Koyama, and T.Kawai, Jpn. J. Appl. Phys., 27 (8) (1988) L1576.
4. R.J.Cava, B.Batlogg, J.J.Krajewski, L.W.Rupp, L.F.Schneemeyer, T.Siegrist, R.B.Van Dover, P.March, W.F.Peck, P.K.Gallagher, S.H.Gralum, J.M.Marshall, R.C.Farrow, J.W.Waszczak, R.Hull, and P.Trevor, Nature 336 (1988) 211.
5. T.Rouillon, J.Provost, M.Hervieu, D.Groult, C.Michel, and B.Raveau, Physica C 159 (1989) 201-209.
6. H.Liu, X.Zhan, Y.Chao, G.Zhou, Y.Ruan, Z.Chen, and Y.Zhang, Sol. St. Comm., 69 (1989) 867.
7. N.D.Spencer, Acepted, Jpn. J. Appl. Phys., Vol. 28, *No* 9.
8. Z.Z.Sheng and A.M.Hermann, Nature 332 (1988) 55, 138.
9. S.S.Parkin, Lee V.Y., Engler E.M.,Nazzal A.I., Huang T.C., Gorman G., Savoy R., and Beyers R. , Phys. Rev. Lett. 60 (1988) 2539.
10. M.A.Subramanian, C.C.Torardi, J.Gopalakrishnan, P.L.Gay, J.C.Calabrese, T.R.Askew, R.B.Flippen, and A.W.Sleight, Phys. Rev. Lett., in press.
11. I.Z.Kostadinov, M.D.Mateev, J.Tihov, V.Skumriev, E.Tskin, O.Petrov, E.Dinolova, V.Kovachev, Physica C 162-164 (1989) 995-996.
12. D.-X.Chen and R.B.Goldfarb, J. Appl. Phys., Vol. 66 (6) 2489-2500.
13. V.Skumriev, R.Puzniak, N.Karpe, Han Zheng-he, M.Pont, H.Medelius, D.-X.Chen, and K.V.Rao, Physica C 152 (1988) 315-320.

SYNTHESIS OF $Y_1Ba_2Cu_3O_x$ SUPERCONDUCTING POWDERS BY INTERMEDIATE PHASE REACTIONS

C. Moure, J.F. Fernandez, J. Tartaj, P. Recio and P. Duran

Instituto de Ceramica y Vidrio, C.S.I.C., Electroceramics Department
28500 Arganda del Rey, Madrid, Spain

ABSTRACT

A procedure for synthesizing $Y_1Ba_2Cu_3O_x$ by solid-state reactions has been developed. The method is based on the use of barium compounds, previously synthesized, as intermediate phases for the process. The reaction kinetics of this procedure have been established between 860°C and 920°C. The crystal structure and the presence of second phases have been studied by means of XRD. The sintering behaviour and ceramic parameters were also determined. The orthorhombic type-I structure has been obtained on the synthesized powder and on the sintered bodies after a cooling cycle in air atmosphere. Superconducting transition took place at 91 K. Sintering densities higher than 95% D_{th} were attained at temperatures below 940°C.

1. INTRODUCTION

Since the discovery of High-T_c Superconductivity in the 90 K range in $Y_1Ba_2Cu_3O_x$ compound (1), considerable efforts have been invested toward improving the synthesis process. This represents an important problem, because of the great complexity of the Y_2O_3-BaO-CuO ternary system (2-5). Several routes have been proposed for the consecution of reproducible and reliable synthesis processes, which lead to single-phase superconducting powder and ceramic materials. Most of these routes have two features in common: a) the formation begins from a mixture of three distinct precursors or raw materials; and b) for some of the several steps, barium carbonate is present as a raw material or as an intermediate product from some precursor (6-8). In a previous work (9), a procedure for synthesizing $Y_1Ba_2Cu_3O_x$ via solid-state reaction from intermediate phases was given. In these intermediate phases, the barium cation is fully combined with CuO and/or Y_2O_3 in adequate amounts. By this procedure, $BaCO_3$, which plays a retarding role in the synthesis process, is not present through the reaction pathway. Ruckenstein et al. (10) have studied another of these possible reactions:

$$Y_2Cu_2O_5 + 4BaCuO_2 \longrightarrow 2Y_1Ba_2Cu_3O_x \qquad [1]$$

but the slow formation reaction rate of $Y_2Cu_2O_5$ (4) and the high temperatures in which the reaction [eq. 1] takes place are major problems that hinder their practical application. Better results were obtained for Halasz et al. (11) by means of the use of $Ba_2Cu_3O_5$ as the intermediate synthesized phase, which reacts with Y_2O_3 to give $Y_1Ba_2Cu_3O_x$ according to the reaction sequence:

$$2Ba_2Cu_3O_5 + Y_2O_3 \longrightarrow 2Y_1Ba_2Cu_3O_x. \qquad [2]$$

The reaction [eq. 2] was systematically studied by the present authors in previous work, along with two other possible pathways, based on the use of the oxycarbonates, $Y_2Ba_4O_7.xCO_2$ and $Y_2Ba_2O_5.yCO_2$. The results of the three processes were promising, but the presence of CO_2 in the oxycarbonates was a limiting factor in the reaction kinetics. The third pathway, $Ba_2Cu_3O_5 + 1/2Y_2O_3$,

led to the formation of single-phase $Y_1Ba_2Cu_3O_x$ at 920°C in relatively short times--1 to 2 hours. Nevertheless, the nature of the $Ba_2Cu_3O_5$ synthesis product, which is a mixture of $BaCuO_2$ plus uncombined CuO, gives rise to the formation of intermediate $Y_2Cu_2O_5$ from free Y_2O_3, which was a retarding compound for the reaction.

In the present work, two new reaction pathways have been analyzed for their possible usefulness as adequate synthesis methods for obtaining $Y_1Ba_2Cu_3O_x$, without the presence of barium carbonates or oxycarbonates through the process. Both of them start from stable yttrium-barium phases which react with homogeneous blends of $BaCuO_2$ + CuO, obtained by calcining adequate amounts of $BaCO_3$ and CuO.

2. EXPERIMENTAL METHOD

$BaCO_3$ (Merck), CuO (Merck) and Y_2O_3 (Johnson and Mathey), all of analytical grade, were used as raw materials. Two barium-yttrium compounds were synthesized from stoichiometric mixtures. BaY_2O_4 was obtained from the calcining of the corresponding stoichiometric mixture of $BaCO_3$ and Y_2O_3 at 1350°C for 2 hours, and then quenching to room temperature. $Ba_3Y_4O_9$ was obtained by calcining at 1300°C for 8 hours with subsequent quenching. The calcination temperatures were chosen according to the phase diagram developed by Kwestroo et al. (12). The $BaCO_3$+ 2CuO blend was heat-treated at 920°C for 16 hours, and quenched to room temperature.

The synthesized compound was identified by X-Ray Diffraction (XRD). The powders were ball-milled with isopropanol for 3 hours in a zirconia vibratory mill, and then attrition-milled for 2 hours with alumina balls. Adequate amounts of these compounds were weighted, mixed and homogeneized by wet milling. Isopressed pellets of the blends were heat-treated for different temperatures between 860°C and 920°C, at times from 1 to 8 hours. The heating rate was 10°C/min., and the cooling rate was 5°C/ min., in an air atmosphere. The pellets were ground and the phase evolution was followed by means of powder XRD.

The sintering behaviour was studied on isopressed samples prepared from $Y_1Ba_2Cu_3O_x$ powder, synthesized at the optimum temperature and time, as determined in the kinetic study. Density measurements, XRD patterns, and reflexion optical microscopy (ROM) with polarized light were obtained on sintered bodies. The sintering process was developed in the 920-940°C temperature range, with times varying between 1 and 8 hours. The heating rate was 3°C/ min., and the cooling rate was 1°C/ min. The cooling cycle was carried out in air atmosphere. Oxygen annealing of sintered samples was not performed in any case.

Transition temperature, T_c, was determined on the synthesized powders by magnetic susceptibility measurements performed on a force magnetometer.

3. RESULTS

The XRD patterns of the barium-yttrium compounds showed the formation of the pure compounds BaY_2O_4 and $Ba_3Y_4O_9$, respectively. No trace of $BaCO_3$ was observed. The XRD of the barium-copper blend showed the formation of $BaCuO_2$, which coexists with uncombined CuO, in a very homogeneous mixture. Only small amounts of liquid were observed in these oxide mixtures. $BaCu_2O_3$ was the nominal composition of the barium-copper-oxide combination.

The studied reaction sequences were as follows:

$$BaY_2O_4 + 3BaCu_2O_3 \longrightarrow 2Y_1Ba_2Cu_3O_x \qquad \text{(Route 1)} \qquad [3]$$

$$Ba_3Y_4O_9 + 5BaCu_2O_3 + 2CuO \longrightarrow 4Y_1Ba_2Cu_3O_x \qquad \text{(Route 2).} \qquad [4]$$

Figure 1 shows the XRD patterns of the samples synthesized according to Route 1 for different temperatures and times. It can be already seen at 880°C, that the synthesis reaction is very advanced for relatively short treatment times--2 to 4 hours. Some amount of Y_2BaCuO_5 compound, the "green phase, 2-1-1," was observed for the 2-hour treatment, along with small amounts of unreacted $BaCuO_2$ and CuO. The yttrium-barium phase was not detected for this time. Higher times led to the progressive disappearance of these phases, and for 16 hours, the only observed compound was the 1-2-3 phase.

At 900°C for 2 hours, the reaction was almost complete; only very small amounts of $BaCuO_2$ could be detected. Beyond this time, traces of second phases were not observed from the XRD patterns. Upon raising the temperature, the results were somewhat different. At 920°C for 2 hours, the final product was pure $Y_1Ba_2Cu_3O_x$ compound, but the heat treatment lengthening led to liquid-phase formation, and to the reappearance of small amounts of the green phase. For times of 8 hours or more, the XRD patterns showed a reinforcement of the 0-0-1 peaks, probably due to the preferential growth of crystals, nucleated from the liquid phase. As can be seen from the XRD patterns, the synthesized $Y_1Ba_2Cu_3O_x$ crystallized with an orthorhombic symmetry, type I. Table I shows the lattice parameters for the three temperatures studied at the 2-hour point. According to the calculated values of lattice parameters, the O_2 content can be evaluated as 6.95. The onset temperature was 91 K for the powder synthesized at 900°C for 2 hours, and slightly varies with temperature and time.

TABLE I

Lattice parameters (in Å) and onset temperature (in K) of powders from Route 1

Reaction synthesis	a_o	b_o	c_o	σ*	Onset temperature
880°C 2h	3.8314	3.8897	11.657	1.51	90
900°C 2h	3.8261	3.8957	11.688	1.80	91
920°C 2h	3.8297	3.8949	11.688	1.69	90

$$*\sigma = 2x\frac{b_o - a_o}{b_o + a_o}x100 \quad \text{(orthorhombicity parameter)}$$

Figure 2 shows the phase evolution during the heat treatment of the powders corresponding to Route 2. A different behaviour as compared with Route 1 can be observed. The green phase, which is formed in the first state of the synthesis reaction does not disappear totally through the whole heat treatment study. Along with this phase, CuO and $BaCuO_2$ traces are also present. Nevertheless, no appreciable amount of the green phase for the higher temperatures and times was observed. Preferential growth of the synthesized powders is also seen in the samples heated at 920°C for 4 and 8 hours. The $Y_1Ba_2Cu_3O_x$ synthesized by Route 2 also shows an orthorhombic symmetry, type I, with the lattice parameters given in Table II. The onset temperature was 89 K for the powder obtained at 900°C, 2h.

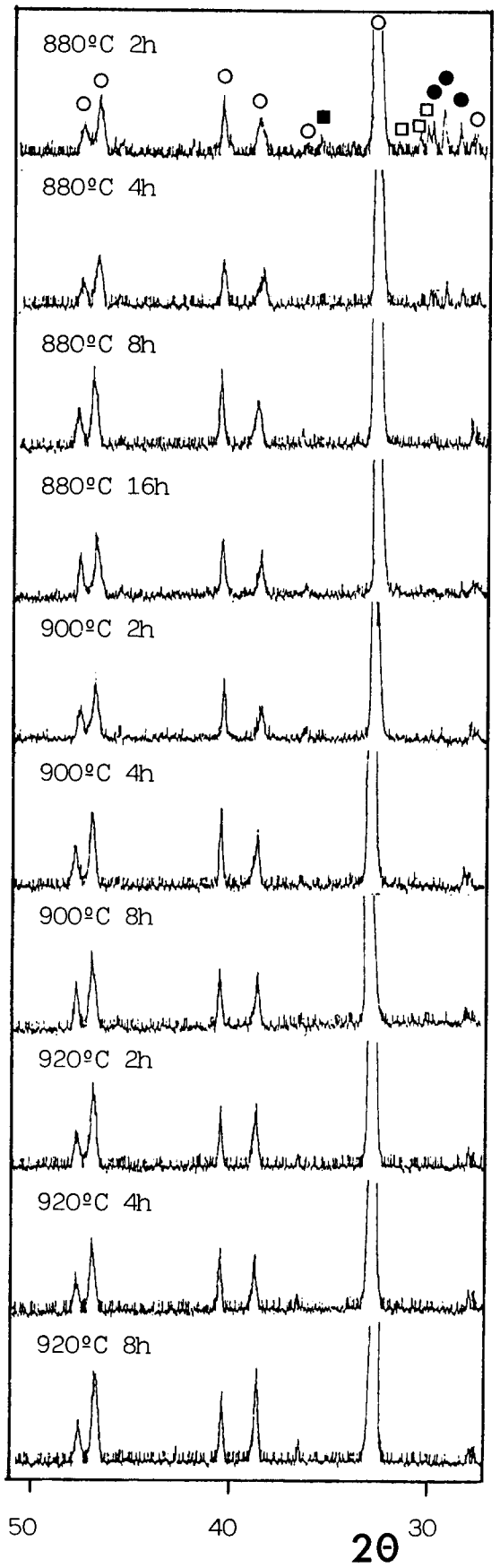


Figure 1. XRD patterns of Route 1, samples heated for different temperatures and times. o $Y_1Ba_2Cu_3$; □ Y_2BaCuO_5; ● $BaCuO_2$; and ■ CuO.

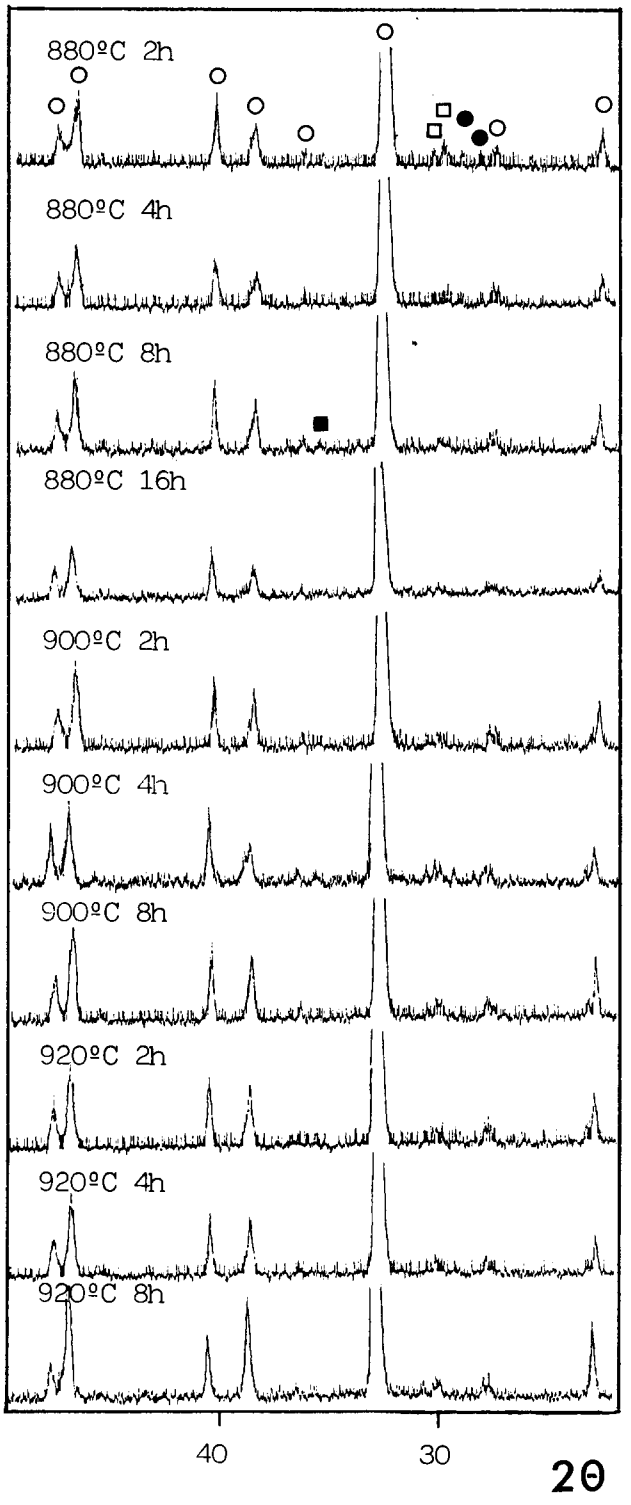


Figure 2. XRD patterns of Route 2 samples heated for different temperatures and times. ■ CuO; o $YBa_2Cu_3O_x$; □ Y_2BaCuO_5; and ● $BaCuO_2$.

TABLE II

Lattice parameters (in Å) and onset temperature (in K) of powders from Route 2

Reaction synthesis	a_o	b_o	c_o	σ	Onset temperature
880°C 2 h	3.8261	3.8956	11.689	1.80	89
900°C 2 h	3.8265	3.8977	11.691	1.84	89
920°C 2 h	3.8245	3.8953	11.691	1.83	88

According to these results, the 900°C, 2-hour schedule was chosen as the better one to obtain synthesis powders for a sintering study. The powders were ball- and attrition-milled, isopressed, and then sintered at different temperatures and times between 920 and 940°C for 1 to 8 hours.

Figure 3 shows the densification curves against temperatures and times for the two synthesis powders. It can be seen that the powder obtained by Route 2 has the best sintering behaviour. It attained a density value of 6.01 gr/cm^3 for 930°C, at 2 hours. By raising the temperature and/or time, somewhat lower density values were attained, but the variation is very smooth. On the other hand, the higher density value for powder synthesized by Route 1 was attained at 940°C for 2 hours, and the value was 5.95 gr/cm^3; smaller than that corresponding to powder 2.

Another important difference between the two materials was the final microstructure and crystal structure. Figure 4 shows ROM micrographs of polished and optically etched, sintered samples. The etching was performed by means of polarized light and crossing nichols. The sample surfaces were not etched by thermal or chemical methods. It can be seen that whereas sample 1 has developed a rather large-grained microstructure with extensive porosity and heavily twinned grains, sample 2 has developed a fine-grained microstructure with scarce porosity and no twinned grains.

The crystal structure of the sintered samples of Route 1 is orthorhombic, with lattice parameters which are in good accordance with type I, as are the synthesis powders. On the other hand, the crystal structure of the sintered samples of Route 2 showed tetragonal symmetry, with lattice parameters which indicated an oxygen content only a little higher than 6.

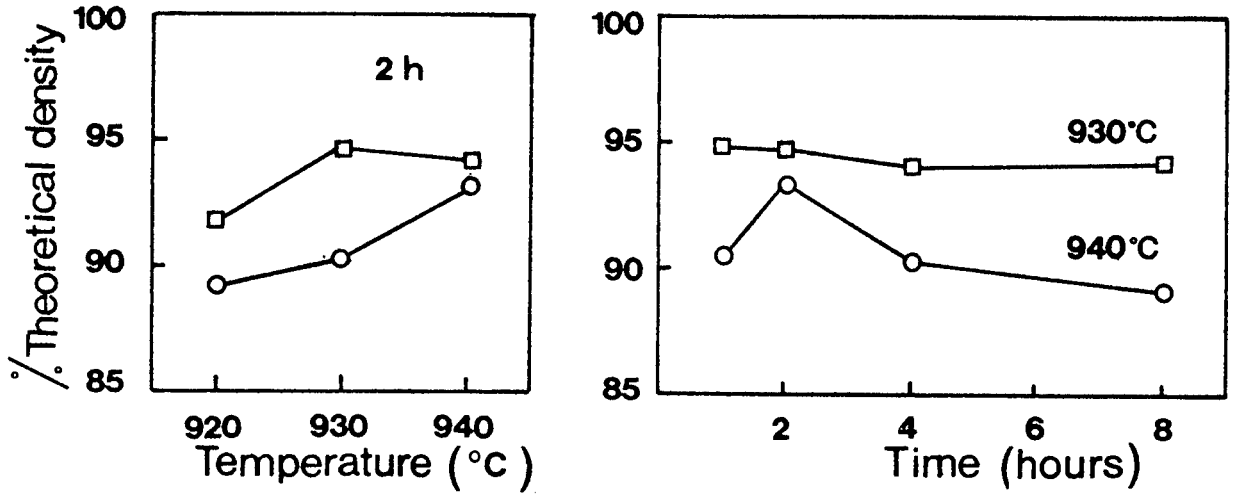


Figure 3. Densification versus sintering temperature and time. o Route 1; □Route 2.

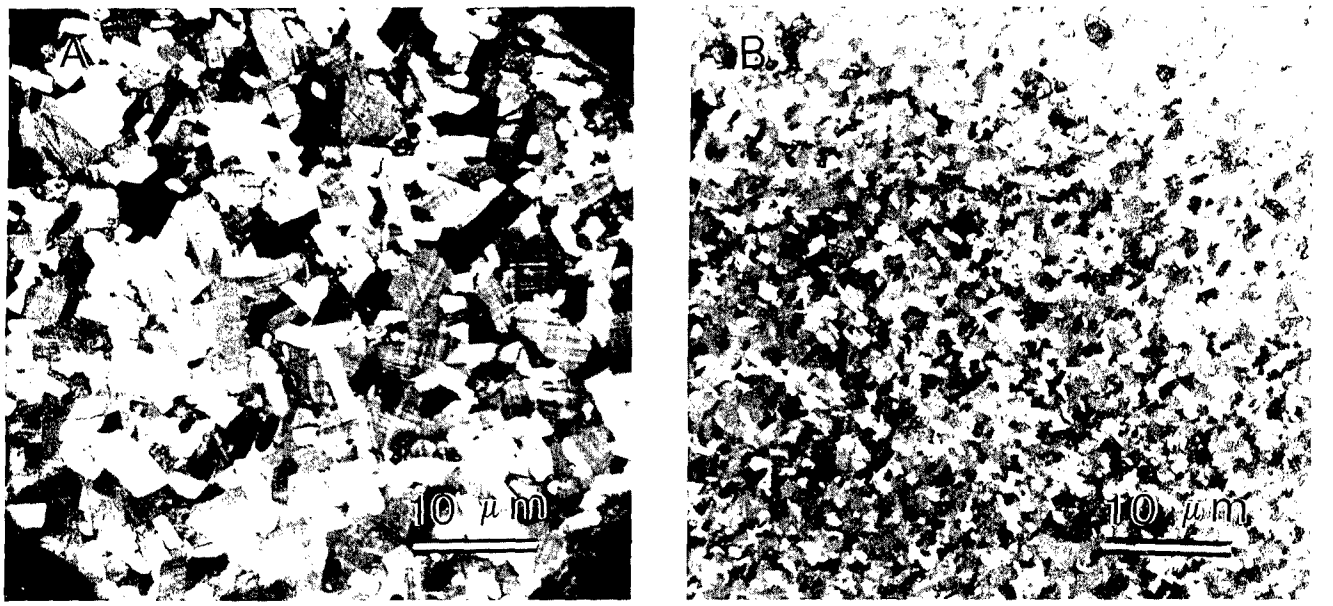


Figure 4. Micrographs of sintered samples: A) Route 1 (940°C); B) Route 2 (930°C)--both for 2 hours.

4. DISCUSSION

$BaCO_3$ has been used as the most reliable source of barium in the forming of $Y_1Ba_2Cu_3O_x$ compound when the solid-state reaction procedure is followed, but as was pointed out above, the sluggish decomposition of the carbonate constitutes a limiting factor in the $Y_1Ba_2Cu_3O_x$ formation. The previous reaction of $BaCO_3$ with Y_2O_3 and/or CuO can avoid this limitation.

The reaction between Y_2BaO_4 and $BaCuO_3$ is very fast and it is possible to obtain pure $Y_1Ba_2Cu_3O_x$ at 900°C for short times; $\leq$ 2 hours. The low temperature for which the reaction is accomplished can be attributed to the presence of the free CuO which is intimately mixed with $BaCuO_2$. The reaction sequence is likely to occur according to the following scheme:

$$3BaCuO_3 + Y_2BaO_4 \text{ ---- } 2Y_1Ba_2Cu_3O_x \qquad [5] \text{ as major reaction}$$

$$CuO + Y_2BaO_4 \text{ ---- } Y_2BaCuO_5 \qquad [6]$$

$$Y_2BaCuO_5 + 3BaCuO_2 + 2CuO \text{ ---- } 2Y_1Ba_2Cu_3O_x \qquad [7]$$

[6] and [7]: as secondary reactions

In this case, the consumption of the green phase is very fast, contrary to the results of Ruckenstein et al. (10), when they studied the reaction shown in eq. 7. The reaction between $Y_4Ba_3O_9$, $BaCu_2O_3$ and CuO is also very fast, probably for the same reasons as those in the first case. The reaction sequence is likely the following:

$$Y_4Ba_3O_9 + 5BaCu_2O_3 + 2CuO \text{ ---- } 4Y_1Ba_2Cu_3O_x \qquad [8] \text{ as major reaction}$$

$$Y_4Ba_3O_9 + 3CuO \text{ ---- } 2Y_2BaCuO_5 + BaCuO_2 \qquad [9]$$

$$Y_2BaCuO_5 + 3BaCuO_2 + 2CuO \text{ ---- } 2Y_1Ba_2Cu_3O_x \qquad [10]$$

[9] and [10]: as secondary reactions

The lack of reaction completeness in the route could be attributed to the instability of the $Y_4Ba_3O_9$ compound, which is the reaction that occurs with the presence of carbonated phases. We think that the results will improve with a striking control of the synthesis procedure and subsequent storage and handling.

The powder from Route 1 shows a sintering behaviour which indicates liquid phase formation with a considerable grain growth. This liquid has been attributed to the reaction with atmospheric carbon dioxide (13) that forms an oxycarbonate which lowers the liquid formation temperature. The interconnected porosity allows the grain boundary diffusion of oxygen to form an orthorhombic material. The grain size is, moreover, small enough to lead to a complete grain oxygenation (Fig. 4).

Powder 2 has a quite different sintering behaviour. This might be explained by the presence of the minor amounts of the green phase. According to the phase diagram, no liquid formation will occur through the sintering process in the studied temperature range, because of the presence of green phase. As a consequence, controlled grain growth takes place, and therefore, it is possible to obtain better densification values (14). Shaw et al. (15) found that small-grained microstructures with high grain-boundary densities favour the oxygenation of the bulk sintered materials, and make the tetragonal-orthorhombic transition easier. In the present case, small grain size could allow the correct oxygenation, but the presence of the second phase in the grain boundaries forms a barrier to the oxygen diffusion, which explains maintenance of the tetragonal symmetry during the slow cooling to room temperature.

4. CONCLUSIONS

Two procedures have been studied for overcoming the presence of $BaCO_3$ during the solid-state reaction of oxides to obtain $Y_2Ba_2Cu_3O_x$. The procedures allow $Y_1Ba_2Cu_3O_x$ synthesis at low temperatures of 900°C, and times of 2 hours, by means of a single-step process. These temperatures and times are well below the eutetic temperature, and therefore, it is possible to avoid particle growth and to maintain a narrow particle size distribution in the synthesized powders.

The effectiveness of the procedures strongly depends on the stability and reliability of the intermediate phases. The Y_2BaO_9 compound fulfills these conditions. On the other hand, $Y_4Ba_3O_9$ is very unstable in moist air, and partially recarbonates if adequate handling care is not taken. Nevertheless, the procedures based on both compounds have led us to obtain superconducting powders through a single cooling cycle in air beyond the synthesis temperature.

The sintering of these powders gives density values near or higher than 95% D_{th}. The presence of small amounts of green phase allows grain size control and higher densities, but the oxygenation process during cooling is hindered by the presence of that second phase. Without green phase development, $Y_1Ba_2Cu_3O_x$ compound superconducts after sintering without a special oxygen treatment.

REFERENCES

1. Wu, W.K., J.R. Ashburn, C.J. Torng, P.H. Hor, R.L. Meng, L. Gao, Z.J. Huang, Y.Q. Wang, and C.W. Chu, 1989, "Superconductivity at 93 K in a New Mixed-Phase Y-Ba-Cu-O Compound System at Ambient Pressure," Phys. Rev. Lett., 58 [9], pp. 908-910.

2. Frase, K.T., E.G. Liniger, and D.R. Clarke, 1987, "Phase Compatibilities in the System Y_2O_3-BaO-CuO at 950°C," J. Am. Ceram. Soc., 70 [9], pp. C204-C205.

3. Roth, R.S., K.L. Davis, and J.R. Dennis, 1987, "Phase Equilibria and Crystal Chemistry in the System Ba-Y-Cu-O," Adv. Ceram. Mater., 2 [3b], pp. 303-312 .

4. Aselage, T. and K. Keefer, 1988, "Liquidus Relations in Y-Ba-Cu Oxides," J. Mater. Res., 3 [6], pp. 1279-1291.

5. Nevriva, N., P. Holba, S. Durcok, D. Zemanova, E. Pollert, and A. Trist, 1989, "On the Melt Equilibria in the Y-Ba-Cu-(O) System," Physica C , 157, pp. 334-340.

6. Itoh, T., M. Uzawa, and H. Uchikawa, 1988, "Formation of Superconducting Ceramic $YBa_2Cu_3O_x$ from a mixture of Y_2O_3, $BaCO_3$ and CuO," J. Master. Sci. Letters, 7, pp. 130-132.

7. Moure, C., R. Duran, S. Vieira, S. Bourgeal, R. Villar, A. Aguilo, and M.A. Ramos, 1988, "Low Temperature Thermal Expansion of a High T_c Superconductor Phase $Y_1Ba_2Cu_3O_{7-\delta}$ Prepared from Oxalate Precursors," Proceedings of Brit. Ceram. Soc. Superconducting Ceramics, Vol. 40, R. Freer, ed., Great Britain Inst. of Ceramics, pp. 237-242 .

8. Chu, Ch-Tse, and B. Dunn, 1987, "Preparation of High-T_c Superconducting Oxides by the Amorphous Citrate Process, " J. Am. Ceram. Soc., 70 [122], pp. C375-C377.

9. Moure, C., J.F. Fernandez, P. Recio, and P. Duran, "A New Route for Synthesizing YBaCuO Superconducting Phases," to be published in Silicates Industriels.

10. Ruckenstein, E., S. Narain, and N-Lih Wu, 1989, "Reaction Pathways for the Formation of the $YBa_2Cu_3O_{7-x}$ Compounds," J. Mater. Res. ,4 [2], pp. 267-72.

11. Halasz, I., I. Kirschenr, T. Porjesz, G. Kavaas, T. Karman, G. Zsolt, C. Sukosd, N.S. Roslosnik, and J. Kurt, "Preparative Chemistry Consequences in Y-Ba-Cu-O Superconducting Compounds," Physica C., 153-155, pp. 179-80.

12. Kwestroo, W., H.A.M. Vauhal, and C. Langereis, 1979, "Compounds in the System BaO-Y_2O_3," Mater. Res. Bull. , 9, pp. 1631-1638.

13. Roth, R.S., C.J. Rawn, F. Beech, J.D. Whitler, and J.O. Anderson, "Phase Equilibria in the System Ba-Y-Cu-O-CO_2 in Air," 1988, Ceramic Superconductors II, M.F. Yan, Ed., The American Ceramic Society, Westerville, Ohio, USA, pp. 13-27.

14. No, K., J.D. Verhoven, R.W. MacCallam, and E.D. Gibson, 1988, "Grain Size Control in Powder Processed $YBa_2Cu_3O_x$," presented at the Appl. Supercond. Conference, San Francisco, Calif., USA, Aug. 21-25, 1988.

15. Shaw, T.M., S.L. Shinde, D. Dimos, R.F. Cook, P.R. Duncombe, and C. Kroll, 1989, "The Effect of Grain Size on the Microstructure and Stress Relaxation in Polycrystalline $YBa_2Cu_3O_{7-x}$," J. Mater. Res., 4, pp. 248-255.

GRAIN ORIENTATION IN HIGH T_c SUPERCONDUCTORS BY MOLTEN SALT POWDER SYNTHESIS

Sudhakar Gopalakrishnan and Walter A. Schulze
New York State College Of Ceramics at Alfred University, Alfred, NY 14802

ABSTRACT

The molten salt or the flux method is utilized in this study to fabricate a grain oriented $YBa_2Cu_3O_{7-x}$ (123) superconductor. Here we suggest a two stage approach in using the "green phase," Y_2BaCuO_5 (211), as seed crystals in the formation of $YBa_2Cu_3O_{7-x}$. The process uses Y_2BaCuO_5 formed by molten salt synthesis. The Y_2BaCuO_5 phase has been observed to be stable in water and in most of the salt systems. Salt processing can can form a small quantity of anisotropic particles of Y_2BaCuO_5. This material can form the 123 phase when tape cast and sintered in the presence of the required levels of Ba and Cu.

INTRODUCTION

The existing anisotropy in the critical current density of $YBa_2Cu_3O_{7-x}$ warrants a grain orientation processing which yields 'textured' microstructure with the aim to enhance the maximum current density of the ceramic[1,2]. Molten salt processing can yield single crystal particles with shape anisotropy which are subsequently aligned by techniques such as tape casting and hot forging. This technique has been applied successfully on a variety of ferroelectric systems[3-5].

Attempts at molten salt synthesis of $YBa_2Cu_3O_{7-x}$ in other ceramic systems has been largely unsuccessful. Studies by others[6,7] revealed the instability of the superconducting phase in NaCl-KCl, LiCl, $BaCl_2$-$CuCl_2$, $CuCl_2$, and Na_2SO_4-K_2SO_4 salts. Certain studies[7] show that the stability of the $YBa_2Cu_3O_{7-x}$ phase might be favored in salt systems with small anion and large cation sizes. $YBa_2Cu_3O_{7-x}$ in powdered form reacts vigorously at room temperature with water[9]. The green phase, Y_2BaCuO_5, is one of the decomposition products of the reaction of $YBa_2Cu_3O_{7-x}$ with water. The stability of the green phase and the anisotropic nature of its grains led us to proceed further with this phase. Moreover molten salt processing of $YBa_2Cu_3O_{7-x}$ requires a complex process for removal of the salts, while in case of the green phase the salts can be removed by washing with water.

The two stage approach to the formation of $YBa_2Cu_3O_{7-x}$ by utilizing the green phase, Y_2BaCuO_5, formed by molten salt synthesis as seed crystals is reported here. The results of our tape casting experiments are also reported here.

EXPERIMENTAL PROCEDURES

Y_2BaCuO_5-Salt Equilibrium

The first experiment tested the stability of preformed 211 in vaious salts to determine the best salts for forming the 211 powders. In the first method precursor materials $BaCO_3$, Y_2O_3 and CuO were taken in stoichiometric proportions of Y_2BaCuO_5 and ball milled in ethanol for 12 hours with YTZ ceramic balls. After drying, the batch was calcined at 960°C for 12 hours and annealed at 530°C for 6 hours in flowing oxygen atmosphere. X-ray diffraction studies confirmed the phase purity of the sample. The preformed 211 powders was then mixed with various salt systems and heat treated in closed magnesia crucibles at temperatures above the melting point of the salt systems[10] used. Table 1 gives all the details of all salt systems used and the resultant phases after heat treatment.

Ratio	Salt	Temp	Time	Resulting Phases	
Salt:211	Systems	$°C$	Hrs.	Oxides	Other Phases
1:1	NaCl	825	3	211	NaCl
1:1	KCl	825	3	211	KCl
1:1	LiCl	825	3	$Cu_2Y_2O_5$, Y_2O_3	LiCl
1:1	NaCl-KCl-LiCl	825	3	$Cu_2Y_2O_5$, Y_2O_3	NaCl, KCl
1:1	Li_2SO_4	975	3	$Cu_2Y_2O_5$,	$BaSO_4$
1:1	Na_2SO_4	975	3	211	Na_2SO_4
1:1	Li_2SO_4-Na_2SO_4-K_2SO_4	975	3	211, $Cu_2Y_2O_5$,	$BaSO_4$
1:1	Na_2SO_4	1050	4	211	Na_2SO_4
1:1	K_2SO_4	1050	4	211	K_2SO_4
1:1	Li_2SO_4-Na_2SO_4-K_2SO_4	1050	4	Y_2O_3	K_2SO_4
1:1	Na_2SO_4	1100	4	211, Y_2O_3	Na_2SO_4
1:1	K_2SO_4	1100	4	211, Y_2O_3	K_2SO_4
1:1	NaCl-KCl	900	2	211	NaCl-KCl
2:1	NaCl-KCl	900	2	211	NaCl-KCl
3:1	NaCl-KCl	900	2	211	NaCl-KCl

Table 1: Stability of Preformed 211 Phase in Molten Salt systems

The salts promising the best stability of 211 phase were then studied as fluxes in producing 211 powders from raw materials. In this method precursor materials $BaCO_3$, Y_2O_3 and CuO in the stoichiometric proportions of Y_2BaCuO_5 were mixed with various salt systems and ball milled in ethanol for 12 hours. The dried batch was then heat treated in closed magnesia crucibles. Table 2 gives details of the salt systems used, the temperature and time of the heat treatment and the resultant phases.

Ratio Salt:211	Salt Systems	Temp °C	Time Hrs.	Resulting Phases	
				Oxides	Other Phases
1:1	NaCl-KCl	850	4	$Cu_2Y_2O_5$, Y_2O_3	$BaCO_3$, NaCl, KCl
1:1	NaCl	850	3	211	NaCl
1:1	NaF	1000	4	Y_2O_3, $Cu_2Y_2O_5$	NaF, $BaCO_3$
1:1	KI	825	4	211	KI
3:1	K_2SO_4	1050	4	211, Y_2O_3	K_2SO_4, $BaCO_3$
3:1	Na_2SO_4	1050	4	211, Y_2O_3	Na_2SO_4, $BaCO_3$
3:1	NaCl-KCl	1000	4	211, Y_2O_3	$BaCO_3$, NaCl, KCl

Table 2: Stability of 211 Phase in Precursor-Salt Systems

The high stability of Y_2BaCuO_5 in water enabled easy removal of the salts by repeatedly washing with water. X-ray diffraction studies were used to confirm the removal of the salts. The washed samples were then observed under the scanning electron microscope.

To test the proof of concept that the green phase, Y_2BaCuO_5 can be used as seed crystals in the formation of the superconductor, the resultant pure Y_2BaCuO_5 was mixed with reagent grade $BaCO_3$ and CuO in the required molar proportions as given by the following reaction:

$$Y_2BaCuO_5 + 3BaCO_3 + 5CuO \longrightarrow 2YBa_2Cu_3O_{7-x} + 3CO_2 \quad (1)$$

The batch was calcined at 960°C for 12 hours and annealed at 530°C for 6 hours in oxygen atmosphere. The results was positive and the 123 material was then formed by tape casting proceedure.

Tape Casting

To test the total concept, 123 ceramic was formed using tape casting technique. The batch containing the required amounts of Y_2BaCuO_5, $BaCO_3$ and CuO, was ball milled in ethanol for 12 hours to ensure homogeneity, dried and sized to 325 mesh to ensure uniform small particle size.

Commercially available binder (Metoramic Sciences, Inc., Clandan Product No. B73210) was used in order to supply the necessary rheological properties required in tape casting. Binder additions to the above batch were made in the amount of 40-45% by weight and Toluene in the amount of 5-7% by weight was also added to adjust the viscosity. This batch was then ball milled for 12 hours with zirconia balls and tape cast on glass using a hand held doctor blade. The blade height was consistently set at 0.25 mm. A solution of pure lecithin dissolved at a 1.5 weight percent ratio with 1,1,1 trichloroethane was used as a releasing agent.

The green tapes were cut into one inch square pieces and laminated in a one inch square die with between 15-20 layers. The die was brought to a stable temperature near the glass transition of the binder through the use of heating plates on a hydraulic press. The lamination temperature used was between 60 and 65°C while the pressure was 5000 psi and the time

varied from 2 to 3 minutes. The resulting monolith showed no evidence of individual layers. The monoliths were then trimmed on all edges and diced into individual compacts. The rate of heating for the binder burnout, as determined from TGA analysis of the green tape, was regulated at 20°C per hour upto 500°C and held there for 1 hour. The compacts were then taken to the calcination temperature of 960°C at a rate of 100°C/hr and held there for 12 hours and then annealed at 530°C for 12 hours in flowing oxygen atmosphere. X-ray diffraction analysis revealed the presence of a nearly single phase $YBa_2Cu_3O_{7-x}$.

RESULTS AND DISCUSSION

Tables 1 and 2 show the stability of Y_2BaCuO_5 in most of the salt systems. This green phase was observed to degrade mostly in those salt systems that contained lithium salts. It was also observed that batches heat treated in uncovered crucibles showed appreciable weight loss, nearly an order of magnitude higher than those runs conducted with covered crucibles. The salts could be easily removed by repeated washing of the heat treated batch with water. The SEM micrographs shown in figures 1-3 are of the samples heat treated at 1000°C at times of 4, 12 and 32 hours respectively. From the micrographs it can be seen that there is a small presence of anisotropic particles at 4 hours which increases by a great amount at 12 hours while for still longer times they tend to be more rounded or equiaxed.

The process of combining the 211 powders from the salt synthesis with $BaCO_3$ and CuO and calcining revealed a phase pure $YBa_2Cu_3O_{7-x}$ with no or very little of Y_2BaCuO_5 phase.

Tape cast mixtures of 211 with $BaCO_3$ and CuO also revealed a nearly phase pure $YBa_2Cu_3O_{7-x}$. Figure 4 shows the XRD pattern of a calcined tape cast sample. From this X-ray diffraction plot it can be seen that peaks belonging to the 00l lines have increased intensity compared to a calculated pattern. This gives an idea of the degree of orientation and the Lotgering's factor[11] calculated for this pattern gives a factor of 0.27 which actually represents a moderate degree of orientation. The density of the calcined tapes was about 80-85% of the theoretical density. Resistivity measurements using a four point probe method performed on the tape cast samples show a T_c at 86 K for zero resistivity. The plot of resistivity against temperature is shown in figure 5. Figure 6 reveals the microstructure of a tape cast sample seen through a surface pore. The pore is surrounded by large grains with some platy morphology and appears consistent with a Lotgering orientation factor of 0.27.

CONCLUSIONS

The Y_2BaCuO_5 phase showed good stability in the salts and its stability in water facilitated in easy removal of the salts. Anisotropy depends on the growth kinetics as evident in times upto 12 hours. Longer soak times tended to produce more equiaxed particles. It was seen that the crucibles need to be covered during to minimize the weight loss of the batch on heat treatment. It has been shown here that Y_2BaCuO_5 can be used as seed crystals in the formation of $YBa_2Cu_3O_{7-x}$ superconductor. As further proof of concept we have shown

that tapes made of precursor materials can be easily converted to superconducting tapes. Moderate degree of orientation can be achieved in the tapes. Resistivity measurements show a T_c of 86 K for these tapes.

ACKNOWLEDGEMENTS

We would like to acknowledge with thanks New York State Institute of Superconductivity for financial support for this work.

REFERENCES

1. T.R. Dinger, T.K. Wothington, W.G. Gallagher, amnd R.L. Sandstrom, "Direct Observation of Electronic Anisotropy in Single Crystal $YBa_2Cu_3O_{7-x}$", Phys. Rev. Lett., 58 [25] 2687-90 (1987).

2. Y. Enomoto, T. Murakami, M. Suzuki, and K. Moriwaki, "Largely Anisotropic Superconducting Critical Current in Epitaxially Grown $Ba_2YCu_3O_{7-x}$ Thin Films", Jpn. J. Appl. Phys., 26 [7] L1248-50 (1987).

3. T. Kimura and T. Yamaguchi, "Morphology Control of Electronic Ceramic Powders by Molten Salt Synthesis", in Advances in Ceramics, Vol. 21, ed. by G.L. Messing, K.S. Mazkiyasni, J.W. McCauley and R.A. Haber, American Ceramic Society, Columbus, Ohio 1987, pp. 169-77.

4. S.H. Lin, S.L. Swartz, W.A. Schulze and J.V. Biggers, "Fabrication of Grain-Oriented $PbBi_2Nb_2O_9$", J. Amer. Ceram. Soc., 66 [12] 881-84 (1983).

5. M. Holmes, R.E. Newnham and L.E. Cross, "Grain-Oriented Ferroelectric Ceramics", Am. Ceram. Soc. Bull., 58 [9] 872-73 (1979).

6. C.T. Decker, V.K. Seth and W.A. Schulze, "Feasibility of Synthesis of Anisotropic Morphology $Ba_2YCu_3O_{7-x}$ Powder by Molten Salt Technique", in Advanced Superconductors II, ed. by M.F. Yan, American Ceramic Society, Westerville, Ohio, 1988, pp.169-76.

7. D.B. Knorr and C.H. Raeder, "Stability of Yttrium Barium Cuprate in Molten Salts", in Superconductivity and Applications, ed. by H.S. Kwok, Plenum Press, NY, 1990.

8. R.L. Barns and R.A. Laudise, "Stability of Superconducting $YBa_2Cu_3O_7$ in the Presence of Water", Appl. Phys. Lett., 51 [17] 1373-75 (1987).

9. E.M. Levin, C.R. Robbins, H.F. McMurdie, Phase Diagrams for Ceramists, 1969 Supplement, M.K. Reser, ed., The American Ceramic Society, Columbus, Ohio, 1969.

10. F.K. Lotgering, "Topotactical Reactions with Ferrimagnetic Oxides having Hexagonal Crystal Structures-I", J. Inorg. Nucl. Chem., 1959, Vol. 9, pp. 113-23.

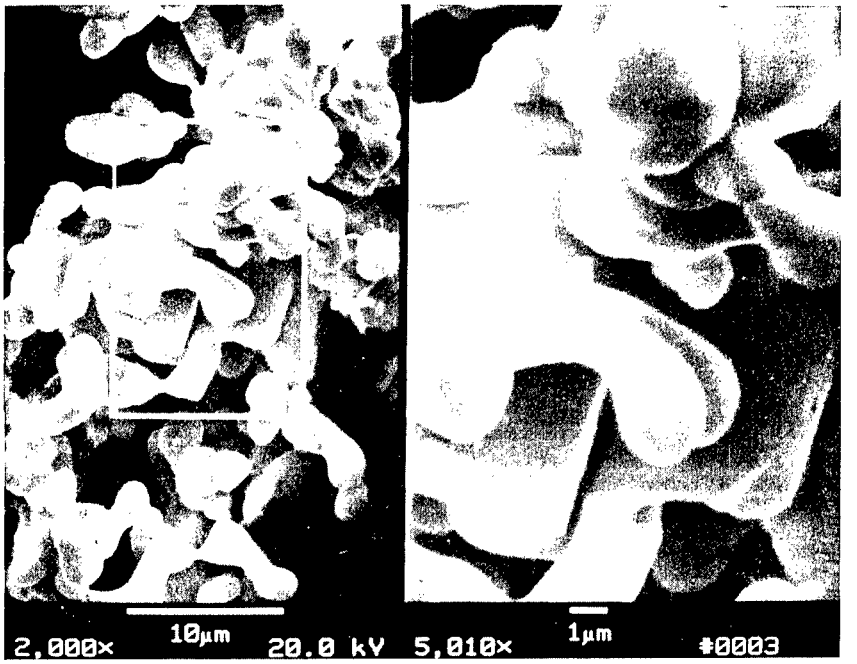


Figure 1: **SEM micrograph of sample containing precursor (211) materials and NaCl-KCl salt system heat treated at 1000°C for 4 hours**

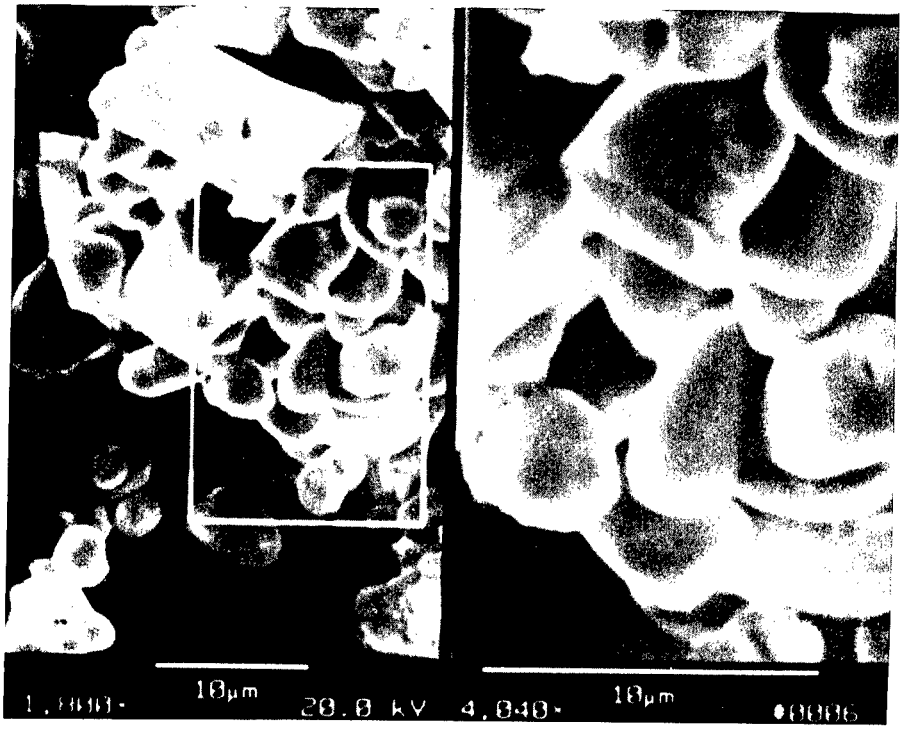


Figure 2: **SEM micrograph of sample containing precursor (211) materials and NaCl-KCl salt system heat treated at 1000°C for 12 hours**

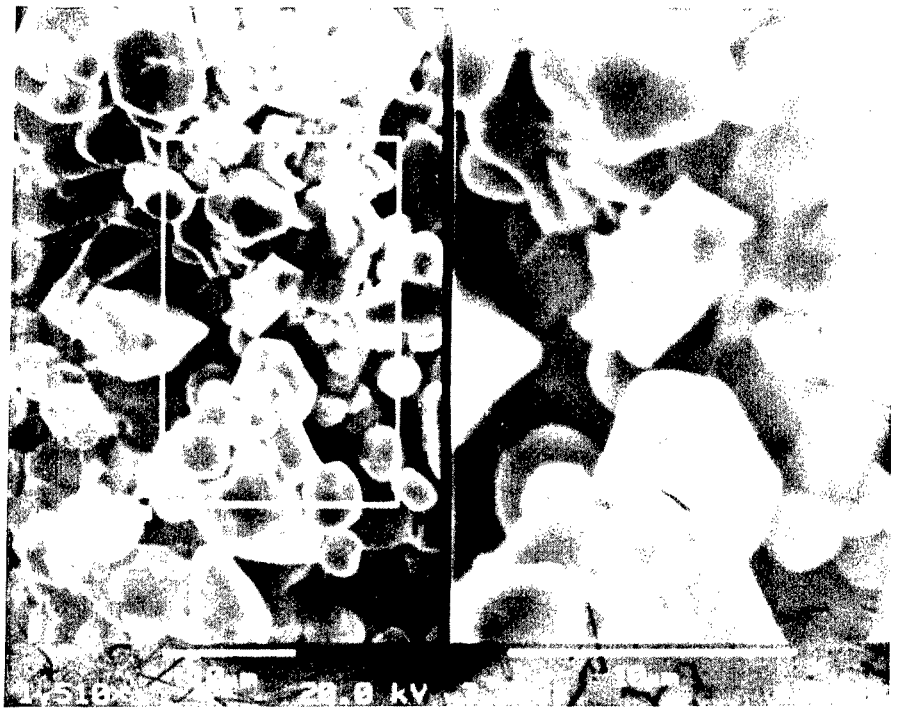


Figure 3: **SEM micrograph of sample containing precursor (211) materials and NaCl-KCl salt system heat treated at 1000°C for 32 hours**

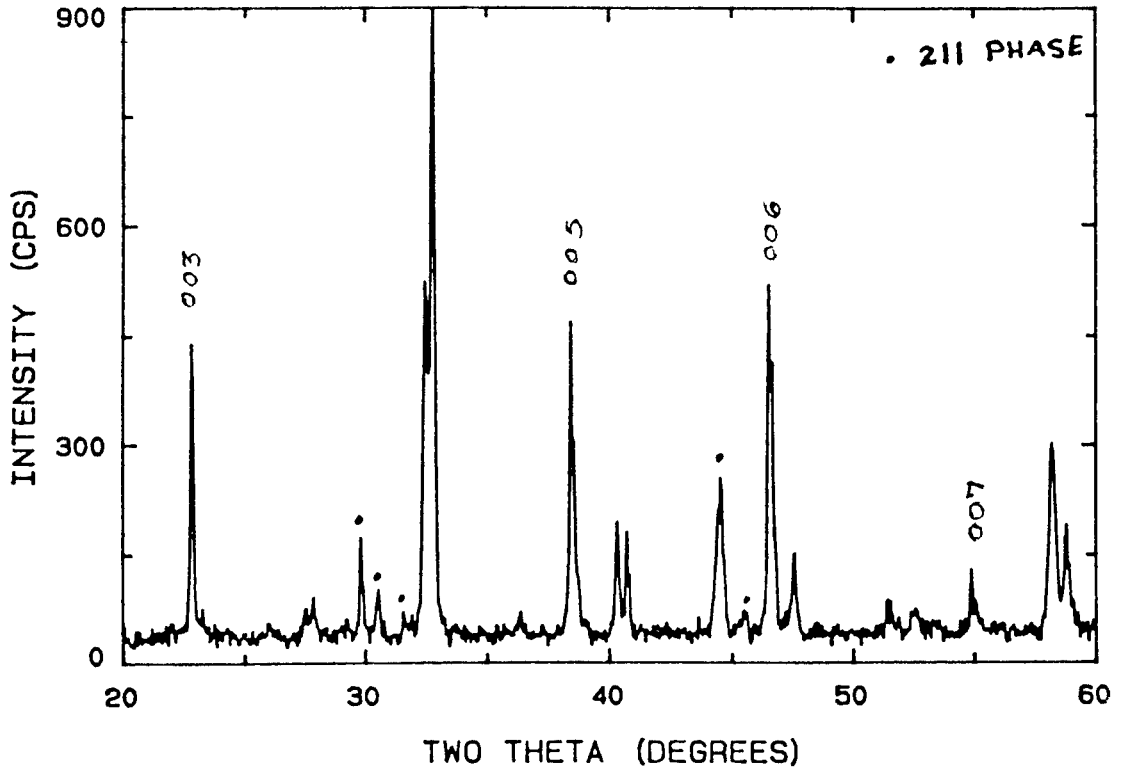


Figure 4: **XRD pattern for $YBa_2Cu_3O_{7-x}$ formed from calcination of tapes of Y_2BaCuO_5 with $BaCO_3$ and CuO**

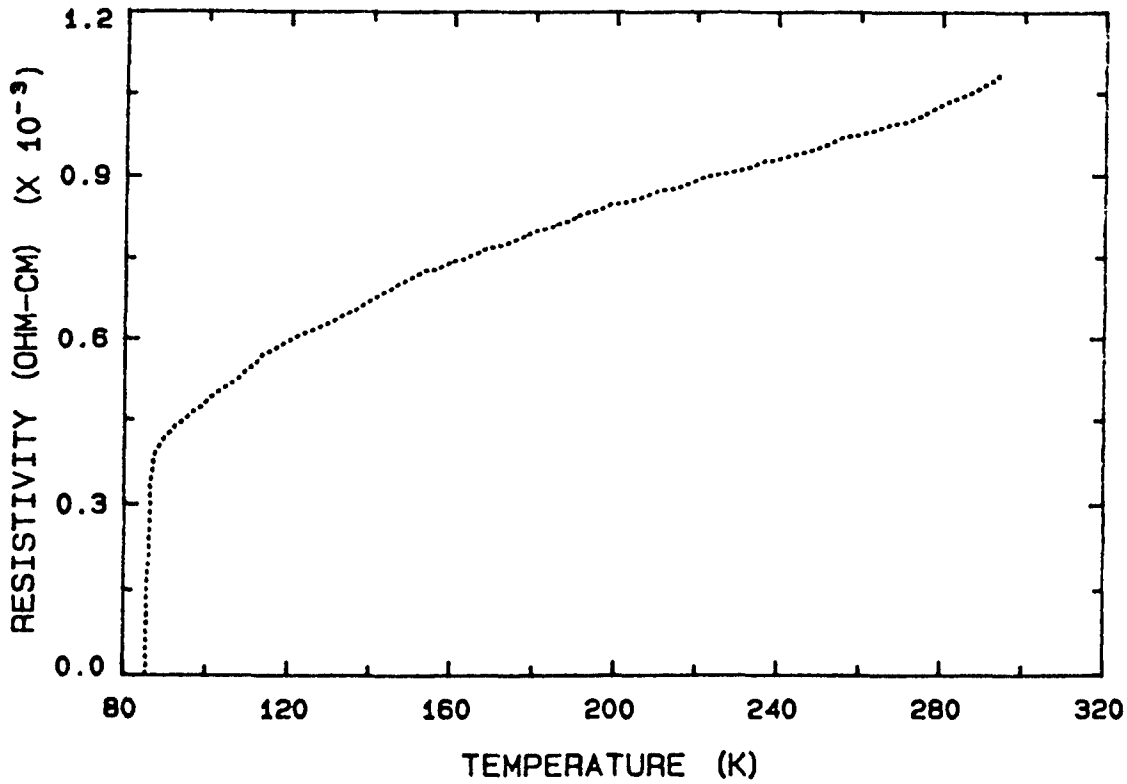


Figure 5: **Plot of resistivity versus temperature of a tape cast sample**



Figure 6: **SEM Micrographs of a tape cast sample as seen through a surface pore for ceramic sintered at 960°C for 12 hours**

LEVITATION OF SUPERCONDUCTING COMPOSITES

C. K. Chiang, M. Turchinskaya, L. J. Swartzendruber,
R. D. Shull, and L. H. Bennett

Material Science and Engineering Laboratory
National Institute of Standards and Technology
Gaithersburg, MD 20899

ABSTRACT

The inverse levitation of a high temperature superconductor-polymer composite consisting of powdered quench-melt-growth $Ba_2YCu_3O_{7-\delta}$ and cyanoacrylate is reported. Magnetic hysteresis loop measurements for the composite are compared to those measured for the bulk material prior to powdering. Differences in the flux pining capibility between the two material forms are small but significant.

INTRODUCTION

The recently developed polycrystalline $Ba_2YCu_3O_{7-\delta}$ high temperature superconductor made by the quench-melt-growth technique (QMG) possesses very effective mechanisms for pinning magnetic flux lines.[1,2] This material requires no external additive such as silver, and still posseses a very large critical current and displays a sizeable levitation effect. The source of flux pinning is attributed to the small non-superconducting Ba_2YCuO_5 phase which is trapped inside the QMG superconductor. The present investigation was initiated to study sample size effects on macroscopic properties and to determine the effectiveness of the QMG superconductor as a component in a superconductor-polymer composite.

EXPERIMENTS

A polycrystalline $Ba_2YCu_3O_{7-\delta}$ ($\delta \sim 0$) sample was prepared by the quench-melt-growth technique.[1,2] A large grain, 5 mm x 3 mm x 1 mm, was chosen from the sample and used for this study. The grain was split into two parts of equal weight. One part was set aside for comparison (hereafter referred to as the bulk sample). The other part was ground into powder using a mortar and pestle. The particle size of the powder was distributed from less than 1 μm to as large as 500 μm. The average size of the particles was estimated to be 70 μm. The powder was made into superconductor-polymer composite by infiltrating the powdered superconductor (80 weight percent) with an insulating liquid cyanoacrylate (20 weight percent). The composite was curred at abient temperature, (hereafter referred to as the composite sample). The volume of the composite sample was slightly larger than the bulk sample.

Low alternating field (ac) susceptibility measurements were performed on both samples using a Hartskorn-type bridge operated at 0.5 Oe rms and at 1.68 kHz. Electrical resistivity of the bulk sample was measured using a standard four-probe dc technique. Magnetic hysteresis measurements were done at 77 K using a vibrating sample magnetometer after cooling the samples in zero applied field.

RESULTS AND DISCUSSION

Figure 1 shows the temperature dependence for the electrical resistivity and the ac susceptibility of the bulk QMG $Ba_2YCu_3O_{7-\delta}$ sample. The data suggest that the bulk sample is of high quality. The ac susceptibility data indicates a large decrease in magnetic susceptibility on decreasing temperature at 92 K. This is consistent with the observed decrease in electrical resistivity . Both results indicate a transition width about 1 K. The ac susceptibility data also indicate the fraction of superconductor was near 100% for the bulk sample at 77K. (there are small fractions of non-superconducting Ba_2YCuO_5 and CuO.)

Two experiments were performed using the bulk and the composite samples. First a permanent magnet was used to test both the levitation and inverse levitation phenomena.[3] Figure 2 shows a photograph of the composite suspended below a small magnet. There appeared to be no qualitative difference in either the levitation or inverse levitation properties between the bulk and the composite samples.

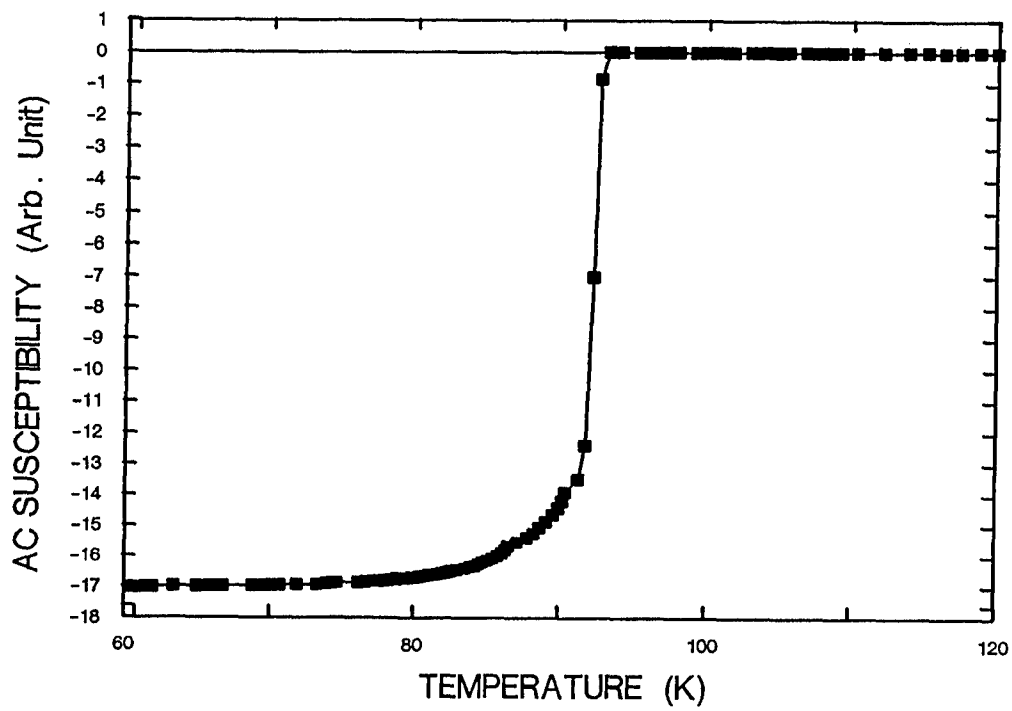


Figure 1a Magnetic susceptibility of the bulk QMG $Ba_2YCu_3O_{7-\delta}$ as a function of temperature.

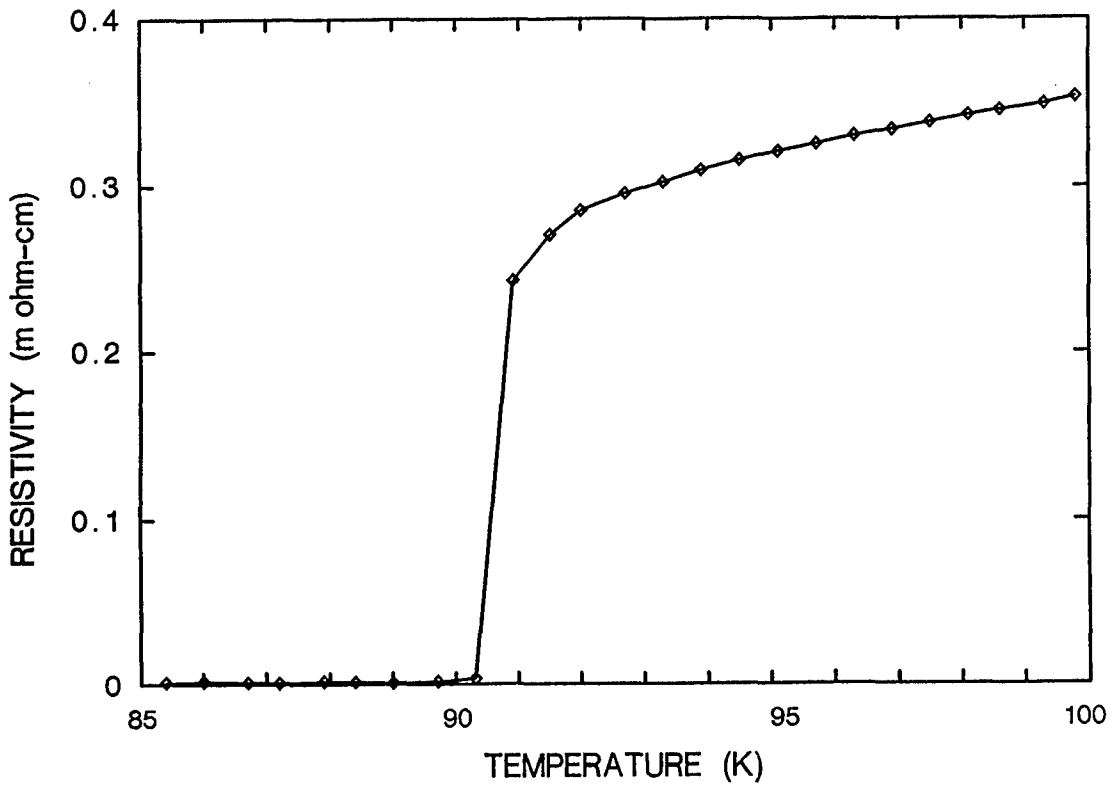


Figure 1b Electrical resistivity of the bulk QMG $Ba_2YCu_3O_{7-\delta}$ as a function of temperature.

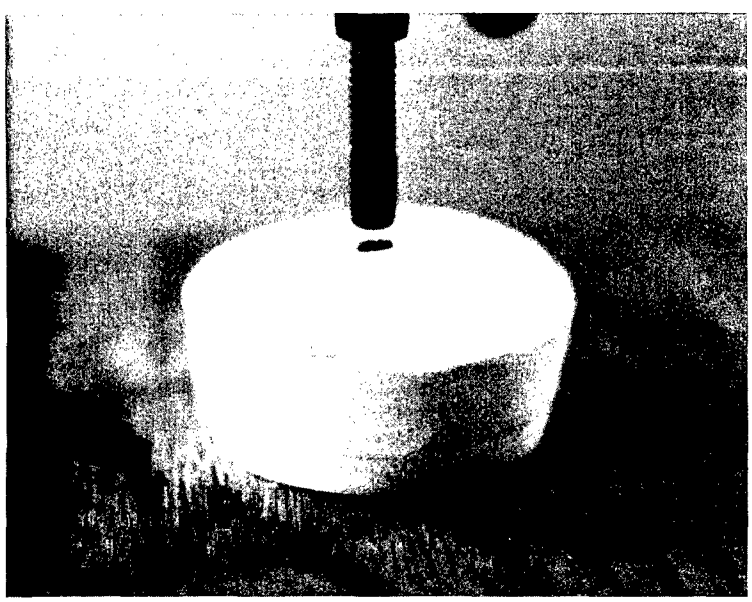


Figure 2 Inverse levitation of a QMG $Ba_2YCu_3O_{7-\delta}$ superconductor/polymer composite.

Figure 3 shows a comparison of the magnetic hystersis loops for the bulk QMG $Ba_2YCu_3O_{7-\delta}$ and the composite sample. A loop for a typical sintered $Ba_2YCu_3O_{7-\delta}$ sample is also included for comparison. The loop for the bulk and the composite are similar, both possesing a large remanent magnetization and a large amount of enclosed area. This indicates a significant amount of magnetic flux pinning. It also indicates that powdering the bulk QMG $Ba_2YCu_3O_{7-\delta}$ sample and isolating each particle in the polymer does not destroy the inherent flux pinning capibility of the superconductor. The small differences which are apparent in the hysteresis loops for these two forms of samples, are likely caused by differences in sample shape, size and texture. These parameters were not controlled in the present study. However, both of these hysteresis loops are significantly different from that typical of a sintered sample, which has little flux pinning capibility.

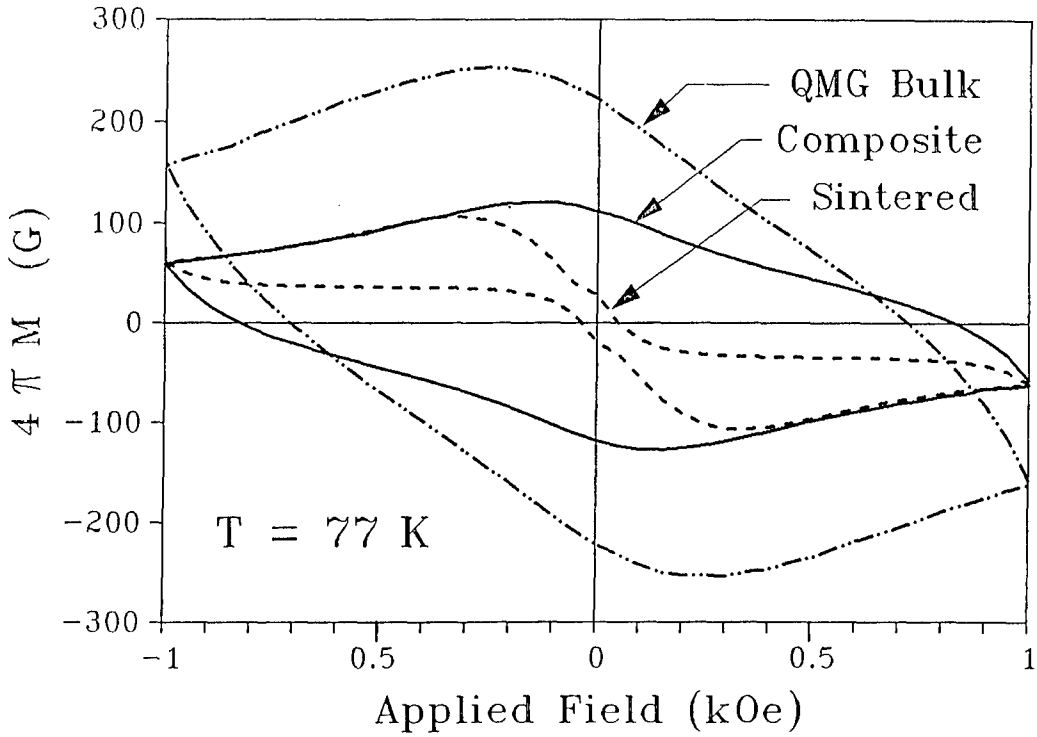


Figure 3 Comparison of the magnetic hystersis loops for the bulk QMG $Ba_2YCu_3O_{7-\delta}$, the composite and a sintered sample.

In the case of the inverse levitation effect, the balance of forces can be written as[3]

$$M(H)[dH/dz]_{-Z_o} = g \qquad <1>$$

where M(H) is magnetization per unit volume. dH/dz is the field gradient where the sample is located and g is the acceleration of gravity. Equation <1> requires positive non-zero value for M(H) in the first quadrant of the hysteresis loop for the inverse levitation to be possible.

Figure 3 shows that the powdering of a bulk sample only has a limited effect on reducing M(H) in this quadrant. The particle size effect on M(H) may be estimated from the field dependence of the magnetization of a superconductor. From Bean's model[4] we have

$$J_c = Km/a \qquad <2>$$

or equivalently,

$$m = J_c a/K \qquad <3>$$

where m is the vertical width of the hysteresis loop, Jc is the critical current for the superconductor, a is the particle diameter and K is a constant depending on the geometry of sample. For a given material the Jc is fixed for the tempeature of measurement, and m will depend on the size of sample through the parameters a anf K. If we take a cubic bulk sample of magnitization m_b cut into n^3 equal cubic particles, the magnetization of each particle will be on the order of $m_n = m_b/n$. The total magnetization per unit volume achievable by the n^3 particles is thus reduced by a factor of n, whereas the volume of each particle has been reduced by a factor of n^3. This simple analysis suggests that the reduction of the magnetic moment is much slower than the reduction of the volume of particles. For the simple study here, the change of total magnetic moment from the bulk sample to the composite sample is much smaller than the factor 1/n, suggesting that that either the bulk sample meight be somewhat granular in nature or the geometric factor K is not the same for the bulk sample and the composite sample, or a combination of both. Obviously, the use of composites for levitation must be weighed against many other factors, such as sample size, synthesis method and engineering designs.

It is also noted that the particle size effect is reflected in the shape of the hysteresis loop. The loop for the composite sample is not identical to that of the bulk. The composite loop appears to reach a saturation at a lower field that of bulk. While the penetration of the field occurs at a higher field for the bulk sample. Consequently, upon the application of field, the composite which is composed of smaller superconducting particles will begin to lose its superconductivity before the bulk $Ba_2YCu_3O_{7-\delta}$ does. However, for some practical application involving levitation using superconducting materials, this reduced performance at high fields may not be a critical factor.

REFERENCE

1. M. Murakami, M. Morita, K. Doi, and K. Miyamoto, Jpn, J. Appl. Phys. 28, 1189, (1989).
2. M. Murakami, M. Morita, N. Koyama, Jpn, J. Appl. Phys. 28, L1125, (1989).
3. C.Y.Huang, Y. Shapira, E. J. McNiff, Jr., P. N. Peters, B. B. Schwartz, M. K. Wu, R.D.Shull, and C. K. Chiang, Mod. Phys. Lett., B2, 869, (1988).
4. C. P. Bean, Rev. Phys. Lett., 8, 250, (1962); Rev. Mod. Phys., 36, 31, (1964)

SECTION 2:
FLUX DYNAMICS

FLUX CREEP IN $Bi_2Sr_2Ca_1Cu_2O_{8+x}$ SINGLE CRYSTALS

E. Agostinelli, D. Fiorani, A.M. Testa, and J. Tejada*

I.T.S.E.--C.N.R., P.B. 10, 00016 Monterotondo Stazione (Italy)
* Dept. of Physics, University of Barcalona (Spain)

ABSTRACT

Dissipative effects have been investigated in $Bi_2Sr_2Ca_1Cu_2O_{8+x}$ single crystals by critical current and magnetic relaxation measurements. Activation energies for the flux motion have been determined from the temperature dependence of the critical current and from the time decay of the zero field cooled and the remanent magnetization. The effective activation energy has been found to increase with temperature, in agreement with the existence of a distribution of activation energies (E_o 20 meV at 4.2 K for H=10 kOe applied parallel to the c-axis).

1. INTRODUCTION

A great deal of effort has been recently devoted to the study of the large relaxation effects seen in the oxide superconductors (1-3). Relaxation processes, associated with the thermally activated flux motion, have been commonly observed in conventional superconductors. However, due to the high activation energy (1 eV) compared to the low thermal energy at 4.2 K, these processes are tolerably slow. Unfortunately, the picture is quite different for high-T_c superconductors. In fact, due to the short coherence length (e.g., $2A < \xi < 40A$), which presumably affects the spatial range of pinning forces, and to the higher absolute operating temperatures, dissipative effects are certainly one of the most serious obstacles to applications requiring high magnetic fields.

In any superconductor in the mixed state, the flux lines are pinned by various types of inhomogeneities (impurities, grain boundaries, extended defects, etc.). Therefore, a number of different mechanisms are possible sources of the interaction between flux lines and defects and, in general, any theoretical description of flux pinning is simplified by assuming that the microscopic defect dimensions are small compared to the flux line lattice parameter. At present, the critical current density in bulk oxide superconductors at 77 K is far below the level of Nb-Ti at low temperatures, mainly because of the weak link nature of grain boundaries in high-T_c materials. However, high critical current densities have been observed in single crystalline thin films (4) and in bulk textured materials. Therefore, because of ambiguity in the morphology and the density of the dominant pinning centers, the nature of the pinning mechanism in high-T_c superconductors has not been clarified.

Much experimental evidence of large dissipative effects has been reported in high-T_c superconductors by different measurement techniques such as DC resistivity (5-8), DC susceptibility (3), time dependence of magnetization (9), and mechanical oscillator (10, 11). In this paper, we will focus our attention on the relaxation properties of a $Bi_2Sr_2Ca_1Cu_2O_{8+x}$ (nominal composition) single crystal. The study has been performed by measuring both the critical current density and the time decay of the magnetization as functions of temperature.

2. RESULTS AND DISCUSSION

2.1 Sample characterization

A single crystal (platelet of dimensions 2.2x1.7x0.3 mm^3) grown by a flux technique (12) has been selected for the measurements. The analysis of the X-ray diffraction pattern indicated the presence of the 2212 phase only. This result has been further supported by the magnetic characterization carried out by AC susceptibility measurements (mutual inductance bridge, with H_{ac} = 1 Oe at ν = 200 Hz) and by DC magnetization measurements (commercial S.H.E. SQUID magnetometer), with the magnetic field applied both parallel and perpendicular to the c axis of the crystal. Both the AC (fig. 1) and the DC curves show only one transition at 85 K without any detectable drop at 110 K, thus confirming the absence of any contribution from the higher T_c phase. The lower critical fields at 4.2 K have been deduced by analysis of the low field region of the magnetization cycle; the H_{c1} values, estimated by the deviation from linearity of the M vs H plot, are H_{c1} (//c)=880 Oe and H_{c1} ($\perp$c)=140 Oe (corrected for the demagnetization factor). Values of H_{c1} reported in the literature commonly range from 10 Oe to 1000 Oe; however, the lowest values should actually reflect flux penetration through non-superconducting phases or intergrowths within the 2212 phase, and are not an intrinsic feature of the material itself.

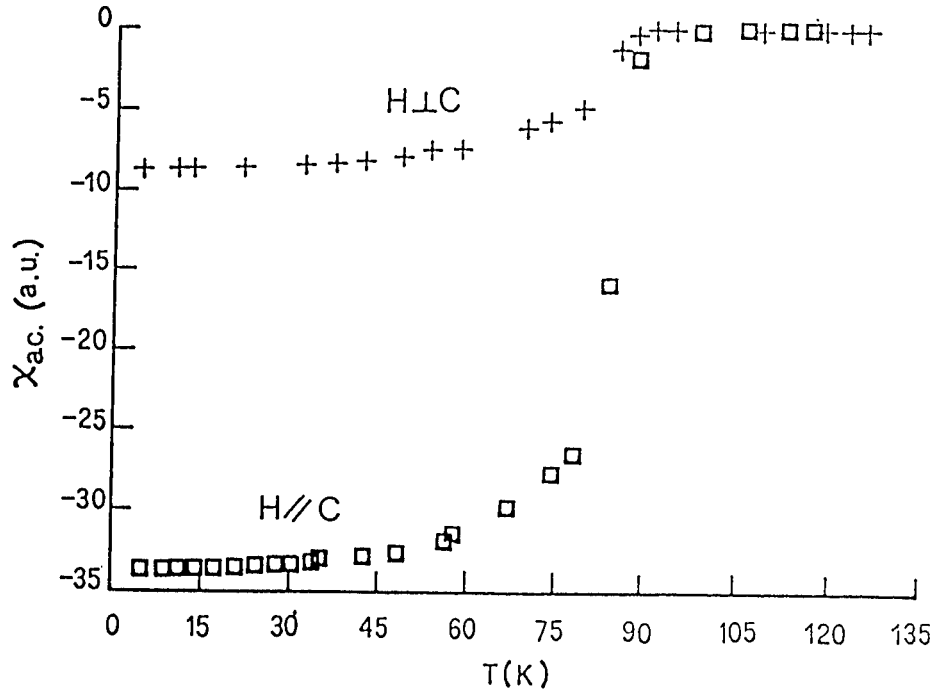


Figure 1. AC susceptibility curves.

2.2 Critical current measurements

Magnetization cycles up to 5 T have been performed at different temperatures (fig. 2). The cycle amplitude, connected to J_c in the Bean critical state model (13), decreases rapidly with increasing temperature. This results in an irreversible regime restricted only to low fields, thus indicating a strong field dependence of J_c even at temperatures well below T_c. This effect is also shown in fig. 3, where the magnetization at 2 kOe is reported as a function of temperature. The lower branch corresponds to the magnetization measured after increasing the field up to 2 kOe, while the upper one corresponds to the magnetization measured after a cycle 0->20 kOe->2 kOe. At 2 kOe there is no longer irreversibility above 20 K.

The Bean model approach, which assumes that the flux gradient is normal to the sample surface and has a magnitude of $4\Pi J_c$, allowed us to determine the critical current density J_c from the volume magnetization. For the H//c case, J_c is isotropic in the CuO_2 plane, allowing us to appproximate our sample as an isotropic cylinder of radius R=0.1 cm. For the H⊥c case, the sample cross section can be considered as a rectangle; this results in a current flowing both parallel as well as perpendicular to the planes and therefore not isotropic. Following Biggs et al. (14), the sample has been approximated as an infinite slab (thickness D=0.2 cm, in our case). J_c in zero field was measured by two different procedures. In the first case, the remanent magnetization was measured at 4.2 K after a cycle up to 5 T and then warming up to T_c. In the second case, after zero field cooling, a cycle has been performed at each temperature and the magnetization measured. The same behaviour was observed in both cases, thus reflecting that the temperature effect is much more important than the time effect. J_c decreases very rapidly with increasing temperature, revealing a high degree of thermal activation for flux motion across the energy barriers.

The temperature dependence of J_c is well decribed by the phenomenological law:

$$J_c(T) = J_c(0)\ [1- T/T_c]^s \qquad (1)$$

as reported for YBaCuO (9). Actually, with increasing temperature, the applicability of the Bean model becomes questionable as the flux creep rate should be higher than the rate of field variation. Anyway, the phenomenological relation (1) gives an estimate of the rate of the temperature decrease of J_c with respect to conventional superconductors, where the exponent has been found to lie in the range of 1-2.5. The low temperature behaviour of T_c has been analyzed in the framework of the thermally activated flux creep model (15). Thermal activation increases the flux creep rate thereby reducing the observed critical current density, which is given by (15):

$$J_c(T) = J_{co}\ [1-(kT/U_o)1n(t/t_o)] \qquad (2)$$

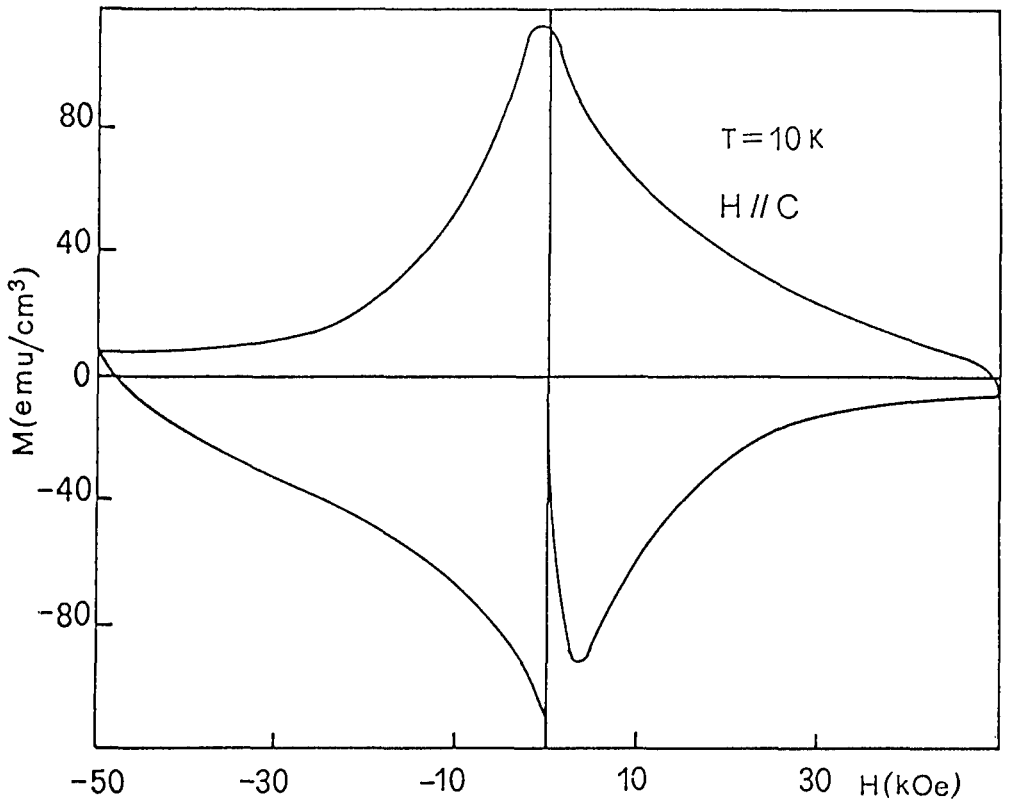


Figure 2. Magnetization cycle at 10 K.

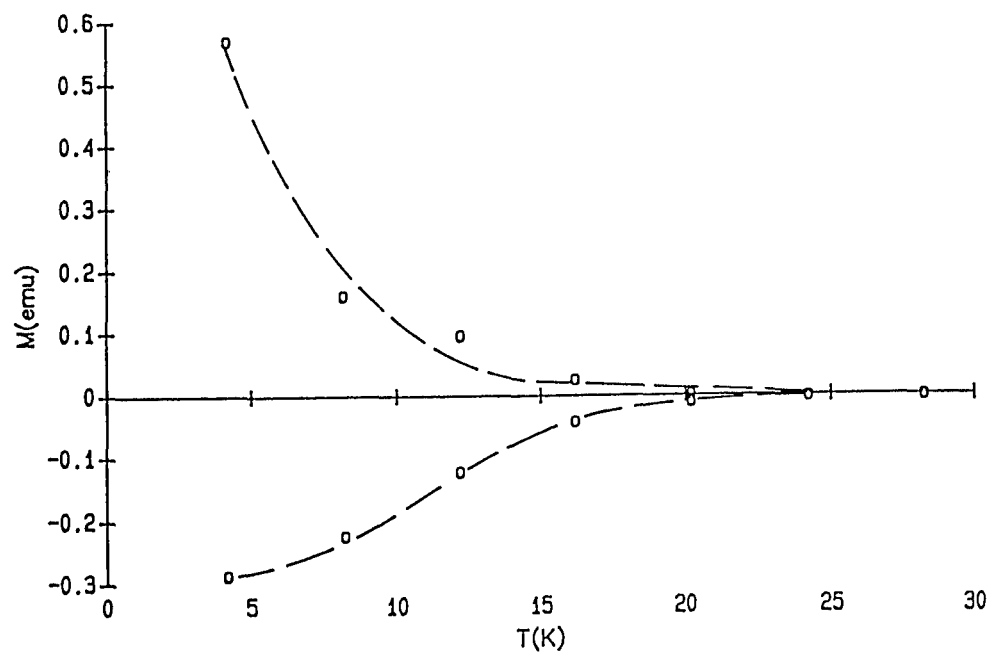


Figure 3. M(H=2 kOe) vs. T (see text).

where J_{co} is the value of J_c in the absence of thermal activation of flux lines, U_o is the depth of the pinning potential, t is a characteristic time for the experiment, and t_o is a constant which depends on parameters such as the fluxon oscillation frequency, the average hopping distance of the fluxons, etc. (15). As a consequence of equation (2), the temperature dependence is much stronger than the time dependence and therefore, to a first approximation, J_c is time independent and linear in T at low temperatures. From the intercept of the straight line at T=O K, the following values of J have been deduced: $J_{co}(//c) = 1.1 \cdot 10^5$ A/cm^2 and $J_{co}(\perp c) = 1.5 \cdot 10^4$ A/cm^2. From the observed slope, at $t \approx 10^4$ s and assuming $t_o \approx 10^9$ s (14), the activation energy has been determined for both orientations: $U_o(//c) = 36$meV and $U_o(\perp c) = 37$ meV. The absence of anisotropy in U_o would suggest that the flux motion perpendicular to the Cu-O planes is negligible; fluxons essentially move along the Cu-O planes even when the field is applied perpendicular to the c-axis (14).

However, it should be noted that equation (2) was deduced assuming a linear current dependence of U_o; this approximation is correct only for the case of a square-shaped flux line potential, which could not reflect the physics of the actual pinning mechanism.

2.3 Relaxation measurements

The relaxation properties of the Bi-Sr-Ca-Cu-O crystal have been investigated by measuring the time decay of the zero field cooled magnetization (M_{zfc}) and of the remanent magnetization (M_r). In the former procedure, the sample has been first cooled in zero field from above T_c and then, at different temperatures, a field H=10 kOe has been applied parallel to the c axis; in the latter one, the decay has been recorded in zero field, after a magnetization cycle up to 5 T. In fig. 4, the time decay of the magnetization, normalized to the first measured value, is reported. The observed relaxation rate is very fast (e.g., at T = 15 K after one hour, the relative decrease of the magnetization is 48%), which is consistent with the vanishing of J_c in low fields well below T_c.

The relaxation data have been analyzed in two ways, both within a thermally activated motion picture. In the first one, the classical flux creep model, which assumes the existence of energy barriers of the same height, has been applied. We substituted equation (2) into the Bean equations (which assume J_c independent of H) (13); for the H//c case, using the cylinder approximation and ignoring H_{c1}, the relaxation rate is given at the lowest order in kT/U_o by (9):

$$d(4\pi M)/d\ln t = -(H^2/H^*)[1-2/3(H/H^*)]kT/U_o \qquad H<H^* \qquad (3a)$$

$$d(4\pi M)/d\ln t = -(H^*/3)kT/U_o \qquad H \geq H^* \qquad (3b)$$

where $H^* = 4\pi J_{co}R/10$ is the field at which flux first penetrates entirely through the sample. In our case, the applied field (10 kOe) is much larger (after the correction for the demagnetization factor) than H^*. From equation (3b), a value of $U_o = 10$ meV at 4.2 K has been deduced. Yeshurun et al. (16) have developed a more realistic model, which takes into account the field dependence of J_c and the onset of irreversibility at H_{c1}. In particular, they developed a formula for the magnetization of a slab in a field lying in the slab plane, with J_c taking the form $J_c = J_{c1}(H_{c1}/h)^n$ for $h>H_{c1}$, where J_{c1} is the maximum critical current at a given temperature, h is the local field

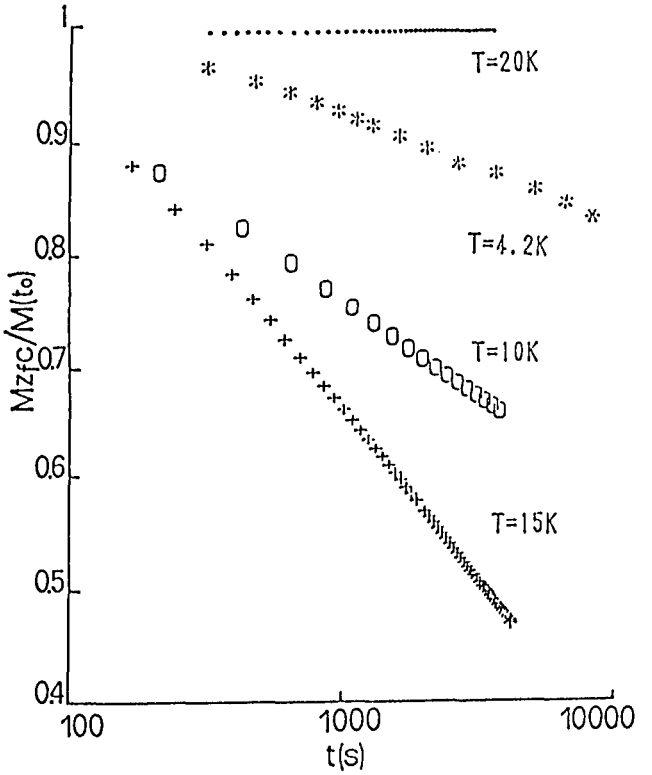


Figure 4. Time dependence of the ZFC magnetization for H=10 kOe //c.

at a distance,x, from the slab edge, and n, a phenomenological power. They found n=1 for YBCuO (with an U_o value differing only by a factor of two from that deduced from the original Bean model) and n=0 (thus recovering the original Bean equations) for Bi-Sr-Ca-Cu-O single crystals (3). Moreover, the temperature dependence of the relaxation rate, going through a maximum, is only partially reproduced by the model.

On the other hand, assuming the existence of a distribution of activation energies as in the Hagen-Griessen model (17), the temperature dependence of the relaxation rate can be well described in the whole temperature range. According to this model, the relaxation rate (S) has the form:

$$S = |dM/(MdInt)|t_o = - [E_o(T)/kT - \ln(t_o/\tau)]^{-1} \qquad (4)$$

where t_o is the starting time for the decay recording, τ is a characteristic relaxation time which is presumably in the range of 10^{-12} s-10^{-6} s (this uncertainty does not affect the deduced $E_o(T)$ values by more than 10%), and $E_o(T)$ is an effective temperature-dependent activation energy; i.e., a weighted average of the local activation energies. The deduced values of $E_o(T)$ at T=4.2 K are the following: $E_o(//c)= (18\pm2)$ meV and $E_o(\perp c)= (37\pm2)$ meV from the relaxation of M_{zfc}; $E_o(//c)=(20\pm2)$ meV and $E_o(\perp c)=(56\pm2)$ meV from the relaxation of M_r. Our data are consistent with a distribution of activation energies peaked at E=40 meV, as found by Hagen and Griessen in their analysis of Yeshurun's relaxation data (3,17). Furthermore, our results confirm the absence of significant anisotropy in the observed E_o which is found to increase with temperature ($E_o \approx 3$ eV at 20 K), as implied in the Hagen-Griessen model. The activation energy of a single pinning center should decrease with temperature and therefore, the observed increase of $E_o(T)$ must be related to the existence of a distribution of activation energies.

must be related to the existence of a distribution of activation energies.

Some processes occur on a time scale shorter than the typical SQUID measuring time and, at higher temperatures, the measured relaxation is essentially that associated with the high-energy characteristic tail of the predicted distribution.

Another explanation of the observed increase in $E_o(T)$ and of the maximum commonly observed in S(T), has been attempted by Larkin and Geshkenbein (L.G. model) (18) generalizing the Anderson's flux creep model. This generalization is based on the assumption that there exist two kinds of pinning centers: many weak centers with rather low activation energy and few strong centers with high activation energy. At low temperatures, weak centers give the main contribution to the pinning and creep and S(T) monotonically increases with temperature. At high temperatures, the weak centers are excluded and the critical current is determined by strong centers for which creep is much slower. This results in a decrease of S(T) and in the observed increase of the effective activation energy $E_o(T)$, which is in turn, related to the existence of high barriers between equilibrium states of the vortex lattice. However, in the L.G. model, the kind of centers for which the pinning energy is high or low, is not clarified.

We would finally remark that the Anderson-Kim model and its extensions do not take into account possible collective effects of the vortex lines, i.e., the existence of interactions between bundles of flux lines. In fact, in the flux creep picture, flux lines are considered as "point particles." In a bulk superconductor, vortex lines are of course, one-dimensional objects but due to the presence of defects, they experience different pinning surroundings. Taking into account collective effects of the flux lines, novel flux states have been predicted (19,20), which are different from the conventional Abrikosov flux lattice. Recently, experimental evidence in favour of the existence of a "vortex glass" phase, implying both collective effects and the existence of a random potential, has been reported for epitaxial films of YBaCuO (21). Although these new concepts certainly require a more complex analysis of experimental data, their applicative implications are an intriguing object of debate.

3. CONCLUSIONS

Almost completely reversible magnetization cycles, except for low fields, above 30 K and a very strong relaxation of the magnetization have been observed in a $Bi_2Sr_2Ca_1Cu_2O_{8+x}$ single crystal. These results, compared with those reported for YBaCuO single crystals (9), indicate that in Bi-based compounds, the dissipative effects are much stronger and that they take place at much lower temperatures, well below T_c. While a significant difference between the values of the critical current at 4.2 K is not generally observed, the temperature dependence in the presence of magnetic fields is very different, thus revealing a much faster thermally activated flux motion in the Bi-based compounds. The difference in the pinning energies between BiSrCaCuO and YBaCuO compounds could be, in principle, associated with the different defect structures. In BiSrCaCuO, the pinning centers are supposed to be weak and randomly distributed point defects (e.g., cross substitutions, intergrowths, etc.). On the other hand, extended defects such as twin planes are present in $YBa_2Cu_3O_7$. Recent experiments on a series of YBaCuO single crystals with different twin boundary densities have shown that the magnetically deduced J_c at 4.2 K is not significantly affected by the presence of twin boundaries (22). However, a smaller irreversibility regime was found in the region near T_c for an untwinned crystal, thus implying lower pinning energies. At such high temperatures, the lattice defects with low pinning energy become less active and the twin boundaries can play an effective role.

The great difference in the electronic anisoptropy (a value of $3 \cdot 10^3$ for the superconducting effective mass anisotropy has been reported for BSCCO (23)) could be the main reason for the different pinning energies and therefore, for the different dissipative behaviour shown by BSCCO and YBCO. A large electronic anisotropy can indeed result in a reduction of the correlation length along the flux lines (L_c), implying a decrease in correlation between vortices in adjacent planes.While in YBCO the coherence length is comparable to the interplanar spacing, in BSCCO it is four times smaller, thus implying a more two-dimensional character.

A shorter correlation length along the vortices results in a smaller flux bundle volume and, consequently, in smaller activation energies: $U_o = J_c \chi B d^2_c L_c r_p$, where dc is the correlation length of the vortices in the planes and r_p is the spatial range of the pinning potential (24). Large dissipative effects are thus favored by small values of L_c, an intrinsic feature of anisotropic compounds and thin films, and by a short coherence length which holds for large K superconductors, including high-T_c materials.

Acknowledgements--We wish to thank Mr. P. Filaci for his technical assistance.

REFERENCES

1. Palstra, T.M., B. Batlogg, L.F. Schneemeyer, J.V. Waszczak, 1988, *Phys. Rev. Lett.*, **61**, p. 1662.

2. Zeldov, E., N.M. Amer, G. Diren, A. Gupta, R.J. Gambino,and M.W. McElfresh, 1989, *Phys. Rev. Lett.*, **62**, p. 3043.

3. Yeshurun, Y., A.P. Malozemoff, T.K. Worthington, R. Dinger, R.M. Yandrofki, L. Krusin-Elbaum, F.H. Holtzberg, and G.V. Chandrasekhar, 1989, *Cryogenics*, **29**, p. 258.

4. Tanaka, S., and H. Itozaki, 1988, *Jpn. J. Appl. Phys.*, **27**, p. L-622.

5. Tinkham, M., 1988, *Phys. Rev. Lett.*, **60**, p. 1658.

6. Palstra, T.M., B. Batlogg, R. Van Dover, L. Schneemeyer, and J. Waszczak, 1989, *Appl. Phys. Lett.*, **54**, p. 763.

7. Hettinger, J., A. Swanson, W. Skocpol, J. Brooks, J. Graybeal, P. Mankiewich, R. Howard, B. Straughn, and E. Burkhardt, 1989, *Phys. Rev. Lett.*, **62**, p. 2044.

8. Sun, J., K. Char, M. Hahn, T. Geballe, and A. Kapitulnik, 1989, *Appl. Phys. Lett.*, **54**, p. 663.

9. Yeshurun, Y., A.P. Malozemoff, F. Holtzberg, and T.R. Dinger, 1988, *Phys. Rev.*, **B38**, p. 11828.

10. Gammel, L. Schneemeyer, J. Waszczak, and D.J. Bishop, 1989, *Phys. Rev. Lett.*, **61**, p. 1666.

11. Gregory, S., C. Rogers, T. Venkatesan, X. Wu, A. Inam, and B. Dutta, 1989, *Phys. Rev. Lett.*, **62**, p. 1548.

12. Balestrino, G., U. Gambardella, Y. Liu, M. Marinelli, A. Paoletti, P. Paroll, and G. Paterno, 1988, *J. of Crystal Growth*, **92**, p. 678.

13. Bean, C.P., 1962, *Phys. Rev. Lett.*, **8**, p. 250.

14. Biggs, B.D., M.N. Kunchur, J.J. Lin, S.J. Poon, T.R. Askew, R.B. Flippen, M.A. Subramanian, J. Gopalakrishnan, and A.W. Sleight, 1989, *Phys. Rev.*, **B39**, p. 7309.

15. Campbell, A.M., and J.E. Evetts, 1972, *Adv. Phys.*, **21**, p. 199.

16. Yeshurun, Y., A.P. Malozemoff, F. Holtzberg, and T.R. Dinger, 1988, *Phys. Rev.*, **B38**, p. 11828.

17. Hagen, C.W., and R. Griessen, 1989, *Phys. Rev. Lett.*, **62**, p. 2857.

18. Larkin, A., and V.B. Geshkenbein, preprint.

19. Nelson, D., 1988, *Phys. Rev. Lett.*, **60**, p. 1973.

20. Fisher, M.P.A., 1989, *Phys. Rev. Lett.*, **62**, p. 1415.

21. Koch. R.H., V. Foglietti, W.J. Gallagher, G. Koren, A. Gupta, and M.P.A. Fisher, 1989, *Phys. Rev. Lett.*, **63**, p. 1511.

22. Dinger, T.R., G.J. Dolan, D. Keane, T.R. McGuire, Y. Yeshurun, T.K. Worthington, and R.M. Yandrofski, 1989, in Proceedings of the Annual Meeting of TMS-AIME, Las Vegas, (February 27-March 3, 1989).

23. Farrell, D.E., S. Bonkham, J. Foster, Y.C. Chang, P.Z. Jiang, K.G. Vandervoort, D.J. Lam, and V.G. Kogan, 1989, *Phys. Rev. Lett.*, **63**, p. 782.

24. Palstra, T.T.M., B. Batlogg, R.B. Van Dover, L.F. Schneemeyer, and J.V. Waszczak, 1989, *Phys. Rev. B*, in press.

ELLIPTICAL FLUX VORTICES IN $YBa_2Cu_3O_7$

H. Hickman, A.J. Dekker, and T.M. Chen

Department of Electrical Engineering
University of South Florida, Tampa, Florida 33620

Abstract- The most energetically favorable vortex in $YBa_2Cu_3O_7$ forms perpendicular to an anisotropic plane. This vortex is elliptical in shape and is distinguished by an effective interchange of London penetration depths from one axis of the ellipse to the other. By generalizing qualitatively from the isotropic to the anisotropic case, we suggest that the flux flow resistivity for a vortex that forms perpendicular to an anisotropic plane should have a preferred direction. Similar reasoning indicates that the Kosterlitz-Thouless transition temperature for a vortex mediated transition should be lower if the vortex is elliptical in shape.

Introduction

The free energy per unit length of an isolated Abrikosov vortex in a type II superconductor is given by [1]

$$\epsilon_1 = \frac{H_{c1}\Phi_o}{4\pi}, \tag{1}$$

where H_{c1} represents the lower critical field and Φ_o represents a single flux quantum. Single crystal $YBa_2Cu_3O_7$ can be viewed as a type II superconductor that contains one plane in which the superconducting properties are isotropic (ab plane) and two planes in which the superconducting properties are equivalently anisotropic (ac and bc). If ϵ_1^{ab} represents the free energy associated with a vortex that forms perpendicular to the isotropic plane, and $\epsilon_1^{ac} = \epsilon_1^{bc}$ represents the free energy associated with a vortex that forms perpendicular to an anisotropic plane, then for $YBa_2Cu_3O_7$ [2]

$$\frac{\epsilon_1^{ac}}{\epsilon_1^{ab}} = \frac{H_{c1}^{ac}}{H_{c1}^{ab}} = \frac{0.05T}{0.5T} = 0.1. \tag{2}$$

Equation (2) indicates that the formation of a vortex perpendicular to the anisotropic plane requires only 1/10 of the energy required by the formation of a vortex perpendicular to the isotropic plane.

But in order for a vortex to form perpendicular to an anisotropic plane, the anisotropic plane has to be incident on a non-superconducting region. This is certainly the case in an a (or b) axis oriented thin film, where almost the entire surface is an anisotropic plane. Further, for bulk $YBa_2Cu_3O_7$, studies indicate that as many as 75 % of the grain boundaries in a "shake and bake" sample contain ab planes [3], while, depending on the density, 18 to 35 % of the bulk sample consists of empty pockets or voids [4]. If many of the isotropic ab planes are incident on other grains, then many of the anisotropic ac and bc planes should be incident on the voids. Evidently there is ample opportunity for the formation of vortices perpendicular to anisotropic planes, even inside bulk $YBa_2Cu_3O_7$.

Discussion

The London theory solution for the magnetic flux density around a vortex that forms perpendicular to an isotropic plane indicates that [5]

$$B \propto K_o\left(\frac{r}{\lambda}\right), \tag{3}$$

where r is the cylindrical coordinate, λ is the London penetration depth, and K_o is a modified Bessel function of the second kind. The London theory solution for the magnetic flux density around a vortex that forms perpendicular to an anisotropic plane indicates that [6,7]

$$B \propto K_o\left(\sqrt{\left(\frac{x}{\lambda_{yy}}\right)^2 + \left(\frac{y}{\lambda_{xx}}\right)^2}\right), \tag{4}$$

where B is z-directed and λ_{yy}, λ_{xx} are the London penetration depths in the y and x directions.

Apart from the fact that the contour lines are elliptical in shape, the most interesting aspect of equation (4) is that it predicts an effective interchange of penetration depths around the vortex. In $YBa_2Cu_3O_7$ for example, measurements by Worthington *et al.* reveal that the longest penetration depth is in the c direction while the longest coherence length is in the a (or b) direction [2]. These data should lead to a "cat's eye" vortex model as shown in Figure 1a. (Here x is identified with the c direction while y could be either the a or the b direction.) The orientation of penetration depths ought to demand that $B(0,\lambda_{yy}) = B(\lambda_{xx},0)$. Instead as shown in Figure 1b, equation (4) predicts that $B(0,\lambda_{xx}) = B(\lambda_{yy},0)$. This remarkable shift has actually been observed by Dolan *et al.*, who report oval vortices with penetration depths that are shortest in the c direction [8].

The fact that the most energetically favorable vortex in

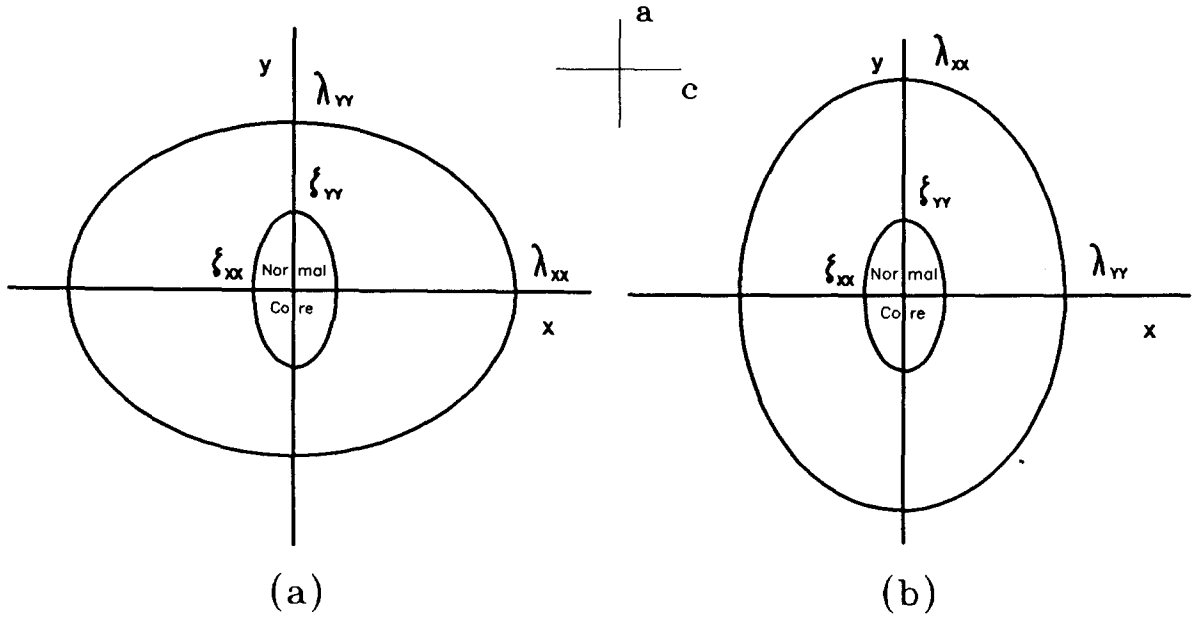


Figure 1 An Abrikosov Vortex in the Anisotropic Plane of $YBa_2Cu_3O_7$
(a) Anticipated Structure Based on Measurements of H_{c1}
(b) Actual Structure Based on London Theory and Observation

$YBa_2Cu_3O_7$ forms perpendicular to an anisotropic plane and is elliptical in shape, ought to have important physical consequences. By way of suggesting directions for future study, we now examine two expressions that were derived from isotropic considerations, and, in lieu of presenting a rigorous anisotropic treatment, we will *qualitatively* extend these equations to the anisotropic case.

Working from the Bardeen-Stephen model, Tinkham gives the following expression for flux flow resistivity in an isotropic superconductor [9]

$$\rho_f \propto \rho_n \left(\frac{B}{H_{c2}}\right), \tag{5}$$

where ρ_n is the normal state resistivity, B is the space averaged magnetic flux, and H_{c2} is the upper critical field. For $YBa_2Cu_3O_7$, ρ_n along c is large compared to ρ_n along a (or b) [10], while H_{c2} along c is small compared to H_{c2} along a (or b) [2]. Applied to (5), these differences lead to

$$\rho_{fc} > \rho_{fa} = \rho_{fb}. \tag{6}$$

Equation (6) indicates that the flux flow resistivity in the a (or b) direction is less than the flux flow resistivity in the c direction. Equation (4) indicates that the vortex is elongated in the a (or b) direction. Evidently, under the influence of a driving force, the vortex will move most easily in the direction of its own elongation. This prediction appears compatible with an argument given by Clem, in which the entropy flow from the trailing to the leading edge of a moving vortex results in dissipation [11]. An elliptical vortex should create the least amount of entropy flow (and hence the least dissipation) when it moves in the direction of its own elongation.

The phase transition of an ultra thin superconducting film is another phenomenon that might be affected by the formation of elliptical vortices. For an isotropic thin film, the Kosterlitz-Thouless transition temperature, T_{KT}, is given by [12]

$$k_B T_{KT} = \frac{\Phi_o^2}{32\pi^2}\frac{d}{\lambda^2}, \tag{7}$$

where d is the film thickness, and λ is the bulk penetration depth. In a c-axis oriented thin film, $\lambda = \lambda_a = \lambda_b$. For an a (or b) axis oriented film, it seems appropriate to replace $1/\lambda^2$ by an effective value. For example,

$$\left(\frac{1}{\lambda^2}\right)_{effective} \approx \frac{1}{2}\left[\frac{1}{\lambda_a^2} + \frac{1}{\lambda_c^2}\right]. \tag{8}$$

Since $\lambda_c > \lambda_a$, one concludes that

$$(T_{KT})_{\text{a axis oriented}} < (T_{KT})_{\text{c axis oriented}}.$$

If a vortex mediated KT transition does in fact take place in high T_c superconducting thin films, then the above argument suggests that the transition region in an a-axis oriented thin film would be wider than the transition

region in a c-axis oriented thin film.

Conclusion

The fact that the most energetically favorable vortex in $YBa_2Cu_3O_7$ is elliptical in shape should have important physical consequences. By qualitatively generalizing from the isotropic to the anisotropic case, we note for example, that both the Kosterlitz-Thouless transition temperature and the flux flow resistivity could be affected by vortex shape.

Acknowledgement

This work was partially supported by DARPA grant no. MDA972-88-J-1006.

References

1. M. Tinkham, Introduction to Superconductivity, p. 144, Robert E. Krieger Publishing Company, Inc., Malabar, Florida, 1980.

2. T.K. Worthington, W.J. Gallagher, T.R. Dinger, and R.L. Sandstrom, "Anisotropy in Single-Crystal $Y_1Ba_2Cu_3O_{7x}$,"in: Novel Superconductivity, edited by S.A. Wolf and V.Z. Kresin, pp. 781-785, Plenum Press, New York, 1987.

3. S. Nakahara, G.J. Fisanick, M.F. Yan, R.B. van Dover, and T. Boone, "On the Defect Structure of Grain Boundaries in $Ba_2YCu_3O_{7x}$," Journal of Crystal Growth, **85**, pp. 639-651, 1987.

4. R.N. Shelton, D. Andreasen, and P. Klavins, "Microstructure and Superconducting Properties of High-Density Consolidated $YBa_2Cu_3O_x$," Journal of the American Ceramic Society, **71**, pp. C487-C489, 1988.

5. B.B. Goodman, "Type II or London Superconductors," Reviews of Modern Physics, pp. 12-19, January 1964.

6. H. Hickman and T.M. Chen, "London Theory Solutions for the Magnetic Flux Density and the Supercurrent Density Around an Elliptical Abrikosov Vortex," scheduled for the January 1990 issue of the IEEE Transactions on Magnetics.

7. V.G. Kogan, "London approach to anisotropic type-II superconductors," Physical Review B, **24**, pp. 1572-1575, 1981.

8. G.J. Dolan, F. Holtzberg, C. Feild, and T.R. Dinger, "Anisotropic Vortex Structure in $Y_1Ba_2Cu_3O_7$," Physical Review Letters, **62**, pp. 2184-2187, 1989.

9. M. Tinkham, Introduction to Superconductivity, p. 165, Robert E. Krieger Publishing Company, Inc., Malabar, Florida, 1980.

10. T. Penney, S. von Molnar, D. Kaiser, F. Holtzberg, and A.W. Kleinsasser, "Strongly anisotropic electrical properties of single-crystal $YBa_2Cu_3O_{7x}$, Physical Review B, **38**, pp. 2918-2921, 1988.

11. J.R. Clem, "Local Temperature-Gradient Contribution to Flux-Flow Viscosity in Superconductors," Physical Review Letters, **20**, pp. 735-737, 1968.

12. M.R. Beasley, J.E. Mooij, and T.P. Orlando, "Possibility of Vortex-Antivortex Pair Dissociation in Two-Dimensional Superconductors," Physical Review Letters, **42**, pp. 1165-1168, 1979.

VORTEX MOVEMENT AND MAGNETIZATION OF HIGH Tc SUPERCONDUCTORS

A.L. Roytburd and M.J. Turchinskaya*
Engineering Materials Program
Department of Chemical and Nuclear Engineering, University of Maryland
College Park, MD 20742-2111
*Metallurgical Division, NIST, Gaithersburg, MD 20899

ABSTRACT

The basic characteristics of the thermoactivated vortex mobility in $Y_1Ba_2Cu_3O_7$ are determined by measurement of the kinetics of magnetization in two time regimes. The analysis of the kinetics of the approach of the equilibrium results in the activation energy, while the measurement of the log-creep rate allows determination of the activated moment. It is shown that the movement of vortices can be regarded as the diffusion process.

INTRODUCTION

The problem of vortex pinning is of great importance for the application of oxide high Tc superconductors. In comparison with pinning of dislocations, interface boundaries or domain walls, the pinning problem for vortices is much more complex because the density of vortices is large and adequate to produce strong interactions between the vortices in many practical important cases.

In accordance with the effects of vortex-vortex interactions on pinning two different cases can be considered. The first one corresponds to strong pinning centers with the spacing much larger than the distance between vortices. In this case the system of vortices can be considered an equilibrium phase (crystal, glass or melt), and the interaction of this phase with randomly distributed pinning obstacles can be analyzed. A classic example of such an approach is the Labusch theory of pinning for an elastic vortex lattice.[1] Another example is Nelson's melt theory,[2] which pretends to the explanation of the very weak pinning at temperatures above the reversibility temperature. Note that before melting, a great number of dislocations must be formed in the vortex crystal, and the real problem of the dynamics of the vortex medium in this case is the problem of movement and pinning of dislocations in the vortex lattice. In other words the trend to melting has to be manifested by a transition from a laminar flow of the vortex medium to a turbulent one. This problem seems very important in the case of pinning by interfaces or particles with spacing larger than a distance between vortices.[3]

However, the problem of intrinsic pinning in oxide superconductors may be closer to reality in the other case, where the individual vortices are pinned by the obstacles, and the distance between the obstacles is comparable with the distance between vortices. Collective effects of the vortex-vortex interactions are important in this case also, but we can expect that they manifest themselves in the renormalization of parameter values rather than in the alteration of the physical picture of the vortex motion. This case of small vortex density is under consideration in the paper. Our goal is to obtain basic characteristics of vortex mobility from the study of the magnetization of zero-field cooled samples.

THEORETICAL CONSIDERATION

The penetration of magnetic flow into a superconductor during its magnetization in an external magnetic field, Fig. 1, is similar to the flux flow diffusion,[4,5] and is described by the generalized diffusion equation:

$$\partial B/\partial t = \nabla(D_{eff}\ \nabla B), \tag{1}$$

where $D_{eff}=vB/\nabla B$ is the effective flux diffusion coefficient, B is the local induction, ∇B is the gradient of the induction, and v is the flux velocity.

The equation (1) is correct if there is no nucleation, multiplication or annihilation of vortices inside the sample, i.e. there are no weak links within a superconductor. The flux velocity for the thermoactivated movement of a vortex through an array of pinning obstacles can be determined as

$$v = v_o \exp(-U/kT)\sinh(\alpha\nabla B/kT). \tag{2}$$

This equation is obtained under the assumption that the energy barrier ΔF, which has been overcome for a vortex displacement, is disturbed under the driving force (∇B), and it is an analytical function of ∇B at $\nabla B=0$:[4,6]

$$\Delta F^{\pm}(\nabla B) = \Delta F(0) \mp \alpha\nabla B, \quad \Delta F(0) \equiv U, \tag{3}$$

where + corresponds to displacements with ∇B, - to the opposite direction, U is the activation energy, and α is the activated moment. $\alpha=m\ell_1$, $m=\phi_o n\ell_2$, where m is the magnetic moment of the vortex or vortex bundle, $\phi_o=2{,}7\times10^{-7}$ Gcm^2 is the flux of one vortex, n is the number of the vortices in the bundle, ℓ_1 is the displacement of the bundle or vortex at an activation event, ℓ_2 is the effective length of a displaced section of the bundle or vortex, factually the distance between the nearest pinning points along the vortex, (Fig. 2). v_o in Eq.(2) is the limiting velocity which equals $\ell_1\nu$, where ν is the frequency of vibration of the vortex section, ℓ_2. Assuming $\nu\sim(\xi/\ell_2)\nu_{at}$, where ξ is the coherence length or vortex "radius" ($\sim10^{-8}$cm), ν_{at} is the atomic vibration frequency $\sim10^{13}$s^{-1}, we get for $v_o\simeq\xi\nu_{at}\simeq10^5$cm/s, a value on the order of the sound velocity.

If the driving force is larger than the critical force, $\nabla B>\nabla B_{cr}=U/\alpha$, the movement of the vortex is overbarrier. The vortex movement is not described by Eq. (2) because it is controlled not by the frequency of fluctuation depinning events but by the rate of the dissipation of the vortex energy. In this case $v=(1/\gamma)\nabla B$, where γ is the viscosity.[7,8]

The vortex velocity, v(∇B), and the corresponding diffusion coefficient, $D_{eff}(\nabla B)$, are given in Fig. 3. There are three regions for which the solution of Eq. (1) can be obtained analytically.

The first one corresponds to the distribution of magnetic induction with $\nabla B>\nabla B_{cr}$. This is the so called flux flow region when $D_{eff}=D_f=B/\gamma$ is independent on ∇B.

The second region corresponds to the near critical state, when $\alpha\nabla B/kT\gg1$, and $\sinh(\alpha\nabla B/kT)\simeq\exp(\alpha\nabla B/kT)$. In this region the total magnetization of a superconductor, or its average induction, is proportional to the logarithm of

time:[4,6]

$$M(t) \simeq P \ln t, \quad P = dM/d\ln t \simeq kTR/(\partial\Delta F/\partial\nabla B) = (kTR/\alpha(R)), \tag{4}$$

where R is the radius of the sample, $\alpha(R)$ is the activated moment at its surface, where the induction B(R) is closed to the equilibrium one, B_o.

The third region corresponds to the constant D_{eff}=D at the small ∇B again:

$$D = (B_o\alpha v_o/kT)\exp(-U/kT) = D_o\exp(-U/kT), \quad D_o \equiv B_o\alpha v_o/kT \tag{5}$$

This regime of ordinary diffusion flow was named the thermally assisted flux flow (TAFF).[8]

It is important to note, that all of these regimes can be observed by measuring the magnetization as a function of time of the zero-field cooled superconductor sample. At the first moment after applying the magnetic field, ∇B is great and is larger than the critical value. Unfortunately, this stage is difficult to study because of nonstationary effects while the field is turned on. The sample then goes through the near critical state, where linear behaviour of magnetization vs. logarithm of time has been expected. At last, in the final stage, the magnetization approaches to the equilibrium saturation, M_o(or B_o), at $t>t^*$, and the kinetics of the magnetization is described by the equation:

$$M(t) = M_o + M'\exp(-t/\tau), \tag{6}$$

where M' is a constant. The relaxation time, τ , is connected with the diffusion coefficient, $D(B_o)$, by the relation $\tau = R^2/D$, where R is the sample radius. It is necessary to stress that this near equilibrium asymptotic behaviour does not depend on the distribution of the local induction at the moment t*, when the exponential stage begins, provided the induction is closed to B_o ($R\nabla B/B_o \ll 1$).

Thus the study of the kinetics of the magnetization at the different stages gives the opportunity to find the basic characteristics of the vortex mobility, α and U, without any additional assumption about the distribution of the induction within the sample. The results of such a kind of study are represented below.

SAMPLES AND EXPERIMENTAL METHOD

Three different $Y_1Ba_2Cu_3O_7$ samples with sharp transitions at Tc=93K were under investigation: a single crystal, a sintered polycrystal and a sample of quench,melt and growth (QMG) material.[10] The QMG sample is a bar of 0.9x0.9x5.8 mm, which was cut from a grain of a polycrystal. The sample has no weak links,[11] making it possible to determine its effective radius, R (R≈0.45 mm). Our single crystal sample contains some fraction of normal phase. So, the single crystal as well as sintered samples were not good for quantative estimates.

The samples were cooled in zero magnetic field. The magnetic field was then applied, and the magnetization was measured as a function of time using either a vibrating sample magnetometer, (VSM), or a SQUID system. The magnetic field was directed along c axes of the single crystal sample and perpendicularly to c axes of the QMG sample.

EXPERIMENTAL RESULTS

Approach to Equilibrium Magnetization, M_o. Diffusion Coefficient, D. Magnetization versus time, M(t), curves were measured at rather high temperatures (70 and 80K) and for long exposures (up to 340 ksec) at relatively weak magnetic fields (2 and 4 kOe), so the density of vortices was small up to approaching the equilibrium magnetization. M(t) data for all the samples at 70K and 2 kOe are plotted in curves (a) of Figures 4,5 and 6 for the QMG, single crystal and sintered samples, respectively. M vs. log-time data are plotted in curves (b). Curves obtained for the other temperature and field setting have the same shape as in these Figures: for all the curves there are log-time dependences M(t), and at much longer times, $t>t,^*$ there are stages of the approach to the equilibrium magnetization, M_o. In these stages the magnetization shows the exponential behaviour:

$$\ln[M(t)/M_o - 1] - \ln(M'/M_o) = -t/\tau, \qquad (7)$$

where $\ln(M'/M_o)$ are constants. In curves (c) of Fig.4,5 and 6, where the calculated data of $\ln[M(t)/M_o-1]$ vs. time for all the samples are plotted, it can be seen that at $t>t^*$ there are linear dependences of $\ln[M(t)/M_o-1]$ on time. The result of the determination of τ depends strongly on the choosen value of M_o, and a special asymptotic method was used[12] for the correction the values of M_o. For the QMG sample we obtained the values of M_o=-3.87 (emu/gr) at 70K and 2 kOe, and M_o=-2,5 (emu/gr) at 70K and 4 kOe.

The values of the relaxation time, τ, were obtained as a slope of the linear portion of the curves (c), and the diffusion coefficients, $D=R^2/\tau$, where R is the effective radius of the sample, were calculated. For the QMG sample at 70K we obtained $D\simeq 6.7\times10^{-9}$ cm^2/s for 2 kOe, and $D\simeq 7.8\times10^{-9}$ cm^2/s for 4 kOe.

Activated Moment, α, Activated Length, ℓ, and Intervortex Spacing, a. The logarithmic creep rate P=dM/dlnt for the QMG and sintered samples was measured in the temperature interval 6-80K.[10] The results are given in Fig. 7,a and in Fig. 7,b, respectively. For the QMG sample we calculated the values of the activated moment, α (using the relation α=kTR/P, Eq. (4)). Derived values of α/ϕ_o, where ϕ_o is the flux of one vortex, for the QMG sample are plotted in Fig. 8.

Values of the average activated length, $\ell=(\alpha/\phi_o)^{1/2}$, are displayed in Fig. 9 together with values of the distance between vortices, $a=(B_o/\phi_o)^{1/2}$. B_o was obtained from measuring the equilibrium magnetization, M_o: $B_o=4\pi M_o+H$.

Activation Energy, U, and Pre-exponential Factor, D_o. Obtaining τ and α from the kinetics of the magnetization, it is possible to estimate the activation energy of the thermoactivated movement of the vortex bundle, U, from the Eq. (5):

$$U/kT = \ln(D/D_o) = \ln(\tau v_o B_o \alpha/kTR^2). \qquad (8)$$

Assuming that $v_o=10^5$ cm/s, we obtained, with log-accuracy by v_o, $U/kT\simeq 33$, $U\simeq 0.19$ eV, and the pre-exponential factor $D_o=B_o\alpha v_o/kT\simeq 6\times10^5$ cm^2/s for the QMG sample at 70K and 2 kOe. For 70K and 4 kOe $U\simeq 0.2$ eV, $D_o\simeq 4\times10^6$ cm^2/s.

DISCUSSION

The exponential approach to equilibrium is evidence of the linear dependence between the vortex velocity and the driving force and supports the assumption of Eq .(3). Taking into account the relation between D_{eff} and resistance, ρ : $\rho = D/c^2$, where c is the velocity of light, we have to admit that at 70 and 80K and H=2 and 4 kOe the QMG sample of $YBa_2Cu_3O_7$ manifests small but finite resistivity. From the point of view of vortex mobility in this stage, the vortex medium is rather "melt" than "glass" (in terms of M.Fisher's theory[13]) or "crystal" with collective pinning.[14] For both these models ΔF must be the divergent function of ∇B at $\nabla \to 0$: $\Delta F \sim 1/\nabla B^{\beta}$, $\beta > 0$ for the vortex glass state, or $\sim \ln \nabla B$ for the collective pinning model.

By "vortex melt", we imply that the effects of correlations between the individual thermoactivated depinning events are small.[15] To prove this suggestion it is necessary to consider the pre-exponential factor, D_o, in Eq. (5) in more detail, rewriting it through the activated length, ℓ, and the intervortex distance, a , as

$$D_o = (\phi_o^2/kT)(\ell^2/a^2)v_o = Lv_o(\ell^2/a^2). \qquad (9)$$

The term, $\phi_o^2/kT \equiv L$, has the dimension of length (e.g. $L \simeq 4$ cm at 70K). From Fig. 10 it is clear that up to 70K at 2 kOe and 60K at 4 kOe, $\ell < a$, i.e. a bundle consists of only one vortex, and ℓ is the weak function of temperature. Then ℓ rises rapidly, i.e. the number of vortices in the bundle increases. For n=1, $\ell = (\ell_1 \ell_2)^{1/2}$, that is, ℓ is close to an average distance between pinning points.

At 70K and higher temperatures, all the pinning centers are occupied by vortices, and the pinning-depinning movements of vortices with the driving force ∇B can be interpreted as back-directed diffusion of pinning points in vortex medium. Indeed, the velocity of the point flow is determined by the Einstein diffusion relation:

$$v_p = (D_p/kT)\nabla\mu \approx (D_p/kT)(\alpha \nabla B/a), \qquad (10)$$

where $D_p = a^2 \nu \exp(-U/kT)$ is the point diffusion coefficent, and $\nabla\mu$ is the gradient of chemical potential of the pinning points in the magnetic field. The point velocity, v_p, is equal numerically to the vortex velocity, v:

$$-v_p = v = D\nabla B/B \qquad (11)$$

(the relation between D and v arises from the definition of D_{eff} in Eq. (1)). If we take into account that $a\nu = v_o$, it follows from Eqs. (10) and (11) that the vortex diffusion coefficient, D, is determined by Eq. (5). At $\ell \simeq a$, $D_o \simeq Lv_o \simeq 10^6 cm^2/s$: that is in accordance with the experimental determination of D_o through measuring α and B_o.

It is clear that the penetration of the flux flow into a sample during magnetization can be considered in terms of the diffusion theory for polycrystal samples with weak grain boundaries too. For this case it would be necessary to bring into consideration the vortex diffusion along the grain boundaries as well as the bulk grain diffusion. Of course the diffusion description may be not

complete if the nucleation of vortices is possible inside "bad" samples.

CONCLUSION

1. It is shown that approach to equilibrium magnetization with time of the zero-field cooled QMG, single crystal and sintered samples of $YBa_2Cu_3O_7$ proceeds according to the exponential law. The equilibrium values of the induction, relaxation time and vortex diffusion coefficient are determined for the QMG sample at 70 and 80K and 2 and 4 kOe.

2. Log-creep rate was measured at 2 and 4 kOe for a set of temperatures between 6 and 80K. From these data the activated moment α was found. The analysis of α shows that an activated vortex bundle contains only one vortex at the temperatures and fields under consideration. An activation length, $\ell = (\alpha/\phi_o)^{1/2}$, is almost constant up to 70 or 80 K. Beyond these temperatures the distance between vortices becomes smaller than ℓ. Up to these temperatures ℓ is likely the average distance between effective pinning points. At temperatures higher than 70K at field 2 kOe and temperatures ~75K at 4 kOe the number of vortices in a bundle grows, as does ℓ.

3. Using B_o and D, which are obtained from the approach to the equilibrium , and α from the log-creep stage, the activation energy, U, has been determined for the QMG sample.

4. The character of vortex movement during magnetization with time at 70 and 80K and 2 and 4 kOe is in good agreement with the diffusion picture, which does not take into account the effects due to the correlation between individual thermoactivation events.

ACKNOWLEDGEMENT

We are very grateful to L.H. Bennet and L.J. Swartzendruber for their friendly collaboration and to K. Sawano, D.L. Kaiser, J.E. Blendell, and C.K. Chiang for the samples.

REFERENCES

1. R. Labusch, Phys. Stat. Sol. 32, 439 (1967), Crystal Lattice Defects 1, 1 (1969).
2. D.R. Nelson and H.S. Seung, Phys. Rev. B39, 9153 (1989).
3. M.J. Turchinskaya and A.L. Roytburd, JETP Lett. 20, 79 (1974).
4. M.R. Beasly, R. Labusch, W.W. Webb, Phys. Rev. 181, 681 (1969).
5. E.M. Brandt, Z. Physik B., in press.
6. P.W. Anderson, Phys. Rev. Lett., 9, 309 (1962).
7. M. Tinkham, Phys. Rev. Lett., 13, 804 (1964).
8. L. Bardeen and M.J. Stephen, Phys. Rev. 140, A1197 (1965).
9. P.H. Kes, J. Aarts, J. van der Berg, and J.A. Mydosh, Supercond. Sci. Technol., 1, 242, (1989).
10. M.J. Turchinskaya, L.H. Bennet, L.J. Swartzendruber, A. Roytburd, C.K. Chiang, M. Hill, J.E. Blendell, and K. Sawano, High-Temperature Superconductors: Fundamental Properties and Novel Materials Processing. MRS Symp. Proc. 169, in press, (1990).
11. M. Murakami, M. Morita, and N. Koyama, Jpn. J. Appl. Phys., 28, L1125 (1989).
12. M.J. Turchinskaya, A.L. Roytburd, L.H. Bennett, L.J. Swartzendruber, and K.

Sawano, in preparation.
13. M.P.A. Fisher, Phys. Rev. Lett., 62, 1425 (1989).
14. M.V. Feigelman, V.B. Geshkenbain, A.L. Larkin, and V.M. Vinocur, Phys. Rev. Lett., 63, 2303 (1989).
15. A.L. Roytburd, M.J. Turchinskaya, L.H. Bennett, and L.J. Swartzendruber, submitted for publication.

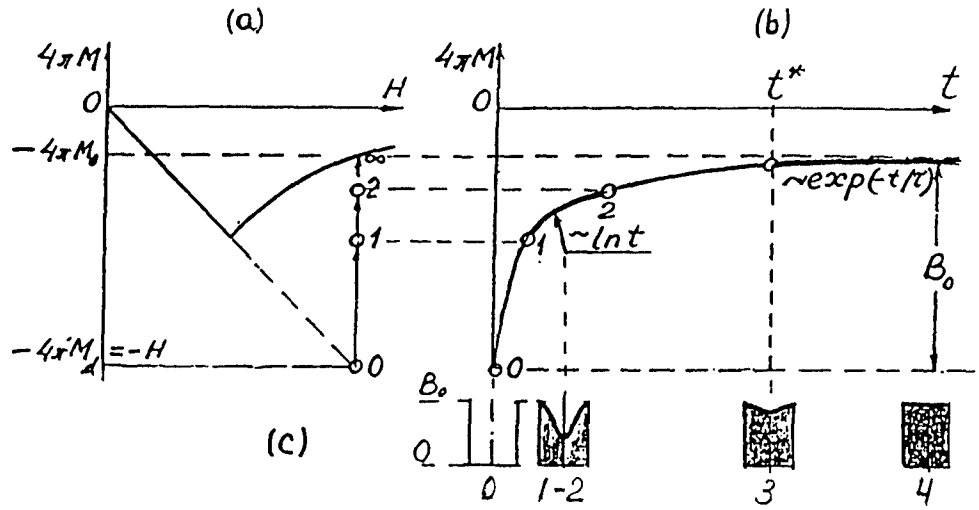


Fig. 1. Kinetics of magnetization of a zero-field cooled sample.
a. Equilibrium magnetization dependence on magnetic field.
b. Time dependence of magnetization.
c. Distribution of magnetic induction.
0 - the initial diamagnetic state, 1~2- the near critical state ($\nabla B \leq \nabla B_{cr}$), 3 - the near equilibrium state, 4 - the equilibrium state ($\nabla B = 0$, $B = B_0$).

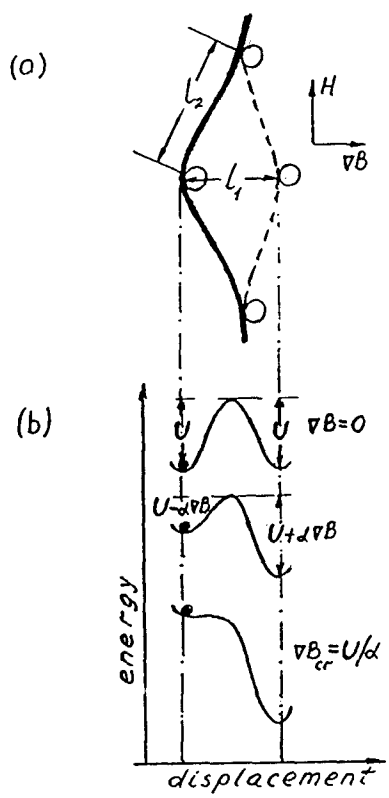


Fig. 2.

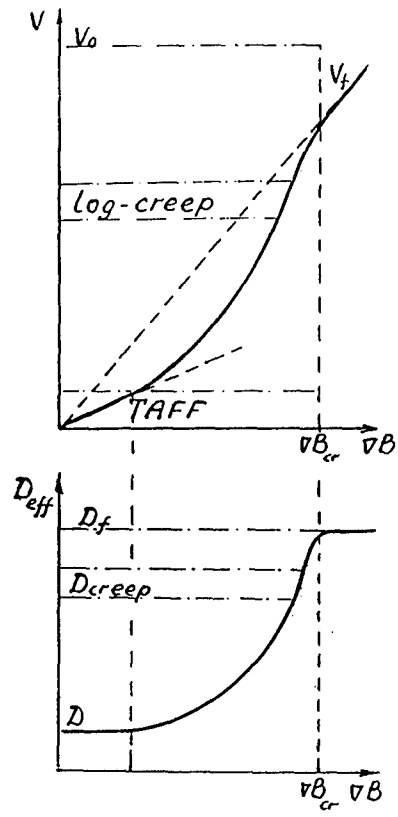


Fig. 3.

Fig. 2. Thermoactivated movement of a vortex. a. A vortex section, ℓ_2, pinned by obstacles, b. Energy as function of a vortex displacement.
Fig. 3. Vortex velocity, v, and vortex diffusion coefficient, D_{eff}.

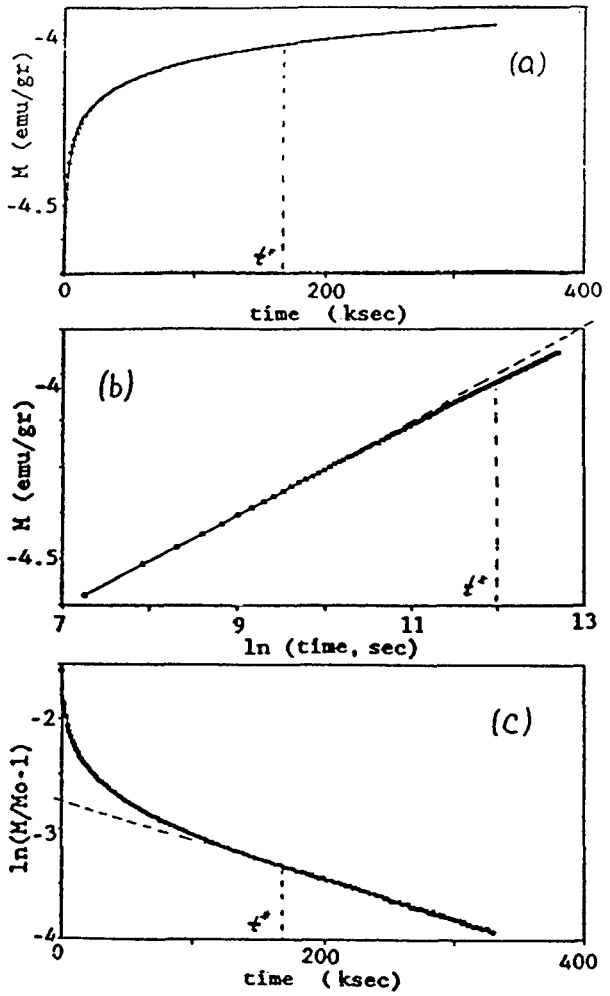


Fig. 4.

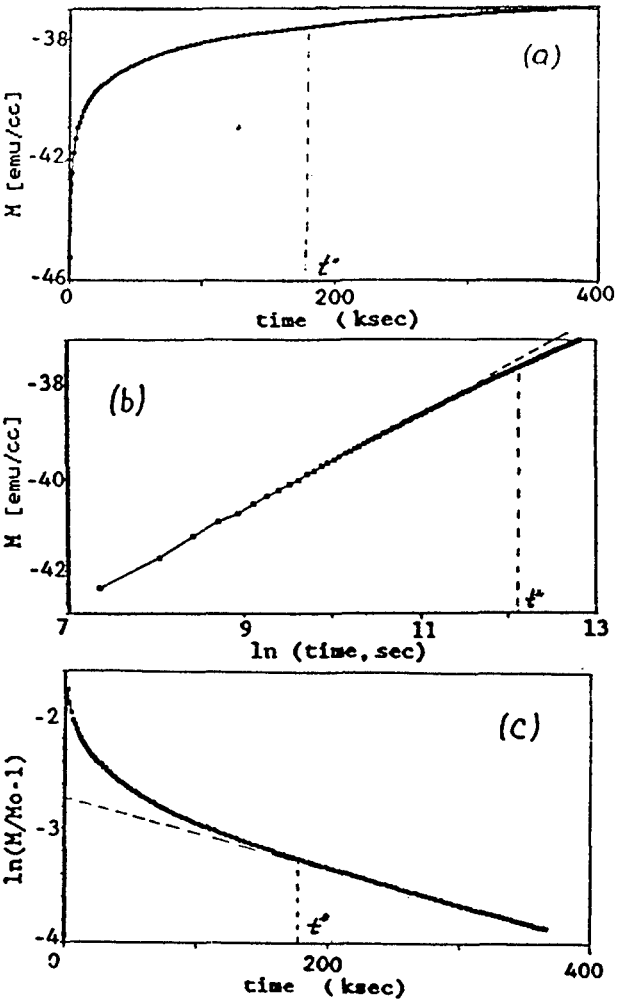
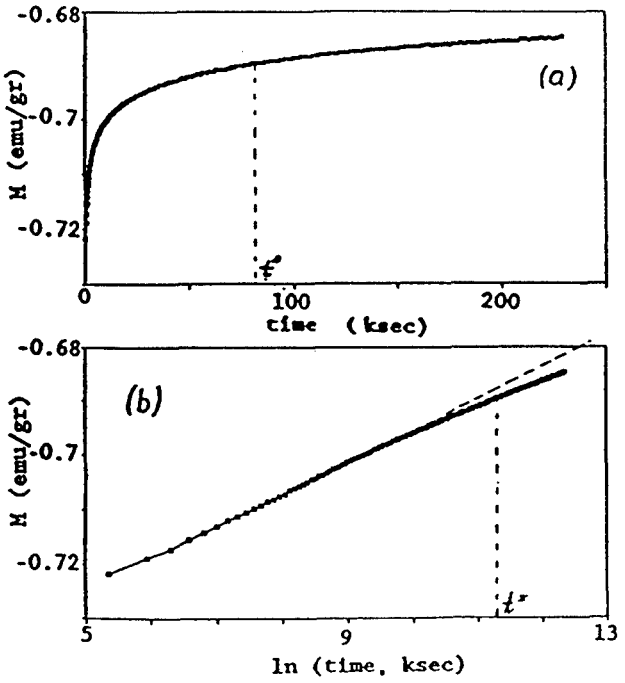


Fig. 5.



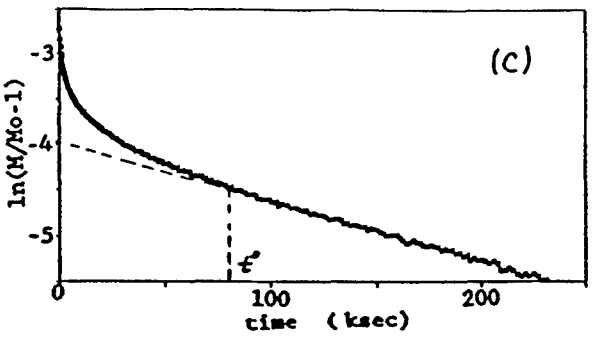
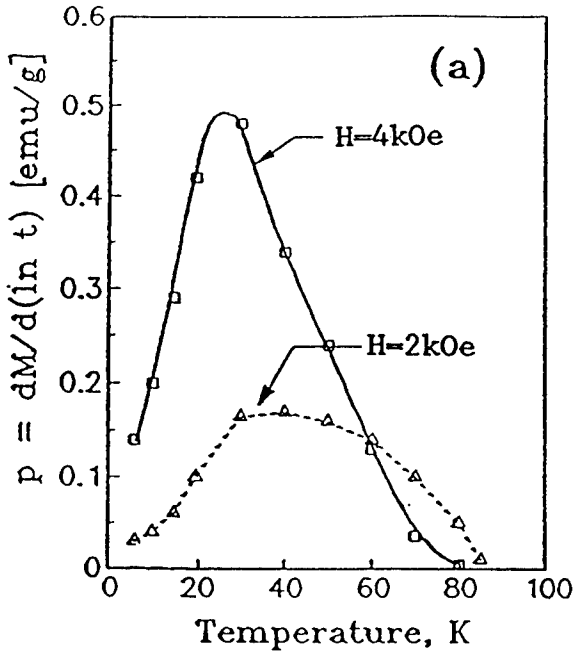


Fig. 6.

Fig. 4. Kinetics of magnetization of the QMG sample, M_o=-3.87(emu/gr).
Fig. 5. Kinetics of magnetization of the single crystal sample, M_o=-36.25 [emu/cc] .
Fig. 6. Kinetics of magnetization of the sintered sample, M_o=-0.68 (emu/gr).



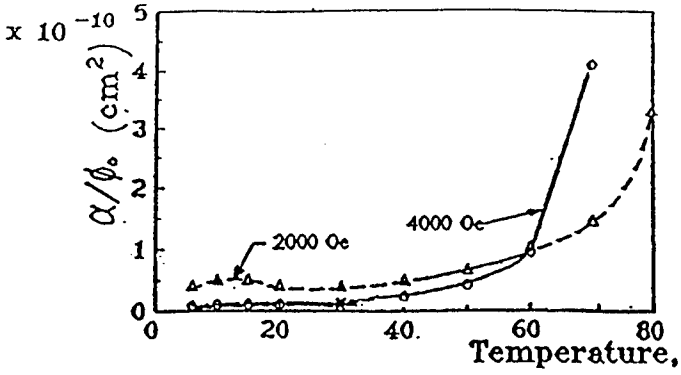


Fig. 8.

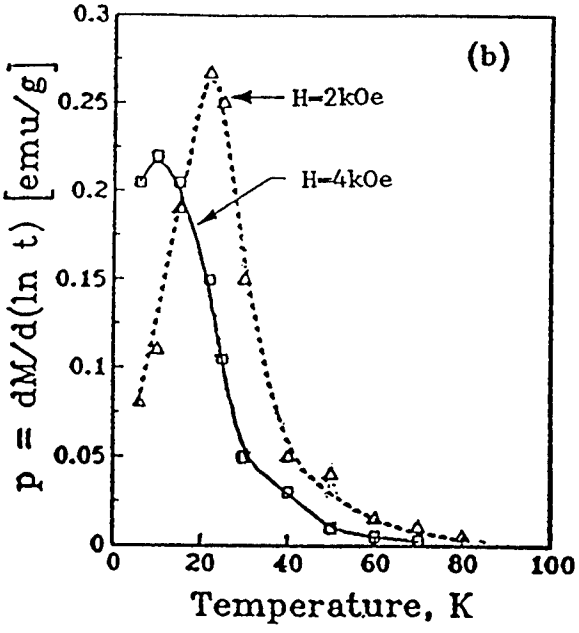


Fig. 7.

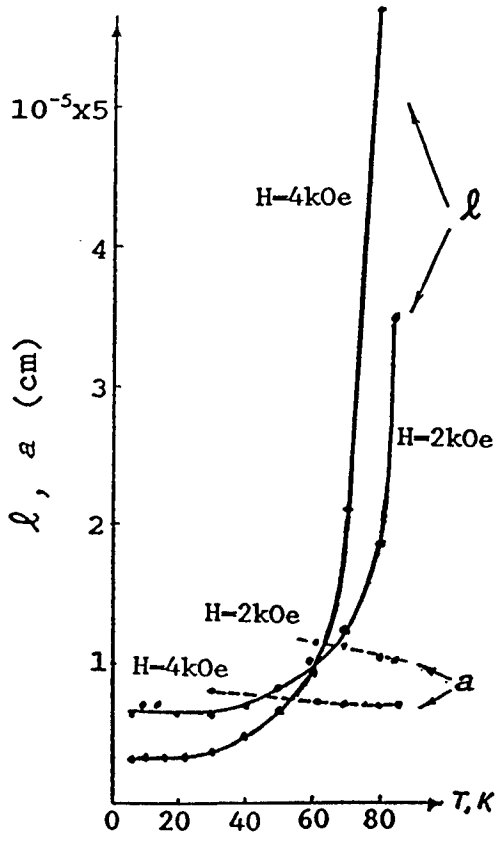


Fig. 9.

Fig. 7. Logarithmic rate of magnetization, P.
a. the QMG sample, b. the sintered sample.
Fig. 8. Temperature dependence of α/ϕ_o for the QMG sample at 2 and 4 kOe.
Fig. 9. Temperature dependence of average activated length, ℓ, and intervortex spacing, a, for the QMG sample at 2 and 4 kOe.

FLUX FLOW AND FLUX DYNAMICS IN HIGH-T_C SUPERCONDUCTORS

L.H. Bennett, M. Turchinskaya, L.J. Swartzendruber, A. Roitburd, D. Lundy,
J. Ritter, and D.L. Kaiser

Materials Science and Engineering Laboratory
National Institute of Standards and Technology
Gaithersburg, MD 20899

Many of the potential applications of the high-temperature superconductors require a pinning mechanism for flux lattice stabilization in the mixed state in order to provide high critical currents and high levitation forces. Three aspects of flux pinning are reviewed here:

(i) The magnetic properties of single crystals of YBCO, including such topics as anisotropy in the flux pinning and in the critical current density, and the effects of twins on the flux pinning and on the lower critical field.

(ii) A critical field for depinning, H_{cp}, can be defined as that field at which the hysteresis loop changes from irreversible to reversible. Measuring BSSCO as a function of temperature, H_{cp} can be described by a power law with an exponent of 1.5.

(iii) When the applied field is changed rapidly, the time dependence of flux change can be divided into three regions, an initial region which occurs very rapidly, a second region in which the magnetization has a ln(t) behavior, and a saturation region at very long times.

INTRODUCTION

When a magnetic field, H, is applied to a type II superconductor which has been cooled below its critical temperature in zero magnetic field, all magnetic flux is excluded from the specimen for $H<H_{c1}$, where H_{c1} is the lower critical field. For $H>H_{c1}$, magnetic flux penetrates the specimen, and a vortex state of mixed normal and superconducting regions exists up to the upper critical field, H_{c2} [1]. In this mixed state, superconducting currents circulate in planes perpendicular to the magnetic flux lines and form vortices threading the specimen. These vortices can be anchored by defects in the material called pinning centers. This pinning inhibits movement of vortices into or out of the specimen. Thermal activation of the vortices over the pinning centers results in flux creep. The flux gradient that occurs due to the presence of pinning forces gives rise to hysteresis in the magnetization vs applied field curve. At any given applied field, the width of this hysteresis loop is proportional to the "magnetic critical current", J_c. At high fields (but still with $H<H_{c2}$), the forces on the vortices can exceed the pinning forces. The width of the hysteresis loop then shrinks to zero and J_c vanishes, and in the sense that transport current will not flow without resistance, the material is no longer "superconducting". Finally, for $H>H_{c2}$, the density of vortices becomes so large that the individual vortices overlap, resulting in complete penetration of the field and a loss of superconductivity.

Because high-temperature superconductors, including $YBa_2Cu_3O_{6+x}$ (YBCO) and Bi-Sr-Ca-Cu-O (BSCCO), are type II superconductors with relatively low H_{c1} values and high H_{c2} values, they will be in a "critical state" for many of their applications. In the critical state, with the effective field between H_{c1} and H_{c2}, flux lines have penetrated the material and are pinned by structural defects, chemical inhomogeneities, and impurities. A detailed knowledge of how flux penetrates the materials and its behavior under the influence of applied fields and current flow, and the effect of material processing on these properties, is required in order to apply, and to improve, the properties of these superconductors.

SINGLE CRYSTAL YBCO

YBCO single crystals have been grown from the melt using a technique described by Kaiser *et al.* [2]. The plate-like morphology of some of these crystals can be seen in Figure 1. Magnetization studies have established that flux pinning in YBCO single crystals is highly anisotropic [3-8]. When a magnetic field is applied parallel to the c-axis, the flux lines are strongly pinned, contributing to high critical currents within the Cu-O planes. In contrast, weak pinning between the Cu-O planes contributes to low critical currents for applied fields perpendicular to the c-axis. This difference in pinning manifests itself in a large anisotropy in the hysteresis loops when a magnetic field is applied parallel to and perpendicular to the c-axis of the crystal, as is evident in Figure 2 [9]. These loops were measured on a nearly cubic single crystal (120x135x120 μm^3). The cubic morphology of the crystal has allowed a clear determination of the anisotropy of the critical current density without the complication of large, and differing, demagnetization factors. Our measured anisotropy, (Jc//c)/(Jc $\perp$ c), is 62 at 10K in an applied field of 10 Oe, which is higher than that reported previously for comparable conditions.

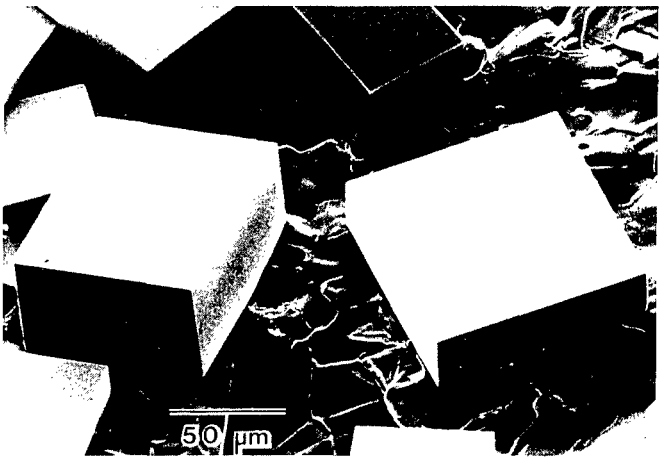


Figure 1. Scanning electron micrograph of some single crystals of YBCO grown from the melt [2].

The observed anisotropy in flux pinning suggests directionality in the distribution or strength of pinning centers. One proposed anisotropic pinning center in single crystals is twin boundaries [4,10] which form in the material during cooling through the tetragonal to orthorhombic transition. The (110) and ($1\bar{1}0$) twin planes lie parallel to the c-axis, with typical spacing between planes of 20 to 2000 nm [2]. A difference in the interaction energy of flux lines and twin boundaries would be expected for flux lines threading through the crystal parallel and perpendicular to the twin planes.

Several high-resolution Bitter-pattern studies [11, 12] have shown that twin boundaries

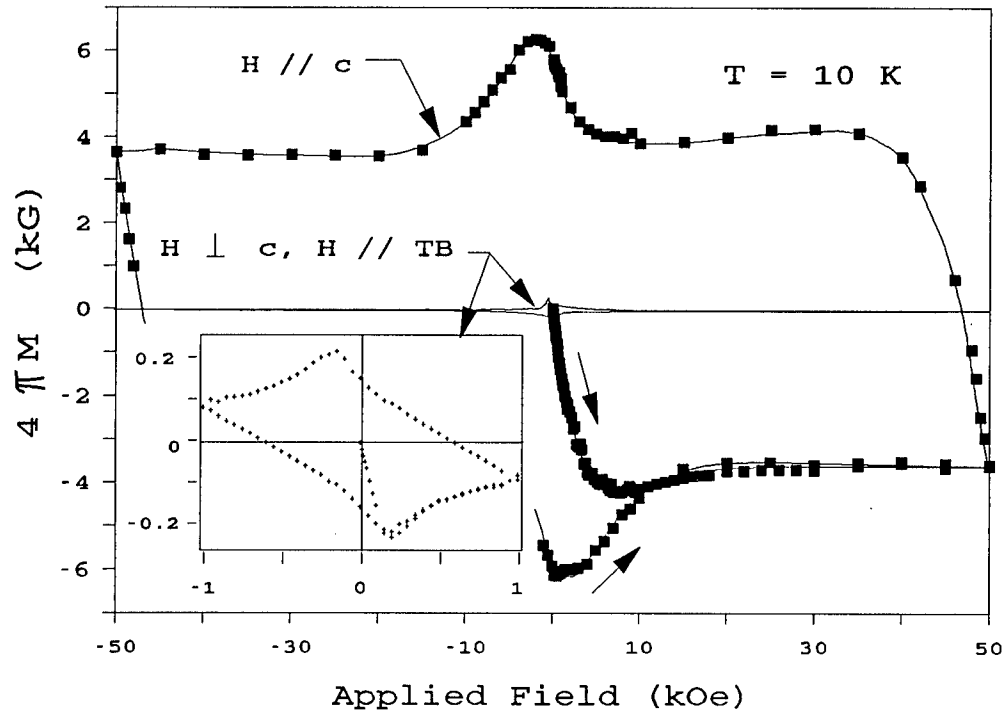


Figure 2. Hysteresis loops at 10K for a YBCO single crystal for fields applied parallel to and perpendicular to the c-axis. The large difference in the widths of the two loops is due to anisotropy of the critical current.

do indeed pin flux lines, resulting in vortex lattices which are clearly correlated with the twin boundary orientation. However, well-developed vortex lattices have also been observed in twin-free regions [12], indicating that other intrinsic crystalline defects such as oxygen vacancies act as pinning centers. Gyorgy et al. [13] recently determined that there was not a significant difference between the critical current densities for flow within the Cu-O planes with an applied field parallel and perpendicular to the c-axis of a twinned crystal, leading them to conclude that twin boundaries are not the dominant pinning centers.

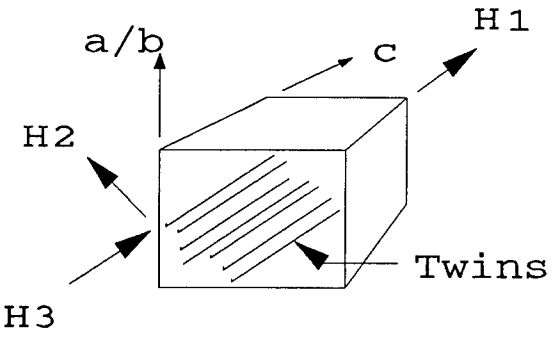


Figure 3. Geometry used to study the effect of twin boundaries on flux pinning. H1 is a field // to both the c axis and the twin boundaries; H2 is ⊥ to both c and the twins; H3 is ⊥ to c and // to the twins.

To study the effect of the twins on the flux pinning, the magnetic properties of the YBCO crystal whose hysteresis loops are shown in Figure 2 was investigated [9]. This crystal had predominantly one variant of twin boundary. Its geometry is sketched in Figure 3. Small differences in magnetic behavior were observed when the field was applied perpendicular to the c-axis and either parallel or perpendicular to the predominant twin boundary orientation, showing that twins have a direct measurable (but small) effect on flux pinning. An example is shown in Figure 4, where the shielding behavior of the crystal in the H1 direction (// to the c axis) is different than for the magnetic field ⊥ to the c axis, for either the H2 (⊥ to the twin planes) or

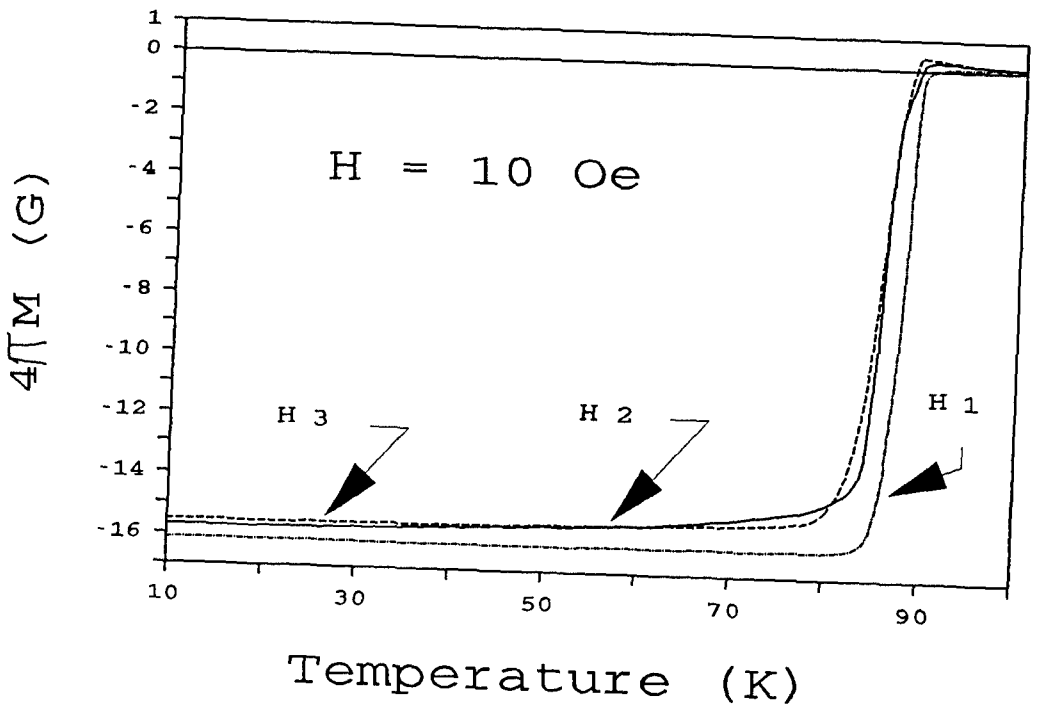


Figure 4. Shielding measurements for the same crystal taken upon heating in a field of 10 Oe, after cooling in zero field. H1, H2, and H3 are magnetic field directions defined in Figure 3.

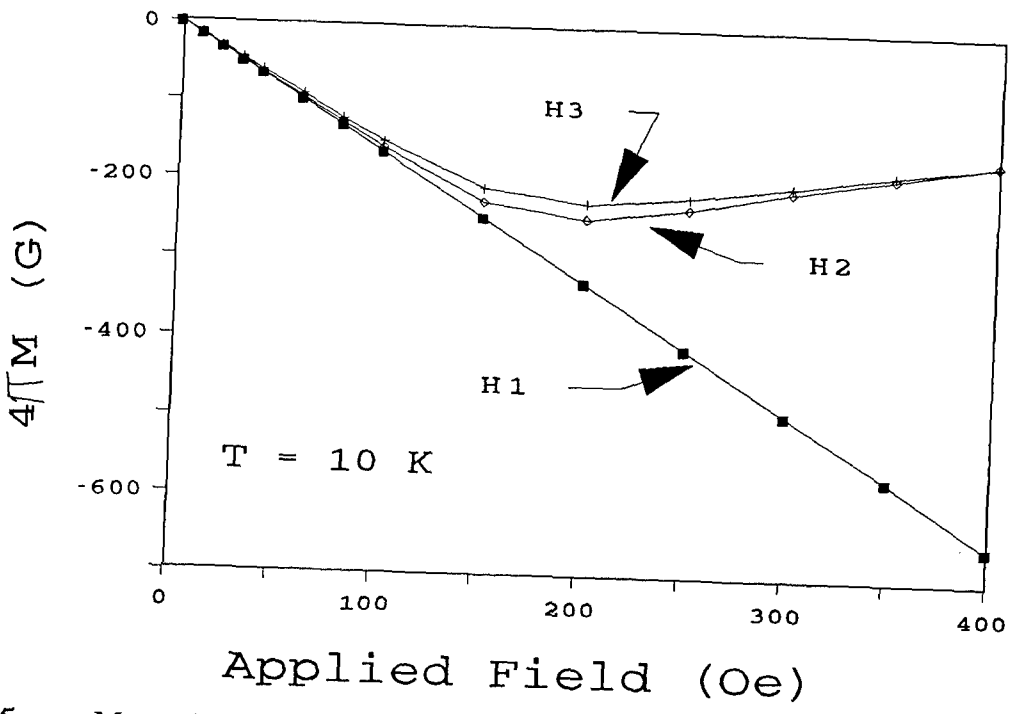


Figure 5. Magnetization curves after zero field cooling for the same crystal, with H1, H2, H3 as defined in Figure 3. H2 and H3 differ due to a difference in flux pinning for vortices ⊥ and // to the twin boundaries.

the H3 direction (// to the twin planes). A second example is shown in the magnetization curves depicted in Figure 5, where a magnetic field is applied to the zero-field-cooled sample for the three directions. Again the largest difference is due to crystalline anisotropy, whereas the behavior with respect to the twins is small, but real. The flux-vortex pinning is greater when the applied magnetic field is perpendicular to the twin boundaries at 10K. However this effect is temperature dependent and reverses at $\approx$80K [14], as is illustrated in Figure 6.

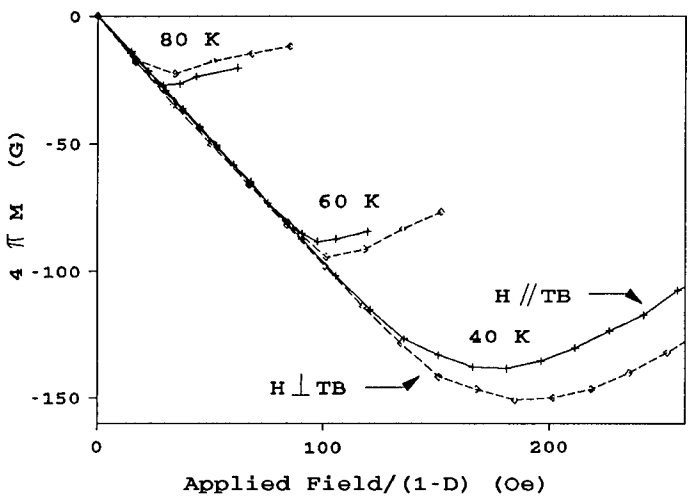


Figure 6. Magnetization vs applied field for two orientations of the same crystal. The applied field has been corrected for demagnetization (D=3).

The pinning mechanisms responsible for the high critical currents, J_c, seen in single crystals is of considerable interest. Although some of the highest J_c's for YBCO at 77K reported to date have been in single crystals, not all crystals have the same J_c. (We refer here to fully oxygenated single crystals, since J_c at 77K is lowered when the oxygen content is decreased enough to lower T_c below 90K.) A case in point is displayed in Figure 7, which shows a 77K hysteresis loop for a different YBCO single crystal than that shown in Figures 2-6. This crystal had dimensions of 200x178x75 μm^3, and has a higher T_c (93K) than the "cube" (T_c=89K) because of its lower concentration of impurities (trace amounts of Al, Si, Ca). The narrowness and characteristic shape of this loop shows that this crystal must have only a small amount of pinning. From this loop and the sample geometry with H//c, it can be estimated that this crystal has a magnetic J_c of $5x10^3 A/cm^2$ for H=0. This value is less than that reported for many single crystals and for quench and melt growth samples. It is larger than obtained in sintered samples (which show J_c's at 77K on the order of 100-1000A/cm^2)

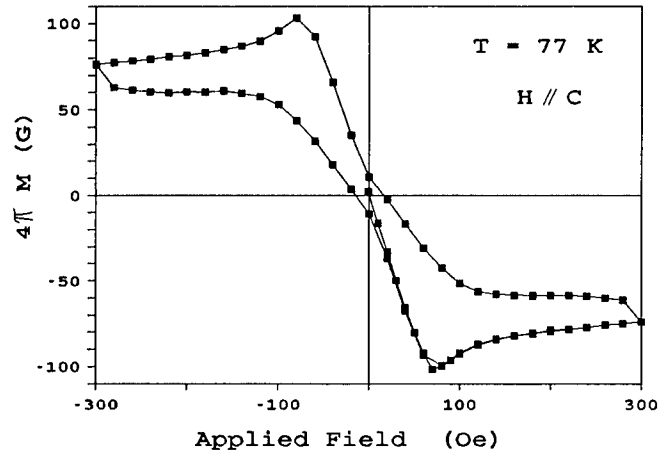


Figure 7. Hysteresis loop of a different single crystal of YBCO taken with the field applied parallel to the c axis.

Although no firm conclusions can be drawn at present, our experience indicates that the more perfect (geometry, purity, etc.)single crystals tend to have much lower J_c's, whether or not they contain twins. Further examples are given elsewhere in this conference, where the lower critical field was measured with high precision, and the temperature dependence of the Ginzburg-Landau parameter derived [15].

FLUX DEPINNING IN Bi SUPERCONDUCTORS

The occurrence of flux depinning, at a critical magnetic field which varies with temperature, has been observed in hysteresis loops of the high-T_C superconductors. The critical field for depinning is relatively low for the bismuth superconductors, with implications for both scientific understanding and technological applications. We report here on the results of magnetic measurements on a bismuth-based superconductor which displays three distinct phases.

The BSCCO superconducting oxides [16,17] have certain advantages over the 1-2-3 materials of which $YBa_2Cu_3O_7$ is the prototype. Among these advantages are a phase with a higher superconducting transition temperature (T_c), the lower cost of bismuth as compared to yttrium, ease of processing particularly with respect to annealing and in forming thin films, and indications of a higher stability with respect to air and moisture. Along with these advantages is the inherent disadvantage associated with the observed magnetic field dependence of their superconducting properties.

Many applications of the high T_C superconductors require the capability of carrying large currents. The critical current density arises from the equilibrium between the Lorentz force exerted by the transport current and the pinning forces operating on the magnetic flux lines. The flux lines often form a flux lattice so that a small number of pinning centers can pin many flux lines. The observation of a hysteresis loop conforming to the Bean critical-state model suggests the presence of strong flux pinning in $YBa_2Cu_3O_7$ [18]. In this model, the magnetic critical current is derivable from the loop parameters. In particular, the width of the hystresis loop at a given magnetic field can be used to calculate a critical current (generally referred to as the "magnetic critical current").

In conventional superconductors, the movement of flux lines occurs by flux "creep" when pinning is strong [19] and by flux "diffusion" when the transport current is large enough to overcome the pinning forces [20]. Both of these dissipative phenomena were observed [18] in the same sample of the high-T_C superconductor, $YBa_2Cu_3O_7$. In addition to these dynamic effects, a novel behavior is observed in the high T_C superconductors, namely a reversible-irreversible transition which was first found by Müller, Takashige, and Bednorz [21] during temperature sweeps in La_2CuO_{4-y}. At a given temperature, flux is depinned for fields higher than a critical field. A de Almeida-Thouless-like behavior was found to describe [22] the separation between reversible and irreversible behavior in the susceptibility. Similar flux depinning was also measured by a number of different kind of experiments in Y-Ba-Cu-O [23,24] and in Bi-Sr-Ca-Cu-O [24-28] high temperature superconductors.

One sample of a Bi-Pb-Sr-Ca-Cu-O high-T_C superconductor, with starting composition $Bi_{1.7}Pb_{0.25}Sb_{0.1}Ca_2Sr_2Cu_2O_x$, is particularly interesting in that it displays three distinct superconducting phases. The critical field for flux depinning found in this sample was low enough to permit its determination over a wide temperature range. We find that the temperature dependence of the critical field for flux depinning can be described by a 3/2 power law for all three phases.

The real and imaginary parts of the ac susceptibility were measured in a Hartshorn-type bridge with an applied ac field of about 40A/m (0.5Oe) at a frequency of 1.68kHz. The hysteresis loops were obtained in a vibrating sample magnetometer. The real part of the ac susceptibility reveals three distinct temperature ranges associated with three superconducting

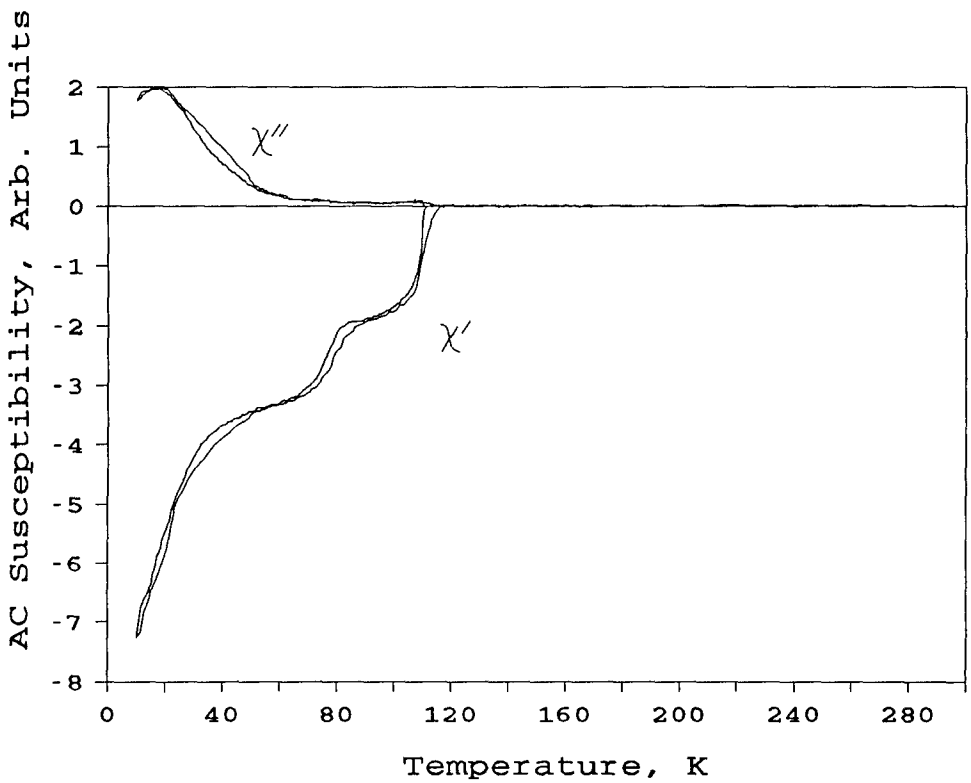


Figure 8. AC susceptibility of a Bi-oxide superconductor. The double traces are up and down temperature sweeps. The real part, χ', shows three distinct regions of superconductivity. The imaginary part, χ'', has less obvious peaks.

phases: (i) a fairly sharp diamagnetic transition starting above 110K, a second transition starting above 80K, and a third broad transition below 60K (see Figure 8). The imaginary part of the ac susceptibility shows a weak peak at about the center of the 10%/90% range of the 110K transition and a stronger peak associated with the 60K transition. These observations indicate that the sample was predominately three phase, but with a distribution of transition temperatures, most likely due to compositional variations within each phase.

Figure 9 shows a hysteresis loop at 105K for the same material used for the measurements in Figure 8. This loop is narrow, indicating the presence of only a small amount of flux pinning. In addition, the loop is constricted in the center, indicating the probable existence of dynamic effects similar to those found [18] in $YBa_2Cu_3O_7$. The hysteresis disappears in this loop for applied fields above $\approx$70Oe. This effect was observed previously (at somewhat different fields) in the hysteresis loops of Bi-Ca-Sr-Cu-O samples prepared by other techniques [27, 28].

Examination of the plots shown in Figures 9 and 10 suggests the existence of a critical depinning field, H_{cp}, above which flux pinning vanishes. The exact definition of such a critical field in our experiment has some uncertainty since the transition is gradual. We define the

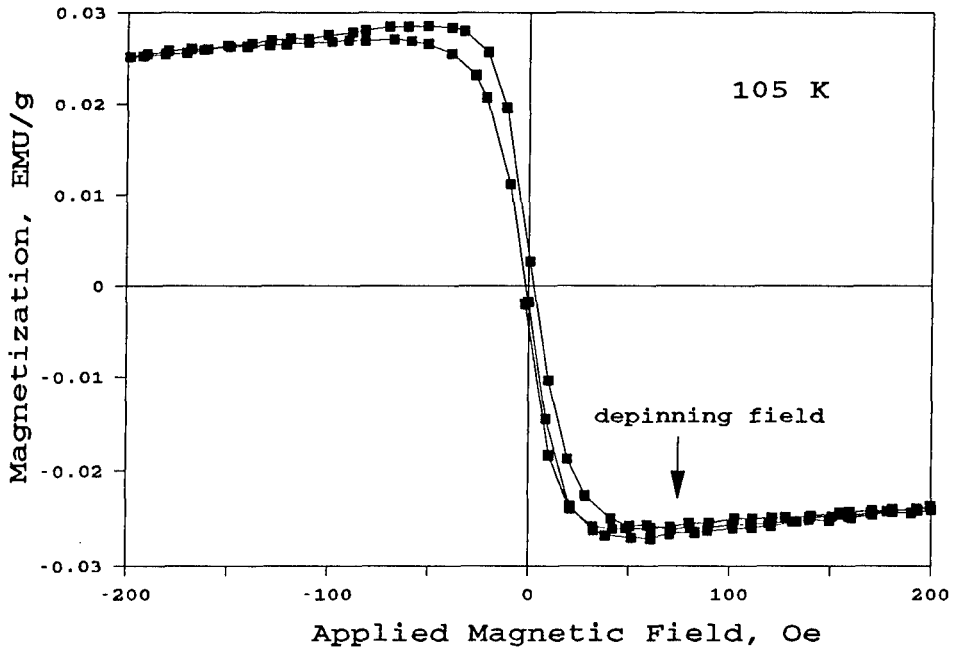


Figure 9. Hysteresis loop at 105K of the same Bi-oxide superconducting material as whose ac susceptibility is shown in Figure 1.

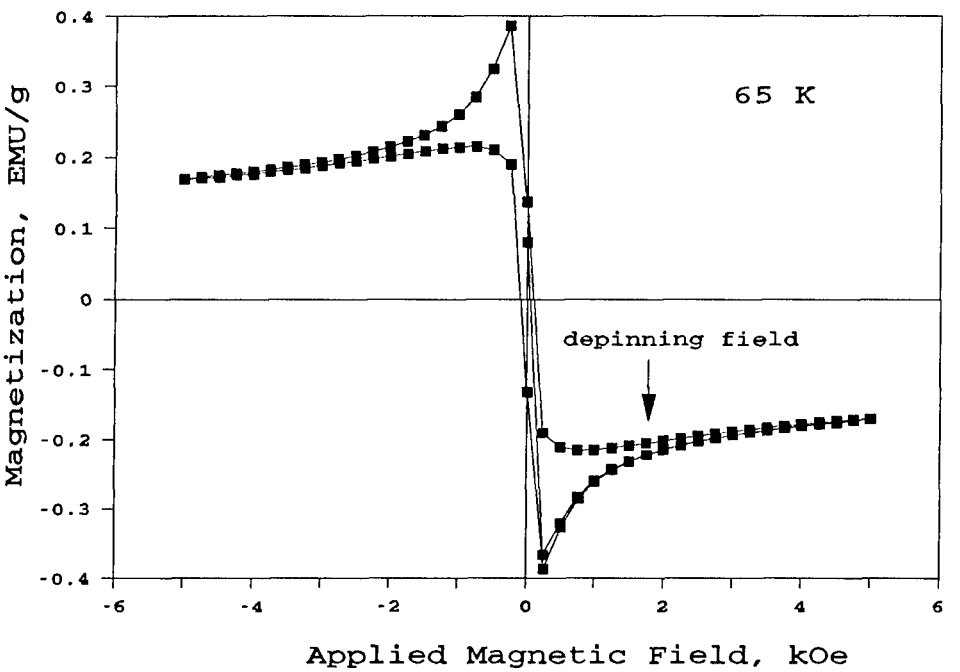


Figure 10. Hysteresis loop at 65K of the same Bi-oxide superconductor.

critical field, H_{cp}, as the field at which the separation between the magnetization for increasing and decreasing fields is less than one-twentieth the peak magnetization (see Figures 9 and 10). For a single phase sample (with a single value of T_c), a log-log plot of the critical field versus the temperature interval below the critical temperature should be a straight line, i.e.,

$$H_{cp}=H_{cp_o}(1-T/T_c)^n \qquad (1)$$

where the prefactor H_{cpo}, the value of H_{cp} at T=0, is a measure of the pinning strength for that superconducting phase. The appearance of a straight line when plotting $\ell(H_c)$ versus $\ell n(1-T/T_c)$ is very sensitive to the value of T_c chosen. The experimental data for our three-phase sample do not form a straight line, no matter what T_c is chosen.

We can, however, interpret the results as made up of three straight lines, the first obtained by plotting against $\ell(1-T/115)$, the second obtained by using $\ell(1-T/91)$, and the third using $\ell(1-T/52)$. An example is shown in Figure 11, for the data in the temperature range 35K to 85K. It is seen that the data between 50K and 80K fall on a straight line. All of the observed data, and the three fits, are displayed in Figure 12. Note that the straight line of Figure 11 appears as a curved line in Figure 12, since the abscissa is different.

The three numbers, 115K, 91K, and 52K, were chosen to give the three best linear fits for which the slope (exponent) is 1.5. When these temperatures are overlayed on the real part of the ac susceptibility results of Figure 8, Figure 13 is obtained. It then appears to be reasonable to consider these numbers as the real "onset" temperatures for the three superconducting phases. They have somewhat higher values than what might have have been chosen directly from the data of Figure 8.

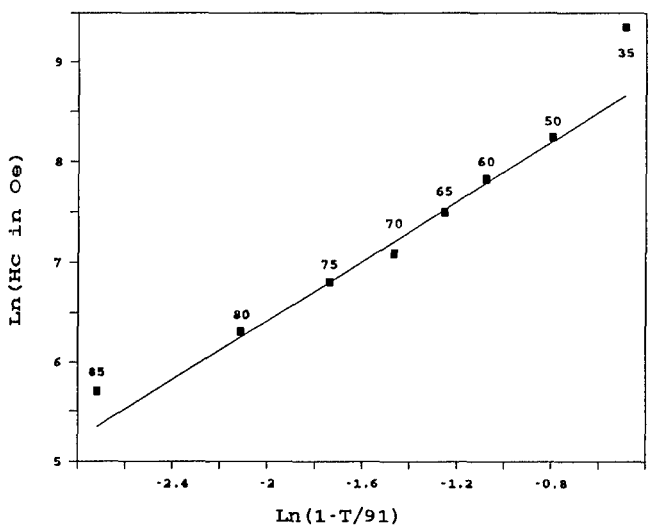


Figure 11. Log-log plot of critical field for flux depinning versus reduced temperature, assuming a critical temperature of 91K. The solid line is a linear fit for temperatures from 50 to 80K.

It is interesting to compare these results with earlier work [26] on magnetic measurements of the superconducting properties of a crystalline chunk, consisting of many small crystals, prepared by casting from the oxide melt with a starting composition of $Bi_3Ca_2Sr_2Cu_3O_x$. AC susceptibility revealed an onset temperature of 82 K and a transition width of $\approx$10 K. Hysteresis loops at 70 K showed a very small hysteresis, indicating a low density of effective flux pinning sites at this temperature, similar to the behavior observed for some superconducting samples of the Bi-Ca-Sr-Cu-O system prepared by other techniques. However, the magnetization at 10 K showed no hysteresis for fields greater than $\approx$3.5 kOe, a much smaller value than observed in the Bi sample reported on above. This critical field for

flux depinning, H_{cp}, appeared to vary with temperature as $H_{cp} = 4980(1-T/82)^{2.5}$. The exponent is very similar to what Lundy et al observed [27] in a different sample, but the prefactor is considerably different in the two samples. If, however, as discussed in [26], it is assumed that each sample consists of more than one phase, with more than one T_c, another interpretation of the data is posssible. Instead of fitting the data to one line, the H_{cp} values could be subdivided into several lines, each with a smaller slope than the average value. It thus appears that these data are also consistent with an exponent of 1.5.

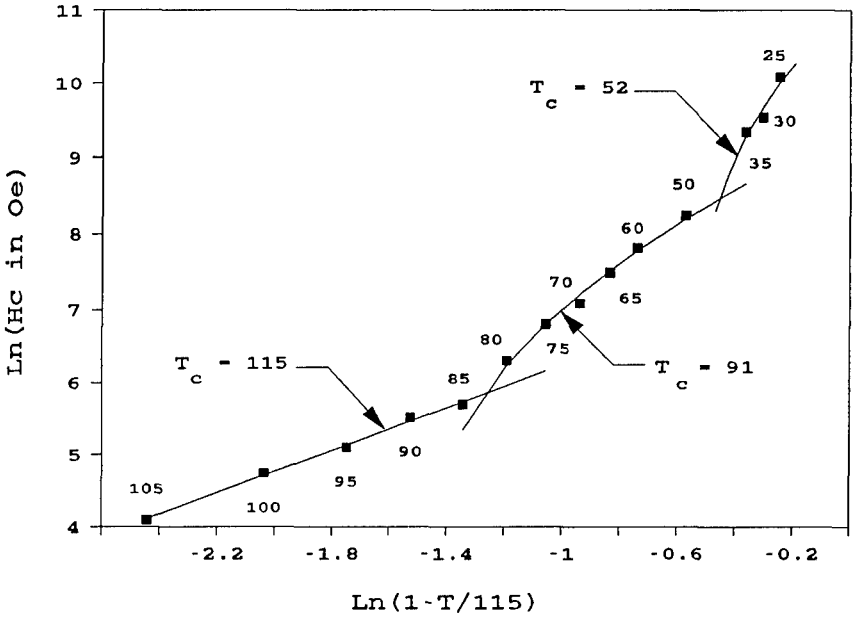


Figure 12. Log-log graph of critical field for flux depinning versus reduced temperature. The three solid lines are linear (see text) least square fits to the data points in their range.

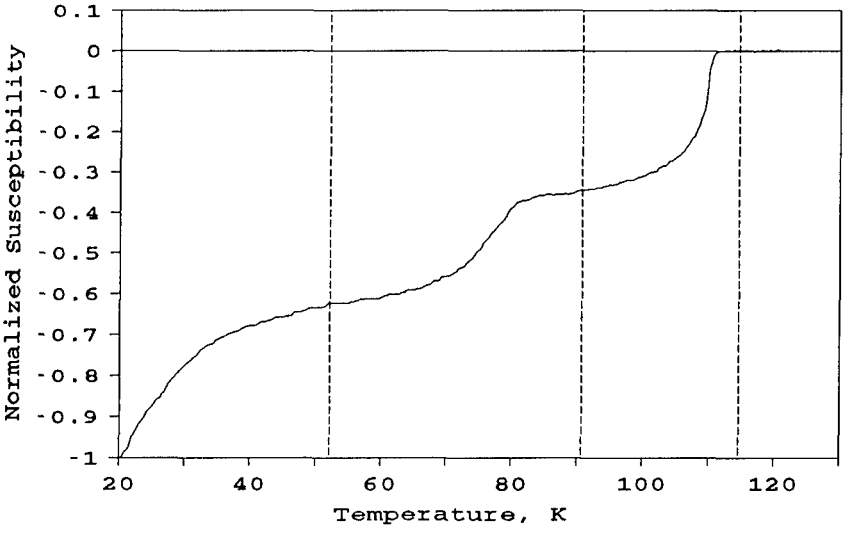


Figure 13. Real part of the ac magnetic susceptibility of the present sample. The three vertical lines are obtained as described in the text.

IV. FLUX DYNAMICS IN HIGHLY-PINNED YBCO

One of the important technological requirements of a superconductor is stability of the flux lattice. When the applied magnetic field is changed suddenly, a transient behavior is observed whereby the magnetization which is initially induced in the superconductor decays exponentially. This "flux flow" was observed to occur in YBCO [18] in the first 10 seconds or so, the actual time depending on the pinning, the field and the temperature. Following this dynamic transient diamagnetic effect, the magnetization decays with a ln(t) behavior as predicted by the Anderson-Kim [19,20] thermally activated flux creep model. Theoretical consideration of the thermoactivated movement of vortices which occur upon application of a magnetic field to a zero-field-cooled high-Tc superconducting sample predicts a further stage in the kinetics of magnetization: following the logarithmic decay with time, (after ~10^5s), equilibrium is approached exponentially [29]. (It is possible that there are two different logarithmic decays asssociated with flux creep in grains and grain boundaries. This is now under investigation.)

Studies of the kinetics of the magnetization allows the pinning characteristics to be determined. From the logarithmic stage of the magnetization vs time curve, it is possible to obtain an activation moment, α = kTR/P, where k is the Boltzmann constant, T is the temperature, R is the effective radius of the sample, and P is the log-creep rate (P=dM/dln(t)). Since the magnitude of P also depends linearly on R, α will not depend on the size of the sample and hence is an intensive characteristic of the material. From the exponential stage, it is possible to obtain the equilibrium magnetization, M_0 (or induction, B_0), the time of relaxation, τ, and a vortex diffusion coefficient, $D \simeq R^2/\tau$. Knowing these parameters allows an estimation of the activation energy for the thermoactivated vortex, or vortex bundle, movement, $U = kT \ln (T \cdot V_0 \cdot B_0 \cdot \alpha / kT)$, where V_0 is the limiting vortex bundle velocity. V_0 is close to the sound velocity [30,31].

These two stages were found by measuring the magnetization as a function of time at different temperatures and applied fields for three samples of $YBa_2Cu_3O_7$ prepared by different processes including a single crystal, a sintered powder, and one prepared by the quench, melt and growth (QMG) method [29,32]. All three samples displayed the same superconducting onset temperature, T_c=93K.

The first sample was a bar 0.9x0.9x5.1 mm^3, with the c direction generally in the plane perpendicular to its long axis, cut from a single grain of a polycrystal produced by the QMG process by K. Sawano of the Nippon Steel Co. The sample can be considered as a bulk superconductor without weak links [32]. The second sample was a bar 2.3x1.7x5.8 mm^3 produced by solid state sintering by J. Blendell of NIST. The sample had a uniform grain structure with a grain size less than 5 μm. The third sample was a single crystal plate 0.9x0.8x0.06 mm^3 prepared at NIST.

Of the three samples studied, only the QMG sample allowed a determination of the effective radius, R, and thus a quantitative estimation of the pinning parameters: activation moment, α, vortex diffusion coefficient, D, and activation energy, U. For a more detailed discussion, see [30]. For the sintered sample, the weak links associated with the grain boundaries causes the effective radius to be a function of magnetic field [33]. The effective radius associated with the single crystal is undetermined because only a portion of it was superconducting.

The samples were cooled to the measuring temperature in zero magnetic field. The magnetic field was then applied and the magnetization, M(t), measured as a function of time

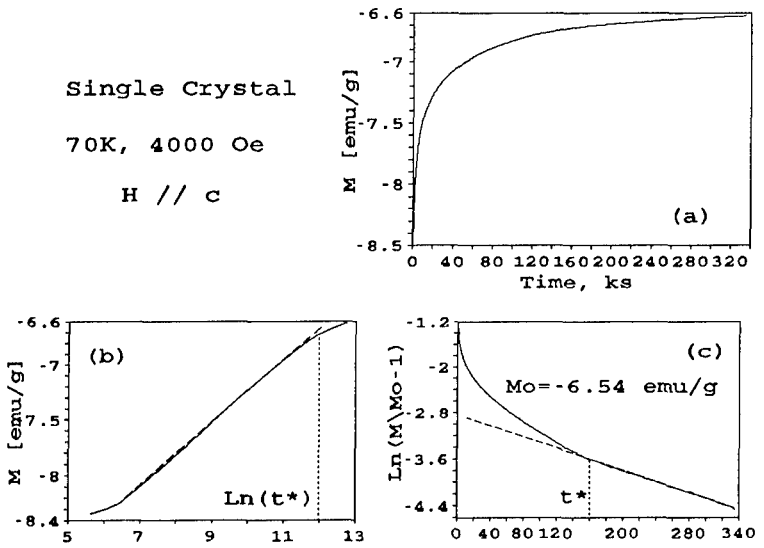


Figure 14. (a) Magnetization, M, vs time, (b) M vs logarithm of time, and (c) logarithm of (M/Mo-1) vs time. The time t* marks the beginning of the approach-to-equilibrium stage. The dashed lines are linear best fits.

using a vibrating sample magnetometer (VSM) for the shorter times, and a commercial SQUID magnetometer for longer times. To approach the equilibrium magnetization, high temperatures (70 and 80K) and long-times (about four days) were necessary. The magnetic fields were applied parallel to the long axis of the bar samples, and perpendicular to the single crystal plate. Magnetization vs time data for the single crystal at 70K and 4kOe, for the sintered sample at 80K and 2kOe, and for the QMG sample at 80K and 2kOe are plotted in Figures 14a, 15a and 16a, respectively. Curves obtained for other temperatures and applied magnetic fields have approximately the same shape as in these Figures: for all the curves there are log-time dependencies in M(t), and for much longer times ($t > t^*$), there are exponential approaches to the equilibrium magnetization, M_0. The magnetization vs logarithm of time curves are displayed in Figures 14b, 15b, and 16b. It is seen, that after about 700 seconds, there are two stages of M(t): (i) a log-time dependence, and (ii) at longer times (after t*) a deviation from the log-time dependence during which the approach to the value of the equilibrium magnetization is obtained [29]. In this time regime, the magnetization, M(t), as illustrated by Figures 14c, 15c, and 16c, obeys an exponential law $M(t) = M_0 + M'\exp(-t/\tau)$, (or $\ln[M/Mo-1] \propto -t/\tau$), where M' is a constant and τ is the relaxation time, for all the samples. The values of the relaxation time, τ, are obtained as the slope of the linear portion of the curves in (c).

Measurements in the logarithmic stage give the log-creep rate, P. The temperature dependences of P are plotted at a number of magnetic fields for the QMG and the sintered sample in Figure 17. These curves are similar to those shown earlier in conventional [34] and high-temperature single crystal [23] and

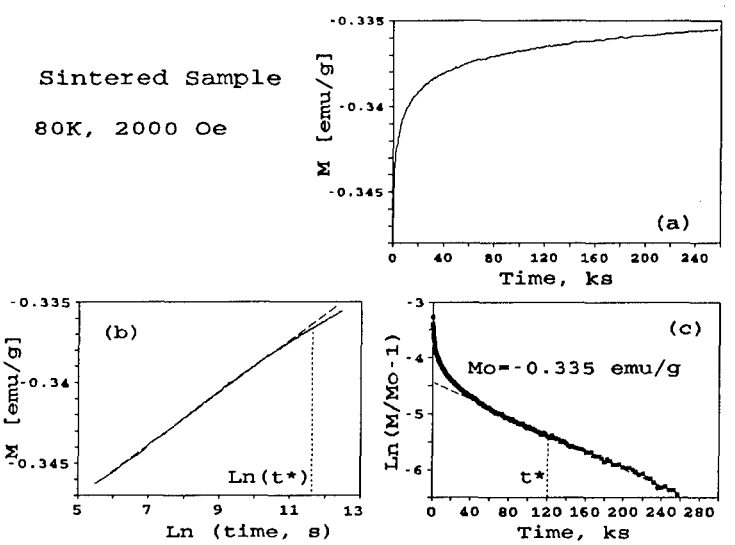


Figure 15. (a) Magnetization, M, vs time, (b) M vs logarithm of time, and (c) logarithm of (M/Mo-1) vs time. The time t* marks the beginning of the approach-to-equilibrium stage. The dashed lines are linear best fits.

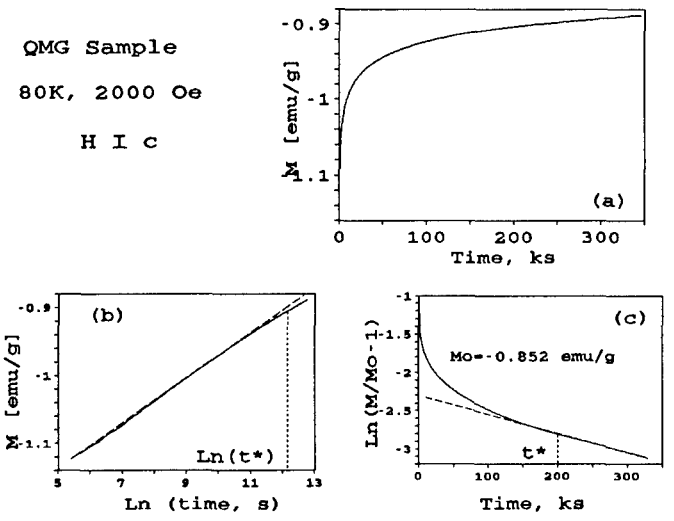


Figure 16. (a) Magnetization, M, vs Time, (b) M vs logarithm of time, and (c) logarithm of (M/Mo-1) vs time. The time t* marks the beginning of the approach-to-equilibrium stage. The dashed lines are linear best fits.

thin film [35] superconductors. For the QMG sample with its effective radius, $R \approx 0.045$ cm, α can be derived. Values of the activation moment α, normalized to ϕ_o (the magnetic flux of one vortex $=2.07\text{x}10^{-7}$ Gcm^2) are plotted in Figure 18. It is seen that, for large enough fields (2 and 4 kOe), α is almost independent of temperature for temperatures below where the maximum in P occurs. Taking into account that $\alpha/\phi_o = n \cdot \ell 1 \cdot \ell 2$, where n is the number of vortices in a bundle, $\ell 1$ is the displacement of the vortex or bundle at an activation event, and $\ell 2$ is the effective length of a displaced section of the bundle, it is possible to estimate the parameters of an activation event. For the QMG sample at 4kOe, for example, assuming that $n \simeq 1$, we can conclude that $\ell 1 \simeq \ell 2 \simeq 3\text{x}10^{-6}$cm. The growth of α at higher temperatures is likely due to the increase in the number of vortices in the bundle.

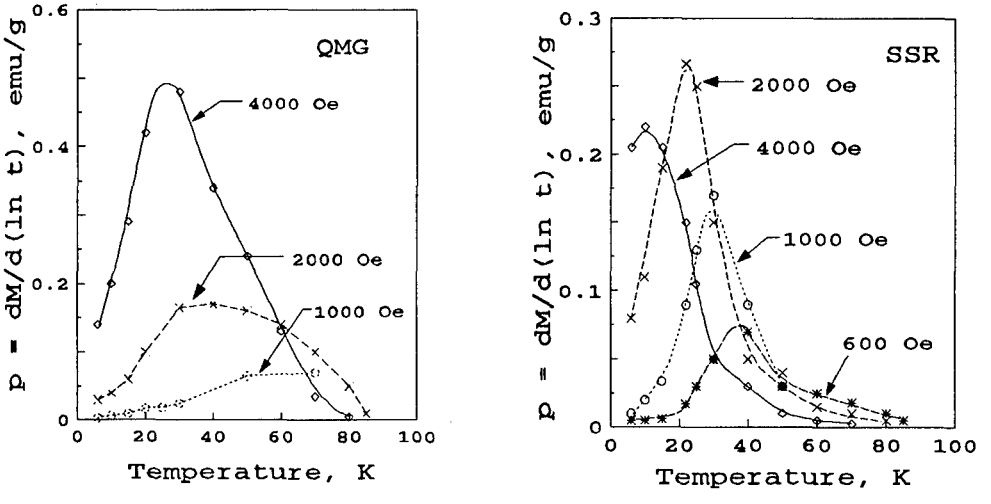


Figure 17. Log-creep rate, P, for the QMG (quench and melt growth) and sintered YBCO samples.

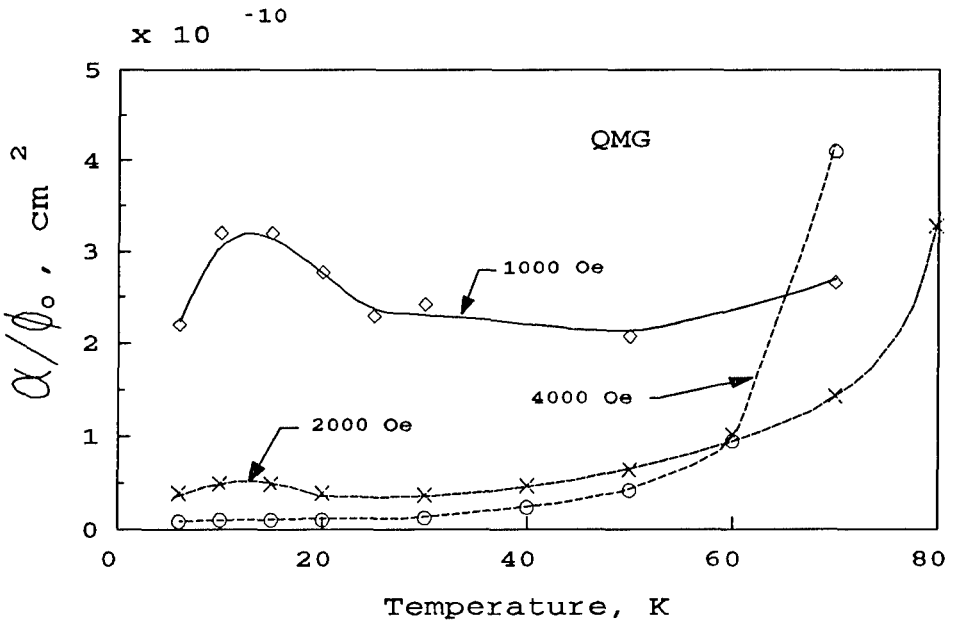


Figure 18. Temperature dependence of α/ϕ_0 at a number of magnetic fields for the QMG sample.

V. SUMMARY

There is still much to be learned concerning the flux flow and flux dynamics in high-temperature superconductors. We have described herein some recent studies on YBCO single crystals which show that twin planes have a small, but measureable, effect on flux pinning. Single crystals with a high degree of perfection appear to have considerably reduced pinning at higher temperatures.

In samples of Bi-Sr-Ca-Cu, we found that there was a critical field for flux depinning which was sample dependent and which could be described by a power law in the reduced temperature using an exponent of 1.5.

Samples of $YBa_2Cu_3O_{6+x}$ prepared by three different techniques were found to display a universal magnetization vs time behavior: after an initial transient at small enough times there is a log-time stage. At much longer times, M(t) approaches equilibrium exponentially [29]. The log-rate of magnetization P=dM/dln(t), can be used to determine the "activation moment", if the effective radius of a sample is known [29]. By analysis of kinetics of both the log-stage and the approach to equilibrium it is possible to determine an activation energy for the vortex movement. Details are given in [30,31].

VI. ACKNOWLEDGEMENTS

The various results described in this paper were carried out in close cooperation with many colleagues and coworkers from NIST and elsewhere. We want to especially acknowledge the following people from National Institute of Standards and Technology - R.D. Shull, D. Lundy, C.K. Chiang, F. Gayle, J.E. Blendell, J. Ritter, J.S. Wallace, W. Wong-Ng, R.S. Roth, L.P. Cook, A.J. Shapiro, R. Brown, R. Drew, D. Mathews, T. Chen, E. Keisman, and M. Hill; from The Johns Hopkins University/Applied Physics Lab - K. Moorjani, J. Bohandy, B.F. Kim, F.J. Adrian, T.E. Phillips, W.J. Green, and E. Agostinelli; from the Naval Research Laboratory - M. Rubinstein; from the Nippon Steel Corporation - K. Sawano; from the Israel Nuclear Center - U. Atzmony, M. Melamed, and H. Ettedgui, and from Superconix, Inc - C.F. Gallo

REFERENCES

1. A.A. Abrikosov, Soviet Physics JETP, 5, 1442 (1957).

2. D.L. Kaiser, F. Holtzberg, B.A. Scott, and T.R. McGuire, Appl. Phys. Lett., 51, 1040 (1987); D.L. Kaiser, F. Holtzberg, M.F. Chisholm, and T.K. Worthington, J. Cryst. Growth 85, 593 (1987).

3. T.R. Dinger, T.K. Worthington, W.J. Gallagher, and R.L. Sandstrom, Phys Rev. Lett. 58, 2687 (1987).

4. G.W. Crabtree, J.Z. Liu, A. Umezawa, W.K. Kwok, C.H. Sowers, S.K. Malik, B.W. Veal, D.J. Lam, M.B. Brodsky, and J.W. Downey, Phys. Rev. B, 36, 4021 (1987).

5. W.J. Gallagher, J. Appl. Phys., 63, 4216 (1988).

6. T.W. Worthington, Y. Yeshurun, A.P. Malozemoff, R.M. Yandrofski, F.H. Holtzberg, and T.R. Dinger, J. de Phys. 49, C8-2093 (1988).

7. T.K. Worthington, W.J. Gallagher, D.L. Kaiser, F.H. Holtzberg, and T.R. Dinger, Physica C, 153-155, 32 (1988).

8. L. Fruchter, M. Oussena, C. Giovannella, and I.A. Campbell, Supercond. Sci. Technol., 1, 75 (1988).

9. L.J. Swartzendruber, A. Roitburd, D.L. Kaiser, F.W. Gayle, and L.H. Bennett, Phys. Rev. Lett. 64, 483 (1990).

10. P.H. Kes, Physica C 153-155, 1121 (1988).

11. L.Ya. Vinnikov, L.A. Gurevich, G.A. Yemelchenko, and Yu.A. Ossipyan, Solid State Comm., 67, 421 (1988).

12. G.J. Dolan, G.V. Chandrashekhar, T.R. Dinger, C. Feild, and F. Holtzberg, Phys. Rev. Lett., 62, 827 (1989).

13. E.M. Gyorgy, R.B. van Dover, K.A. Jackson, L.F. Schneemeyer, and J.V. Waszczak, Appl. Phys. Lett. 55, 283 (1989).

14. A. Roitburd, L.J. Swartzendruber, D.L. Kaiser, F.W. Gayle, and L.H. Bennett, Phys. Rev. Lett. 64, 2962 (1990).

15. D. Kaiser, these proceedings.

16. H. Maeda, Y. Tanaka, M. Fukutomi, and T. Asano, Jap. J. Appl. Phys. Lett. 27, L209 (1988).

17. C. W. Chu, L. Bechtold, L. Gao, P. H. Hor, Z. J. Huang, et al., Phys. Rev. Lett. 60, 941 (1988).

18. U.Atzmony, R.D. Shull, C.K. Chiang, L.J. Swartzendruber, L.H. Bennett, and R.E. Watson, J. Appl. Phys. 63, 4179 (1988).

19. P.W. Anderson, Phys. Rev. Lett. 9, 309 (1964).

20. Y.B. Kim, C.F. Hempstead, and A.R. Strnad, Phys. Rev. Lett. 12, 145 (1964).

21. K.A. Müller, M. Takashige, and J.G. Bednorz, Phys. Rev. Lett. 58, 1143 (1987).

22. I. Morgenstern, K.A. Müller, and J.G. Bednorz, Z. Phys. B 69, 33 (1987).

23. Y. Yeshurun and A.P. Malozemoff, Phys. Rev. Lett. 60, 2202 (1988).

24. P.L. Gammel, L.F. Schneemeyer, J. V. Waszczak, and D. J. Bishop, Phys. Rev. Lett. 61, 1666 (1988).

25. T.T.M. Palstra, B. Batlogg, L.F. Schneemeyer, and J.V. Waszczak, Phys. Rev Lett. 61, 1662 (1988).

26. L.J. Swartzendruber, L.H. Bennett, and C.F. Gallo, in "Proceedings of High-T_c Superconductors: Magnetic Interactions" edited by L.H. Bennett, Y. Flom, and G.C. Vezzoli (World Scientific Publishing Co., New Jersey, 1989). p.303

27. D.R. Lundy, J. Ritter, L.J. Swartzendruber, R.D. Shull, and L.H. Bennett, in "Proceedings of High-T_c Superconductors: Magnetic Interactions" edited by L.H. Bennett, Y. Flom, and G.C. Vezzoli (World Scientific Publishing Co., New Jersey, 1989). p.263

28. F.J. Adrian, J. Bohandy, B.F. Kim, K. Moorjani, J.S. Wallace, R.D. Shull, J.J.

Swartzendruber, and L. H. Bennett, Physica C 156, 184 (1988).

29. M. Turchinskaya, L.H. Bennett, L.J. Swartzendruber, A. Roitburd, C.K. Chiang, M. Hill, J.E. Blendell, and K. Sawano, in "High-Temperature Superconductors: Fundamental Properties and Novel Materials Processing" Mat. Res. Soc. Symp. Proc. 169, 957 (1990).

30. A.L. Roitburd, and M.T. Turchinskaya, these proceedings.

31. A.L. Roitburd, M.T. Turchinskaya, L.H. Bennett, and L.J. Swartzendruber, "Vortex Diffusion Coefficient in YBaCuO", Phys. Rev. Lett. in press (1990).

32. M. Murakami, M. Morita, and N. Koyama, Jpn. J. Appl. Phys., 28, L1125 (1989).

33. J.W. Ekin, T.M. Larson, A.M. Herman, Z.Z. Sheng, K. Togano, and H. Kumakura, Physica C (in press).

34. M.R. Beasley, R. Labush, and W.W. Webb, Phys. Rev. 181, 682 (1969).

35. C. Rossel and P. Chaudhari, Physica C, 153-155, 306 (1988).

RIGID LEVITATION, FLUX PINNING, THERMAL DEPINNING AND FLUCTUATION IN HIGH-T_C SUPERCONDUCTORS

E.H. Brandt

Max-Planck-Institut für Festkörperforschung
Heisenbergstr. 1, D-7000 Stuttgart 80, FRG

Abstract: The motionless and very stable levitation of high-T_c superconductors above a not rotationally symmetric magnet, and of a magnet above a flat superconductor, demonstrates that pinning and forced depinning of the magnetic flux lines (the Abrikosov vortices) in these type-II superconductors plays a decisive rôle here. Flux pinning causes a *hysteresis* of the magnetization curves, and thus hysteretic force–displacement curves when the superconductor is moved in an inhomogeneous magnetic field. This hysteresis stabilizes the levitation of type-II superconductors and strongly damps its vibration, rotation, and orbiting in fields of low symmetry. In perfectly rotationally symmetric magnetic fields, however, any superconductor can rotate without such friction; this allows the construction of superconducting bearings.

At temperatures sufficiently close to the transition temperature T_c, *flux creep* caused by thermally activated depinning may *decrease* the levitation force. A sharp transition to an effectively pin-free reversible state is observed above a (frequency and geometry dependent) *depinning line* in the induction–temperature plane. This onset of *thermally assisted flux flow* (TAFF), with the flux-line lattice obeying a linear diffusion equation, has been erroneously interpreted as "melting" of the flux-line lattice. It is not clear at present whether an ideally pin-free and strongly fluctuating vortex lattice would melt, what this melting really means (flux lines can cut and reconnect), and how it could be detected.

1. SUPERCONDUCTOR LEVITATING ABOVE A MAGNET

Since the discovery of high-T_c superconductors which stay superconducting above the temperature of liquid nitrogene [1], the free levitation of a superconducting disk above a permanent magnet is one of the most impressive demonstration experiments [2-15]. A ceramic disk of $YBa_2Cu_3O_7$ may be cooled in liquid nitrogene and put above an appropriately shaped magnet where it floats motionless (or rotates, orbits, or vibrates) for several seconds until it warms up to its transition temperature $T_c \approx 92$K and then drops on the magnet (Figure 1). This experiment demonstrates superconductivity directly on a table, not behind the windows of a helium cryostat.

By permanently cooling the superconductor in a stream of evaporating nitrogene gas, the levitation continues as long as desired. Alternatively, a magnet at room temperature may be levitated above a large flat superconductor which may sit in a closed vessel with liquid nitrogene [2, 15]. Apart from cooling, superconducting levitation requires no energy input. Applications of superconducting levitation for frictionless bearings or contact-free positioning of samples will be dealt with in other contributions to this conference. Levitation of tiny superconducting crystallites may be used to separate these or to measure their magnetization [14].

Perhaps the most fascinating feature of levitating high-T_c superconductors is that, above magnets with strong transverse field gradients and without rotational symmetry, the floatation is *completely motionless.* One may push the levitated disk to a wide range of positions and orientations where it will continue to levitate rigidly [3]. This levitation is thus very stable. A superconductor levitating above a low-symmetry magnet [4], and also a magnet levitating above a ceramic superconductor [2], feels an invisible friction as if it were embedded in sand. The levitating body "digs its own potential well" wherever it sits (self trapping). The friction is so strong that the force may become *attractive.* A superconductor may thus be suspended *below* a magnet [6–10] or a magnet below a superconductor [12–13]. Various types of levitation and suspension with superconductors are visualized in Figure 2.

In general, a levitating superconductor will not rotate frictionless even if it is perfectly round [9–10]. On the other hand, a levitating round magnet will rotate frictionless above a flat or arbitrarily shaped superconductor. Rotation of a levitated superconductor (round or of any shape) is frictionless only when it levitates in a position where the magnetic field exhibits rotational symmetry. A residual, velocity-independent friction is then caused only by deviations from perfect rotational symmetry of the magnetic field. A further weak friction proportional to the velocity, in principle may originate from eddy currents which are induced in the surrounding conductors by the magnetic field of a not perfectly symmetric rotating superconductor or magnet.

In this paper I will show that the strong velocity-independent frictional force on a levitating superconductor, and on any type-II superconductor moving in an inhomogeneous magnetic field, is caused by pinning and depinning of the magnetic flux lines in its interior. Levitation may thus be used to investigate the pinning properties of a superconductor, and friction in a superconducting bearing may be minimized by choosing appropriate materials and geometries.

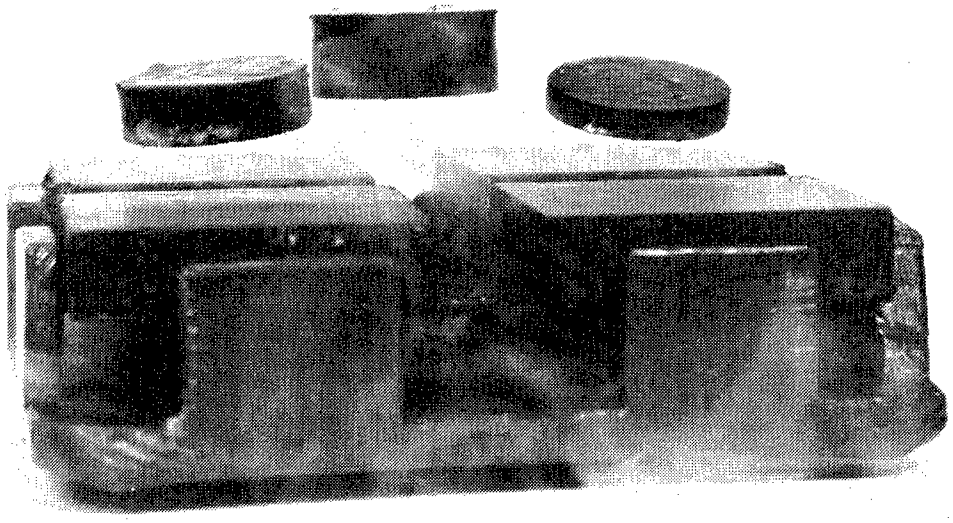


Fig.1. Disks of the high-T_C superconductor $YBa_2Cu_3O_7$ (12 mm diameter) levitating above four strong 2×2 cm magnets sitting with north pole up on an iron plate above a bowl with liquid nitrogene. A screw in the middle is the south pole. Above such a magnet with no rotational symmetry the disks can float motionless in a continuous range of positions and inclinations as if they were stuck in sand.

2. FLUX FLOW

All high-T_c superconductors, even as most superconducting alloys and superconducting compounds, are type-II superconductors. In magnetic fields exceeding the lower critical field of the material $B_{c1} \approx 0.02\mathrm{T}$, magnetic flux penetrates a type-II superconductor in form of magnetic flux lines. These are tiny current vortices which repel each other and tend to arrange into a more or less perfect triangular lattice. Each vortex carries a quantum of magnetic flux $\Phi_0 = h/2e = 2.07 \times 10^{-15}\mathrm{Tm}^2$. The radius of the (usually strongly overlapping) flux tubes is $\lambda \approx 2 \times 10^{-7}\mathrm{m}$ (the penetration depth for weak magnetic fields) and the radius of the vortex core is $\approx \xi = (\Phi_0/2\pi B_{c2})^{1/2} \approx 1 \times 10^{-9}\mathrm{m}$ in the oxide superconductors, where both λ and ξ are highly anisotropic (by factors of ≈ 5 or more).

When the external field is increased, e.g., by pushing the superconductor closer to the magnet, more flux lines penetrate. In high-T_c superconductors, due to their very large Ginzburg-Landau parameter $\kappa = \lambda/\xi \approx 200$, the internal magnetic field B_{rev} in equilibrium practically equals the applied field B_a as soon as B_a moderately exceeds B_{c1}. Ideal (pin-free, reversible) superconductors at $B_a > 2B_{c1}$ exhibit a reversible magnetization

$$-\mu_0 M_{rev}(B_a) \;=\; (B_a - B_{rev})/(1-N) \;\approx\; 0.3\,(1 - B_a/B_{c2})\,B_{c1} \qquad (1)$$

where $B_{c2} \approx (2\kappa^2/\ln\kappa)B_{c1}$ is the upper critical field of the material and N is the demagnetization factor of the specimen ($N = 0$ for cylinders or slabs in longitudinal field, $N = 1/3$ for a sphere, $N = 1/2$ for cylinders in transversal field, and $1 - N \ll 1$ for flat disks in transversal field). $B = |\mathbf{B}(\mathbf{r})|$ is the magnetic field inside the superconductor averaged over several flux-line spacings and assumed to be spatially constant in (1).

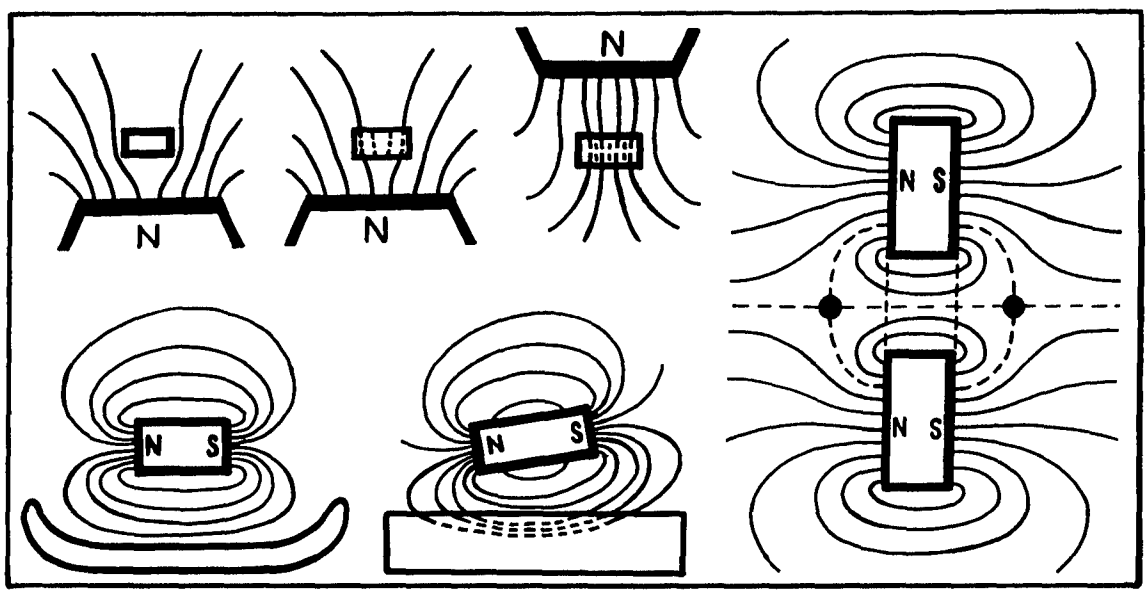


Fig.2. **Top left:** A type-I superconductor and a type-II superconductor levitating above a magnet; a type-II superconductor with positive magnetization (trapped flux) suspended below a magnet. The solid lines indicate magnetic field lines and the dashed lines flux lines. **Bottom left:** Magnets levitating above a bowl of a type-I superconductor and above a flat type-II superconductor. **Right:** The field of an axially magnetized ring magnet has two isolated zeros. In the field minima superconductors in the Meissner state (black dots) can levitate freely even below the ring. This type of suspension thus does not demonstrate attractive forces on a superconductor.

If $\mathbf{B}(\mathbf{r})$ is not constant (due to flux pinning, Section 3), or if an electric current with local density $\mathbf{J}(\mathbf{r}) \approx \mu_0^{-1} \nabla \times \mathbf{B}(\mathbf{r})$ is applied, a Lorentz force $\mathbf{P} = \mathbf{J} \times \mathbf{B}$ acts on the flux lines and causes them to drift with velocity $\mathbf{v} = \mathbf{P}/\eta_{FF}$. The viscosity η_{FF} is related to the flux-flow resistivity $\rho_{FF} \approx \rho_n B/B_{c2}$ by $\eta = B^2/\rho_{FF} \approx B\,B_{c2}/\rho_n$ where ρ_n is the normal conductivity at the same temperature T [16]. This flux drift generates an electric field $\mathbf{E} = \mathbf{B} \times \mathbf{v}$. Thus,

$$\mathbf{E} = \mathbf{B} \times \mathbf{v} = \mathbf{B} \times \mathbf{P}/\eta_{FF} = \mathbf{B} \times (\mathbf{J} \times \mathbf{B})/\eta_{FF} = \rho_{FF} \mathbf{J}_\perp \qquad (2)$$

is proportional to, and directed along, the current-density component $\mathbf{J}_\perp$ perpendicular to the flux lines. This means, *the presence of mobile flux lines destroys the ideal conductivity.* The resulting flux-flow resistivity is *anisotropic*: only currents perpendicular to the applied field cause a voltage drop and a dissipation JE, but currents parallel to the flux lines are loss free.

A more careful analysis reveals that, in ideal superconductors, a longitudinal current density $\mathbf{J}_{||} = \hat{\mathbf{B}}(\mathbf{J}\hat{\mathbf{B}})$ ($\hat{\mathbf{B}} = \mathbf{B}/B$) may cause the flux lines to distort spontaneously into helices which blow up until they cut each other or the surface of the specimen [17–19]. This *helical instability* induces flux-line motion and thus dissipation. However, even as in the usual flux flow, because of flux pinning this dissipation occurs only when the current density exceeds a (longitudinal) critical current density. For a recent contribution and a compilation of references on longitudinal currents in superconductors see [20].

The dissipation caused by flux motion in type-II superconductors in general is due to eddy currents, which form a dipolar pattern around isolated vortices when $\kappa \gg 1$. Part of the dissipation originates since the induced current flows also through the normal conducting core [21]. A further contribution, approximately of the same size, originates from the relaxation of the superconducting order parameter Δ: When the flux-line core passes a fixed position in the material Δ goes to zero for a short time $\approx \xi/v$ [22]. Both dissipation effects are incorporated in the solution of the time-dependent Ginzburg-Landau theory for a moving vortex [23] or vortex lattice [24]. For a review on moving vortices see [25].

There has been some discussion recently whether dissipation in the highly anisotropic high-T_c superconductors is always caused by flux flow. Several experiments (e.g. [26]) seemed to indicate that the flux-flow concept cannot explain the measured resistivity, which was independent of the angle between $\mathbf{B}$ and $\mathbf{J}$, both chosen in the a-b plane of the crystal. However, as shown by Kes et al. [27], a small perpendicular (to the a-b plane) field component, which should always be present in imperfect crystals, can explain these observations by the usual flux-flow dissipation (Section 8).

3. FLUX PINNING

In all *real* superconductors the flux lines cannot move completely freely because they interact with material inhomogeneities, e.g., precipitates, interstitials, vacancies, dislocations, grain boundaries, and in $YBa_2Cu_3O_7$ with twin boundaries, oxygen vacancies, and, due to the extremely small vortex core, even with the atomic lattice cell and the CuO_2 planes. This means, their energy depends on the position of the vortex core. Therefore, when the driving force density P is less than a critical value BJ_c, or the current density less than a critical value J_c, the vortices will be pinned and do not move [28–30]. There is thus no voltage drop and no dissipation for $J < J_c$ (for simplicity I shall now write J for $J_\perp$). This result will be modified at finite temperatures in high-T_c superconductors, where thermally activated depinning occurs (Section 8).

The summation of elementary pinning forces (which often are estimated from the Ginzburg-Landau theory) is a complicated statistical problem [28–30]. A soft flux-line lattice is more effectively pinned since the flux lines can adjust better to the pins. J_c thus depends crucially on the elastic properties of the vortex lattice [28–31].

When J exceeds J_c the flux lines are depinned and move as discussed above, but with a nonlinear resistivity, $E \approx \rho_{FF}(J^2 - J_c^2)^{1/2}$. The dissipation EJ is still caused by the viscous motion of the

vortices, but now the vortex velocity is not constant. Near some pins, the flux lines are "plucked", i.e., during depinning they jump with a much higher than the average velocity $\bar{v} = E/B$. In particular, immediately above J_c, E and thus $\bar{v}$ are small, whereas the jumping velocity v_{max} is of the order of $\rho_{FF}J_c/B$. v_{max} depends on the elastic restoring force acting during the jump but (almost) not on J or E.

4. EFFECTS OF FLUX PINNING ON THE LEVITATION

The depinning jumps forced by sufficiently large flux gradients or currents inside superconductors cause the observed frictional damping of levitating superconductors or magnets. As a consequence, the levitation is *stable in a finite range of heights, lateral positions, and orientations* of the levitating body. This behavior in principle can be calculated from the hysteretic magnetization curve $M(B_a)$ of the superconductor. The general expression for the force $\mathbf{F}$ exerted by a magnetic field $\mathbf{B_a}$ on the current density $\mathbf{J(r)}$ inside the superconductor (surface shielding currents and vortex currents) is

$$\mathbf{F} = \int_V \mathbf{J(r)} \times \mathbf{B(r)}\, d^3r. \tag{3}$$

When $B_a(\mathbf{r}) = |\mathbf{B_a(r)}|$ has nearly constant gradient over the volume V of the superconductor one may approximate (32) by

$$\mathbf{F} = (\mathbf{m}\nabla)\,\mathbf{B_a(r)} = \nabla[\mathbf{m}\,\mathbf{B_a(r)}] \approx MV\,\nabla B_a(\mathbf{r}) \tag{4}$$

where $\mathbf{m} \approx \mathbf{M}V$ is the magnetic moment of the superconductor with magnetization $\mathbf{M} = -(\mathbf{B_a} - \mathbf{B})$ $/(1-N)\mu_0$, and $M = |\mathbf{M}|$. The second identity in (3) follows from $\nabla \mathbf{B_a} = 0$, and the third one holds when $\mathbf{M}$ is nearly parallel to $\mathbf{B_a}$.

According to Eq. (1) the magnetization M_{rev} of an ideal type-II superconductor is always *negative*. For real materials, however, $M(B_a)$ is a non-unique function due to flux pinning and may also be positive. One has $-M \geq -M_{rev}$ when B_a is increased (since flux penetration is impeded by pinning), and $-M \leq -M_{rev}$ when B_a is decreased (since the flux does not want to move out). This hysteresis of $M(B_a)$ causes a hysteresis of the force (3) as a function of $B_a(z)$ or of the height z above the magnet. There exists, therefore, a continuous range of equilibrium positions for a levitating superconductor.

In general, whenever the specimen is moved vertically or horizontally in a field gradient, flux is forced to enter or exit. This causes depinning and thus a friction which holds a levitating superconductor in place. An even stronger friction occurs when a magnet levitates above a flat superconductor. One may say that the magnetic field lines are "anchored" inside a type-II superconductor since they are materialized by pinned flux lines.

5. LEVITATION OF TYPE-I SUPERCONDUCTORS

A pinning-caused friction does not occur in type-I superconductors (e.g., lead or tin) since these do not contain flux lines. Type-I superconductors expell the magnetic flux completely when $B_a < (1-N)B_c$ where B_c is the thermodynamic critical field. In the field interval $(1-N)B_c < B_a < B_c$ type-I superconductors with demagnetization factor $N > 0$ are in the *intermediate state* [16, 30] containing superconducting lamellae or tubes (with $B = 0$) surrounded by normal conducting regions (with $B = B_c$), or normal tubes or lamellae in a superconducting matrix. These tubes, with diameters of many λ, can move and be pinned similarly as flux lines in type-II superconductors, but the pinning force is much weaker. The magnetization curves of type-I superconductors are, therefore, reversible and a levitated type-I superconductor has only one (or several discrete) positions of stable levitation but not a continuous range.

In the classical demonstration of superconducting levitation a magnet levitates over a concave bowl of lead or tin in a Helium cryostat. Levitation of a magnet over a *flat* type-I superconductor is *unstable* since the magnetic field lines are expelled from the type-I superconductor and the magnet "rolls" on its compressed field lines over the edges of the superconductor (Figure 2).

6. SUSPENSION OF A SUPERCONDUCTOR BELOW A MAGNET

When the pinning-caused magnetic hysteresis is sufficiently strong, a superconductor can be freely *suspended below* a magnet [6–7, 9–10]. When the superconductor is moved towards the pole of the magnet, more and more flux penetrates; the maximum flux density is somewhat smaller than the field at the pole. When the superconductor is removed from the pole, the internal field initially stays constant due to flux pinning; the force, proportional to $(B - B_a)\,\partial B_a/\partial z$, therefore changes from repulsive to attractive when $B - B_a$ changes sign. Even as the leviation, the suspension of a superconductor below a magnet is *vertically stable* since the attractive force *increases* when the superconductor is moved away from the pole. Horizontal stability of suspension is obvious.

In contrast, a piece of iron cannot be suspended stably below a magnet since the attractive force *decreases* when the iron is moved away from the pole. Stability is the main problem also with other types of levitation [9]: *Aerodynamic* levitation in a fluid jet; *acoustic levitation* by intensive sound waves; *radiometric levitation* by heat radiation in a low-pressure atmosphere; *optical levitation* by laser light; *electric levitation* in combined dc and ac electric fields; *magnetic levitation* of diamagnets by permanent magnets or coils; *radio-frequency levitation* of solid or liquid metals in appropriately shaped coils.

7. SUSPENSION BY A RING MAGNET

The levitation of a superconductor by an axially magnetized ring magnet is an interesting special case (Figure 2). The magnetic field of a ring has two minima (even zeros) on its axis at distances of ≈ 0.4 hole diameters from its flat surfaces [11]. Near such a minimum, the magnetic field is quadrupolar, e.g., $E = \nabla(x^2 + y^2 - 2z^2)$ in appropriate coordinates. Quite generally, electric and magnetic fields in free space cannot have isolated maxima but only minima since $\nabla^2(E^2) \geq 0$ and $\nabla^2(H^2) \geq 0$ [32].

Any diamagnetic material is attracted to a minimum in the magnetic field and can levitate there when the magnetic force exceeds the gravitational force. Therefore, the free levitation of a superconductor by a ring magnet is *not* indicative of attractive forces or a positive magnetization. Any superconductor in the Meissner state, even a type-I superconductor, can levitate *above, beside, or below* a strong ring magnet.

8. THERMALLY ACTIVATED DEPINNING

Due to flux pinning, a type-II superconductor generally is not in thermodynamic equilibrium with the applied field B_a. After a change of B_a, magnetic flux enters or exits the specimen such that the internal field $\mathbf{B}(\mathbf{r})$ exhibits a gradient which, like the slope of a sand pile, does not exceed a critical value; one has $|\nabla \times \mathbf{B}| \approx |\nabla|\mathbf{B}|| \leq \mu_0 J_c$ everywhere in the specimen [16, 28, 33].

At temperatures $T > 0$ the thermal motion of flux lines "shakes" the flux-line lattice such that some of the pinned flux lines may overcome the pinning potential [34]. The flux-density gradient and the current density $\mathbf{J} = \mu_0^{-1}\nabla \times \mathbf{B}$ will then decrease gradually by thermally activated depinning. This phenomenon of *flux-creep* (e.g. a slow decrease of trapped flux with a logarithmic time law [35]) is observed also in *"classical" superconductors* (e.g. Nb, Nb_3Sn, and Nb-Ti alloys), but only close to their transition temperature T_c, where the pinning potential is weak. In *high-T_c*

superconductors flux creep is observed in a much larger temperature interval below T_c because (a) T is higher and (b) the pinning energy $U \approx B_c^2 \xi^3/\mu_0$ is much smaller due to the very short coherence length $\xi \approx 10$Å (in Nb, $\xi \approx 1000$Å) [36-40]. The jumping probability $\propto \exp(-U/k_BT)$ is thus much higher.

According to Anderson's idea [34], the net jump rate ν of flux lines or flux-line bundels is the difference of the jump rates along and against the driving force density $\mathbf{J} \times \mathbf{B}$,

$$\nu = \nu_0 \exp[-(U - \delta U)/k_BT] - \nu_0 \exp[-(U + \delta U)/k_BT]. \quad (5)$$

In (5) ν_0 is an attempt frequency, which I interpret as the typical frequency of the thermal fluctuations of the ideal vortex lattice, $2\pi\nu_0 = \Gamma_1 = B^2/\mu_0\lambda'^2\eta = \rho_{FF}/\mu_0\lambda'^2 \approx \rho_n b(1-b)/\mu_0\lambda^2$ where $b = B/B_{c2}$ and $\lambda'^2 = \lambda^2/(1-b)$ [41]; U is an activation energy; $\delta U = JBVl$ is the work done by a jumping vortex bundle with volume V and jump width l. The interpretation of U, V, and l is not clear at present. Recent scaling theories [42] yield a current dependent $U(J)$ diverging as $J \to 0$ and thus predict zero resistivity at $J = 0$. These extensions of the successful *theory of collective pinning* [29] assume purely elastic deformation of the flux-line lattice and thus disregard its plastic deformation. Experiments yield *constant* resistivity over several decades of J at small J in $YBa_2Cu_3O_7$ single crystals [39]. A *spectrum* of activation energies is considered in [40].

Introducing *heuristic parameters* $J_c = U/BVl$ (critical current density) and ρ_c (resistivity at $J = J_c$) one gets for the drift velocity $v = \nu l$ and electric field $E = Bv$ from (5)

$$E(J) = 2\rho_c J_c \exp(-U/k_BT) \sinh(JU/J_c k_BT). \quad (6)$$

This result means that at $J \approx J_c$, $E(J)$ increases exponentially with J (flux creep) but for $J \ll J_c k_BT/U$, $E(J)$ is linear. This regime of *thermally asissted flux flow* (TAFF) [38] is a new phenomenon observed in the high-T_c superconductors at low current densities, e.g., when the smeared transition $\rho(T)$ is measured with B as parameter [38–39]. From(6) and the flux flow approximation at $T = 0$ (Section 3) one gets the general picture for voltage–current curves (Figure 3):

$$E = (2J\rho_c U/k_BT)\exp(-U/k_BT) = J\rho_{TAFF} \quad \text{for } J \ll J_c \quad \text{(TAFF)} \quad (7)$$

$$E = J\rho_c \exp[(J/J_c - 1)U/k_BT] \quad \text{for } J \approx J_c \quad \text{(flux creep)} \quad (8)$$

$$E = \rho_{FF}(J^2 - J_c^2)^{1/2} \approx J\rho_{FF} \quad \text{for } J \gg J_c \quad \text{(flux flow).} \quad (9)$$

In the linear regime $J \ll J_c$ (6) (even as for $J \gg J_c$) the flux density obeys a diffusion equation $\partial\mathbf{B}/\partial t = D\nabla^2\mathbf{B}$ [38] provided a term $\propto \nabla \times \mathbf{J}_{||}$ (Section 2) may be disregarded [43]. The diffusion constant is given by the TAFF resistivity, $D = \rho_{TAFF}/\mu_0$. This *flux diffusion* is discussed by Kes [38] and in a forthcoming paper [43]. As one consequence, the relaxation time $\tau_0 = L^2/\pi^2 D$ for flux-density gradients and current densities, and also the frequency $(2\pi\tau_0)^{-1}$ where maximum dissipaton occurs in ac experiments, depend on the *geometry and size (L)* of the specimen. These are thus *not* mere material parameters as is often assumed.

9. DOES THE FLUX-LINE LATTICE MELT ?

The thermal fluctuation $\langle \mathbf{u}^2 \rangle$ of the flux lines ($\mathbf{u}$ = displacement of vortex cores) is given by k_BT times the trace of the reciprocal elastic matrix $\Phi_{\alpha\beta}(\mathbf{k})$ of the vortex lattice integrated over (k_x, k_y) in the Brillouin zone and over $|k_z| < \xi^{-1}$: $\langle \mathbf{u}^2 \rangle = k_BT \int (\Phi_{xx}^{-1} + \Phi_{yy}^{-1})\, d^3k/8\pi^3$ [41, 44–46]. In high-T_c superconductors $\langle \mathbf{u}^2 \rangle$ is much larger than in classical superconductors since

(a) T can be high;

(b) the shear modulus c_{66} of the vortex lattice is small, $c_{66} \approx BB_c/4\sqrt{2}\kappa\mu_0$ ($B \ll B_{c2}$);

(c) the elasticity is highly *nonlocal*, i.e., the tilt modulus of the flux-line lattice $c_{44}(k) \approx (B^2/\mu_0)/(1+$

$k^2\lambda'^2$) depends on the wavelength $2\pi/k$ of the tilt strain, and little energy is required to tilt the vortex lattice locally [31, 45];

(d) the pronounced anisotropy of these oxides reduces $c_{44}(k)$ even more (not at $k = 0$ as argued by [44] but at $k > 1/\lambda'$ [45–46]) and thus increases $\langle \mathbf{u}^2 \rangle$;

(e) the small pinning energy cannot reduce the short-wavelength thermal fluctuations.

It has been argued [44] that the vortex lattice might *melt* when $\langle \mathbf{u}^2 \rangle^{1/2}$ reaches ≈ 0.1 times the vortex spacing $a = 1.075(\Phi_0/B)^{1/2}$. From this Lindemann criterion, and from other melting criteria (fluctuating vortex distance and shear strain) [41, 45] one may derive a "melting temperature" $T_m(B)$, which decreases when the flux density B increases. It is sometimes assumed that a "melted flux lattice" cannot be pinned since it can flow between the pins [47]. This would be true if there were much less pins than flux lines. However, in real materials and in three dimensions there are many pins per flux line, and a soft flux-line lattice is even *stronger pinned* since it can adjust better to the pins [28–30, 48]. The vibrator experiments [47], therefore, did not measure a "melting line" $T_m(B)$ but rather the usual "irreversibility line" or "depinning line" above which thermally activated depinning makes the pins ineffective (Section 8). As shown by Esquinazi [48], the data of [47] coincide with the depinning lines obtained for the same materials by measurements of resistivity, magnetization, and damping and frequency enhancement of superconducting vibrating reeds [48–49].

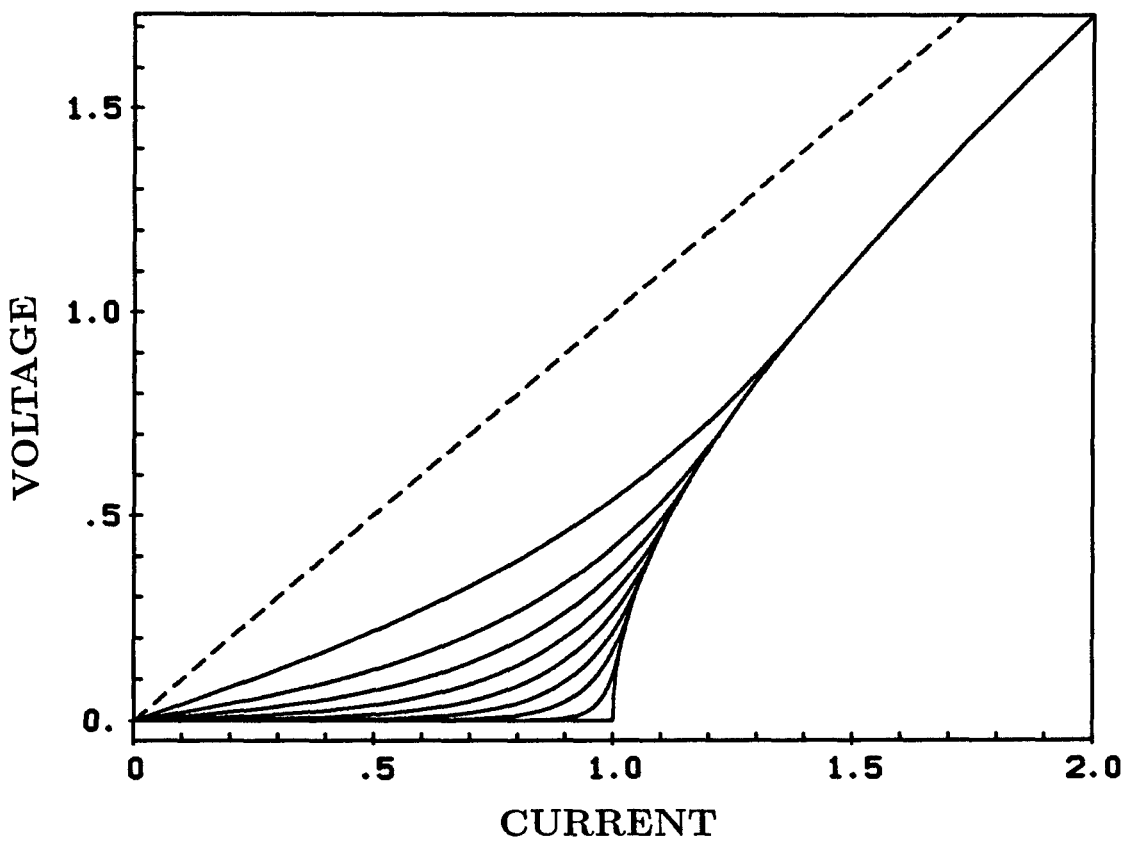


Fig.3. Voltage–versus–current curves due to flux-line drift at various temperatures T and inductions B, Eqs. (7)–(9), in reduced units $E/\rho_{FF}J_{c0}$ versus J/J_{c0} with $J_{c0} = J_c$ at $T = 0$. Larger T and B yield smoother curves. The dashed line shows $E = \rho_{FF}J$.

Due to the always present pinning-caused disorder it is not clear how one should observe "flux melting" and separate it from thermal depinning. It is even not clear what melting of a line lattice really means. In the melting theory [4] a simple stiff-vortex interaction has been assumed rather than the correct three-dimensional interaction between line elements [30–31]. If melting is defined by the vanishing of a shear modulus, one should consider that the shear stiffness of a vortex lattice containing defects depends on both *time and length scale* of the deformation since screw dislocations in the vortex lattice can move freely (they see no Peierls potential). An important difference to the atomic lattice is that some topological defects can easily vanish by cutting and reconnection of flux lines. More work has to be done in order to clarify this melting concept. Probably there is no sharp melting transition but a gradual increase of thermal disorder.

The thermally activated flux motion and the melting speculation concern monocrystals or single grains of ceramic superconductors. The influence of the granular structure [50] on the magnetic and levitation properties has not been dealt with in this contribution due to limited space, but the levitation behavior of ceramic superconductors in principle can be explained from the measurements of intergrain critical currents [51] and irreversible magnetization curves [52].

References

[1] M.K. Wu et al., *Phys. Rev. Lett.* **58**, 908 (1987).

[2] F. Hellman et al., *J. Appl. Phys.* **63**, 447 (1988).

[3] F.C. Moon, M.M. Yanoviak and R. Ware, *Appl. Phys. Lett.* **52**, 1534 (1988).

[4] E.H. Brandt, *Appl. Phys. Lett.* **53**, 1554 (1988).

[5] P.N. Peters et al., *Appl. Phys. Lett.* **52**, 2006 (1988).

[6] C.Y. Huang et al., *Modern Physics Lett. B* **2**, 869 (1988); Y. Shapira et al., *J. Magn. Magn. Mat.* **78**, 19 (1989).

[7] C. Politis and F. Stubhan, *Modern Physics Lett. B* **2**, 1119 (1988).

[8] W.G. Harter, A.M. Herman and Z.Z. Sheng, *Appl. Phys. Lett.* **53** , 1119 (1988).

[9] E.H. Brandt, *Science* **243**, 349 (20 Jan. 1989).

[10] E.H. Brandt, *Am. J. Phys.* **58**, 43 (Jan. 1990).

[11] H. Kitaguchi et al. *Physica C* **157**, 267 (1989).

[12] D. Burton and P.J. Ouseph, *J. Appl. Phys.* **66**, 5063 (1989); P.J. Ouseph, *Am. J. Phys.* **57**, 955 (Oct. 1989).

[13] V.V. Nemoshkalenko et al., *Solid St. Comm.* **xx**, xxx (1989); preprint (Ukrainian Acad. of Science, Institut of Metalphysics. Kiew, USSR, 1989) (a nice treatise, in Russian); V.V. Nemoshkalenko, G.A. Klimenko and B.G. Nikitin, *Metallofisika* **11**, 124 (1989) (in Russian).

[14] E. Walker, P. Monnerat and M. Peter, *Physics C* **153-155**, 1425 (1988); G.S. Grader, A.F. Hebard and R.H. Eick, *Appl. Phys. Lett.* **53**, 2238 (1988).

[15] Z.J. Yang et al., *Physica C* **160**, 461 (1989).

[16] M. Tinkham, *Introduction to Superconductivity*, McGraw-Hill, New York 1975.

[17] J.R. Clem, *Phys. Rev. Lett.* **24**, 1424 (1977).

[18] E.H. Brandt, *J. Low Temp. Phys.* **44**, 33, 59 (1981).

[19] J.R. Clem, *J. Low Temp. Phys.* **38**, 353 (1980); E.H. Brandt, *J. Low Temp. Phys.* **39**, 41 (1980); J.R. Clem, *Physica* **107B**, 453 (1981).

[20] A. Pérez–González and J.R. Clem, *Phys. Rev. B*, submitted.

[21] J. Bardeen and M.J. Stephen *Phys. Rev.* **140**, A1197 (1965)

[22] M. Tinkham, *Phys. Rev. Lett.* **13**, 804 (1964).

[23] C.-R. Hu and R.S. Thompson, *Phys. Rev. B* **6**, 110 (1972); A.I. Larkin and Yu.N. Ovchinnikov, *Sov. Phys.-JETP* **37**, 557 (1973).

[24] R.S. Thompson and C.-R. Hu, *Phys. Rev. Lett.* **20**, 1352 (1971).
[25] For reviews on vortex motion see: A.I. Larkin and Yu.N. Ovchinnikov, in: *Nonequilibrium Superconductivity*, D.N. Langenberg and A.I. Larkin, eds. (Elsevier, Amsterdam, 1986), p. 493; L.P. Gor'kov and N.B. Kopnin, *Sov. Phys.-Uspechi* **18**, 496 (1976); see also: J. Bardeen, *Phys. Rev. B* **17**, 1472 (1978), and references therein.
[26] Y. Iye, S. Nakamura and T. Tamegai, *Physica C* **159**, 433 (1989).
[27] P.H. Kes, J. Aarts, V.M. Vinokur and C.J. van der Beek, *Phys. Rev. Lett.* **64**, 1063 (1990).
[28] A.M. Campbell and J.E. Evetts, *Adv. Phys.* **21**, 199 (1972).
[29] A.I. Larkin and Yu.N. Ovchinnikov, *J. Low Temp. Phys.* **43**, 109 (1979).
[30] E.H. Brandt and U. Essmann, *phys. stat. sol. (b)* **144**, 13 (1987) (a review on the flux-line lattice); E.H. Brandt, *J. Low Temp. Phys.* **64**, 375 (1986).
[31] E.H. Brandt, *J. Low Temp. Phys.* **26**, 709, 735 (1977); **28**, 263, 291 (1977); *Phys. Rev. B* **34**, 6514 (1986).
[32] T.B. Jones, *J. Appl. Phys.* **50**, 5057 (1979).
[33] C.P. Bean, *Phys. Rev. Lett.* **8**, 250 (1962); *Rev. Mod. Phys.* **36**, 31 (1964); *J. Appl. Phys.* **41**, 2482 (1970); L. Ji et al., *Phys. Rev. B* **40**, 10936 (1989).
[34] P.W. Anderson, *Phys. Rev. Lett.* **9**, 309 (1962); P.W. Anderson and Y.B. Kim, *Rev. Mod. Phys.* **36**, 39 (1964).
[35] M.R. Beasley, R. Labusch and W.W. Webb, *Phys. Rev.* **181**, 682 (1969).
[36] D. Dew-Hughes, *Cryogenics* **28**, 674 (1988).
[37] Y. Yeshurun and A.P. Malozemoff, *Phys. Rev. Lett.* **60**, 2202 (1988).
[38] P.H. Kes et al., *Supercond. Sci. Technol.* **1**, 242 (1989).
[39] T.T.M. Palstra et al., *Phys. Rev. Lett.* **61**, 1662 (1988); T.T.M. Palstra et al., *Appl. Phys. Lett.* **54**, 763 (1989); *Phys. Rev. B*, in print.
[40] C.W. Hagen and R. Griessen, *Phys. Rev. Lett.* **62**, 2857 (1989).
[41] E.H. Brandt, *Physica C* **162-164**, 257, 1167 (1989).
[42] M.V. Feigel'man et al., *Phys. Rev. Lett.* **63**, 2303 (1989); T. Nattermann, *Phys. Rev. Lett.*, submitted.
[43] E.H. Brandt, *Proceedings of NATO Workshop "Relaxation and Related Topics in Complex Systems", 16-22 Oct. 1989 in Torino, Italy* (Plenum Press), in print, and to be published.
[44] D.R. Nelson and H.S. Seung, *Phys. Rev. B* **39**, 9153 (1989).
[45] E.H. Brandt, *Phys. Rev. Lett.* **63**, 1106 (1989).
[46] A. Houghton, R.A. Pelcovits and A. Sudbø, *Phys. Rev. B* **40**, 6763 (1989).
[47] P.L. Gammel et al., *Phys. Rev. Lett.* **61**, 1666 (1988); R.N. Kleinmann et al., *Phys. Rev. Lett.* **62**, 2331 (1989) (reply).
[48] E.H. Brandt, P. Esquinazi and G. Weiss, *Phys. Rev. Lett.* **62**, 2330 (1989) (comment); A. Gupta, P. Esquinazi and H.F. Braun, *Phys. Rev. Lett.* **63**, 1869 (1989); P. Esquinazi, *Solid State Comm.*, in print.
[49] E.H. Brandt, P. Esquinazi and H. Neckel, *J. Low Temp. Phys.* **63**, 187 (1986); E.H. Brandt et al., *Phys. Rev. Lett.* **56** 89 (1986); E.H. Brandt, *J. de Physique, Colloque* **C8**, 31 (1987); P. Esquinazi, C. Durán and E.H. Brandt, *J. Appl. Phys.* **65**, 4936 (1989).
[50] J.R. Clem, *Physica C* **153-155**, 50 (1988); M. Tinkham and C. Lobb, *Solid State Physics* (Academic Press, San Diego, 1989), Vol. 42, pp. 91–134.
[51] H. Küpfer, *Cryogenics* **26**, 650 (1988); **29**, 268 (1989).
[52] H. Dersch and G. Blatter, *Phys. Rev. B* **38**, 11391 (1988).

COMPARATIVE STUDY OF FLUX PINNING, CREEP AND CRITICAL CURRENTS BETWEEN YBaCuO CRYSTALS WITH AND WITHOUT Y_2BaCuO_5 INCLUSIONS

Masato MURAKAMI, Satoshi GOTOH, Hiroyuki FUJIMOTO, Naoki KOSHIZUKA
and Shoji TANAKA
International Superconductivity Technology Center,
Superconductivity Research Laboratory,
1-10-13 Shinonome, Koto-ku, Tokyo 135 JAPAN

ABSTRACT It is possible to distribute fine Y_2BaCuO_5 inclusions into $YBa_2Cu_3O_7$ crystals by a melt process utilizing a peritectic reaction: $Y_2BaCuO_5 + L \rightarrow 2YBa_2Cu_3O_x$. We prepared Y-Ba-Cu-O crystals with and without Y_2BaCuO_5(211) inclusions and compared critical currents and flux creep. It was found that the crystal with fine 211 inclusions exhibit much higher Jc values and lower flux creep rate than the crystal without 211 inclusions. This result indicates that fine dispersion of 211 inclusions can contribute to flux pinning as in the case of conventional superconductors.

1. INTRODUCTION

In type II superconductors, the introduction of effective pinning centers is required in order to obtain high critical current density(Jc). However, in the case of high Tc oxide superconductors, it is not yet clear whether the conventional pinning theory can explain their critical current characteristics or not. It is also believed that extremely small coherence length and high anisotropic nature in electric conduction may play a dominant role in flux pinning. However, it has been reported that the introduction of pinning centers either through neutron irradiation[1,2] or metallurgical process[3] can help increase critical current density.

We have recently found a novel melt processing technique which enables us to fabricate large Y-Ba-Cu-O crystals with various volume fractions of Y_2BaCuO_5 inclusions[4]. It is known that non-superconducting inclusions can work as effective pinning centers in conventional superconductors[5]. They are also expected to contribute to flux pinning in oxide superconductors.

In this study, we prepared two kinds of Y-Ba-Cu-O crystals with and without Y_2BaCuO_5 inclusions by the Melt-Powder-Melt-Growth (MPMG) process. Then we compared critical currents and flux creep between them in order to clarify if fine dispersion of 211 inclusions is beneficial to flux pinning.

2. EXPERIMENTAL

2.1. Sample preparation - MPMG process[4]

Y-Ba-Cu-O powders with nominal compositions of $YBa_2Cu_3O_x$ and $Y_{1.4}Ba_{2.2}Cu_{3.2}O_y$ were prepared by mixing Y_2O_3, $BaCO_3$ and CuO and calcining at 950°C for 8h. Then they were subjected to the MPMG process schematically illustrated in Fig. 1. The powders were heated to temperatures above 1300°C and held until the powders reacted and melted completely in platinum crucibles. The melt was cooled rapidly by quenching using cold copper plates. The quenched plates

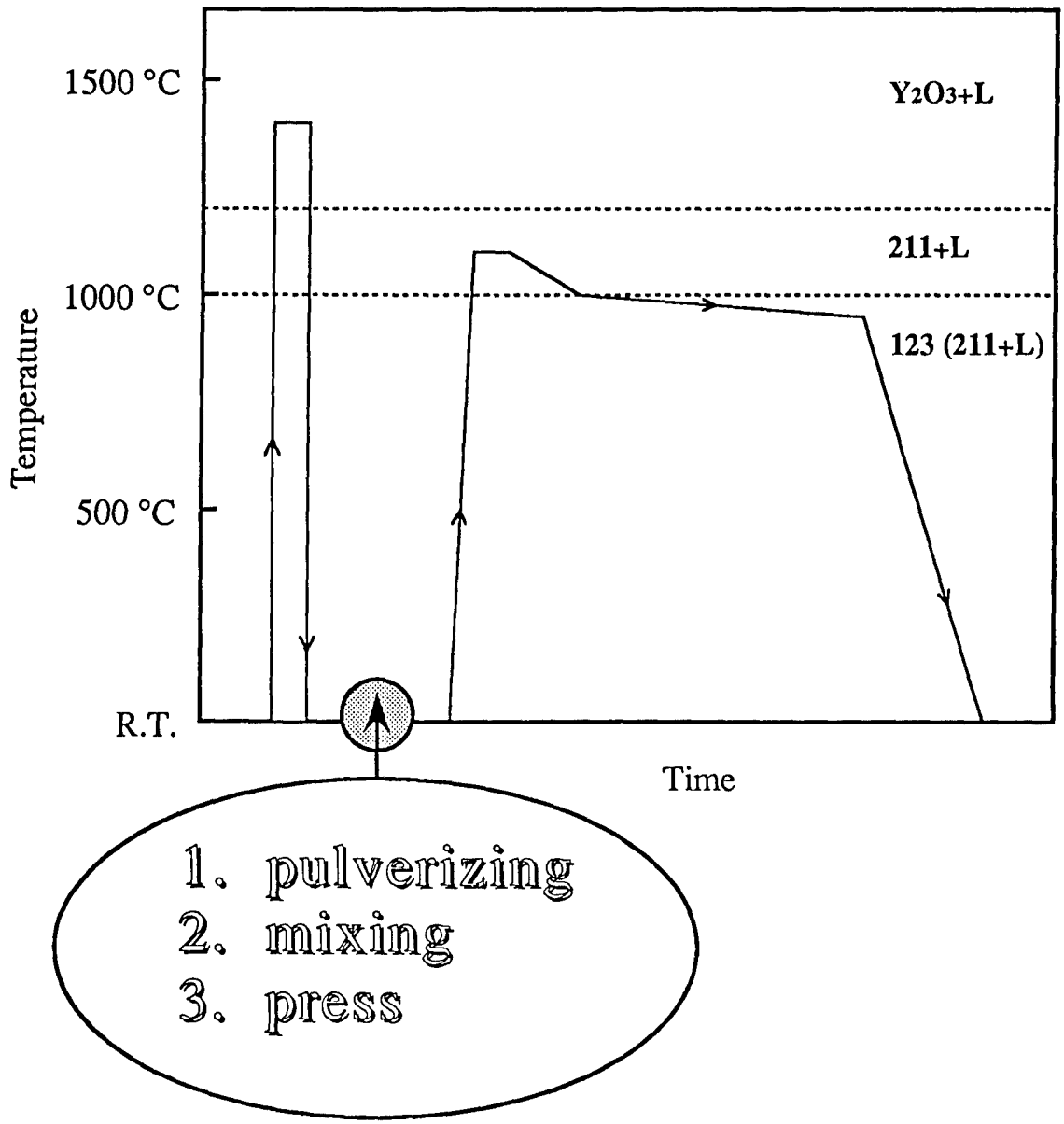


Fig. 1. Schematic illustration for Melt-Powder-Melt-Growth (MPMG) process. Y-Ba-Cu-O calcined powders are heated to temperatures above 1300°C where Y_2O_3 and liquid are stable. The melt is cooled down to room temperature then ground and mixed well in order to refine and homogenize the distribution of Y_2O_3. The melt powders are pressed into various shapes such as pellets and then reheated to around 1100°C where Y_2BaCuO_5(211) and liquid are stable. At this stage 211 nucleates from Y_2O_3 as fine whiskers. The sample is cooled down to 1000°C followed by slow cooling. During the slow cooling below 1000°C, $YBa_2Cu_3O_7$ phase nucleates and grows continuously. When we start with the compositions off the stoichiometry toward 211 rich region, fine dispersion of 211 phase is possible in the 123 matrix. After the process, the sample is annealed at 600°C for 1h and furnace cooled in flowing oxygen to incorporate oxygen into the sample.

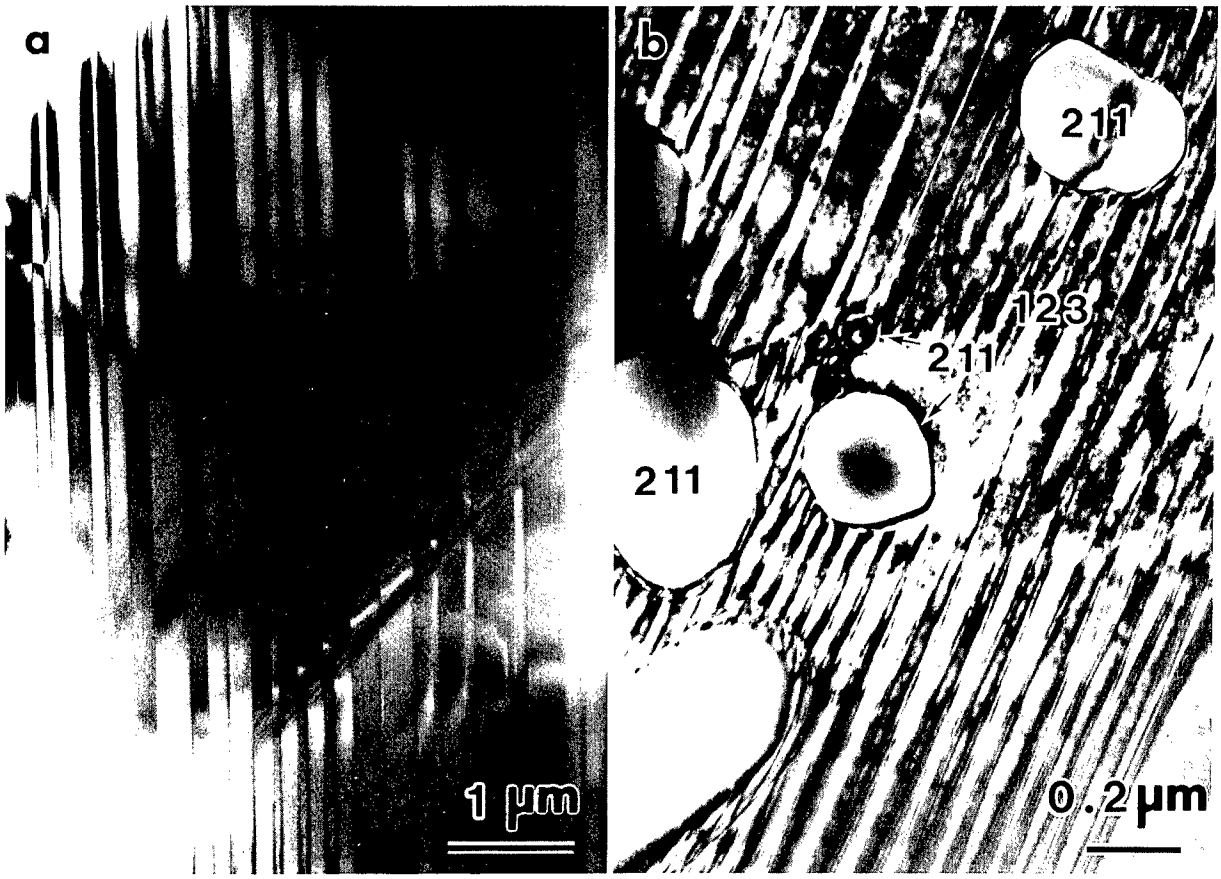


Fig. 2. Transmission electron micrographs for microstructures of (a) $YBa_2Cu_3O_7$ crystal and (b) $Y_{1.4}Ba_{2.2}Cu_{3.2}O_y$ crystals.

were then ground to powders about 1 μm in diameter and mixed well and pressed into pellets 2 cm in diameter and 5 mm in thickness. The pellets were again heated to 1100°C for 20 min and cooled down to 1000°C at a rate of 100°C/h followed by slow cooling at a rate of 1°C/h down to 950°C and furnace cool. The whole process was done in air. Finally the pellets were annealed at 600°C for 1h and slow cooled in flowing oxygen to incorporate oxygen into the samples. Fig. 2 shows transmission electron micrographs for the Y-Ba-Cu-O crystals with 1:2:3 and 1.4:2.2:3.2 compositions. It is noticeable that the former does not contain 211 inclusions, while the latter contain about 20% volume fraction of fine 211 inclusions.

2.2 Physical properties

Critical current densities were obtained from magnetization loops by using the following relations[6,7]:

$$4\pi(M^+ - M^-) = (4\pi/10)\, J_c(d/2) \qquad (1)$$

where M^+ and M^- are magnetization in the increasing and decreasing field processes in emu/cm^3, Jc is critical current density in A/cm^2 and d is sample thickness in cm. The samples were cut from MPMG processed pellets into thin plate of 2 x 2 x 0.4 mm^3 so that the c axis was perpendicular to the surface plane. Magnetic field was applied parallel to the surface plane and therefore

perpendicular to the c axis.

Flux creep measurements were conducted with monitoring time decay of magnetization. The pinning energy U was obtained according to the following relation[8,9]:

$$dM(t)/M_0 = -(kT/U)\, d\ln t \qquad (2)$$

where M_0 is the initial magnetization, t is time, k is Boltzmann constant and T is temperature.

3. EXPERIMENTAL RESULTS

3. 1. Magnetization measurements

Fig. 3 shows magnetization loops for Y-Ba-Cu-O crystals with and without 211 inclusions. It is clear that the crystal with 211 inclusions exhibits much larger magnetic hysteresis and therefore larger J_c values. Fig. 4 shows magnetic field dependence of J_c for these two crystals obtained from magnetization results.

3.2. Flux creep measurements

Fig. 5 shows time decay of magnetization for the Y-Ba-Cu-O crystals under magnetic fields of 1kOe and 5kOe at 77K. The relaxation takes place logarithmically with time as shown in the figure. It is also clear that the crystal with 211 inclusions with higher critical current shows lower flux creep rate or higher pinning energy. Fig. 6 shows magnetic field dependence of the pinning energy U for the crystals at 77K obtained using the relation (2). The pinning energy scales with $B^{-1/2}$ in the both samples. These results support that the fine dispersion of 211 inclusions into the 123 matrix can contribute to flux pinning.

4. DISCUSSION

4.1. Theoretical estimation of Jc[10,11]

It is known that non-superconducting phase can work as a strong pinning center in conventional superconductors. When the size of pinning center is d, the elementary pinning energy U_p is obtained as

$$U_p = (H_c^2/8\pi)\pi\xi^2 d \qquad (3)$$

where H_c is the thermodynamical critical magnetic field, ξ is Ginzburg-Landau coherence length. Then the elementary pinning force f_p is given by

$$f_p = U_p/2\xi = (H_c^2/16)\xi d \qquad (4)$$

In order to obtain bulk pinning force F_p per unit volume, we need to sum up f_p considering the contribution of various pinning centers. In the case of non-superconducting inclusions with density N_p and d in size. F_p is obtained as

$$F_p = (N_p d/a_f) f_p \qquad (5)$$

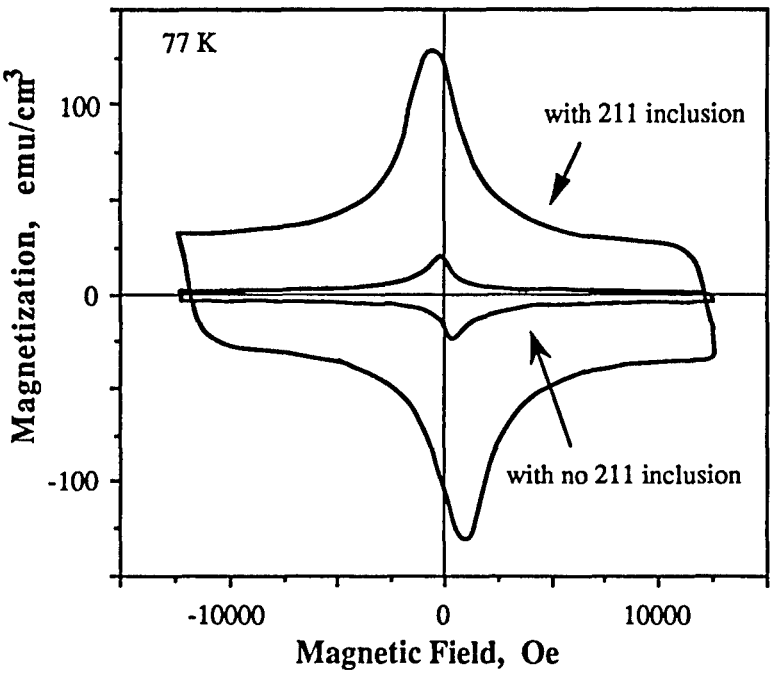


Fig. 3. Magnetization loops for the Y-Ba-Cu-O crystals with and without 211 inclusions. Note that the crystal with 211 inclusions exhibits larger hysteresis.

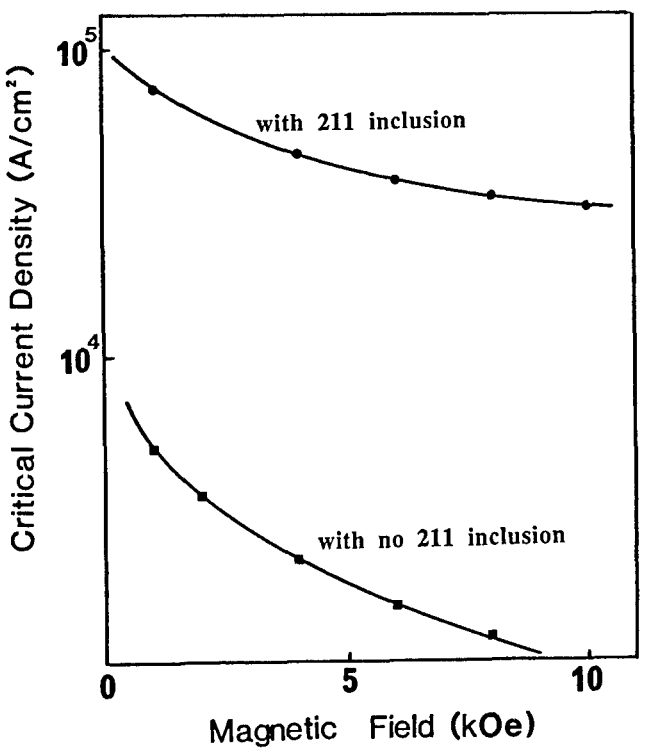


Fig. 4. Magnetic field dependence of J_c for the Y-Ba-Cu-O crystals with and without 211 inclusions. Note that the crystal with 211 inclusions exhibits much higher J_c values.

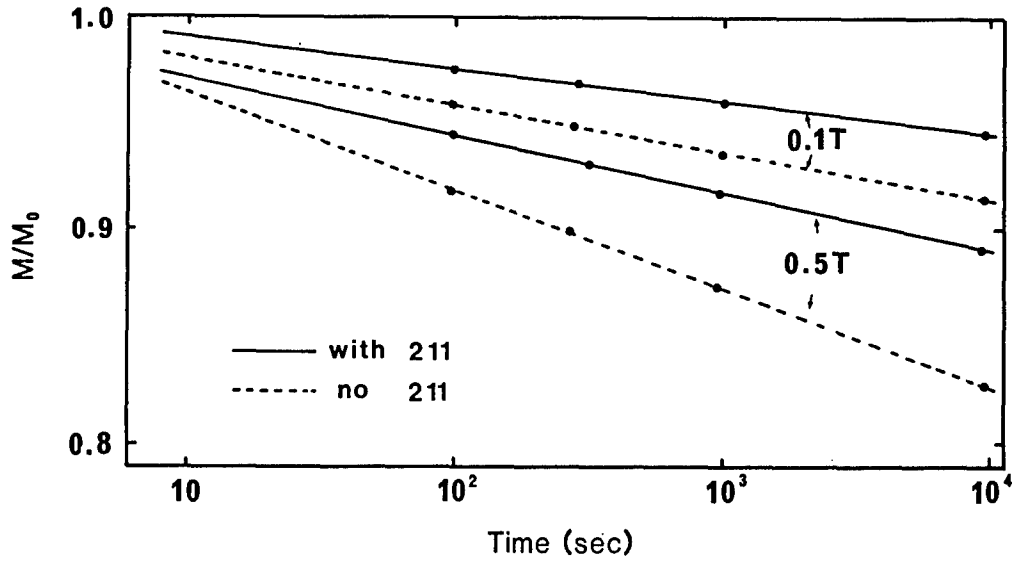


Fig. 5. Time decay of magnetization for the Y-Ba-Cu-O crystals with and without 211 inclusions under magnetic field of 1kOe and 5kOe at 77K. Note that the flux creep rate is smaller in the crystal with 211 inclusions exhibiting higher J_c values. This result indicates that the flux creep rate can be reduced by increasing J_c or the pinning force.

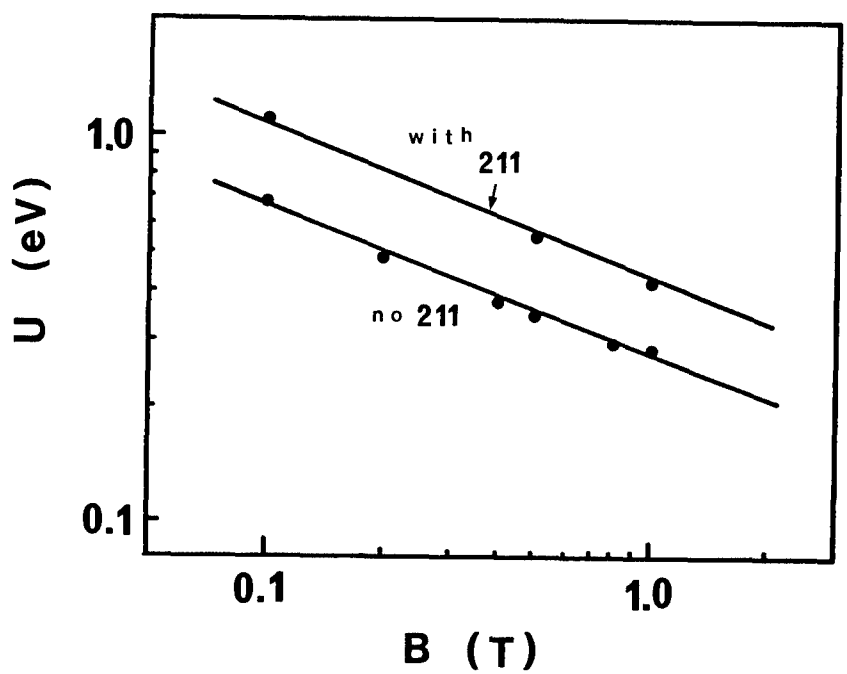


Fig. 6. Magnetic field dependence for the pinning energy U in the Y-Ba-Cu-O crystals with and without 211 inclusions. U scales with $B^{-1/2}$ in the both samples.

where a_f is the flux lattice spacing and given by $a_f=(\phi_0/B)^{1/2}$. On the other hand, Jc is obtained from the relation $Fp=J_c B/10$ and therefore a Jc value expected from the contribution of 211 inclusions is obtained as

$$J_c = 10F_p/B = (10N_p d^2/a_f)(H_c^2 \xi/16B) \qquad (6)$$

In the case of the crystal with 211 inclusions studied in this paper, the volume fraction of 211 inclusions is about 0.2 and the average 211 particle diameter is about 2.5 μm. For the estimation of Jc we used Hc value of 30000e and the coherence length of 20 A at 77K. Then we obtain a Jc value of 35000 A/cm^2 at 77K and 10kOe, which is in good agreement with the experimental results.

The fact that the crystal without 211 inclusion exhibit a Jc value of order 10^3 A/cm^2 indicates that other defects such as twin planes and dislocations can also contribute to flux pinning, although the effect is much smaller than the contribution of 211 inclusions.

4.2. Flux pinning and creep

According to the thermally activated flux creep model[12], flux creep rate v is given by

$$v = v_0 \exp(-E/kT) \qquad (7)$$

where v_0 is the flux creep rate when no pinning barrier exists and E is an effective pinning barrier and given as E=U-JBVx. U is the pinning energy, V is the activation volume of flux bundle which hops collectively and x is the distance for the bundle to move. Jc or magnetization M is considered to decay with time because of flux creep. Time relaxation of M(t) is given by relation (2). Experimental data seem to follow logarithmic time dependence. In the critical state, the effective barrier becomes zero, and therefore the pinning energy U is obtained as

$$U = J_c BVx \qquad (8)$$

V and x are closely related to the stiffness of flux line lattice and depend on B. According to Matsushita's analysis[13]

$$U = \text{const.}\ J_c^{1/2} B^{-1/4} \qquad (9)$$

This relation indicates that the pinning energy can be increased with increasing Jc, which is consistent with the present results.

It is also found from Fig. 4 that J_c scales with $B^{-1/2}$ in MPMG processed crystals. From this dependence and relation(9) it is found that U scales with $B^{-1/2}$. As already presented in Fig. 6, U scales empirically with $B^{-1/2}$, which is also compatible with Matsushita's analysis[13].

Consequently, we can conclude that flux creep is strongly affected by flux pinning and therefore microstructure. It is also clear that flux creep rate can be reduced by the introduction of effective pinning centers.

5. CONCLUSIONS

Through the comparison of critical currents and flux creep between the Y-Ba-Cu-O crystals with and without 211 inclusions, it can be concluded that the fine dispersion of 211 inclusions can help increase J_c in the Y-Ba-Cu-O system. We believe that non-superconducting phase can work as pinning centers even in high Tc oxide superconductors, although other defects can also contribute to flux pinning. It is also concluded that large flux creep rate is not inherent to Y-Ba-Cu-O superconductors even at 77K since the flux creep rate can be decreased by increasing flux pinning force through the microstructural control.

Acknowledgment We would like to thank Mr. K. Yamaguchi of Superconductivity Research Laboratory and Mr. M. Saga of Nippon Steel Corporation for transmission electron microscopic observation. We are also grateful to Mr. T. Oyama and Dr. Y. Shiohara of Superconductivity Research Laboratory for their help in sample preparation.

REFERENCES

1) H. Kupfer, I. Apfelstedt, R. Flukiger, C. Keller, R. Meiner-Hirmer, B. Runtsch, A. Turowiski, U. Wiech and T. Wolf:"Intragrain junctions in $YBa_2Cu_3O_{7-x}$ ceramics and single crystals" Cryogenics 29 (1989) 268.
2) R. B. van Dover, E. M. Gyorgy, L. F. Schneemeyer, J. W. Mitchell, K. V. Rao, R. Puzniak and J. V. Waszczak: Nature 342 p. 55 (1989).
3) M. Murakami, M. Morita, K. Doi and K. Miyamoto: "A New Process with the Promise of High J_c in Oxide Superconductors", Jpn. J. Appl. Phys. 28 pp. 1189-1194 (1989).
4) H. Fujimoto, M. Murakami, S. Gotoh, T. Oyama, N. Koshizuka, Y. Shiohara, and S. Tanaka: "Melt Processing of YBaCuO Superconductors", Proc. ISS 89 (Springer-Verlag, 1990) to be published.
5) R. I Coote, J. E. Evetts and A. M. Campbell:"Flux Line Pinning by Large Normal Particles in Type-II Superconductors", Canad. J. Phys. 50 pp. 421-427 (1972).
6) C. P. Bean:"Magnetization of Hard Superconductors", Phys. Rev. Lett. 8 pp. 250-253 (1962).
7) M. Murakami, M. Morita and N. Koyama: "Magnetization of a $YBa_2Cu_3O_7$ Crystal Prepared by the Quench and Melt Growth Process", Jpn. J. Appl. Phys. 28 pp. L1125-L1127 (1989).
8) A. M. Campbell and J. E. Evetts: "Flux Vortices and Transport Currents in Type II Superconductors", Adv. Phys. 21 pp. 199-427 (1972).
9) M. Murakami, M. Morita and N. Koyama: "Flux Creep in High J_c $YBa_2Cu_3O_7$ Crystals", Jpn. J. Appl. Phys. 28 pp. L1754-1756 (1989).
10) M. Murakami, S. Gotoh, N. Koshizuka, S. Tanaka, T. Matsushita, S. Kambe and K. Kitazawa:"Critical Currents and Flux Creep in Melt Processed High Tc Oxide Superconductors", Cryogenics (1990) to be published.
11) T. Matsushita: Jpn. J. Appl. Phys. 20 p. 1955 (1981).
12) P. W. Anderson:"Theory of Flux Creep in Hard Superconductors", Phys. Rev. Lett. 9 pp. 309-311 (1962).
13) T. Matsushita:"Flux Pinning Mechanism and Critical Current Density in High-Temperature Superconductors", Proc. ISS 89 (Springer-Verlag,1990)to be published.

LOWER CRITICAL FIELD MEASUREMENTS IN $YBa_2Cu_3O_{6+x}$ SINGLE CRYSTALS

D.L. Kaiser, L.J. Swartzendruber, F.W. Gayle and L.H. Bennett
Materials Science and Engineering Laboratory
National Institute of Standards and Technology
Gaithersburg, MD 20899

The temperature dependence of the lower critical field in $YBa_2Cu_3O_{6+x}$ single crystals has been determined by magnetization measurements with the applied field parallel and perpendicular to the c-axis. Results were compared with data from the literature and fitted to Ginzberg-Landau equations by assuming a linear dependence of the parameter κ on temperature. A value of 7 ± 2 kOe was estimated for the thermodynamic critical field at T = 0 by comparison of calculated H_{c2} values with experimental data from the literature.

INTRODUCTION

The lower critical field (H_{c1}) of the high temperature superconductor $YBa_2Cu_3O_{6+x}$ (YBCO) is an intrinsic material property which depends upon temperature and crystallographic orientation. Accurate measurement of H_{c1} is complicated by flux pinning and edge effects (as illustrated in Fig. 1) and by uncertainty in the demagnetizing factor. Consequently, early reported H_{c1} values in single crystals[1-5] were up to an order of magnitude larger than later values.[6-12]

In this study, H_{c1} measurements were made on twinned and detwinned crystals and the data were compared with results of previous investigations for orientations with the applied field parallel and perpendicular to the c-axis of the crystal. The experimental data were fitted to Ginzberg-Landau equations for the dependence of H_{c1} on temperature and upper critical field (H_{c2}) values were calculated for the two orientations of interest.

EXPERIMENTAL PROCEDURE

The YBCO crystals used in the present study (Fig. 2) were grown from Y-Ba-Cu-O melts[13] and subsequently annealed in oxygen gas at 420°C for 80 h to obtain superconducting transition temperatures $T_c > 90$ K. (Thus, the oxygen content $6+x > 6.85$[14]). Two crystals were selected for measurement. The first crystal (AN3-5) exhibited characteristic {110} twin planes and was nearly cubic with dimensions 120 × 135 × 120 μm^3 (c-dimension = 120 μm). Due to the cubic morphology, the demagnetizing factors were nearly identical in all three dimensions. The second crystal (AN9-5) was fully detwinned via a thermo-mechanical process developed in our laboratory[15] and had dimensions a × b × c = 200 × 250 × 100 μm^3.

Magnetic measurements were made using a superconducting quantum interference device (SQUID) magnetometer, with the c-axis of the crystal aligned either perpendicular or parallel to the applied field H. The crystal was first cooled in zero field to a predetermined temperature and the magnetization was then measured as the applied field was increased to a value in excess of H_{c1}. For temperatures greater than about 60 K, sharp breaks from linearity in the M vs. H curves were observed for both crystals, making the estimation of H_{c1} relatively precise. Below 60 K, the

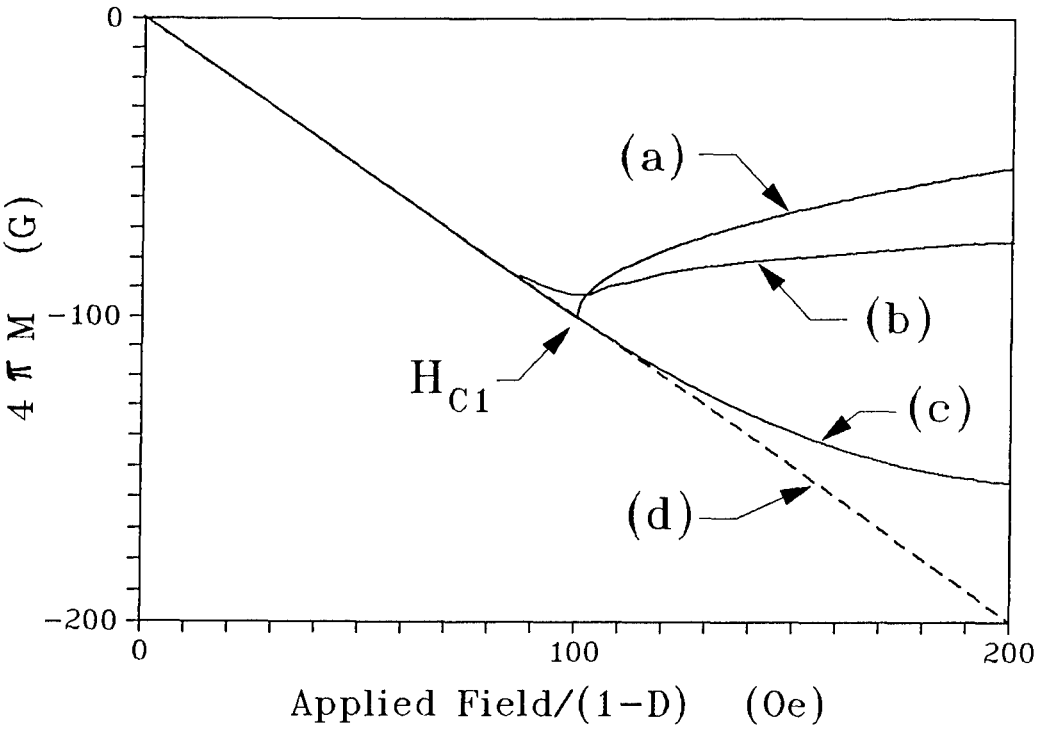


Fig. 1. Hypothetical magnetization curves after cooling in zero field for a sample: (a) at equilibrium (i.e., an ellipsoid with no flux pinning); (b) with some pinning and edge effects; (c) with strong pinning; and (d) with perfect diamagnetic character (i.e., magnetization is proportional to the applied field after correction for the demagnetizing factor, D). For the equilibrium case (a), there is a well-defined, sharp break at H_{c1}, which allows for an accurate determination of H_{c1}. Pinning and edge effects (b and c) make it difficult to estimate the true H_{c1}. In case (b), the observed onset occurs at applied fields below H_{c1} due to flux penetration at the sharp edges and corners of the crystal. In case (c), pinning causes a gradual departure from linearity, making the estimate of H_{c1} less accurate.



Fig. 2. Scanning electron micrograph of as-grown YBCO single crystals. The smallest dimension of a crystal generally lies along the c-axis of the unit cell.

departure from linearity was more gradual and H_{c1} was estimated from the initial point of departure from linearity.

RESULTS AND DISCUSSION

Temperature-dependent H_{c1} data from the present study and previous investigations[4,6-8,10-12] for $H \parallel c$ and $H \perp c$ are presented in Fig. 3. The earliest reported H_{c1} values[1-3,5] were erroneously high due to difficulties in defining H_{c1} and are not included in the two plots. The curves shown in each plot were obtained by fitting all displayed data points using the Ginzberg-Landau equation[16]

$$H_{c1} = H_c(\ln \kappa + 0.08)/\sqrt{2}\,\kappa, \qquad (1)$$

where H_c is the thermodynamic critical field at temperature T as given by

$$H_c = H_{c0}\,(1 - t^2). \qquad (2)$$

Here H_{c0} is H_c at T = 0, t is the reduced temperature T/T_c and κ is the Ginzberg-Landau parameter (the ratio of the penetration depth λ to the coherence length ξ). Data for both $H \parallel c$ and $H \perp c$ can be well-fitted by assuming that κ varies linearly with temperature:

$$\kappa = a + bt. \qquad (3)$$

Good fits of Eq. (1) may be obtained for a wide range of H_{c0} values, leading to a wide range of values for the parameters a and b in Eq. (3). The range of permissible H_{c0} values is limited considerably by requiring that H_{c2} values calculated from a second Ginzberg-Landau equation

$$H_{c2} = \sqrt{2}\,\kappa\,H_c \qquad (4)$$

be in reasonable agreement with experimental H_{c2} data from the literature. This comparative analysis yields a value of 7 kOe for H_{c0}, $\kappa = 100 + 85t$ for $H \perp c$ and $\kappa = 22 + 22t$ for $H \parallel c$. The calculated curves and data for H_{c2} are compared in Fig. 4. Considering the large uncertainties in the experimental H_{c2} data and the obvious differences in T_c for samples from different studies, agreement of the calculated curves with the data is a matter of judgement. The maxima seen in the calculated H_{c2} curves are unphysical, indicating that the linear form used for κ should be modified, e.g., by the addition of a quadratic term in t. However, the large uncertainty in the H_{c0} value used here (7 ± 2 kOe) does not justify such an additional term. Considering the large variations in the experimental H_{c2} data, our H_{c0} value is in reasonable agreement with the value of 10 kOe estimated by Worthington et al.[6] The resulting uncertainties in κ values calculated from our equations are also of order ±30%.

Our H_{c1} data for the detwinned crystal AN9-5 shown in Fig. 3a ($H \parallel c$) are in good agreement with the data of Krusin-Elbaum et al.[10] for twinned crystals. This result indicates that twin boundaries have only a small effect on H_{c1}, as noted in our earlier investigation.[17] Our H_{c1} data for the twinned crystal AN3-5 shown in Fig. 3b ($H \perp c$) are in reasonable agreement with the data from previous investigations.[4,6-8,10-12] Anisotropy in H_{c1} ($H_{c1} \parallel c / H_{c1} \perp c$) as calculated from the two curves in Fig. 3 was 3.1 ± 0.1 for 10 K < T < 80 K.

The calculated H_{c2} values for $H \parallel c$ (Fig. 4a) are in reasonable agreement with the data of Welp et al.[18] near the superconducting transition and follow the general trend of the data of Iye et al.[19] and Worthington et al.[2]. For $H \perp c$ (Fig. 4b) the calculated values at high temperature show good agreement with the experimental data of Gallagher et al.[3] and Welp et al.[18] Anisotropy in H_{c2} ($H_{c2} \perp c / H_{c2} \parallel c$) as calculated from the two curves in Fig. 4 was 4.3 ± 0.2 for 10 K < T < 80 K.

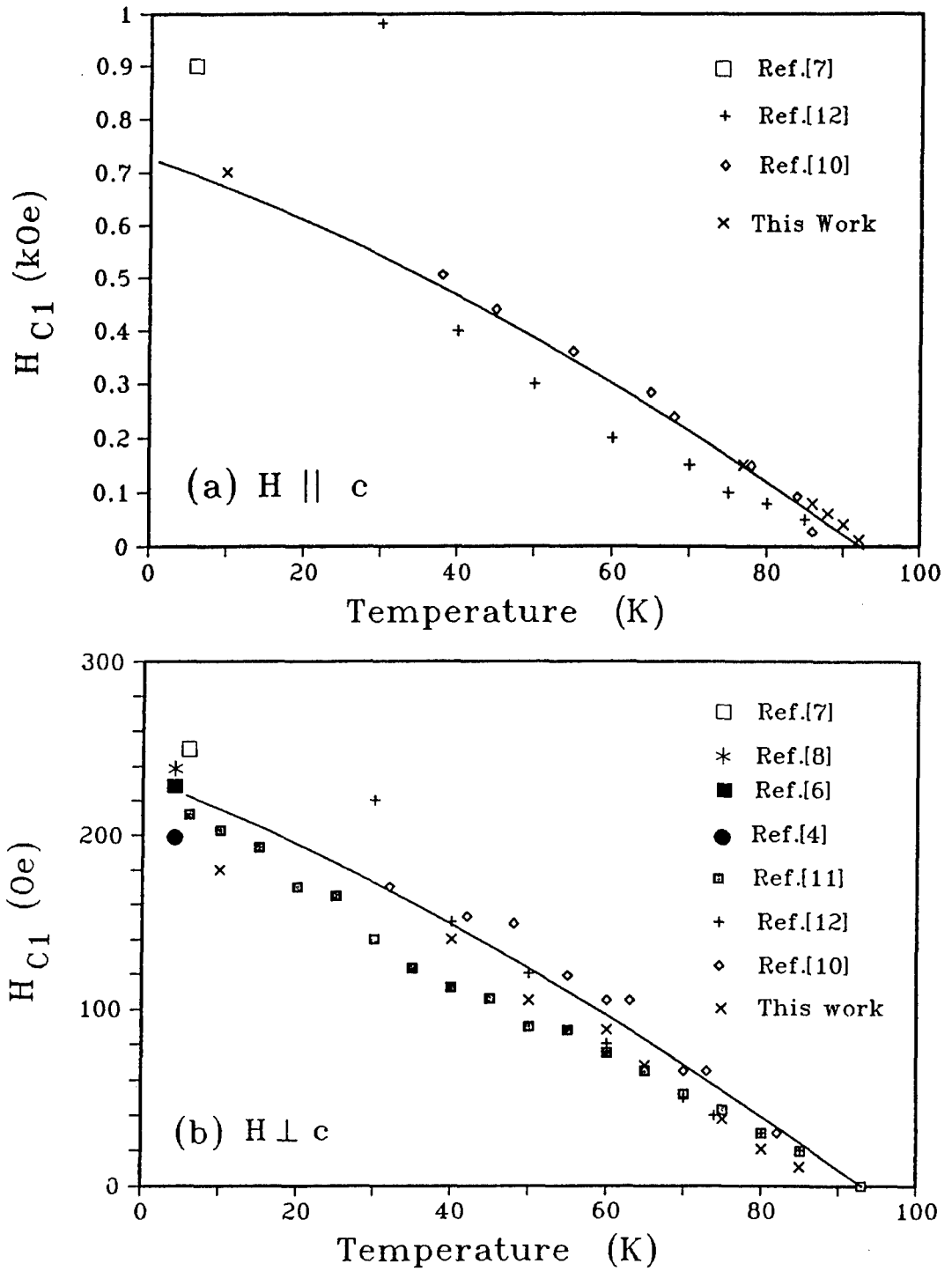


Fig. 3. Temperature-dependent H_{c1} data for (a) H ∥ c (strong pinning) and (b) H ⊥ c (weak pinning). Our data are for (a) the detwinned crystal AN9-5 and (b) the twinned crystal AN3-5. The curves were generated by fitting the data to the Ginzberg-Landau equation for H_{c1} and temperature-dependent κ equations given by (a) $\kappa = 22 + 22t$, and (b) $\kappa = 100 + 85t$ ($t = T/T_c$).

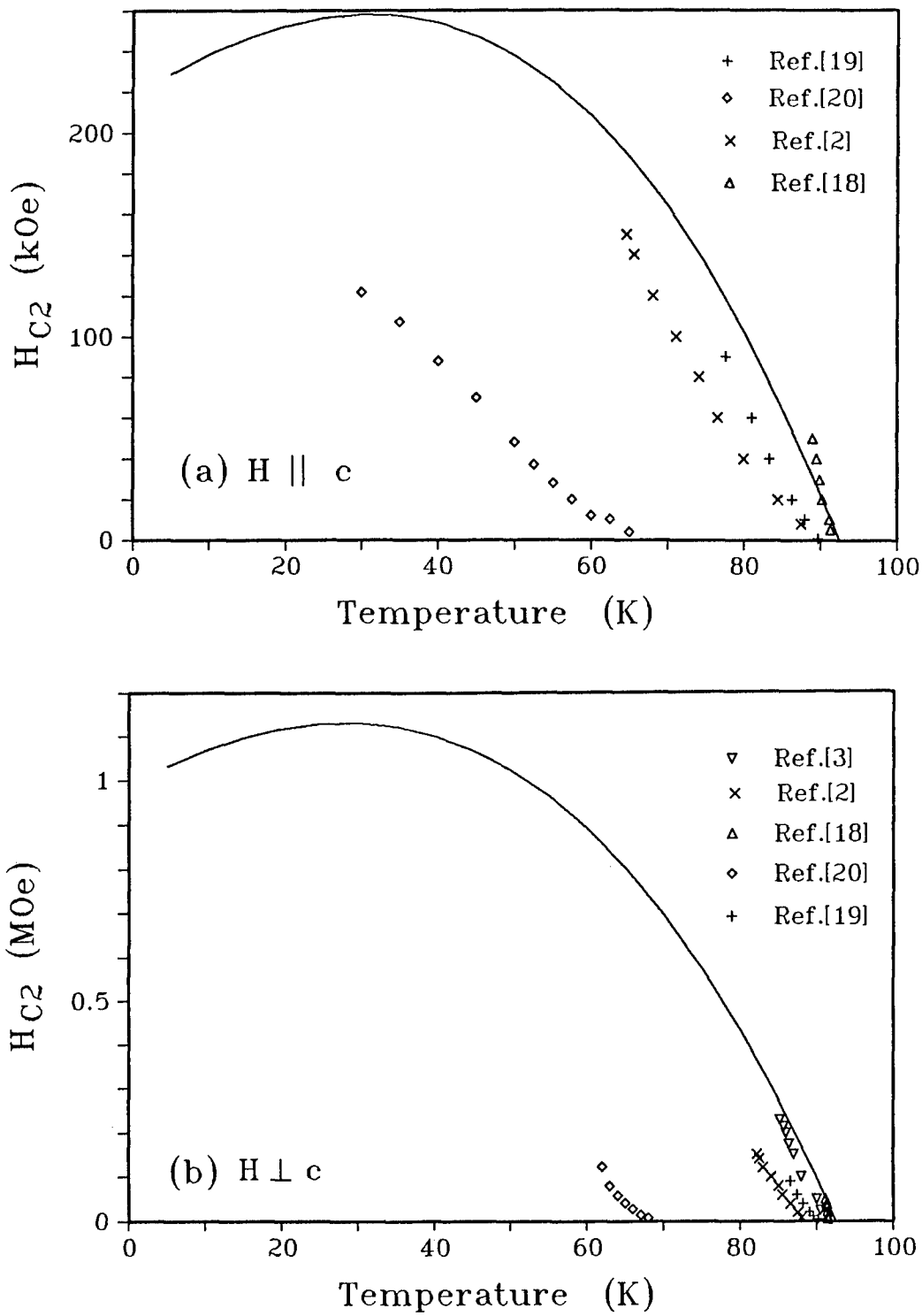


Fig. 4. Temperature-dependent H_{c2} curve (solid line) calculated from the Ginzberg-Landau equation for H_{c2} and the temperature-dependent κ equation for (a) H $\parallel$ c and (b) H $\perp$ c. Experimental H_{c2} data from the literature are shown for comparison. The extrapolations to lower temperatures (T < 60 K) are unreliable and the maxima in the curves probably do not exist.

CONCLUSIONS

Temperature-dependent H_{c1} results were determined from magnetization measurements on detwinned and twinned single crystals of YBCO for H ∥ c and H ⊥ c. The results from the present study and previous investigations for each orientation were fitted to Ginzberg-Landau equations assuming a linear temperature dependence for the parameter κ. H_{c2} values calculated from the Ginzberg-Landau equation and the temperature-dependent κ relations were in reasonable agreement with experimental H_{c2} data from the literature near the superconducting transition temperature. Values of $H_{c0} = 7 \pm 2$ kOe, $\kappa = 100 + 85t$ for H ⊥ c, and $\kappa = 22 + 22t$ for H ∥ c were estimated from the analysis.

Acknowledgments

We gratefully acknowledge the technical assistance of H.J. Brown with the magnetization measurements.

References

1. T.R. Dinger, T.K. Worthington, W.J. Gallagher, and R.L. Sandstrom, "Direct Observation of Electronic Anisotropy in Single-Crystal $Y_1Ba_2Cu_3O_{7-x}$," *Phys. Rev. Lett.* **58**, 2687-2690 (1987).
2. T.K. Worthington, W.J. Gallagher, and T.R. Dinger, "Anisotropic Nature of High-Temperature Superconductivity in Single Crystal $YBa_2Cu_3O_{7-x}$," *Phys. Rev. Lett.* **59**, 1160-1163 (1987).
3. W.J. Gallagher, T.K. Worthington, T.R. Dinger, F. Holtzberg, D.L. Kaiser, and R.L. Sandstrom, "Anisotropy in the Magnetic Properties of Single-Crystal $Y_1Ba_2Cu_3O_{7-x}$," *Physica* **148B**, 228-232 (1987).
4. T.R. McGuire, T.R. Dinger, P.J.P. Freitas, W.J. Gallagher, T.S. Plaskett, R.L. Sandstrom, and T.M. Shaw, "Magnetic Properties of Y-Ba-Cu-O Superconductors," *Phys. Rev. B* **36**, 4032-4035 (1987).
5. R.N. Shelton, R.W. McCallum, M.A. Damento, K.A. Gschneider, Jr., H.C. Ku, H.D. Yang, J.W. Lynn, W.-H. Li, and Q. Li, "Effects of Crystal Anisotropy on Magnetization and Magnetic Order in Superconducting $RBa_2Cu_3O_{7-x}$," *Physica B* **148B**, 285-288 (1987).
6. T.K. Worthington, Y. Yeshurun, A.P. Malozemoff, R.M. Yandrofski, F. Holtzberg, and T.R. Dinger, "The Effect of Flux Pinning and Flux Creep on Magnetic Measurements of Single Crystal $Y_1Ba_2Cu_3O_{7-x}$," *J. de Phys.* **49**, C8-2093-2098 (1988).
7. Y. Yeshurun, A.P. Malozemoff, F. Holtzberg, and T.R. Dinger, "Magnetic Relaxation and the Lower Critical Fields in a Y-Ba-Cu-O Crystal," *Phys. Rev. B* **38**, 11828-11831 (1988).
8. L. Fuchter, C. Giovannella, G. Collin, and I.A. Campbell, "Lower Critical Fields and Pinning in $Y_1Ba_2Cu_3O_{7-x}$," *Physica C* **156**, 69-72 (1988).
9. A. Umezawa, G.W. Crabtree, J.Z. Liu, T.J. Moran, S.K. Malik, L.H. Nunez, W.L. Kwok, and C.H. Sowers, "Anisotropy of the Lower Critical Field, Magnetic Penetration Depth, and Equilibrium Shielding Current in Single-Crystal $YBa_2Cu_3O_{7-x}$," *Phys. Rev. B* **38**, 2843-2846 (1988).
10. L. Krusin-Elbaum, A.P. Malozemoff, Y. Yeshurun, D.C. Cronemeyer, and F. Holtzberg, "Temperature Dependence of Lower Critical Fields in Y-Ba-Cu-O Crystals," *Phys. Rev. B* **39**, 2936-2939 (1989).
11. A. Umezawa, G.W. Crabtree, K.G. Vandervoort, U. Welp, W.K. Kwok, and J.Z. Liu, "Temperature Dependence of the Lower Critical Field of Single Crystal $YBa_2Cu_3O_{7-x}$," *Physica C* **162-164**, 733-734 (1989).
12. H. Adrian, W. Assmus, A. Hohr, J. Kowalewski, H. Spille, and F. Steglich, "Anomalous $H_{c1}(T)$ Behavior of Single Crystalline $YBa_2Cu_3O_{7-x}$," *Physica C* **162-164**, 329-330 (1989).
13. D.L. Kaiser, F. Holtzberg, B.A. Scott, and T.R. McGuire, "Growth of $YBa_2Cu_3O_x$ Single Crystals," *Appl. Phys. Lett.* **51**, 1040-1042 (1987); D.L. Kaiser, F. Holtzberg, M.F.

Chisholm, and T.K. Worthington, "Growth and Microstructure of Superconducting $YBa_2Cu_3O_x$ Single Crystals," *J. Cryst. Growth* **85**, 593-598 (1987).
14. R.J. Cava, B. Batlogg, C.H. Chen, E.A. Rietman, S.M. Zahurak, and D. Werder, "Single-phase 60-K Bulk Superconductor in Annealed $Ba_2YCu_3O_{7-x}$ ($0.3 < x < 0.4$) with Correlated Oxygen Vacancies in the Cu-O Chains," *Phys. Rev. B* **36**, 5719-5722 (1987).
15. D.L. Kaiser, F.W. Gayle, L.J. Swartzendruber, and R.S. Roth, "Thermomechanical Detwinning of Superconducting $YBa_2Cu_3O_{7-x}$ Single Crystals," *J. Mater. Res.* **4**, 745-747 (1989).
16. A.A. Abrikosov, Fundamentals of the Theory of Metals,p. 325 (North Holland, Amsterdam, 1988).
17. L.J. Swartzendruber, A. Roitburd, D.L. Kaiser, F.W. Gayle, and L.H. Bennett, "Direct Evidence for an Effect of Twin Boundaries on Flux Pinning in Single-Crystal $YBa_2Cu_3O_{6+x}$," *Phys. Rev. Lett.* **64**, 483-486 (1990).
18. U. Welp, W.K. Kwok, G.W. Crabtree, K.G. Vandervoort, and J.Z. Liu, "Magnetic Measurements of the Upper Critical Field of $YBa_2Cu_3O_{7-x}$ Single Crystals," *Phys. Rev. Lett.* **62**, 1908-1911 (1989).
19. Y. Iye, T. Hiroyuki, H. Takeya, and H. Takei, "The Anisotropic Upper Critical Field of Single Crystal $YBa_2Cu_3O_x$," *Jap. J. Appl. Phys.* **26**, 1057-L1059 (1987).
20. Y. Hidaka, Y. Enomoto, M. Suzuki, M. Oda, A. Katsui, and T. Murakami, "Anisotropy of the Upper Critical Magnetic Field in Single Crystal $YBa_2Cu_3O_{7-x}$," *Jap. J. Appl. Phys.* **26**, L726-L728 (1987).

OXIDE SUPERCONDUCTORS UNDER MAGNETIC FIELD

K. Kitazawa, Department of Industrial Chemistry, University of Tokyo, 7-3-1 Hongo, Bunkyo-Ku, Tokyo, 113 Japan

One of the current most serious problems for the oxide superconductors from the standpoint of practical application is the various novel features derived mainly from their extremely short coherence. In particular, the coherence length so far observed in the cuprate superconductors is in the range of 0.1 nm perpendicular to the CuO_2 plane. This seems to be creating most of the difficulties in the device fabrication and in the performance under the magnetic field.

In this report, some of the superconducting properties under the magnetic field will be discussed in terms of the short coherence length. First of all, it is pointed out that the widely accepted criterion on the Meissner fraction to represent the quality of the specimen is baseless unless very special precautions are taken. The Meissner fraction has been systematically measured under various intensities of the magnetic field and for various morphologies of the samples, including powder, poly- and single-crystals of different superconducting oxides. It is strongly dependent on the field intensity and the size of the specimen. A model will be presented based on the gradual strengthening of the pinning force with decrease in temperature and the weak coupling at the grain boundaries.

Secondly, the broadening of the superconducting transition under the magnetic field is discussed. This is observed significantly only when the field is applied perpendicular to the basal plane and the relative orientation of the current to the field is insignificant in determining the extent of the broadening. Besides, the change in the strength of the pinning force does not affect the width of the broadening. From these observations discussions will be made on a model based on the "giant fluctuation". Based on this model, it is predicted that the coherence length along the c-axis will be the single most important material parameter to determine the performance of the superconductor under a strong magnetic field. It seems that BYCO is superior in this regard to Bi- or Tl-systems as far as the performance at 77K is considered, although another material with the coherence length slightly longer along the c-axis is still highly desired.

SECTION 3:
THIN FILMS

MICROWAVE CONDUCTIVITY OF LASER ABLATED $YBa_2Cu_3O_{7-\delta}$ SUPERCONDUCTING FILMS AND ITS RELATION TO MICROSTRIP TRANSMISSION LINE PERFORMANCE

K. B. Bhasin, J. D. Warner, C. M. Chorey*, B. T. Ebihara, R. R. Romanofsky and V. O. Heinen
National Aeronautics and Space Administration
Lewis Research Center, Cleveland OH., 44135

* Sverdrup Technology/LeRC Group
Cleveland OH., 44142

F. A. Miranda and W. L. Gordon
Department of Physics
Case Western Reserve University, Cleveland OH., 44106

ABSTRACT

We report on the values of the microwave conductivity in the normal (σ_N) and superconducting ($\sigma^*=\sigma_1-j\sigma_2$) states of two laser ablated $YBa_2Cu_3O_{7-\delta}$ thin films at 35 GHz, in the temperature range from 20 to 300 K. The films (0.7 and 0.4 μm) were deposited on $LaAlO_3$ by laser ablation. The conductivity was obtained from the microwave power transmitted through the films and assuming a two fluid model. Values of $\sigma_N \sim 2.3 \times 10^5$ S/m at room temperature for both films, and of $\sigma_1 \sim 6.3 \times 10^5$ and 4.6×10^5 S/m at temperatures around 80 K were obtained for the 0.7 and 0.4 μm films respectively. For σ_2 values of 4.9×10^6 and 5.4×10^6 S/m were obtained for the 0.7 and 0.4 μm films at 80 K. The expected conductor losses and Q-factor of a superconducting ring resonator were calculated using these conductivity values. The theoretical values were then compared with the experimental results obtained for a resonator fabricated from one of these films.

The discovery of high transition temperature (T_c) superconductors has raised the possibility of a new class of microwave and millimeter wave devices operating at temperatures considerably higher than liquid helium temperatures. Therefore, materials properties such as microwave conductivity (σ), critical current density (J_c), microwave surface resistance (R_s), transport anisotropies, thermal expansion, and others have to be well characterized and understood. To date, measurements of R_s at microwave and millimeter wave frequencies and of J_c of $YBa_2Cu_3O_{7-\delta}$ superconducting oxides have been very abundant.[1-3] Nevertheless, reports on the microwave conductivity of these new oxides have been rare.[4,5] The need for more data on the microwave conductivity of these oxides arises from the fact that knowledge of this parameter provides a way to calculate other relevant properties such as the normal skin depth (δ_n) and the magnetic penetration depth in the superconducting state (λ_s). From the practical application point of view, it provides valuable aid for the design of microwave devices and circuits, based on superconducting microstrip lines.[6,7]

In this paper we report on the microwave conductivity of laser ablated $YBa_2Cu_3O_{7-\delta}$ superconducting thin films at 35 GHz in the temperature range from 20 to 300 K. The values of the conductivities were obtained from the microwave power transmitted through the film, assuming a two-fluid model. The expected conductor losses and Q-factor of a superconducting ring resonator were calculated using

these conductivity values. The theoretical values were then compared with the experimental results obtained for a resonator fabricated from one of these films.

The pulsed laser ablation technique is similar to that reported by other researchers.[8,9] The deposition was performed at a substrate temperature of 750° C at an ambient oxygen pressure of 170 mtorr. The laser wavelength was 248 nm, the pulse length and rate were 20 to 30 ns and 4 pps respectively. During this process the distance between the target and the sample was kept at 7.5 cm and the laser fluence on the target was maintained at 2.0 J/cm^2 per pulse. The laser beam was continually scanned 1 cm across the target using an external lens on a translator. When the deposition was finished, the oxygen pressure was raised to 1 atm and the temperature was lowered to 450° C at a rate of 2° C/min. The temperature was held at 450° C for two hrs before it was lowered to 250° C at the same rate already mentioned. Finally, the heater power was turned off and the sample was allowed to cool to 40° C or less before it was removed from the chamber. This deposition process is explained in more detail in reference 10.

Two $YBa_2Cu_3O_{7-\delta}$ superconducting thin films, deposited by laser ablation on $LaAlO_3$, have been considered in this study. The films' thicknesses were 0.7 and 0.4 μm respectively. $LaAlO_3$ is a convenient substrate because of its perovskite crystal structure and its lattice constant of a=5.357 Å which match very well with the lattice constant of the $YBa_2Cu_3O_{7-\delta}$ superconducting oxide. Also, its low dielectric constant (~22) makes it suitable for microwave device applications. The films were analyzed by X-ray diffraction, dc resistance versus temperature measurements and scanning electron microscope (SEM). Transitions temperatures (T_c , R=0) of 89.7 and 86.0 K were measured for the 0.7 and 0.4 μm thin films respectively. The dc resistance versus temperature curves are shown in fig.1. The X-ray diffraction pattern revealed that both films are single phased with a strong c-axis orientation. Both films exhibit a very smooth surface as observed from scanning electron micrographs. A grain size of ≈¼ μm was observed for both films.

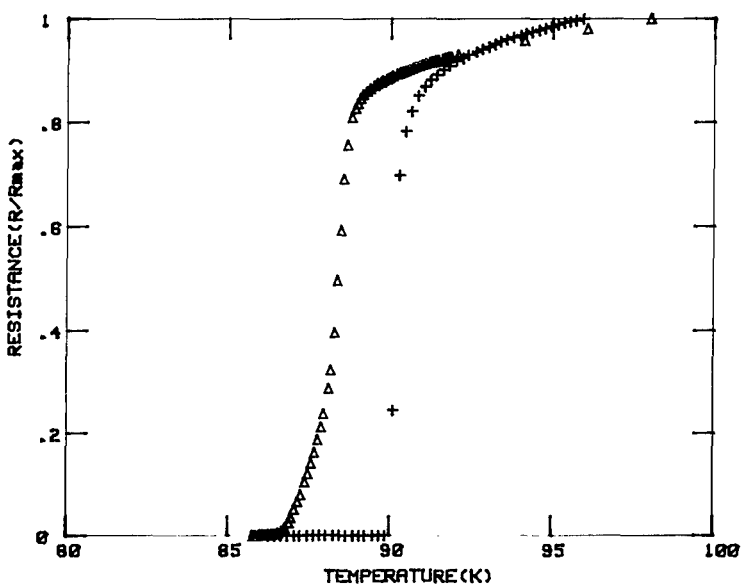


FIGURE 1. Dc resistance versus temperature of 0.7 μm (+) and 0.4 μm (Δ) laser ablated $YBa_2Cu_3O_{7-\delta}$ thin films on $LaAlO_3$.

The power transmission measurements were performed using an HP-8510 network analyzer connected to a helium gas closed cycle refrigerator by Ka-band (26.5 to 40.0 GHz) waveguides. All the measurements were taken under vacuum ($<10^{-3}$ torr) in a custom designed vacuum chamber. Inside the vacuum chamber the sample was clamped between two waveguide flanges mounted on top of the cold finger of the refrigerator. The waveguides were made of stainless steel to minimize heat conduction from the external waveguide arrangement and their inner surfaces were gold-plated to reduce microwave energy losses. Vacuum was maintained at the waveguide feedthroughs by means of 'O' rings and mica sealing windows. The temperature of the sample was monitored using silicon diode sensors mounted on the waveguide flanges supporting the sample. All the measurements were taken during sample cooling.

The measured temperature dependence of the transmitted power through the sample for both films under consideration is shown in fig.2 . Note that for the 0.7 μm film both, the onset temperature for the transition from the normal to the superconducting state (~91 K) and the transition temperature T_c (89.7 K), are clearly observed in this measurement. For the thinner film a sharp drop in transmitted power is observed below the onset temperature, with an attenuation of approximately 20 dB at temperatures around 80 K. The most relevant feature of the power versus temperature curve for this film is the sudden increase in transmitted power at temperatures below 80 K. This feature is an indication of the formation of a leakage source (micro-crack or pinhole) which broadens as the temperature decreases allowing more power to leak through the film. At temperatures below 50 K the amount of power leaking through the film reaches a constant value suggesting no significant variation of the leakage sources as a function of temperature in this temperature region.

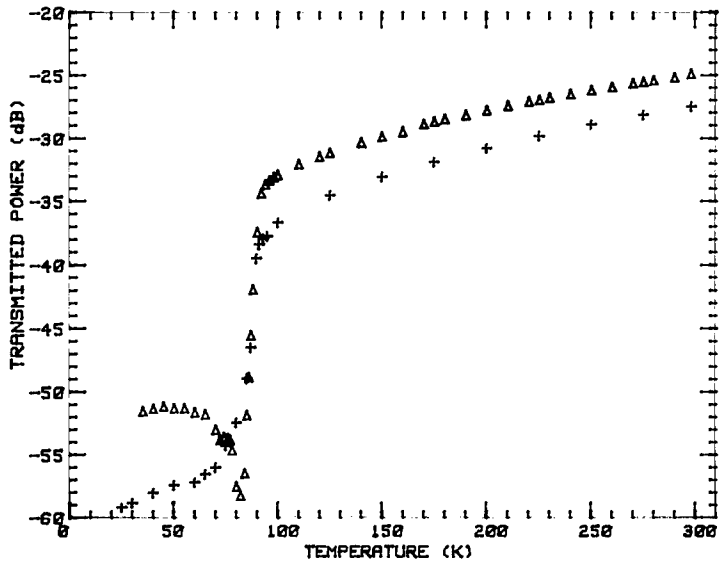


FIGURE 2. Transmitted power versus temperature of 0.7 μm (+) and a 0.4 μm (Δ) laser ablated $YBa_2Cu_3O_{7-\delta}$ thin films on $LaAlO_3$ at 35 GHz.

The normal state microwave conductivity, σ_N, was obtained from the power transmitted through the sample in the normal state, P_N, according to the expression[5]

$$\sigma_N=(-RP_N + [(RP_N)^2-4GP_N(HP_N-8n^2)]^{\frac{1}{2}})/2GP_NdZ_c \quad (1)$$

where

$$G=(n^2+1)+(n^2-1)\cos(2k\ell) \quad (1.a)$$
$$R=2(3n^2+1)+2(n^2-1)\cos(2k\ell) \quad (1.b)$$
$$H=n^4+6n^2+1-(n^2-1)^2\cos(2k\ell) \quad (1.c)$$

with Z_c the characteristic impedance of the waveguide, d the film thickness, ℓ and n the substrate thickness and the index of refraction respectively, and k the wave number. At temperatures below the beginning of the transition, the microwave conductivity takes the form $\sigma^*=\sigma_1-j\sigma_2$. We have calculated σ_1 by using $\sigma_1=\sigma_N(T/T_c)^4$, as defined under the two-fluid model approximation. Values of σ_2 were obtained using the relation[5]

$$\sigma_2/\sigma_c= -\beta/(2\sigma_cdZ_c) + \{[(\beta/2)^2-\gamma]/(\sigma_cdZ_c)^2 -\alpha\sigma_1/\sigma^2dZ_c -(\sigma_1/\sigma_c)^2 +\ldots \ldots (P_c/P_s)[1+\alpha/\sigma_cdZ_c + \gamma/(\sigma_cdZ_c)^2\}^{\frac{1}{2}} \quad (2)$$

with P_s the power transmitted through the film for $T<T_c$, σ_c and P_c are the conductivity and transmitted power respectively at $T=T_c$, $\alpha=R/G$, $\gamma=H/G$ and $\beta=[-2n(n^2-1)\sin(2k\ell)]/G$.

Figure 3 shows the temperature dependence of σ_r ($\sigma_r=\sigma_N$ for $T>T_c$ and $\sigma_r=\sigma_1$ for $T<T_c$) for the samples under study. The conductivities (~2.3 X 10^5 S/m) at room temperature are in close agreement for the two films considered. These values also compare favorably with reported values for the dc conductivity in this type of film.[11] Hence, using the value of σ_N we found a typical resistivity, ρ, of about 435 $\mu\Omega$-cm at room temperature and of 133 and 160 $\mu\Omega$-cm at temperatures around 100 K, for the 0.7 and 0.4 μm films respectively. These resistivity values are on average a factor of 1.5 greater than the values for ρ (ρ~290 $\mu\Omega$-cm at 300 K and ρ~95 $\mu\Omega$-cm at 100 K) obtained from surface resistance (R_s) measurements in strongly c-axis oriented $YBa_2Cu_3O_{7-\delta}$ thin films on $SrTiO_3$ as reported by Klein, et al.[12] The normal conductivity of both films exhibit a metallic behavior with decreasing temperature, reaching values of ~7.7 X 10^5 S/m for the thicker film and of ~6.3 X 10^5 S/m for the thinner one, at the onset temperature. Below T_c, the values of σ_1 were obtained using the value of the conductivity at the onset temperature in the expression $\sigma_1=\sigma_N(T/T_c)^4$. Values for σ_1 of ~6.3 X 10^5 and 4.6 X 10^5 S/m were obtained at 85 K for the 0.7 μm and 0.4 μm films respectively. At temperatures around 50 K and below the values for σ_1 for the 0.7 μm film has decreased by one order of magnitude. Because the 0.4 μm film exhibited leakage of microwave power below 80 K, no data are shown below this temperature.

Figure 4 shows the imaginary part of σ^* for both films. For the 0.7 μm film, values for σ_2 of ~4.9 X 10^6 and 7.0 X 10^6 S/m were obtained at temperatures around 80 and 50 K respectively. These values are greater than those obtained for $YBa_2Cu_3O_{7-\delta}$ laser ablated films deposited on MgO and ZrO_2.[5] Due to the leakage sources formed in the 0.4 μm film, we were unable to obtain values of σ_2 at temperatures below 80 K. A value of 3.5 X 10^6 S/m was obtained just below the onset temperature (~92 K) and of 5.4 X 10^6 S/m at 85 K. Note that the increase

of σ_2 with decreasing temperature corresponds to an increase in electron pairs which implies a reduction of the normal carrier density.

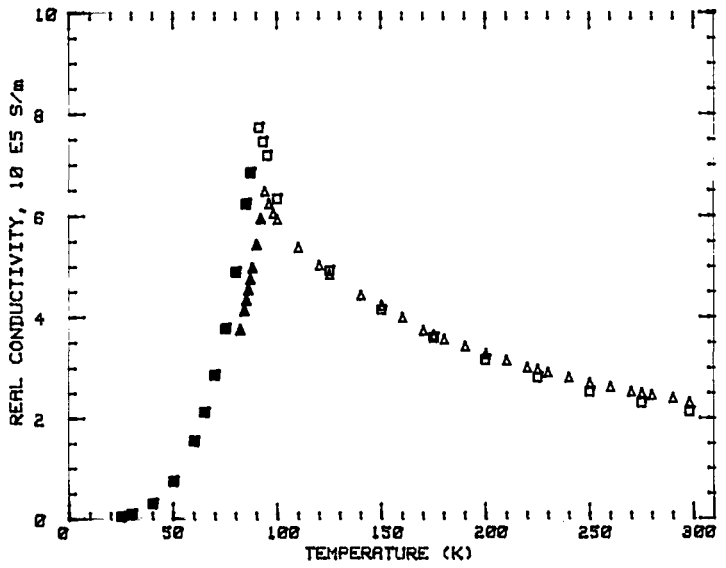


FIGURE 3. Real part of the conductivity, σ_r, versus temperature for 0.7 μm (□) and 0.4 μm (Δ) laser ablated $YBa_2Cu_3O_{7-\delta}$ thin films on $LaAlO_3$ at 35 GHz; $\sigma_r=\sigma_N$ for $T>T_c$ and $\sigma_r=\sigma_1$ for $T<T_c$. Open symbols represent values of the conductivity calculated directly from power transmission measurements and filled symbols represent values of the conductivity calculated using the two-fluid model.

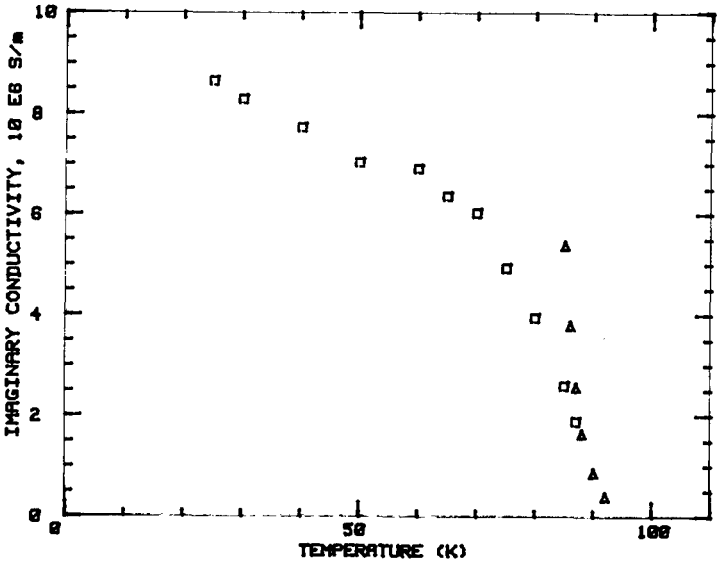


FIGURE 4. Imaginary part of the conductivity, σ_2, versus temperature for 0.7 μm (□) and 0.4 μm (Δ) laser ablated $YBa_2Cu_3O_{7-\delta}$ thin films on $LaAlO3$ at 35 GHz.

The values of σ_1 and σ_2 have been used to estimate values for the magnetic penetration depth λ and the surface resistance R_s.[13] Values of λ_o=0.67 μm and R_s~9mΩ at 77 K were obtained. These values are in close agreement with those obtained by other researchers.[12]

The conductivity values have been used to calculate the Q-factor of a ring resonator, which has a superconducting strip and a normal conducting ground plane. This resonator is shown in figure 5 and consists of a microstrip ring with a circumference that is three wavelengths in length at the design frequency of 35 GHz. Straight lengths of superconducting strip provide input to the ring with coupling achieved by small capacitive gaps. The substrate is 10 milliinch thick lanthanum aluminate; and the characteristic impedance of the line is 45 ohms.

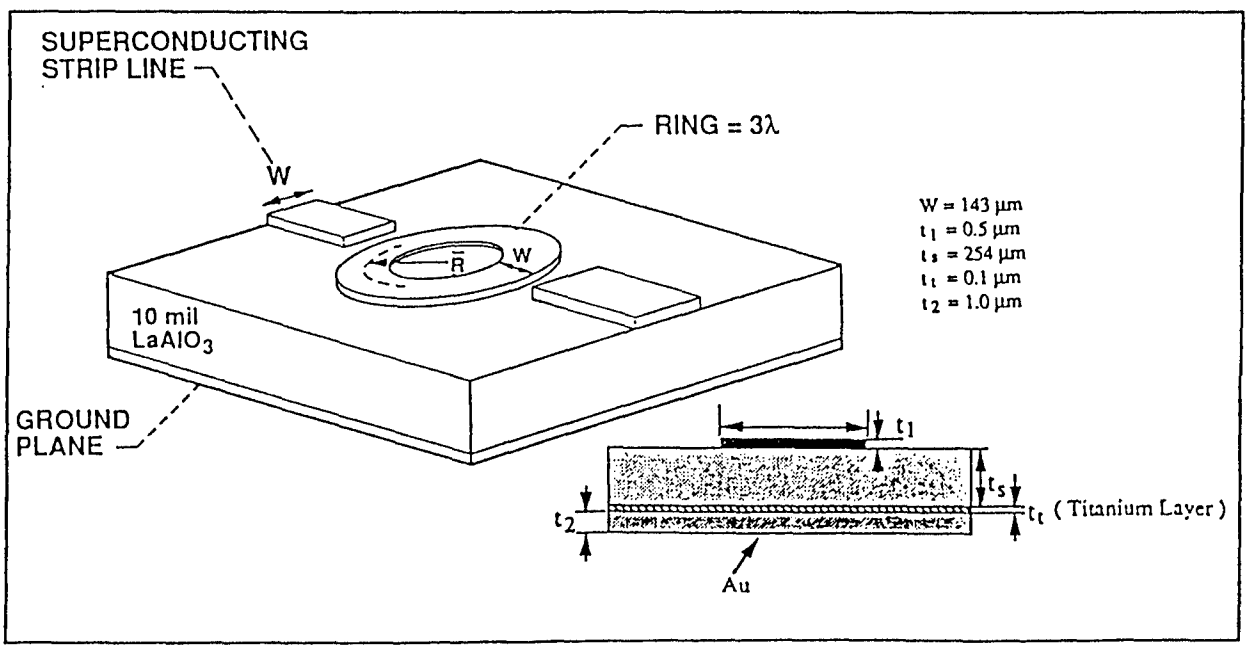


FIGURE 5. 35 GHz ring resonator microstrip transmission line circuit.

The "Q" of the ring is determined by two major loss mechanisms, 1) dielectric loss in the substrate and 2) resistive losses in the conductors. Radiation loss is assumed to be negligible in this case since the resonator, when being measured experimentally, is shielded by a section of waveguide below cutoff which acts to suppress radiation by the circuit. Dielectric losses can be calculated using:

$$\alpha_d = 3.15\ (q^*\epsilon/\epsilon_{eff})\ (\tan\ \delta/\lambda g)\quad \text{Nepers/m} \qquad (3)$$

where α_d[14] is the attenuation constant due to dielectric loss, 'q' is a geometrical 'filling factor', ϵ and ϵ_{eff} are the static and effective dielectric constants, tan δ is the dielectric loss tangent and λ_g is the transmission line wavelength. In these calculations we have used a value of 5.8 x 10^{-4} for tan δ15 but it should be noted that authoritative values for the loss tangent have not been established.

The conductor losses were calculated by the Phenomenological Loss Equivalence Method (PEM), an analytical solution for loss in microstrip lines that accounts for thin conductors. The attenuation due to the loss in the conductors is given by :

$$\alpha_c = Z_{ri}/(2*Z_c) \quad \text{Nepers/m} \tag{4}$$

where Z_{ri} is the real part of the internal impedance of the strip and ground plane and Z_c is the characteristic impedance of the line. The internal impedance (Z_i) is obtained through the PEM where:

$$Z_{ix} = Z_{sx} * G_x * \coth(Z_{sx} * \sigma_x * G_x * A) \tag{5}$$

G_x is a geometrical factor, A the cross sectional area of the strip, Z_{sx} is the surface impedance and σ_x the conductivity of the conductor material of the strip or ground plane (x denotes different values for strip and ground plane). The σ values are obtained from the transmission data and the surface impedance is calculated from them. The "Q" of the ring is calculated as:

$$\frac{1}{Q} = \frac{2(\alpha c + \alpha d)}{\beta} \tag{6}$$

where β is the propagation constant of the line.

Using values of the conductivity obtained form the .7μ film and the tan δ as noted above, the "Q" values were calculated and compared to results obtained from a resonator made from a film fabricated under similar conditions (figure 7). Also shown are the measured "Q" values for a resonator with a normal metal (gold) strip and ground plane. While the superconducting strip performs better than the normal metal, the measured "Q" values do not follow those predicted by the calculations using the transmission conductivity values.

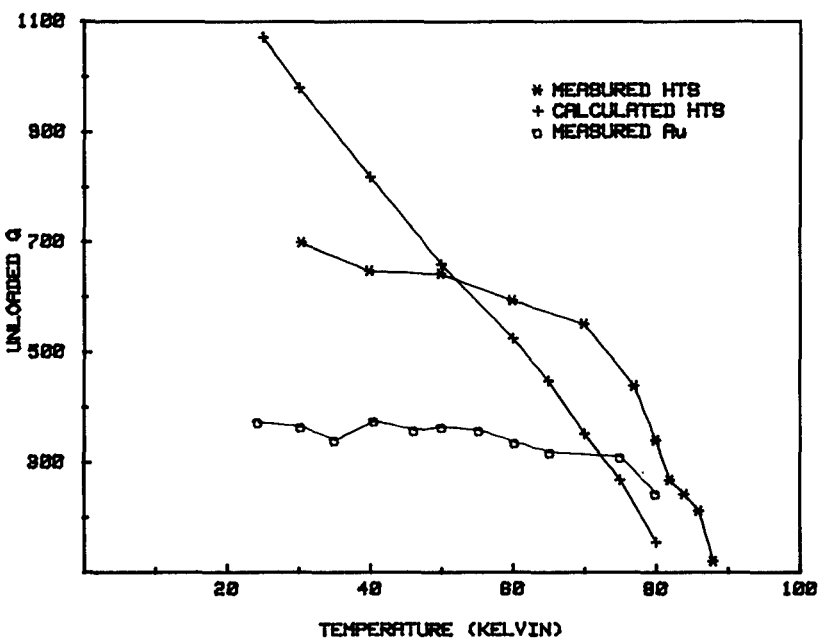


FIGURE 6. Measured and calculated values of unloaded Q for superconducting and normal resonators.

In summary, we have obtained the microwave conductivity at 35 GHz of laser ablated $YBa_2Cu_3O_{7-\delta}$ thin films in the temperature range from 20 to 300 K. The conductivity values at room temperature are in close agreement with dc values reported for the same type of material. Comparing the values for σ_1 and σ_2 for both films with those previously reported for laser ablated $YBa_2Cu_3O_{7-\delta}$ thin films on MgO and ZrO_2 suggest that $LaAlO_3$ is a superior substrate for microwave applications. From these conductivity values, values for the zero-temperature magnetic penetration depth λ_0 and the surface resistance R_s, fundamental in the design of microwave devices and circuits, have been obtained. We have used the conductivity values to obtain conductor losses and Q-factors of a microwave transmission line. However, predicted and experimentally observed values are not in good agreement. Further work is needed in developing an accurate correlation between measured conductivity values and microstrip performance.

REFERENCES

1. J. P. Carini, A. M. Awasthi, W. Beyermann, G. Gruner, T. Hylton, K. Char, M. R. Beasley and A. Kapitulnik, "Millimeter-wave surface resistance measurements in highly oriented $YBa_2Cu_3O_{7-\delta}$ thin films", Phys. Rev. B. 37 (16), 9726-9729 (1988).

2. N. Klein, G. Muller, H. Piel, B. Roas, L. Shultz, U. Klein and M. Peiniger, "Millimeter wave surface resistance of epitaxially grown $YBa_2Cu_3O_{7-x}$ thin films", Appl. Phys. Lett. 54 (8), 757-759 (1989).

3. H. Kupfer, C. Keller, K. Salama and V. Selvamanickam, "Inductive current measurements in an oriented grained $YBa_2Cu_3O_x$ superconductor", Appl. Phys. Lett. 55 (18), 1903-1905 (1989).

4. P. H. Kobrin, W. Ho, W. F. Hall, P. J. Hood and A. B. Harker, Presented at the M^2S-HTSC Conference, Stanford Ca., July 24-28, 1989. To be published in Physica C.

5. F. A. Miranda, W. L. Gordon, K. B. Bhasin, V. O. Heinen, J. D. Warner and G. J. Valco, NASA TM-102345 (1989).

6. F. Huret, D. Kinowski, P. Pribetich and P. Kennis, "Spectral domain analysis of a microstrip thin superconducting line laid on GaAs substrate", Microwave and Optical Tech. Lett. 2 (6), 205-208 (1989).

7. K. B. Bhasin, C. M. Chorey, J. D. Warner, R. R. Romanofsky, V. O. Heinen, K. S. Kong, H. Y. Lee and T. Itoh, NASA TM-102526 (1990).

8. A. Inam, M. S. Hedge, X. D. Wu, T. Venkatesan, P. England, P. F. Miceli, E. W. Chase, C. C. Chang, J. M. Tarascon and J. B. Watchman, "As-deposited high T_c and J_c superconducting thin films made at low temperatures", Appl. Phys. Lett. 53 (10), 908-910 (1988).

9. B. Roas, L. Schultz, and G. Endres, "Epitaxial growth of $YBa_2Cu_3O_{7-x}$ thin films by a laser evaporation process", Appl. Phys. Lett. 53 (16), 1557-1559 (1988).

10. J. D. Warner, J. E. Meola and K. A. Jenkins, NASA TM-102350 (1989).

11. R. T. Collins, Z. Schlesinger, R. H. Koch, R. B. Laibowitz, T. S. Poaskett, P. Freitas, W. J. Gallacher, R. L. Sandstrom and T. R. Dinger, "Comparative study of superconducting energy gaps in oriented films and polycrystalline bulk samples of Y-Ba-Cu-O", Phys. Rev. Lett. 59 (6), 704-707 (1987).

12. N. Klein, G. Muller, S. Orbach, H. Piel, H. Chaloupka, B. Roas, L. Schultz, U. Klein and M. Peiniger, "Millimeter wave surface resistance and London penetration depth of epitaxially grown $YBa_2Cu_3O_{7-x}$ thin films", Physica C 162-164, 1549-1550 (1989).

13. F. A. Miranda, W. L. Gordon, K. B. Bhasin, J. D. Warner and V. O. Heinen, "Microwave Conductivity of Laser Ablated $YBa_2Cu_3O_{7-\delta}$ Superconducting Thin Film on $LaAlO_3$ Substrate", submitted to Appl. Phys. Lett.

14. R. A. Pucal, D. J. Masse, C. P. Hartwig, "Losses in Microstrip", IEEE Trans. Microwave Theory and Tech., vol. MTT-16, no. 6, 342-350 (1968).

15. R.W. Simon, C. E. Platt, A. E. Lee, G. S. Lee, K. P. Daly, M. S. Wire, J. A. Luine and M. Urbanik, "Low -loss substrate for epitaxial growth of high-temperature superconductor thin films", Appl. Phys. Lett., vol. 53 (26) 2667-2679 (1988).

16. H. Y. Lee and T. Itoh, "Phenomenological Loss Equivalence Method for Planar Quasi-TEM Transmission Line with a Thin Normal Conductor or Superconductor," IEEE Trans. Microwave Theory and Tech., Vol. MTT-37, no. 12, 1904-1909 (1989).

LASER SURFACE INTERACTION OF HIGH-T_C SUPERCONDUCTORS

C. H. Chen, M. P. McCann, and R. C. Phillips

Chemical Physics Section, Oak Ridge National Laboratory
Oak Ridge, Tennessee 37831-6378

ABSTRACT

During the past two years, one of the most exciting research fields in science has been the study of the newly discovered high-T_c metal oxide superconductors. Although many theoretical models were proposed, there has been no general agreement on any theory to expain these materials. One of the "peculiar" features of these high-T_c materials is the noninteger number of oxygen atoms. The oxygen content is extremely critical to the superconductive properties. Our results from mass spectroscopy of laser desorbed species indicate that significant quantities of oxygen molecules are trapped in the bulk of these superconductors. It appears that these trapped oxygen molecules may play key roles in superconductive properties.

INTRODUCTION

In 1986, Bendorz and Muller[1] discovered that metallic oxide with a perovskite structure in the La-Ba-Cu-O system exhibited superconductivity at 20°K. In early 1987, Chu and his co-workers[2] made a $YBa_2Cu_3O_{7-x}$ compound which had a T_c higher than the temperature of liquid nitrogen. Since these discoveries, the research and development of high-T_c superconductors has aroused unpecedented attention, not only from the scientific community, but also from various industries and governments. As these new superconducting materials are in general very "brittle" and difficult to machine, it is extremely difficult to fabricate them into thin wires. In addition, practical use of new high-T_c superconductors will require materials with very high critical current density. Thus thin film preparation is particularly important for many applications of superconductors, such as electronics for the computer industry. Films with high superconducting transition temperatures have been prepared by electron beam evaporation, organometallic chemical vapor deposition, DC sputtering, molecular beam epitaxy, and laser evaporation and deposition processes. For example, Rice *et al.*[3] used electron beam and thermal evaporation to produce Ca-Sr-Bi-Cu-O superconducting films from CaF_2, SrF_2, Bi, and Cu targets. Berry *et al.*[4] produced a superconductive film by organometallic chemical vapor deposition. Hellman *et al.*[5] used molecular beam epitaxy to produce a $DyBa_2Cu_3O_{7-x}$ film on a $SrTiO_3$ substrate. Lynds *et al.*[6] used a Nd-YAG laser beam to do laser evaporation and deposition to prepare a $YBa_2Cu_3O_{7-x}$ thin film from targets of Y_2O_3, Ba_2CO_3, and CuO. Kwok *et al.*[7] applied a homogeneous excimer laser to obtain a film with the right stoichiometry of $YBa_2Cu_3O_{7-x}$. However, most of the films in the works cited above need to be annealed in an oxygen environment in order to produce superconductivity. Recently, several research groups obtained superconductive films of $YBa_2Cu_3O_{7-x}$ by raising the temperature of the substrate and introducing oxygen into the chamber during the thin film preparation process.[8] However, no superconductive films of the Bi-Sr-Ca-Cu-O or Tl-Sr-Ba-Cu-O systems were obtained without oxygen annealing. Nevertheless, the right ratio of various metal elements is one of the key factors in achieving superconductivity. Superconductive films are usually obtained based on repeated trials and adjustments. Venkatesan *et al.*[9] observed two distinct components during pulsed laser deposition of high-T_c superconductive film. It was pointed out that the quality of the

superconductive film depends on controlling the film stoichiometry. The role of introducing oxygen into the thin film preparation chamber has never been fully understood. Thus, the need for a real-time monitor for high-T_c thin film preparation is quite critical.

In general, the preparation of a superconductive thin film involves the vaporization of various chemicals. The species deposited on substrates include neutral atoms or molecules in ground states, atoms and molecules in excited states, ions in ground states and ions in excited states. An instrument which has the capability of the quantitative determination of atoms, molecules, and ions in various electronic states should provide very detailed information on the mechanism of formation of superconductive films. A position sensitive monitor of various oxide compounds relative to the flow and pressure of oxygen should reveal the role of oxygen in superconductive film preparation. An ideal method of monitoring the deposition process is to continuously track the deposition *in situ* and automatically maintain optimum film growth. With this goal in mind, we have investigated several diagnostic methods. In this work, fluorescence spectra are presented which indicate suitability for monitoring excited atoms, molecules, and ions; mass analysis of laser desorbed ions is described; and the application of resonance ionization spectroscopy (RIS) to monitor desorbed neutral atoms and molecules is discussed.

One of the "peculiar" features of these high-T_c materials is the noninteger number of oxygen atoms. The oxygen content is extremely critical to the superconductive properties. All of the bulk metal oxide superconductors need to be annealed in an oxygen environment for an extensive period of time in order to achieve superconductivity. The oxygen content is equally critical to bulk and thin film superconductors. Take $YBa_2Cu_3O_{7-x}$ as an example. Its superconductive properties disappear whenever x is larger than 0.5. The samples not only need to be sintered in the oxygen environment, but also need to be cooled down slowly to take up oxygen.[10]

Batlogg *et al.*[11] and Leary *et al.*[12] observed a very small isotopic effect by replacing ^{16}O with ^{18}O for the $YBa_2Cu_3O_{7-x}$ system and concluded that weak electron-phonon coupling cannot be used to explain this observation. The crystal structures of $YBa_2Cu_3O_{7-x}$ have been studied very extensively by X-ray diffraction and neutron diffraction.[13] It was confirmed as orthorhombic for $x = 0$ in $YBa_2Cu_3O_{7-x}$. However, the crystal structure becomes tetragonal when $x \geq 0.5$. It was widely speculated that the change in crystal structure was responsible for the loss of superconductivity. However, experimental results by Xiao *et al.*[14] indicate that the crystal structure is not the key for superconductivity. It was pointed out that the T_c of $YBa_2Cu_3O_{7-x}$ is determined mostly by the actual oxygen content rather than its configuration and that the oxygen-vacancy order was found to be insignificant for high-T_c superconductors. From the viewpoint of valence numbers for the $YBa_2Cu_3O_{7-x}$ compound, the number of oxygen atoms should be 6.5 (i.e., $YBa_2Cu_3O_{6.5}$). Unfortunately, it has been proven experimentally that a single crystal of $YBa_2Cu_3O_{6.5}$ does not demonstrate superconductivity. The number of O atoms needs to be higher than 6.5 for $YBa_2Cu_3O_{7-x}$ to achieve superconductivity. A similar situation is true for all other high-T_c metal oxide superconductors. Thus the existence of Cu^{+3} in these high-T_c superconductors was suggested in order to account for the chemical structure. However, Sarma and Rao[15], as well as Horn *et al.*[16] used X-ray photoelectron spectroscopy (XPS) and Auger electron spectroscopy (AES) to investigate the chemical state of the copper ion. They found that Cu^{+3} was not present in these superconductors. Instead, Cu^{+} was observed. It is well known that high-T_c superconductors in an oxygen-free atmosphere will lose oxygen. It has been assumed that the oxide anion (O^{-2}) in the CuO plane is in equilibrium with oxygen molecules in the gas phase at the same temperature and a fixed partial pressure. It is known that these metal oxide superconductors are, in general, very porous and that there are many

deficit sites in the crystal. However, the possible existence of trapped O_2 molecules in the bulk or thin film materials has been ignored. During the development of the present monitor for superconductive films preparation, we observed the existence of trapped O_2 in superconductors.[17] The trapped O_2 gas can possibly have significant implications for the nature of the superconductivity of these high-T_c materials.

EXPERIMENTAL RESULTS AND DISCUSSION

A schematic of the experimental apparatus is shown in Fig. 1. A Nd:YAG laser beam was used to do laser ablation of samples. A quadrupole mass spectrometer was used to monitor the desorbed ions directly. The desorbed neutral atoms or molecules were ionized by electron impact or by a laser resonance ionization method. Fluorescence spectra were obtained from excited atoms and molecules.[18] Different samples of superconductors were used in this work. One was produced from an aqueous solution containing Y, Ba, and Cu salts and oxalic acid via a homogeneous coprecipitation technique using urea. Others were made by a standard solid-state chemistry approach. Transition temperatures of samples for $Y-Ba-Cu-O$ and $Bi-Sr-Ca-Cu-O$ were measured as $\sim 92°K$ and $\sim 125°K$, respectively. Most fluorescence data were taken using laser ablation of the superconductor sample by the fundamental of a Nd:YAG laser beam. Most secondary ion spectra were obtained using the second harmonic of the Nd:YAG laser beam. However, the data obtained with different harmonics show very little dependence on the frequency of the laser beam. The laser beam power density on the superconductor target was varied from 5×10^5 W/cm^2 to 1×10^9 W/cm^2. In general, breakdown occurs when the laser power density is higher than 1×10^7 W/cm^2. Insufficient photons could be detected to monitor fluorescence in the absence of laser-induced breakdown. However, the fluorescence spectra remain constant as long as laser-induced breakdown occurs. The laser energy per pulse was measured by a Scientech calorimeter. The laser beam pulse duration was 5–7 ns which was measured by a fast response photodiode. A Pellin-Broca prism was used to separate different harmonics of the laser beams. Since this laser utilized an unstable resonator, the typical laser beam distribution was a doughnut shape. Fluorescence spectra were obtained by using a GCA McPherson spectrometer which can be scanned automatically. The resolution of the monochromator was fixed at 4 cm^{-1}. A photomultiplier (RCA 31034) which has an almost flat response for visible and near-infrared (IR) photons was used to detect the wavelength-resolved photons. Since the laser beam was pulsed, the fluorescent light detected by the photomultiplier was gated for 20 μs so that the background from room light or dark current of the phototube could be neglected. The output of the phototube went through a charge-sensitive preamplifier followed by a pulse-shaping amplifier. It then went to a sample and hold circuit which drove a recorder.

The entire fluorescence spectra in the visible and near-IR region for $YBa_2Cu_3O_{7-x}$ and Tl-Ba-Ca-Cu-O are shown in Fig. 2 and Fig. 3. The fluorescence spectra of CuO, Y_2O_3, CaO, and $BaCO_3$ were also obtained as an aid in the identification of the peaks in the fluorescence spectra of these two superconductors. The emission due to different metal elements was identified from atomic spectra. Many different transitions for Y, Ba, and Ca were observed. However, no definite indication of transitions due to copper atoms, which had been suggested as the key element for superconductive properties, was observed. No clear spectra corresponding to CuO transitions were identified. The complete fluorescence spectra of high-T_c superconductors are quite complicated. However, the sharp transition lines, especially in the red and near-IR spectral regions, should be convenient for use in monitoring the concentration of most metal elements, since the broad continuum emission due to the plasma can be neglected in this region. The fluorescence band for YO was also observed in the Y-Ba-Cu-O system. Absolute fluorescence quantum yields can be obtained

by using the fluorescence of a dye solution excited by the frequency doubled Nd:YAG laser beam.[19]

Elements which provide low emission intensity such as Cu and Tl can be monitored by desorbed ion spectra. Ion spectra of laser-ablated Y-Ba-Cu-O and Tl-Ca-Ba-Cu-O are shown in Fig. 4(b) and Fig. 4(c) with a laser power density of 2 $\times 10^7$ W/cm^2. YO^+ signals were observed to be much stronger than the signal of BaO^+ for the Y-Ba-Cu-O system for a modest ablation laser energy. No CuO^+ signals were observed for the Y-Ba-Cu-O or Tl-Ca-Ba-Cu-O systems. The crystal structure of Y-Ba-Cu-O has been extensively studied by X-ray diffraction and neutron scattering methods.[20] There were no oxide atoms on the Y plane. Thus the formation of YO^+ was thought to be either from peroxide or from trapped oxygen molecules. For the Tl-Ca-Ba-Cu-O system, CaO^+ was observed, although X-ray diffraction data indicate that there are no oxides on the Ca plane. The formation of YO^+ and CaO^+ can possibly come from the chemical reaction between Ca or Y atoms with oxygen in the plume just above the surface. Secondary ion spectra obtained in this work are much simpler than the results from atom probe experiments.

The major species detected following laser ablation of superconductors are neutral atoms and molecules in the ground state. However, it is difficult to detect most of these desorbed species by a conventional mass spectrometer with an electron impact ionizer due to the low density of the desorbed neutral molecules. However, RIS has been demonstrated to have the capability of detecting a single neutral metal atom.[21] Recently, the detection of Bi atoms from the Bi-Sr-Ca-Cu-O system was demonstrated. Different laser excitation schemes for various metal elements are given in Table 1. It shows that commercially available lasers can be used to detect all desorbed neutral atoms and molecules. With an arrangement of multiple laser beams to do resonant excitation and ionization, several metal elements can be probed at the same time. Then, a real-time monitor for a superconductive thin film preparation can be achieved.

Table 1
Resonance ionization schemes for various metal elements
in metal oxide superconductors

						λ
Ba ($6s^2$)	$\xrightarrow{h\nu}$	Ba (6s 7p)	$\xrightarrow{h\nu}$	Ba^+		324.5 nm
Tl ($6s^2$ 6p)	$\xrightarrow{h\nu}$	Tl ($6s^2$ 7s)	$\xrightarrow{h\nu}$	Tl^+		377.6 nm
Pb ($6s^2$ $6p^2$)	$\xrightarrow{h\nu}$	Pb ($6s^2$ 6p 7s)	$\xrightarrow{h\nu}$	Pb^+		283.3 nm
Bi ($6p^3$)	$\xrightarrow{h\nu}$	Bi ($6p^2$ 7s)	$\xrightarrow{h\nu}$	Bi^+		306.8 nm
Ca ($4s^2$)	$\xrightarrow{h\nu}$	Ca (4s 5p)	$\xrightarrow{h\nu}$	Ca^+		273.6 nm
Y (4d $5s^2$)	$\xrightarrow{h\nu}$	Y (4d 5s 5p)	$\xrightarrow{h\nu}$	Y^+		359.4 nm
Cu ($3d^{10}$ 4s)	$\xrightarrow{h\nu}$	Cu ($3d^{10}$ 4p)	$\xrightarrow{h\nu}$	Cu^+		324.8 nm
Sr ($5s^2$)	$\xrightarrow{h\nu}$	Sr (5s 6p)	$\xrightarrow{h\nu}$	Sr^+		295.2 nm

It was observed that a large amount of O_2 was desorbed during the laser ablation process. the amount of desorbed O_2 was estimated as $\sim 10^{10}$ molecules per pulse from laser ablation of a $YBa_2Cu_3O_{7-x}$ target at 22°K with a very modest laser power density of 1×10^6 W/cm^2. With this laser power level, there should be no significant destruction of any chemical bonds. No significant numbers of atoms, molecules, or ions other than O_2 were observed, as shown in Fig. 4(a). This process of desorption should be due to a heating effect. Since the desorption of O_2 was observed for laser ablation by the fundamental Nd:YAG laser beam at 1064 nm, it is very unlikely the desorption was due to bond breaking of a metal oxide by the one-photon absorption process. The bond strength of Cu-O and Cu-O^- were estimated by Sawyer[22] to be 2.8 and 3.1 eV, respectively. Thus, the present results indicated that O_2 molecules were loosely trapped in these superconducting materials. Even a mild heating process is enough to drive out significant quantities of oxygen molecules trapped in these materials. The average velocity of desorbed O_2 was estimated as $\sim 7 \times 10^4$ cm/sec which indicated that the surface temperature was less than 300°C. There was a concern that the observed neutral O_2 molecules could be due to the adsorption of O_2 on the surface of the superconductor sample. To minimize this concern, a power density of 1×10^9 W/cm^2 was used to vaporize the top layers of material for several minutes before making measurements of desorbed O_2. We also carefully checked to see that there was no H_2O, N_2, or CO desorbed from the target to assure that the laser was probing below the original surface layer. These procedures rule out the possiblity of O_2 being adsorbed just on the surface. Therefore, the fact that oxygen molecules are trapped in $YBa_2Cu_3O_{7-x}$ and Tl-Ca-Ba-Cu-O superconductors is confirmed.

It has been known for two decades that O_2 can be trapped in an alkali-halide crystal.[23] Consequently, it should be much more likely that O_2 can be trapped in loosely packed and very porous superconductor materials, which were produced and sintered either in air or in a pure oxygen environment. From our results, the existence of trapped O_2 in the bulk of these superconductive materials is confirmed. The implication of trapped O_2 inside of the bulk of superconductors can be quite significant. It has long been considered that the existence of Cu^{+3} accounts for the excess of oxygen in $YBa_2Cu_3O_{7-x}$. The nominal composition suggests that 33% of the copper is in the +3 state. However, no Cu^{+3} ions were observed by X-ray photoelectron spectroscopy. With the trapped molecular oxygen, there is no need to have Cu^{+3} account for the number of oxygen atoms to be higher than 6.5. This should have an important effect on the calculation of the electronic structure of these crystals. Since a very small isotope effect was observed for $YBa_2Cu_3O_{7-x}$, conventional BCS theory regarding electron-phonon coupling can not be used to account for this observation. However, if the trapped O_2 molecule plays an important role in superconductivity, the isotopic effect can be expected to be much smaller if trapped O_2 has only weak coupling to the crystal lattice. If the trapped O_2 is critical for the superconductivity, the conservation of O_2 in superconductive film becomes very critical for any practical application for these newly invented superconductors.

ACKNOWLEDGEMENTS

This research was sponsored by the Office of Health and Environmental Research, U.S. Department of Energy, under contract number DE-AC05-84OR21400 with Martin Marietta Energy Systems, Inc. M. P. McCann, present address: Southern Arkansas University, Magnolia, Arkansas 71753.

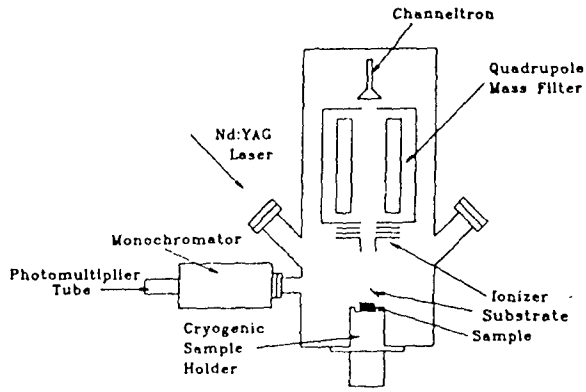


Fig. 1. Experimental schematic for fluorescence spectra, desorbed ion spectra, and resonance ionization spectra for laser ablation of the superconductors.

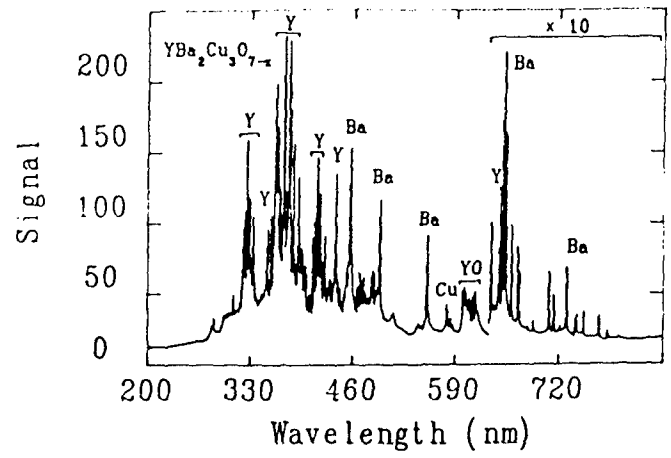


Fig. 2. Emission spectrum of laser ablation of $YBa_2Cu_3O_{7-x}$.

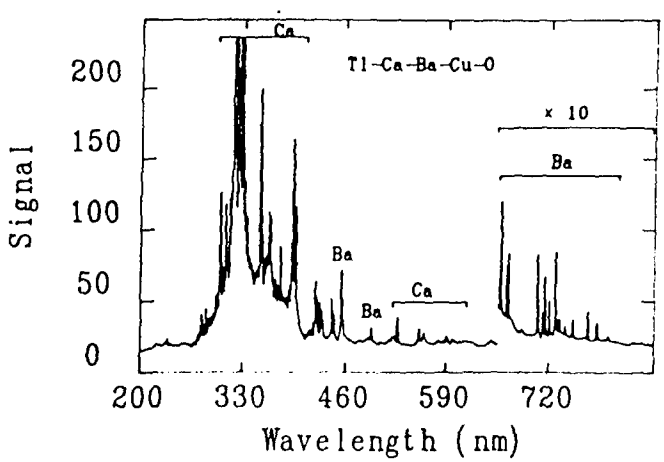


Fig. 3. Emission spectrum of laser ablation of Tl-Ba-Ca-Cu-O superconductors.

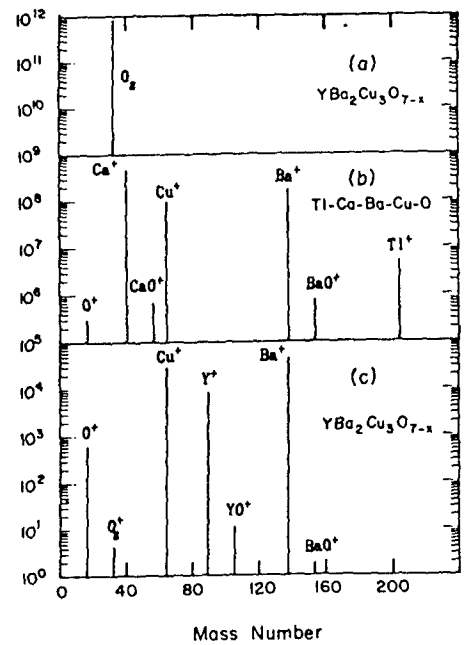


Fig. 4. Desorbed mass spectra from a laser ablation process of superconductor targets. (a) represents mass spectrum from $YBa_2Cu_3O_{7-x}$ target with laser density at 2 x 10^6 W/cm^2, the desorbed neutral O_2 molecules were ionized by electron impact ionization. No other desorbed ions or molecules were observed. (b) and (c) represent desorbed ion spectra from $YBa_2Cu_3O_{7-x}$ and Tl-Ca-Ba-Cu-O targets, respectively. The ablation laser power density was 2 x 10^7 W/cm^2. Filament was off.

REFERENCES

1. J. G. Bednorz and K. A. Müller, "Possible High T_c Superconductivity in the Ba-La-Cu-O System," *Z. Phys. B*, 64 (2) , pp. 189-193, 1986.

2. M. K. Wu, J. R. Asburn, C. J. Torng, P. H. Hor, R. L. Meng, L. Gao, Z. J. Huang, Y. Q. Wang, and C. W. Chu, "Superconductivity at 93 K in a New Mixed-Phase Y-Ba-Cu-O Compound System at Ambient Pressure," *Phys. Rev. Lett.*, 58 (9), pp. 908-910, 1987.

3. C. E. Rice, A.F.J. Levi, R. M. Fleming, P. Marsh, K. W. Baldwin, M. Anzlowar, A. E. White, K. T. Short, S. Nakahara, and H. L. Stormer, "Preparation of superconducting thin films of calcuim strontium bismuth copper oxides by coevaporation," *Appl. Phys. Lett.*, 52 (21), pp. 1828-30, 1988.

4. A. D. Berry, D. K. Gaskill, R. T. Holm, E. J. Cukauskas, R. Kaplan, and R. L. Henry, "Formation of high-T_c superconducting films by organometallic chemical vapor deposition," *Appl. Phys. Lett.*, 52 (20), pp. 1743-45, 1988.

5. E. S. Hellman, D. G. Schlom, N. Missert, K. Char, J. S. Harris, Jr., M. R. Beasley, A. Kapitulnik, T. H. Geballe, J. N. Eckstein, S.-L. Weng, and C. Webb, "Molecular-beam epitaxy and deposition of high-T_c superconductors," *J. Vac. Sci. Technol. B*, 6 (2), pp. 799-803, 1988.

6. L. Lynds, B. R. Weinberger, G. G. Peterson, and H. A. Krasinski, "Superconducting thin films of Y-Ba-Cu-O produced by neodymium:yttrium aluminum garnet laser ablation," *Appl. Phys. Lett.*, 52 (4), pp. 320-322, 1988.

7. H. S. Kwok, P. Mattocks, L. Shi, X. W. Wang, S. Witanachchi, Q. Y. Ying, J. P. Zheng, and D. T. Shaw, "Laser evaporation deposition of superconducting and dielectric thin films," *Appl. Phys. Lett.*, 52 (21), pp. 1825-1827, 1988.

8. H. S. Kwok, J. P. Zheng, S. Witanachchi, P. Mattocks, L. Shi, Q. Y. Ying, X. W. Wang, and D. T. Shaw, "Growth of highly oriented CdS thin films by laser-evaporation deposition," *Appl. Phys. Lett.*, 52 (13), pp. 1095-1097, 1988.

9. T. Venkatesan, X. D. Wu, A. Inam, and J. B. Wachtman, "Observation of two distinct components during pulsed laser deposition of high T_c superconducting films," *Appl. Phys. Lett.*, 52 (14), pp. 1193-1195, 1988.

10. X. D. Chen, S. Y. Lee, J. P. Golben, S. Lee, R. D. McMichael, Y. Song, T. W. Noh, and J. R. Gaines, "Practical preparation of copper oxide superconductors," *Rev. Sci. Instrum.*, 58 (9), pp. 1565-1571, 1987.

11. B. Batlogg, R. J. Cava, A. Jayaraman, R. B. van Dover, G. A. Kourouklis, S. Sunshine, D. W. Murphy, L. W. Rupp, H. S. Chen, A. White, K. T. Short, A. M. Mujsce, and E. A. Rietman, "Isotopic Effect in the High-T_c Superconductors $Ba_2YCu_3O_7$ and $Ba_2EuCu_3O_7$," *Phys. Rev. Lett.*, 58 (22), pp. 2333-2336, 1987.

12. K. J. Leary, H. Loye, S. W. Keller, T. A. Faltens, W. K. Ham, J. N. Michaels, and A. M. Stacy, "Observation of an Oxygen Isotope Effect in $YBa_2Cu_3O_7$," *Phys. Rev. Lett.*, 59 (11), pp. 1236-1239, 1987.

13. J. D. Jorgensen, H. B. Schüttler, D. G. Hinks, D. W. Capone, K. Zhang, M. B. Brodsky, and D. J. Scalapino, "Lattice Instability and High-T_c Superconductivity in $La_{2-x}Ba_xCuO_4$," *Phys. Rev. Lett.*, 58 (10), pp. 1024-1027, 1987.

14. G. Xiao, M. Z. Cieplak, A. Gavrin, F. H. Streitz, A. Bakhshai, and C. L. Chien, "High-Temperature Superconductivity in Tetragonal Perovskite Structures: Is Oxygen-Vacancy Order Important?" *Phys. Rev. Lett.*, 60 (14), pp. 1446-1449, 1988.

15. D. D. Sarma and C.N.R. Rao, "Nature of the Copper Species in Superconducting $YBa_2Cu_3O_7^+$," *Solid State Commun.*, 65 (1), pp. 47-49, 1988.

16. S. Horn, J. Cai, S. A. Shaheen, Y. Jeon, M. Croft. C. L. Chang, and M. L. denBoer, "High-temperature superconductivity in the presence of O 2p-Cu 3d holes: A spectroscopic study," *Phys. Rev. B*, 36 (7), pp. 3895-3898, 1987.

17. C. H. Chen, R. C. Phillips, and M. P. McCann, "Observation of trapped O_2 in high-T_c metal oxide superconductors," *Phys. Rev. B*, 39 (4), pp. 2744-2747, 1989.

18. C. H. Chen, M. P. McCann, and R. C. Phillips, "Real-time monitoring of laser ablation deposition of superconductors by fluorescence and secondary-ion spectra," *Appl. Phys. Lett.*, 53 (26), pp. 2701-2703, 1988.

19. C. H. Chen and M. P. McCann, "Laser-Induced pH Change in Solution," *Chem. Phys. Lett.*, 153 (4), pp. 338-340, 1988.

20. J. D. Jorensen, M. A. Beno, D. G. Hinks, L. Soderholm, K. J. Volin, R. L. Hitterman, J. D. Grace, Ivan K. Schuller, C. U. Segre, K. Zhang, and M. S. Kleefisch, "Oxygen ordering and the orthorhombic-to-tetragonal phase transition in $YBa_2Cu_3O_{7-x}$," *Phys. Rev. B*, 36 (7), pp. 3608-3616, 1987.

21. G. S. Hurst, M. G. Payne, S. D. Kramer, and C. H. Chen, "Counting the Atoms," *Phys. Today*, 33 (9), pp. 24-29, 1980.

22. Donald T. Sawyer, "Nature of the Bonding and Valence for the Oxygen and Copper in High-Temperature Superconductors," *J. Phys. Chem.*, 92 (1), pp. 8-9, 1988.

23. J. Rolfe, F. R. Lipsett, and W. J. King, "Optical Absorption and Fluorescence of Oxygen in Alkali Halide Crystals," *Phys. Rev.*, 123 (2), pp. 447-454, 1961.

PERSPECTIVES ON HIGH-TEMPERATURE SUPERCONDUCTING ELECTRONICS

T. Venkatesan
Bellcore
Red Bank, New Jersey

ABSTRACT

The major challenges in making HTSC electronics viable are predominantly materials problems. Unlike their predecessors, the metal oxide-based superconductors are integratable with other advanced technologies such as opto- and micro-electronics. The materials problems to be addressed relate to the epitaxial growth of high-quality films, highly oriented films on non-lattice-matched substrates, heterostructures with atomically sharp interfaces for junctions and other novel devices, and the processing of these films with negligible deterioration of the superconducting properties.

I illustrate these issues with results based on films prepared in situ by a pulsed laser deposition process. Films with zero-transition temperatures of 90 K and critical current densities of 5*10E6 A/cm^2 at 77 K have been prepared by this technique. Ultra-thin films--less than 100 A--show $T_c > 80$ K, supporting the idea of two-dimensional transport in these materials. By the use of appropriate buffer layers, films with T_c of 87 K and J_c of 6*10E4 A/cm^2 have been fabricated on silicon substrates. Submicron structures with J_c >2*10E7 at 10 K have been fabricated.

Results on nonlinear switching elements, IR detectors and microwave studies will be briefly summarized.

PREPARATION AND CHARACTERISTICS OF SUPERCONDUCTING CUPRATE THIN FILMS: $Nd_{2-x}Ce_xCuO_4$ AND SUBSTITUTED Bi-SYSTEM

H.Adachi, S.Hayashi, K.Setsune, S.Kohiki, Y.Ichikawa and K.Wasa
Central Research Laboratories, Matsushita Electric Industrial Co., Ltd.
Moriguchi, Osaka 570, Japan

ABSTRACT Characteristics of the electron-doped-type $Nd_{2-x}Ce_xCuO_4$ system and substituted Bi-system have been studied using the high quality thin-film samples grown by rf-magnetron sputtering and/or subsequent heat-treatment. The $Nd_{2-x}Ce_xCuO_4$ samples with excellent superconducting properties were obtained in thin films and their optical and X-ray photoelectron spectroscopy (XPS) studies were performed in regard to the Ce content and reducing treatment. Substituted Bi-Sr-Ln-Cu-O thin films have also been prepared and growth conditions for Bi-system with 2-2-1-2 and 2-2-2-2 phases were found. Moreover, new 2-2-1-2 phase in the simple Bi-Sr-Cu-O system was fabricated by thin-film processing and 80-K superconductivity was obtained.

1. INTRODUCTION

A great deal of interests have been focused to the thin films processing of high-Tc superconductors for not only the viewpoint of device applications but the scientific research. Thin-film processing has an ability to create a metastable phase which cannot be made by solid state reaction technics, i.e. ceramics method. For instance, 1-2-4 phase ($YBa_2Cu_4O_y$) or 2-2-3-4 phase ($Bi_2Sr_2Ca_3Cu_4O_y$) was firstly prepared in the thin film samples [1,2]. In addition to the fabrication of new phases, thin film processing enable the preparation of superconducting samples with excellent quality. High Jc (critical current density) samples were realized in the single-crystalline thin films epitaxially grown on adequate single crystal substrates [3]. For electron-doped $(Nd,Ce)_2CuO_4$ system, excellent superconducting properties were easily obtained in thin films rather than in bulk ceramic samples, which may be responsible for the facility of reducing treatment in the films [4]. Thus, in some cases, thin films and thin-film processing are very useful for the research on the nature of high-Tc superconductors.

In this paper, we describe the thin films of two systems; one is electron-doped $(Nd,Ce)_2CuO_4$ system with a variety of Ce content and the other is the lanthanoid (Ln) substituted bismuth-system, Bi-Sr-Ln-Cu-O. Their preparation methods, electric properties, x-ray photoemission were studied.

2. FILM PREPARATION

Thin films were prepared by the rf-planar magnetron sputtering and subsequent annealing. Targets were complex oxides of constituents, which were made by calcining the adequate mixture of each oxides. The diameter of the target was 100 mm. Substrates used were (100) plane of MgO or (100) plane of $SrTiO_3$ single crystals and heated at 400-700°C during deposition. Sputtering was carried out in the argon and oxygen mixed atmosphere with an input power of about 150 W and gas pressure of 0.5 Pa. The appeared phases in the films were controlled during the deposition or the post-annealing procedures.

One of the compounds we intended to prepare is $(Nd,Ce)_2CuO_4$ system which was found to be the "n-type" material with electrons as the charge carriers [5]. Since excellent superconductivity is easily obtained in film samples of this system, $(Nd,Ce)_2CuO_4$ thin films are suitable for a basic research. The other compounds are Bi-based materials with lanthanoid substitution, Bi-Sr-Ln-Cu-O. The interesting viewpoint is the feasibility of "n-type" in the Bi-system. From the similar consideration to the $(Nd,Ce)_2CuO_4$ system, we dealt with Bi-Sr-(Nd,Ce)-Cu-O thin films. Appearance of crystal phases in thin films of this system was studied. Moreover in the course of the experiments, construction of metastable structure in Bi-based thin films with no lanthanoid elements, i.e. simple Bi-Sr-Cu-O system, was investigated.

3. $(Nd,Ce)_2CuO_4$ THIN FILMS

3.1 SUPERCONDUCTING PROPERTIES

The $Nd_{2-x}Ce_xCuO_4$ thin films with various Ce content, x, have been prepared. (100) plane of perovskite $SrTiO_3$ were selected as a substrate and heated at around 500°C during deposition. The crystallinity of the as-deposited films showed the polycrystalline structure of the T' phase (Nd_2CuO_4 structure) with weakly preferred c-axis orientation. In order to improve crystallinity, the films were post-annealed at 1100°C for 2 hours in air, followed by quenching. The films showed a highly oriented structure with the c-axis normal to the substrate after the annealing, as shown in Fig.1 for the x=0.15 film. As x increased from 0 to 0.18, the c-axis lattice constant decreased from 1.215 nm to 1.203 nm. The electric properties of the films showed semiconductor-like behavior. Superconductivity was induced by the subsequent reducing treatment. This treatment was done by annealing the films in a vacuum (10^{-1} -10^{-4} Pa).

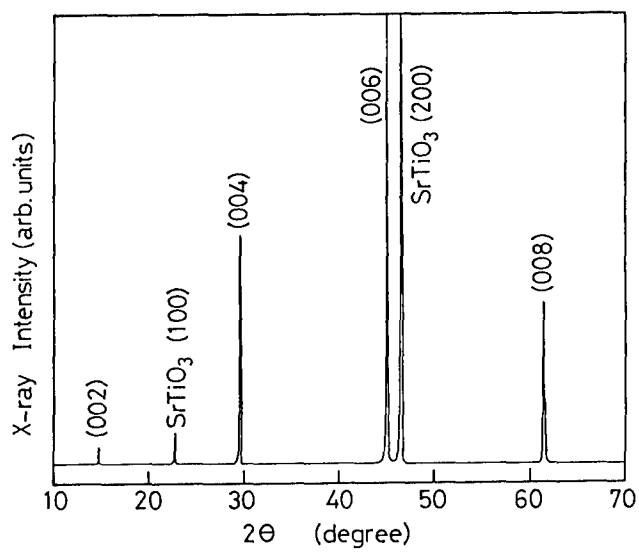


Fig.1. X-ray diffraction pattern of the $Nd_{1.85}Ce_{0.15}CuO_4$ film.

Figure 2 shows the temperature dependence of the resistivity for the films with various Ce content x ($0 \leq x \leq 0.23$) after reduction. Metallic behavior was observed for $x \geq 0.10$. Superconductivity was observed for $0.14 \leq x \leq 0.18$. With increasing x from 0.14 to 0.18, Tc tended to lower, similarly to bulk samples [6]. The Hall coefficient R_H was negative in the normal state, indicating that the charge carriers are electrons.

The diamagnetism (shielding effect) of the films were measured by an rf SQUID magnetometer under a magnetic field of 10 Oe. Figure 3 shows the temperature dependence of the diamagnetization for the films with various x after the reduction. For the x=0.15 film, the diamagnetization rapidly decreased at around 20 K with increasing the temperature and was observed up to 25 K. According to Bean's formula, the diamagnetization at 4.2 K for the

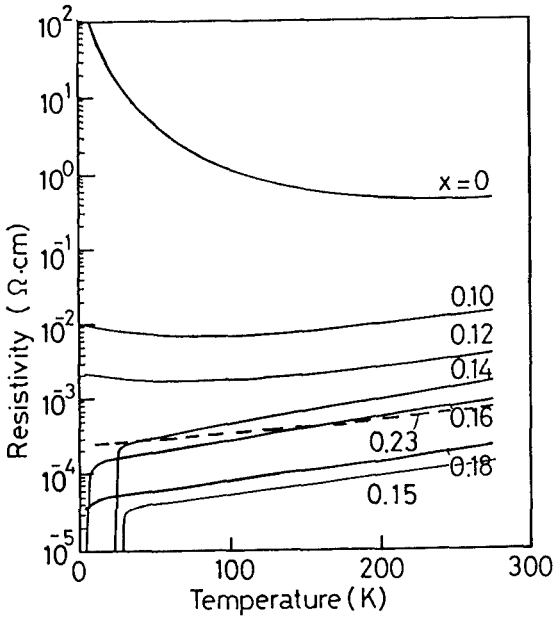


Fig.2. Temperature dependence of the resistivity for $Nd_{2-x}Ce_xCuO_4$ films after reduction.

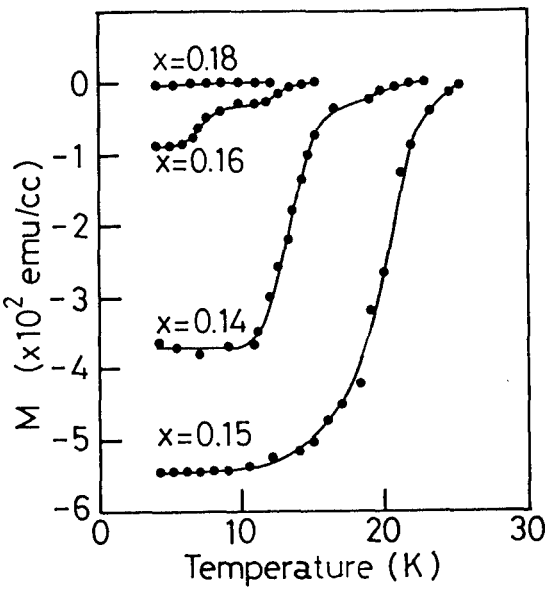


Fig.3. Temperature dependence of the diamagnetization for $Nd_{2-x}Ce_xCuO_4$ films.

x=0.15 film corresponds to a critical current density of 7×10^5 A/cm^2, which is consistent with the result of electrical measurement. The diamagnetization is highly dependent on x. The value at 4.2 K remarkably decreased as x deviates from 0.15.

3.2 OPTICAL PROPERTIES

To investigate the change of the electronic state by the Ce doping, optical properties such as reflectivity and absorption spectra were measured from 0.4 to 2.5 μm [7]. The polarization of the incident light was normal to the c-axis. There was no appreciable change in spectra before and after reduction except for the x=0 film.

Figure 4 shows the reflectivity spectra. For the Nd_2CuO_4 film (x=0), some features were observed, but no sign of plasma reflection. With increasing the Ce content x up to 0.12, a Drude-like plasma reflection appeared. At higher x of $0.14\leq x\leq0.16$, the reflection became much clearer with a plasma edge at around 1.0 μm. The solid lines in this figure are the Drude fits. The plasma frequency w_p was estimated to be 1.1 eV, and was almost constant over the range of $0.14\leq x\leq0.18$. The w_p value is about 0.2 eV larger than that of $(La,Sr)_2CuO_4$ system [8], but its constant behavior against dopant concentration is common.

Figure 5 shows the absorption spectra. A solid line for x=0 shows the absorption spectrum of the Nd_2CuO_4 film before reduction. The intense absorption below 1 μm seems to originate from the interband transition with an energy gap of 1.3eV. According to the Mott-Hubbard energy scheme, it may be interpreted as a charge transfer excitation between the O 2p states (valence band) and the upper Hubbard band (conduction band). Suzuki [8] reported an

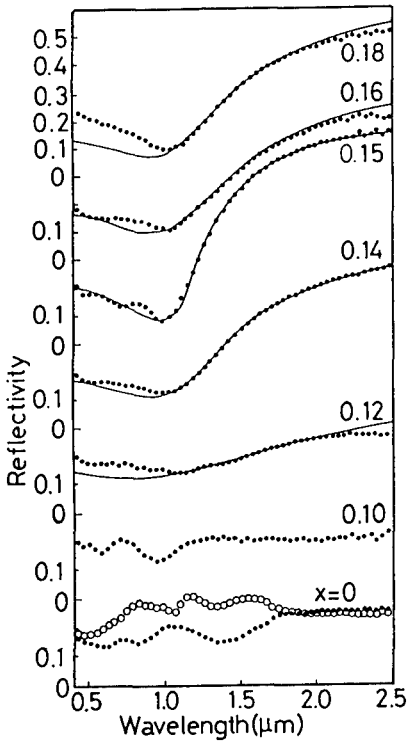


Fig.4. Optical reflectivity spectra for the $Nd_{2-x}Ce_xCuO_4$ thin films.

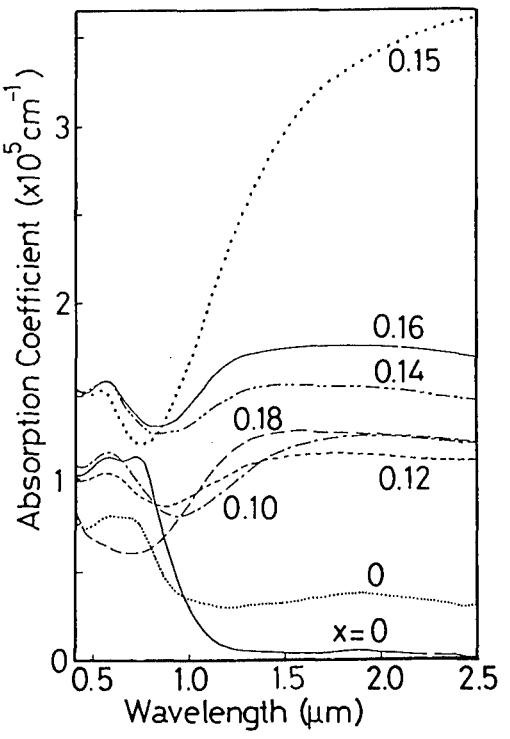


Fig.5. Optical absorption spectra for the $Nd_{2-x}Ce_xCuO_4$ thin films.

energy gap of 2.0 eV for La_2CuO_4 single crystal film, and Tajima et al. [9] observed charge transfer excitation at 2.0 and 1.5 eV for La_2CuO_4 and Nd_2CuO_4 single crystals, respectively. These gap energies may be inherent in different Cu-O configurations, octahedra for La_2CuO_4 and squares with no apical oxygen for Nd_2CuO_4.

As x increases from 0 to 0.12, the interband absorption decreased and a broad absorption appeared in the near-infrared region. In the superconducting compositional region, $0.14 \leq x \leq 0.18$, the spectra were dominated by the near-infrared absorption and the interband absorption was completely suppressed at x=0.18.

These features reflect the change of the electronic state by the electron doping into the conduction band, which evolves from the semiconducting state to the metallic state. The integrated oscillator strength in this spectral region was enhanced in the superconducting compositional region. This may suggest the development of density states and its correlation with Tc.

3.3 X-RAY PHOTOEMISSION STUDY

X-ray photoemission spectra were measured with a hemispherical electron spectrometer in a vacuum pressure less than 3×10^{-8}Pa. The measurement of the spectra was carried out after in-situ scrape of the film surface with a diamond file until no further change in the photoemission spectra was observed. The Cu $2p_{3/2}$ electron spectra for the $Nd_{2-x}Ce_xCuO_4$ films where x is 0, 0.15 and 0.23 were collected after the reducing treatment. Figure 6 (a), (b), and (c) shows the results for x=0, 0.15, and 0.23 thin films, respectively. From the observed binding energies and line widths of peaks, it

was revealed that electron doping from the semiconducting Nd_2CuO_4 (x=0), where Cu valence is +2, gave rise to Cu^{1+} ion formation [10]. The valence for Cu of the $Nd_{1.85}Ce_{0.15}CuO_4$ superconducting film is +1. However, further doping of Ce seemed to result in the recreation of Cu^{2+} as shown in the x=0.23 film because the satellite peak is observed.

Then, the effect of reducing treatment was studied by the XPS using $Nd_{1.85}Ce_{0.15}CuO_4$ thin films of before and after the reduction. Before the reducing treatment, there existed Cu^{2+} species although Cu valence was entirely +1 after the treatment. It was found that the reduction eliminates the remaining +2 species. It is important to distinguish superconductivity-correlated behavior from simple doping dependence and oxygen stoichiometry dependence.

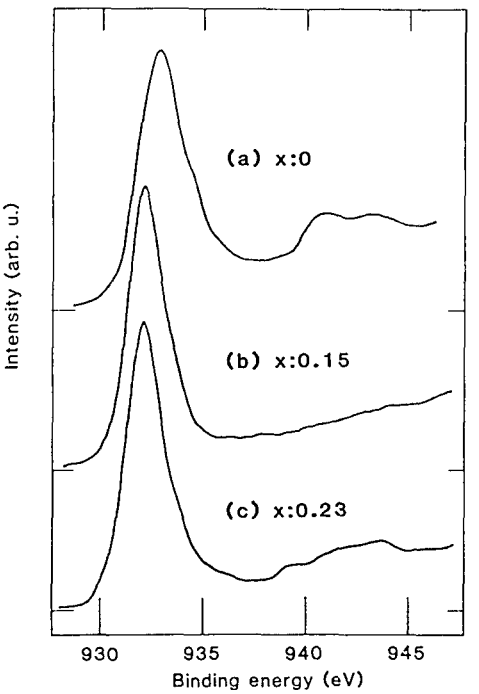


Fig.6. The Cu $2p_{3/2}$ spectra of the $Nd_{2-x}Ce_xCuO_4$ thin films.

4. Bi-BASED THIN FILMS

4.1 LANTHANOID SUBSTITUTED Bi-Sr-Ln-Cu-O THIN FILMS

For the lanthanoid element, we chose a series of (Nd,Ce) similar to the electron-doped $(Nd,Ce)_2CuO_4$ system. The construction of crystal phases in Bi-Sr-(Nd,Ce)-Cu-O films on MgO (100) substrates was investigated. Ordinarily, 2-2-1-2 phase was easily obtained in this system when the deposition was carried out at the substrate temperature of 600-700°C, or amorphous films deposited at 400°C were annealed at a temperature of 800-900°C. In this 2-2-1-2 phase, lanthanoid elements are supposed to occupy the intermediate site between two CuO_2 planes. When the annealing procedure of amorphous film was carried out at higher temperature (1100°C), other phase was created. This crystal structure was found to be 2-2-2-2 phase recently discovered by Tokura et al. [11], where two CuO_2 planes are separated by two lanthanoid layers and a oxygen layer. Figure 7

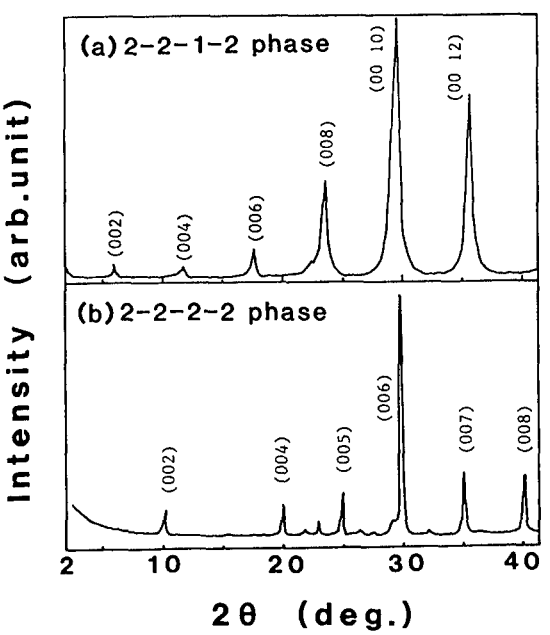


Fig.7. X-ray diffraction patterns for the Bi-Sr-(Nd,Ce)-Cu-O thin films.

shows the X-ray diffraction patterns of Bi-Sr-(Nd,Ce)-Cu-O thin films with (a) 2-2-1-2 phase and (b) 2-2-2-2 phase. c-axis orientation normal to the substrates was confirmed in both films, and lattice constant c was estimated to bi 3.02 nm for 2-2-1-2 phase and 1.77 nm for 2-2-2-2 phase. Although we also tried to prepare Bi-Sr-Ln-Cu-O system with three CuO_2 planes, it seems to be very difficult when lanthanoid elements were doped in the Bi-system.

Detailed experiments were done on the 2-2-1-2 phase of Bi-Sr-(Nd,Ce)-Cu-O system. Figure 8 shows the relation between Ce content x and lattice constant c of the films. The lattice constant c lengthens with the increase of content x, i.e. substitution of Ce for Nd. In the case of $Nd_{2-x}Ce_xCuO_4$ superconducting system, where the valence of Ce is +4, the lattice constant c shrinks with Ce content x [6]. The results shown in Fig.8 is opposite to the case for the electron carrier type superconductor of $Nd_{2-x}Ce_xCuO_4$ system. From the consideration of ion radius, where $Ce^{4+}<Nd^{3+}<Ce^{3+}$, the valence of Ce in the 2-2-1-2 phase of Bi-Sr-(Nd,Ce)-Cu-O is supposed to be +3. This speculation agreed with the result of XPS study. The valence of the site between two CuO_2 planes seems not to exceed +3.

Figure 9 shows the room-temperature resistivity of the Bi-Sr-(Nd,Ce)-Cu-O films at various x. The resistivity decreases with the Ce content x, which may indicate that the carrier is supplied by doping of Ce to insulating $Bi_2Sr_2NdCu_2O_y$ structure. Post-treatment study showed that the reducing treatment did not change or somewhat increase the resistivity, on the other hand the oxidizing treatment decreased resistivities of the films for every Ce content x remaining the same tendency. Since the valence of Ce in the $Bi_2Sr_2(Nd,Ce)Cu_2O_y$ system was found to be same as Nd, +3, it is unlike to supply charge carrier by Ce doping. More detailed research such as oxygen stoichiometry is desired to elucidate the decrease of the resistivity with Ce content.

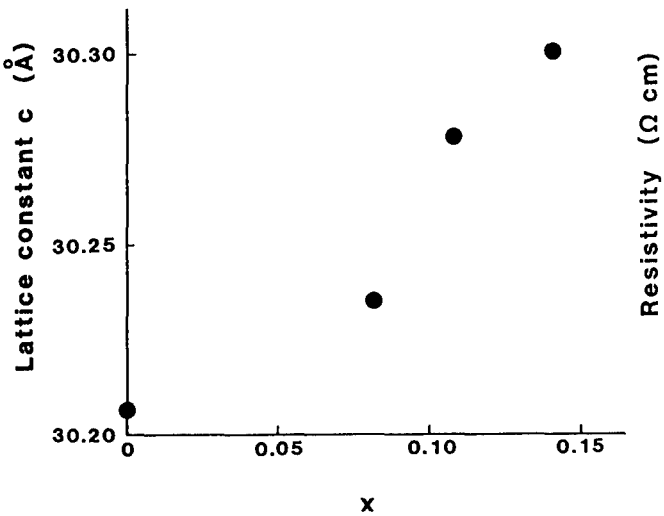


Fig.8. The relation between Ce content x and lattice constant c for the $Bi_2Sr_2Nd_{1-x}Ce_xCu_2O_y$ films.

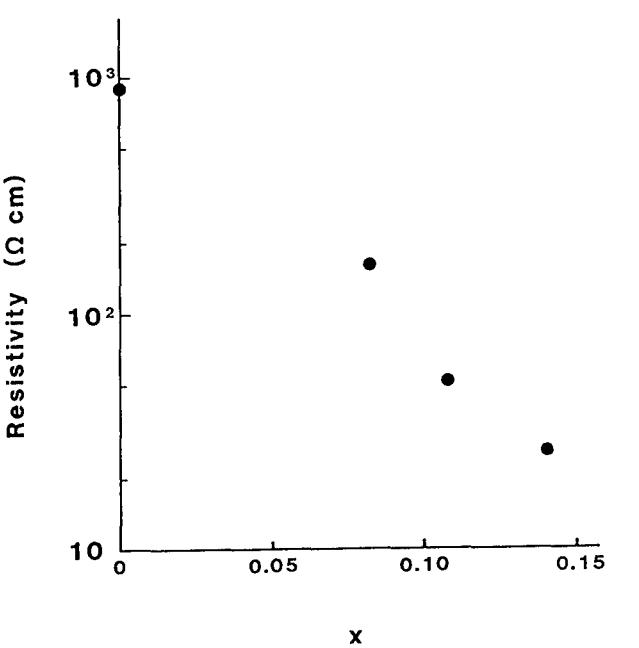


Fig.9. The relation between Ce content x and the resistivity for the $Bi_2Sr_2Nd_{1-x}Ce_xCu_2O_y$ films.

4.2 Bi-Sr-Cu-O THIN FILMS

The another advantage of the thin-film samples is construction of metastable state since novel crystal structures of unequilibrium state are sometimes created in thin films. In the course of the experiment of the Bi-Sr-Ln-Cu-O system, we dealt with no lanthanoid composition. The Bi-Sr-Cu-O system is known as the 10 K superconductor in the $Bi_2Sr_2CuO_y$ (2-2-0-1) phase [12,13]. New superconducting phases were investigated in this simple Bi-Sr-Cu-O system.

Thin films were prepared onto MgO (100) substrates. When the substrate temperature was elevated at around 600-650°C, new crystal structure having a long c-axis was created in addition to the ordinary 2-2-0-1 phase. By adjusting the film composition and the substrate temperature, almost single phase of the new structure was obtained at the substrate temperature of 630°C [14]. The chemical composition of the films was found to be nearly Bi:Sr:Cu=2:3:2.5. Figure 10 shows the X-ray diffraction pattern of the film. Bismuth-oxide layered structure with c-axis orientation normal was confirmed. The lattice constant c was estimated to be 3.12 nm, which was fairly larger than 2-2-0-1 phase (2.46 nm) and suggested the creation of 2-2-1-2 phase in the simple Bi-Sr-Cu-O system. By the present sputtering method, the metastable phase such as the 2-2-1-2 structure in the Bi-Sr-Cu-O system was successfully formed.

The as-deposited films exhibited a semiconductor-like temperature dependence of the resistivity. In order to improve the electric properties, films were heat-treated at 750°C for 30 min in oxygen. Figures 11 shows the

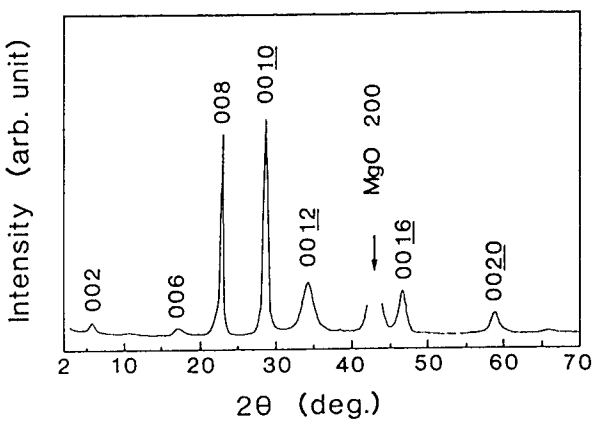


Fig.10. X-ray diffraction pattern for the Bi-Sr-Cu-O thin film with 2-2-1-2 phase.

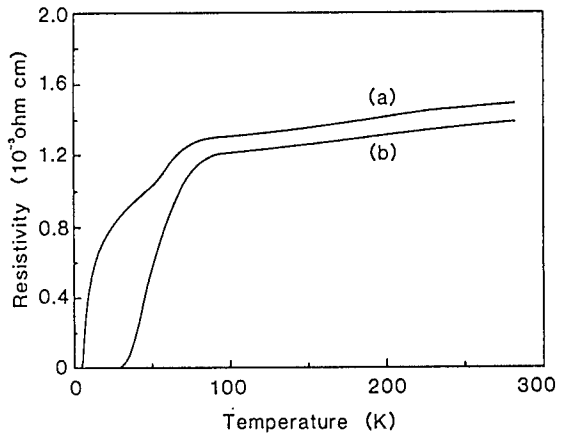


Fig.11. Temperature dependence of the resistivity for the Bi-Sr-Cu-O thin film with 2-2-1-2 phase.

temperature dependence of the resistivity. The film of the new phase exhibited superconductivity with an onset temperature as high as 80 K. However, the transition width is not so sharp, and the zero-resistance state was achieved below 29 K.

Transmission electron microscopy (TEM) analyses operated at 350 kV were carried out. Figure 12 shows the lattice image of the film including c axis. The major length between Bi_2O_2 layers is 1.5 nm, which is consistent with the X-ray diffraction pattern. Intergrowths of the other units were also observed in the figure (1.2 nm and 1.9 nm). The 1.2-nm phase is the conventional $Bi_2Sr_2CuO_y$ which has a single CuO_2 plane between Bi_2O_2 layers. The phases with the units of 1.5 nm and 1.9 nm are similarly considered to have double and triple CuO_2 planes between Bi_2O_2 layers in the Bi-Sr-Cu-O system, respectively. The broad superconducting transition may be due to the random intergrowth of multiphases with different CuO_2 planes. Figure 13 shows the electron diffraction pattern taken with incidence [001] showing the a^*-b^* reciprocal lattice of the subcell with a=b=0.54 nm. The long period modulation of 2.6 nm which corresponds to 4.8b is observed along b^* as commonly observed in the $Bi_2Sr_2CuO_y$ or $Bi_2Sr_2CaCu_2O_y$ system.

In this experiment, there remain several subjects; for instance, occupancy of oxygen in the intermediate Sr layer, optimization of annealing, or formation of the structure with more than three CuO_2 planes. Further investigation is expected to discuss the superconductivity in this simple Bi-Sr-Cu-O system.

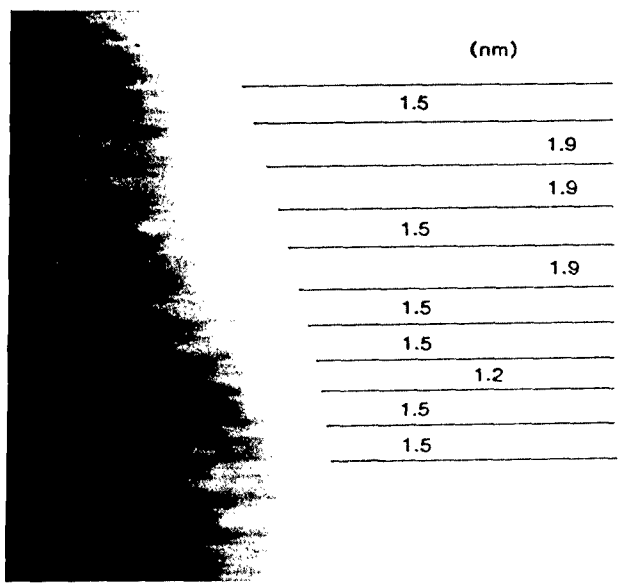


Fig.12. Lattice image of the Bi-Sr-Cu-O thin film including c-axis.

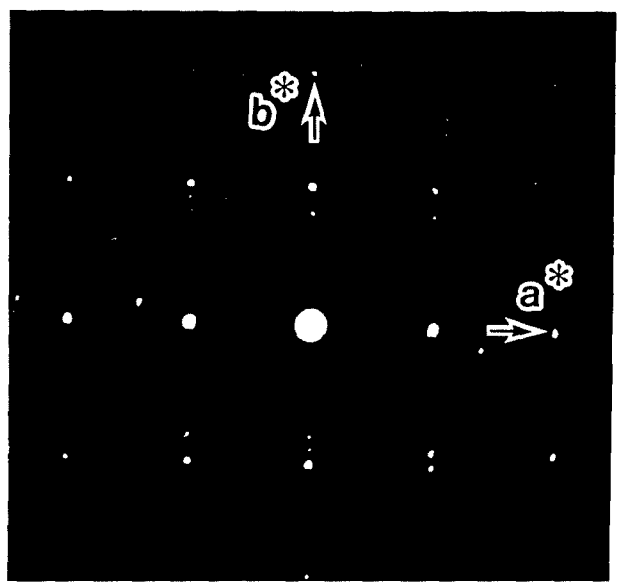


Fig.13. Electron diffraction pattern of the Bi-Sr-Cu-O film with 2-2-1-2 phase.

5. SUMMARY

By taking advantage of thin film samples, several experiments have been carried out. Thin films of electron-doped-type $(Nd,Ce)_2CuO_4$ were prepared with excellent quality and their superconducting, optical, and XPS properties were revealed. Lanthanoid substituted Bi-system of Bi-Sr-(Nd,Ce)-Cu-O films were firstly prepared and conditions of phase creation such as 2-2-1-2 and 2-2-2-2 phases were found. Moreover, metastable 2-2-1-2 phase were obtained in simple Bi-Sr-Cu-O system by the thin-film processing and 80-K superconductivity was confirmed. The present thin-film processing will be one of the most useful methods to prepare new superconducting phases, which will give much information on the nature of cuprate superconductors.

ACKNOWLEDGMENTS

The authors would like to thank Dr. T.Nitta for his support. We also thank Drs. S.Hatta, S.Adachi, K.Hirochi, T.Matsushima and C.C.Almasan for useful discussions, and M.Onoda for TEM analyses.

REFERENCES

[1] A.F.Marshall, R.W.Barton, K.Char, A.Kapitulnik, B.Oh, R.H.Hammond, and S.S.Laderman, "Ordered-defect structure in epitaxial $YBa_2Cu_3O_{7-x}$ thin films", Phys. Rev. B **37**, 9353 (1988).

[2] H.Adachi, S.Kohiki, K.Setsune, T.Mitsuyu, and K.Wasa, "Formation of superconducting Bi-Sr-Ca-Cu-O thin films with controlled c-axis lattice spacings by multitarget sputtering", Jpn. J. Appl. Phys. **27**, L1883 (1988).

[3] Y.Enomoto, T.Murakami, M.Suzuki, and K.Moriwaki, "Largely anisotropic superconducting critical current in epitaxially grown $Ba_2YCu_3O_{7-y}$ thin film", Jpn. J. Appl. Phys. **26**, L1248 (1987).

[4] H.Adachi, S.Hayashi, K.Setsune, S.Hatta, T.Mitsuyu, and K.Wasa, "Superconducting $(Nd,Ce)_2CuO_4$ thin films grown by rf magnetron sputtering", Appl. Phys. Lett. **54**, 2713 (1989).

[5] Y.Tokura, H.Takagi, and S.Uchida, "A superconducting copper oxide compound with electrons as the charge carriers", Nature **337**, 345 (1989).

[6] H.Takagi, S.Uchida, and Y.Tokura, "Superconductivity produced by electron doping in CuO_2-layered compounds", Phys. Rev. Lett. **158**, 1197 (1989).

[7] K.Hirochi, S.Hayashi, H.Adachi, T.Mitsuyu, T.Hirao, K.Setsune, and K.Wasa, "Optical properties of $Nd_{2-x}Ce_xCuO_4$ thin films", Physica C **160**, 273 (1989).

[8] M.Suzuki, "Hall coefficients and optical properties of $La_{2-x}Sr_xCuO_4$ single-crystal thin films", Phys. Rev. B **39**, 2312 (1989).

[9] S.Tajima, H.Ishii, T.Nakahashi, S.Uchida, M.Seki, S.Suga, Y.Hidaka, M.Suzuki, T.Murakami, K.Oka, and H.Unoki, "Extensive study of the optical spectra for high-temperature superconducting oxides and their related materials from the infrared to the vacuum-ultraviolet energy region", J. Opt. Soc. Am. B **6**, 475 (1989).

[10] S.Kohiki, S.Hayashi, H.Adachi, S.Hatta, K.Setsune, and K.Wasa, "Electron spectroscopy of $Nd_{2-x}Ce_xCuO_{4-y}$ (x=0, 0.15, and 0.23) thin films", J. Phys. Soc. Jpn. **58**, 4139 (1989).

[11] Y.Tokura, T.Arima, H.Takagi, S.Uchida, T.Ishigaki, H.Asano, R.Beyers, A.I.Nazzal, P.Lacorre, and J.B.Torrance, "New double-sheet copper oxide compounds with BiO or TlO bilayers", Nature **342**, 890 (1989).
[12] C.Michel, M.Hervieu, M.M.Borel, A.Grandin, F.Deslandes, J.Provost, and B.Raveau, "Superconductivity in the Bi-Sr-Cu-O system", Z. Phys. B **68**, 421 (1987).
[13] J.Akimitsu, A.Yamazaki, H.Sawa, and H.Fujiki, "Superconductivity in the Bi-Sr-Cu-O system", Jpn. J. Appl. Phys. **26**, L2080 (1987).
[14] H.Adachi, Y.Ichikawa, K.Hirochi, T.Matsushima, K.Setsune, and K.Wasa, "80 K superconductivity in Bi-Sr-Cu-O thin films", Jpn. J. Appl. Phys. **29**, L81 (1990).

HIGH-T_c SQUID APPLICATION IN MEDICINE AND GEOPHYSICS

V.N.POLUSHKIN, S.V.UCHAIKIN B.V.VASILIEV

JINR, Laboratory of Neutron Physics, Dubna,
101000,Head Post Office, P.O. Box 79, Moscow, USSR

In our Laboratory a high-T_c one-hole squid was built from $Y_1Ba_2Cu_3O_{7-x}$ ceramics obtained by a standard procedure of solid state reaction [1]. The ceramics with critical current density $J_c>100$ A/cm^2 was selected.

In the middle of 10× 10× 2mm ceramics pellet a 0.8mm hole was drilled in which superconducting loop of the squid was located. Between the hole and the edge of the pellet a cut was mechanically filed out with a bridge inside it connecting the superconducting ring. The bridge with characteristic size of 10μm must have the critical current $I_c\simeq 10\mu$A for the squid hysteretic parameter $\beta=2\pi L_S I_c/\phi_o$ to be less than (5÷10). Here - L_S - quantum loop inductance, ϕ_o - magnetic flux quantum. The squid is depicted in fig.1. In order to provide the mecanical stability $Y_1Ba_2Cu_3O_x$ dielectric phase was used.

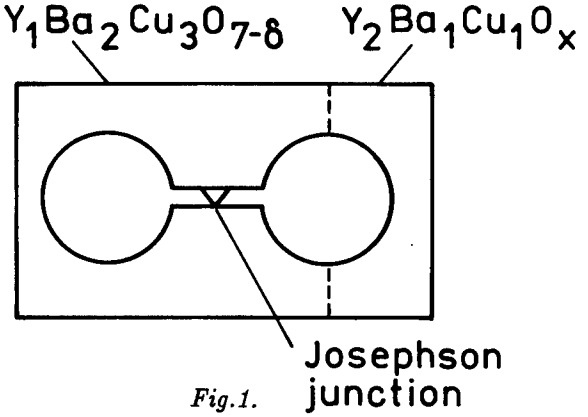


Fig.1.

In fig.2 a scheme of the magnetometer is presented. The squid - 1 was pumped, as usual, at high frequency ($f_p \simeq 20$MHz) by the rf-generator - 2 and was tested by the tank circuit $L_T C_T$ - 3, inductively coupled with it which was tuned on resonant frequency - ω_p. In order to obtain the maximum response the coefficient of coupling is chosen by the relation $K^2 Q \simeq \pi/2$, where Q is the quality factor of the circuit. The circuit voltage is amplified by a low-noise rf-amplifier - 4 and is detected by an amplitude detector - 5. The detected signal is transformed by low frequency units - 6,7, which provide flux-locked regime to the magnetometer. All these units are completely identical to electronic units of low-temperature squids.

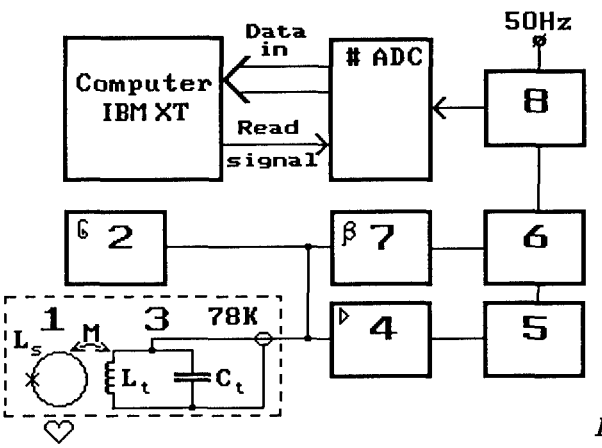


Fig.2.

Main characteristics of the magnetometer

The squid inductance can be measured experimentally, by the method described before. The resonant frequency shift of the tank circuit, which arise influenced by the squid, the connection of the squid with this circuit and the squid inductance are evaluated:

$$L_S = I_o^2 C_T / \phi_o^2 (\omega_{p1}^{-2} - \omega_{p2}^{-2}),$$

where I_o - current value through the L_T, changing the squid flux on ϕ_o;

C_T - tank circuit capacity;

ω_{p1} -tank circuit resonant frequency measured at a low pumping level when the contact remains superconductive and dissipative processes in the squid are not observed;

ω_{p2} -tank circuit resonant frequency measured at a high pumping level when Josephson contact is not superconducting.

The measurements have shown that at superconducting ring diameter of 0.8mm $I_o \simeq (0.8 \pm 0.1)\mu A$, $k \simeq (0.15 \pm 0.01)$, $C_T \simeq (220 \pm 10)pF$, $f_{p1} = (17.7 \pm 0.1)MHz$, $f_{p2} = (17.35 \pm 0.1)MHz$ and squid self inductance $L_S = (2.5 \pm 0.1) \times 10^{-10} H$.

Spectral noise density dependence on magnetic flux $\phi_N \simeq 4.5 * 10^{-4}\ \phi_o/\sqrt{Hz}$. The calculations give us energy resolution in the white noise region $\varepsilon = \phi_N^2 / 2L_S \simeq 9 \times 10^{-28} J/Hz$.

The calibration in the Helmholtz rings has shown the volt-oersted field period to be $B_o = 3.8 \times 10^{-10} T$, knowing which one can easily obtain the estimate of the squid field sensitivity: $\langle B_N \rangle = \langle \phi_N \rangle B_o / \phi_o$.

In fig.3 the spectral noise density on magnetic field of the magnetometer based on the high-T_c (T=77K) one-hole squid is shown (lower curve). It is evident that in the white noise region self field sensitivity is $\sim 10^{-13} T/Hz^{1/2}$. Thus, even today the high-T_c squids are inferior only to the best low-temperature squids at T=4.2K. For comparison spectral noise density of the traditional magnetometers is given in fig.3.

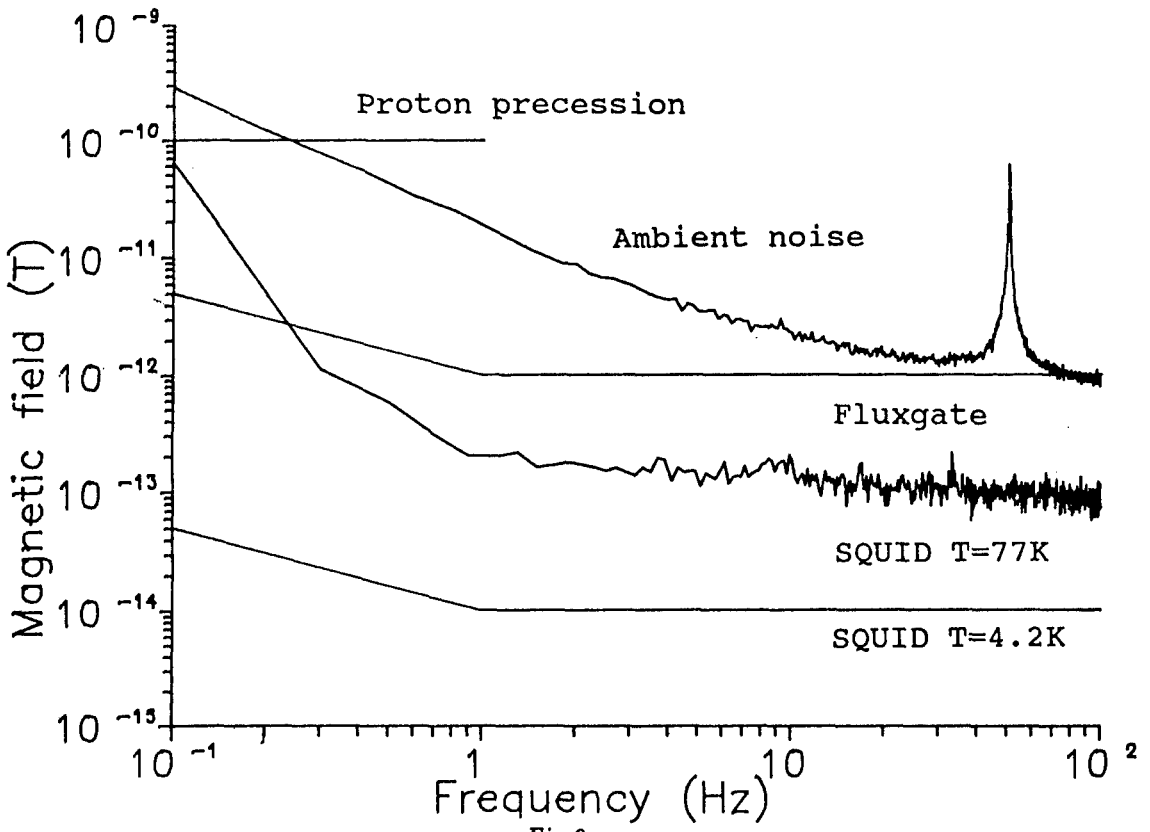


Fig.3.

In fig.3 the ambient noise spectrum is depicted (upper curve), which was read at night at a distance of 20m from the nearest Laboratory building in Dubna. It is clearly seen, that the ambient noise is considerably higher than the squid self-noise. Thus, we can suppose that such a magnetometer can be used for geophysical investigations.

One of the most interesting fields of the squid-based magnetometer application is biomagnetism, particularly, the human heart magnetocardiogram measuring. The low-temperature squids for a long time have been used in this area and to the present moment many interesting and important scientific results have been obtained.

In fig.4 a magnetocardiogram is shown , which was recorded by the above described magnetometer in a bandwidth of 60Hz (upper curve). The magnetocardiogram was taken in an aluminium box (~5mm wall) within 50m from the nearest Laboratory building.

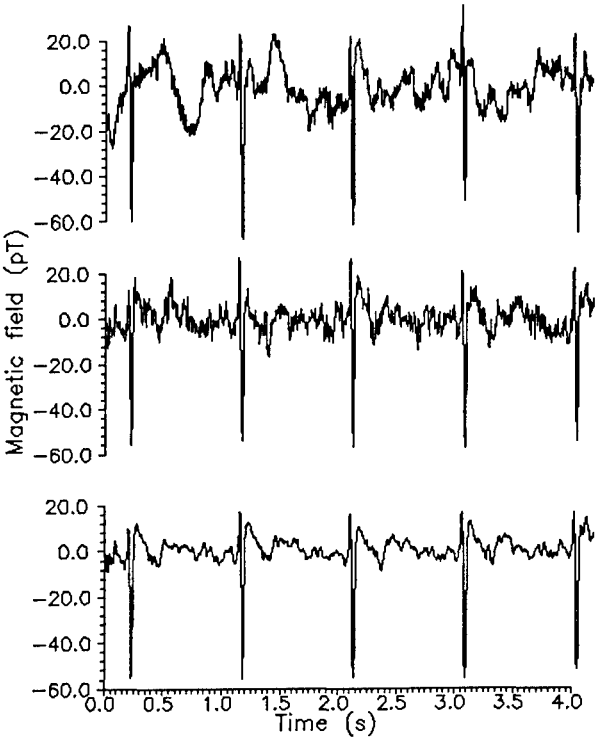


Fig.4.

As a sensitive element, as mentioned before, one-hole squid was operating. The squid inside the sealed copper thinwall container was placed on the bottom of the biomagnetic nitrogen cryostat. The squid was placed ~25mm above the human chest.

The observations have shown that the main noise contribution was not due to the squid but to the Earth's magnetic field variations, industrial inductions and mainly to the vibrations caused by liquid nitrogen boiling and by vibrations of the box. Further attempts in our work are needed in view to reduce the magnetic noise inductions. Nevertheless, the estimations promise us the maximum signal/noise relation of the high-T_c squid-magnetocardiometer to be (at the MCG amplitude - 20pT) not less than 10:1 in a bandwidth of 60Hz. Apparently, such resolution would be enough not only for steady cardiogram reading but even for thin structure investigation at average technique application.

When this paper was ready a new magnetocardiogram was measured with two high-temperature one-hole squids. In fig.4 (middle curve) a MCG in a real scale of time in a bandwidth of 60 Hz, and the same magnetocardiogram after four period average (lower curve) are given.

Microstructures and properties of superconducting Y-ErBaCuO thin films obtained from disordered Y-ErBaF_2Cu films

P. Cikmach, M. Diociaiuti*, A. Fontana, C. Giovannella, M. Iannuzzi, C. Lucchini, V. Merlo, R. Messi, L. Paoluzi, L. Scopa+, P. Tripodi

Dip. di Fisica, Sez. INFN e Sez. INFM, II Università di Roma "Tor Vergata", Via E. Carnevale, 00173 Roma, Italia
*Istituto Superiore di Sanità, Via Regina Margherita, 00193 Roma, Italia
+IESS - CNR, Via Cineto Romano 42, 00156 Roma, Italia

1. INTRODUCTION

High T_c Superconducting thin films can be prepared either by an ex-situ or an in-situ process. Although the latter route is more appropriate in applications that require samples of small areas (or preparation of superlattices) the former still mantain a certain appeal for those applications in which a single layer of films of large area are needed, e.g., coating of radiofrequency cavities. Moreover the use of BaF_2 in the preparation of the precursor films, used in the ex-situ preparation process, makes these films much more moisture-resistent. Here we describe in all the details the preparation procedure used to obtain superconducting thin films by R.F. magnetron sputtering of a single mosaic target composed by (Y-Er), BaF_2 and Cu. There have been several reports[1-15] on the production of high T_c superconducting thin films obtained from precursor films composed by Y, BaF_2, and Cu, but to our knowledge this is the first case in which such films are obtained simply by means of sputtering of a single mosaic target[12,13].

2. SPUTTERING CONDITIONS AND PRECURSOR FILMS

The R.F. magnetron target has been made by sticking small pieces of Yttrium-Erbium and Barium Fluoride on a Copper disk whose diameter is 200 mm. Standard R.F. discharge conditions are: 5×10^{-3} Torr, 400 Watt, pure Argon gas. The precursor films obtained have the expected 1:2:3 composition on a diameter of about 100 mm. Typical X-ray spectra of the precursor films are shown in fig. 1. Oxygen passivation is needed in order to obtain films with a smooth surface. The X-ray spectra of a precursor film with a smooth surface (curve A) show only the 111 line characteristic of the BaF_2 cubic structure. X-ray spectra of

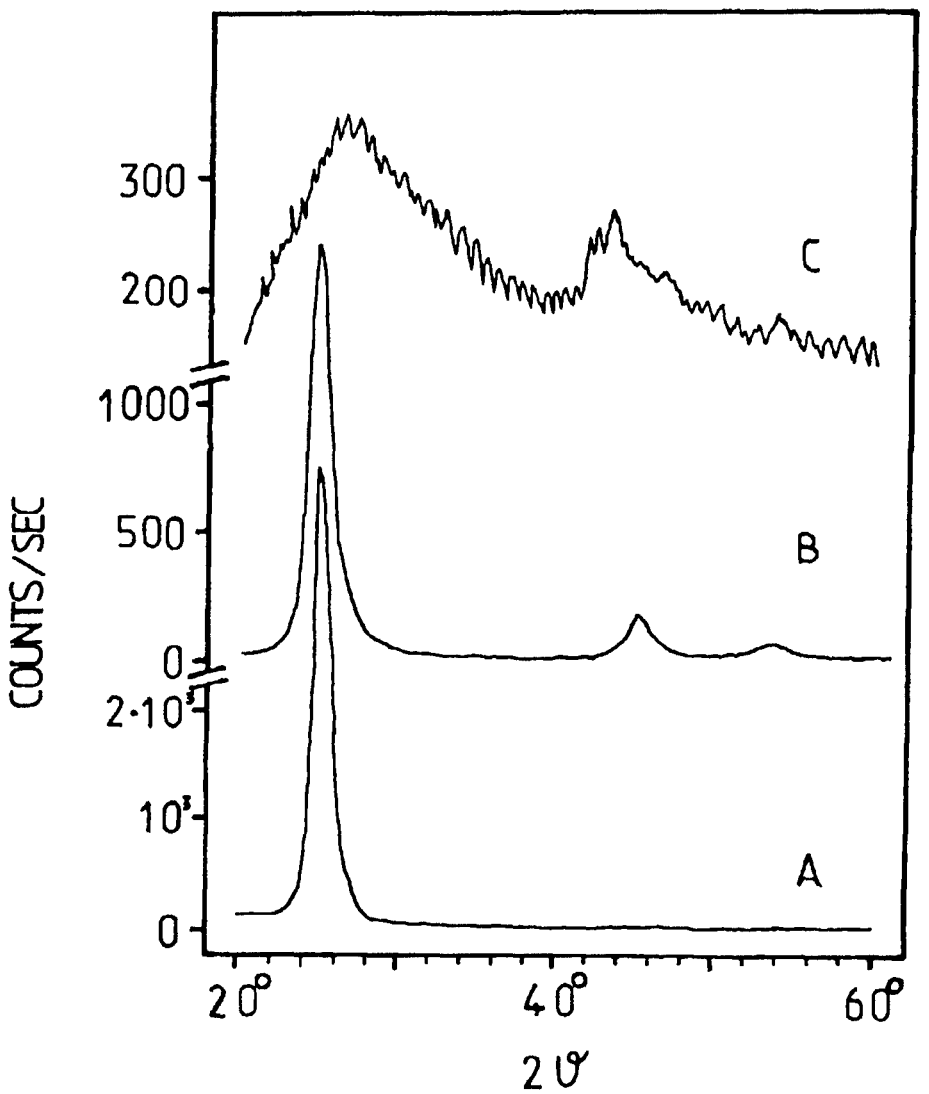


Fig. 1 - X-ray spectra of precursor films: A - passivated sample, B - unpassivated sample, C - unpassivated sample after two month.

unpassivated samples evidentiate a much less intense 111 BaF_2 line and bumps characteristic of the Cu f.c.c. structure indicating a partial copper segregation.

3. ANNEALING PROCEDURE

A typical annealing profile is shown in fig. 2: note the use of water in order to remove the Fluorine from the sample. The pictures of fig. 3 show how the temperature of the higher plateau affects the formation of the crystallites in the case of a sample 7500 A thick.In fig. 3a

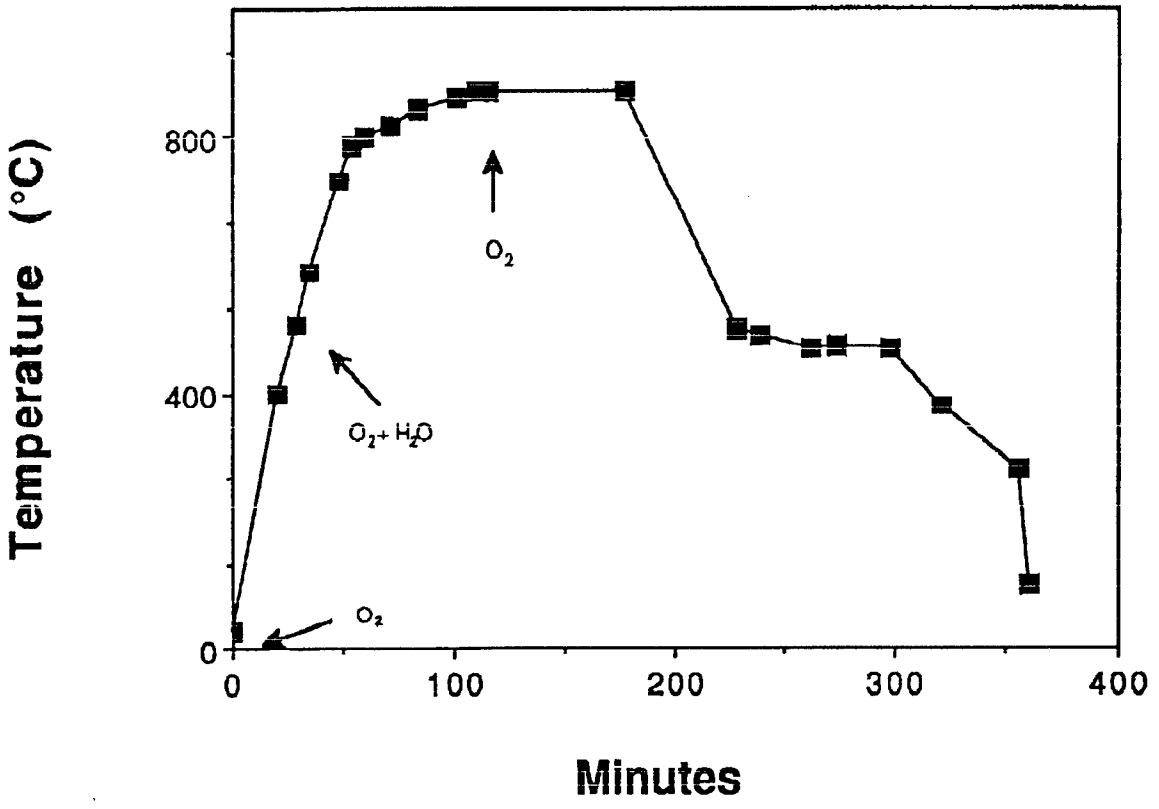
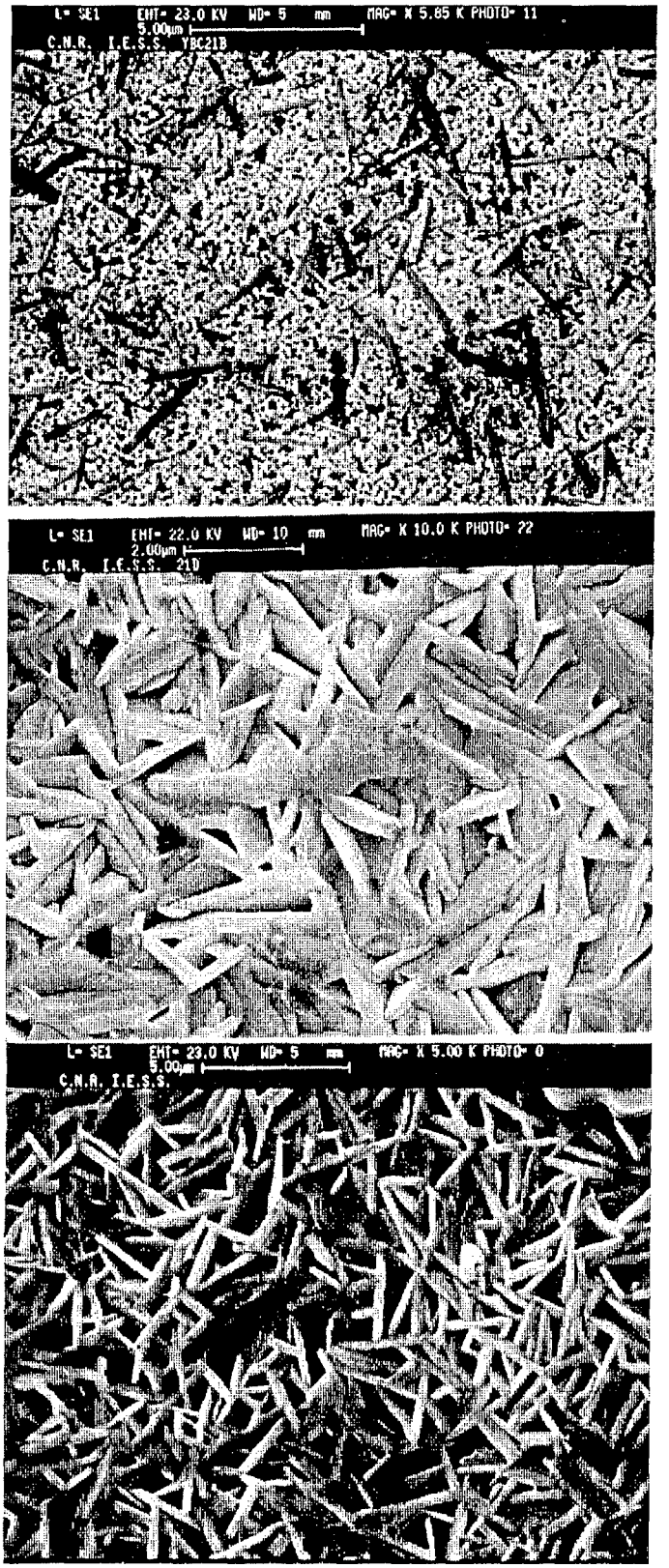


Fig. 2 - Typical annealing profile.

we observe a certain amount of crystallites that, we believe, enucleate either from the surface of the substrate and from the bulk of the film; the black spots also visible are superconducting areas from which the formation of the crystallites develops.

Fig.s 3b and 3c correspond to top-plateau temperatures of 830 and 850 °C respectively; in the latter we observe fully developed crystallites. They are randomly oriented and from their size we can deduce that the growth rate in the direction of the a-b plane is at least a factor 10 higher than in the c direction. In correspondence with the increasing degree of crystallinity of

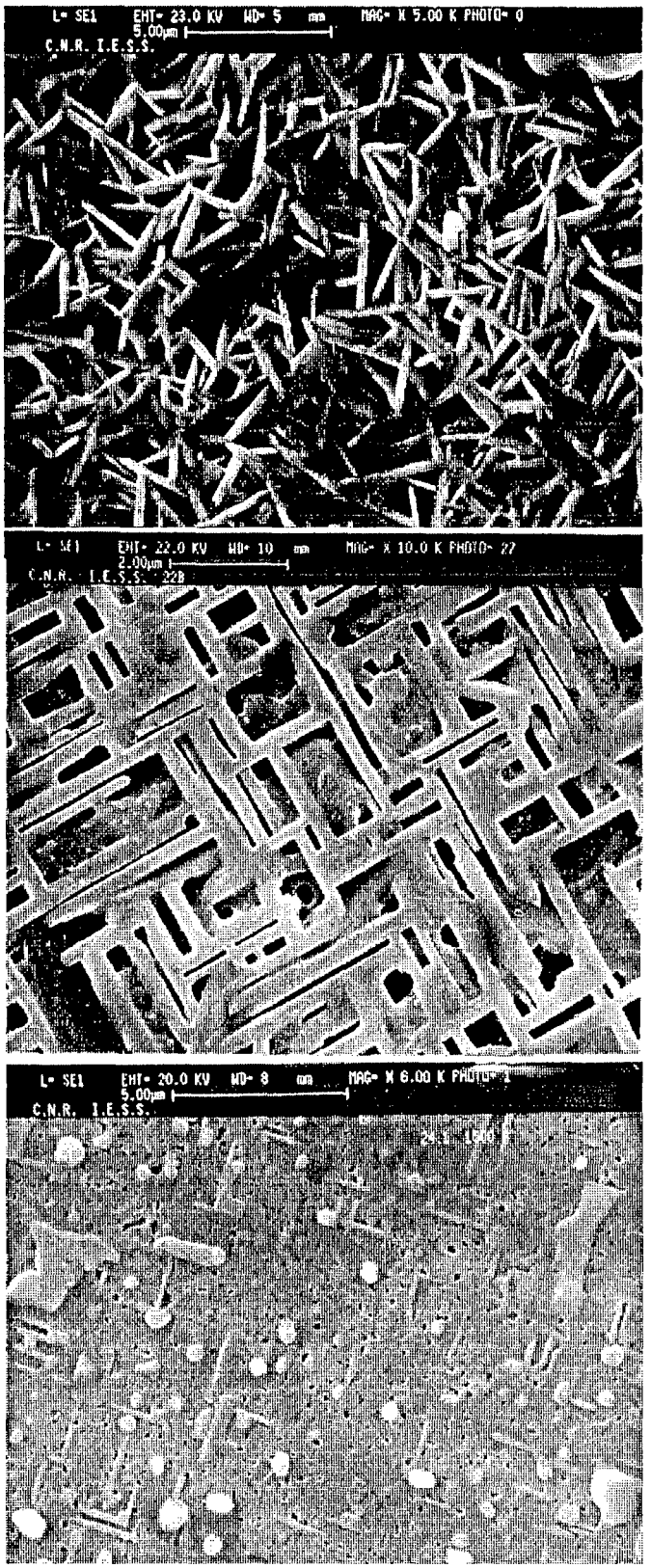


a

b

c

Fig. 3 - SEM pictures of samples , all having the same thickness (7500 A) but that have been subjected to annealing cycles having a different temperature of the top-plateau (see fig. 2): a - 820 °C, b - 830 °C, c - 850 °C. Note the different scale used for sample b.



a

b

c

Fig. 4: SEM pictures of samples having different thickness
a: 7500 A, b: 3000 A, c: 1500 A.

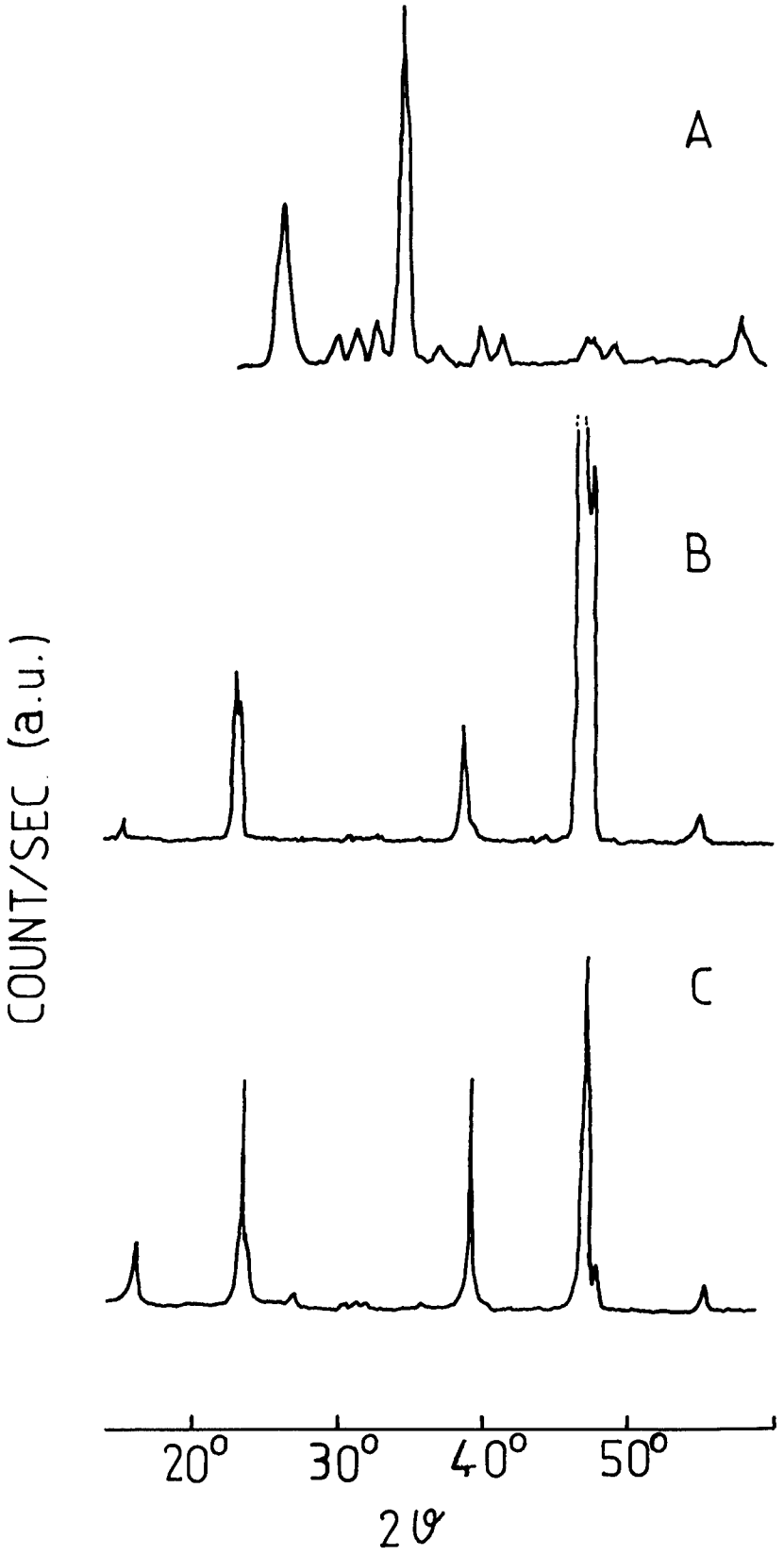


Fig. 5: X-ray data of thin films whose SEM pictures are shown in fig. 4

the film we observed in the x-ray spectra, as expected, a decrease down to zero of the intensity of the 111 BaF_2 line.

4. EFFECT OF SAMPLE THICKNESS

In fig. 4 we show SEM pictures of samples having different thicknesses, but submitted to the same annealing conditions (fig. 2). The corresponding X-ray data are reported in fig. 5. Sample a is clearly composed by random crystallites. To a first glance the X-ray spectra corresponding to samples b and c suggest the presence of a c-texture. However the SEM-picture of sample b clearly shows a cross-linked structure typical of crystallites having the c-axis lying along the plane of the substrate and the a-axis perpendicular to it;[10] their dimensions confirms the slower growth rate along t he c-axis of factor between 5 and

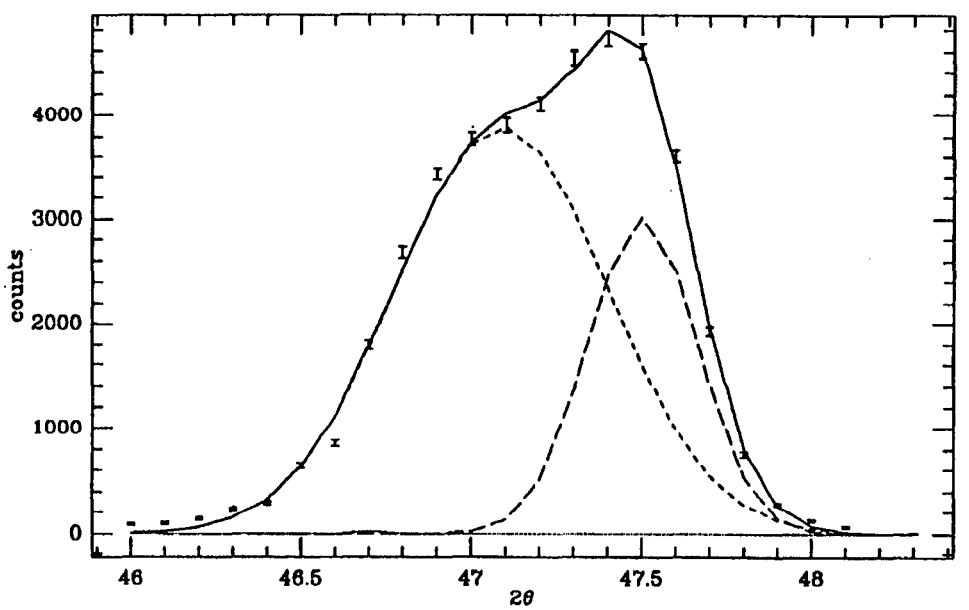


Fig. 6 - Three-gaussian fit to the x-ray line-shape for the sample in fig.4b; the two peaks around $2\theta = 47°$ and $2\theta = 47.5°$ are the (200) and (006) lines respectively. The third peak, around $2\theta = 46.7°$, barely visible on the scale of the plot, is the (200) line from the substrate.

20.[16,17] An accurate analysis of the line-shape observed around $2\theta = 47°$ (see fig. 6), shows indeed the existence of both textures. In sample c a-textured crystallites that nucleate

directly from the substrate are rare although not completely absent, and the sample results to be almost fully c-textured. The fact that in the thinner sample we observe basically only c-oriented crystallites leads us to suggest that sample b is constituted by a c-textured layer grown epitaxially on the substrate and by an a-textured layer heteroepitaxially grown on the top of the c-textured one. The onset temperature of the resistive transition for these three samples are 86.8 K, 86 K, and 80.5 K respectively. The sharpness of the resistive transition as well as the onset temperature are, basically, correlated with the quality of the surface layer (i.e. that visible in the SEM pictures) but not necessarly with the X-ray spectra. Indeed we observed also cases in which the X-ray spectra show sharp 00n peaks, in contrast with the SEM picture showing a random surface with poorly formed crystallites; furthermore, the offset temperatures in such cases are lower than 77 K.

5. CONCLUSIONS

We have shown that a combination of several techniques is necessary to characterize properly each step of the preparation of the high T_c superconducting thin films. C-textured films are easily obtained in the thickness range 1000 - 2000 Å while thicker films are constituted by a heteroepitaxial a-textured layer grown on the top of a c-textured one. This is an extremely important observation because it might explain several discrepancies reported in the measurements of physical quantities obtained from nominally (but not fully characterized) c- or a-textured samples. For thicknesses higher than 4000 - 5000 Å the samples are randomly oriented.

6. REFERENCES

1) Mankiewich P M, Scofield J H, Skocpol W J, Howard A H, Dayem A H, and Good,E : Appl.Phys.Lett. 51 (1987) 1753.

2) Cabanel R, Hirtz J P, Etienne P, Fruchter L, Giovannella C, and Creuzet G.: Physica C153-155 (1988) 1473.

3) Mogro-Campero A, Turner L G, Hall E L, and Burrell M C: Appl.Phys.Lett. 52 (1988) 2068 and references therein.

4) Desantolo A M, Mandich M L, Sunshine S, Davidson A B, Fleming M R, Marsh P, and Kometani T Y: Appl. Phys. Lett. 52 (1988) 1995.

5) Stormer H L, Levi A F J, Baldwin K W, Anzlowar M, and Boebinger G S: Phys.

Rev. B38 (1988) 2472.
6) Siu-Wai Chan, Bagley B G, Greene L H, Giroud M, Feldmann W L, Jenkin K R, and Wilkins B J: Appl. Phys. Lett. 53 (1988) 1443.
7) Feenstra R,Budai J D, Christen D K, Chisolm M F, Boatner L A, Galloway M D, and Poker D B: preprint on "Microstructure and critical currents of YBaCuO thin films on $SrTiO_3$ and a new substrate $KTaO_3$".
8) Valco G J, Roher N J, Pouch J J, Warner J D, Bhasin K B, : preprint on "Characterization of ZrO_2 buffer layers for sequentially evaporated YBaCuO on Si and Al_2O_3 substrates"
9) Cabanel R, Hirtz J P, Giovannella C, Dubreuil D, and Creuzet J: "Superconducting thin films of YBaCuO and ErBaCuO grown by MBE", proceedings of the TMS conference New Brunswick, May 1988.
10) D.X. Li, X.K. Wang, D.Q. Li, R.P.H. Chang, J.B. Ketterson, J. Appl. Phys. 66 (1989) 5505
11) Mogro-Campero A., Turner L.G., Hall E.L., Garbauskas M.F., Lewis N., Appl. Phys. Lett. 54 (1989) 2719
12) Cikmach P, Diociaiuti M, Fontana A, Gauzzi F, Giovannella C, Iannuzzi M, Lucchini C, Merlo V, Messi R, Paoluzi L, Petrocco G: "Modern aspects of superconductivity", ed. by R. Suryanarayan, IITT Publisher (1989), 277.
13) Cikmach P, Giovannella C, Iannuzzi M, Merlo V, Messi R, Paoluzi L, Gauzzi F, Petrocco G, Scopa L: "On the oriented (Y-Er)-BaCu0 superconducting thin films obtained by a single mosaic target", Satt 3 Conference, World Scientific, in press.
14) Mombourquette C M, Berry J G, Brown D R, Lemons R A, Raistrick I D: prepint on "Processing and patterning techniques for thin films of YBCO"
15) Asher S E, Nelson A J, Mason A R, Swartzlander A B, Dhere R, Kazmerski L L, Halbritter J, Harvey T E, Beall J A, Ono R H: preprint on "Analysis of the YBCO/$SrTiO_3$ interface as a function of post-deposition annealing temperature"
16) Kaiser D L, Holtzberg F, Scott B A, McGuire T R, Appl. Phys. Lett. 51 (1987) 1040
17) Scheemeyer L F, Wasczak J V, Siegrist R, VanDover B, Rupp W, Batlogg B, Cava R J, Murphy D W, Nature 328 (1987) 601

OPTICAL AND MICROWAVE DETECTION USING Bi-Sr-Ca-Cu-O THIN FILMS

B.E. Grabow
Department of Electrical and Computer Engineering, Johns Hopkins University
3400 N. Charles St, Baltimore, 21218, MD

R.M. Sova, and B.G. Boone
Electro-Optical Systems Group

K. Moorjani, B.F. Kim, J. Bohandy, F. Adrian, and W.J. Green
Microphysics Group

Johns Hopkins University Applied Physics Laboratory, Johns Hopkins Rd., Laurel, MD, 20707

Abstract

Recent progress at the Johns Hopkins University Applied Physics Laboratory (JHU/APL) in the development of optical and microwave detectors using high temperature superconducting thin films will be described. Several objectives of this work have been accomplished, including: deposition of Bi-Sr-Ca-Cu-O thin films by laser abation processing; development of thin film patterning techniques, including in-situ masking, wet chemical etching and laser patterning; measurements of bolometric and non-bolometric signatures in patterned Bi-Sr-Ca-Cu-O films using optical and microwave sources, respectively; analysis and design of an optimized bolometer through computer simulation; and investigation of its use in a Fourier transform spectrometer. This paper will focus primarily on our fabrication developments and results from the measurement of the bolometric and non-bolometric response.

Introduction

The development of high temperature superconducting (HTSC) thin film devices for electro-optical and radio-frequency sensors is probably one of the most likely near-term outcomes of recent breakthroughs in the field of superconductivity [1]. Among the many potential devices we have considered at APL passive thin-film devices such as detectors of electromagnetic radiation are favored. We are investigating near-term application of HTSC detectors to laboratory instrumentation for microwave and infrared spectrometry. Response times are on the order of milliseconds to microseconds, depending on the detection mode and wavelength. Operating temperatures are 77 K for bolometric detection, however, the relative sensitivity of the non-bolometric mode of detection requires operation below 77 K.

HTSC materials are expected to exhibit excellent performance as quantum (Josephson junction) radiation detectors, in which case they should operate at extremely high frequencies reaching into the far-infrared band, limited ultimately by the very high superconducting energy gap found in these new materials ($\leq$ 50 meV). Ideal sensitivity should also be good for these type of detectors ($\leq 10^{15}$ photons cm^{-2} sec^{-1} in a 1 kHz bandwidth for a 10^{-4} cm^2 detector area, as calculated by Forrester and Talvacchio [2]), but it will be worse than low temperature superconducting (LTSC) devices (by the square root of the temperature ratio for noncoherent detection). Fabrication of prescribed (ideal) Josephson junctions is, however, very difficult because the junction size must be on the order of the coherence length, which is extremely short ($\leq$ 20 nm) in these materials. Granular film (multiple Josephson junction) detectors, on the other hand, may, be competitive as detectors, as suggested by Wolf [3].

HTSC bolometers have been proposed [4] because they are easy to fabricate. They operate on the principle that incident radiation of virtually any wavelength will induce a resistive transition from a virtual superconducting state to normal state in a thin piece of superconducting film. The substrate must be coupled to a thermal reservior and have a low heat capacity to yield the best possible response to

incident radiation in the shortest possible response time. Thus there is a tradeoff between response time and sensitivity in bolometric (type II) detectors, which limits their performance relative to ideal quantum detectors. By making the HTSC bolometric element very small and impedance matching it to an efficient antenna structure, better performance should be obtained. Calculated ideal sensitivity [4] (measured by noise equivalent power (NEP)) is in the range of 1-20 x 10^{-12} W $Hz^{-1/2}$.

We report here results of our investigations of the bolometric and non-bolometric modes of detection in Bi-Sr-Ca-Cu-O thin films. We find that both detection modes appear in the same sample under mutually exclusive conditions (bolometric with light and nonbolometric with microwaves). Konopka, Jung, et al [5-7] have measured the microwave response of Y-Ba-Cu-O and Bi-Sr-Ca-Cu-O films and clearly observed similar behavior in Y-Ba-Cu-O films. Our measurements indicate that the non-bolometric mode of detection obviates the thermal response-time tradeoff of the bolometric mode, a result which offers promise for application to laboratory instrumentation. Recent progress will be described, including: deposition of Bi-Sr-Ca-Cu-O thin films by laser ablation processing [8,9]; development of several thin film patterning techniques, including in-situ masking, wet chemical etching, and laser patterning; and measurements of bolometric and non-bolometric signatures in patterned Bi-Sr-Ca-Cu-O thin films using optical and microwave sources. Possible mechanisms for the non-bolometric detection mode are reviewed and future measurements to determine performance limits are discussed.

Deposition and Patterning Techniques

Among the several laser beam processing techniques developed at APL, the deposition of thin films by laser ablation processing (LAP) was the first and most important. In that method (Fig. 1) a pulsed beam from an excimer laser is focused onto a pressed pellet of superconducting oxide that is mounted in a vacuum cell, and ablated material is collected on a substrate a few centimeters away tilted at ~ 30° relative to the target. The excimer laser operates at 193 nm, in the ultraviolet region of the spectrum, with a pulse frequency of nominally 10 Hz and an energy of approximately 150 mJ per pulse. During the deposition, the target is translated stepwise so that the beam focal spot of approximately 0.5 mm^2 resides at any single location on the target material for 30-100 seconds, which improves the stochiometry of the film. In addition, the substrate can be heated, and new samples or new targets introduced without breaking vacuum by using a carousel sample support. Substrates can also be translated during deposition to improve thickness uniformity.

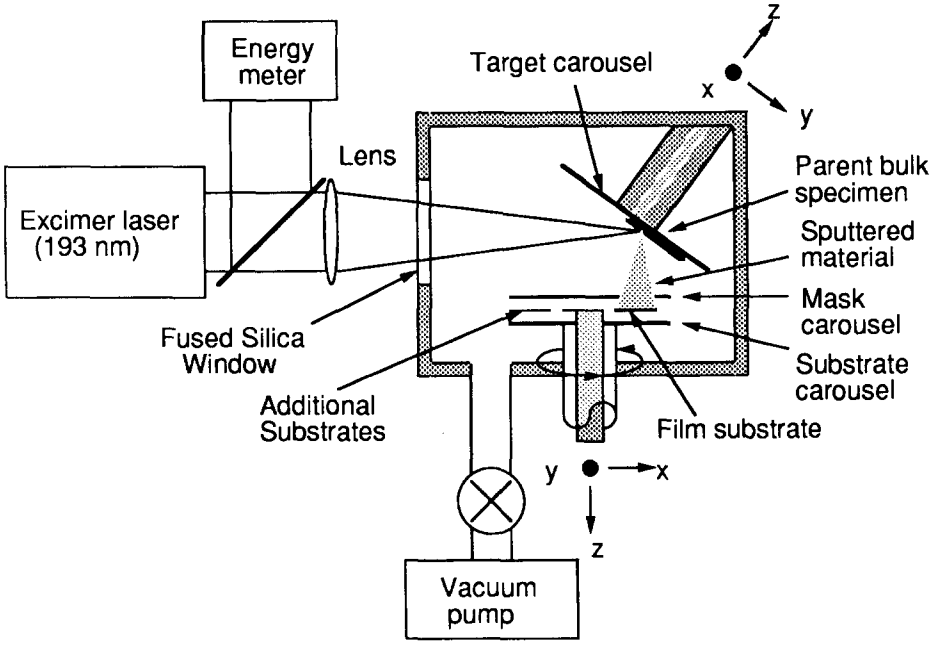


Fig. 1: Laser ablation processing cell used to deposit superconducting thin films.

The laser ablation processing technique has been used to deposit thin films of La-Sr-Cu-O, Y-Ba-Cu-O, and Bi-Sr-Ca-Cu-O on a variety of substrates that include fused quartz, zirconia buffered quartz, crystalline silicon, sapphire and oriented crystals of strontium titanate, zirconium oxide (ZrO_2), and magnesium oxide (MgO) [9-10]. The quality of the film depends on the substrate as well as deposition parameters, such as substrate temperature during deposition, and the post-deposition annealing temperature.

For the optical and microwave results reported here the Bi-Sr-Ca-Cu-O films were deposited on MgO and ZrO_2. An example of one of our early Bi-Sr-Ca-Cu-O films on ZrO_2 is shown in Fig. 2, showing the texture and granularity of these films. Film thickness was 1-2 μm and average grain size was estimated at 3-5 μm. A "slow" annealing schedule was established to achieve better film properties, as measured by resistivity. The annealing schedule consisted of a 25° to 810 C° ramp-up for 1 hour, a soak at 810 C° for 10 minutes, followed by a 810° to 25° C ramp-down for 3 hours. Earlier measurements of the resistive transition curve and the magnetically modulated microwave absorption (MAMMA) response reveal a transition temperature (T_c) of ~ 77 K. From this earlier work [9,10] the benefit of heating the substrate during deposition was clearly established. Heating the substrate makes the resistive transition narrower and helps to achieve smoother and more oriented films.

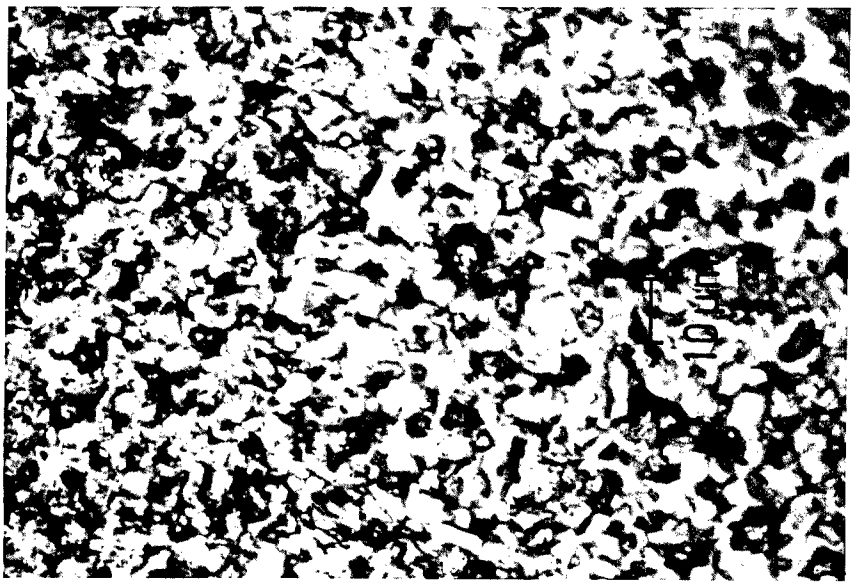


Fig. 2: Optical microscope photograph of a Bi-Sr-Ca-Cu-O thin film under 2500X magnification showing grain sizes on the order of 3-5 μm. This sample was used for subsequent testing.

Several patterning techniques have been tried, including in-situ deposition masking, wet chemical etching, and laser patterning. These tools are available individually or in combination to pattern complex planar structures, such as meanderlines and microstrip. In-situ masking was our earliest attempt at patterning, and it was used to achieve 625 μm linewidths, which are sufficient to make simple detector elements and striplines. A 50 μm thick Kovar mask was used. The limitations of using a shadow mask are that line-widths are limited to 50 μm or more, and complex patterns cannot be made. Thus procedures for wet-chemical etching of Bi-Sr-Ca-Cu-O films were developed. These procedures incorporated a Shipley 21822 photoresist and a selection of acid etches. Choice of the acid etch depends on film type (Y-Ba-Cu-O or Bi-Sr-Ca-Cu-O) and whether the film had been previously annealed. Then linewidths of 1 μm can be achieved. An example of wet chemical etching is shown in Fig. 3, illustrating a prototype meanderline element to be used as a bolometer.

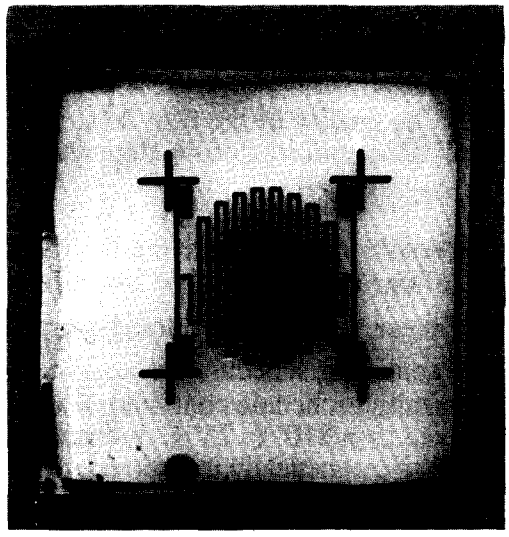


Fig. 3: Bi-Sr-Cu-Ca-O meanderline bolometer element patterned by wet-chemical etching. Linewidth and thickness are 200 μm and 0.7 μm, respectively.

To achieve finely controlled, complex patterns on very small substrates (~1 mm x 1 mm) a laser patterning system was developed as shown in Fig. 4 [11]. Similar efforts by other groups have been applied to Y-Ba-Cu-O films [12,13]. Rothschild, et al [12] and Liberts, et al [13] show that by using an oxygen atmosphere while exposed to a laser beam the film can be locally heated and consequently annealed. By using a reducing atmosphere (including nitrogen) an initially superconducting film can be driven back into the normal phase. For our initial testing we increased the laser power to a relatively low threshold level so that the film could actually be etched in ambient air. Thus finely sketched (computer controlled) patterns can be produced on substrates too small to be patterned by conventional wet chemical etch procedures. This approach employs an Argon ion laser operated at 514.5 nm with a $\leq$ 10 μm spot size and 7 x 10^5 W/cm ^{2} maximum irradiance on the substrate. Laser modulation is enabled electro-mechanically (or acousto-optically). Substrate positioning is achieved with a computer-controlled x-y translation stage, which has a 0.1 μm stepping resolution. A vacuum cell with multi-axis optical access is used to house the film. Partial pressure of oxygen and/or nitrogen from ~ 100 mTorr to one atmosphere can also be maintained during operation, in order to explore local annealing of Bi-Sr-Ca-Cu-O films. The sample is monitored under reflected ambient light using a charge coupled device (CCD) camera and telephoto/zoom lens combination, and the transmitted power is measured with a photodetector.

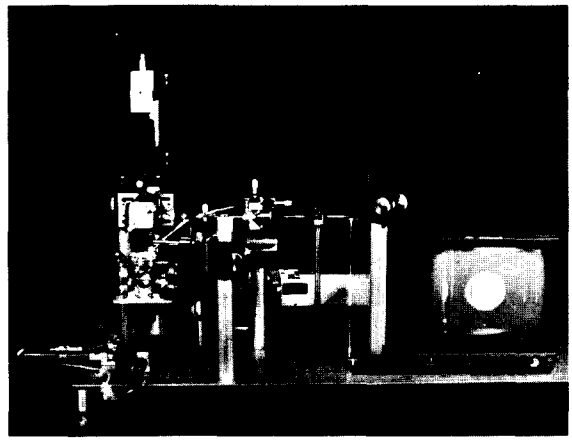


Fig. 4: Laser patterning system developed for sketching and locally annealing patterns on very small substrates.

In a new on-going effort [11], a meanderline HTSC bolometer was developed using the LAP cell and wet chemical etching as shown in Fig. 3. A computer program for calculating bolometer response was developed to support the design of the bolometer, which included a noise budget. The particular design pictured in Fig. 3 (5 x 5 mm) is not the smallest that can be achieved and will be reduced by a factor of 5 to achieve our desired performance goal. The requirement to reduce substrate size in order to reduce heat capacity will dictate the use of our laser patterning system. Our goal is that the HTSC detector should be at least as sensitive as the pyroelectric detector (deuterated triglycerine sulfide (DTGS)) and cover a broader spectral range, extending beyond the DTGS range of 0.25-500 μm. This design will be isolated thermally to achieve a desired response time (τ = 10 msec) and intefaced to a low temperature JFET preamp to achieve low noise (NEP = 10^{-10} W $Hz^{-1/2}$).

To demonstrate the use of the laser patterning system, a simple meanderline pattern was sketched on a Y-Ba-Cu-O thin film, as shown in Fig. 5. The laser was guided by computer between the two closest contacts (spaced apart by ~ 1600 μm). The linewidth of the meanderline was 400 μm, and the furrows created by the laser beam were ~ 10 μm wide. This sample and another were tested and results indicate that they have good electrical isolation, increased resistance over the unpatterned sample (by one to two orders of magnitude), and a bolometric response.

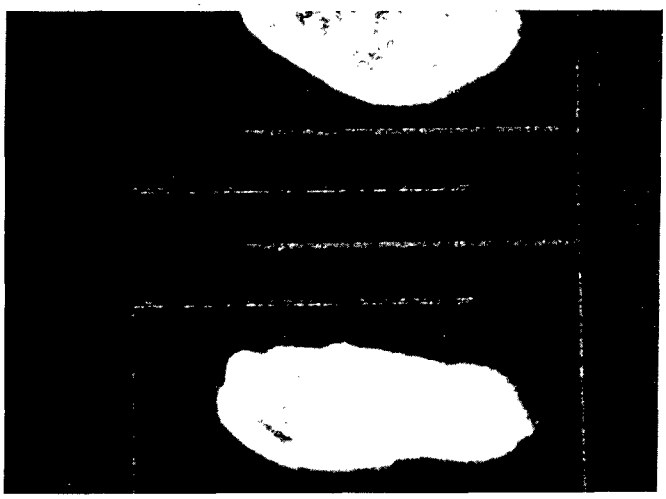


Fig. 5: Simple meanderline element sketched on Y-Ba-Cu-O on MgO using Argon ion laser beam.

Optical and Microwave Detection Measurement Results

Many investigators[14-19] are interested in developing a practical high temperature superconducting detector. APL is interested in detectors that can be used in lieu of a conventional bolometer in a laboratory Fourier transform spectrometer (FTS). Testing and design work are underway to ultimately integrate a very small meanderline element, similar to the prototype shown in Fig. 3 with a low-temperature JFET amplifier (and other electronics), which will yield signal levels compatible with the A/D converters on our FTS. We are also interested in developing detectors for similar microwave instrumentation. In a preliminary effort described below we have measured the optical and microwave response of simpler patterned Bi-Sr-Ca-Cu-O films using a standard four-point probe configuration.

Two of the samples tested in these preliminary measurements consisted of a small section of a patterned Bi-Sr-Ca-Cu-O film deposited in the LAP cell on a single crystal MgO substrate at 300 °C and on single crystal ZrO_2 at room temperature. Film thicknesses were 2 μm and 1.3 μm, and film areas were 2000 by 600 μm and 1500 by 370 μm, respectively. These samples were shadow-masked during deposition and annealed as previously described. Silver epoxy contacts were placed on the sample and annealed-in during film annealing, a procedure that almost always eliminates contact resistance problems. Typical

contact resistances varied from a few ohms at room temperature to approximately 0.1 ohm at 13 K. In addition, we find that the samples can be thermally recycled many times with little degradation of the contacts or the intrinsic film properties, and they can be re-used after a long (~ 6 month) shelf-life.

For optical detection, a 4 mW, 633 nm helium-neon laser was chopped at 26 Hz and focused onto the center of the sample. For microwave detection, a 9 GHz microwave signal was generated with a microwave oscillator and square wave modulated at 40 Hz with a PIN diode modulator. The signal was then amplified and fed into an X-band horn positioned directly in front of the sample. In both cases the induced output voltage from the sample was synchronously detected with a lockin amplifier. See Fig's. 6(a) and 6(b) for details.

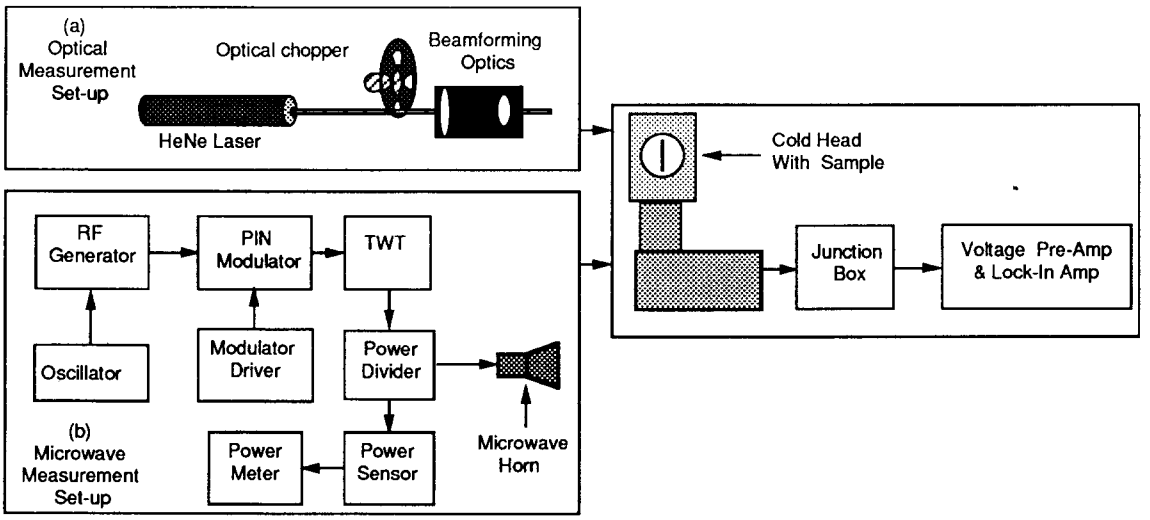


Fig.6: (a) Bolometric response measurement set-up and (b) microwave response measurement set-up, shown adjacent to cold head and post detection electronics.

Results for the optical detection experiment shown in Fig. 7 indicate a response peak located at the center of the transition region. From standard bolometric theory, it is known that the bolometric response is proportional to the derivative of the resistance curve. Calculated derivatives of the resistance curves correlate well with the measurements, as shown. In addition, measurements of the lockin response versus chopper frequency shown in Fig. 8 indicate response times (~ 5.7 and 11.5 msec) consistent with a thermal response mechanism dominated by substrate characteristics.

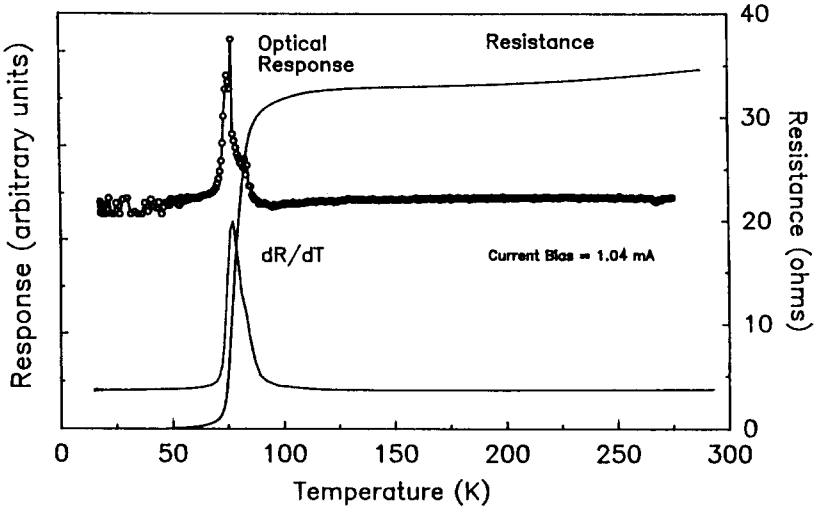


Fig. 7: Optical response, resistance, and dR/dT versus temperature of Bi-Sr-Ca-Cu-O sample. Bias current was set to a relatively high value (1.04 mA).

Unlike the optical response, the peak in the microwave response is located (in temperature) in the region of the resistive tail well-below T_c as shown in Fig. 9 and clearly separated from the optical bolometric response peak shown previously in Fig. 7. This implies that the microwave response is non-bolometric. As expected, the width of the resistive tail increases with increasing microwave power, and the peak of the response increases until saturation, as shown. In addition, lockin response to microwaves does not rolloff with chopper frequency (up to 50 kHz) as did the optical response, implying the microwave response mechanism is not thermal.

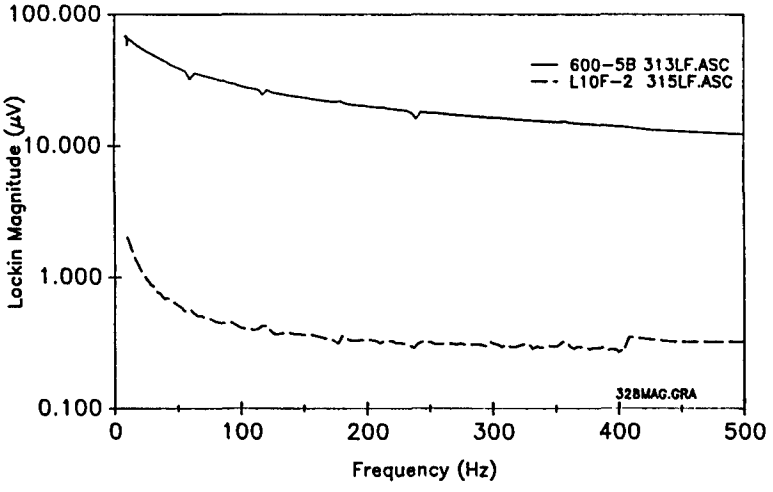


Fig. 8: Optical bolometric response versus chopper frequency for two Bi-Sr-Ca-Cu-O samples.

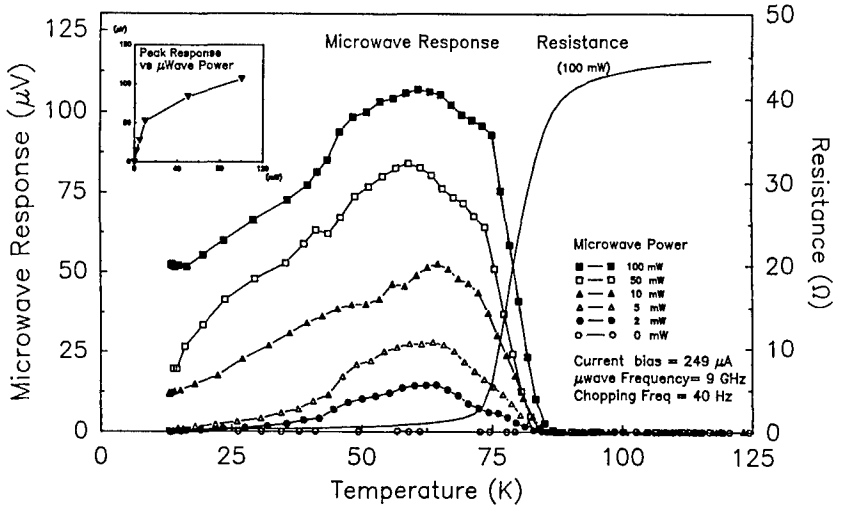


Fig. 9: Microwave response of Bi-Sr-Ca-Cu-O sample versus temperature for different microwave powers. The inset is a plot of the peak response vs microwave power.

Noise voltage measurements were also taken with the lockin amplifier using a low noise pre-amplifier and biasing with a battery source. Similar microwave noise emission results were observed by Konopka, et al in Y-Ba-Cu-O films. [7] For our measurements, the equivalent noise bandwidth was set to 1 Hz and the chopping frequency was set to 40 Hz. Even with no illumination the sample has a response, and it is in the resistive tail region as shown in Fig. 10. In addition, peak excursions of the noise voltage observed in the region of the peak were much higher than the RMS noise voltage levels. This behavior would be expected if individual transient fluctuations occur in the film over very short time intervals, perhaps associated with flux motion and dissipation induced by bias current flow.

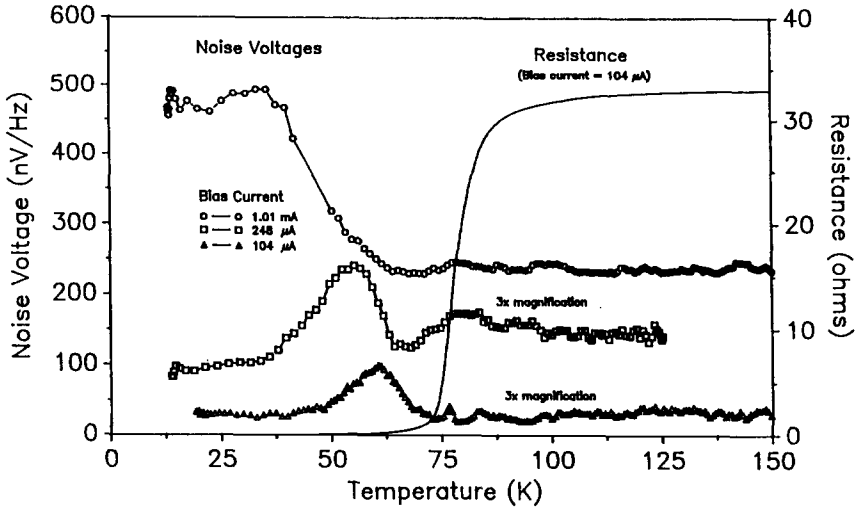


Fig. 10: Noise voltage versus temperature for Bi-Sr-Ca-Cu-O sample for various bias currents. The R(T) curve is shown for comparison.

Models of Response Mechanism

Several hypotheses have been put forward to explain the microwave response peak. It could be ascribed to flux-flow within a weakly-coupled granular weak-link array. Some of the evidence used to support this vortex-antivortex dissociation mechanism (also known as the Kosterlitz-Thouless model) includes the presence of a resistive tail below the superconducting transition[20], which we observe. In addition to evidence for this type of response in granular Y-Ba-Cu-O films noted by Culbertson, et al [18], Zeldov et al[21] have observed a non-bolometric response in epitaxial Y-Ba-Cu-O films, and they explain their results on the basis of photoenhanced flux creep. This mechanism, however, is not likely to be the cause of the optical response seen in our granular films since the peak location and response time are consistent with the thermal (bolometric) response, but it may be a mechanism for the microwave response. In fact, earlier work by Voss et al [22] in granular aluminum films demonstrated an almost identical behavior to our microwave results. Recent results of Konopka, et al [5-6] and Jung, et al [7] also reveal similar behavior in Y-Ba-Cu-O films, as well as Bi-Sr-Ca-Cu-O films, but the results for the noise emission in Bi-Sr-Ca-Cu-O were barely detectable. We observe clear indications of microwave noise emission in our samples.

The responsivity of the bolometric detection mode using HeNe laser light (633 nm) was calculated from the experimental parameters. Values of 5 mV/W (Bi-Sr-Ca-Cu-O on MgO) and 250 mV/W (Bi-Sr-Ca-Cu-O on ZrO_2) were obtained for a chopper frequency of 20 Hz. In contrast, the responsivity of the nonbolometric mode using a X-band (9 GHz) horn was calculated to be 20-120 V/W (Bi-Sr-Ca-Cu-O on MgO) independent of chopper frequency up to the limit set by our current experimental apparatus (50 kHz), which is considerably higher than the bolometric mode. Of course, the bolometric mode was not optimized for maximum responsivity in these preliminary samples. Nor was the microwave response necessarily optimized, but the means to optimize it are not as clear because the exact mechanism is not known. Gallop, et al [23] offer a plausible explanation based on their measurements of the differential resistance (dV/dI) of Y-Ba-Cu-O samples and the idea that microwave radiation synchronizes with the weak fluxon lattice likely present in the granular film. Fluxons move, creating a Faraday voltage due to the Lorentz force and a consequent dissipation measured by dV/dI. If the rate of passage of fluxons across the sample is proportional to the microwave frequency (f) then the corresponding voltage drop across the sample is $V = n\Phi_0 f$, where n is an integer and Φ_0 is the flux quantum. This result is similar to the Josephson relation for Shapiro steps, except that the resulting dV/dI indicates a dissipation rather than a supercurrent at voltage values proportional to frequency. We strongly expect to see similar results in our samples as we measure the frequency dependence of the nonbolometric response.

Summary

Deposition and patterning techniques have been developed based on the use of lasers, which are very effective and flexible in developing practical HTSC thin film detectors. We are continuing to refine these techniques to implement detectors for laboratory-based infrared and microwave spectroscopy. Measurements of Bi-Sr-Ca-Cu-O patterned thin films reveal the presence of optical bolometric and microwave nonbolometric responses in the same samples. The nonbolometric response appears to be a faster, more sensitive mechanism than the bolometric response by over three orders of magnitude in these preliminary results, but further design refinements and measurements will determine the actual relative performance. Measurements will be made by varying the microwave frequency and static applied magnetic field. These proposed measurements should help resolve issues regarding the response mechanism.We also plan to use fast rise-time microwave excitation to attempt to determine the ultimate bandwidth.

Acknowledgements

The authors would like to thank A. Razavi and T.J. Hughes of Wilkes University for their contribution of Y-Ba-Cu-O films and support for laser patterning.

References

1. B.G. Boone, "Application of High Temperature Superconducting Thin Film Devices to Electro-Optical and Electronic Warfare Systems", JHU/APL Technical Report TG-1377 (Feb 1990)

2. M.G. Forrester and J. Talvacchio, "Photon Detection by High-Temperature Superconducting Films: Fundamental Limits", Proc. M^2S-HTSC, Stanford, CA, July 1989, submitted to Physica C

3. S.A. Wolf, "Making Sense of Superconducting Infrared Sensors", 13th International Conf. on Infrared and Millimeter Waves, R.J. Temkin, ed., Dec. 5-9, 1988, Honolulu, Hawaii, SPIE Vol. 1039

4. P.L. Richards, J. Clarke, R. Leoni, Ph. Lerch, S. Verghese, M.R. Beasley, T.H. Geballe, R.H. Hammond, P. Rosenthal, and S.R. Spielman, "Feasibility of High T_c Superconducting Bolometer", Appl. Phys. Lett. 54, 283-285 (1989)

5. J. Konopka, R. Sobolewski, A. Konopka, and S. Lewandowski, "Microwave Detection and Mixing in Y-Ba-Cu-O Thin Films at Liquid Nitrogen Temperatures", Appl. Phys. Lett. 53, 796-798 (1988)

6. J. Konopka, G. Jung, P. Gierlowski, W. Kula, A. Konopka, R. Sobolewski, and S.J. Lewandowski, "Interaction of Microwave Radiation with High-T_c Films of Different Microstructures", Physica C, 162-164 , pp. 1041-1042 (1989)

7. G.Jung, J. Konopka, P. Gierlowski, and W. Kula, "Microwave Noise Emission from High T_c Thin Films", Appl. Phys. Lett. 54, 2355-2357 (1989)

8. K. Moorjani, F.J. Adrian, B.F. Kim, J. Bohandy, T.E. Phillips, W.J. Green, E. Agostinelli, B.G. Boone, and R.M. Sova, "High Temperature Superconductivity", JHU/APL Tech. Dig. 11, No. 1 (Jan-Mar 1990)

9. K. Moorjani, F. J. Adrian, B. F. Kim, J. Bohandy, T. E. Phillips, W. J. Green, E. Agostinelli, and B. G. Boone, "High-Temperature Superconducting Thin Films," JHU/APL Tech. Dig. 9, 174-188 (1988)

10. B.G. Boone, K. Moorjani, R.M. Sova, B.F. Kim, J. Bohandy, F.J. Adrian, W.J. Green, and R.L. Edwards, "Development of Bi-Sr-Ca-Cu-O Thin-Film Devices for Microelectronic Applications", 175th Electrochemical Society Meeting, Los Angeles, CA (May 7-12, 1989)

11. R.M. Sova, B.G. Boone, K. Moorjani, B.E. Grabow, R.C. Meitzler, T.J. Hughes, and A. Razavi, "Development of High Temperature Superconducting Thin Film Detectors", abstract submitted to 177th Electrochemical Society Meeting, High T_c Superconducting Technology Program, to be held May 6-11, 1990, Montreal, Canada

12. M. Rothschild, J.H.C. Sedlacek, J.G. Black, and D.J. Ehrlich, "Laser Patterning of Metal Oxide Superconductor Films by Reactive Solid-State Transfomation", IEEE Trans. Electron Device Lett., 9, 68 (1988),

13. G. Liberts, M. Eyett, and D. Bauerle, "Direct Laser Writing of Superconducting Patterns into Semiconducting Ceramic Y-Ba-Cu-O", Appl.Phys. Lett. A 46, 331 (1988)

14. P.L. Richards, S. Verghese, T.H. Geballe, and S.R. Spielman, "The High T_c Superconducting Bolometer", IEEE Trans. on Magnetics, 25, 1335-1338 (1989)

15. W.S. Broklesby, D. Morris, A.F.J. Levi, M.Hong, S.H. Liou, J. Kwo, and C.E. Rice, "Electrical Response of Superconducting $YBa_2Cu_3O_{7-\delta}$ to Light", Appl. Phys. Lett. 54, 1175-1177 (1989)

16. A. Frenkel, M.A. Saifi, T. Venkatesan, C. Lin, X.D. Wu, and A. Inam, "Observation of Fast Nonbolometric Optical Response of Nongranular High T_c $Y_1Ba_2Cu_3O_{7-x}$ Superconducting Thin Films", Appl. Phys. Lett. 54, 1594-1596 (1989)

17. M.G. Forrester, J. Talvacchio, and A.I. Braginski, "Electrical Response of High-T_c Superconducting Films to Laser Radiation", Proc. GACIAC Workshop on High-T_c Superconductivity, Huntsville, AL, May 1989

18. J.C. Culbertson, U. Strom, S.A. Wolf, P. Skeath, E.J. West, and W.K. Burns, "Nonlinear Optical Response of Granular Y-Ba-Cu-O Films", Phys. Rev. B 39, 12359-12362 (1989)

19. H.S. Kwok, J.P. Zheng, and Q.Y. Ying, "Nonthermal Optical Response of Y-Ba-Cu-O Thin Films", Appl. Phys. Lett. 54, 2473-2475 (1989)

20. M. R. Beasley, J. E. Mooij, and T. P. Orlando, "Possibility of Vortex-Antivortex Pair Dissociation in Two-Dimensional Superconductors," Phys. Rev. Lett. 42, pp. 1165-1168 (1979)

21. E. Zeldov, N. M. Amer, G. Koren, and A. Gupta, "Nonbolometric Optical Response of $YBa_2Cu_3O_{7-\delta}$ Epitaxial Films," Phys. Rev. B 39, pp. 9712-9714 (1989)

22. R. F. Voss, C. M. Knoedler, and P. M. Horn, "Vortex Noise at the Superconducting Transition in Granular Aluminum Films," in *Inhomogeneous Superconductors-1979*, D. U. Gubser, T. L. Francavilla, J. R. Leibowitz, and S. A. Wolf, eds., American Institute of Physics, New York, pp. 314-318 (1980)

23. J.C. Gallop, W.J. Radcliffe, C.D. Langham, R. Sobolewski, W. Kula, and P. Gierlowski, "Josephson Effects and Microwave Response of HTS Thin Films", Physica C 162-164, 1545-1546 (1989)

IN-SITU INTEGRATED PROCESSING AND CHARACTERIZATION OF THIN FILMS OF HIGH TEMPERATURE SUPERCONDUCTORS, DIELECTRICS AND SEMICONDUCTORS BY MOCVD

R. Singh, S. Sinha, N.J. Hsu, R.P.S. Thakur, P. Chou, and A. Kumar, School of Electrical Engineering and Computer Science, University of Oklahoma, Norman, OK, 73019 and J. Narayan, Materials Science and Engineering Department, North Carolina State University, Raleigh, NC 27695-7916

Low temperature deposition, high throughput, sharp interfaces, selective deposition with direct ion, electron, and photon beam controlled techniques, and deposition in conventional as well as atomic layer epitaxy mode are some of the attractive features of MOCVD. In addition to the well established role in semiconductor and optoelectronics industry, MOCVD is expected to play a significant role in high temperature superconductor industry. High temperature superconducting thin films as well as semiconductors and/or dielectrics are essentially required for the fabrication of superconductor and hybrid superconductor/semiconductor devices. From materials compatibility point of view, the interface between two disimilar materials (e.g.superconductor/dielectric, semiconductor/dielectric, etc.) should have chemical, physical, and thermal integrity during and after the processing of materials. In our strategity of depositing the basic building blocks of superconductors, semiconductors, and dielectric having common elements, we have deposited superconducting films of Y–Ba–Cu–O, semiconductor films of Cu_2O, and dielectric films of BaF_2 and Y_2O_3 by MOCVD. By switching source materials entering the chamber, and by using direct writting capability complex device structure like three terminal hybrid semiconductors/superconductors transistors can be fabricated. The Y–Ba–Cu–O superconducting thin films on BaF_2/YSZ substrates show a T_c of 80K and are textured with most of the grains having their $c-axis$ or $a-axis$ perpendicular to the substrate. In this paper, we will report electrical characteristics as well as structural characteristics of superconductors and related materials obtained by X-ray deffraction, SEM, TEM, and energy dispersive X-ray analysis.

This work was supported by Defense Advanced Research Agency (DARPA) contract number MDA972–88–D–0004

MAGNETIC RELAXATION IN THE 110 K SUPERCONDUCTING PHASE in Bi-Sr-Ca-Cu-O THIN FILMS

Atsushi Tanaka, Jason Crain, Nobuo. Kamehara and Koichi Niwa

FUJITSU LABORATORIES LTD.

10-1, Morinosato-Wakamiya, Atsugi, 243-01, Japan

Abstract

We have investigated the time dependence of remnant moment decay in a highly oriented, nearly single high Tc phase Bi-Sr-Ca-Cu-O thin film. A strictly logarithmic time dependence was observed over a 20 K temperature range for observation intervals of 2000 seconds. The normalized decay rate exhibits a peak around 14 K and has a relatively weak magnetic field dependence. These data are then compared with existing data on the YBCO and Eu - based superconductors.

Introduction

Unusually large thermally activated flux creep in a single crystal of $YBa_2Cu_3O_7$ (YBCO)[1] as well as a reported peak in the temperature dependence of the normalized relaxation rate[2] has prompted investigation into the time dependence of remnant magnetization in that system and in other high Tc superconductors[3,4,5]. However, the high Tc phase of the Bi-based material, especially in thin film form, has gone largely uninvestigated. We report here the results of magnetic relaxation experiments on highly oriented, polycrystalline films of the high Tc phase of Bi-(Pb)-Sr-Ca-Cu-O (BSCCO).

Sample fabrication

The BSCCO film was fabricated by rf magnetron sputtering onto single crystal MgO. A composite target with composition $Bi_{3.00}Sr_{1.90}Ca_{2.00}Cu_{3.00}$ was used. In addition, a PbO target and a CuO target were used to dope Pb in desired amounts and to optimize the Cu composition. Details of the sample synthesis are reported elsewhere[6]. The post-anneal composition was $Bi_{1.94}Pb_{0.08}Sr_{2.00}\ Ca_{2.04}Cu_{3.30}O_x$. The film used for this study exhibited zero resistance at 106.2 K and was c-axis oriented, nearly single phase, high Tc material as determined by X-ray diffraction.

Procedure

The magnetic measurements were performed by weak-field (approximately 2 Oe) cooling the sample from room temperature in a squid magnetometer. A magnetic field was applied for ten minutes parallel to the c-axis and then removed. The time decay of the remnant moment was measured at several temperatures and at fields of 0.5 kOe and 1 kOe.

Results and discussion

The decay was observed to obey a strictly logarithmic time dependence during observation intervals of 2000 seconds as shown in Figure 1. The normalized decay rate R and average pinning potential Uo were calculated from the Anderson-Kim model[7] using the relations:

$$M(t) = M_o\{1 - \frac{k_bT}{U_o}\ln(\frac{t}{\tau})\} \qquad \text{(Eqn. 1)}$$

and

$$\mathcal{R} = \frac{1}{M_0}\frac{\partial M(t)}{\partial(\ln(t))} = \frac{k_bT}{U_o} \qquad \text{(Eqn. 2)}$$

and a linear least squares fit to the data. The value of Mo was defined as the t = 1 second extrapolation of the linear fit. As single crystals of the high Tc phase have not yet been synthesized, the question of whether Uo represents a parameter intrinsic to the high Tc phase or is dominated by grain boundary structure remains an open one.

The temperature dependence of the normalized decay rate obtained at 0.5 kOe and 1 kOe is shown in Fig. 2. A sharp peak followed by a rapid drop is a qualitative feature of both sets of data. This phenomena has been reported in bulk polycrystals of YBCO[2] after field cooling in 0.5 kOe. A weak field dependence of peak position is also observed. The temperature at which the maximum normalized rate occurs shifts from 14K to 12 K as the field is increased from .5 kOe to 1 kOe. There are notable differences between these results and those reported for YBCO

material. The peak is much more broad in the YBCO material than in the Bi-film and the temperature at which the maximum normalized rate occurs is roughly 15 K lower in the Bi film than in the YBCO sample for the same applied field.

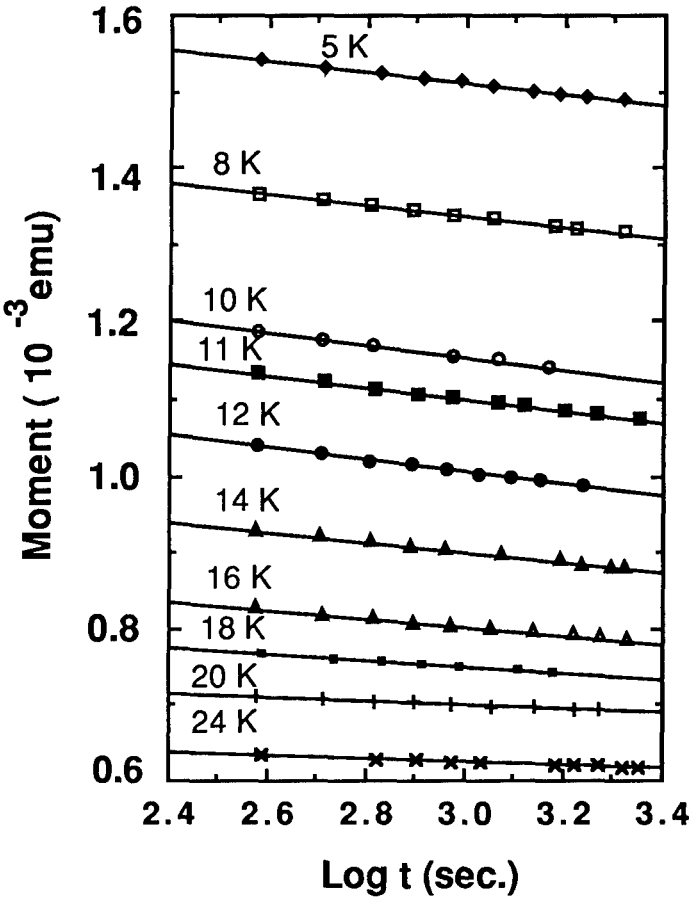


Fig.1. Time dependence of the remnant magnetic moment after a ten-minute application of a 1 kOe field parallel to the film's c-axis. The lines represent a least squares fit.

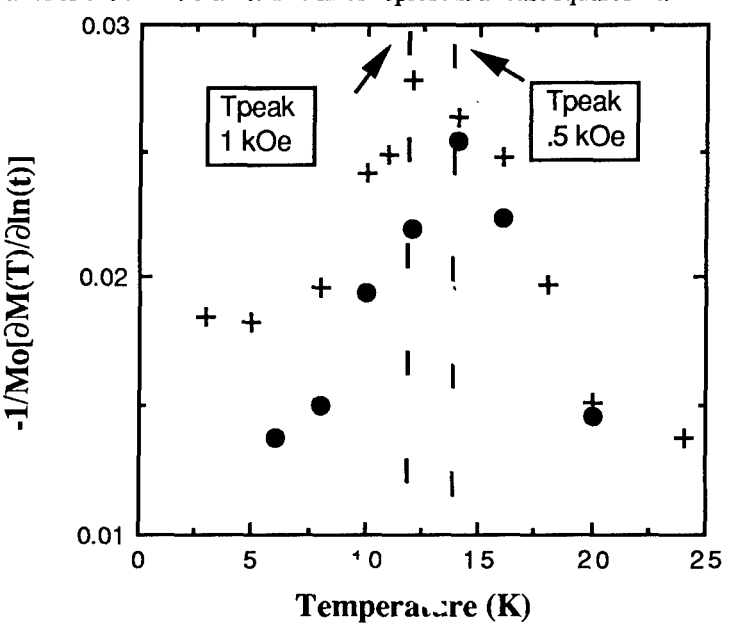


Fig. 2. Temperature dependence of the normalized relaxation rate of a highly c-axis oriented BSCCO thin film. The plus signs and filled circles indicate relaxation measured from applied fields of 1 kOe and .5 kOe respectively.

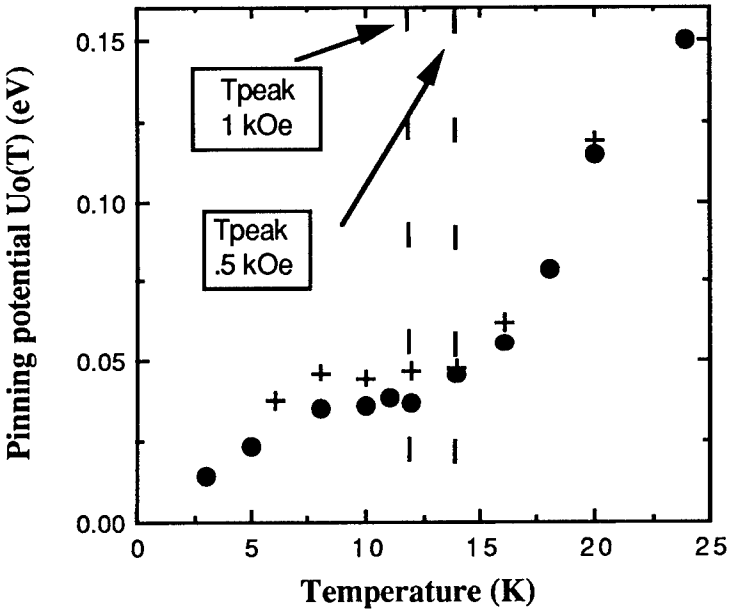


Fig. 3. Temperature dependence of the pinning potential Uo(T). The plus signs and filled circles indicate relaxation measured from applied fields of 1 kOe and .5 kOe respectively.

The temperature dependence of Uo is shown in Fig. 3. It is observed that the pinning potential had a nearly constant value of 40 meV between 8 K and 14 K regardless of the field from which relaxation was measured. The average pinning potential at 10 K was approximately 40 meV. It should be noted that at temperatures above T_{peak}, the pinning potential monotonically increases with temperature. This apparent inconsistency with the Anderson-Kim model of thermally activated flux creep makes the validity of the model, and hence the definition of Uo, questionable above T_{peak}.

Several theoretical models have been proposed in an attempt to explain the origin of the peak in the temperature dependence of the normalized rate. In one such model[8], based on a theory of the elastic moduli of the vortex lattice, the pinning potential is related to temperature-dependent critical current, effective radius of pinning and the average volume of flux bundles. Using this model the expression arrived at for the temperature dependence of the normalized rate is

$$\mathfrak{R} = \text{const.} \times \left[1 - \frac{T}{T_c(B_e)}\right]^{\frac{n(B_e)}{2}-1} \left[1 + \left(\frac{T}{T_c(B_e)}\right)^2\right]^{-2} \qquad \text{(Eqn.3)}$$

where Be is the external flux density and n(Be) can be determined from critical current measurements. We used n(Be) as an adjustable parameter but were not able to simultaneously reproduce the qualitative structure of the peak for any reasonable choice of n(Be) using this model. It is possible that this model may be satisfactory for a very rigid lattice and that the fields used in this investigation were not sufficiently strong to generate a vortex structure for which Eqn. 1. is applicable.

Another model[9] involving a distribution of activation energies ρ(Uo) has also been proposed and has been used to analyze relaxation results similar to ours for thin films of $ErBa_2Cu_3O_{7-d}$[10]. For the Eu-based films, the pinning energy distribution function obtained from an inversion of that data exhibits a peak at roughly 40 meV. This is similar to the estimated average value of the pinning potential for our sample in the range of 8 - 14 K, suggestive of certain underlying similarities in the pinning mechanisms between the two materials. This model is based on the idea that as temperature is increased, low energy pinning sites become increasingly less effective until only very high energy pinning centers can pin vortices. The weak but observed magnetic field dependence of the peak position, however, is not explicitly included in the energy distribution model.

Summary and Conclusions

We have observed logarithmic decay of remnant magnetization in thin films of the high Tc phase in the Bi superconducting system and we report the first observation in this material of a peak in the temperature dependence of the normalized rate. The peak occurred at a lower temperature and was sharper than that of YBCO for relaxation measured from the same field. The average pinning potential of the sample was the same as that calculated for Eu-based superconducting films. Of the present theoretical attempts to explain the origin of the peak and the relevant energy scales for pinning, we find the model of a distribution of activation energies most satisfactory.

References

[1]Y. Yeshurun and A.P. Malozemoff, "Giant flux creep and irreversibility in an Y-Ba-Cu-O crystal: An alternative to the superconducting-glass model", Phys. Rev. Lett. **60** (1988) 2202.

[2]M. Tuominen, A.M.Goldman, M.L.Mecartney, "Time-dependent magnetization of a superconducting glass",Phys. Rev B 37, 548 (1988).

[3]T. Kotani, K. Ohkura H. Takei, and T Tada,"Magnetic properties of Bi- and Tl -based single crystals", To appear in Proceedings of ISS 1989.

[4]S. Hatta, Y. Ichikawa, H. Adachi, and K. Wasa:, "Magnetic aftereffects in high Tc superconducting thin films", Japn J. Appl. Phys. 28 (1989) L 422-423.

[5]H. Kumakura, K. Togano, E. Yanagisawa, K. Takahashi, M. Nakao, H. Maeda, Magnetic relaxation in high-Tc oxide superconductors", Japn. J. Appl. Phys **28** (1989) L 24-26.

[6]A.Tanaka, N. Kamehara and K.Niwa,"Composition dependence of high Tc phase formation in Pb-doped Bi-Sr-Ca-Cu-O thin films""Appl. Phys. Lett. **55**, 1252 (1989).

[7]P. W. Anderson, "Theory of flux creep in hard superconductors",Phys. Rev. Lett. **9**, 309 (1962).

[8]T. Fujiyoshi, K. Toko, T. Matsushita, and K. Yamafuji, "Temperature dependence of flux creep in high Tc superconductors", Jpn. J. Appl. Phys. **28** (1989) L 1906-1908.

[9]C. W. Hagen and R. Griessen, "Thermally avtivated magnetic relaxation in high Tc superconductotrs", Studies of high temperature superconductors, Nova Science Publishers Inc.

[10]H. Furukawa, K. Kawaguchi, and M. Nakao, "Distribution of flux pinning energies in superconducting thin films", To appear in Proceedings of ISS 1989.

In-Situ Deposition of YBCO High-Tc Superconducting Thin Films by MOCVD and PE-MOCVD

J. Zhao, D.W. Noh*, C. Chern**, Y.Q. Li*, P.E. Norris, B. Kear**, B. Gallois*
EMCORE Corporation, 35 Elizabeth Ave.,Somerset, N.J. 08873
*Stevens Institute of Technology, Hoboken, NJ 07030
**Rutgers, The State University, New Brunswick, NJ 08854

The development of a successful low temperature, in-situ process for the formation of high temperature superconducting (HTSC) thin films is crucial for the early application of copper oxide-based ceramics. Such a process should permit the deposition of high quality, high density, HTSC films which have smooth sufaces, on a variety of substrates. Metal-Organic Chemical Vapor Deposition (MOCVD) process technology offers the advantages of a high degree of compositional control, adaptability for large scale production and the potential for low temperature fabrication. The capability of operating at high oxygen partial pressure is particularily suitable for in-situ formation of HTSC films. Use of a plasma-enhanced (PE) process substitutes electron kinetic energy for conventional thermal energy and enhances compound formation by introducing activated oxygen generated from dissociation of oxidizer constituents. This permits the use of lower temperature deposition conditions. In addition, the CVD process offers the advantage of easy transfer from R&D applications to low cost, large scale fabrication.

Our preliminary results demonstrate that high density, mirror smooth, low carbon YBCO films can be formed in-situ at reduced substrate temperatures, as low as 570°C. Further reductions in deposition temperature by increasing microwave plasma power are expected. Our results indicates that this method is a promising process for superconducting device technology.

Our approach involves the use of Metalorganic Chemical Vapor Deposition (MOCVD), which has been successfully employed in the production of III-V compound semiconductor devices. A novel variation on MOCVD, is the use of a microwave plasma to enhance the growth rate at low substrate temperatures. In addition, such a plasma-enhanced MOCVD (PE-MOCVD) process produces excited oxidizer species which, being more reactive than O_2, result in a higher degree of oxidation at low growth temperatures.

Comparisons of Deposition Techniques: PVD and CVD

To date, efforts to fabricate high T_c superconducting films at low temperature without post annealing have primarily involved activated physical vapor deposition (PVD) processes in which excited species were present such as plasma-assisted laser deposition,[1] activated reactive evaporation,[2] rf planar magnetron sputtering,[3] and electron cyclotron resonance with oxygen plasma-assisted evaporation.[4] These methods all have the drawbacks of requiring high vacuum, being limited to line-of-sight deposition, having low deposition rates, and having limited adaptability to flexible, large-scale production processes. Chemical Vapor Deposition (CVD), in principle, overcomes the above limitations. In addition, CVD offers accurate compositional control, through controlling the mass transport of individual precursors, and the fabrication of abrupt interfaces, due to the ability to rapidly change gas phase composition, which leads to the potential for creating metastable structures.

At the beginning of 1988, a few groups (including EMCORE)[5] independently succeeded in the preparation of high T_c oxide films by MOCVD. In less than a year, Y-Ba-Cu-O films had been prepared with T_c higher than 90K and J_c = 1.9x10^6 A/cm^2 at 77K,[6] which is comparable to that obtained by PVD. Today, more than twenty research groups have joined this promising field which is currently dominated by the Japanese scientific community, with at

least ten laboratories active in the growth of HTSC thin-films using MOCVD. However, unlike PVD, no activated CVD method has been fully developed, hence, a deposition temperature of more than 800°C is still required to obtain high quality, in-situ HTSC films using MOCVD. However, YBCO films can be formed at temperatures around 600°C using activated PVD.[1,2] Due to the strong chemical reactivity of HTSC materials, a deposition temperature around 600°C is still too high to prepare superconducting thin films on some technologically important, but more highly reactive substrates, such as Si.

MOCVD, which has the capability of operating at high oxygen partial pressure, is particularly suitable for in-situ formation of HTSC films. Fig.1 shows a plot of oxygen partial pressure vs. temperature indicating the location of the phase transitions of $YBa_2Cu_3O_y$ together with experimental data points from the literature[7] for several reports of successful in-situ growth. The critical phase stability boundary is at $y = 6.0$. Below y=6.0, YBCO is unstable and disproportionates into Y_2BaCuO_5, $BaCuO_2$ and Cu_2O. At an oxygen content of 6.5 a phase transition from tetragonal to a orthorhombic structure occurs, with a T_c of about 50K. At $y = 6.9$, the superconducting transition temperature increases to about 90K. As indicated in Fig.1 by the filled circle, the proposed low temperature deposition process (PE-MOCVD) is the first deposition process to form the orthorhombic superconducting phase in the as-deposited state. The filled circle in Fig.1 represents our present growth conditions. By further decreasing the deposition temperature, the in-situ formation of YBCO superconducting films with y =6.9 will be possible and an in-situ, low temperature MOCVD growth process for $T_c \geq$ 90K HTSC thin films should result.

PE-MOCVD of YBCO using Nitrous Oxide

In PE-MOCVD, the presence of a plasma changes the chemistry of film formation from atom-atom to atom-ion or ion-ion, which is much more energetically favorable for compound formation. It has been shown that high quality films of a variety materials such as diamond and SiC can be deposited at significantly reduced temperatures using PE-MOCVD.[8,9,10] The application of PE-MOCVD process to HTSC thin films should emerge as an exciting method to prepare oxide superconducting thin films with desired properties at much reduced deposition temperatures. $YBa_2Cu_3O_{7-x}$ films prepared by PE-MOCVD at deposition temperatures as low as 580°C by and having $T_c = 82K$ and $J_c = 10^5 A/cm^2$ at about 50K have recently been reported by Hitachi using oxygen as a reactant gas.[11] Nitrous oxide (N_2O) is known to be relatively inert to metalorganic precursors yet highly reactive when dissociated to atomic and ionic oxygen.[12,13] Superconducting $YBa_2Cu_3O_{7-x}$ films formed at 650°C by MOCVD using N_2O as reactant gas have been reported recently.[14] Hence, by combining plasma activation and N_2O, we are seeking to develop a novel PE-MOCVD deposition technique for in-situ formation of superconducting high T_c oxide films at significantly reduced deposition temperatures. By employing higher microwave power levels (up to 500 W) and N_2O reactant gas, deposition temperatures as low as 400°C may be achieved. This technique will permit the deposition of high quality HTSC films on a variety of substrate materials such as Si and sapphire, which will have a significant impact on the early device applications of HTSC thin films.

Our preliminary work has demonstrated the feasibility of the proposed process. $YBa_2Cu_3O_{7-x}$ superconducting films have been deposited, in-situ, at a substrate temperature of 570°C by PE-MOCVD using remote microwave (100W) plasma-activated nitrous oxide as a reactant gas. The use of a remote plasma avoids the direct, intense ion bombardment of the film surface. The deposition temperature was measured by a thermocouple in contact with the substrates.

PE-MOCVD System Development

A prototype EMCORE System 5000 MOCVD[15] with a remote plasma coupling system was developed for the deposition of HTSC films. The system incorporated a resistance heated, high speed (0 - 2000 rpm) rotating-disk in a vertical, cylindrical cold wall growth chamber. The internal components of the reactor were chosen for their resistance to high temperature oxidation. The 5 inch diameter wafer carrier was configured to allow simultaneous growth on multiple substrates including (100) MgO, (1$\bar{1}$02) Sapphire, (100) $SrTrO_3$, YSZ, and Si wafers.

A N_2O plasma was generated by a 2.45 GHz microwave cavity mounted above the growth chamber with a special designed quartz injector tube which uniformly distributes the activated species. The cavity was powered by a modified microwave source with a variable power output of 10 - 100 Watts. Oxygen was uniformly introduced through the top of the chamber at 2 - 6 slm. The three precursors were transported by N_2 carrier gas, to individual dividing flow manifolds (injectors) mounted 120° apart. The separate injector arrangement for each source was chosen to minimize the possibility of gas phase reactions and to give additional degrees of freedom for optimizing compositional uniformity[16]. The vapor phase precursors were injected with a velocity of over 3 m/s. This high velocity significantly reduces the possibility of prereaction, resulting in a significant improvement in deposition efficiency.

Among the possible volatile organometallic precursors for high T_c MOCVD, metal ß-diketonates are attractive since they are easily synthesized, purified, and handled in air. In order to form superconducting films in the as-deposited state, ß-diketonate complexes $Y(dpm)_3$, $Ba(dpm)_2$, and $Cu(dpm)_2$ (dpm = dipivaloymethanate), were used as yttrium, barium, and copper precursors, respectively. The bubblers for the copper and yttrium sources were specially designed to yield a constant mass transport rate since they are solid at these temperatures. $Ba(dpm)_2$ is the only known non-fluorocarbon-based ß-diketonate complex which has significant volatility. However, $Ba(dpm)_2$ partially decomposes during the evaporation process, which causes its partial pressure to drop as a function of time at a constant source temperature. An apparatus for adding DPM ligand vapor to the source carrier gas was developed to stabilize the evaporation rate of $[Ba(dpm)_2]_2$, thereby ensuring that its vapor pressure remained constant.[17] Also THF (tetrahydrofuran) was added to the $Ba(dpm)_2$ along with N_2 carrier gas to increase the volatility of $Ba(dpm)_2$. THF, which has a low boiling point and high volatility can attach to a conventional-diketone metal complex. All transport lines and valves were maintained at ≈10°C above the bubbler temperature to avoid decomposition or condensation of the precursors in the gas transport system.

Deposition was carried out at a system pressure of 10 - 76 Torr and substrate temperature of 550°C - 850°C with a rotation speed of 1100 rpm. After deposition, the films were slowly cooled to 100°C under one atmosphere of oxygen. Plasma power was 100W with 1.5 slm flow of N_2O gas. Film deposition rate was controlled at 0.5 - 1µm/hour and the films were usually 0.5 - 1µm thick.

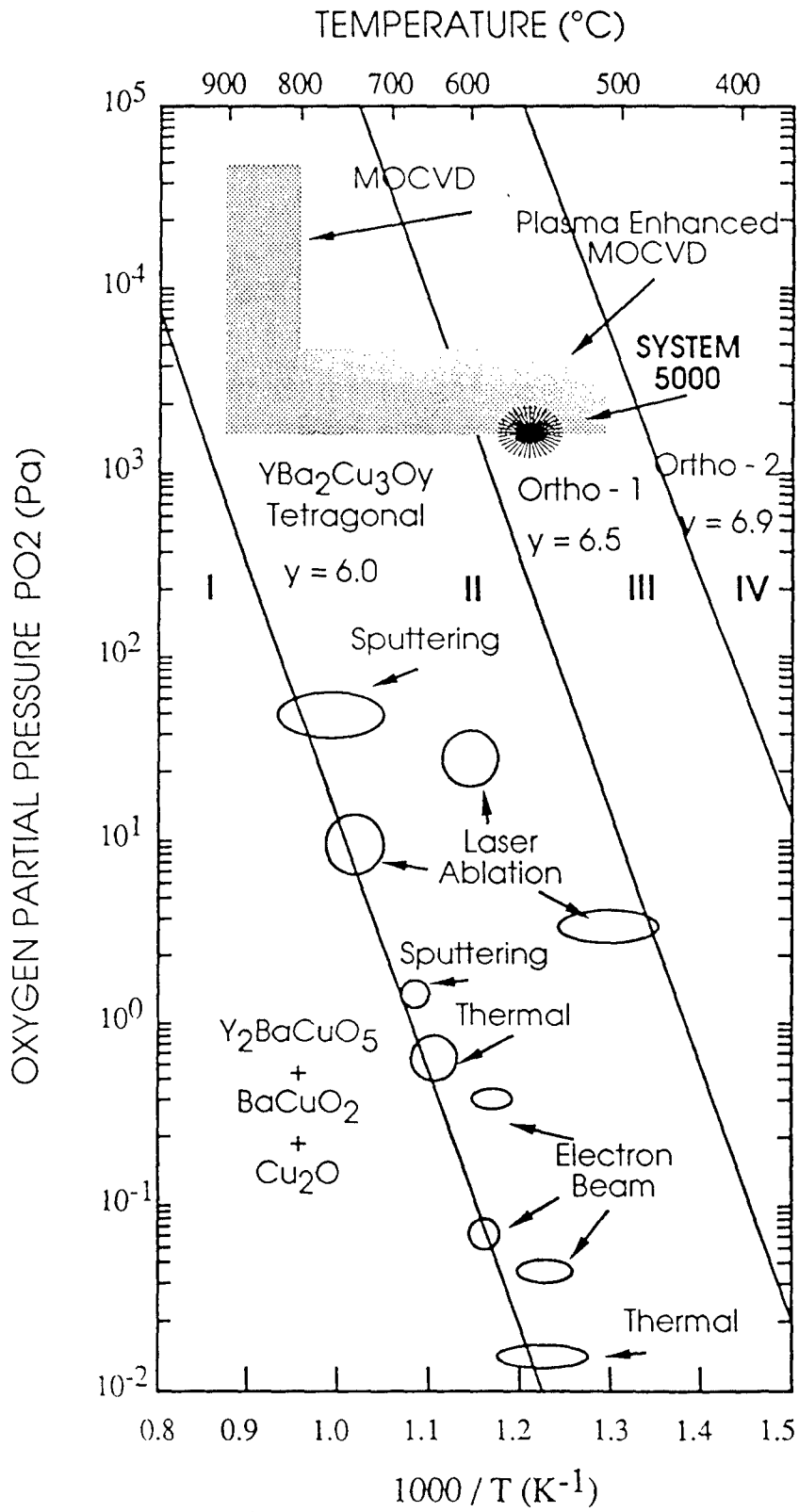
$YBa_2Cu_3O_{7-x}$ superconducting thin films with T_c above 90 K and J_c above $10^4 A/cm^2$ were reproducibly deposited in-situ on YSZ substrate at 850°C in our MOCVD system. Fig. 2 is a variable temperature resistance measurement of an as-deposited film. It shows that this film has a metallic resistance behavior with extrapolation of the normal state resistance curve to zero resistance. This film has the onset of the superconducting transition at about 94K and attainment of zero resistance by 92K with a sharp transition width of 2K.

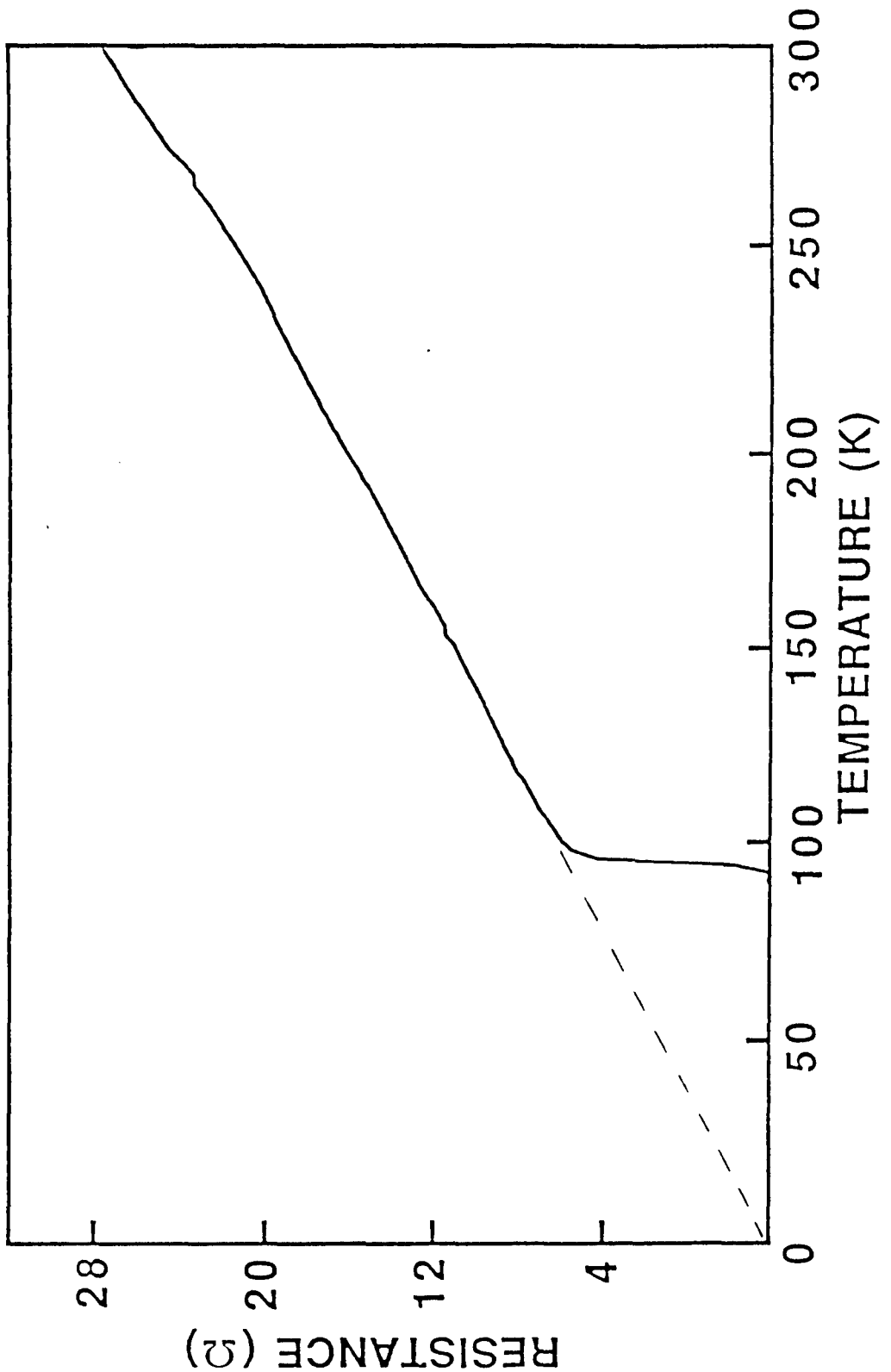
PE-MOCVD PROCESS

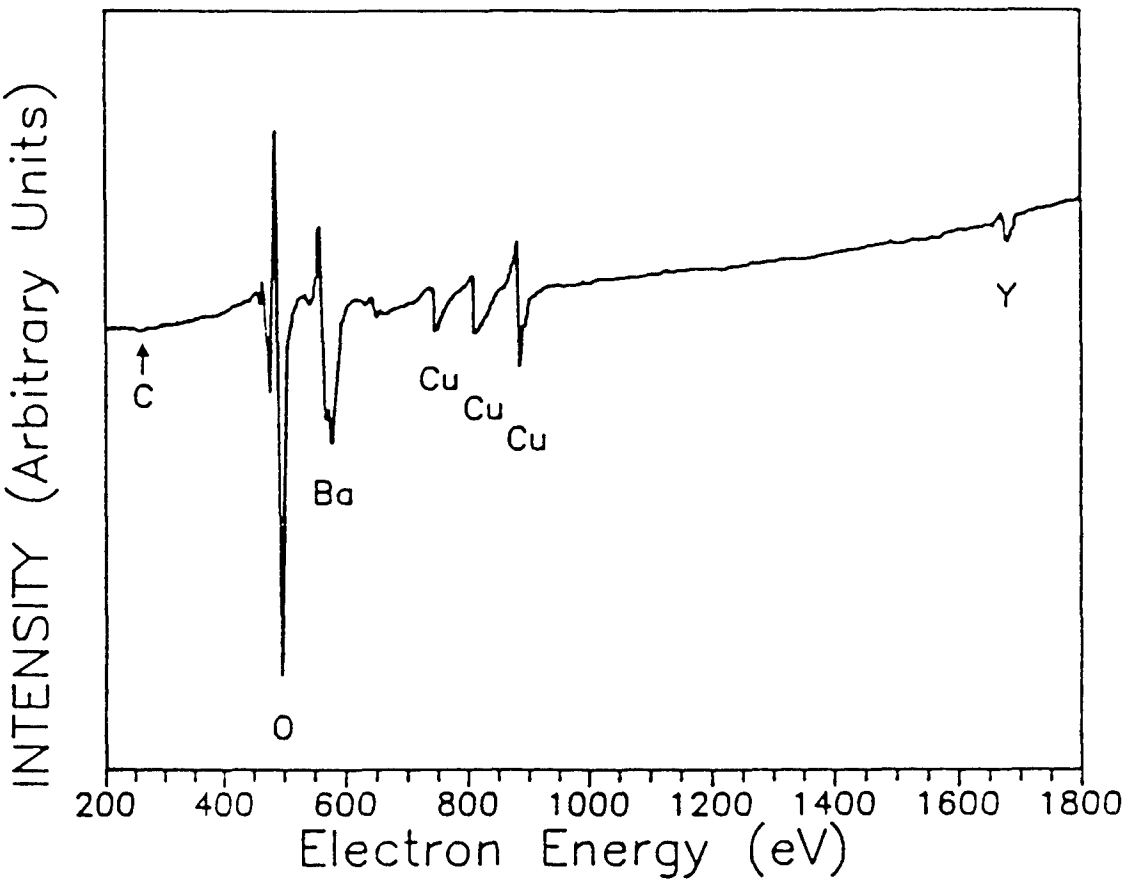
Carbon is a common impurity in films prepared by MOCVD processes, especially for films deposited at low temperatures. Fig. 3 is the Auger electron spectrum of the superconducting film formed at 610°C by PE-MOCVD with activated N_2O. With an instrumental sensitivity of 0.5 atomic percent, the barely detected carbon peak indicates that carbon content in the film is significantly less than one atomic percent. This result indicates great promise for this low temperature deposition technique. A smoothly dense film structure which is free of voids was obtained by the PE-MOCVD process, an important result for device technology. As shown in Fig. 4, the films show a sharp resistance transition, with a transition width of about 5K. However, the zero transition temperature of the initial films prepared by PE-MOCVD is 72K, which may be due to slight deviations in the film stoichiometry or to an oxygen deficiency in the film resulting from improper cooling.

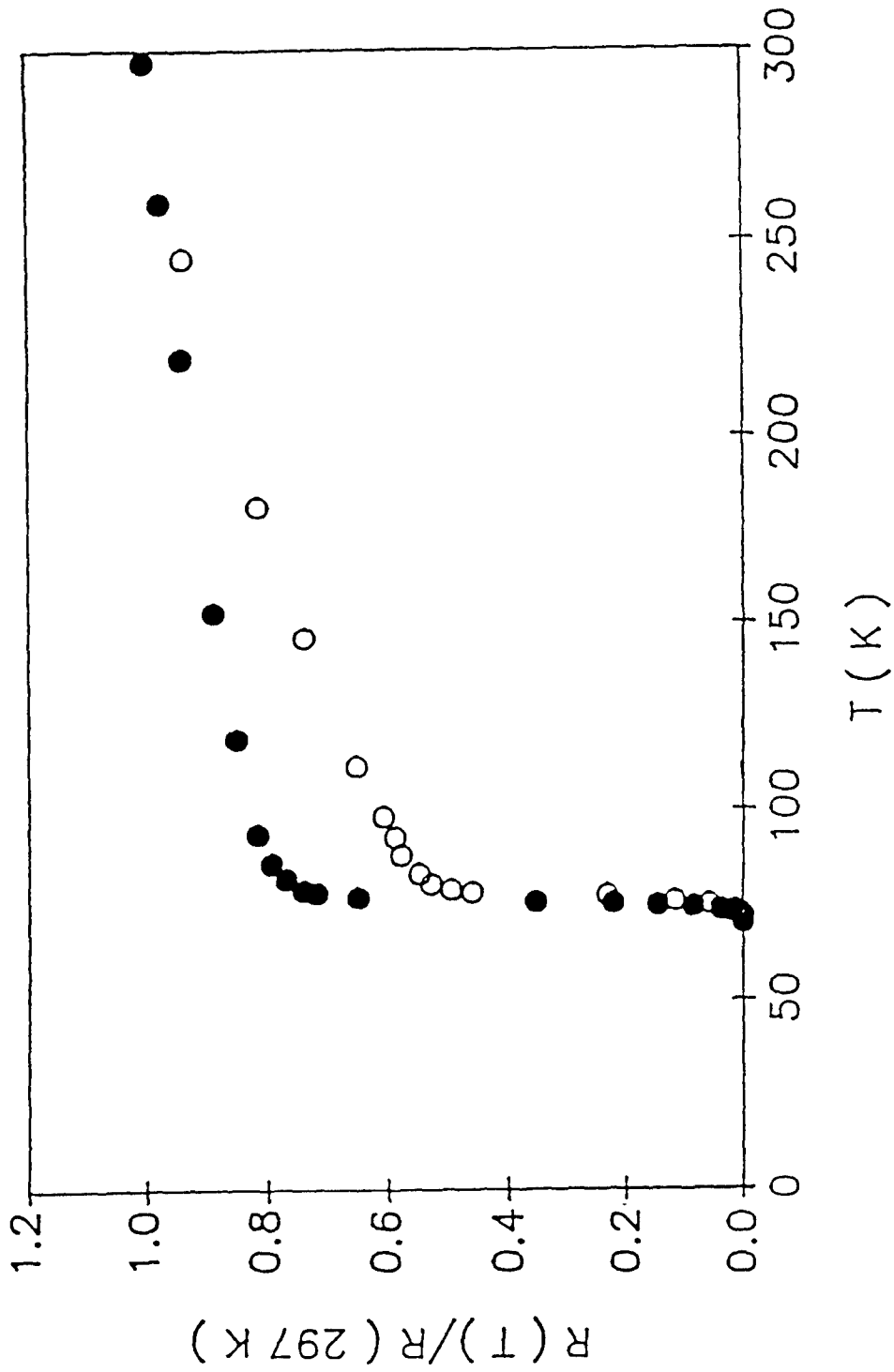
Section 4.1 REFERENCES

1. S. Witanchchi, H.S. Kwok, X.W. Wang and D.T. Shaw Appl. Phys. Lett. 53, 234 (1988)
2. S. Prakash; D.M. Umarjee; H.J. Doerr.; C.V. Deshpadey and R.R. Bunshah Appl. Phys. Lett. 55, 31 (1989)
3. K. Mizuno, M. Miyauchi, K. Setsune and K. Wasa, Appl. Phys. Lett. 54, 383 (1989)
4. T. Aida, A. Tsukamoto, K. Imagawa, T. Fukazawa, S. Satito, K. Shindo, K. Takagi and K. Miyauch, Jpn. J. Appl. Phys 28, L635 (1989)
5. P. Zawadzki, G. Tompa, D. Noh, B. Gallois, C. Chern, and B. Kear, High Temperature Superconducting Technologies Symposium, Spring ECS Meeting, Los Angeles, May, 1989.
6. H. Yamane, H. Masumoto, T. Hirai, H. Iwasaki, K. Watanabe, N. Kobayashi and Y. Muto, AppL. Phys. Lett. 53, (1988) 1548; SUPERCONDUCTOR WEEK, 3, October 9, 1989.
7. R. H. Hammond and R. Bormann to be published in Appl. Phys. Lett.
8. M. Kamo, Y. Sato, S. Matsumoto, and N. Setaka, J. Cryst. Growth, 62, 642(1983).
9. A. Inspektor, U. Carmi, A. Raveh, Y. Weitzmann, N. Mayo, and R. Avni, Proc. of the Sixth European Conf. on CVD, edited by R. Porat (Iscar Ltd. Nahariya, Israel, 1987.
10. M. Shimizu, Y. Matsueda, T. Shiosaki and A.J. Kawabata, Crystal Growth 71, 209 (1985)
11. N. Sugii and K. Miyauchi, M7.172, MRS 1989 Fall Meeting Proceding.
12. Hanbook of Thin-Film Deposition Processes and Techniques, Noyes Publication (1988), Edited by K. Klaus K. Schuegraf.
13. X.D. Wu, A. Inam, M.S. Hegde, B. Wilkens, C.C. Chang, D.M. Hwang, L. Nazar, T. Venkatesan, S. Miura, S. Matsubara, Y. Miyasaka, and N. Shohata, Appl. Phys. Lett. 54, 754 (1989)
14. T. Tsuruoka, R. Kawasaki, and H. Abe, Jpn. J. Appl. Phys. 28, L607, 1989.
15. J. Zhao, D. Noh, C. Chern, Y.Q.Li, B. Gallois, P. Norris and B. Kear, submmited Appl. Phys. Lett.
16. G.S. Tompa, M.A. McKee, C. Beckham, P.A. Zadwadzki, J.M. Colabella, R.A. Stall, and P.E. Norris, J Cryst. Growth 93 (1988) 220-227.
17. P.H. Dickinson, T. H. Geballe, A. Sanjurjo, D. Hildenbrand, G. Graig, M. Zisk, J. Collman, S.A. Banning, and R.E. Sievers, J. Appl. Phys, 66, 444, 1989.


TEMPERATURE (°C)
900
800
700
600
500
400
10^5
10^4
10^3
10^2
10^1
10^0
10^{-1}
10^{-2}
OXYGEN PARTIAL PRESSURE PO2 (Pa)
MOCVD
Plasma Enhanced MOCVD
SYSTEM 5000
YBa_2Cu_3Oy Tetragonal
y = 6.0
Ortho - 1
y = 6.5
Ortho - 2
y = 6.9
I
II
III
IV
Sputtering
Laser Ablation
Sputtering
Thermal
Y_2BaCuO_5 + $BaCuO_2$ + Cu_2O
Electron Beam
Thermal
0.8
0.9
1.0
1.1
1.2
1.3
1.4
1.5
1000 / T (K^{-1})


RESISTANCE (Ω)
28
20
12
4
0
50
100
150
200
250
300
TEMPERATURE (K)


INTENSITY (Arbitrary Units)
C
O
Ba
Cu
Cu
Cu
Y
200
400
600
800
1000
1200
1400
1600
1800
Electron Energy (eV)


R (T)/R (297 K)
1.2
1.0
0.8
0.6
0.4
0.2
0.0
0
50
100
150
200
250
300
T (K)

An explanation for the rise in T_c in the Tl- and Bi-based high temperature superconductors

S.M. Bose

Department of Physics and Atmospheric Science

Drexel University, Philadelphia, Pennsylvania 19104

and

P. Longe

Institut de Physique, B5

Universite′ de Liege, Sart-Tilman, B-4000 Liege, Belgium

Using the plasmon exchange model for the high T_c superconductor, we show that the T_c rises with an increase in the number of CuO layers per unit cell, which is in agreement with recent observations in the Tl- and Bi-based compounds. Our calculation also suggests that the sample will become superconducting in successive stages and that there is a saturation effect, i.e. that T_c cannot be raised indefinitely by increasing the number of CuO layers.

CRITICAL CURRENTS AND HIGH-TEMPERATURE SUPERCONDUCTORS

P. Chaudhari
IBM Research Division
Thomas J. Watson Research Center
Yorktown Heights, New York

ABSTRACT

In this talk I shall summarize the experimental information on critical currents and epitaxial thin films of high-temperature superconductors. I also describe experiments carried out to measure critical currents across single grain boundaries. A variety of mechanisms responsible for limiting currents in films as well as across grain boundaries are presented and their predictions compared with experimental data.

SECTION 4:
THEORY

THE SUPERCONDUCTING STATE OF THE HIGH-TRANSITION TEMPERATURE SUPERCONDUCTORS: EXPERIMENTAL BASIS

W. A. Little
Physics Department
Stanford University, Stanford CA 94305

Abstract

Experiments on the high-T_c cuprate superconductors continue to narrow the possible theoretical explanations of the phenomenon. Experimental evidence to date points to a BCS-like state, with pairs in singlet s-states, the familiar gap in the excitation spectrum, Type II behavior in a magnetic field and a normal state with fermi liquid origins. Several other features of the superconducting state in the cuprates, however, appear to differ from those of conventional alloy superconductors - these relate to the detailed structure of the gap and to the nature of the coupling mechanism. Recent experiments have helped clarify what these differences are, and together with the earlier experiments, they now impose still stronger constraints on theories of these superconductors. These and other developments will be reviewed.

PHENOMENOLOGICAL THEORY OF THE NORMAL AND SUPERCONDUCTIVE STATES OF Cu-O AND Bi-O METALS

C.M. Varma
AT&T Bell Laboratories
Murray Hill, New Jersey 07974

ABSTRACT

The universal normal state anomalies in the Cu-O metals follow from a marginal Fermi-liquid hypothesis: there exists a contribution to the polarizability over most of momentum space proportional to ϖ/T for $\varpi/T \ll 1$ and constant thereafter up to a cutoff ϖ_c. Using the same excitation spectrum, the properties of the superconductive state have been calculated. We can obtain the right order of T_c, the zero-temperature gap, $2\Delta(o)/T_c$ and the nuclear relaxation rate near T_c.

I will discuss the possible microscopic physics leading to the marginal Fermi-liquid hypothesis.

CHARGE TRANSFER POLARISATION WAVE IN HIGH T_c OXIDES AND SUPERCONDUCTIVE PAIRING

B.K. Chakraverty - CNRS - LEPES -
25 avenue de Martyrs - BP 166 - 38042 Grenoble Cedex

ABSTRACT

A general formalism of quantised charge transfer polarisation waves has been developed. The nature of possible superconductive pairing between oxygen holes is discussed. Unlike optical phonons these polarisation fields will give rise to dielectric bipolarons or bipolaron bubbles. In the weak coupling limit a new class of superconductivity is to be expected.

INTRODUCTION

The relevance of charge transfer excitation to superconductivity was first pointed out by Varma [1] et al. The idea of such a local short range interaction has since been extended to a variety of charge transfer excitations [2] in the high T_c oxides. This paper has its inspiration in the idea of polarisation waves that goes back to Hopfield [3] and revived recently by Aschcroft [4] with respect to the high T_c oxides. The basic notion of long range dipole-dipole interaction giving rise to a collective and quantised charge transfer wave is the key ingredient. Some of the detailed calculations are presented elsewhere [5].

A - POLARISATION WAVE FORMALISM

We want to make essential points clear. In the Hartree-Fock approximation, the state of an **Unit Cell of CuO_2** square is a Slater determinant of the occupied lowest energy orbital states. Consider an excitation α corresponding to moving one electron from a ground state to an excited state orbital costing an energy α. Figure 1 gives the relevant energy levels [6] ; figure 1a shows the charge transfer insulator gap energy E_g for zero-doping, while the arrows in figure 1b indicate the charge transfer excitation energy ω_g to the Fermi level on p-type doping (l signifying a ligand hole or $2p^5$ configuration).

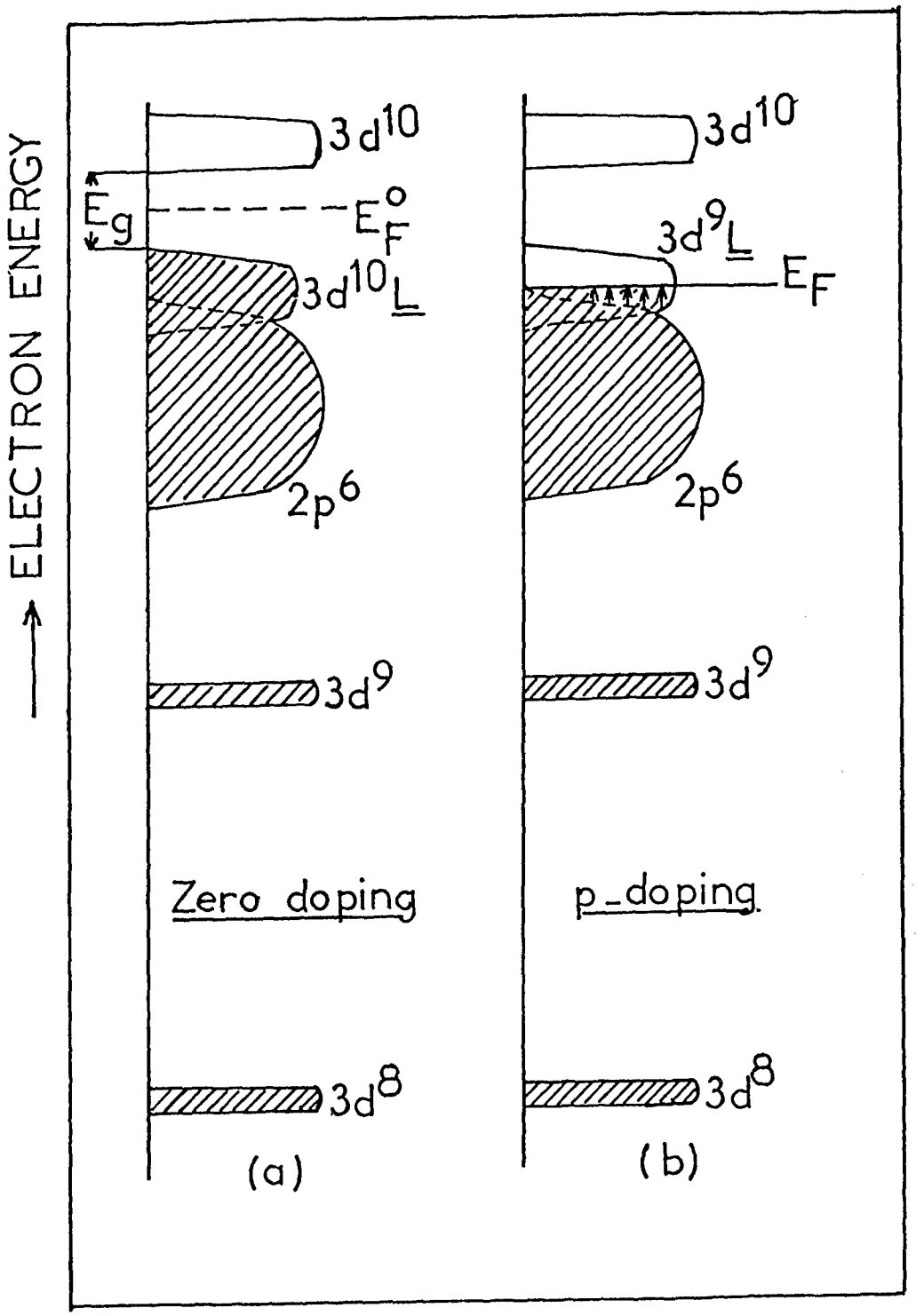


Figure 1a. Energy band--updoped material
Figure 1b. Energy band--doped material

We define by b_α^+ the operator to describe this excitation, which can be written in terms of the operator a_n of the electronic state

$$b_\alpha^+ = a_m^+ a_n \tag{1}$$

We approximate Hamiltonian of a **single cell** by

$$H = E_g + \sum_\alpha \omega_\alpha b_\alpha^+ b_\alpha \tag{2}$$

E_g : ground state energy

Define a **dipole matrix element**

$$\mu(\alpha) = \int d^3 r \ \phi_m^*(r) \ \vec{x} \ \phi_n(r) \tag{3}$$

Where the two orbitals ϕ_n and ϕ_m differ by one unit of angular momentum. Introduce the **polarisation operator** in the vector direction $\vec{x}$ for the unit cell by

$$P_x = e \sum_\alpha \mu_x(\alpha) \ (b_\alpha + b_\alpha^+) \tag{4}$$

This operator has the units of polarisation, which is charge times length - analogous to the displacement operator for a harmonic oscillator, which has the unit of length $\sim \left(\frac{\hbar}{2 m \omega}\right)^{\frac{1}{2}}$. We use the symbol $G_{xy}(i\omega)$ to denote the denote the retarded correlation function of the P operator with itself by

$$G_{xy}^0(i\omega) = - \int_0^\beta e^{i\omega\tau} \left\langle T_\tau \ P_x(\tau) \ P_y(0) \right\rangle d\tau \tag{5}$$

It is easily evaluated for the non interacting Hamiltonian (2).

$$G_{XY}^0(i\omega) = \sum_\alpha \frac{2 e^2 \ \mu_x \mu_y \omega_\alpha}{(i\omega)^2 - \omega_\alpha^2} \tag{6}$$

The quantity $- G^0(i\omega)$ is **actually the polarisability $\alpha^0(i\omega)$ of the unit cell.**

Assuming isotropy

$$\alpha(i\omega) = 2e^2 \sum_{\alpha} \frac{\mu^2(\alpha)\,\omega_\alpha}{\omega_\alpha^2 - (i\omega)^2} \qquad (7)$$

So far our discussion has been confined to the properties of a single unit cell CuO_2. However when one excites dipoles in a cell i, it has **long-range dipole-dipole interaction** with dipoles of the cell j, given by

$$H' = \vec{X_i} \cdot \phi(R_i - R_j) \cdot \vec{X_j} \qquad (8)$$

Where :

$$\phi_{xy}(R) = \frac{\delta_{xy}}{R^3} - \frac{3R_x R_y}{R^3} \qquad (8a)$$

Defining a Fourier transform

$$T_{xy}(k) = \frac{\Omega_0}{4\pi} \sum_{l} \phi_{xy}(R_l) \exp ik \cdot R_l \qquad (8b)$$

We get the resultant Hamiltonian in the k-space as

$$H = E_g + \sum_{\alpha,k} \omega_\alpha b^+_{\alpha k} b_{\alpha k} + \frac{1}{2} \sum_{k,\alpha\beta} V_{\alpha\beta}(k) \left[b_{\alpha,k} + b^+_{\alpha,-k}\right]\left[b_{\beta,-k} + b^+_{\beta,k}\right] \qquad (9)$$

where :

$$V_{\alpha\beta}(k) = \frac{4\pi e^2}{\Omega_0} \sum_{xy} \mu_x(\alpha)\, T_{xy}(k)\, \mu_y(\beta) \qquad (9b)$$

Thus the Dyson equation for the correlation function is the matrix equation

$$G_{xy}(k, i\omega) = G^0_{xy}(k, i\omega) + \frac{4\pi}{\Omega_0} \sum_{x'y'} G^0_{xx'}(k, i\omega)\, T_{x'y'}(k)\, G_{yy'}(k, i\omega) \qquad (10)$$

Solution of this equation will give us the collective excitation wave, that we have called charge transfer polarisation waves. In a cubic symmetry, it is solved to give

$$G_{xy} = -\frac{\alpha}{1 - \frac{4\pi\alpha}{3\Omega_0}} \left[\delta_{\mu\nu} - \frac{\frac{4\pi\alpha}{\Omega_0}}{\left(1 + \frac{8\pi\alpha}{3\Omega_0}\right)} \frac{k_x k_y}{k^2}\right] \qquad (11)$$

The quantity-G_{xy} is the **static polarisability of the solid**, just as - G^0_{xy} is the static polarisability of the unit cell. This gives us the dielectric function at long wave-length which has the Lorentz-Lorentz form

$$\varepsilon(\omega) = \frac{1 + \frac{8\pi}{3\Omega_0}\ \alpha(k,\omega)}{1 - \frac{4\pi}{3\Omega_0}\ \alpha(k,\omega)} \qquad (12)$$

The pole and zero of the dielectric function gives us the transverse and longitudinal charge transfer polarisation waves respectively.

$$\omega_t^2 = \omega_g^2 - \frac{1}{3}\ \Omega_p^2$$

$$\omega_l^2 = \omega_g^2 + \frac{2}{3}\ \Omega_p^2 \qquad (13)$$

B - THE GAP EQUATION

Interaction between two carriers due to the longitudinal charge transfer waves is given by

$$V(q,\omega) = \frac{4\pi e^2}{q^2\ \varepsilon(q,\omega)} \qquad (14)$$

Where $\varepsilon(q,\omega)$ is the dielectric constant as shown in fig (2), for a finite value of ω_t.

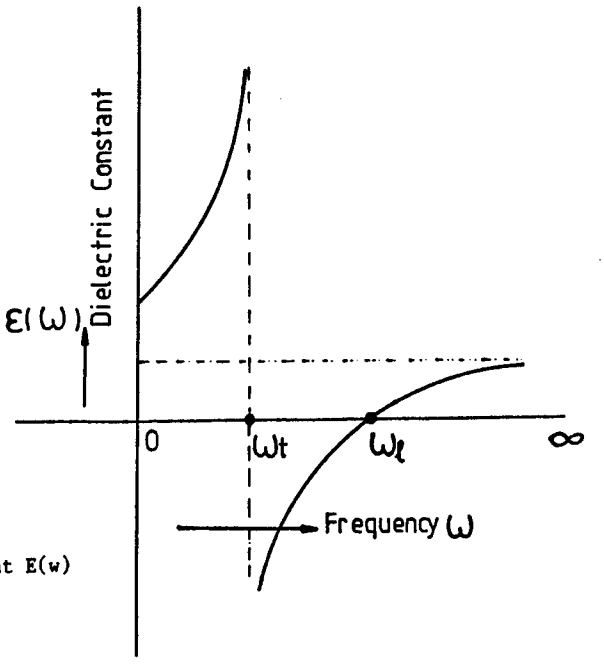


Fig. (2) - Long wave length dielectric constant E(w)

We see immediately **that excitations up to $\omega = \omega_t$ has repulsive interactions** between two carriers and is attractive between ω_t and ω_l. A **B.C.S. like gap nonetheless appears at the Fermi Surface.** The gap equation is given by

$$\Delta(\xi) = - \int_0^{\infty} \frac{K(\xi, \xi')}{\sqrt{\Delta^2(\xi') + \xi'^2}} \tanh \left[\frac{\sqrt{\Delta^2(\xi') + \xi'^2}}{2kT} \right] d\xi' \qquad (15)$$

We can mimic the repulsive interaction at frequencies $0 < \omega < \omega_t$ and an attractive interaction between $\omega_t < \omega < \omega_l$, by two **piecewise constant Kernels**

$$\begin{aligned} k(\xi,\xi') &= \lambda_1 && 0 < \xi,\xi' < \omega_1 \\ &= -\lambda_2 && \omega_1 < \xi,\xi' < \omega_2 \end{aligned} \qquad (16)$$

We also assume two energy gaps

$$\begin{aligned} \Delta(\xi) &= \Delta_1 && 0 < \xi < \omega_1 \\ &= \Delta_2 && \omega_1 < \xi < \omega_2 \end{aligned} \qquad (17)$$

The gap equation is easily solved to give these two gaps Δ_1 and Δ_2.

We have $$kT_c = 1.14\ \omega_1 \exp - \frac{1}{\tilde{\lambda}} \qquad (17a)$$

where $$\frac{1}{\tilde{\lambda}} = \frac{\lambda_2 g - 1}{D}$$

With $$g = \ln \frac{\omega_2}{\omega_1}$$

and $$D = \lambda_1 - \lambda_2^2 g$$

For $\frac{\omega_2}{\omega_1} = 6$, $\lambda_1 = 0.5$, $\frac{\lambda_2}{\lambda_1} = 0.76$ and $\hbar\omega_1 = 0.5$ eV, we obtain a $T_c \sim 300°$ k.

The same formalism will apply for optical phonons. Using $\hbar\omega_1 = 0.1$ eV, $\frac{\omega_2}{\omega_1} = 2.25$ (corresponding to $\frac{\varepsilon_0}{\varepsilon_\infty} = 5$), $\lambda_1 = 0.3$, $\lambda_2 = 0.7$ gives a $\tilde{\lambda} = 0.6$ and a zero temperature gap $\Delta_1 = 36$ m eV. We thus see that a dipole lattice or a **Lorentz lattice in general** can give rise to a B.C.S. kind of pairing and an energy gap at the Fermi surface, inspite of a net repulsive interaction in the small frequency range, and the most general solution admits at least more than one energy gap ($\Delta_2 > \Delta_1$).

C - DIELETRIC POLARONS AND BIPOLARONS

The interaction of the carriers with the longitudianl polarisation field gives rise to polarons (Feynmann [7]). Will it give rise to bipolarons ? The literature is quite scarce on the subject. While the answer is quite affirmative with the acoustic bipolarons, it seems to be less so with its optical counterpart. Early [8] calculations seemed to indicate that for a favorable range of the dielectric constant ratios ($\frac{\varepsilon_0}{\varepsilon_\infty} \sim$ 10 - 20) we may be able to have a dielectric bipolaron. More recent path [9] integral calculations put this ratio even higher. What is certain [10] is that if the carrier behaves like a localized classical charge (i.e its interaction with polarisation field is recoil less), the phonon-mediated interaction will at best reduce the coulomb repulsion between the two charges form $\frac{e^2}{\varepsilon_\infty r}$ to $\frac{e^2}{\varepsilon_0 r}$ but does not lead to any attraction. We can see from figure 1b, that as the p-type doping is increased, there is an increasing component of low energy excitation ω_g (ω_g going down with ε_F) such that we expect $\omega_t \rightarrow 0$, at some critical doping value x_c, given by equation [13]. With the longitudinal frequency $\omega_l \rightarrow \sqrt{\frac{2}{3}}\,\Omega_p$ and because of the collapse of the Lorentz lattice, we can have the whole frequency range up to ω_l where the dielectric constant is negative. This low frequency attraction will give **instantaneous local interaction** between carriers, giving rise to (fig. 4b) **dielectric bipolarons or bipolaron bubble** (if its energy is embedded in the continuum of 1-particle states). We can model the effective Hamiltonian by

$$H_{eff} = \sum \varepsilon_k C_k^+ C_k - V \sum C_{k\sigma}^+ C_{k'\sigma'}^+ C_{k'\sigma'} C_{k\sigma} \qquad (18)$$

This Hamiltonian is strikingly different form the B.C.S Hamiltonian in not having the ω-cut off and its general behavior pattern has been indicated [11]. In the usual weak-coupling approximation and when the dielectric bipolaron interaction energy $V << \varepsilon_F$, the superconductivity gap equation has been solved [5] to give

$$\Delta = 8\,\varepsilon_F \exp -\frac{\varepsilon_F}{\varepsilon_c} \qquad (19)$$

Where ε_c is an energy cut-off.

It is necessary to recall the essential ingredients leading to the equation (18) signifying an instantaneous attractive interaction V between two carriers.

We can define two key dimensionless parameters in the pairing scenarios.

- The dimensionless coupling constant

$$\lambda = \frac{V}{E_F} \qquad (20a)$$

- Antiadiabaticity parameter

$$\gamma = \frac{\hbar\omega}{E_F} \qquad (20b)$$

Signifying ratio of boson frequency to the Fermi energy.

There are several interesting differences of the electronic properties in the normal state between the adiabatic ($\gamma << 1$) and the antiadiabatic ($\gamma >> 1$) regime. These differences[12] are shown schematically in figure (3a) and (3 b), as well as in fig. (4a) and (4b).

(a) The effective mass ratio $\frac{m^*}{m}$ is exponentially large (Holstein factor) around $\gamma = 1$ ($\lambda < 1$) but is completely unrenormalised in the antiadiabatic limit [5] (fig. 3a).

(b) The electron life time τ at the Fermi surface is quite different in the two regimes. In the adiabatic regime $\frac{1}{\tau} << kT \sim \frac{T^2}{E_F}$, which gives the usual metallic conductivity. In the antiadiabatic regime $\frac{1}{\tau} >> kT$ (fig. 3b) and is conjectured to be $\sim T$, if it behaves as a marginal Fermi liquid [13].

(c) In the adiabatic regime, the usual electron-phonon interaction (fig. 4a) gives the **retarded non local** attraction between electron-pairs. In the antiadiabatic regime the attraction is expected to be instantaneous and local (fig. 4b), forming a real-space electron-pair or a **dielectric bipolaron bubble. The** resulting normal and superconducting properties are bound to be different from the classical B.C.S. behavior.

In the B.C.S. behavior

$$\frac{kT_c}{E_F} = \gamma \exp - \frac{1}{\lambda} \qquad (21a)$$

In the other limit, $\gamma >> 1$

$$\frac{kT_c}{E_F} \doteq \exp - \frac{1}{\lambda} \qquad (21b)$$

In summary, we can say that presence of high frequency bosons ($\hbar\omega > E_F$) will lead to quasiparticules which are dielectric polarons with properties in the normal and superconducting states quite different from usual metals.

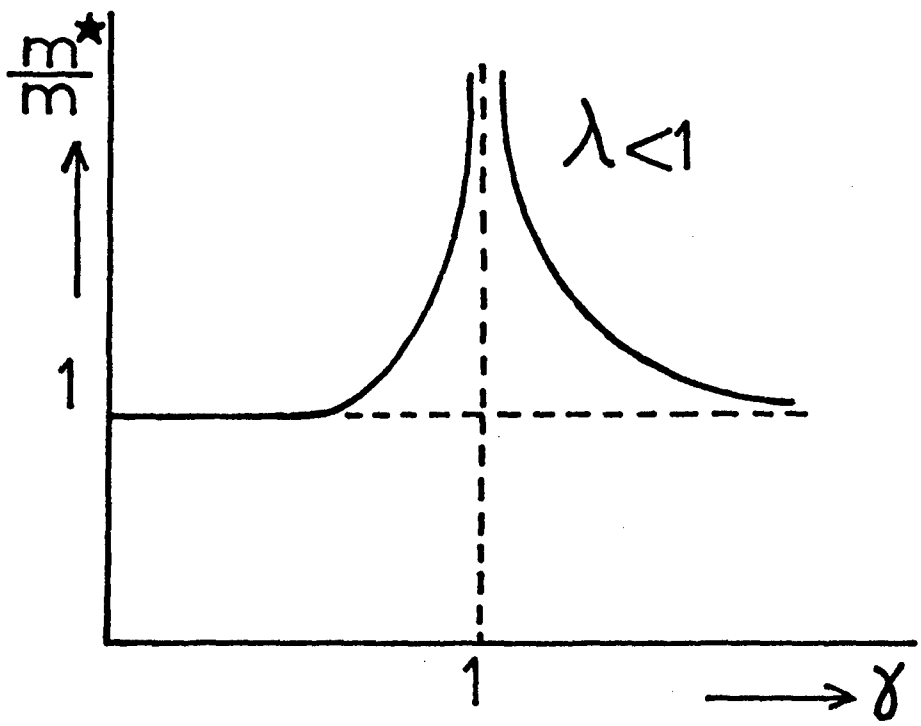


Fig. 3a

Fig. (3a) - Effective mass of carriers as function of $\gamma = \frac{\hbar\omega}{E_F}$ or antiadiabaticity.

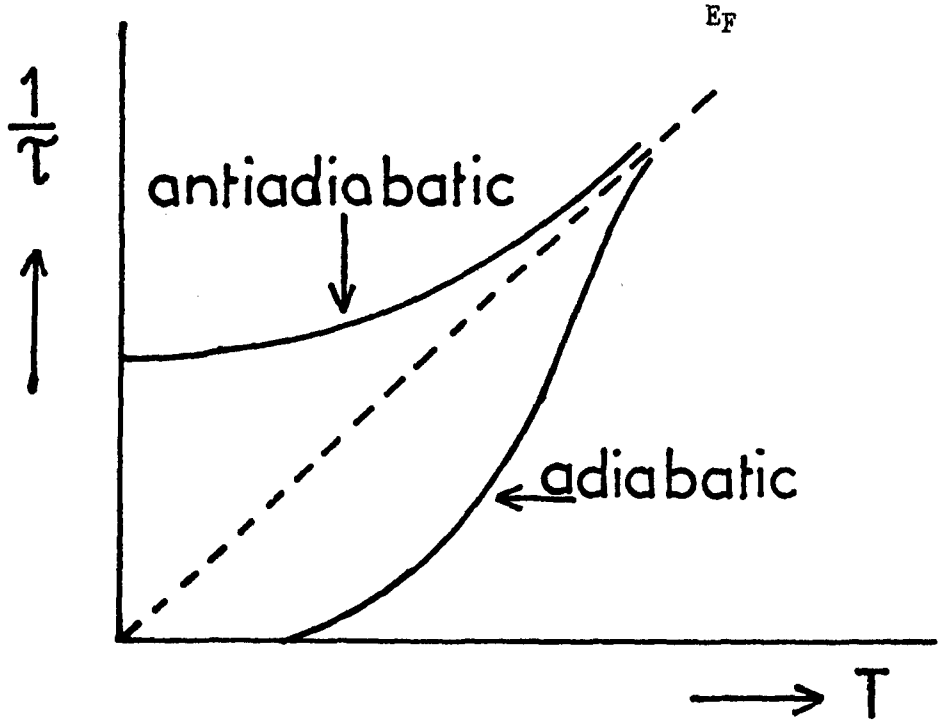


Fig. 3b

Fig. (3b) - A carrier life time τ as function of temperature

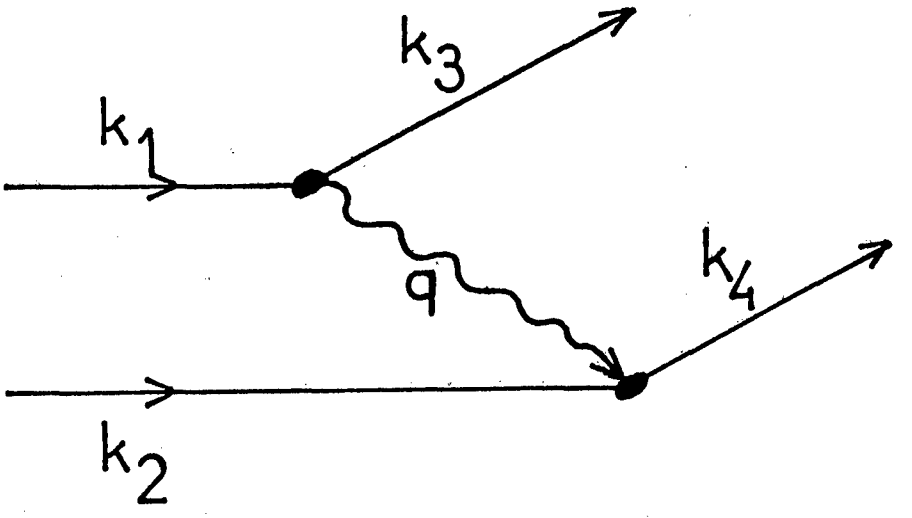


Fig. 4a

Fig. (4a) - Electron-electron interaction in the adiabatic regime

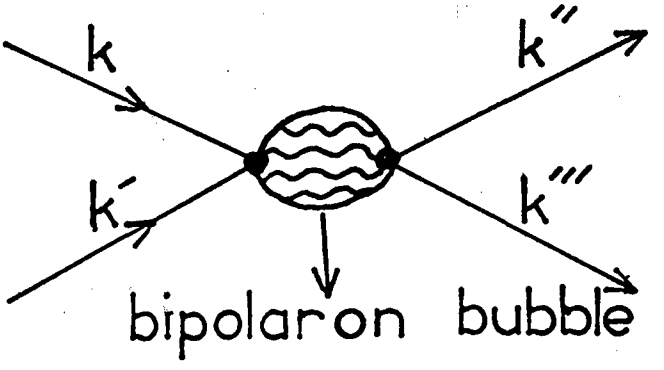


Fig. 4b

Fig. (4b) - Electron-electron interaction in the antiadiabatic regime

REFERENCES

1 - C.M.Varma, S. Schmitt-Rink and E. Abrahams
Sol. St Comm. 62, 681 (1987).

2 - B.K. Chakraverty, D. Feinberg, H. Zheng and M. Avignon
Sol. St Comm. 64, 1147 (1987.

W. Weber, Zeit Physik B 70, 323 (1988)/

J.E. Hirisch and S. Tang, Sol. St. Comm. 69, 987 (1989).

3 - J.J. Hopfield, Phys. Rev. 112, 1555 (1955).

4 - N.W. Aschcroft, "Recent Progress in Many body theories "vol. I Edited by E. Pajanne and R.F. Bishop (Plenum Publishing, N.Y. 1988) p 39.

5 - B.K. Chakraverty, Phys. Rev. B, April 1990.

6 - A. Bianconi et al
"Procceding Adriatico Research Conf. on High Temperature Superconductors"
Trieste Italy 6-8 July 1989
Edited Y. Lu, M. Tosi and E. Tosatti, World Scientific 1988.

7 - R.P. Feynman, Phys. Rev. 97, 660 (1955).

8 - V.L. Vinetskii and M. Sh. Giterman
J. Expt. Theoret. Phys. (USSR) 33, 560 (1958).

V.L. Vinetskii
Soviet Physics JETP, 13, 1023 (1961).

9 - H. Hiramoto and Y. Toyozawa
Jl. Phys. Soc. Jap 54, 245 (1985).

10 - W. Kohn
Phys Rev. 110, 857 (1958).

11 - Ph. Nozières and S. Schmitt-Rink
Jl Low Temp. Phys. 59, 195 (1985).

12 - D. Feinberg, S. Ciuchi and F. de Pasquale
Int. Jl. Modern Phys. B (1990 to be published.
Also
S. Aubry et al
"Workshop "Non-Linear Coherent Structures" Montpellier, France 1989 (Verlag-Springer)

13 - C.M. Varma et al
Phys. Rev. Letter 63, 1996 (1989).

Correlation of Normal and Superconducting Properties and Unified Approach to the Description of High T_c Oxides

V.Z. Kresin* and S.A. Wolf**

*Lawrence Berkeley Laboratory, Berkeley CA 94720
**Naval Research Laboratory, Washington, DC 20375-5000

ABSTRACT

We present a unified approach based on the Fermi liquid picture which allows us to describe the normal as well as the superconducting properties of the doped cuprates.

1. Introduction

The theory presented in this paper is for the doped compounds which are metallic. One can distinguish two interrelated, but nevertheless, different directions in the physics of high T_c [1,2], one involving the problem of carrier doping and the transition to the metallic state and the second being the description of the metallic state. It is important that this metallic phase undergoes the transition into the superconducting state; as a result, our analysis is directly related to the origin of high T_c. We are using a quasi-2D Fermi liquid model to estimate the fundamental parameters of these very interesting materials. We find that this description is able to describe these materials and also that phonons and plasmons play a major role in the mechanism of high T_c.

2. Normal Properties

The most efficient way to analyze the anisotropy and to evaluate the normal parameters is to describe the system in momentum (reciprocal) space; our method is based on the use of Fermiology. The anisotropy of the system is reflected in the topology of the Fermi surface (FS): $\varepsilon(p)=\varepsilon_F$.

Our approach [3] is based on Fermi liquid theory. According to the Fermi liquid theory which has been developed by Landau and describes strongly correlated Fermi systems, the low lying excitation of the system can be classified in the same way as a Fermi gas. It means that such concepts as disper-

sion relation, Fermi surface and Fermi velocity have a direct meaning. We certainly followed this approach in our previous paper [3]. Recent experimental photoemission data on 1:2:3 [4] shows the presence of a sharp Fermi edge. These data present direct experimental support for an approach based on these concepts.

The usual methods for studying the Fermi surface require the sample to be normal at low temperatures, otherwise the intensive thermal motion smears out the relevant signals. An unconventional and explosive technique to produce very large magnetic fields (megagous) has been successfully utilized to demon-strate De Haas-Van Alphen oscillations in grain-aligned crystals of Y-Ba-Cu-O [F. Mueller et al. 1990] [5]. This result unambiguously demonstrates the exis-tence of a Fermi surface in this material.

The La-Sr-Cu-O system has a layered structure, so that the interlayer distance $d_c >> d_a, d_b$. The dispersion relation $\varepsilon(p)$ is highly anisotropic, where $p=\{k, p_z\}$ is a quasi-momentum (k is a 2D momentum); the Z axis has been chosen to be perpendicular to the layers. As a first approximation, one can assume the Fermi surface to be cylindrically shaped which corresponds to neglecting the interlayer transitions. Of course the interlayer transitions lead to small deviations from the cylindrical shape. It is important that we are not assuming the Fermi curve (the Fermi curve is defined as the cross-section of the FS by the plane p_z = constant) to be a circle. It is appears that one can estimate the values of the Fermi energy ε_F and the effective mass m*(its defin-ition see below, Eq.(2)) without specifying the shape of the Fermi curve. In the case of cylindrically shaped FS the dispersion relation is $\varepsilon(k)$ and does not de-pend on p_z. A large anisotropy of the normal conductivity justifies such an approximation. One should note that this approach is applicable to hole as well as to electron carrier types of materials. For example, the hole surfaces at the corners of the first zone can be viewed in the quasi-2D case as a cylinder as can be seen from a simple translation in momentum space. One can derive the following relations [3].

$$m^* = 3\,(h^2/\pi)\,k_B^{-2}\,d_c\,\gamma \qquad (1)$$

$$\varepsilon_F = (\pi^2 k_B^2/3)\,n/\gamma \qquad (2)$$

Here n is the carrier concentration, and γ is the Sommerfeld constant.

Equations (1) and (2) express m* and ε_F in terms of the experimentally measured quantities d_c, n, and γ. These values of m* and ε_F do not depend on any assumption about the shape of the Fermi curve. On the contrary, these values should be taken into account when reconstructing the Fermi surface.

The values of γ and n can be determined from heat capacity data (see e.g. the review 6) and Hall effect measurements. The comparison of the evaluated major normal parameters of the high T_c material and the usual normal metal can be seen in Table I.

TABLE I. Comparison of normal-state properties of conventional metals with $La_{1.8}Sr_{0.2}CuO_4$.

Quantity	Conventional Metals	$La_{1.8}Sr_{0.2}Cu$-O_4
m*	(1-15) m_e	$5m_e$
$k_{F\ (cm^{-1})}$	10^8	3.5×10^7
$v_{F\ (cm\ sec^{-1})}$	(1-2) $\times 10^8$	8×10^6
ε_F (eV)	5-10	0.1

We think that small values of ε_F and v_F along with the anisotropy are key physical properties of the new high T_c oxides.

The cuprates are characterized also by unusual spectra of the collective excitation. Speaking of phonon spectrum, one should stress the existence of low frequency optical nodes and the presence of strong anharmonicily. As a result, one could expect the strong electron-phonon coupling (see below). In addition they contain the quasi-2D low-lying acoustic plasmon branch which has a slope of the same order of magnitude as the Fermi velocity (see e.g.,

Ref. [7]). This small slope of the "electronic sound" makes the branch similar to the usual phonon acoustic branch.

3. Superconducting Parameters

According to our analysis, the Fermi velocity v_F is small relative to the values in conventional metals. For La-Sr-Cu-O (see Table I) $v_F \cong 8 \times 10^6$ c m sec^{-1}. One can see that a such small value along with a large value of T_c leads to a short coherence length. Indeed, if we use the expression $\xi_c = 0.18\, h v_F / k_B T_c$ we obtain $\xi_0 \cong 25$Å.

A small value of the Fermi energy ε_F has also had a strong impact on the superconducting properties. The ratio $\Delta(0)/\varepsilon_F$ in conventional superconductors is small ($\sim 10^{-4}$), whereas in the high T_c oxides ε_F and Δ are comparable ($\Delta(0)/\varepsilon_F \leq 10^{-1}$). A small value of the ratio $\Delta(0)/\varepsilon_F$ means that only a small number of states near the FS are involved in pairing. The picture is different in the oxides. A large value of the ratio corresponds to a situation when a significant fraction of the carriers are paired. This of course means a short coherence length is directly related to the quasi-2D structure of the cuprates. Indeed, in conventional superconductors ($\Delta/\varepsilon_F << 1$) pairing can occur only near the Fermi surface. (Cooper theorem). The states on the Fermi surface form a quasi 2D system in momentum space. This is an important factor because in the 2D case, any attraction leads to the formation of bound states (see e.g. Ref. [8]). The presence of the layered structure makes pairing possible even for states which are distant from the Fermi surface; this corresponds to the picture in the cuprates.

A large value of $\Delta(0)/\varepsilon_F$ leads to an unusual critical behavior near T_c. This has been predicted in Ref. [9] and observed experimentally in Ref. [10]. In addition the observation of a shift in the positron-annihilation lifetime in the high T_c oxides, such as La-Sr-Cu-O, Y-Ba-Cu-O or Tl-Ba-Ca-Cu-O [11] is directly related to the small value of their Fermi energy. The shift $\Delta\tau/\tau$ is equal to [12].

$$\frac{\Delta\tau}{\tau} = \gamma \left(\frac{\Delta}{\varepsilon_F}\right)^2 \ln \frac{\varepsilon_F}{\Delta} \qquad (3)$$

where $\gamma \cong \tau$; in addition $\gamma \sim m^*$. Therefore the sign of the shift is directly related to the sign of the carriers. For conventional superconductors

$(\Delta/\varepsilon_F)^2 \cong 10^{-8}$, whereas for La-Sr-Cu-O $\Delta/\varepsilon_F \cong 10^{-1}$ and this leads to the possibility of observing the shift.

4. Strength of the Coupling

Using heat capacity and neutron spectroscopy data, one can evaluate the strength of the electron phonon coupling: $\lambda = [\gamma(0)/\gamma(T_c)-1]$.

1. Using the data [5], we obtain $\lambda_{\varepsilon-ph} \cong 2.5$ and this means the presence of strong coupling. Nevertheless, based on the expression [13]

$$T_c = \frac{0.25\,\tilde{\Omega}}{[e^{\frac{2}{\lambda^{0.8}}}-1]^{\frac{1}{2}}} \qquad (4)$$

one can conclude that there is a need for an additional mechanism. We think that the additional attraction is mediated by a peculiar acoustic plasmon branch [12] with weak additional coupling λ_{pl}. A small value of λ_{pl} does not mean that the contribution to T_c is also small. In fact, it depends not only on the strength of the coupling but to its corresponding energy scale. A noticeable contribution of plasmons to T_c arises from the large scale of the plasmon energy relative to the phonon energy. This can be seen directly from the equation [3, 7]

$$T_c = T_c^{ph}\left(\frac{\tilde{\omega}_{pl}}{T_c^{ph}}\right)^{\upsilon} \qquad (5)$$

where $\upsilon = \lambda_{pl}\,(\lambda_{ph} + \lambda_{pl})$. Here $T_c{}^{ph}$ is described by eq. (12) and λ_{pl} is the electron-plasmon coupling constant and $\tilde{\omega}_{pl} \approx \langle\omega\rangle_{pl}$.

Therefore, a high T_c is due to a generalized phonon mechanism, that is caused by a strong interaction with phonons and low lying phonon-like plasmon mode ("electronic-sound").

5. Multigap Structure

A multigap structure is caused by the presence of overlapping energy bands; each band is characterized by its own energy gap. Differences in densities of states, pairing interactions, etc. lead to distinct values of the gaps. It should be noted that the overlap of the energy bands is a typical situations for conventional metals including superconductors. Nevertheless, the properties of conventional superconductors have been described accurately by a one-gap model. This is due to their large coherence length ξ_o; namely, the inequality $l << \xi_o$ (l is a mean free path) which holds for most conventional superconductors leads to averaging [17], because of interband scattering and as a result to the applicability of a one-band model. One exception is Nb doped $SrTiO_3$, for which a two gap structure was observed [18].

The situation in the high T_c oxides is entirely different. The coherence length is small and the criterion $l > \xi_o$ can be easily met. As a result there is an unique opportunity to observe the effects due to multigap structure.

One should note that La-Sr-Cu-O has a relatively simple band structure and as a result, its properties can be adequately described by the one band model. The situation is different for Y-Ba-Cu-O and Bi-S-Ca-Cu-O. Note also that the effect of the multigap structure is similar to the effect of an energy gap anisotropy. In both cases we are dealing with a deviation of the Fermi surface from a spherical shape. The multiband structure implies the existence of several sections of the Fermi surface even for a fixed direction in momentum space. This effect is stronger than the usual anisotropy and leads to a larger spread of the values of the energy gaps.

Let us consider two overlapping energy bands. The pairing is described by the order parameters $\Delta_1(\vec{p}, \omega_n)$ and $\Delta_2(\vec{p}, \omega_n)$, where $\vec{p}$ is a quasi-momentum, and $\omega_n = (2n + 1)\pi T$. They are solutions of the following equations in an analytical form:

$$\Delta_i(\vec{p}, \omega_n) Z_i = T \sum_{\omega_{n'}} \sum_{l=1,2} \int d\vec{p}' \, \Gamma_{il}(\vec{p}, \omega_n ; -\vec{p}, -\omega_n ; \vec{p}', \omega_{n'} ; -\vec{p}', -\omega_{n'}) \frac{\Delta(\vec{p}', \omega_{n'})}{\sqrt{\omega_{n'}^2 + \Delta^2(\vec{p}', \omega_{n'})}}$$

$i = \{1, 2\}$.

If we study the usual phonon mechanisms, then $\Gamma_{il} = \lambda_{il} D$, where $D = \Omega^2(q)\,[\Omega^2(q) + (\omega_n - \omega_n)^2]^{-1}$; $\vec{q} = \vec{p}\,' - \vec{p}$ and Ω is the phonon frequency; we assume a summation over all phonon branches. As a result, we obtain the Eliashberg equation generalized for the case of several gaps T_c is described by the expression:

where
$$T_c = 1.14\,\tilde{\Omega}\,\exp\left(-1/\tilde{\lambda}\right) \tag{6}$$

$$\tilde{\lambda} = \frac{1}{2}\left\{\lambda_{11} + \lambda_{22} + \left[(\lambda_{22} - \lambda_{11})^2 + 4\lambda_{12}\lambda_{21}\right]^{1/2}\right\} \tag{7}$$

Note also that usually $p_{F1} \neq p_{F2}$, and as a result, one can neglect interband pairing.

6. The Ratios $\varepsilon_i(0)/T_c$

Let us now evaluate the ratio $\varepsilon_1(0)/T_c$ and $\varepsilon_2(0)/T_c$ in a two-gap model. This problem is of definite interest, because these ratios can be determined experimentally. As is well known, the ratio $\varepsilon(0)/T_c$ in a one-gap theory allows one to determine the strength of the coupling.

In the two-band case we have three independent coupling constants (λ_{11}, λ_{22}, λ_{12} ; $\lambda_{21} = \lambda_{12}\,\nu_1/\nu_2$). That's why the correspondence between $\varepsilon_i(0)/T_c$ and λ_{il} is not simple and must be treated carefully one can formulate the following theorem: one of the gaps in a two-gap system is always smaller than the BCS value ($\Delta(0) = 1.76\ T_c$), whereas the other gap is larger. Note that

$$\frac{\Delta_1}{\Delta_2}\Big|_{T_c} = \frac{\Delta_1(0)}{\Delta_2(0)}$$ as has already been shown [16].

Assume for concreteness that $\tau < 1$ ($\varepsilon_1 > \varepsilon_2$). Then

$$(2\varepsilon_1/T_c) > a_{BCS};\ (2\varepsilon_2/Tc) < a_{BCS} \tag{8}$$

Note that the value $2\varepsilon_1/T_c$ exceeds a_{BCS}, but such behavior does not mean strong coupling, as in the one-band case (see Eq. (8)). This deviation from the BCS value is caused by the presence of a multigap structure.

Consider the following example: $\lambda_{11}>>\lambda_{12}, \lambda_{21}; \lambda_{22} = 0$. This means that the superconducting state of the second band is due to the interband transitions only. This model is realistic for cuprates (see below). In this case we obtain:

$$\tau \equiv \lambda_{21}/\lambda_{11} << 1 \qquad (9)$$

Therefore, the ratio Δ_2/Δ_1 is small;. This means (see Eq. (14)) that the values of the energy gaps may noticeably differ from each other.
In the strong coupling limit

$$\tau = \frac{\varepsilon_2(0)}{\varepsilon_1(0)} \cong \frac{\lambda_{21}(1+\lambda_{11})}{\lambda_{11}} \qquad (10)$$

In a weak coupling approximation $\lambda_{11} << 1$ and we obtain the expression (9).

The presence of strong coupling leads to the factor $1 + \lambda_{11}$. This factor is important if we are interested in the relative value of the energy gaps. For example, if $\lambda_{11} = 1.5$ and $\lambda_{21} = 0.3$, then the weak coupling approximation (see Eq. (17)) leads to the value $\tau = 0.2$, whereas the correct value obtained with consideration of the strong coupling effects (see Eq. (10)) is $\tau = 0.5$. The strong coupling tends to decrease the relative difference in the values of the energy gaps in order to observe the multigap structure one should meet the criterion $1>\xi_0$. The cuprates are characterized by short coherence length and as a result it is perfectly realistic to observe a multigap structure in the high T_c oxides. Of course, this possibility implies the overlap of different energy bands. Such a situation is realized in Y-Ba-Cu-O system and probably in the Bi-S-Ca-Cu-O. As for the La-Sr-Cu-O compound it is characterized by a relatively simple band structure (see e.g. the review [19]), and its properties can be described by a one- gap model. The weak temperature dependence of the Hall coefficient (see Ref.[20]) is a manifestation of such a structure. A detailed description of this system is given in our paper [4].

The situation with Y-Ba-Cu-O is entirely different and it is connected with presence of the chain structure. As a result, we have two different energy bands; they have a quasi-2D and a quasi-1D nature. The presence of such a two-band picture is manifested in a strong temperature dependence of the Hall effect and it is supported by the band structure calculations [19] The Fermi surface in this system consists of a cylindrical piece and two planar pieces as we have described previously [3].

As a result, one should observe two energy gaps in the Y-Ba-Cu-O superconductor. There were several experimental papers indicating the presence of the two-gap structure. The most convincing evidence comes from NMR experiments [20, 21].

A more recent detailed investigation carried out in [21] and describing the temperature dependence of the Knight shift clearly demonstrated the presence of two energy gaps. Therefore, the Y-Ba-Cu-O compound is characterized by two superconducting subsystems, two different bands with different energy gaps. The authors [21] can definitely distinguish the presence of two gaps; as for their numerical values, there are some experimental uncertainties. For the smaller gap Δ_{ch}/T_c is of the order of 3.5. The value of Δ_{pl}, according to [21] lies between 4 T_c and 6 T_c.

7. The Parameters of $Y_1Ba_2Cu_3O_7$

In our papers [3, 4]we evaluated the major normal and superconducting parameters of the La-Sr-Cu-O system. Based on the two band model, one can estimate the parameters of Y-Ba-Cu-O.

According to heat capacity data the Sommerfeld constant for Y-Ba-Cu-O is equal to $\gamma \cong 16$ mJ/mole K^2. In the presence of two bands $\gamma = \gamma_{pl} + \gamma_{ch}$. The Fermi surface for Y-Ba-Cu-O compound consists of two parts: a cylindrical part and a set of planes. The cylindrical part, which corresponds to the quasi-2D band (planes) is similar to the quasi-2D band of La-Sr-Cu-O. Based on the relation [3] : $\gamma = (\pi/3\ h^2)\ k_B^2\ m^* d_c^{-1}$ and assuming that the value of the effective mass m^* of the carriers in the planes is the same as for La-Sr-Cu-O ($m^* \cong 5\ m_e$) we obtain $\gamma_{pl} \cong 0.04$ mJ/cm^3 K^2. Correspondingly $\gamma_{ch} \cong 0.15$ mJ/cm^3 K^2. Assuming also that the hole concentration is similar to that in the $La_{1.85}Sr_{0.15}CuO_4$ compound ($n_h \cong 3 \times 10^{21}$cm^3) we obtain $k_{F;pl} \cong (2\pi\ nd_c)^{1/2} \cong 4.7 \times 10^7$ cm^{-1} and $v_{F;pl} \cong 10^7$cm/s^{-1}. The Fermi energy appears to be equal to $E_F \cong 0.2$ eV in accordance with a previous calculation by G.

Deutscher and the present authors using a different method[3]. It is remarkable that the photoemission data [4] also gives the same value for the Fermi energy.

A small value of the Fermi energy is a very important feature of the cuprates [3, 21].

Using the values of the parameters obtained above, one can estimate the value of the in-plane coherence length $\xi_{pl} = hv_F/\pi\ \Delta(0)$, and we obtain $\xi_{pl} \cong 10$ Å.

Let us consider the carriers in the quasi-1D band (chains). Using the value of γ obtained above, one can evaluate the Fermi velocity (see [3]) and we obtain $v_{F;ch} \cong 5 \times 10^6$ cm s^{-1}. This leads to a very small value of the coherence length $\xi_{ch} \cong 7$Å. The carrier concentration, n_{ch}, is unknown. In the presence of two bands the Hall effect depends strongly on temperature and it cannot be used to determine n directly. It is probable that $m^*_{ch} >> m^*_{pl}$; e.g. if $n_{ch} \cong n_{pl} \cong 3 \times 10^{21}$, we obtain $m^*_{ch} \cong 25\ m_e$.

The nature of the carriers on the chains is a very interesting question. This question can be answered by analyzing the positron annihilation data. According to [11] the shift in the positron annihilation lifetime $\delta\tau \sim m^*$. Therefore the sign of the shift is directly related to the sign of m*. For La-Sr-Cu-O the positron comes to rest near the planes and in Y-Ba-Cu-O the positron comes to rest near the chains [11]. The shifts in the lifetime have opposite signs [11] and we know that the carriers in the Cu-O planes in La-Sr-Cu-O are holes therefore, we are dealing with n-type of conductivity in the chain structure.

8. Conclusion.

We described the unified approach in the theory of high T_c based on strong correlation of normal and superconducting properties. The main results can be summarized as follows:

1. Small values of ε_F and v_F along with high anisotropy are key properties of the oxides.

2. The calculated value of the coherence length (Sec. III.2) appears to be small. A small value of ε_F leads to a peculiar picture of the pairing when a significant part of the carriers are paired. The quasi-2D nature of the system is favorable for the pairing.

3. The small value of ξ_0 leads to a unique opportunity to observe the multigap structure.

4. The materials are characterized by strong electron-phonon coupling. However, the coupling is not strong enough to provide such a high T_c. There is a need for an additional attraction, such as a plasmon mechanism.

We think that small values of ε_F and v_F along with the anisotropy are key physical properties of the new high T_c oxides. The cuprates are characterized also by unusual spectra of the collective excitation. Speaking of phonon spectrum one should stress the existence of low frequency optical modes and the presence of strong anharmonicity. As a result, one should expect the strong electron-phonon coupling (see below). In addition, these materials contain a quasi-2D low lying acoustic plasmon branch which has a slope of the same order of magnitude as the Fermi velocity (see, e.g., Refs7). This small slope of the "electronic-sound" makes the branch similar to the usual phonon acoustic branch.

References

1. J. Bednorz and K. Muller, Z Phys., B 64, 189 (1986).

2. M. Wu et al., Phys. Rev. Lett. 58, 908 (1987); H. Maeda et al., J. Appl. Phys. Lett. 27, 1209 (1989)' Z. Sheng and A. Herman, Nature 332, 138 (1988).

3. V.Z. Kresin and S.A. Wolf, Solid State Commun. 63, 1141 (1987); Novel Superconductivity, Ref., 3, p. 287; J. Superconductivity 1, 143, (1988); Physica C 158, 76 (1989); Phys. Rev. B 41, 4278 (1990).

4. Y.A. Arko et. al. Phys. Rev. B 40, 2268 (19879).

5. F. Mueller et al. Bull. Am. Phys. Soc. 35, 4550 (19). Preprint.

6. R. Fisher et al., J of Superconductivity 1, 231 (1988).

7. V. Kresin and H. Morawitz, Phys. Rev. B37, 7584 (1988), J. of Superconductivity 1, 108 (1988), Phys. Lett A (to be published).

8. L. Landau and E. Lifshitz, Quantum Mechanics (Pergamon, Oxford, 1977) p. 163.

9. G. Deutscher, Novel of Superconductivity, Ref., 3, p. 293, Physica C 153 - 155, 15 (1988).

10. S. Inderhees et al., Phys. Rev. Lett. 60, 1178 (1988); R. Fisher et. al., Physics 153 - 155C 1092 (1988); A. Voronel, ibid 153-155C, 1086 (1988).

11. Y. Jean et al., Phys. Rev. Lett. 60, 1069, (1988); preprint.

12. V. Kresin, H. Morawitz, J. of Superconductivity (to be published).

13. V.Z. Kresin, Phys. Lett. A 122. 434 (1987).

14. H. Suhl, B. Mattias and L. Walker, Phys. Rev. Lett., 3, 552 (1959).

15. V. Moskalenko, Fizika Metal Metalloved, 8, 503 (1959).

16. B. Geilikman, V. Kresin, Kinetic and Non Stationary Phenomena in Superconductors, Wiley, NY (1974); V. Kresin, J. Low Temp. Phys. 11, 519 (1973).

17. P. Anderson, J. Phys. Chem. Sol. 11, 26 (1959).

18. G. Binnig et. al., Phys. Rev. Lett. 45, 1352 (1980); we are grateful to Don Ginsberg for bringing this paper to our attention.

19. W. Pickett, Rev. Mod. Phys., 61, 433 (1989).

20. W. Warren et al., Phys. Rev. Lett. 59, 1860 (1987).

21. S. Barrett et. al., Phys. Rev. Lett 59, 1860 (1987).

22. V. Kresin, G. Deutcher, and S.A. Wolf, J. of Superconductivity, 1, 327 (1988).

Electronic Structure Fermi Liquid Theory of High T_c Superconductors; Comparison of Predictions with Experiments

Jaejun Yu and **A.J. Freeman**
Department of Physics and Astronomy and Materials Research Center
Northwestern University, Evanston, IL 60208-3112

Abstract

Predictions of local density functional (LDF) calculations of the electronic structure and transport properties of high T_c superconductors are presented. As evidenced by the excellent agreement with both photoemission and positron annihilation experiments, a Fermi liquid nature of the 'normal' state of the high T_c superconductors become clear for the metallic phase of these oxides. In addition, LDF predictions on the normal state transport properties are qualitatively in agreement with experiments on single crystals. It is emphasized that the signs of the Hall coefficients for the high T_c superconductors are not consistent with the types of dopants (e.g., electron-doped or hole-doped) but are determined by the topology of the Fermi surfaces obtained from the LDF calculations.

INTRODUCTION

The most exciting issues in the microscopic theory of high T_c superconductivity are embodied in the questions: "What are the mechanisms of high T_c ?" and "What is the nature of the normal state of the Cu-oxide superconductors ?" A major issue is the understanding of the normal state of these systems, and, in particular, how well a Fermi liquid picture —in which for instance the quasiparticle energy band structure is approximated by the eigenvalues obtained within the local density approximation (LDA)— works in describing their normal state properties.

For years, there has been controversy and confusion among theorists as well as experimentalists on whether the 'normal' state of the Cu-oxide superconductors is a Fermi liquid or some other exotic ground state. Recently, however, some experimentalists (including Arko *et al.*[1]) are clarifying the nature of the normal state of the high T_c superconductors, surmounting the experimental difficulties in producing clean, well characterized surfaces so as to obtain meaningful high-resolution angle-resolved photoemission data. Their results agree with earlier positron-annihilation experiments[2]. Hence it has become apparent that, while the antiferromagnetic properties of the parent insulating compounds are not accounted for by present implementations of the local spin density approximation[3], the properties of these materials in the metallic region are well described by LDA band theory — as evidenced by the agreement between predictions of theory with both photoemission and positron annihilation experiments.

Recently, for $Nd_{2-x}Ce_xCuO_4$ systems, we obtained a positive Hall coefficient for the magnetic field oriented perpendicular to the Cu-O planes. This is to be compared with a negative experimental value found for $x < 0.18$ and recent experiments which show a change of sign of this Hall coefficient (from negative to positive with increasing x) for $x = 0.18$. Moreover, the measured Hall coefficient for the non-Cu based $Ba_{1-x}K_xBiO_3$ system was found to be negative, which agrees with our energy band results[4]. In addition, LDA predictions on the normal state transport properties for $La_{2-x}Sr_xCuO_4$ and $YBa_2Cu_3O_7$ by Allen

et al.[5] These results on Hall coefficients indicate a trend (previously found for $La_{2-x}Sr_xCuO_4$) toward a regime where the conventional band theoretical description come into better agreement with experiment.

In this paper, we present the results of the local density functional calculations of the electronic structure and transport properties of high T_c superconductors and compare them with recent experiments. A Fermi liquid picture of the 'normal' metallic state of the high T_c superconductors is established through a detailed comparison of high-resolution angle-resolved photoemission spectra with our predictions of energy band dispersions and Fermi surfaces. In addition, we report a band theory based calculation of the Hall coefficients for cubic perovskite $Ba_{1-x}K_xBaO_3$ and for $Nd_{2-x}Ce_xCuO_4$ following those of Allen *et al.*[5] for the transport properties of $La_{2-x}Sr_xCuO_4$ and $YBa_2Cu_3O_7$. The LDA predictions of the normal state transport properties are qualitatively in agreement with experiments on single crystals. Particularly it is emphasized that the signs of the Hall coefficients for the high T_c superconductors are not consistent with the types of dopants (e.g., electron-doped or hole-doped) but are determined by the topology of the Fermi surfaces.

LDA BAND STRUCTURE

For the electronic structure calculations, we used the highly precise full-potential linearized augmented plane wave (FLAPW) method [6] within the local density approximation (LDA) and the Hedin-Lundqvist form for the exchange-correlation potential. In the FLAPW approach no shape approximations are made to either the charge density or the potential. Results obtained on the high T_c Cu-oxides we studied — La_2CuO_4, $YBa_2Cu_3O_{7-\delta}$, $Bi_2Sr_2CaCu_2O_8$, $Tl_2Ba_2CaCu_2O_8$ and $Tl_2Ba_2Ca_2Cu_3O_{10}$ — indicate a number of common chemical and physical features, especially the role of intercalated layers such as the CuO chains, Bi_2O_2 and Tl_2O_2 rock-salt type layers. In the following, we provide a brief summary of the results on the electronic structure of $YBa_2Cu_3O_7$ as an illustrative example, compare them with experiments, and discuss its implication on the nature of the normal ground state of the high T_c Cu-oxides.

The calculated band structure[7, 8] of stoichiometric $YBa_2Cu_3O_7$ along high symmetry directions in the bottom ($k_z = 0$) plane of the orthorhombic Brillouin zone is shown in Fig. 1. As seen, a remarkably simple band structure near E_F emerges from this complex set of 36 Cu-O hybrid bands. Four bands — two each

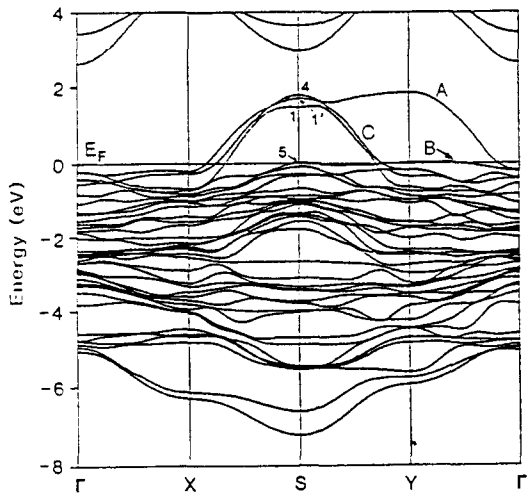


Figure 1: Band Structure of $YBa_2Cu_3O_7$ along symmetry directions in the $k_z = 0$ plane of the orthorhombic Brillouin zone

consisting of Cu(2) d - O(2) p - O(3) p orbitals and Cu(1) d - O(1) p - O(4) p orbitals — cross E_F. Two strongly dispersed bands labelled C ($S_{1'}$ and S_4 in Fig. 1; the labels are given by their character at S) consist of Cu(2) $d_{x^2-y^2}$ - O(2) p_x - O(3) p_y combinations and have the 2D character, which is also common in other high T_c Cu-oxide systems. Significantly, the Cu(1) $d_{z^2-y^2}$ - O(1) p_y - O(4) p_z anti-bonding band labelled A (S_1 in Fig. 1) shows the (large) 1D dispersion expected from the Cu(1)-O(1)-Cu(1) linear chains but is almost entirely unoccupied. This band is in sharp contrast to the π anti-bonding band labelled B (formed form the Cu(1) d_{zy} - O(1) p_z - O(4) p_y orbitals) which is almost entirely occupied in the stoichiometric ($\delta = 0$) compound.

In Fig. 2, our predicted Fermi surfaces (FS) of $YBa_2Cu_3O_7$ determined from our band structure are compared with experimental Fermi surfaces determined by high-resolution angle-resolved photoemission (ARPES) experiments by Campuzano *et al.*[9]. Filled circles indicate the points at which bands are found to cross the Fermi level. The open circles are the points in the Brillouin zone at which bands crossing E_F are not detected. (The size of the circles represents the experimental uncertainty in momentum.) The dashed lines are the predicted FS in Ref. [8]. Two 2D Cu-O $dp\sigma$ bands yield two rounded square FS's centered around S. It is remarkable that these 2D FS's have strong nesting features along the (100) and (010) directions, which are commonly found in other high T_c Cu-oxides except for the case of La-Sr-Cu-O. In addition, the 1D elec-

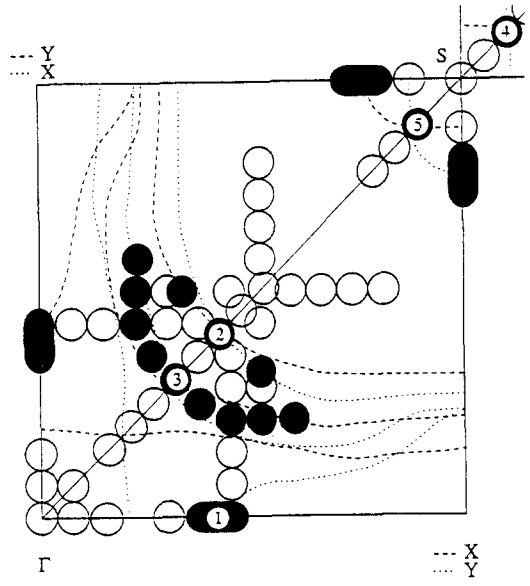


Figure 2: Comparison of the calculated Fermi surfaces with the experimentally determined Fermi surfaces of $YBa_2Cu_3O_7$. See the text for details. (This figure is taken from the paper by Campuzano *et al.*[9])

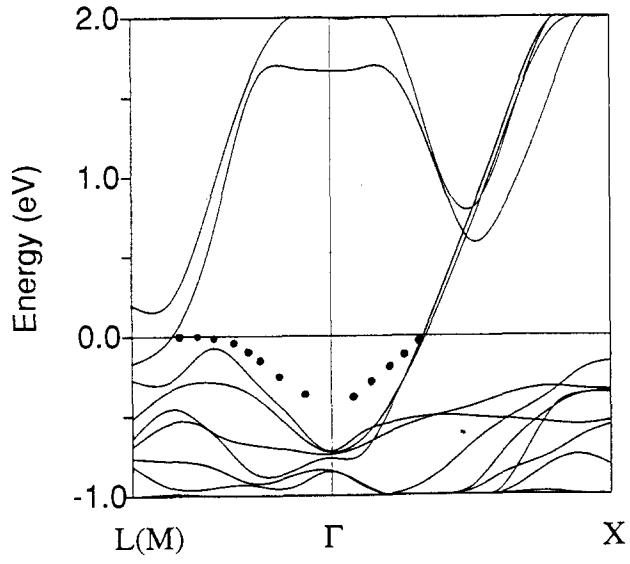


Figure 3: Comparison of the calculated energy bands with the measured bands in the ARPES experiments for $Bi_2Sr_2CaCu_2O_8$.

tronic structure also gives a 1D FS with again strong nesting features along the (010) direction. There are additional hole pockets around S(R) which come from the flat $dp\pi$ bands (band **B**) at E_F. In general, there is a remarkable agreement between the ARPES measurement of FS and our theoretical predictions on the FS of $YBa_2Cu_3O_7$. All of the predicted FS are observed in the experiment. Furthermore, there is also good agreement between the FS measured in the ARPES experiment and the FS obtained by positron annihilation experiment by Smedskjaer *et al.*[2]. These results demonstrate that the observed Fermi surfaces in $YBa_2Cu_3O_7$ are in agreement with LDA band calculations and consistent with the Luttinger theorem, where the large FS volume, which should be unaffected by the interaction, indicates the Fermi liquid nature of the normal ground state of these high T_c superconductors. It is important to note that the confirmation of the FS results has significant impact on several theories, which deny the Fermi liquid nature of the normal ground state in the Cu-oxide superconductors.

Another detailed ARPES study has been carried out on the $Bi_2Sr_2CaCu_2O_8$ system by Olson *et al.*[10] and leads to a good agreement with the LDA calculated band dispersions and Fermi surfaces. Fig. 3 shows a comparison of the calculated energy bands with the observed bands by Olson *et al.*[10]. (Filled circles in Fig 3 represent the observed band dispersions.) The agreement on the FS dimension between the experiment and the LDA band calculations is good, as also expected from the case of $YBa_2Cu_3O_7$. The observed band dispersions along major symmetry lines are large and indicate an enhanced effective mass, which may come from the renormalization effects due to electron-phonon interactions or Coulomb correlations.

The existence of Fermi surfaces and the large band dispersions observed in $YBa_2Cu_3O_7$ and $Bi_2Sr_2CaCu_2O_8$ together with such good agreement between LDA band theory and experiment strongly supports a Fermi liquid description of these high T_c superconductors.

NORMAL STATE TRANSPORT PROPERTIES

Normal state transport properties are of course an important test of the band theory of high T_c superconductors. The calculations based on the band theory have previously been performed for $La_{2-x}M_xCuO_4$ and $YBa_2Cu_3O_7$ by Allen *et al.*[5], and gave important results; these included a prediction of a change of sign in the current carriers at $x \approx 0.24$ for La-M-Cu-O, and the positive and negative signs for the Hall coefficients in $YBa_2Cu_3O_7$ when the magnetic field is aligned parallel and perpendicular to the c-axis, respectively. The

latter prediction has been confirmed by single crystal experiments[22], while the actual x value at which R_H changes sign is larger ($x \approx 0.3$) in experiments[11] on La-M-Cu-O.

An interesting test system for theory is the Ba-K-Bi-O system, for which it is a matter of discussion whether the conventional electron-phonon mechanism produces superconductivity, or if a different mechanism, possibly common to the cuprates, is necessary. In any event, if the K substitution into the insulating parent compound $BaBiO_3$ were regarded as hole-doping (i.e., if $Ba_{1-x}K_xBiO_3$ were a hole-doped superconductor), one would expect a positive Hall coefficient for the positive current carriers in $Ba_{1-x}K_xBaO_3$. Instead, the measured Hall coefficient (R_H) for the $Ba_{1-x}K_xBaO_3$ system was found to be negative[12, 13], which is in agreement with the calculated electron-like Fermi surface of this system[14] as shown in Fig. 4.

Another system obtained by electron doping of the parent compound, Nd_2CuO_4, is the recently discovered Nd-Ce-Cu-O superconductor[15]. In contrast to the case of $Ba_{1-x}K_xBiO_3$, if the Ce substitution into the insulating compound Nd_2CuO_4 were regarded as electron-doping, one would expect a negative Hall coefficient for the negative current carriers in $Nd_{2-x}Ce_xCuO_4$. There are, however, only few uncertain experiments available to date.

We present results in Tables 1 and 2 of a band theory based calculation of the Hall coefficients for cubic perovskite $Ba_{1-x}K_xBaO_3$ and for $Nd_{2-x}Ce_xCuO_4$ together with those of Allen *et al.*[5] for $La_{2-x}Sr_xCuO_4$ and $YBa_2Cu_3O_7$. Our approach is based on the Bloch-Boltzmann theory, and rests on the Midgal approximation, where the sign of the Hall coefficients is mainly determined by the curvature of FS, i.e., the FS topology. Thus, one expects to have a positive R_H from the hole-like FS and a negative R_H from the electron-like FS, while the open FS can give rise to either positive or negative R_H depending on details of the FS geometry.

The Hall coefficient of the $Ba_{1-x}K_xBaO_3$ system in its cubic perovskite structure, as a function of K concentration, was calculated[4] within a rigid-band model (which was shown to be a good approximation for this system by a supercell calculation[16]). Our results are expected to reflect the experimental situation only in the region $x > 0.25$, since, as is well known, pure $BaBiO_3$ is an insulator and its structure has a monoclinic distortion. In the metallic region, the Hall coefficient is seen to be negative, and varies substantially with x. A negative sign of the Hall coefficient for $x > 0$ is, of course, expected from the electron-like Fermi surface of this system[14], as shown in Fig. 4.

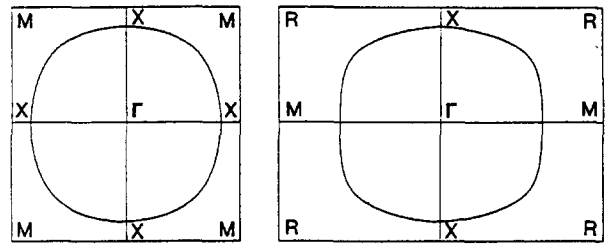


Figure 4: Fermi surface of $Ba_{1-x}K_xBiO_3$ ($x = 0.29$) within a rigid band model.

Experimentally, Sato *et al.*[12] measured a negative Hall coefficient in a single crystal, for $x \sim 0.39$ The measured R_H value ranges around $-4 \times 10^{-4}cm^3C^{-1}$ and with a weak temperature dependence. The sign of the measured R_H is in perfect agreement with our calculated electron-like FS, although the magnitude of the calculated R_H is larger than the measured R_H by a factor of ~ 2. Note, however, that this kind of disagreement in the magnitude of R_H between theory and experiment is not new. For instance, the calculations of Beaulac and Allen[17] showed that a factor of ~ 2 between theory and experiment exists for pure Pd if an isotropic scattering assumption is used, and that by contrast the inclusion of a moderate anisotropy gives good agreement with experiment.

The first thing to be pointed out for $Nd_{2-x}Ce_xCuO_4$ is the highly anisotropic nature of its transport properties. This is made apparent by comparison of the Fermi surface (FS) cuts on the basal and top planes of the Brillouin zone[18], plotted in Fig. 5 for x = 0.15. The mid-plane FS (not shown in Fig. 5 for clarity) lies in between those plotted. The striking closeness of these two curves illustrates the nearly vanishing dispersion along k_z of the Cu-O dps band near E_F. This feature is also common[19] to the $Tl_2Ba_2CaCu_2O_8$ system, for which a partial confirmation exists from preliminary positron annihilation measurements of the FS[20]. No such feature is found in $La_{2-x}Sr_xCuO_4$[21].

The calculated Hall coefficients for $Nd_{2-x}Ce_xCuO_4$ as a function of x (in a rigid band scheme) over a range including the superconducting region show, due to tetragonal symmetry, two independent components, $R_{xyz} = R_{yzx} \neq R_{xyz}$. R_{xyz} has a positive sign, as expected from the hole-like two-dimensional projection of the Fermi surface (cf. Fig. 5). On the other hand,

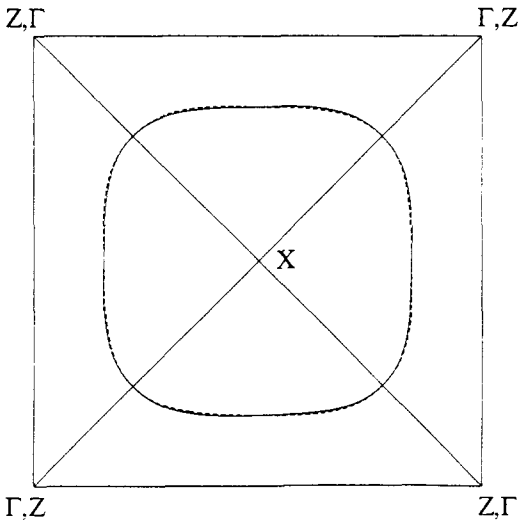


Figure 5: Fermi surface of $Nd_{2-x}Ce_xCuO_4$ ($x = 0.15$) plotted on the basal (solid line) and on the top (dashed line) planes of the Brillouin zone. A rigid band model is used.

this hole-like FS exists in $La_{2-x}M_xCuO_4$ only for a restricted range of $x < 0.24$[5, 21]. This difference relative to the "hole-analog" compound, La-M-Cu-O, is not surprising, since its Fermi surface[21] is quite different from that of $Nd_{2-x}Ce_xCuO_4$, and in particular shows a change of topology with compositions corresponding to the presence of a saddle point singularity in its band structure. The dependence of R_{xyz} on Ce concentration is rather weak.

The two other components ($R_{zxy} = R_{yzx}$) for $Nd_{2-x}Ce_xCuO_4$ are negative, and their magnitudes are comparable to that of R_{xyz}. A negative sign for these Hall coefficients, which correspond to the case of an in-plane magnetic field, is common to all the cuprate superconductors for which such calculations[5] have been performed, and was experimentally verified on single crystals of $YBa_2Cu_3O_7$ by Tozer *et al.*[22]. In fact, the magnetic field applied parallel to the Cu-O plane corresponds to the open topology of the zx-cross section of the Fermi surface.

Only a few experiments are available to date for the Nd-Ce-Cu-O system. In the semiconducting region ($x = 0.12$), single crystal measurements[23] showed a negative Hall coefficient, with a value consistent with the Ce concentration. Measurements on polycrystalline samples by Takagi *et al.*[24] showed that the charge carriers are electrons over a wide range of x values, but a departure from the $R_H \approx 1/n$ behavior was apparent. On the other hand, in the metallic (or superconducting) region ($x > 0.14$), recent measurements on single crystals showed interesting behavior of the Hall coefficients. The measurements by Takagi *et al.*[24] on polycrystalline samples and single crystals (with the magnetic field oriented parallel to the c-axis) showed a negative Hall coefficient but a change of sign (from negative to positive) for $x \approx 0.18$. Furthermore, the Hall coefficients measured by Ong *et al.*[25] are found to be positive for many superconducting samples of $Nd_{2-x}Ce_xCuO_4$ ($x \sim 0.15$).

Actually, this transition from the insulating ($x <\sim 0.14$) region, characterized by a negative Hall coefficient, to the metallic region, in which band structure effects should (according to our calculation) produce a positive R_{xyz} value, needs to be clarified from the theoretical point of view. The fact that experimentally a negative sign persists over the insulating and superconducting range might be due to an inhomogeneous Ce distribution over the sample, resulting in a clear departure of R_{xyz} from $1/n$ behaviour but still keeping a negative value. Further experimental work might clarify the situation.

A brief summary of both theoretical and experimental results on the Hall coefficients is given in Table 1 and 2. Note that the "doped-insulator" picture of high T_c superconductors is in disagreement with the experimental observations. On the other hand, the LDA band theory gives correct predictions on the signs of the Hall coefficients as determined by the FS topologies. For example, although the $Ba_{1-x}K_xBiO_3$ is regarded as "hole-doped", the Hall coefficient is not positive, but negative in agreement with the LDA calculations. Comparing the results of Hall coefficient measurements with the (p-type or n-type) "doped-insulator" picture, we are led to the conclusion that a separation of carriers into positive and negative in the spirit of the effective mass approximation is not possible for these copper oxides.

CONCLUSIONS

The energy band dispersions and Fermi surfaces observed in ARPES experiments are in good agreement with the predictions of LDA band theory. Further, the LDA predictions of the normal state transport properties are qualitatively in agreement with experiments on single crystals. In particular, it is emphasized that the signs of the Hall coefficients for the high T_c superconductors are not consistent with the types of dopants (e.g., electron-doped or hole-doped) but are determined by the local density functional calculations of the topol-

Table 1: Hall coefficients with **H** || **c**

	"doped" carrier	Fermi surface topology	band theory	experiment
$Ba_{1-x}K_xBiO_3$	hole	electron	$-$ [a]	$-$
$Nd_{2-x}Ce_xCuO_4$	electron	hole	$+$ [a]	$+$(?)
$La_{2-x}Sr_xCuO_4$	hole	hole $\rightarrow$ electron	$+ \rightarrow -$ [b]	$+ \rightarrow -$
$YBa_2Cu_3O_7$	hole	hole	$+$ [b]	$+$

[a] Ref. [4]
[b] Ref. [5]

Table 2: Hall coefficients with **H** $\perp$ **c**

	"doped" carrier	Fermi surface topology	band theory	experiment
$Ba_{1-x}K_xBiO_3$	hole	electron	$-$ [a]	$-$
$Nd_{2-x}Ce_xCuO_4$	electron	open	$-$ [a]	(?)
$La_{2-x}Sr_xCuO_4$	hole	open	$-$ [b]	$-$
$YBa_2Cu_3O_7$	hole	open	$-$ [b]	$-$

[a] Ref. [4]
[b] Ref. [5]

ogy of the Fermi surface.

The existence of Fermi surfaces and large band dispersions observed in $YBa_2Cu_3O_7$ and $Bi_2Sr_2CaCu_2O_7$ together with such good agreement between LDA band theory and experiment strongly supports a Fermi liquid description of these high T_c superconductors. As a Fermi liquid (metallic) nature of the 'normal' state of the high T_c superconductors becomes clear, these experimental observations have served to confirm the predictions of our local density functional calculations and hence the energy band approach as a valid natural starting point for further studies of their superconductivity.

ACKNOWLEDGMENTS

We thank S. Massidda, N. Hamada and D.D. Koelling for collaboration on the work reported here. Work supported by the National Science Foundation (through the Northwestern University Materials Research Center, Grant No. DMR88-21571) and by a grant of computer time at the NASA Ames Supercomputing Center and the National Center for Supercomputing Applications, University of Illinois at Urbana-Champaign.

References

[1] R.S. List, A.J. Arko, Z. Fisk, S.-W. Cheong, S.D. Conradson, J.D. Thompson, C.B. Pierce, D.E. Peterson, R.J. Bartlett, N.D. Shinn, J.E. Schirber, B.W. Veal, A.P. Paulikas and J.C. Campuzano, Phys. Rev. B38, 11966 (1988); A.J. Arko, R.S. List, Z. Fisk, S.-W. Cheong, J.D. Thompson, J.A. O'Rourke, C.G. Olson, A.-B. Yang, Tun-Wen Pi, J.E. Schirber and N.D. Shinn, J. Mag. Magn. Matter. 75, L1 (1988).

[2] L. Hoffmann, A.A. Manuel, M. Peter, E. Walker and M.A. Damento, Europhys. Lett. 6, 61 (1988); L.C. Smedskjaer, J.Z. Liu, R. Benedek, D.G. Legnini, D.J. Lam, M.D. Stahulak, H. Claus and A. Bansil, Physica C156, 269 (1988); A. Bansil, R. Pankaluoto, R.S. Rao, P.E. Mijnarends, W. Dlugosz, R. Prasad and L.C. Smedskjaer, Phys. Rev. Lett. 61, 2480 (1989).

[3] W.E. Pickett, Rev. Mod. Phys. 61, 433 (1989).

[4] S. Massidda, N. Hamada, J. Yu and A.J. Freeman, Phys. Rev. B (to appear).

[5] P.B. Allen, W.E. Pickett and H. Krakauer, Phys. Rev. B36, 3926 (1987); P.B. Allen, W.E. Pickett and H. Krakauer, Phys. Rev. B37, 7482 (1987).

[6] H.J.F. Jansen and A.J. Freeman, Phys. Rev. B30, 561 (1984), and references therein.

[7] S. Massidda, J. Yu, A.J. Freeman and D.D. Koelling, Phys. Lett. **122**, 198 (1987)

[8] J. Yu, S. Massidda, A.J. Freeman and D.D. Koelling, Phys. Lett. **122**, 203 (1987)

[9] J.C. Campuzano, G. Jennings, M. Faiz, L. Beaulaigue, B.W. Veal, J.Z. Liu, A.P. Paulikas, K. Vandervoort, H. Claus, R.S. List, A.J. Arko and R.J. Bartlett, Phys. Rev. Lett. **64**, 2308 (1990).

[10] C.G. Olson, R. Liu, D.W. Lynch, B.W. Veal, Y.C. Chang, P.Z. Jiang, J.Z. Liu, A.P. Paulikas, A.J. Arko and R.S. List, Physica C **162-164**, 1697 (1989); C.G. Olson, R. Liu, A.-B. Yang, D.W. Lynch, A.J. Arko, R.S. List, B.W. Veal, Y.C. Chang, P.Z. Jiang and A.P. Paulikas, Science **245**, 731 (1989).

[11] M. Suzuki, Phys. Rev. B39, 2312 (1989); H. Takagi, T. Ido, S. Ishibashi, M. Uota and S. Uchida, Phys. Rev. B40, 2254 (1989).

[12] H. Sato, S. Tajima, H. Takagi and S. Uchida, Nature 338, 241 (1989); H. Sato, S. Tajima, H. Takagi and S. Uchida, Proceedings of 2nd Intl. Conf. on Materials and Mechanisms of Superconductivity: High-Temp. Superconductors (Stanford, 1989).

[13] S. Kondoh, M. Sera, Y. Ando, and M. Sato, Physica C157, 469 (1989).

[14] N. Hamada, S. Massidda, A.J. Freeman and J. Redinger, Phys. Rev. B40, 4442 (1989).

[15] Y. Tokura, H. Takagi and S. Uchida, Nature 337, 345 (1989).

[16] L.F. Mattheiss and D.R. Hamann, Phys. Rev. Lett. 60, 2681 (1988).

[17] T.P. Beaulac and P.B. Allen, J. Phys. F, 13, 383 (1983).

[18] S. Massidda, N. Hamada, J. Yu and A.J. Freeman, Physica C157, 571 (1989).

[19] J. Yu, S. Massidda, and A.J. Freeman, Physica C 152, 273 (1988).

[20] L.C. Smedskjaer, (private communication).

[21] J.-H. Xu, T.J. Watson-Yang, Jaejun Yu and A.J. Freeman, Physics Lett. A120, 489 (1987).

[22] S.W. Tozer, A.W. Kleinsasser, T. Penney, D. Kaiser and F. Holtzberg, Phys. Rev. Lett. 59, 1768 (1987).

[23] Y. Hidaka and M. Suzuki, Nature 338, 635 (1989).

[24] H. Takagi, S. Uchida and Y. Tokura, Phys. Rev. Lett. 62, 1197 (1989); S. Uchida, H. Takogi and Y. Tokura, Proceedings of 2nd Intl. Conf. on Materials and Mechanisms of Superconductivity: High-Temp. Superconductors (Stanford, 1989).

[25] N.P. Ong *et al.*, (preprint).

INCOHERENT VS. COHERENT BEHAVIOR IN THE NORMAL STATE OF COPPER OXIDE SUPERCONDUCTORS +

Zlatko Tesanovic
Department of Physics and Astronomy
The Johns Hopkins University
Baltimore, Maryland 21218

The self-consistent quantum fluctuations around the mean-field Hartree-Fock state of the Hubbard model provide a very good description of the ground state and low-temperature properties of a two-dimensional itinerant antiferrogmagnet.[1,2,3] Very good agreement with numerical calculations and experimental data is obtained by including the one-and two-loop spin wave corrections to various physical quantities. In particular, the destruction of the long-range order above the Neel temperature can be understood as a spontanteous generation of a length-scale ϵ (T), which should be identified as the spin correlation length.[4] For finite doping, the question of the Hartree-Fock starting point becomes a more complex one since an extra hole tends to self-trap in antiferromagnetic background. Such quantum defects in an underlying antiferromagnetic state can be spin-bags[5] or virtex-like sturctures[6] and tend to suppress the long-range order. If motion of the holes occurs on a time-scale shorter than the one associated with the motion of these quantum defects of a spin background, one obtains several important empirical features of the normal state of CuO superconductors like linear T-dependence of resistivity, the cusp in the tunneling density of states, etc.[4] As opposed to a familiar Fermi-liquid behavior the phenomenology of the above system is dominated by a large incoherent piece of a single hole propagator, resulting in many unusual normal state properties.

The work reported here was done in collaboration with A. Singh. The author acknowledges support of the David and Lucile Packard Fellowship.

+ Invited Talk

References:

[1]A. Singh and Zlatko Tesanovic, Phys. Rev. **B41**, 614 (1990).

[2]A. Singh and Zlatko Tesanovic, Phys. Rev. **B** to appear.

[3]A. Singh, Zlatko Tesanovic, H. Tang, G. Xiao, C. L. Chien, and J. C. Walker, Phys. Rev. Lett. **64**, 2571 (1990).

[4]A. Singh and Zlatko Tesanovic, submitted to Phys. Rev. **B**.

[5]J. R. Schrieffer, X-G. Wen, and S.-C. Zhang, Phys. Rev. Lett. **60** 944 (1988).

[6]A. R. Bishop, F. Guinea, P. S. Lomdahl, E. Louis, and J. A. Verges, submitted to Phys. Rev. Lett.

THE ELECTRONIC HAMILTONIAN FOR CUPRATES

James F. Annett
The Pennsylvania State University
University Park, PA

A.K. McMahan
Lawrence Livermore National Laboratory
Livermore, CA

Richard M. Martin
University of Illinois at Urbana-Champaign
Champaign, IL

A realistic many-body Hamiltonian for the cuprate superconductors should include both copper d and oxygen p states, hopping matrix elements between them, and Coulomb energies, both on-site and inter-site. We have developed a novel computational scheme for deriving the relevant parameters *ab initio* from a constrained occupation local density functional. The scheme includes numerical calculation of appropriate Wannier functions for the copper and oxygen states. Explicit parameter values are given for La_2CuO_4. These parameters are generally consistent with other estimates, and with the observed superexchange energy.

Secondly, we address the question: can this complicated multi-band Hamiltonian be reduced to a simpler one with fewer basis states per unit cell? We propose a mapping onto a new two-band effective Hamiltonian with one copper d and one oxygen p derived state per unit cell. This mapping takes into account the large oxygen-oxygen hopping given by the *ab initio* calculations.

Supported in part at Lawrence Livermore National Laboratory by Contract No. W-7405-ENG-48 to the US Department of Energy, and at the University of Illinois by National Science Foundation Grant No. NSF-DMR86-12860.

THE RELATION BETWEEN FERROELASTICITY AND SUPERCONDUCTIVITY

A. Molak and R. Mańka
Silesian University
Institute of Physics
Univovyteche 4, Katoevice, Poland

ABSTRACT

The high-temperature superconductivity is explained widely by the layered crystallic structure. The one- and two-dimensional subsystems and their interaction are investigated in this work. It is assumed that the high-Tc superconductivity takes place in the two-dimensional subsystem [1] and the increase of the phase transition temperature from 60 K up to 90 K is the consequence of turning on the influence of one-dimensional chains. The interaction between the two subsystems is transferred along the c axe by the phonons of breathing mode, what causes the hybridization of the electronic bonds between these subsystems [2].

The experimental works indicate that the existence of both the chains Cu(1)-O [3] and their interaction with the superconducting plane of Cu(2)-O modify the temperature of the transition to the superconducting state. It is seen from the neutron scattering data that the rates of the interatomic distance dependencies on temperature are changed around 240 K and 90 K [4]. The "zig-zag" order in Cu(1)-O chains has been postulated [4], but, on the other hand, the vibrations with a large amplitude only were reported [5].

The bi-stabilized situation of the oxygen ions can be caused by the change of distance between these ions and the Ba ions [4]. It leads to the appearance of a two-well potential [6]. Its parameters depend on temperature and the determine the dynamics of the oxygen ions' movement. They can induce the antipolar order, which can be, however, more or less chaotic.

The investigation of the ferroelastic properties of Y-Ba-Cu-O samples lead to the conclusion that they are related to jumps of ions inside the given chain and not to a diffusion between different sites in the ab plane [7]. We deduce thus that the fluctuating oxygen ions from these chains create dipols in the ab plane. They can be described with the pseudo-spin formalism / - Pauli matrices/. The system can be described with Ising model:

$$H_s' = -\frac{1}{2} J \sum_{ij} \sigma_{3j} \sigma_{3j} \qquad (1)$$

The pseudo-spins interact with phonons and influence the superconductivity in the second subsystem:

$$H_{sI} = \sum_{q} \sum_{i} \gamma_i(q) \sigma_3 \{ b_{q,3} + b_{-q,3} \} \qquad (2)$$

The Ising model in the molecular field approximation / though fully correct in the one-dimensional case/ gives the phase transition for the anti-polar order parameter:

$$\langle \sigma_{3i} \rangle = (-1)^i \eta \neq 0 \tag{3}$$

The effective field conjugated to the pseudo-spin interacts with the ferroelastic order like an external magnetic field with a real spin system:

$$H' = B_z \sigma_3 \tag{4}$$

$$B_z = 2 \xi_o \gamma(o) = A' u \tag{5}$$

where u denotes condensation of phonons of breathing mode /deformation of pyramids/:

$$u = (h/2M)^{1/2} \{ \xi_o + \xi_o^+ \} \tag{6}$$

We obtain the description of the relation between the superconductivity and ferroelasticity in such a way.

References

[1] S. Robaszkoewicz et al., Phys. Rev. B 36 (1987) 180.

[2] R. Mańka, A. Molak, Phys. Lett. A 134 (1989) 497.

[3] M.A. Alario-Franco et al., Physica C156 (1988) 455.

[4] M. Francois et al., Solid State Commun. 66 (1988) 1117.

[5] B. Rupp, Physica C156 (1988) 559.

[6] S.K. Kurtz et al., Ferroelectrics 87 (1988) 29.

[7] H. Schmid et al., Physica C157 (1989) 555.

High Tc Superconductors: The Scaling of Tc with the Number of Bound Holes Associated With Charge Transfer Neutralizing the Multivalence Cations

G. C. Vezzoli, M.F. Chen, and F. Craver
U.S. Army Materials Technology Laboratory
Materials Science Branch, Watertown, Mass

ABSTRACT

It is observed that for the known high-Tc Cu-, Tl-, and Bi-based superconductors, Tc scales consistently with the number of bound holes per unit cell which arise from charge transfer excitations of frequency $\sim 3X10^{13}$ that neutralize the multivalence cations into diamagnetic states. The resulting holes are established on the oxygens. Extrapolation of this empirical fit in the up-temperature direction suggests a Tc of about 220-230K at a value of 25 holes/unit cell (approximately the maximum that can be materials-engineered into a high-Tc K_2MnF_4 or triple Perovskite structure). In the down-temperature direction the extrapolation gives a Tc of about 25K for a normal metal of zero holes. These extrapolations are in accord with experimental data suggesting maximum Tc in the vicinity of 235K for the Y-Ba-Cu-O system as well as the known maximum temperature of 23K for low-Tc materials shown by Nb_3Ge. The approach is also consistent with the experimental findings that only multivalence ions which are diamagnetic in their atomic state (Cu, Tl, Bi, Pb, Sb) associate with high-Tc compounds.

(1) THE DIFFERENCE IN SCALING PARAMETERS FOR HIGH- AND LOW- Tc

(A) Low-Tc

Since conventional low-Tc superconductors are known to be governed by the strong-coupled electron-phonon mechanism, and since we believe that such coupling cannot fully explain the properties and mechanism of high-Tc superconductors[1,2], we search for a scaling parameter related to vibration of atoms and to low-Tc that does not scale in a similar manner for high-Tc.

In Fig 1A we plot Tc versus density (ρ) for conventional low-Tc superconductors. These show a peaking Tc at densities of 6-9 gm/cm^3 for materials with positive magnetic susceptibility at room temperature and at about 11-14 gm/cm^3 for materials with negative magnetic susceptibility (circled in Fig 1A). In the inset to Fig. 1A the plot of Tc vs weight is given. The peaking of Tc with density can be understood in terms of the dependency of the frequency term (in the Debye temperature relationship) with density. Plotting Tc vs atomic weight for the A15 superconductors (Nb_3X or V_3X) shows a generally decreasing trend with atomic weight.

The critical field above which magnetic flux can no longer be excluded from the interior of a superconductor is given by $H_c=H_o(1-(T/Tc)^2)$ In Fig. 1B, H_o is shown vs the number of missing electrons that would fill the partially-filled subshells for the superconducting elements. There is a general dependence of H_o on this number. The exceptions Ti, Th, Zr, and Pa (not plotted) have a d^2 state in their outershell configuration which presumably adds another unique factor. Hg being the other exception has vastly differing electronic properties than the other metals. The fit in Fig. 1B suggested searching for related scaling in high-Tc.

(B) HIGH-Tc SUPERCONDUCTING SCALING

A rather clearcut general increase of Tc with molecular weight is shown for all of the known high-Tc superconducting oxides except for $Bi_2Sr_2Cu_1O_6$ and possibly $Ba(PbBi)O_3$ (which may be largely phonon-induced superconductors). This mass or weight dependence is very different from that in low-Tc superconductors given in Fig. 1A, suggesting a very different role of the mass parameter in the two types of superconductors. In the high-Tc materials, the mass dependence seems related to the added complexity of the two (or three) different types of polyhedral building blocks and more extensive layering in substances having a greater number of ions per unit cell.

In Fig. 2 we plot Tc versus the total number of bound holes (P(b)) per unit cell associated with the ionization of the multivalence cations and associated with charge transfer from the oxygens.[3] We define the number of bound holes associated with a charge transfer excitation as the number of resulting holes on the oxygens when a multivalence cation is transiently ($3X10^{13}$ times per sec) neutralized by the excitation. Thus for $Y_1Ba_2Cu_3O_{7-}$ which for charge neutrality can be written as $Y^{3+}{}_1Cu^{3+}{}_1Ba^{2+}{}_2Cu^{2+}{}_2\,O_{7-}$ we illustrate how a maximum of seven bound holes are created: the charge transfer $Cu^{3+} + O^{2-} + O^{2-}$ yields $Cu^{o} + O^{o} + O^{-}$ thus creating three bound holes on oxygens; the charge transfer $Cu^{2+} + O^{2-}$ yields $Cu^{o} + O^{o}$ creating two holes on oxygens. Since there are 2 Cu^{2+} and only 1 Cu^{3+} we sum 2(2)+3=7. The apical oxygen (O(4)) in the CuO_5 pyramidal building block is believed to be the optimal candidate ion as the charge transfer agent. There is then by this empirical method of calculating P(b), found to be a linear correlation for the high-Tc superconductors in Tc vs P(b) as shown in Fig. 2. The correlation is described by the least-square best fit as Tc=7.9 P(b) + 27.2. For P(b)=0, characteristic of low-Tc superconductors, the fit in Fig 2 gives Tc=27.2K which is approximately the maximum Tc for electron-phonon induced superconductivity (experimentally 23K). On the other hand a theoretical superconducting high-Tc lattice involving the highest valence states of the functioning ions such as Bi^{5+} and Sb^{5+}, and having the 2223X form, could achieve a maximum of about 25 holes/unit cell which according to Fig 2 would lead to a Tc of about 225K. According to Ref 4, this is the maximum Tc for superconductivity derived from an excitonic mechanism, such a mechanism necessarily requiring the existence of bound holes. Since $SrTiO_3$, $Ba(PbBi)O_3$, and $Bi_2Sr_2Cu_1O_6$ do not fit the straight line representation in Fig 2, we suspect that superconductivity in those materials is governed largely by electron-phonon coupling rather than by bound holes or exciton. The value of P(b) =7 for $Y_1Ba_2Cu_3O_7$ implies a maximum allowable carrier concentration in the normal state of about $10^{22}cm^{-3}$. In our previous work (5) we show that near Tc the actual positive carrier concentration is 10^{21} to $10^{22}cm^{-3}$.

Recently the compound $Y_5Ba_6Cu_{11}O_y$ has been synthesized and shown under oxygen overpressure to have a transition to zero electrical resistance at 235-265K (Ref. 6). For charge balance with this stoichiometry, and considering a K_2MnF_4 type structure, the value of P(b) would be expected to be 25-27 leading to a Tc in Fig. 2 of about 235K. Presently this phase seems to be of a filamentary or interfacial nature and has not been formed in high enough yield to derive conclusions regarding Meissner exclusion, however, the correlation with the empirical fit indeed exists.

References

1. J. Bednorz and K. Mueller, Z Phys. B64, 189 (1986).
2. C. W. Chu, P. Hor, R. Meng, L. Gao, Z. Hueng and Y. Wang, Phys. Rev. Lett. 58(4), 405, and 58(9), 908 (1987).
3. G. C. Vezzoli, M.F. Chen, F. Craver, W. Stanley, M. Shoga, A. Safari, T. Burke, B. Moon and B. Lalevic, Proc. of MRS Boston Meeting Dec 1989.
4. L.V. Keldysh and A. N. Kozlov, JETP Lett 5, 190 (1967), and A. A. Abrikosov, Zh. Eksp. Teor. Fiz Pis'ma Red 27, 37 (1978).
5. G. C. Vezzoli, T. Burke, B. Moon, A. Safari, H. Hundyar, B. Lalevic, R. Bonometti, C. Alexander, C. Rau, and K. Waters, J. Magnetism and Magnetic Materials 79, 146 (1989).
6. J. T. Chen, L-X Qian, L-Q Wang, L. E. Wenger, and E.M. Logothetis, Mod. Phys. Lett B (in press)

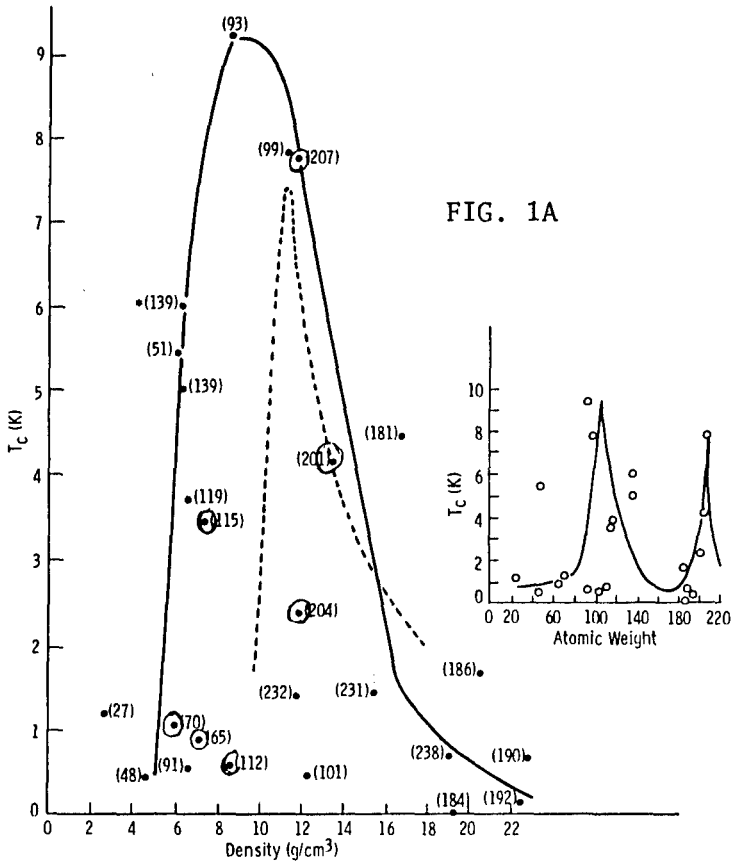


FIG. 1A

FOR CONVENTIONAL LOW-T_c ELEMENTAL SUPERCONDUCTORS VERSUS DENSITY (WEIGHT IS IN PARENTHESES)

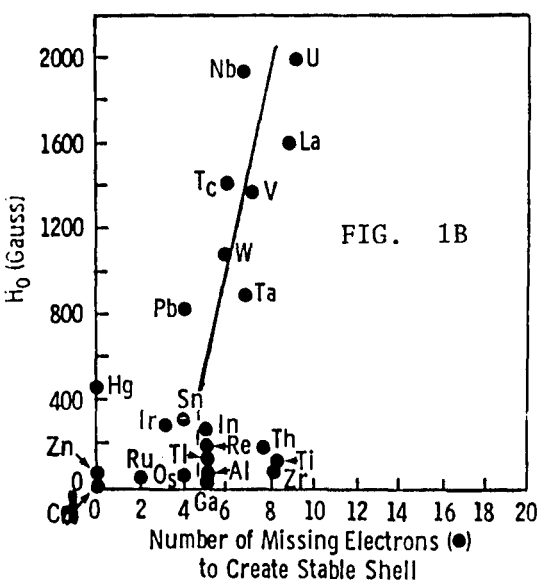
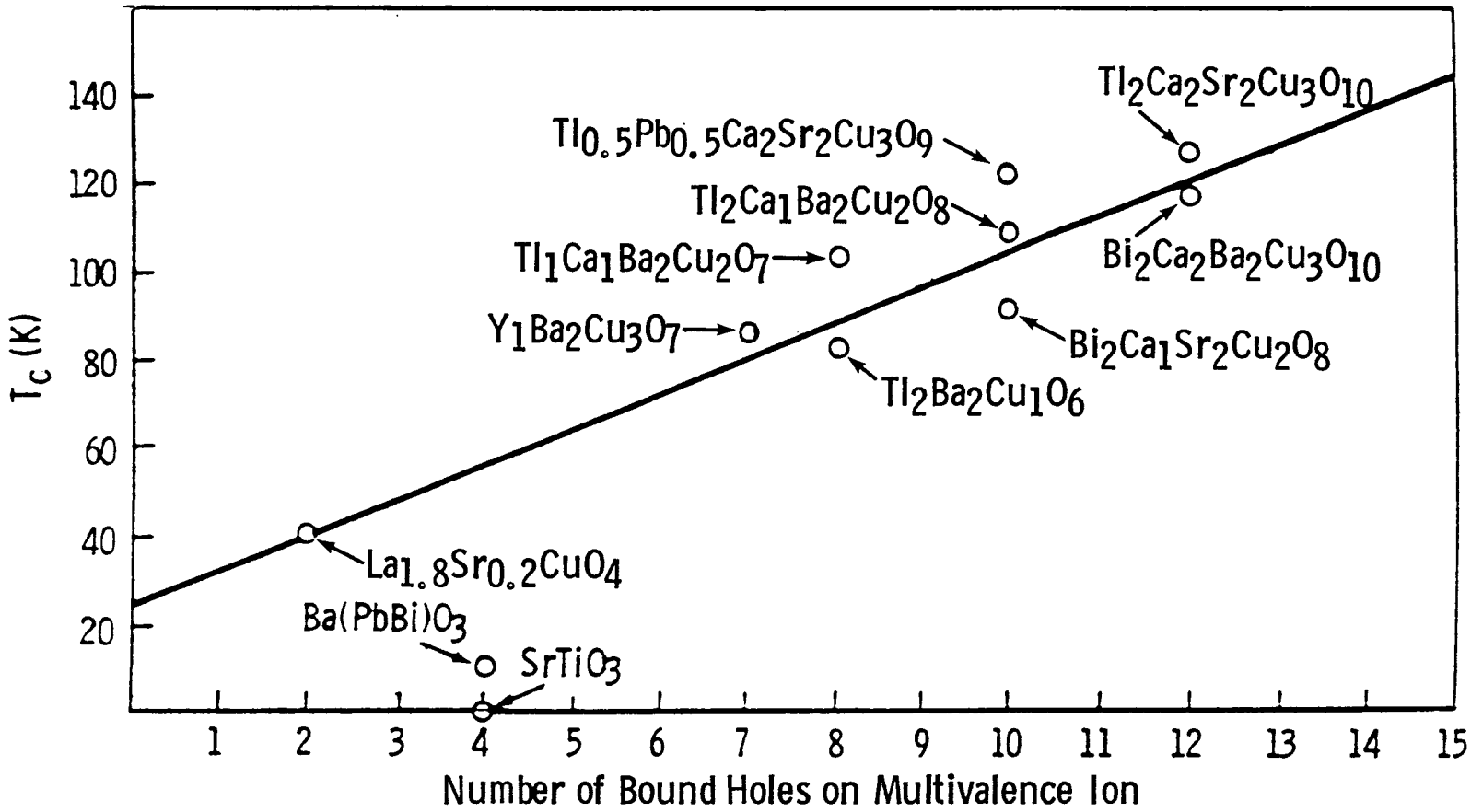


FIG. 1B

H_0 VERSUS NUMBER OF MISSING ELECTRONS TO FORM STABLE SHELL IN LOW-T_c ELEMENTAL SUPERCONDUCTOR



(These holes can be the core of bound excitons on the multivalence cations)

TRANSITION TEMPERATURE FOR HIGH-T_c MATERIALS VERSUS NUMBER OF HOLES DUE TO IONIZATION OF MULTIVALENCE METAL ATOM

FIG. 2

ELECTRON ENERGY SPECTRUM AND MAGNETIC INTERACTIONS IN HIGH-T_c SUPERCONDUCTORS

S.A.Turshevski, A.I.Liechtenstein, V.P.Antropov, V.A.Gubanov

Institute of Chemistry and Institute of Metal Physics,

Ural Science Center, Academy of Sciences, Sverdlovsk, USSR

The character of magnetic interactions in La-Sr-Cu-O and Y-Ba-Cu-O systems is of primary importance for analysis of high-T_c superconductivity in these compounds. Neutron diffraction experiments showed the antiferromagnetic ground state for nonsuperconducting La_2CuO_4 and $YBa_2Cu_3O_6$ with the strongest antiferromagnetic superexchange being in the ab plane [1,2]. Nonsuperconducting "1-2-3" system has even two Neel temperatures T_{N1} and T_{N2}. The first one corresponds to the ordering of Cu atoms in the CuO_2 planes, T_{N2} reflects the antiferromagnetic ordering of magnetic moments in CuO chains relatively to the moments in the planes T_{N1} and T_{N2} depend strongly on the oxygen content [3] (T_{N1}=450 K for x=0,1 and T_{N2}=80 K, but T_{N1}=230 K and T_{N2}=10 K for x=0.35).

We have tried to describe magnetic interactions in high-T superconductors basing on theLMTO band structure calculations. Exchange interaction parameters can be defined from the effective Heisenberg hamiltonian:

$$H_{ex} = -1/2 \sum_{ij} J_{ij} \vec{S}_i \vec{S}_j \qquad (1)$$

When the magnetic moments are not too large, as copper magnetic moments in superconducting oxides, J_{ij} parameters can be defined through the non-local magnetic susceptibility of spin-restricted solution for the crystal [4,5]:

$$J_{ij} = \frac{1}{2} \frac{I_i \cdot I_j}{S_i \cdot S_j} \sum_{LL'} \chi^{ij}_{LL'}, \qquad (2)$$

where

$$\chi^{ij}_{LL'} = 1/\pi \int^{E_F} \mathrm{Im}\, G^{ij}_{LL'}(E) \cdot G^{ji}_{L'L}(E)\, dE \quad , \qquad (3)$$

$$G^{ij}_{LL'} = 1/\Omega_{BZ} \int_{BZ} d\vec{k} \sum_n \frac{\psi_{nL}(\vec{k}) \psi^*_{nL'}(\vec{k})}{E - E_n(\vec{k})} e^{i\vec{k}\cdot\vec{R}_{ij}} \qquad (4)$$

- is the nondiagonal Green function which can be calculated through the energy spectrum $E_n(\vec{k})$ and $\psi_{nl}(\vec{k})$ of the LMTO-hamiltonian. I_i in formulae (2) is interatomic exchange parameters of atom i. Due to the sharp dependence of nondiagonal Green function $G^{ij}_{LL'}(E)$ on the E the integral (3) should be calculated as contour integral in complex plane.

The results of nonlocal magnetic susceptibility calculation and the values of exchange interaction parameters for La CuO and $YBa_2Cu_3O_7$ systems are given in the Table.

Strong anisotropy of exchange interactions in the ab plane and along the c axis in La_2CuO_4 is obviously seen. The value of Neel temperature found agrees well with the experimental data available. In the $YBa_2Cu_3O_7$ system there is strong antiferromagnetic Cu-O-Cu interaction in the CuO_2 plane, which results in antiferromagnetic ground state of $YBa_2Cu_3O_6$. Superexchange of Cu1-O4-Cu2 type is antiferromagnetic also, in accordance with the experiment. Using the simplest mean field approximation $T_N = \frac{1}{3}|J|zS(S+1)$, where z is the number of the nearest magnetic neighbours, it is possible to estimate Neel temperature values. They are T_{N1} = 265-314 K, T_{N2} = 61 K agree well with the experimental data. Large ferromagnetic moment exchange in Cu1-O4-Cu1 chains (which follows from NMR experiments [6] also) does not influence antiferromagnetic ordering, as when δ = 1 all the chaines are broken.

In the planes of "1-2-3"system there are quite strong antiferromagnetic Cu-O and O-O interaction which appear due to holes in oxigen subbands. These results are in line with the magnetic model of oxigen holes pairing in high-T_c superconductor suggested in [7].

We have performed also a number of LMTO spin-polarised calculations for $GdBa_2Cu_3O_6$ and $GdBa_2Cu_3O_7$ both for ferromagnet and antiferromagnetic ordering of magnetic moments. For antiferromagnetic state the energy gap of 0,04 ev is formed at the Fermi level. Spin splitting of Gd f-states equals to 5 ev, a magnetic moment of Gd atoms is 7.3 μ_B. The estimation of stabil parameters [8] leads to the conclusion of more stable antiferromagnetic ordering: the difference of J_0 parameters is 230 K (O_6) and 180 K (O_7). The value of s-f integral in antiferromagnetic phase of $GdBa_2Cu_3O_7$ appears to be about 20 K, and correspond to small changes of T_c when Gd atoms enter the crystal lattice.

Reproduced From
Best Available Copy

Table. Exchange interaction parameters for $YBa_2Cu_3O_7$ and La_2CuO_4 (for s=1/2 and I_{Cu}=0,07 Ry, I_O=0,11 Ry)

pair	$\hat{R}_{ij}$	$\chi^{ij}_{dd(p)}$ (mRy^{-1})	J^{ij} (K)
$YBa_2Cu_3O_7$			
Cu2-O2-Cu2	(0 1 0)	-50,8	-157
Cu2-O3-Cu2	(1 0 0)	-42,8	-132
Cu1-O4-Cu2	(0 0 1)	-9,9	-31
Cu1-O1-Cu1	(0 1 0)	72,5	225
Cu2-O2	(0,5 0 0)	112,3	545
O2-O2	(0,5 0,5 0)	35,5	270
La_2CuO_4			
Cu-O1-Cu	(1 0 0)	-73,5	227
Cu-O2-Cu	(0 0 1)	-0,45	1,4

REFERENCES

[1] D.Vaknin, S.K.Sinha, D.E.Moncton et.al. Phys.Rev.Lett.58(1987)2801
[2] W.I.F.David, W.T.A.Harrison, J.M.F.Gunn. Nature 327(1987)310
[3] G.Shirane, ICM'88, Paris, Abstracts, p.295
[4] V.A.Gubanov, S.A.Turshevski et.al. Physica C, 153-155(1988)123
[5] K.Terakura, N.Hamada et.al.J.Phys.F.12(1982)1661
[6] B.A.Aleksashin, A.M.Bogdanovich et.al.Pisma v ZETF,48(1988)263
[7] G.Chen and W.A.Goddard, Science 239(1988)899
[8] Liechtenshtein A.I., Katsnelson M.I. et al. JMMM,65(1987)41

COUPLED BIPOLARONS AND OPTICAL PHONONS AS A MODEL FOR HIGH-T_c SUPERCONDUCTORS

J. Kasperczyk

Phys. Inst., Ped. University, Zawadzkiego 13/15, PL-42201 Czestochowa (Poland)

1. INTRODUCTION.

All known up-to-date high-temperature superconductors are oxides (mainly copper oxides although compounds without copper were obtained, e.g. $BaKBiO_3$). On the other hand, more than 95 % of all ferroelectric compounds are also oxides or contain oxygen ion [1] . Therefore, the problem of mutual relation between ferroelectricity and superconductivity is of great theoretical interest.

The electron-phonon interaction is important in both phenomena. In ferroelectrics a cubic electron-phonon and/or a quartic electron-two-phonon interactions play an essential role [1] . In classical superconductors (of the BCS type) a cubic electron-one-phonon interaction leads to the formation of Cooper pairs of two electrons with opposite momenta and spins . The average distance (in real space) between the two electrons is of order of the so-called coherence length ξ which is much greater than lattice constant of such a classical superconductor. However, the coherence length of the new high-temperature superconductors reaches very small value which is comparable to the dimensions of unit cell of these compounds [3] . This means that a pair consists of two holes occupying the same site or two adjacent sites . Such a situation seems to be described by a model of the local-pairs (bipolarons) [2,3].

The origin of local-pair may come not only from strong enough electron or hole-phonon interaction but also from other interactions . Independently of a specific nature of such local-pairs, they can undergo a Bose-like condensation to the superconducting state at a critical temperature which is usually much lower than the temperature of the pair formation.

In this paper an interplay of ferroelectric and superconducting properties is considered within the model of hole-like local-pairs interacting with optical phonons . Therefore, we extend the usual local-pair Hamiltonian [2] by including an direct interaction between the local-pairs and the optical phonons. These optical phonons are known to play an important role in the ferroelectric transition if any and they transform into an additional pseudo-acoustic branch at the ferroelectric critical temperature [1] (this is associated with arising of nonzero electric polarization due to existence of two separate lattices composed of negative and positive ions, respectively).

2. HAMILTONIAN OF INTERACTING LOCAL-PAIRS AND OPTICAL PHONONS.

The Hamiltonian of our system is as follows

$$H = - w_o \sum_i \sum_j (N_i N_j - A_i^+ A_j) + \sum_i (h\nu_o b_i^+ b_i - \mu N_i - \lambda N_i (b_i^+ + b_i)),$$ where

$A_i^+(A_i)$,$b_i^+(b_i)$ are creation (annihilation) operators for the local-pair and the optical phonon (with frequency ν_o) at the i-th site, respectively, $N_i = A_i^+ A_i$, w_o is a local-pair bandwidth and μ denotes the chemical potential.An analysis

of the above Hamiltonian can be carried out on the ground of the Bogolyubov's inequality [4] for the free energy $F \leq F_t = F_0 + \langle H \rangle_0 - \langle H_t \rangle_0$, with the trial Hamiltonian in which the local-pairs and the phonons are decoupled

$$H_t = \sum_i (- W_i A_i^+ - W_i^* A_i - Q_i N_i + h\nu_o B_i^+ B_i) = H_{pair} + H_{ph}$$

where W_i , W_i^* and Q_i stand for variational parameters and B_i^+ (B_i) are new creation (annihilation) operators for phonon at the i-th site . The thermal averages of the $\langle \quad \rangle_0$ type are defined as usual, e.g., $\langle H \rangle_0 = Tr (\varrho_0 H)$, $\varrho_0 = \exp(-\beta H_t) / Tr(\exp (-\beta H_t))$, $\beta = (k_B T)^{-1}$, k_B - the Boltzmann's constant . Within the single site approximation which is equivalent to the mean-field approximation (MFA)

$$F_0 = - \beta^{-1} \sum_i \ln Z_0 \qquad \text{with the single-site partition function}$$

$$Z_0 = (\exp(-\beta\varepsilon_1) + \exp(-\beta\varepsilon_2)) / (1 - \exp(-\beta h\nu_o)) \quad ,$$

where ε_1 and ε_2 are the eigenvalues of the Hamiltonian H_{pair} calculated in the basis of states consisting of two single-site states : φ_o and φ_1 which describe a given site occupied (φ_1) or unoccupied (φ_o) by a local-pair . A straightforward diagonalization of the H_{pair} matrix $\begin{pmatrix} 0 & -W^* \\ -W & Q \end{pmatrix}$ leads to the following eigen-energies

$$\varepsilon_1 = (- Q - (- Q^2 + 4| W |^2)^{1/2}) / 2$$
$$\varepsilon_2 = (- Q + (- Q^2 + 4| W |^2)^{1/2}) / 2$$

The variational parameters Q, W and W^* should be calculated by minimizing the trial free energy F_t . One obtains the mean-field Hamiltonian H_{MFA} by means of the following decouplings

$$\sum_i \sum_j A_i^+ A_j \Rightarrow \sum_i \sum_j \langle A_i^+ \rangle A_j + \sum_i \sum_j A_i^+ \langle A_j \rangle = \sum_i z (\alpha A^+ + \alpha^* A)$$

$$\sum_i \sum_j N_i N_j \Rightarrow \sum_i \sum_j \langle N_i \rangle N_j + \sum_i \sum_j N_i \langle N_j \rangle = 2z\nu \sum_i N_i$$

where $\alpha=\alpha_i=\langle A_i \rangle=\langle A \rangle$ is the superconducting order parameter, $\nu=\nu_i=\langle N_i \rangle=\langle N \rangle$ is the concentration of the local-pairs per one site and z denotes a coordination number (a number of the nearest neighbours of a given site). In the result

$$H_{MFA} = \sum_i (- w (\alpha A^+ - \alpha^* A) + 2w\nu N + h\nu_o b^+ b - \mu N - \lambda N (b^+ + b))$$

with the parameter $w = z w_o$.

3. FREE ENERGY AND COUPLING EQUATIONS.

In this section we determine the trial free energy according to the

above Hamiltonian. The trial energy per one site $f_t = F_t / \sum_i 1$ takes the form

$$f_t = -\beta^{-1}\ln(\exp(-\beta\varepsilon_1) + \exp(-\beta\varepsilon_2)) + \beta^{-1}\ln(1-\exp(-\beta h\nu_o)) + W\alpha^* + W^*\alpha -$$
$$-2w|\alpha|^2 + 2w\nu^2 + (Q-\mu)\nu + h\nu_o\,(\langle b^+b\rangle_0 - \langle B^+B\rangle_0) - \lambda\langle N\,(b^+ + b)\rangle_0$$

In order to calculate the necessary averages let us introduce the new states

$$\Phi_1 = c_{1o}\varphi_o + c_{11}\varphi_1 \qquad \Phi_2 = c_{2o}\varphi_o + c_{21}\varphi_1$$

for which the matrix of H_{pair} has a diagonal form. The coefficients c_{kl} can be obtained from the equation : $H_{pair}\Phi_i = \varepsilon_i\Phi_i$,i.e.

$$\begin{pmatrix} -\varepsilon_i & -W^* \\ -W & Q-\varepsilon_i \end{pmatrix}\begin{pmatrix} c_{io} \\ c_{i1} \end{pmatrix} = 0$$

Taking into account the normalization condition for eigenfunctions Φ_1 and Φ_2 one obtains in the result :

$$c_{io} = (\,1 + |\varepsilon_i/W^*|^2\,)^{-1/2} = (W/(Q-\varepsilon_i))\,(\,1 + |W^*/(Q-\varepsilon_i)|^2\,)^{-1/2}$$

$$c_{i1} = (\,1 + |W^*/(Q-\varepsilon_i)|^2\,)^{-1/2} = (-\varepsilon_i/W^*)\,(\,1 + |-\varepsilon_i/W^*|^2\,)^{-1/2}$$

Consider the quantities $\xi_k = \langle\Psi_k|b-B|\Psi_k\rangle$, where Ψ_k are the phonon eigenfunctions i.e. $H_{ph}\Psi_k = kh\nu_o\Psi_k$ ($k = 0,1,2,\ldots$) . Let us assume for simplicity that $\xi_k = \xi$ and $\langle\Psi_{k-1}|b-B|\Psi_k\rangle = 0$ for all values of k. The parameter ξ can be treated as a non-variational quantity which is proportional to a lattice deformation . This deformation can be associated with arising a nonzero dipole electric moment, i.e. with a ferroelectric phase transition. After some algebra one comes to the following :

$$\langle b^+b\rangle_0 - \langle B^+B\rangle_0 = \xi^*\xi .$$

Using the calculated coefficients c_{i1} one obtains :

$$\langle N\,b\rangle_0 = \xi/2 + \xi Q(Q^2+4|W|^2)^{-1/2}\left[\,2-\tanh(\beta(Q^2+4|W|^2)^{1/2})\right]/2$$

The trial reduced free energy is then readily written as

$$f_t = -\beta^{-1}\ln(\exp(-\beta\varepsilon_1) + \exp(-\beta\varepsilon_2)) + \beta^{-1}\ln(1-\exp(-\beta h\nu_o)) + W\alpha^* + W^*\alpha - 2w|\alpha|^2 +$$
$$2w\nu^2 + (Q-\mu)\nu + h\nu_o\xi^*\xi - \lambda(\xi^*+\xi)\left[\,1 + Q\,(Q^2+4|W|^2)^{-1/2}\left[\,2-\tanh(\beta(Q^2+4|W|^2)^{1/2})\right]\right]/2$$

A minimization of the above thermodynamic potential with respect to W, W^*, α, α^*, Q and ν leads to the following coupling equations

$$(2w)^{-1} = (Q^2+4|W|^2)^{-1/2}\tanh(\beta(Q^2+4|W|^2)^{1/2}) - \lambda(\xi^*+\xi)Q(Q^2+4|W|^2)^{-3/2}$$
$$\tanh(\beta(Q^2+4|W|^2)^{1/2}) + \lambda(\xi^*+\xi)\beta Q(Q^2+4|W|^2)^{-1}\left[\,\cosh(\beta(Q^2+4|W|^2)^{1/2})\right]^{-2}/2$$

$$2\nu - 1 = Q(Q^2+4|W|^2)^{-1/2}\tanh(\beta(Q^2+4|W|^2)^{1/2}) + 4\lambda(\xi^*+\xi)|W|^2(Q^2+4|W|^2)^{-3/2}$$
$$\tanh(\beta(Q^2+4|W|^2)^{1/2}) + \lambda(\xi^*+\xi)\beta Q^2(Q^2+4|W|^2)^{-1}\left[\,\cosh(\beta(Q^2+4|W|^2)^{1/2})\right]^{-2}/2$$

$$W = 2w\alpha \qquad Q = -4w\nu + \mu \qquad + c.c .$$

It is easily seen that $W=W^*$ and $\alpha=\alpha^*$. The above set of equation should be

self-consistently solved.

4. GROUND STATE .

By taking the limit $T \Rightarrow 0$, the energy of a ground state per one site is given by

$$E = \langle H \rangle_o / \sum_i 1 = - 2w\alpha^2 + 2w\nu^2 - \mu\nu + h\nu_o\xi^2 + \lambda\xi\,(1+Q/(Q^2+4W^2)^{1/2})$$

Let us consider the purely superconducting ground state for which the ferroelectric order parameter ξ disappears ($\xi=0$) . The superconducting order parameter strongly depends on the local-pair concentration , i.e. $\alpha^2 = \nu(1-\nu)$. The energy of the superconducting ground state is as follows

$$E_{sc} = - 2w\alpha^2 + 2w\nu^2 = 2w\,(2\nu-1)\nu \quad .$$

For the purely ferroelectric ground state the superconducting order parameter disappears ($\alpha=W=0$) and the energy is given by

$$E_{fe} = 2w\nu^2 + h\nu_o\xi^2 - \lambda\xi\,(1+Q/(Q^2)^{1/2}) \quad .$$

The normal state , i.e. non-superconducting and paraelectric ($\alpha=0$ and $\xi=0$), has the energy $E_n = 2w\nu^2$. It is clearly seen that normal state cannot be realized because of the lower energy of the superconducting state , at least ($E_{sc} < E_n$). Nevertheless, an competition is possible between superconducting and ferroelectric ground states. The superconducting state is prefered if $2\nu(1-\nu) > (2\lambda\xi - h\nu_o\xi^2)/w$.

5. SUPERCONDUCTING TRANSITION

Let us return to finite temperatures. To get the superconducting critical temperature T_c we assume that superconducting order parameter disappears ($\alpha=\langle A \rangle=0$). The reduced critical temperature is thus given by

$$t_c = k_B T_c/w = q \,/\, \ln((1+Z)/(1-Z)),$$

where $q = Q/w = 2\nu-1+((2\nu-1)^2-4pZ)^{1/2}$, $p = \lambda\,\xi\,/w$ and the quantity Z can be numerically calculated from the additional condition

$$0 = q^2/2 - (q-2p)Z - p(1-Z^2)\,\ln((1+Z)/(1-Z)) \quad .$$

It can be shown that maximum critical temperature is strongly enhanced due to the rather moderate interaction up to $p \cong 0.3$. However, a nonzero value of ξ, i.e. temperature below ferroelectric transition temperature, is necessary. For stronger coupling and/or smaller bandwidth w , this effect weakens . On the other hand , the high-temperature superconductivity is rather restricted to the regions far from half-filling ($\nu \neq 1/2$).

REFERENCES

[1] H.Bilz, G.Benedek & A.Bussmann-Holder, *Phys. Rev.* B35 (1987) 4840.
[2] I.O. Kulik, *Physica* 126 B (1984) 280.
[3] J.Kasperczyk, submitted to the IMF'7,Saarbrücken.
[4] R. Mańka & A. Molak, *phys. stat. sol. (b)* 129 (1985) 369.

XES STUDIES OF DENSITY OF STATES OF HIGH TEMPERATURE SUPERCONDUCTORS

Gabriel Jasiolek
Institute of Physics
Polish Academy of Sciences
02-668 Warszawa, Poland

ABSTRACT

X-ray emission spectroscopic studies concerning the superconducting crystals, thin films and ceramics of the Y-Ba-Cu-O, Tm-Ba-Cu-O, Bi-Sr-Ca-Cu-O, Bi-Pb-Sr-Ca-Cu-O and Tl-Ba-Ca-Cu-O types are presented. The contributions of the $13d^9L\rangle$, $13d^{10}L\rangle$, $13d^{10}LL\rangle$ and $13d^{10}L^2\rangle$ configurations, where L denotes a ligand hole at the oxygen orbitals, in the spectroscopic pattern of these superconductors is discussed. An attempt to connect the X-ray "as registered" Cu $L\alpha$ emission spectra with the density of states close to the Fermi level, considering an influence of the CuL_3 absorption edge, is presented. The corrected intensity distributions below the Fermi level are found to correspond to the theoretical density of states.

Furthermore, an approach to the average valence of copper basing on the account of the self-absorption and fluorescence effects and on the configurations listed above is shown. The average valence of copper in the materials investigated is estimated to lie in the range of +2.10-2.32 when the formal trivalent copper is considered as this characterized by the $13d^9L\rangle$ configuration. The density of states at the Fermi level was estimated to be 2.4 states/eV-cell for a Bi-Sr-Ca-Cu-O crystal and 3.6 states/eV-cell for a Tl-Ba-Ca-Cu-O ceramic.

PACS: 74.70, 78.70E.

SUPERCONDUCTIVITY IN THE Sn-Ba-Sr-Y-Cu-O SYSTEM

K.S.Aleksandrov, B.P.Khrustalev, S.N.Krivomazov,
M.I.Petrov, A.D.Vasilyev, and S.A.Zwegintsev

Kirensky Institute of Physics, USSR Academy of Sciences,
Siberian Branch, 660036 Krasnoyarsk, USSR

Since Bednorz and Müller /1/ discovered high-T_c superconductivity in the La-Ba-Cu-O compound, several families of superconducting oxides have been synthesized /2/. In this paper we report the results of search for superconductivity in the compounds based on tin which has a lone electron pair like Bi, Tl, Pb.

The following compounds were synthesized: $Sn_1Ba_1Sr_1Cu_3O_x$, $Sn_1Ba_1Ca_1Cu_3O_x$, $Sn_1Ba_1Mg_1Cu_3O_x$, $Sn_1Sr_1Ca_1Cu_3O_x$, $Sn_1Sr_1Mg_1Cu_3O_x$, $Sn_1Ca_1Mg_1Cu_3O_x$. The initial components were oxides and carbonates of the appropriate elements. Standard firing-grinding procedure was used. Final heating was carried out at 960°C during 12 hours. Then the samples were cooled inside the furnace. All the synthesis cycles were carried out in air atmosphere.

Among the synthesized compounds only $Sn_1Ba_1Sr_1Cu_3O_x$ showed remarkable conductivity ($\rho \sim 10$ Ohm·cm). Other compounds were practically dielectrics ($\rho > 1000$ Ohm·cm). Presence of a possible superconductivity in $Sn_1Ba_1Sr_1Cu_3O_x$ was defined by using the Meissner effect. At low temperature a deviation from paramagnetic behaviour is observed. The hysteresis loops obtained at lower temperatures undoubtly testify to the presence of a superconductive phase in the sample. However, the part of the superconductive phase in the $Sn_1Ba_1Sr_1Cu_3O_x$ ceramic turned out to be small, less than 2%, which agrees with the estimation from magnetic data. In order to increase the content of the superconductive phase two-valent cations Ba, Sr were partially substituted by univalent (K) and three-valent ones (Y). Two samples were obtained: $Sn_1Ba_{0.7}Sr_{0.7}K_{0.7}Cu_3O_x$ and $Sn_1Ba_{0.7}Sr_{0.7}Y_{0.7}Cu_3O_x$. The former is a typical paramagnet without any anomaly down to 4.2K. The latter has shown the magnetic and electric properties undoubtly indicating the presence of a superconductivity phase with the onset temperature $T_c \simeq 55$K. The superconductive properties of the sample do not seem to be caused by the phase $YBaSrCu_3O_7$ /3/. This conclusion follows from the study of the $Sn_2Sr_2Ba_{0.5}Y_{0.5}Cu_3O_x$ and $Sn_2Ba_2Sr_{0.5}Y_{0.5}Cu_3O_x$ samples that were synthesized by analogy with the recent communications on superconductivity in $Pb_2Sr_2(Y,Ca)_1Cu_3O_8$ /4,5/. One may expect equal probability of the $YBaSrCu_3O_7$ content for both samples, however their electrical properties are quite different. The compound $Sn_2Sr_2Ba_{0.5}Y_{0.5}Cu_3O_x$ is a good dielectric while $Sn_2Ba_2Sr_{0.5}Y_{0.5}Cu_3O_x$ has clearly expressed superconductive properties 76/. The magnetic moment was measured in an external field H = = 100 Oe. At T < 86K the sample exhibits a clearly defined diamagnetic behaviour characteristic of superconductors. At these temperatures the hysteresis loop has the form typical of high-T_c superconductors. The amount of the superconductive phase in this sample, as a magnetic estimation in powder, is $\sim$15% of the volume of the sample.

A comparative analysis of the X-ray powder diagrams leads us to believe that the main motive of the $Y_1Ba_2Cu_3O_7$ structure is preserved in the structure of $Sn_2Ba_2Sr_{0.5}Y_{0.5}Cu_3O_x$. The unit cell parameters are: a = 4.1 Å, c = 12.4 Å (or multiple).

We have also used the same procedure for $Sn_1Ba_2Sr_{0.5}Y_{0.5}Cu_3O_x$. The sample is a typical paramagnet without any anomaly down to 4.2 K.

The presence of superconductivity in the system based on tin allows us to suggest that other cations, besides the well-known Bi, Tl, Pb, having the lone electron pair effect, should also form superconductive compounds. If we limit ourselves to consideration of copper-containing oxides, we may suppose that definite alkali-earth ions (or their combination) would suit for each of the ions: Hg,Sb,In,... in order to form a superconductive phase.

References

1. J.C.Bednorz and K.A.Müller, Z.Phys.B 64 (1986) 189.
2. A.W.Sleight, Science 242 (1988) 1519.
3. Y.Takeda, R.Kanno, O.Yamamoto, M.Takano, Z.Hiroi, Y.Bando, M.Shimada, H.Akinaga, and K.Takita, Physica C 157 (1989) 358.
4. M.A.Subramanian, I.Gopalakrishnan, C.C.Torardi, P.L.Gai, E.D. Boyes, T.P.Askew, R.B.Flippen, W.E.Farneth, and A.W.Sleight, Physica C 157 (1989) 124.
5. R.I.Cava, M.Marezio, I.I.Krajewski, W.F.Peck Ir., A.Santoro, and F.Beech, Physica C 157 (1989) 272.
6. K.S.Aleksandrov, B.P.Khrustalev, S.N.Krivomazov, M.I.Petrov, A.D.Vasilyev, and S.A.Zwegintsev, Physica C, submitted.

Studies of Local magnetism and Local Structure in $La_{2-x}Sr_xCuO_4$

J. I. Budnick, Z. Tan, and M. Filipkowski
Physics Department, University of Connecticut
Storrs, CT 06269, USA
Ch. Niedermayer, H. Gluckler, A. Weidinger, and E. Recknagel
Fakultat fur Physik, Universitat Konstanz
D-7750 Konstanz, FRG

We have presented the results of studies of magnetic ordering and correlation in $La_{2-x}Sr_xCuO_4$ via muon spin rotation (μSR) and DC magnetization. Evidence for a local structural distortion at the Sr dopant site was also presented. We briefly summarize some of these results in the following.

Early zero-applied-field μSR results demonstrated unambiguously the occurrence of magnetic order in La_2CuO_4 at temperatures below approximately 250 K [1]. It was also determined that the ordered magnetic state is destroyed quickly by Sr doping, with the ordering temperature being reduced to 12 K for x=0.02 and below 6 K for x=0.05. The internal magnetic field probed by the muon precession frequency remains approximately a constant up to x=0.02 despite the rapid suppression of the ordering temperature, suggesting that the magnetic moment on Cu atoms is not reduced appreciably [2]. The suppression of magnetic order by Sr doping is likely a result of a weakening of the effective interaction. For superconducting samples with x = 0.07, x = 0.10, and an x=0.15 sample with T_c=35 K, an observed rapid muon depolarization rate indicates the existence of strong magnetic correlations with an electronic origin. The strength of this magnetic correlation, as measured by the internal field probed by the muons, decreases as T_c increases. In an x=0.15 sample with T_c=39 K, the internal field becomes vanishingly small. At the present time it is not clear whether these magnetic correlations, which are observed at low temperatures (T < 4 K), are related to the superconducting pairing mechanism.

A peak-like anomaly appears.in the temperature-dependent DC magnetization at the onset of antiferromagntic ordering in undoped and lightly doped La_2CuO_4. A similar anomaly was, however, not observed for $x \geq 0.02$ even though a magnetically ordered state was suggested by local probes such as μSR and NQR (4). It is generally speculated that a spin-glass state may exist in the region for $0.05 \geq x \geq 0.02$, bridging the AFM and superconducting phases. During the effort to study the nature of the magnetic state in the spin glass region, we observed a cusp-like anomaly at a temperature $T_f(x)$, similar to the kind expected from a spin-glass transition, in DC magnetization measurements performed on vacuum-annealed x=0.02 and 0.03 samples [4]. In addition, a similar anomaly was clearly observed at T_f in the temperature dependence of the amplitude of an electron spin resonance (ESR) signal also measured in vacuum-annealed samples. There are reasons to believe that this ESR signal is due to spins that give rise to the low temperature magnetic phase measured via NMR, μSR and DC magnetization, with general agreement amongst the values of T_f determined by the four methods . However, the measured temperature dependence of the ESR linewidth and the resonance field do not follow the expected behavior of the usual spin glass system.

Attention has been focused on the homogeneity of the $La_{2-x}Sr_xCuO_4$ material. As an effort to understand the local

structural effect of Sr doping, a series of x-ray absorption measurements at the Sr K-edge have been made on various $La_{2-x}Sr_xCuO_4$ materials. Our Sr x-ray absorption near-edge structure (XANES) results suggest a local structural distortion at the Sr site when a La is replaced by a Sr [5]. The structural distortion leads to a nearly empty apical oxygen site near the Sr dopant in samples prepared under normal conditions. Accompanied with this, it was proposed that an interstitial defect oxygen is trapped near each Sr atom at low doping level. The defect oxygen is more tightly bound in the structure than the apical oxygen. The defect oxygen may serve as a mechanism for hole doping similar to the hole doping by excess oxygen in oxygen-enriched La_2CuO_{4+y}. Evidence for a local structural distortion in the $La_{2-x}Ba_xCuO_4$ compounds was also observed.

Acknowledgements: The work of the Konstanz group has been supported by the Bundesminster Fur Forchung und Technologie. The work of the University of Connecticut Group has been supported by the U. S. Department of Energy under Contracts No. DE-AS05-80-ER10742 and No. DE-AC02-76CH00016, and has also been supported in part by the Department of Higher Education of the state of Connecticut.

References

[1] J. I. Budnick et al. Phys. Lett. 124, 106 (1987).
[2] J. I. Budnick et al. Europhys. Lett. 5, 651 (1988).
[3] A. Weidinger et al. Phys. Rev. Lett. 62, 102 (1989).
[4] M. E. Filipkowski, Physica C 167, 35 (1990), and refernces therein.
[5] Z. Tan et al. Phys. Rev. Lett. 64, 2715 (1990).

MAGNETIC CORRELATIONS IN $La_{2-x}Sr_xCuO_4$ FROM NQR RELAXATION AND SPECIFIC HEAT

F. Borsa
Dipartimento di Fisica dell' Universitá, 27100 Pavia, Italy
and Ames Laboratory and Department of Physics
Iowa State University
Ames, Iowa 50011 USA

and

A. Rigamonti
Dipartimento di Fisica dell' Universitá
27100 Pavia, Italy

ABSTRACT

We review ^{139}La and ^{63}Cu NQR spin-lattice relaxation rates and specific heat measurements as a function of temperature in $La_{2-x}Sr_xCuO_4$ for x ranging from 0 up to 0.3, with particular emphasis on the effect of doping on the Cu^{2+} spins magnetic correlations. In the low doping limit, $x \leq 0.05$, the results can be interpreted consistently in terms of a simple phenomenological "two-fluids" model whereby the effect of thermally-activated mobile O(2p) holes is the one of disrupting locally the Cu^{2+} spin correlations. For $x \geq 0.1$, the results indicate the onset, as $T \rightarrow T_c^+$, of a strong coupling between Cu^{2+} spins and the Fermi liquid of O(2p) holes leading to the apparent disappearance of localized Cu^{2+} moment in connection with the opening of a superconducting gap.

INTRODUCTION

A central issue for the understanding of the microscopic mechanism leading to superconductivity in Cu-base high-T_c superconductors is about the interplay between the O(2p) holes controlling the transport and the effective Cu magnetic moments controlling the magnetic properties. In both $La_{2-x}Sr_xCuO_4$(LaSCO) and $YBa_2Cu_3O_{6+\delta}$(YBCO) systems one can change, as a function of composition, from a planar Heisenberg system of localized Cu^{2+} moments into a metallic system in which a strong coupling exists between the Cu^{2+} d-states and the itinerant O-p states. The true nature of the Cu^{2+} magnetic state and of its correlations in the latter case is still a matter of debate.

NMR-NQR and relaxation measurements have provided enlightening information about the above-mentioned problematic, particularly in the two systems YBCO and LaSCO. The studies of spin dynamics in YBCO by ^{63,65}Cu NMR-NQR have been recently reviewed.[1] Furthermore, ^{89}Y[2,3] as well as ^{17}O NMR[4–6] have proved to be sensitive tools to test the properties of Fermi liquid of O(2p) holes.

In this paper, we present a review of our ^{139}La and ^{63}Cu NQR relaxation measurements in LaSCO.[7] The results are analyzed in terms of a simple phenomenological model which leads to a satisfactory classification of the magnetic correlation properties of the Cu^{2+} d-states as a function of Sr-doping and as a function of temperature.

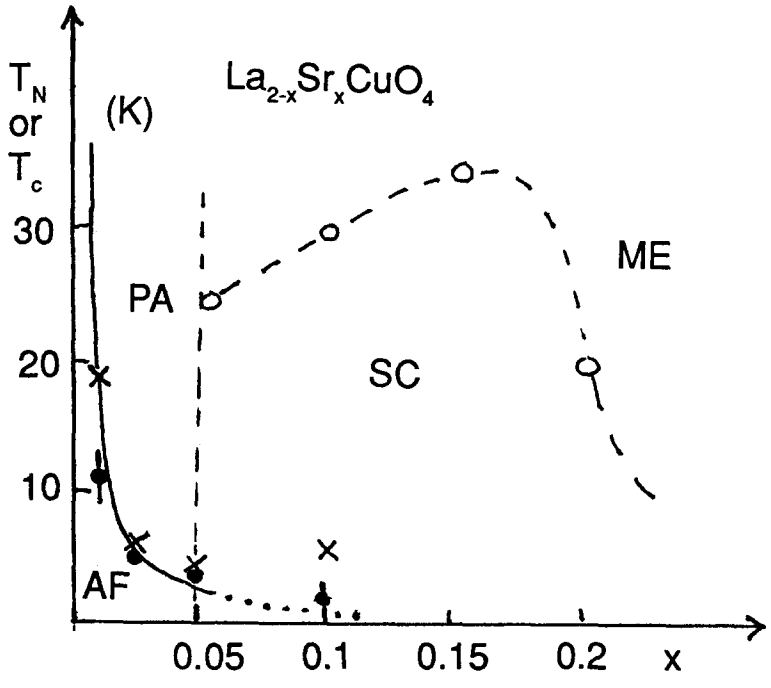


FIG. 1 Phase diagram for LaSC based on results of the present in vestigation (see Ref. 7): (O) Meis ner effect; (x). specific heat; (NQR. The solid line is the the retical result, Eq. (12), in the tex

The phase diagram of LaSCO is shown in Fig. 1. For sake of simplicity, only our dat referring to the samples which were used in the present investigation are indicated. The bounc ary between the paramagnetic (PA) and antiferromagnetic (AF) phase is obtained from NQR and specific heat[8] measurements. The normal metal (ME)-superconductivity (SC) boundar is obtained from Meissner effect measurements.[7] The boundary between semiconducting an metallic phase is not defined by experimental measurements; in the subsequent discussion, w will assume it to be around $x = 0.05$. The boundary between tetragonal and orthoromb structure is not indicated since it is not relevant for the purpose of our investigation. It shou be noted that there exist substantial agreement in the literature about the phase diagram LaSCO except that for two points:

(i) the magnetically ordered phase observed at low temperature for $x \geq 0.01$ can be either spin-glass phase or a disordered antiferromagnetic phase.

(ii) a coexistence of magnetic order and superconductivity has been reported for $x \geq 0.0$ Although we also find this coexistence in both NQR and specific heat measurements, w tend to interpret it as due to phase separation.

In the analysis of NQR T_1 data in LaSCO, it is useful to consider separately two rang of x-doping:

(i) moderate doping, namely $x \leq 0.05$ where the samples are semiconductors and a transitic from the paramagnetic to an ordered phase is observed.

(ii) strong doping, namely $x \geq 0.1$ or metal region, where at T_c one has the transition the superconducting phase.

Reproduced From
Best Available Copy

NQR Relaxation and Spin Dynamics

The ^{139}La NQR spin-lattice relaxation rates are obtained by monitoring the growth of the magnetization due to the population difference between the $\pm$ 5/2 $\leftrightarrow \pm$ 7/2 levels, (frequency separation in the range 18 $\div$ 19 MHz) after a saturating sequence of rf pulses. The same holds for the ^{63}Cu nucleus in terms of the $\pm$ 1/2 $\leftrightarrow \pm$ 3/2 NQR levels (frequency separation in the range 35 $\div$ 38 MHz). The recovery process can be expressed in terms of relaxation transition probabilities W which can be due, in principle, to two mechanisms:

(i) time dependence of the electric field gradient (EFG) components induced by lattice vibrations and/or by defect motion (quadrupole mechanism)

(ii) fluctuations of the local hyperfine field h(t) acting on the nucleus and due to localized and/or itinerant electron spins (magnetic mechanism).

It was found[7] that the dominant mechanism is the magnetic one except, perhaps, for ^{139}La around room temperature.

The dominant magnetic relaxation transition probability driven by the fluctuations induced by the Cu^{2+} electronic spins $\vec{S}(t)$ on the hyperfine field $\vec{h}(t) = h_{eff}\,\vec{S}(t)$ at the nucleus (^{63}Cu or ^{139}La) is:

$$W_M = \frac{1}{4}\gamma_N^2 \int < h_+(0)h_-(t) > \exp(-i\omega_R t)dt \qquad (1)$$

where ω_R is the resonance frequency for a given pair of NQR levels and the z axis is along the maximum component of the EFG tensor in its principal axis frame of reference. By introducing collective spin components $\vec{S}_{\vec{q}}$, in the assumption of isotropic spin fluctuations, and by taking into account that ω_R is much smaller than the characteristic frequencies of the spin fluctuations, the spectral density in Eq. (1) can be rewritten:[9]

$$J(\omega_R \simeq 0) = (h^0_{eff})^2 \frac{1}{N}\int \sum_q < S^z_q(0)S^z_{-q}(t) > dt \qquad (2)$$

where h^0_{eff} represents the hyperfine field at the nucleus for the rigid-lattice AF structure of localized Cu^{2+} magnetic moments (namely for T $\rightarrow$ 0 in the prototype system La_2CuO_4). The result in Eq. (2) is valid only if the hyperfine field is weakly $\vec{q}$ and $\alpha(\pm,z)$ dependent. This condition is fulfilled quite well for ^{63}Cu and approximately at the ^{139}La site.[7c]

By considering the relationship[7c] between W_M and the experimentally measured spin-lattice rates T_1^{-1}, one derives from Eqs. (1) and (2):

$$T_1^{-1} = \frac{1}{N}A\sum_q \int < S^z_q(0)S^2_{-q}(t) > dt = \frac{1}{N}A\sum_q \frac{|S_{\vec{q}}|^2}{\Gamma_q} \qquad (3)$$

where we have assumed that the isotropic collective spin fluctuations decay exponentially with decay rate Γ_q. Here, $A_{La} = 11.5\,\gamma^2_{La}\left(h^0_{eff}\right)^2_{La}$ and $A_{Cu} = 3\gamma^2_{Cu}$. From the splitting of the NQR

line below T_N, one obtains[7a,b] $\left(h^0_{eff}\right)_{La} \simeq 0.1$ Tesla(T) while from the ^{63}Cu zero field–NMR in La_2CuO_4 at 1.3 K one has[10] $\left(h^0_{eff}\right)_{Cu} = 7.8$ T, thus yielding

$$A_{La} = 1.6 10^{14} \quad rad^2 s^{-2} \tag{4a}$$

$$A_{Cu} = 9.10^{17} \quad rad^2 s^{-2} \tag{4b}$$

In normal exchange-coupled insulating magnetic systems, the relaxation rate T_1^{-1} can be related to the magnetic correlation length $\xi = k^{-1}$ in the framework of static and dynamic scaling:[9]

$$|S_{\vec{q}}|^2 = k^{-2+\eta} f_2(q/k) \tag{5a}$$

$$\Gamma_{\vec{q}} = B k^z f_3(q/k) \simeq \omega_e k^z f_3(q/k) \tag{5b}$$

where z and η are characteristic critical exponents.[9] In the assumption $f_2 \cdot f_3 \simeq 1$ and $\eta = 0$ one has:

$$T_1^{-1} = A \frac{k}{\Gamma_c}^{d-2} \tag{6}$$

where $\Gamma_c = \omega_e k^z$ is the frequency corresponding to the critical fluctuations and d is the lattice dimensionality. In the limit of no correlation, i.e., $T >> J/k_B$ where J is the Heisenberg exchange interaction one has:

$$\Gamma_c \simeq \omega_e = \left[\frac{8}{3}\frac{J^2 S(S+1)}{\hbar^2}\right]^{1/2} \tag{7}$$

NQR in the Low-Doping Semiconducting Phase

In the region of moderate doping ($x \leq 0.05$) it was found[7c,d] that the ^{139}La T_1^{-1} data are inconsistent with the predictions of Eq. (6) if one assumes that the correlation length is limited by thermal fluctuations, i.e. $\xi, \propto (T - T_N)^{-\nu}$. On the other hand, the ^{139}La relaxation data can be explained[7c,d] consistently if one assumes that the correlation length is limited by the presence of the mobile 0(2p) holes. This corresponds to the assumption that the local time-dependent correlation function of the Cu^{2+} spins decays exponentially to zero because of "collisions" with mobile defects rather than because of thermal fluctuations.

Then one can write, starting from Eq. (3):

$$T_1^{-1} = A \frac{\tau_d}{\Gamma_c \tau_d + 1} \simeq A\tau_d = A\tau_0 n^{-1} \tag{8}$$

where we introduce a "collision" time $\tau_d = \tau_0 n^{-1}$ inversely proportional to the effective concentration n of mobile defects. The assumption $\Gamma_c \tau_d << 1$ in Eq. (8) reflects the fact that the magnetic correlation is limited by the defects rather than by thermal fluctuations.

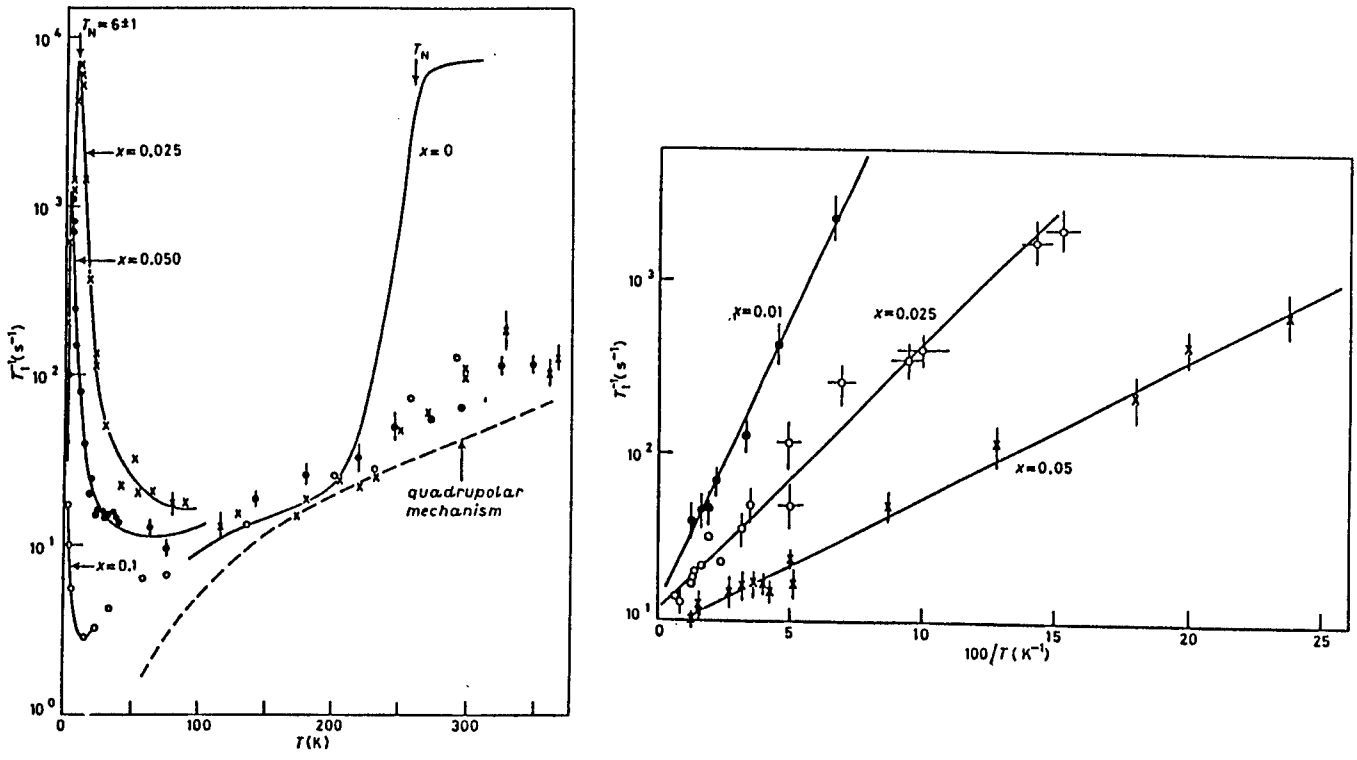


FIG. 2 ^{139}La NQR spin-lattice relaxation rates vs. temperature in $La_{2-x}CuO_4$. (a) The full lines are guides to the eye. The dashed line is the quadrupole contribution to relaxation as estimated theoretically in Ref. 7c. The position of the peak (T_1^{-1} vs. T) corresponds to the temperature T_N at which long range order sets in as reported in Fig. 1. (b) Semilog plot of T_1^{-1} vs T^{-1} used to obtain the activated law for the concentration n of mobile charge defects (see Eq. (9).)

By fitting Eq. (8) to the ^{139}La T_1^{-1} data for x < 0.1 (shown in Fig. 2), it was deduced[7c,d] that the concentration of mobile defects should follow a thermally-activated law

$$n(x,T) = x\exp\left(-0.85/xT\right) \tag{9}$$

with an x-dependent activation energy E(x) = 0.85/x(°K). This implies that as the temperature is lowered well below $\sim$ 0.85/x(K) the mobile defects "freeze" and the magnetic correlation length is no longer limited by the defects thus allowing the system to order at T_N (see Fig. 1). The fit of the ^{139}La T_1^{-1} yields $\tau_0 = 2.10^{-15}$ sec rad^{-1} which corresponds to the inverse of the exchange frequency, ω_c, defined in Eq. (7) for an exchange interaction J = 2700 K.

The present model leads to precise predictions[7c,d] regarding the x and T dependence of the correlation length ξ and of the ordering temperature T_N. Regarding ξ, one can note that the correlation length can be thought as the average distance among defects, i.e., $\xi \propto n^{-(1/d)}$ where d is the lattice dimensionality. Thus from Eq. (8), one has

$$T_1^{-1} = A\tau_0\xi^2 \tag{10}$$

where A is given in Eq. (4), $\tau_0 \simeq \omega_e$ as defined in Eq. (7) and we have taken d = 2 for the CuO_2 planes. From the experimental value for ^{139}La T_1^{-1} (see Fig. 2), one derives for ξ the values shown in Fig. 3. The theoretical curve:

$$\xi = \frac{1}{\sqrt{x}} \exp\left(\frac{0.85}{2xT}\right) \tag{11}$$

follows from our model and the result in Eq. (9). Regarding the x-dependence of T_N, it appears that the magnetic order sets in when the correlation length reaches a certain critical value ξ^* independent of concentration x. Setting $\xi^* = 100$ lattice units in Eq. (11) and solving for T, one has

$$T_N(x) = \frac{0.85}{2x\ell n(100\sqrt{x})} \tag{12}$$

The theoretical curve Eq. (12) is compared with the experimental values in Fig. 1.

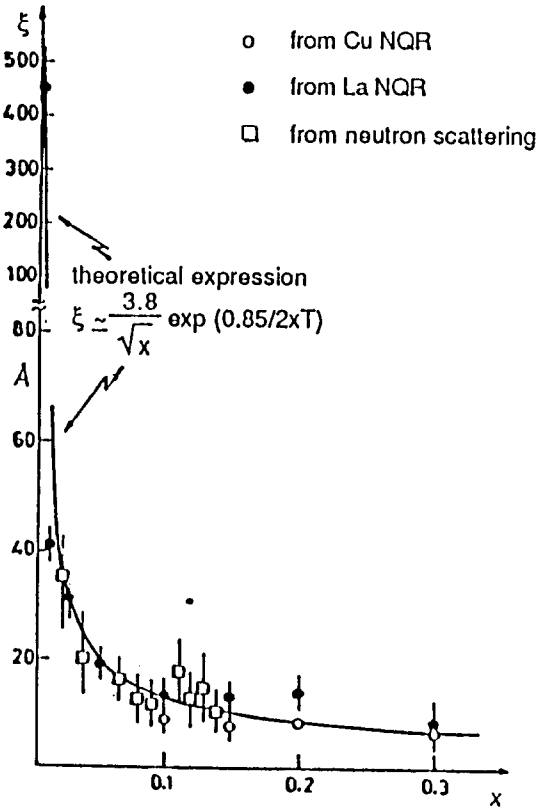


FIG. 3 In-plane magnetic correlation in $La_{2-x}Sr_xCuO_4$ at T = 77 K, in Å, as derived from NQR T_1 for ^{139}La and ^{63}Cu, according to Eq. (10) (the value for nominally pure La_2CuO_4 at $T \geq T_N$ is also reported) and comparison with the results obtained through neutron scattering (R. J. Birgeneau et al. *Phys. Rev. B* **39**, 2868 (1989).

It should be noted that in the analysis outlined above, the amplitude of the hyperfine magnetic field at the nuclear site has been assumed x and T independent and given by h^0_{eff} (see Eq. 4). Therefore, the role of the mobile 0(2p) holes for $x \leq 0.05$ is only the one of disrupting locally the strong AF correlations, without affecting the intrinsic magnetic moment of the Cu^{2+} ions. This corresponds to setting in Eq. (3) $< S_z^2 >= \frac{1}{N}\frac{\sum_i}{q} < |S_q|^2 > = 1$.

NQR in the High-Doping Metallic and Superconducting Phases

The NQR relaxation rates T_1^{-1} for both ^{63}Cu and ^{139}La in samples with $x \geq 0.1$ are characterized by a weakly temperature-dependent region at $T > 100$ K followed by a rapid decrease as the temperature is lowered through the superconducting critical temperature T_c (see Figs. 4 and 5). In order to analyze the data in these large doping metallic samples, one should refer to expressions of T_1^{-1} in terms of an x and T dependent generalized susceptibility $\chi(q,\omega)$ describing the coupled system of Cu 3d and O-2p holes.[11-13] However, since a rigorous treatment of this complex system is not yet available, we chose to interpret the data in terms of our simple phenomenological model which still retains the main physical insights. Starting from the "two fluid" model which appear to be valid in the low concentration semiconducting limit, i.e., $x \leq 0.05$, we write:

$$T_1^{-1} = A < S_z^2 > \tau_d + A_0^2 \chi_s^2(x,T)T \qquad (13)$$

where we neglect the weak q-dependence of the coupling parameter A for both ^{63}Cu and ^{139}La nuclei. Furthermore, the hyperfine interaction A should not change appreciably as a function of temperature as indicated qualitatively by the almost constant value of the quadrupole coupling frequency ν_Q, which, just like A, depends on the symmetry and probability density of the electronic wave function at the nuclear site.[14] The second term in Eq. (13) is the Korringa-type contribution[14] related to the hyperfine interaction, A_0, of ^{63}Cu (or ^{139}La) with the 0-2p Fermi liquid described by the spin susceptibility χ_S.

(a) ^{63}Cu Spin-Lattice Relaxation Rate

The ^{63}Cu NQR relaxation rates are shown in Fig. 4 for $x = 0.15$ and $x = 0.2$. The solid line in Fig. 4 is the theoretical behavior expected for $x = 0.2$ by using for T_1^{-1} the expressions (8) and (9) corresponding to $< S_z^2 > = 1$. With the value of A_{Cu} in Eq. (4b) and $\tau_0 = 2.10^{-15}$ s, one has $T_1^{-1} = 1.8\ 10^3/x$ in satisfactory agreement with the experimental results at high temperature.

As the temperature is lowered, one has a dramatic difference between the samples with low x and the ones at large doping. For $x \leq 0.05$, the relaxation rate becomes so short that the ^{63}Cu NQR signal is undetectable, conforming to the notion that the Cu^{2+} spins retain their localized character, i.e., $< S_z^2 > = 1$. On the contrary, for $x \geq 0.1$, one observes a rapid decrease of T_1^{-1} as $T \rightarrow T_c^+$, opposite to the behavior expected from the solid line in Fig. 4 indicating that the "two fluids" model breaks down in this limit.

The decrease of T_1^{-1} on cooling can be described phenomenologically as due to a decrease of the degree of localization of the Cu^{2+} spins associated with the coupling to the liquid of O-2p holes. Since the contribution to the Cu relaxation rate from the carriers, second term in Eq. (13), is negligible (see Fig. 4), one can derive the temperature dependence of $< S_z^2 > \sim \sum_q \chi(\vec{q},\omega = 0)$ from Eq. (13) and the data in Fig. 4. The results are shown in Fig. 5(a). From the semilog plot of $h_{eff}(x,T) = h_{eff}^0 < S_z^2 >^{1/2}$ vs T^{-1} shown in Fig. 5(b) the temperature dependence appears to be of the form exp $(-\Delta/T)$ with an activation energy which is correlated to T_c: in fact the ratio $2\Delta/T_c$ is close to 3.5 as one would expect for conventional BCS mechanism with gap 2Δ.[15]

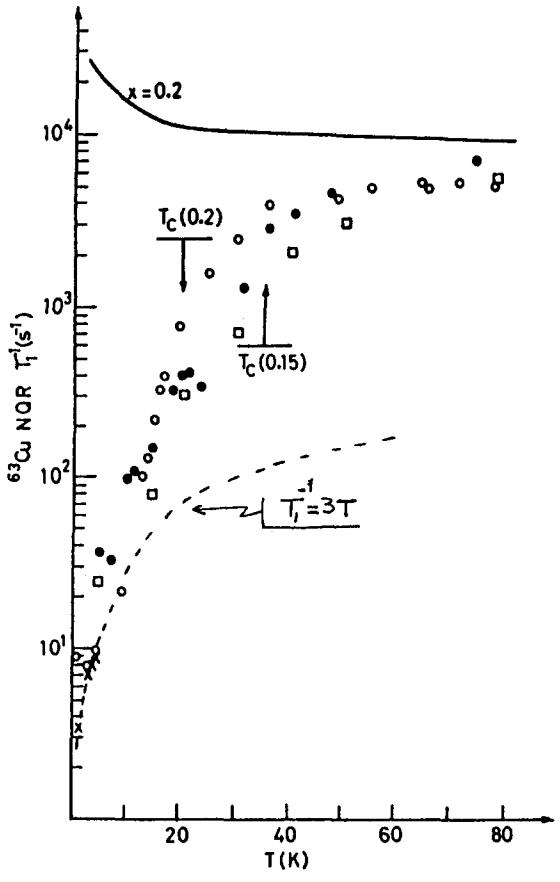


FIG. 4 ^{63}Cu NQR spin-lattice relaxation rates $T_1^{-1} = 6\ W_M$ vs. temperature in $La_{2-x}Sr_xCuO_4$ for: (O) x = 0.2; (●) x = 0.15. A few data from K. Ishida et al., *J. Phys. Soc. Jpn.* **58**, 36 (1989) are reported for comparison (□). The dashed line represents the Korringa-like contribution extrapolated from low temperature data (x) in x = 0.4 (Ref. 21). The solid line is the behavior expected from Eqs. (8) and (9) for a fully localized moment, i.e., $< S_z^2 > = 1$.

It should be emphasized that the physical interpretations of the decrease of $< S_z^2 >$ remains an open question. One could speculate that the apparent disappearance of the Cu^{2+} local moment could be just a way to describe the "quenching" of the local moment susceptibility due to the strong coupling with the conduction charges, a problem reminiscent of the Kondo effect found when a magnetic impurity is dissolved in a normal metal.

(b) ^{139}La Spin-Lattice Relaxation Rate

The ^{139}La NQR relaxation rates are shown in Fig. 6 for x = 0.2. The quadrupole contribution to the relaxation rate can be neglected in this temperature range[7] (see Fig. 2a). Therefore, one can use Eq. (13) to describe the two dominant relaxation mechanisms for ^{139}La. By using the results by Kobayashi et al.[16], for $x \geq 0.3$, one estimates for the ^{139}La Korringa term in Eq. (13), $A_0^2\chi_s^2 = 4.10^{-2}\ s^{-1}K^{-1}$ (a renormalization by a factor 10 is taken into account in this estimate because of a different definition of T_1 in terms of W_M used in Ref. 16). Two theoretical curves have been drawn in Fig. 6 to be compared with the experimental data. The first one (upper curve) is obtained by using Eq. (13) with the $< S_z^2 >$ extracted from the results for ^{63}Cu (see Fig. 5(a)), A from Eq. 4(a), $\tau_d = 10^{-14}x/(s.rad^{-1})$, and $A_0^2\chi_s^2 = 4.10^{-2}s^{-1}K^{-1}$ as given above. The second curve (lower curve in Fig. 6) is obtained as before, except for the scaling of the spin susceptibility in Eq. (13), according to $\chi_s(x,T) = \chi_s^0 < S_z^2 >^{1/2}$. This assumption takes into account the coupling of the Cu^{2+} spin with the O2p holes within the framework of our simple description. Because of the large uncertainty in the experimental results, it is not possible to decide which of the two descriptions is more appropriate. However, in either case, the temperature dependence of ^{139}La NQR relaxation for large x reflects unambiguously the temperature dependence of the localized Cu^{2+} magnetic moment in the same way as for ^{63}Cu NQR T_1.

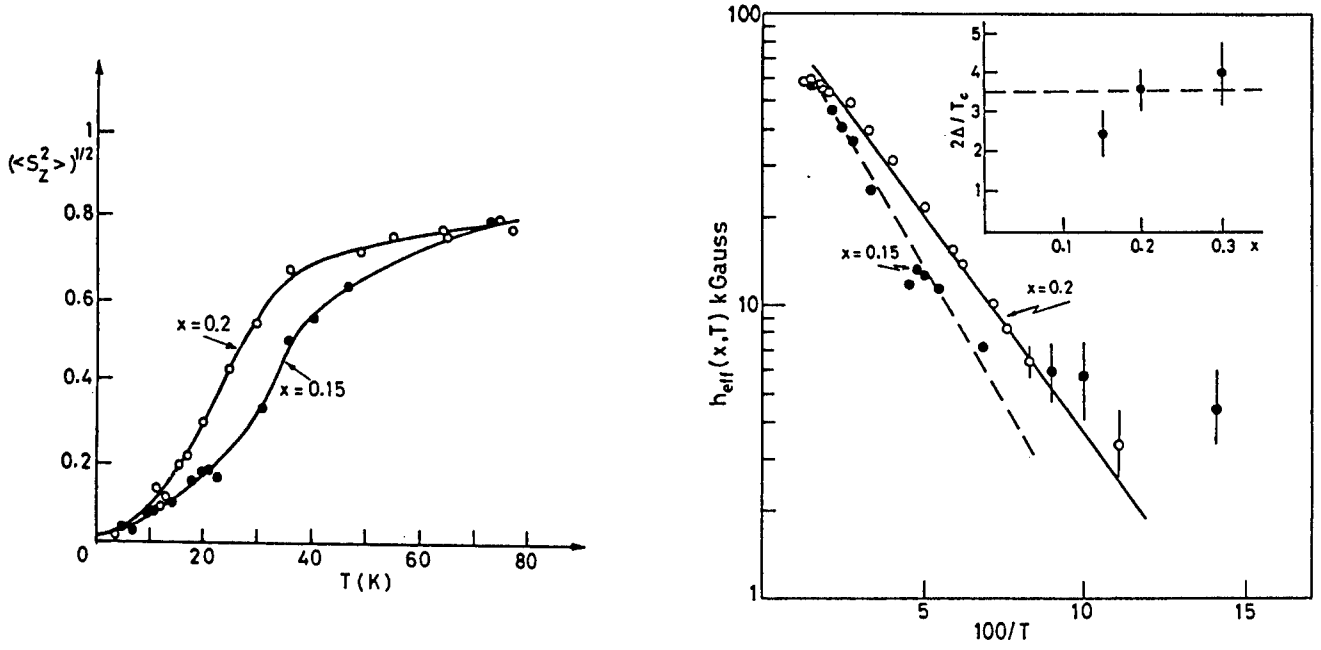


FIG. 5 (a) Temperature dependence of the normalized local Cu^{2+} spin moment, $(< S_z^2 >)^{1/2}$, in $La_{2-x}Sr_xCuO_4$ for x = 0.2 and x = 0.15 as obtained from the experimental data for ^{63}Cu NQR T_1 (Fig. 4) according to Eq. (13) in the text. Note that $T_c(0.2) = 20 \pm 5K$ and $T_c(0.15) = 35 \pm 5K$.

(b) Semilog plot of $h_{eff}(x,T) = h^0_{eff}(< S_z^2 >)^{1/2}$ vs. 100/T obtained by using the temperature-dependence of $< S_z^2 >^{1/2}$ shown in part (a) and $h^0_{eff} = 7.8$ T. The straight lines correspond to activation energies Δ (0.2) = 36 ± 3K and Δ (0.15) = 40 ± 10K. For x = 0.3 one obtains a more uncertain estimate of Δ around 10 K. In the inset, the ratio $2\Delta/T_c$ is shown as a function of x.

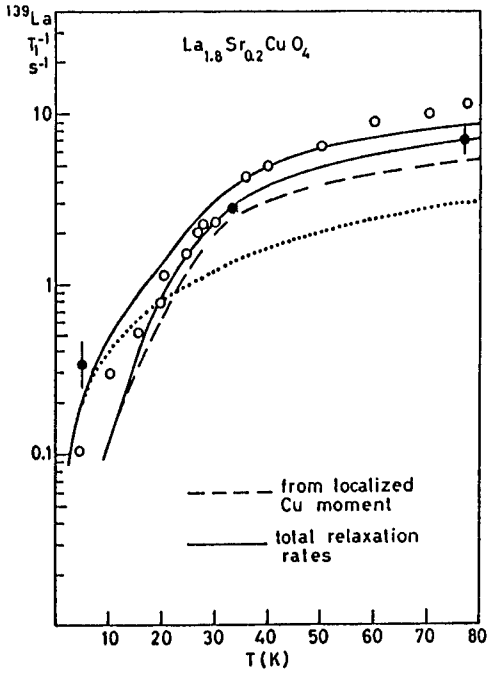


FIG. 6 Temperature dependence of ^{139}LA NQR relaxation rate in $La_{2-x}Sr_xCuO_4$ for x = 0.2. The experimental points are from Ref. 16 (O) with representative points measured by us (●). The dotted line represents the Korringa-like behavior obtained for x = 0.4 and x = 0.3 from Ref. 16 as explained in the text. The dashed line is the theoretical behavior according to the first term in Eq. (13) and using the temperature dependence of $< S_z^2 >$ shown in Fig. 5 (see text.). The two solid lines represent the total rates according to Eq. (13) as explained in the text.

Specific Heat Measurements

The samples with x = 0.01, 0.025, 0.05, and 0.1 show an anomaly in the specific heat which can be ascribed to the onset of long-range magnetic order[8] (see Fig. 7). The corresponding transition temperatures, T_N, derived from the position of the specific heat peak, are plotted in Fig. 1. As can be seen, our results compare well with the ones obtained from other techniques except for x = 0.1. The sharpness of the peak observed in the specific heat is more in favor of a 3D antiferromagnetic transition, as in the prototype La_2CuO_4, rather than a spin-glass type transition. It should be stressed that the anomalies reported here were not observed in the previous measurements, although a specific search for them does not seem to have been done.[17]

At high and intermediate temperatures, the effect of substituting La with Sr should be related mostly to the changes in the phonon spectrum.[8] For T < 15 K and for x = 0.05 and x = 0.025, there seems to be a hint of an x dependent broad maximum superimposed to the background specific heat. This feature could be associated with the excitation spectrum of the O-2p holes and/or the effect of the holes on the Cu^{2+} spin magnetic correlations. The contribution to the specific heat can be estimated in the framework of the heuristic model proposed to explain the NQR results. In such a model, it is hypothesized that the electronic holes are trapped at low temperature and become mobile with an activation energy E_a which is inversely proportional to x. By assuming that the mobile holes behave as a classical gas of noninteracting particles of concentration $\bar{n}$(x,T) one has:

$$\frac{C_v}{k_B} = E_a \frac{\partial \bar{n}(x,T)}{\partial T} = \left(\frac{0.85}{T}\right)^2 \frac{1}{x} \frac{\exp(-0.85/xT)}{(1+\exp(-0.85/xT))^2} \tag{14}$$

where we have used for $\bar{n}$(x,T) the normalized expression (9):

$$\bar{n}(x,T) = \frac{x\exp(-E_a/k_BT)}{1+\exp(-E_a/k_BT)} \tag{15}$$

with E_a/k_BT = b/xT (b=0.85 K). The theoretical behavior of Eq. (14) is compared with the experimental data in Figs. 7a,b. Although the agreement is rather poor, one should keep in mind that Eq. (14) was derived on the basis of an oversimplified model and that the parameters found in the NQR analysis were used without any adjustment.

Reproduced From
Best Available Copy

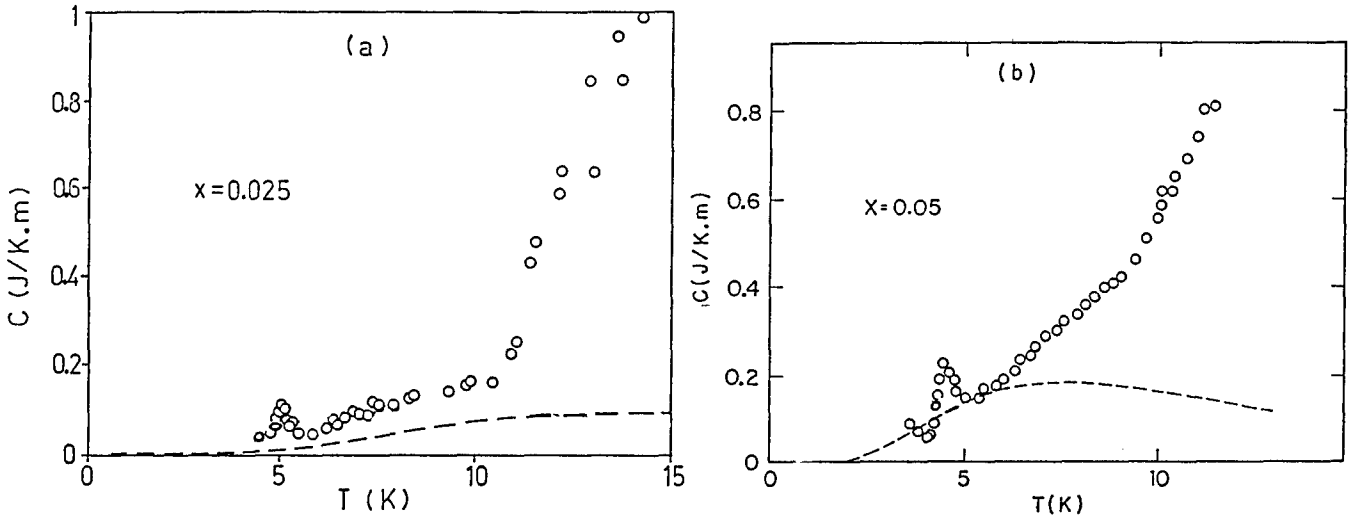


FIG. 7(a,b) Specific heat vs. temperature in $La_{2-x}Sr_xCuO_4$ for two Sr concentrations compared with the theoretical curve (Eq. (14) and (15) in the text) representing the contribution of the thermally excited O 2p mobile holes.

SUMMARIZING REMARKS

It has been shown that in the superconducting $La_{2-x}Sr_xCuO_4$ a decrease on cooling of the effective Cu^{2+} local spin moment occurs, possibly as a result of the pairing processes occurring in the liquid of charge carriers. This reduction, for large doping ($x > 0.1$) is observable well above T_c and it is consistent with susceptibility[18] as well as μSR[19] measurements. The temperature dependence of the effective Cu^{2+} spin appears to be well-described by an activated law, with a gap 2Δ correlated to T_c. If the decrease of $< S_z^2 >^{1/2}$ is indeed related to the opening of a gap, it is remarkable that the effect is observed well above T_c. Analogous "precursor" effects were detected in YBCO ($T_c = 61$ K) in the temperature range $90 \div 100$ K, and interpreted in terms of pair formation and energy gap beginning in the CuO_2 plane above the three-dimensional superconductivity.[1]

Numerical studies of the 2D Hubbard model have produced results for the dependence of the local spin moment from temperature and from the one-site repulsion U.[20] If analogous results could be obtained for the dependence of the Cu^{2+} local spin moment from the coupling to the thermally fluctuating Fermi liquid of O2p holes, they could be used for a more quantitative comparison with our experimental findings.

An important debated issue regards the possible coexistence of superconductivity and long-range magnetic order. Low temperature NQR spectra[21] for $x \geq 0.1$ were interpreted as indicating magnetic ordering, with reduced Cu^{2+} magnetic moments. However, more recent ^{63}Cu NMR-NQR spectra[22] in aligned polycrystalline samples seem to rule out the existence of a sizeable static hyperfine field at $T = 4.2$ K. The peak in the specific heat in the sample at $x = 0.1$ (see Fig. 1 and Ref. 8) could also be interpreted in terms of a phase separation or inhomogenity of the sample (the Meissner effect yielding $T_c = 28$ K for $x = 0.1$ is only partial, i.e., $\simeq 50\%$). Finally, no evidence of a static magnetic moment in $La_{1.85}Sr_{0.15}CuO_4$ at $T = 20$ mK was found in the time evolution of the muon polarization function.[23]

A comparison with recent findings by neutron scattering in LaSCO[24] and in YBCO[25] is in order. While T_1 is sensitive to the q-integrated generalized susceptibility in the MHz range, inelastic neutron scattering yield, in principle, $\chi''(q,\omega)$ in the whole frequency range, for a selected wave vector. However, a frequency resolution limit around 1 meV has to be taken into account, thus making difficult the comparison with the NQR relaxation rate. In particular, neutron scattering seems to indicate that around T_c the spin dynamics of the Cu^{2+} spins undergo a change: the normalized integrated intensity of the magnetic response function exhibits a drastic decrease in the low energy range, while it is not T-dependent for energies larger than about 15 meV, whereby the q-integrated spin is conserved.[25] Since no static hyperfine field at the Cu site can be detected below T_c, these modes would have to be interpreted as paramagnons in a strongly correlated itinerant antiferromagnetic system without long range order. In this case, the decrease of $< S_z^2 >^{1/2}$ observed by us (see Fig. 5) would have to be ascribed to a progressive changeover from a diffusive correlation function centered at zero frequency into an oscillatory correlation function having a power spectrum centered at ω_c, thus far above the NQR resonance frequency. The main conclusions regarding the temperature dependence of the effective hyperfine interaction due to the Cu^{2+} spins and of the spin susceptibility of the Fermi liquid, with the precursor effects above T_c are not modified.

We mention that the physical picture at the basis of the interpretative model outlined in this paper can be used consistently also to explain the ^{63}Cu, ^{89}Y, and ^{17}O NMR-NQR results in YBCO-type systems, as it is discussed elsewhere.[7e]

ACKNOWLEDGMENTS

The work in Pavia was supported by INFN (Grant MSC 1990-92) and by INFM–GNSM (Grant PI 40%). The collaboration with M. Corti, T. Rega, J. Ziolo, S. Aldrovandi, A. Lascialfari, F. Parmigiani, G. Chiodelli, and G. Flor is gratefully acknowledged. Ames Laboratory is operated for the U. S. Department of Energy by Iowa State University under Contract No. W-7405-ENG-82. This work was supported by the Director for Energy Research, Office of Basic Energy Sciences.

REFERENCES

1. W. W. Warren, J. and R. E. Walstedt, *Proceedings of the 10th International Symposium on NQR*, Takayama, Japan, 1989. To appear in *Z. Naturforschung.*

2. H. B. Brom et al., *Physica C* **153**, 753 (1988).

3. H. Alloul, T. Ohno, and P. Mendels, *Phys. Rev. Lett.* **63**, 1700 (1989).

4. Y. Kitaoka et al., Proceedings of *IBM Japan Symposium on Strong Correlation and Superconductivity*, May 1989, Mt. Fuji, Japan.

5. P. Wzietek et al., *Europhys. Lett.* **8**, 363 (1989).

6. M. Takikawa et al., *Phys. Rev. Lett.* **63**, 1865 (1989); *Phys. Rev. Lett.* **63**, 1992 (1989).

7. Most of the measurements reviewed here were reported by us in the following publications:

   a) J. Ziolo, F. Borsa, M. Corti, and A. Rigamonti *Physica C* **153**, 725 (1988).

   b) A. Rigamonti, F. Borsa, M. Corti, T. Rega, J. Ziolo, and G. Flor, in *Magnetic Resonance and Related Phenomena*, North Holland, 1989, p. 611.

c) F. Borsa, M. Corti, T. Rega, and A. Rigamonti, *Nuovo Cimento D* **11**, 1785 (1989).

d) A. Rigamonti, F. Borsa, M. Corti, T. Rega, J. Ziolo, and F. Waldner, in *Early and Recent Aspects of Superconductivity*, Eds. J. G. Bednorz and K. A. Müller (Springer-Verlag, 1990).

e) A. Rigamonti, M. Corti, T. Rega, J. Ziolo, and F. Borsa *Physica C* (in press).

8. S. Aldrovandi, F. Borsa, A. Lascialfari, and V. Tognetti, *J. Appl. Phys.* (in press).

9. See, for example, various contributions in *Local Properties at Phase Transitions*, Eds. K. A. Müller and A. Rigamonti (North Holland) 1976; see also: R. Borsa and A. Rigamonti, in *Magnetic Resonance at Phase Transitions*, Ed. F. J. Owens, C. P. Poole, and H. A. Farach (Academic Press, New York, 1979).

10. T. Tsuda et al., *J. Phys. Soc. Jpn.* **57**, 2908 (1988).

11. F. Mila and T. M. Rice, *Physica C* **157**, 561 (1989); see also *Phys. Rev. B* **40**, 11382 (1989).

12. N. Bulut, D. W. Hone, D. J. Scalapino, and N. E. Bickers, *J. Appl. Phys.* (in press).

13. B. Srizam Shastry, *Phys. Rev. Lett.* **63**, 1288 (1989).

14. G. C. Carter, L. H. Bennet and D. J. Kahan, *Metallic Shifts in NMR*, Progress in Materials Science, Vol. 20, Pergamon Press, 1977.

15. L. C. Hebel and C. P. Slichter, *Phys. Rev.* **113**, 1504 (1959).

16. T. Kobayashi et al., *J. Phys. Soc. Jpn.* **58**, 2662 (1989); *ibid.* **58**, 779 (1989).

17. For an exhaustive review of specific heat measurements in high-T_c superconductors see, for example; R. A. Fisher, J. E. Gordon, and N. Phillips, *J. Superconductivity* (1988).

18. D. C. Johnston, *Phys. Rev. Lett.* **62**, 957 (1989).

19. Y. I. Budnick et al., *Europhys. Lett.* **5**, 651 (1988).

20. J. E. Hirsch, *Phys. Rev. B* **31**, 4403 (1985); R. S. White et al., *Phys. Rev. B* **40**, 506 (1989).

21. K. Kumagai and Y. Nakawura, *Physica C* **157**, 307 (1989); see also Yoshimura et al., *J. Phys. Soc. Jpn.* **58**, 3057 (1989).

22. K. Yoshimura et al., *J. Phys. Soc. Jpn.* **58**, 3057 (1989).

23. R. F. Kiefl et al., *Phys. Rev. Lett.* **63**, 2136 (1989).

24. G. Shirane et al., *Phys. Rev. Lett.* **63**, 330 (1989).

25. J. Rossat-Mignod et al., *International Conference on the Physics of Highly Correlated Electron Systems*, Santa Fe (1989) and private communication.

MAGNETISM AND SUPERCONDUCTIVITY OF SOME Tl-Cu OXIDES

TIMIR DATTA*
Institute of Superconductivity & Physics, and Astronomy Department
University of South Carolina
Columbia, SC 29208

Many copper-oxide based "Thallium" compounds have now been discovered. Of these, the high temperature superconductors (HTSC) may be represented by the homologous series $(Tl_{1-x}A_xO)_m$-$(B_{1-v}C_y)_nCa_{p-1}Cu_pO_{2(p+1)+d}$; if A=Bi or Pb, B=Ba or Sr(5), C=Ce, Zr or Nd; n=2 and p=1-4. In comparison to the Bi-compounds, the Tl-system shows a richer diversity; viz., HTSC can be obtained with either one or two Tl-O layers (m=1,2); also, the triple-digit phases are easier to synthesize. The value of d, the oxygen stochiometry, is critical to achieving superconductivity. The Tl-system is robust to oxygen loss; Tl may be lost or incorporated by diffusion. We determine a diffusion coefficient equal to 10 m s at 900C. Both ortho-rhombic and tetragonal structures are evidenced, but HTSC behavior is indifferent to the crystal symmetry. This system has the highest Tc confirmed. Tc generally increases with p, the number of Cu-O layers, but tends to saturate at p=3. Zero resistance as high as 125K has been observed (1). Most of these HTSC's are hole type, but the Ce-doped specimens may be electronic.

The effort at USC has focused on the magnetic aspects; because in addition to defining the perfectly diamagnetic groundstate as in the conventional superconductors, magnetism of the copper oxides (1) show a surprising variety. This is true of both the normal and the superconducting states. Also, due to the large phonon contribution to the specific heat at the high Tc, accurate thermal measurement of important parameters such as the sp. heat jump, electronic density of states, D(Ef) and coherence length are uncertain, and thus, are estimated from the magnetic results.

We determine for single phase: (i) Tl-Ba; D(Ef)=2.0 states/ev.at. Cu, a BCS sp. ht. jump=6.2 mj/mol.Cu K; and (ii) Tl-(Ba,Ce); D(Ef)=2.2 and a BCS sp. ht. jump=6.8 (same units). For both, the Cu moment is about 0.1-0.4 Bohr mag. The Ce moment is 1.5, representing a charge state higher than 3+. This is indicative of electron doping and is evidence for n-type behavior. Paraconductivity and diamagnetic fluctuations are consistent with the expected two-dimensionality. Flux creep shows trapping potential somewhat stronger than those in Y-123. These and other results from the Tl-system Cu-O, LaBaCu-O,120 and the Bi-CuO compounds will be discussed. The emphasis will be on the role of magnetism in the Tl-CuO HTSC, but technological aspects will also be pointed out.

* In collaboration with A.M. Hermann (U. Colorado) and D.U. Gubser (Naval Research Lab.). Partially supported by USC and SDIO.

(1) Copper Oxide Superconductors, by C.P. Poole, T. Datta, and H.A. Farach, John Wiley & Sons, New York, NY, 1988.

SECTION 5:
APPLICATIONS

A TECHNIQUE TO MEASURE THE THERMAL DIFFUSIVITY OF HIGH T_c SUPERCONDUCTORS

Charles E. Powers
Goddard Space Flight Center
Materials Branch, Code 313
Greenbelt, Md. 20771

High temperature superconducting electrical current leads and ground straps will be used in cryogenic coolers in future NASA Goddard Space Flight Center missions. These superconducting straps will be long, thin leads with a typical diameter of 0.2 cm. A longitudinal method is being developed to measure the thermal diffusivity of candidate materials for this application. This technique will use a peltier junction to supply an oscillatory heat wave into one end of a specimen and will use low mass thermocouples to follow the heat wave along the specimen. The thermal diffusivity will be calculated using both the exponential decay of the heat wave and the phase shift of the wave. Measurements will be done in a cryostat between 10 K and room temperature.

INTRODUCTION

A program has been initiated in the Materials Branch at the Goddard Space Flight Center to develop methods for characterizing candidate high temperature superconducting (HTSC) material for possible space flight use. Part of this program has been directed at measuring various physical quantities of HTSC electrical current leads that may be used in cryogenic coolers. These current leads will typically be between 0.1 and 0.2 cm in diameter. The advantages of using current leads constructed from HTSC material over conventional current leads are higher electrical conductivity and lower thermal conductivity. The disadvantages of using HTSC material are its mechanical properties. Since all HTSC materials are ceramics, they have a low ductility and have a widely varying strength due to inherent defects typical of ceramics.

In this paper, preliminary measurements of the thermal diffusivity, **D**, of a $YBa_2Cu_3O_{7-x}$ specimen are reported. These thermal diffusivity measurements will be used along with thermal conductivity and specific heat measurements, to be made using the same apparatus, to characterize the thermal properties of HTSC specimens.

The technique used to measure thermal diffusivity is an implementation of Angstrom's temperature wave method.[1] A heater is attached to one end of a specimen rod to send a periodic heat wave down the rod. Two thermometers are mounted along the specimen to follow the wave. The phase difference between the temperature oscillations at the two thermometers and the ratio of the amplitudes of these oscillations are used to calculate **D**.

SPECIMEN DESCRIPTION

The HTSC specimen used for these experiments is manufactured by Argonne National Laboratory. The x-ray diffraction pattern for the specimen shows it to be single phase $YBa_2Cu_3O_{7-x}$ with trace amounts of barium oxide and other impurities. AC susceptibility measurements (Figure 1) done at 100 kHz, in the absence of an external magnetic field, show the specimen to have a critical temperature of 90 K and a transition region of about 2 K. The specimen has a cylindrical shape with a diameter of 0.188 cm, a length of 2.556 cm, and a density of 5.93 gm/cm^3.

EXPERIMENTAL METHOD

In this implementation of the temperature wave method, a peltier junction is used to generate a periodic heat wave and two chromel-alumel thermocouples made of 0.0076 cm diameter wire are used to measure the temperature along the specimen rod (Figure 2). One thermocouple is connected to the specimen 0.487 cm from the peltier junction, and the other is 1.799 cm from the peltier junction. The peltier junction is mounted on a block of aluminum that is used to control the absolute temperature at which a measurement is made. Running through the aluminum block are

several copper tubes through which liquid nitrogen is allowed to flow to control the temperature of the peltier junction and specimen rod. Presently, measurements are made in vacuum (10^{-5} torr) between 150 and 300 K. The use of a cryostat in the future will allow measurements to be made between 10 and 300 K. The peltier junction is connected to the block of aluminum and the specimen rod using STYCAST 2850FT epoxy manufactured by Emerson & Cuming. The thermocouples are also connected to the specimen rod using STYCAST 2850FT.

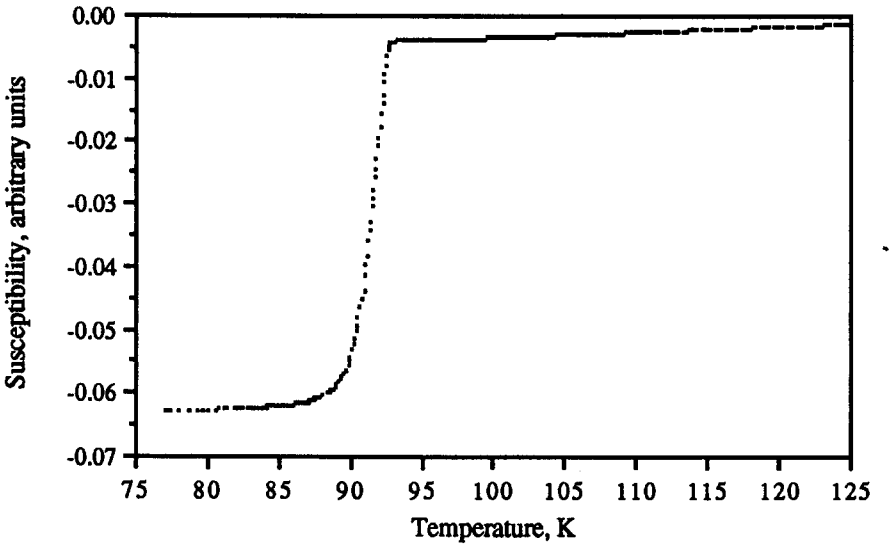


Figure 1. AC susceptibility of the $YBa_2Cu_3O_{7-x}$ specimen used in these experiments.

A Hewlett-Packard 3314A function generator connected to a Kepco BOP 50-2M amplifier are used to produce an oscillating current through the peltier junction. The function generator is capable of generating a sinusoidal signal with a frequency as low as .001 Hz. A Fluke 8505A digital multimeter and a Keithley 196 system digital multimeter are used to measure the voltage across each thermocouple. Both multimeters have a resolution of 100 nV (this is about 0.0025 K for chromel-alumel thermocouples). A Fluke 1722A instrument controller is used to record the measurements from the multimeters.

By controlling the amount of liquid nitrogen that flows through the copper tubes mentioned previously, the absolute temperature at which a diffusivity measurement is made can be set. Once the temperature of the aluminum block and test specimen have reached equilibrium, a periodic current is supplied to the peltier junction to generate a thermal wave through the specimen rod. When the temperature oscillations at each thermocouple reach steady state, a BASIC program is initiated on the Fluke 1722A instrument controller to read and record the voltage across each thermocouple. For these experiments the frequency of oscillation of the thermal wave ranges between .01 and .05 Hz, so the voltage across each thermocouple is sampled once a second giving between 20 to 100 measurements per cycle.

DATA ANALYSIS

To calculate the thermal diffusivity from the voltage measurements mentioned previously, a curve fitting routine is used to determine the magnitude and phase of the temperature oscillations at each thermocouple. These values are then used in the following equation to calculate diffusivity,

$$D = (\pi f L^2)/[\phi \ln(a_0/a_1)] \qquad (1)$$

where f is the frequency of oscillation, L is the distance between the thermocouples, ϕ is phase different between the thermocouples, a_0 is the amplitude of the temperature oscillation at the thermocouple closest to the peltier junction,

and a_1 is the amplitude of the temperature oscillation at the second thermocouple. This equation assumes that the amplitude of the heat wave has decayed to a negligible value at the end of the specimen farthest from the peltier junction.

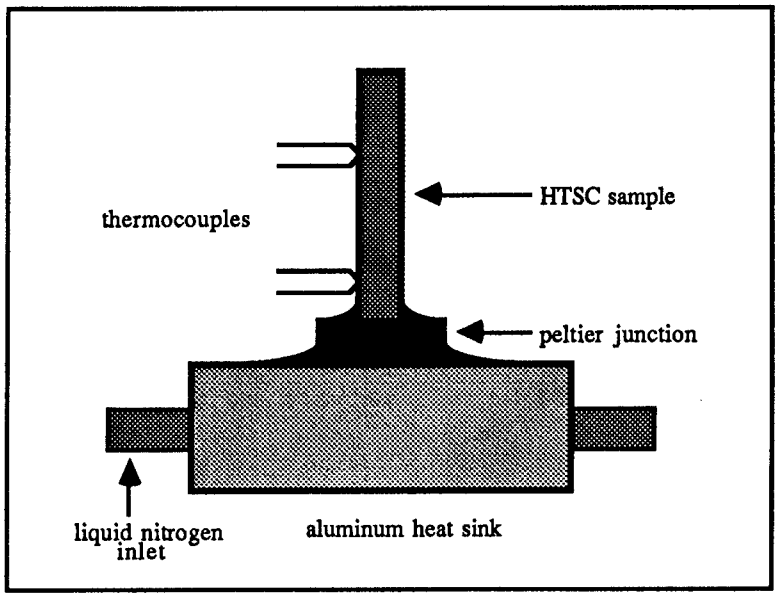


Figure 2. Basic apparatus for measuring thermal diffusivity.

For negligible lateral heat losses to the surrounding environment or thermocouples the phase difference between the thermocouples is approximately equal to the logarithm of the amplitude ratio, and the following equation can be used to calculate diffusivity,

$$\mathbf{D} = (\pi f L^2)/(\phi^2) = (\pi f L^2)/[\ln(a_0/a_1)]^2. \qquad (2)$$

In these experiments, the value of diffusivity calculated using only the phase difference is always about 10% larger than the values calculated using the amplitude ratio, indicating some lateral heat loss. Modified diffusivity calculations which account for losses due to the thermocouples only predict the value calculated from the phase difference to be about 2% larger than the value from the amplitude ratio. This 10% difference is characteristic of a lateral heat loss, which presently has not been identified. Radiative coupling with the surrounding environment could be the cause of this heat loss. During these experiments, measurements below room temperature always had a temperature gradient across the specimen, which can be entirely accounted for by radiative coupling calculations.

Two alternate equations, which account for the reflection of the heat wave at the end of the rod farthest from the peltier junction, can be used to calculate the diffusivity. These equations are,

$$(a_0/a_1) = \tan^{-1}[\tan(kx_0)\tanh(kx_0)] - \tan^{-1}[\tan(kx_1)\tanh(kx_1)] \text{ and} \qquad (3)$$

$$\phi = \sqrt{[\cosh(2kx_0)+\cos(2kx_0)]/[\cosh(2kx_1)+\cos(2kx_1)]} \qquad (4)$$

where $k = \sqrt{\pi f/D}$, and the lengths x_0, x_1 are measured from the free end of the rod to the thermocouples mounted closest and farthest respectively from the peltier junction.[2] The diffusivity values calculated from equation (2) are always within two percent or better of the values calculated with equations (3) and (4), indicating that the amplitude of the thermal wave at the end of the rod farthest from the peltier junction is negligible for these calculations.

The diffusivity of a cylindrically shaped fused SiO_2 specimen (Corning 7940) with a diameter of 0.404 cm and a length of 11.9 cm was measured using this technique to test the accuracy of the technique. The measured values (Figure 3) agree to within ± 6% of the values reported by Luikov, Vasiliev, and Shashkov.[3] Most of the uncertainty in these measurements is due to thermal noise associated with the thermocouple contacts. The amplitude of the temperature wave at the thermocouple closest to the peltier junction is typically 0.6 K (1.2 K peak-to-peak), and the amplitude at the other is typically 0.03 K, while the standard deviation of the noise is 0.015 K. When this noise is simulated using a computer program a ± 5% uncertainty in the generated diffusivity values is observed, which is in good agreement with the measured values.

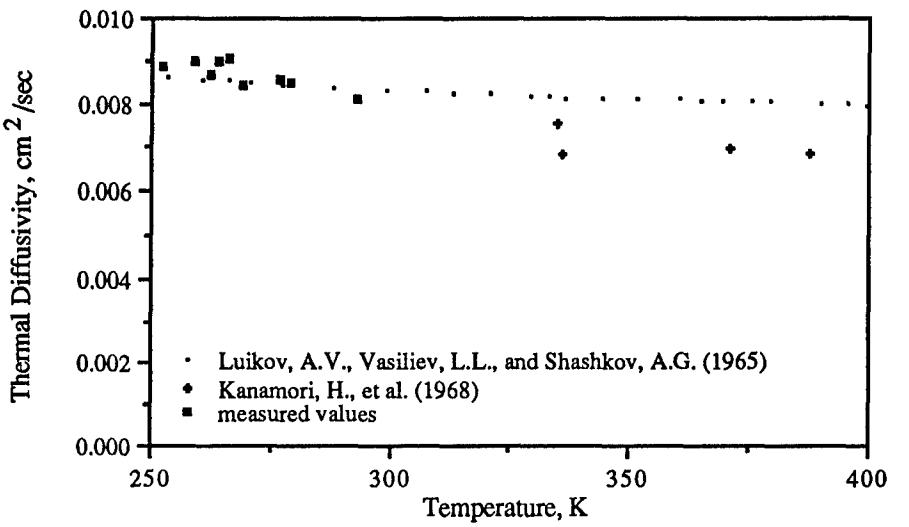


Figure 3. Thermal diffusivity of fused SiO_2.

RESULTS

The thermal diffusivity of the $YBa_2Cu_3O_{7-x}$ specimen, calculated using equation (1), is shown in Figure 4. All measured values of diffusivity are within ± 4% of a second order polynomial fit to the data. Again, the amplitude of the temperature wave at the thermocouple closest to the peltier junction is typically 0.6 K, and the amplitude at the other is typically 0.03 K, but the standard deviation of the noise is only 0.012 K. When this noise is simulated using a computer program a ± 4% uncertainty in the generated diffusivity values is observed, which is in good agreement with the measured values as compared to the polynomial fit.

CONCLUSION

From the measured values of thermal diffusivity for fused SiO_2, as compared to other reported values, it is concluded that the accuracy of this technique is about ± 6%. Further, the agreement in uncertainty between the measured values and the computer simulated values indicate that most of the error is due to noise associated with the thermocouples. There may also be a systematic error of about 2% due the distance measurement between the thermocouples.

To improve the accuracy of this technique, several changes will be made in the future. The first will be the use of a cryostat, which will decrease the amount of radiative coupling of the specimen with the surrounding environment and will allow for measurements down to 10 K with better temperature control. The thermocouples to be used in future measurements will have a diameter of 0.0025 cm, which will decrease heat losses to the thermocouples and will increase the accuracy of the distance measurement between the thermocouples. These thermocouples will also be connected in series with junction thermocouples (that will be connected to the block of aluminum) to eliminate any DC voltage across the thermocouples due to the absolute temperature of a measurement. This voltage is typically

100 times larger than the magnitude of the voltage oscillations due to the heat wave. Eliminating this offset will increase the accuracy of the temperature measurements by allowing the use of voltage amplifiers and filters.

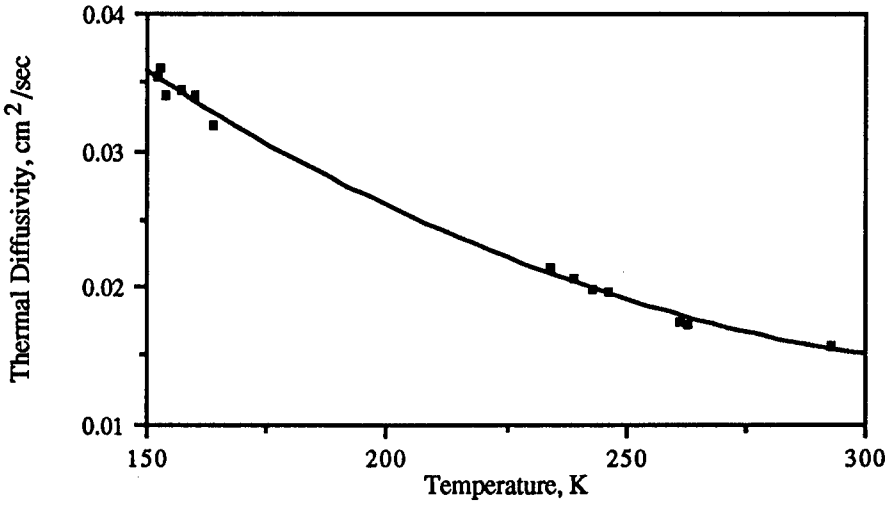


Figure 4. Thermal diffusivity of $YBa_2Cu_3O_{7-x}$ specimen.

ACKNOWLEDGEMENTS

The author would like to thank Mr. C. Clatterbuck for his help in connecting the thermocouples and peltier junction to the specimen rod. The author would also like to thank Mr. S. Pagano for his help with the vacuum system used in these experiments and his efforts in constructing the test apparatus. A thorough and rigorous analysis of the experimental data was made possible through many conversations with Dr. H. Leidecker, with whom most aspects of thermal wave propagation were discussed. Dr. H. Leidecker also first suggested using a peltier junction to generate a heat wave.

REFERENCES

1. Touloukian, Y.S., Powell, R.W., Ho, C.Y., and Nicolaou, M.C., Thermal Diffusivity -- Vol. 10 of Thermophysical Properties of Matter -- The TPRC Data Series, pp. 28a-37a, IFI/Plenum Data Corp., New York, 1973.

2. Howling, D.H., Mendoza, E., and Zimmerman, J.E., "Preliminary Experiments on the Temperature-Wave Method of Measuring Specific Heats of Metals at Low Temperatures", A229, pp. 86-109, 1955.

3. Touloukian, Y.S., Powell, R.W., Ho, C.Y., and Nicolaou, M.C., Thermal Diffusivity -- Vol. 10 of Thermophysical Properties of Matter -- The TPRC Data Series, pp. 399-400, IFI/Plenum Data Corp., New York, 1973.

THE EFFECTS OF SPACE RADIATION ON THIN FILMS OF $YBa_2Cu_3O_{7-x}$

R. Herschitz, A. Bogorad, C. Bowman and S.S. Seehra
General Electric Astro-Space Division
Princeton, New Jersey 08543-0800

A. Mogro-Campero and L.G. Turner
General Electric Research & Development Center
Schenectady, New York 12301

ABSTRACT

Thin films of polycrystalline $YBa_2Cu_3O_{7-x}$ (YBCO) grown on silicon were exposed to Co-60 gamma rays and 780-keV electrons, simulating the effect of low-earth-orbit radiation. Neither a dose of 50 megarads nor a fluence of 10^{15} e/cm^2 produced a significant decrease in critical transition temperature.

INTRODUCTION

High temperature superconducting materials are expected to offer significant improvements in the performance of spacecraft components. Specifically, low surface resistance at high frequencies is expected to result in reduced RF losses in superconducting waveguides, bandpass filters, and antennas.

It is attractive to provide passive cooling to superconductors by locating them on the shaded side of a space vehicle, radiating directly into space. Unfortunately, the technique results in exposure to high radiation dose levels due to trapped electrons and protons in the space environment. The high energy electrons and the protons will lose most of their energy in the first few microns inside the surface. For example, a typical surface dose for a 5-year mission in low earth atmospheric remote sensing orbit is 10^{15} electron/cm^2 which deposits 10 Megarads (10^9 ergs/gram) of energy in surface material. This is two or three orders of magnitude higher than the dose to most satellite electronics, which are shielded by at least several millimeters of material. The effects of space radiation on superconducting properties of YBCO materials are therefore critically important in incorporating these materials into spacecraft systems. The effects of charged particle irradiation on surface morphology of superconducting thin films has been published (1-3).

This investigation had two objectives: (1) to determine the effects of space radiation on superconductor parameters that are most important in space applications and (2) to determine whether this effect can be simulated with Co-60 gamma rays, the standard test method for space materials.

EXPERIMENTAL CONDITIONS

Thin films of YBCO were formed by coevaporation of Y, BaF_2, and Cu and post-annealing in wet oxygen at 850°C for 3.5 h. The substrate used was (100) silicon with an evaporated zirconia buffer layer. Processing and microstructure studies of these types of films have been published (4-7). The zero-resistance transition temperatures of the samples used in this study were 84 to 86K. The samples were characterized by four point probe electrical measurements as a function of temperature. The parameters measured were: the zero-resistance transition temperature (T_c) and the room-temperature resistance. The samples were then exposed to Co-60 gamma rays, in air and in pure nitrogen, and to 780-keV electrons, in air. The parameters were then remeasured.

RESULTS

The results are summarized in Tables 1 and 2.

The results indicate little or no degradation in the parameters measured for samples exposed up to 50 megarads of gamma rays in nitrogen. However, complete degradation of samples exposed to 10 megarads in air was observed. This degradation is preliminarily attributed to the high level of ozone generated in the chamber by the gamma ray interaction with air. Furthermore no degradation in superconducting properties of samples exposed to 10^{15} electrons at 780 keV in air was observed.

DISCUSSION

The radiation tests show that polycrystalline YBCO films on Si are only slightly affected by gamma and electron radiation. Significant changes in the electrical properties of bulk YBCO exposed to 1-MeV electrons have been reported [8]. For these YBCO bulk materials, degradation occurred at a fluence of 6.5 x $10^{11}e/cm^2$. We believe that the relatively good performance of our thin films is related to the use of BaF_2 as an evaporation source.

Even though the annealing of thin films is performed in wet oxygen to remove the fluorine from the films we have found by x-ray photoelectron spectroscopy that about 1 atomic % fluorine abundance remains in the surface region. We speculate that the fluorine improves the degradation performance of these films [9]. As suggestive evidence we cite Tressaud et al, [10], who find that a thin surface layer containing fluorine provides protection against hydrolysis and gas exchange. It has also been suggested [11] that a thin surface layer containing fluorine improves the resistance of YBCO to degradation caused by thermal cycling.

CONCLUSION

It can be concluded that (1) the electron component of space radiation does not degrade the critical temperature of the YBCO films described herein, at least for energies around 800 KeV and doses similar to those received by surface materials on spacecraft in typical remote sensing missions; (2) for qualifying this and other superconducting materials against the space-radiation threat the standard test method used in the aerospace industry, namely, exposure to Co-60 gamma rays in air, may require some further investigation. As a minimum, the sample must be either in vacuum or in positive nitrogen pressure.

The results of this study and that reported in [11] are encouraging for the use of YBCO films in low earth orbit satellites because these films resist degradation from radiation [this paper] and temperature cycling [11]. Thus, even with a lack of protective layers, passive cooling can be provided to the thin YBCO films by exposing them to space without concern about radiation damage.

REFERENCES

1. D.M. Parkin and M. Nastasi, "Radiation induced amorphization in $YBa_2Cu_3O_7$ and $GdBa_2CU_3O_7$ superconductors", Proceedings of the Materials Research Society Meeting, Nov. 28 - Dec. 03, 1988, Boston, MA.

2. N. Nastasi, D.M. Parkin, T.G. Zocco, J. Koike, P.R. Okamoto, "Electron irradiation induced amorphization in $YBa_2Cu_3O_7$ and $GdBa_2CU_3O_7$ superconductors, Appl. Phy. Lett. 53 (14), 1988.

3. B. Egner, J. Geerk, H.C. Li, G. Linker, O. Meyers, B. Strehlau, "The influence of irradiation-induced defects on the superconductivity of $YBa_2Cu_3O_7$", Japanese Journal of Applied Physics, 26, 2141-2142, 1987.

4. A. Mogro-Campero, L.G. Turner, E.L. Hall, and M.C. Burrell, "Characterization of thin films of YBaCuO on oxidized silicon with a zirconia buffer layer", Appl. Phys. Lett. 52 (24), 2068-2070, 1988.

5. A. Mogro-Campero, L.G. Turner, and G. Kendall, "Thickness and annealing dependence of the superconducting transition temperature of $YBa_2Cu_3O_{7-x}$ thin films on oxidized silicon and polycrystalline alumina substrates", Appl. Phys. Lett. 53 (25), 2566-2568, 1988.

6. A. Mogro-Campero, L.G. Turner, and E.L. Hall, "Large differences of critical current density in thin films of superconducting $YBa_2Cu_3O_{7-x}$", J. Appli. Phys. 65 (12), 4951-4954, 1989.

7. A. Mogro-Campero, L.G. Turner, E.L. Hall, M.F. Garbauskas, and N. Lewis "Epitaxial growth and critical current density of thin films of $YBa_2Cu_3O_{7-x}$ on $LaA1O_3$ substrates", Appl, Phys. Lett. 54 (26), 2719-2721, 1989.

8. R. Adem, L. Martinez, J. Rickards, E. Orozco, J. Fuentes-Maya, J.L. Albarran, A. Mendoza, E. Carrillo, L. Cota, J. Reyes-Gasga, J.L. Boldu, R. Perez, J.G. Perez-Ramirez and J. Jose Yacaman, "The effects of electron irradiation in high-T_c oxide superconductors", J. Maters. Res. 3 (5), 807-810, 1988.

9. P.M. Mankiewich, J.H. Scofield, W.J. Skocpol, R.E. Howard, and A.M. Dayem, "Reproducible Technique for fabrication of thin Films of high transition temperature superconductors" App. Phys. Lett. 51 (21), 1753-1755, 1987.

10. A. Tressaud, B. Chevalier, B. Lepine, J.M. Dance, L. Lozano, J. Grannec, J. Etourneau, R. Tournier, A. Sulpice, and P. Lejey, "Passivation process of high T_c superconducting $YBa_2Cu_3O_{7-x}$ by fluorine gas treatment." Modern Phys. Lett. B2 (10), 1183-1188, 1988.

11. A. Mogro-Campero, L.G. Turner, A. Bogorad, R. Herschitz "The effects of temperature cycling typical of low earth orbit satellites on thin films of $YBa_2Cu_3O_{7-x}$", Conference Proceedings of AMSAHTS, April 2-6, 1990, Greenbelt, MD.

	SAMPLE DESCRIPTION	AMBIENT ENVIRONMENT	GAMMA-RAY DOSE (Mrad)	TRANSITION TEMPERATURE (K) BEFORE EXPOSURE	TRANSITION TEMPERATURE (K) AFTER EXPOSURE	COMMENTS
1a)	YBCO on Si	Air	10	86	--	Catastrophic failure
1b)	YBCO on Si	Air	100	85	--	Complete erosion of superconducting film
2a)	YBCO on Si	Nitrogen	10	85	84	No degradation in Tc
	YBCO on Si	Nitrogen	50	85	84	No degradation in Tc
2b)	YBCO on Si with silver pads	Nitrogen	10	86	82	Slight degradation in Tc
		Nitrogen	50	86	81	
3)	YBCO on Si (Control Sample)*	Air	--	85	85	No degradation in Tc (after 21 days)

*The control sample was placed outside of the Co-60 source and its superconducting properties were compared to the exposed samples.

TABLE 1: SUMMARY OF GAMMA-RAY EXPOSURES ON SUPERCONDUCTING MATERIALS

	SAMPLE DESCRIPTION	AMBIENT ENVIRONMENT	ELECTRON DOSE	TRANSITION TEMPERATURE (K) BEFORE EXPOSURE	TRANSITION TEMPERATURE (K) AFTER EXPOSURE	COMMENTS
1)	YBCO on Si	Air	10^{15} electron/cm^2	84	84	No degradation in Tc
2)	YBCO on Si (Control Sample)*	Air	---	85	85	No degradation in Tc

* The control sample was placed outside of the electron generator and its superconducting properties were compared to the exposed samples.

TABLE 2: SUMMARY OF ELECTRON EXPOSURES ON SUPERCONDUCTING MATERIALS

An Instrument for Spatial Conductivity Measurements of High T_c Superconducting (HTSC) Materials

T. Van Sant
Materials Branch, Goddard Space Flight Center
Greenbelt, Maryland 20771

HTSC thin films have been suggested for use in a number of aerospace applications such as an IR bolometer and as electromagnetic shielding. As part of its flight assurance role, the Materials Branch of the Goddard Space Flight Center has initiated development of an instrument capable of measuring variations in conductivity for flat samples using an eddy current testing device and an X-Y positioning table. This instrument has been used to examine bulk HTSC samples. System changes that would enable characterization of thin film materials are discussed.

Introduction

Blendell et al (1) have noted the correlation between room temperature conductivity of $YBa_2Cu_3O_{7-x}$ specimens and transition temperature (T_c). Viens (2) reported success using a simple eddy current scope to distinguish between superconductive and nonsuperconductive $YBa_2Cu_3O_{7-x}$ specimens of identical geometries and that the strength of eddy current readings was directly correlated with room temperature conductivity.

This series of findings led to the suspicion that initial screening of bulk samples using various compositions and processes could then be done quickly at room temperature. It was hoped that combination of precise motion control and a data acquisition system would provide information about the spatial variation in conductivity in flat samples at room temperature.

Instrument Description

The eddy current testing system is shown schematically in Figure 1. A conventional eddyscope is used to generate eddy currents in the HTSC samples. This instrument generates an alternating current in a coil placed over a flat specimen, thereby creating a changing magnetic field. This changing magnetic field in turn creates an electric field and a current flows in response. This current creates a magnetic field which bucks that of the probe. An impedance bridge internal to the eddyscope attempts to balance the impedance of a reference coil and the coupled probe and sample. The eddyscope displays the measured response in two dimensions corresponding to the real and imaginary components of the effect of the specimen impedance.

Probe widths used in this test varied from 50 to 125 mils; driving frequencies ranged from 100kHz to 6MHz. The skin depth (δ) of an electromagnetic field is given by:

$$\delta = \frac{1}{\sqrt{\pi \mu \sigma f}} \qquad (1)$$

where μ is the magnetic permeability, σ the conductivity, and f the frequency of the field (3). Assuming a conductivity of 200 S/cm (1), skin depths could vary from ~1 cm at 100kHz to ~1.5mm at 6MHz. Precise determination of skin depth is difficult since probe width also is a contributing factor. Ultimately, 6MHz proved a suitable frequency for bulk materials (but thin films will require different hardware capable of much higher frequencies).

A scan is accomplished as follows. A flat specimen is positioned on a PC-controlled, XY table. The table's two stepping motors are controlled by separate indexing boards which occupy single slots on the PC

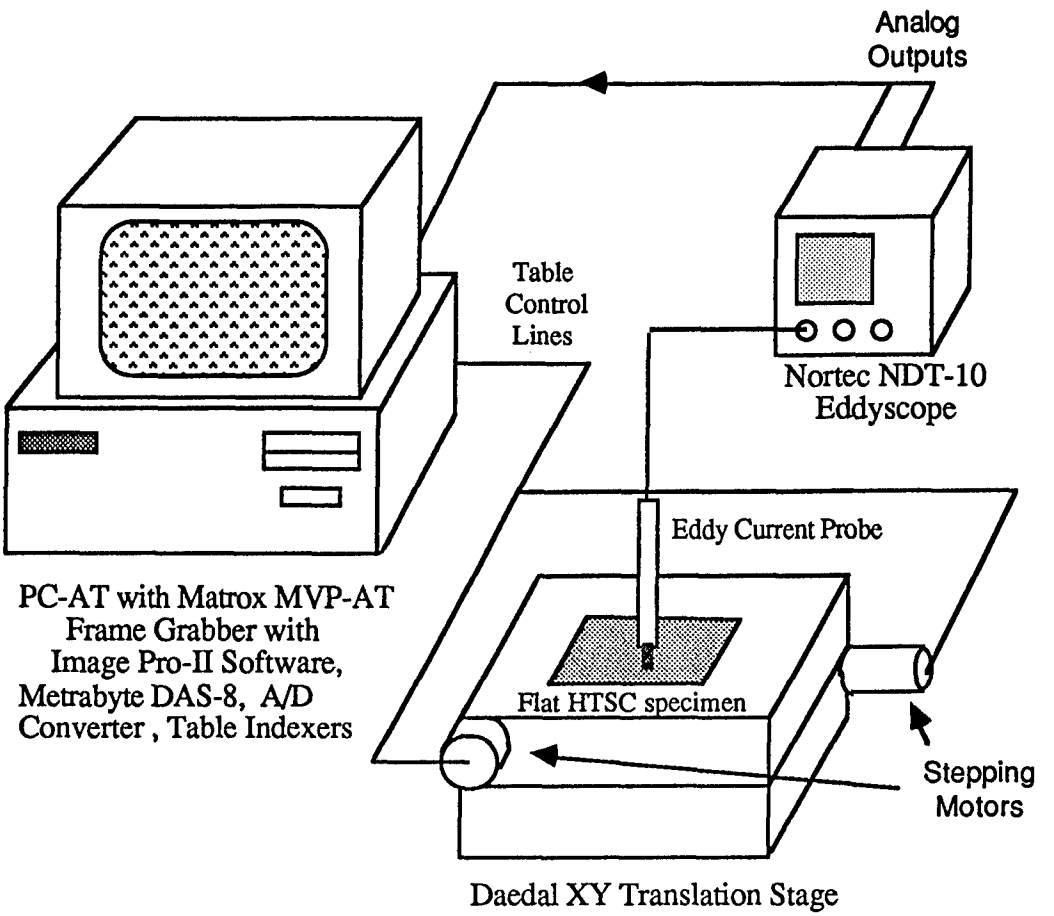


Figure 1 The Eddy Current Scanner

expansion bus. Command of the table is accomplished in software via subroutine calls from a BASIC program.

The scanning control software executes a "raster" scan (unidirectional scans with a non-sampling retrace) of a rectangular area with the range of travel determined at the beginning of run. Digitization of the two eddyscope data channels is done with a 12-bit A/D converter board which resides in the PC. Control of digitization is managed from within the same BASIC program which controls table motion. Scanning dimensions and the distances between columns and rows in the resulting image can be selected prior to scanning. The software automatically computes the required sampling rate for the A/D board and synchronizes data taking so that the resulting image is registered correctly.

Following the run, display of the conductivity map is done with a PC-AT based imaging system using a microcomputer imaging software package. This hardware is capable of displaying 512 x 480 x 8-bit images, but typical image sizes ranged from 100 to 200 pixels on a side. Using information about the dynamic range of the data channels compiled during run-time, a post-run program compresses (or expands) the 12-bit data to fit the 8-bit display range. The two channels from the eddyscope (x and y) can be

displayed separately but only single channel images are presented in this paper since the x and y channel images differ only slightly.*

Results

Some preliminary scans with metal samples were done to assure proper scan line registration. Once image registration was confirmed, scans were done of bulk $YBa_2Cu_3O_{7-x}$ material produced in-house. These were disc-shaped specimens 12.7 mm in diameter and 2 mm thick. An "ideal" scanner would have an infintesimally small probe and a driving frequency such that δ is approximately material thickness. It is expected that an "ideal" scan would produce a circular region with diameter equal to the specimen diameter, would have high contrast compared to its surroundings, and would possess a boundary at the edge of the circle that is quite abrupt. Figure 2a shows the eddy current image of a scan from the disc done with a 0.125" wide probe at 100kHz. This "real" image is dominated by edge effects; the result of the relatively wide probe and low driving frequency (hence large δ) which combine to smear out any detail.

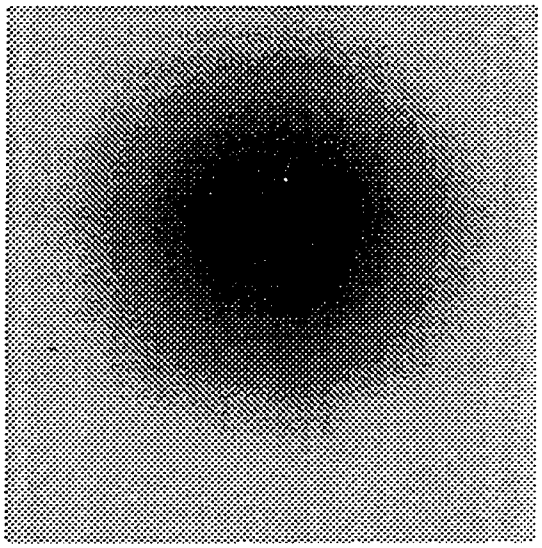


Figure 2a Eddy Current Image of HTSC Disc
Probe width = 0.125"
Frequency = 100 kHz

Figure 2b shows a scan of the same disc using a 0.050" probe at 6MHz. The edges of the disc are clearly visible in this image, as is an intensity gradient running from top to bottom. This gradient represents liftoff of the probe from the surface of the specimen due to a tilted bottom surface. The slightly brighter rectangular area at the top of Figure 3 is not specimen-related; it is the result of manipulation of eddyscope gain during the run.

---

* This is due to the arbitrary rotation one can apply to an eddyscope's display (and hence, its analog outputs). Often the eddyscope operator positions this rotation so that the liftoff phenomenon, generally an undesirable experimental artifact that can obscure information, affects only one channel of data. The channel not "corrupted" by liftoff is then monitored. While interpreting the images that follow please note that a change in image intensity reflects only *some change* in conductivity. Increased brightness does *not necessarily* correspond then to increased conductivity but rather to a conductivity gradient between that region and some other portion of the scan area.

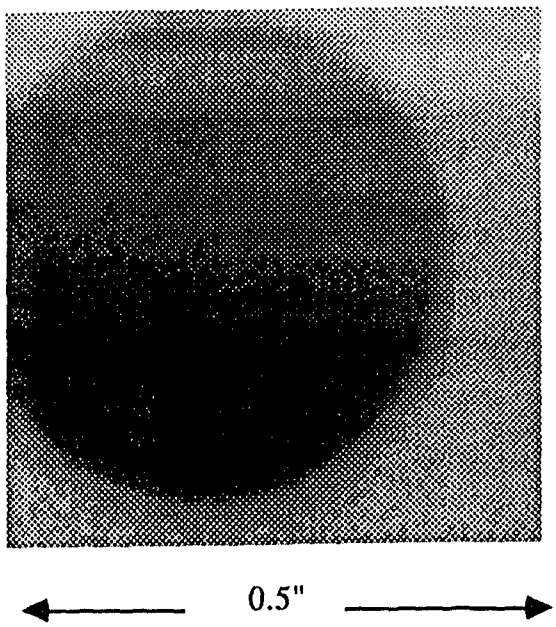


Figure 2b Eddy Current Image of HTSC Disc
Probe width = 0.050"
Frequency = 6 MHz

Another HTSC disc specimen examined (with similar dimensions) had a crack clearly visible on its surface (see the photograph in Figure 3). Figure 4 shows the eddy current image when scanned with a 0.050" probe at 6 MHz. The crack can be seen in the lower right-hand corner running from 3 to 5 o'clock. There is also a slight irregularity in the disc edge to the right of the crack; this corresponds to a small notch in the specimen.

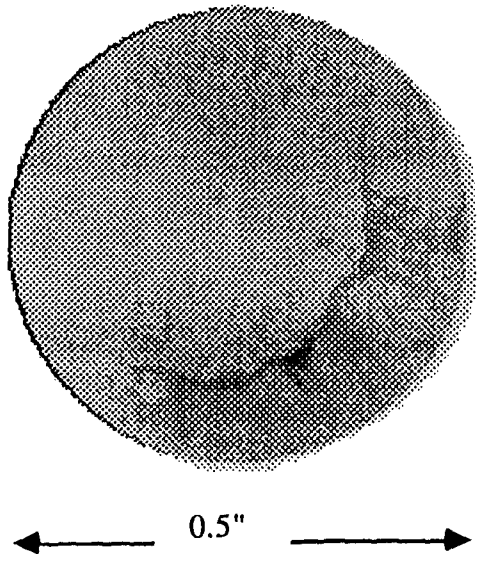


Figure 3 Photograph of HTSC Disc with Crack
Probe width = 0.050"
Frequency = 6 MHz

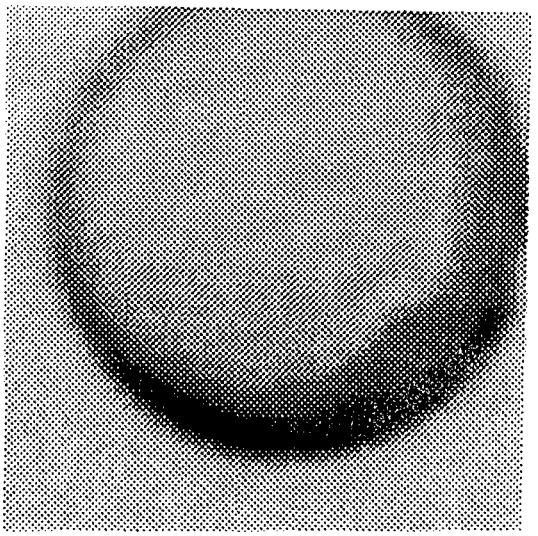


Figure 4 Eddy Current Image of HTSC Disc with Crack
Probe width = 0.050"
Frequency = 6 MHz

Conclusions

A scanning eddy current instrument has been developed and used to inspect bulk HTSC materials. The system produces an image of the spatial variation in eddyscope signal, which corresponds to a mapping of room temperature conductivity. This presently can be done for flat bulk specimens with thicknesses ≥ several millimeters.

Consideration is being given to extension of this technique to use with thin films. If probes suitable for use at 100 MHz can be secured, this would yield a $\delta \approx 350$ μm (.014"). This may be further reduced by thin probes. A digital impedance meter with a high-stability impedance bridge would be needed to replace the eddyscope, which cannot operate at higher frequencies. The impedance values this instrument would provide might provide sufficient data for extraction of absolute room temperature conductivity, which would provide information about spatial variation in superconductive performance.

Acknowledgements

The author would like to acknowledge the invaluable assistance provided by Charles Powers, Gloria Oh, and Michael Viens in the development of this instrument. Dr. Henning Leidecker also provided technical suggestions. This work was also supported in part by the Director's Discretionary Fund and the Office of Flight Assurance of Goddard Space Flight Center.

References

1. Blendell, J.E. et al, "Processing - Property Relations for $Ba_2YCu_3O_{7-x}$ High T_c Superconductors", Advanced Ceramic Materials Vol. 2, No. 33, American Ceramics Society, July 1987, pp. 512-529.

2. Viens, M., "Evaluation of Eddy Current Testing to Characterize Ceramic High Temperature Superconductors (HTS)", internal NASA memorandum, January 1988.

3. Plonus, M.A., **Applied Electromagnetics**,McGraw-Hill Book Company, 1978, p. 301.

PLASTIC SUPERCONDUCTOR BEARINGS
ANY SIZE--ANY SHAPE
77 k and up

Franklin G. Reick
FLUORAMICS, INC.
103 Pleasant Avenue
Upper Saddle River, N.J. 07458
(201)825-8110

ABSTRACT

"Friction free" bearings at 77 k or higher are possible using the high-Tc copper oxide ceramic superconductors (1) (2). The conventional method for making such bearings is to use a sintered ceramic monolith. This puts great restraints on size, shape and post-forming machining. The material is hard and abrasive. It's possible to grind up ceramic superconductors and suspend the granules in a suitable matrix. Mechanical properties improve and are largely dependent on the binder. The Meissner effect is confined to individual grains containing vortices (3). Tracks, rails, levitation areas and bearings can be made this way with conventional plastic molding and extruding machines or by painting. The parts are easily machined. The sacrifice is in bulk electrical property.

A percolating wick feed for LN_2 can be used to cool remote superconductors and large areas quite effectively. A hollow spheroid or cylinder of superconductor material can be molded with the internal surfaces shielded by the Meissner effect. It might be thought of as the DC magnetic analog of the Farady cage and the inside can be called the "Meissner space."

It's selective. AC fields are transmitted with minor attenuation. Particle size and distribution have a profound effect on final magnetic and electrical characteristics.

INTRODUCTION

High-Tc superconductors are usually made of pressed ceramic, vapor-deposited or sputter-deposited films. Some have been made from solutions of the appropriate precursors (4) (5) (6). Most researchers take great pride in making the pressed ceramics as close to "theoretical density" as possible. Their desire is to produce the very best electrical and magnetic properties. However, this is not a field where conventional wisdom necessarily produces the best results. This paper will describe:

1. A technique for controlling the porosity of ceramic high-Tc superconductors to any value desired below the theoretical maximum.
2. Another technique for using granules of superconductive materials in polymers to mold nonconductive plastics that exhibit a strong Meissner effect suitable for bearings, tracks, rails, levitation areas, and DC and magnetic shielding.
3. An LN_2 percolating heat pipe that has been invented for cooling superconductors approximately 2.5 cm above an LN_2 reservoir. It can be bonded to the high-Tc superconductor for remote cooling.
4. A number of applications which are possible for bearings and magnetic shields, as long as high current density is not a requirement and the Meissner effect is of prime concern. This permits great flexibility and ease of manufacture (7) (8) (9).

POROUS HIGH Tc SUPERCONDUCTORS

All of the work in this paper uses the rare earth, barium, copper, oxygen system, particularly the $Y_1Ba_2Cu_3O_7$ variety. The techniques described, however, will work with any ceramic material. We have obtained good results using europium instead of yttrium in some test runs. Many rare earths are reported to work as well (10).

The precursors are carbonates or oxides of the element carefully measured for stoichiometry. They are mixed and presintered in ceramic crucibles with minimum wall contact for 5 hours in dry air to 950 C and cooled in the oven overnight.

A black klinker results. This is ground up in a mortar and pestle to form a powder that will pass about 90% through a 100-mesh sieve. So far, all is conventional. The powder is then mixed with an ash-free spectrographic grade cellulose fiber and a small amount of fluorocarbon resin powder. It is pressed at 30 tons in a 2-cm-diameter die. A cellulose reinforced pellet results.

Figure 1 is a 50X SEM photo of a compressed pellet showing the squashed fibers distributed throughout its body. The fibers are brittle and they lose their identity in the bulk of the molded part. Figure 2, at 1500X SEM, is a broken sample. The cellulose is there but it has been crushed and shattered and is hard to identify. These pellets mold nicely and are easy to handle. The cellulose, crushed or not, reinforces it significantly.

THE SECOND FIRING

The pellets are stacked so gases can flow freely around them and are placed in a silicon carbide resistance-heated tube furnace. Dry air is fed into one end at a relatively slow rate. They are gradually heated to 400 C to allow the cellulose to burn out gently. The gas is switched to O_2, or in some cases to O_3, and heated over a 3-hour period to 950 C. The temperature is then increased gradually to 975 C over a period of 5 hours in flowing oxygen. The oven is then turned off and allowed to cool slowly for 12 hours in flowing oxygen or ozone.

The resulting ceramic buttons are quite porous. A 100X SEM photo (Figure 3A) shows a webwork of channels throughout the matrix. At higher magnification, tubules can be seen throughout the superconductor (Figure 3B). The ceramic grains are cemented together; however, all is electrically continuous.

The effect of PTFE and fiber loading can now be demonstrated. Since the disks are porous, they hold a charge of LN_2 after dipping in a reservoir. The levitation time above a nest of magnets increases since the disks do not warm up as rapidly as those of higher density. Figure 4 shows the levitation to be dramatically increased when .5% of fiber is added to the disk. Figure 5 shows that the electrical characteristics are reflected in the height of the Meissner levitation. It is enhanced by the addition of .5% weight of PTFE powder. The levitation height increases from 2 to 7.5mm--a considerable improvement.

FLUOROCARBON RESIN

The purpose of the fluorocarbon (Teflon) resin inclusion is twofold. First, it acts as a mold lubricant and enhances the compaction of the granules and fiber. Second, it decomposes to form a fluorocarbon gas that greatly improves the electrical and mechanical properties of the final superconductor.

The current belief in our labs is that the fluorocarbon gases reduce the melting temperature of the surface of the granules, which then acts like a solder to assure intimate contact between grains. It might also act as a crystalization flux. Note that in Figure 3B, the granules are nicely cemented together.

We measure the Meissner effect using a standard cobalt samarium magnet above a superconductor. The higher it levitates the better. The inclusion of a moderate amount of PTFE improves the properties significantly (see Figure 5).

THE ADVANTAGE OF POROSITY

Oxygen is an essential component of the high-Tc superconductors. It must diffuse through the body of the superconductor and become part of its crystal structure (2). In a high-density ceramic, this will take much longer than in one with porosity and interlaced diffusion tunnels. The result is very high-quality granular superconductors with extraordinarily strong Meissner effect. The superconductivity is not confined to the surface due to its porosity (11).

When electrical contact is made to the superconductor, the voids allow silver or gold paint to soak in deeply, making good contact to the bulk rather than just to the surface. That's advantage number one. The second advantage is that the porous superconductor acts like a liquid nitrogen (LN_2) sponge. If a pellet is dipped in LN_2, it soaks it up and carries the charge of coolant after it is removed from the coolant reservoir. It will continue to superconduct for 30 seconds to 1 minute, depending on its volume, until the LN_2 has evaporated from the piece. The third advantage is that the final fully formed superconductor is easy to grind up without crushing directly through the crystals. As a result, we can make powders of superconductors, disperse them in suitable plastic binders and make molded plastics and paints that have very high Meissner or shielding effects.

We have used Teflon, polyester, epoxy and silicone rubber successfully for molded bulk items, sheets and paints. The objects are molded with as little binder as possible so the particle density is high. The resulting parts can be drilled, milled and turned on a machine lathe. The bulk electrical property suffers. The parts are essentially high-resistance conductors, depending on the amount of binder that is used. The Meissner effect is degraded slightly since large-diameter vortices and circulating currents cannot exist. Particle size is an important variable.

ANOMALIES

The firing of the superconductor must be carefully controlled. A general rule is that it should end up at the maximum temperature that does not cause measurable shrinkage. When the peak temperature is exceeded, a dramatic shrinkage occurs. Actual meltdown can occur if the temperature is too high. The buttons then assume the appearance of watches painted by Salvador Dali and aren't much good for anything (Figure 7). The voids are greatly reduced in size, resulting in larger crystals with poor "soldering" between crystals for reduced Meissner effect. The liquid phase will have run out and been blotted up by the ceramic supports. Higher bulk room temperature resistance results.

If the heating is performed with the superconductors stacked like bricks, one on top of the other, the second tier down has a granular glitter of microcrystals after processing. The SEM shows a most interesting crystal pattern with laminar planes visible (mica-like) running through the crystals (Figure 8). These do not have the best Meissner effect in spite of particle/particle contact being well formed.

MAGNETIC SUSCEPTIBILITY AND FLUX PENETRATION DEPTH

A fast screening test for superconductors exploits the fact that their weak field magnetic susceptibility is approximately - 1/4Π below Tc (12). We use two pancake coils cut from an RF choke coil. They are mounted on perforated circuit board. The superconductor under test is placed between the coils so that the three are parallel in a sandwich configuration. A standard signal is transmitted through the sample and picked up by the top coil. The two signals are displayed on a twin beam oscilloscope and preserved with an XY recorder (the X scale records temperature). When Tc is passed, the superconductor becomes opaque to the signal and transmission drops to zero. The scope signal on the output coil vanishes. Simple, easy, and fast! And superconductors are the only materials in the world that do this.

However, much to my surprise, the molded plastic granular superconductor remains fairly transparent to alternating fields and doesn't behave like the bulk superconductor on the above test. This is in spite of the fact that magnets levitate above the sample quite nicely. It turns out that their transparency is related to particle size and packing density and is never as good as the unground monolith.

The thickness of the superconductor is also an important variable (Figure 10). Penetration depth of about 8mm is shown in a stack of disks. (We continued stacking until the levitation height of the magnet stabilized.) In metallic superconductors, the super currents are located near the surface--a DC analog of the high-frequency AC skin effects in conventional conductors (13). More powerful magnets can be expected to penetrate deeper and levitate higher. This is an important consideration in bearing design.

MANUFACTURING TECHNIQUES

1. A flexible tape of silicone rubber (RTV) is easily made by mixing the granular superconductor in the RTV and doctoring it onto a carrier strip of fiberglass scrim for strength. Once cured, it can be wrapped on cylinders and spheres and bonded with additional RTV. Thickness, particle size and loading determine the depth of shielding (Figure 11A).
2. Packing--Pack the granular material in a dead soft copper tube, flattening and welding the ends after displacing the interstitial air with O_2. The unit can be squashed flat and hydroformed into complicated dishes and pans. Copper is nonmagnetic so the Meissner effect is pronounced and available in deep drawn shapes, limited principally by the ductility of the container (Figure 11B).
3. Hand layups--The granular material can be mixed into epoxy or polyester resin and hand molded to surfaces for complex shapes. Fiberglass can be incorporated for strength.
4. Molding--The granular material can be mixed into thermo-setting or thermo-plastic resins and molded just like a piece of plastic. Very high production is possible in complex shapes (Figure 11C, both views). Tracks can be extruded.
5. Monoliths--Large-diameter or large-volume containers can be packed with the granular material and vacuum impregnated with suitable plastics and later machined into the final shape.

6. The porous unground ceramic can be vacuum impregnated with plastic. This creates an object that has the strength of the plastic but is electrically conducting across its bulk.

PARTICLE SIZE

In a sense, a monolithic superconductor is a one-particle body. If it is ground up, it becomes many particles of smaller and smaller size as the grinding progresses. Smallest is not necessarily best, since the diameter of a Cooper pair is on the order of approximately 20 A (11). To make a plastic filled with superconductive particles, it is best not to grind too fine or the Cooer pair radius will be encroached. Circulating current and vortices will be adversely affected. Plastics filled with superconductive particles have been made in two ranges of particle sizes:

1. ground and passed through a 100-mesh sieve; and

2. ground and passed through a 16-mesh sieve onto a 100-mesh sieve (removing the fines).

The strongest Meissner effect is from the sample passed through the 100-mesh screen. Apparently, the particles are not yet too small. Packing will be fairly good since a full range of particle sizes passes through the finer sieve. The coarse material has had the fines removed so there is a lot of resin-filled space. The problem is similar to that of making concrete aggregates. A range of particle sizes is required to properly fill the space. The resin should only be used for a binder, not a gap filler.

PERCOLATING HEAT PIPES

A technique has been developed for cooling the plastic superconductors that dies not require them to be dipped directly in liquid nitrogen. The plastic os molded against a wick of nonwoven fabric and copper wire mesh or aluminum foam. The fabric lifts the LN_2 via capillary attraction to the superconductor. The mesh allows vapor to escape.

If small-diameter holes are simultaneously molded in the superconductor, they act as percolation paths. The wick-fed fluid perks up through the holes and cools the superconductor efficiently. So far, this has worked against a pressure head of about 2.5 cm. A "remote" source of LN_2 can therefore be used to cool large areas of superconductors (Figure 12).

WEAK LINKS

Superconductors can handle very high current density (100,000 amps per square cm) in thin films (13) or 200 to 400 amps per square cm in the granular high Tc ceramic (11). This is sufficient if one wishes to use them for high-power applications or bearings. However,the process is more complicated when used for sensors and detectors of various sorts. Their impedance is very low and difficult to work with.

The current must be limited for such applications and it is customary to use a weak link--a Dayem bridge or Josephson device to couple superconductors and reduce the current magnitude to manageable levels. The weak links must be very small (9). The technique described in this paper for controlling the porosity of the ceramic high-Tc superconductor has the possibility, if carried to its extreme, to make devices that contain a multitude of weak links in a "swiss-cheese" or sponge-like structure.

So far, we have been unable to get the circulating currents low enough to measure flux jumps or magnetic flux quanta. This is, nevertheless, an interesting possibility and we will continue to try.

SUMMARY

"WHAT'S IT GOOD FOR?" (14)

Non-conductors that exhibit the exotic magnetic properties of superconductors are very curious materials. In a sense, we can make magnetic field manipulating bodies from molded plastics. Fields can be shoved, molded and concentrated into configurations not normally attainable. For example--

- Possible uses are in levitated bearings, tracks and rails.

- **Gyros come immediately to mind.**

O Beam shapers and plasma bottles are possible. Flux pumps and concentrators are easy to make.

O Magnetic "field-free" regions inside a Meissner bottle are possible. They can be selective in that DC fields are shielded better than AC fields.

O Coils and sensors can be embedded in the plastic.

O A fiber/metal-mesh heat pipe can help remotely cool the superconductor. Percolation holes for LN_2 in the superconductor dramatically improve cooling.

The list goes on and on and the number of applications seems to go up directly with the number of engineers and scientists that are exposed to the possibilities.

There is nothing new about the idea of superconductor bearings. Levitation is as old as the Meissner-Ochsenfeld discovery. It's obvious and dramatic. Readers wishing to delve into the subject further would greatly benefit by reading Newhouse's book (7) first. It has the best coverage of the subject I've discovered so far and has an excellent bibliography.

REFERENCES

1. Muller, K.A. and J.G. Bednorz, 1987, "The Discovery of a Class of High-Temperature Superconductors," Science, September 4, Article 1133.

2. Wu, M.K., P.H. Hor, R.L. Meng, L. Gao, Y.Q. Huang, and C.W. Chu, 1987, "Superconductivity at 93K in a New Mixed-phase Y-Ba-Cu-O Compound System at Ambient Pressure," Phys. Rev. Lett., Vol. 58, No. 9, p. 908.

3. Saint-James, D., G. Sarma, E.J. Thomas, 1969, *Type II Superconductivity*, Pergamon Press, p. 279.

4. Venkatesan, T., 1987, "Laser Deposited High Tc Superconductors," in Thin Films-Solid State Technology, pp. 39-41.

5. Feiglelson, R.S., D. Gazit, D.K. Fork, and T.H Geballe, "Superconducting Bi-Ca-Sr-Cu-O Fibers Grown by the Laser-Heated Pedestal Growth Method," Science, Vol. 24c, p. 1642.

6. Golben, J.P., S. Lee, S.Y. Lee, Y. Song, T.W. Noh, X. Chen, J.R. Gaines, and R. Tettenhorst, 1987, "Superconductivity of the single-phase compound $Er_1Ba_2Cu_3O_{9-8}$ Transport and structural properties," Phys. Rev. B, Vol. 35, No. 16.

7. Newhouse, V.L., 1964, *Applied Superconductivity*, GE Research Laboratory.

8. Gregory, W.N., J.R. Mathews, and E.A. Edelsack, 1973, *The Science and Technology of Superconductivity*, Plenum Press, New York.

9. Foner, S., and B.B. Schwartz, 1974, *Superconducting Machines and Devices: Large Systems Applications*, Plenum Press, New York.

10. Feinberg, E.O., November 15, 1988, High Tc Update, Ames Laboratory, Vol. 2, No. 22. (Note: Preprints are free to any interested party. The literature is expanding so fast that this is the best source of the most current information.)

11. Van Duzer, T. and C.W. Turner, 1981, *Principles of Superconductive Devices and Circuits*, Elsevier North Holland, Inc., New York.

12. Foner, S. and B.B. Schwartz, 1981, *Superconductor Materials Science--Metallurgy, Fabrication and Applications*, Plenum Press, New York, pp. 6-F164.

13. Chaudhari, P.,, R.H. Koch, R.B. Laibowitz, T.R. McGuire, and R.J. Gambino, 1987, "Critical-Current Measurements in Epitaxial Films of $YBa_2Cu_3O_{7-x}$ Compound," Phys. Rev. Lett., Vol. 58, No. 25, p. 2684.

14. Zimmerman, J.E. and T.M. Flynn, 1977, Applications of Closed-cycle Cryocoolers to Small Superconducting Devices, National Bureau of Standards.

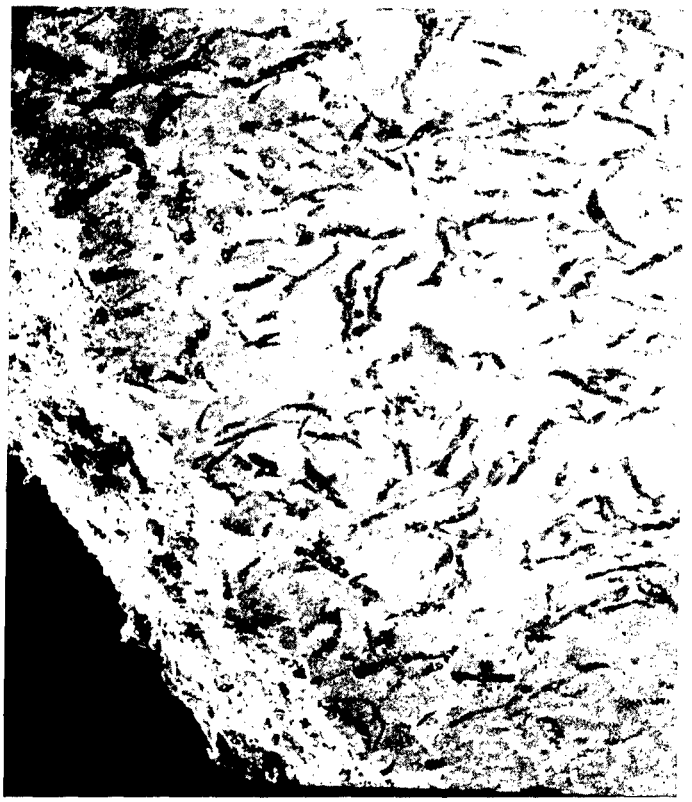


Figure 1. 50X SEM showing cellulose reinforced ceramic after molding and before final firing in O_2.

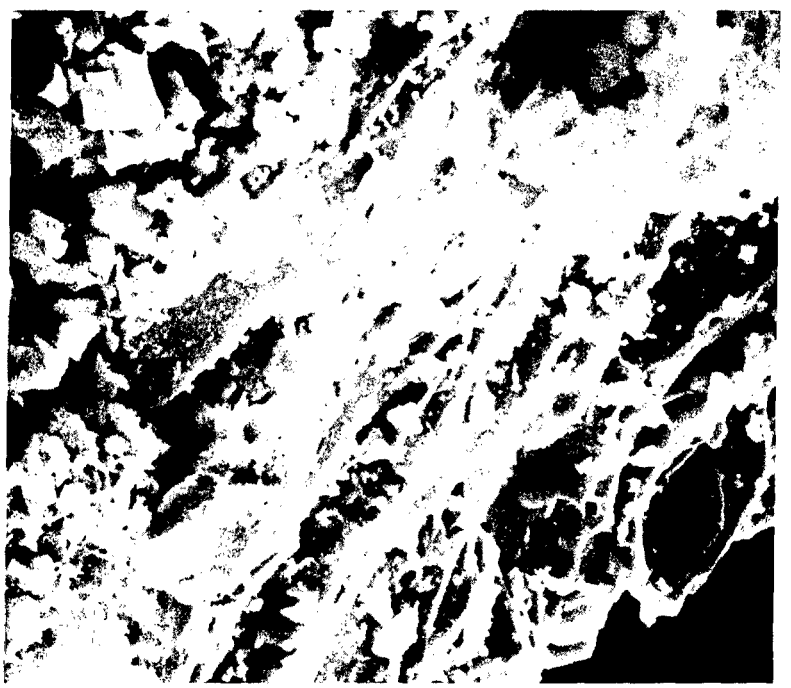
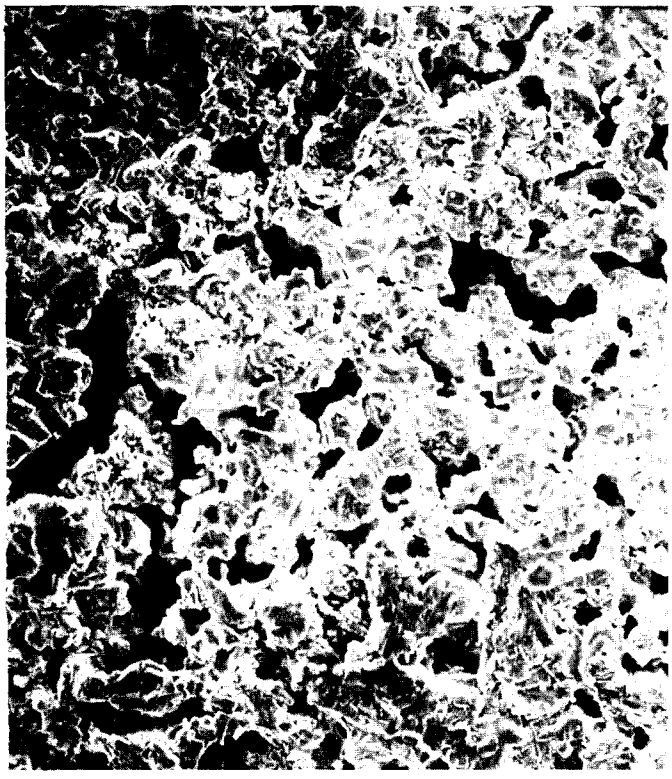


Figure 2. 1500X SEM showing cellulose reinforced pellet before firing. The cellulose is brittle and doesn't show as fibers in the broken section--they are there however.



igure 3A. 100X SEM showing pellet after second ring. The cellulose has burned out and left the pel-et riddled with tunnels.



Figure 3B. 1500X SEM showing a tubule in the ceramic. Note that grains are cemented (soldered) together. The pellet resistance is about .1 ohm at room temperature.



Figure 4. A cobalt samarium magnet levitates well above the porous superconductor. The porosity contributes to fast cooldown and high thermal hysteresis--it's an LN_2 sponge.

Reproduced From
Best Available Copy

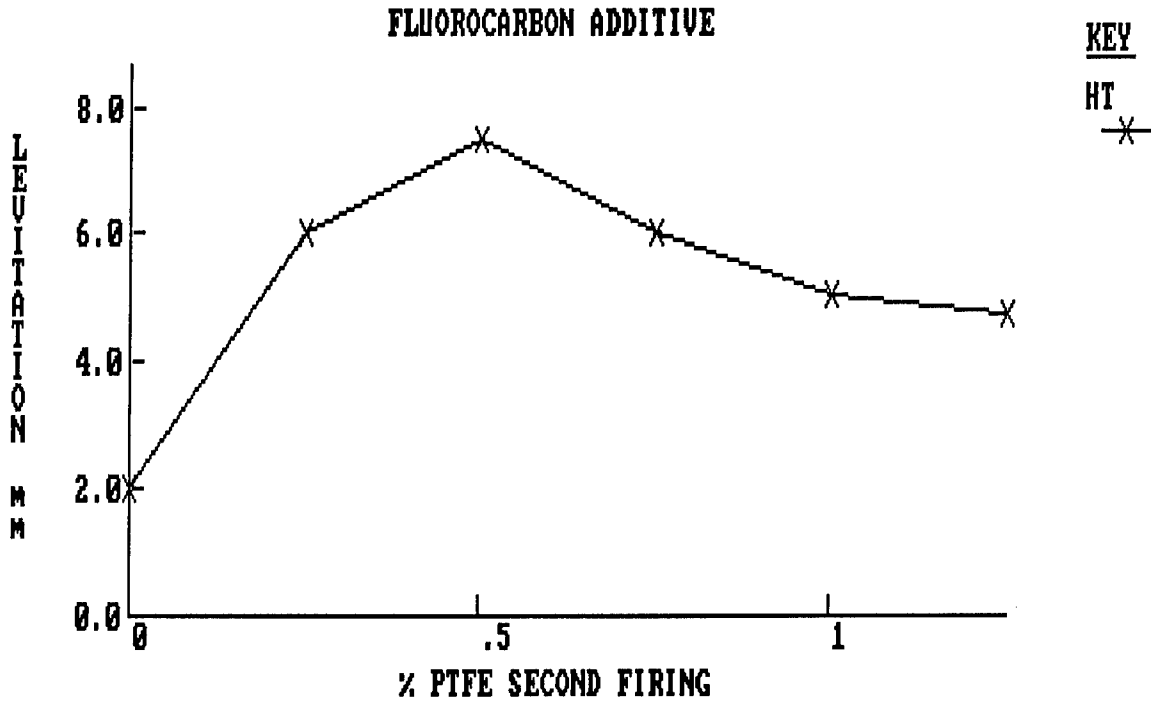


Figure 5A. The addition of PTFE powder to the pellet improves the Meissner effect as measured by the height of levitation of a standard magnet (see Figure 4).

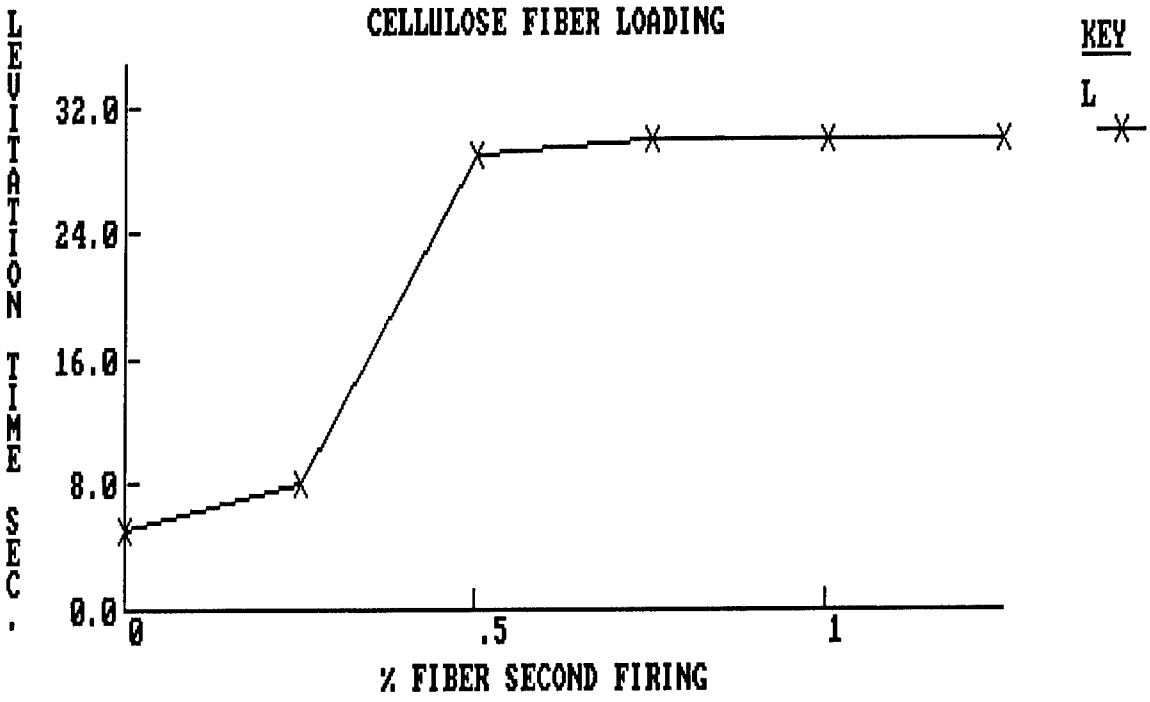


Figure 5B. The effect of cellulose loading.

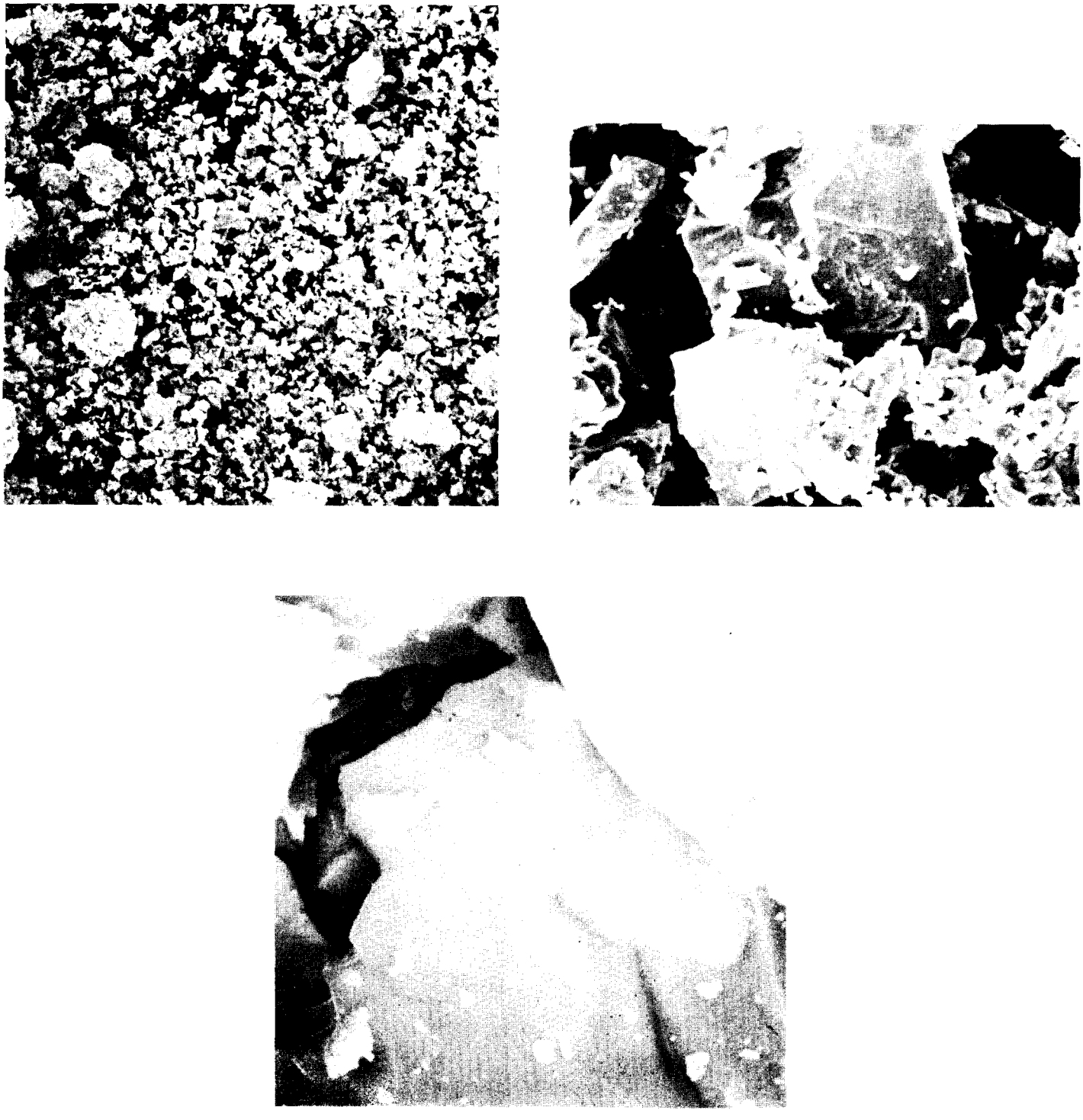


Figure 6. Ground superconductor passed through a 100-mesh sieve: a) 50X SEM; b) 500X SEM; and c) 3000X SEM.

Reproduced From
Best Available Copy

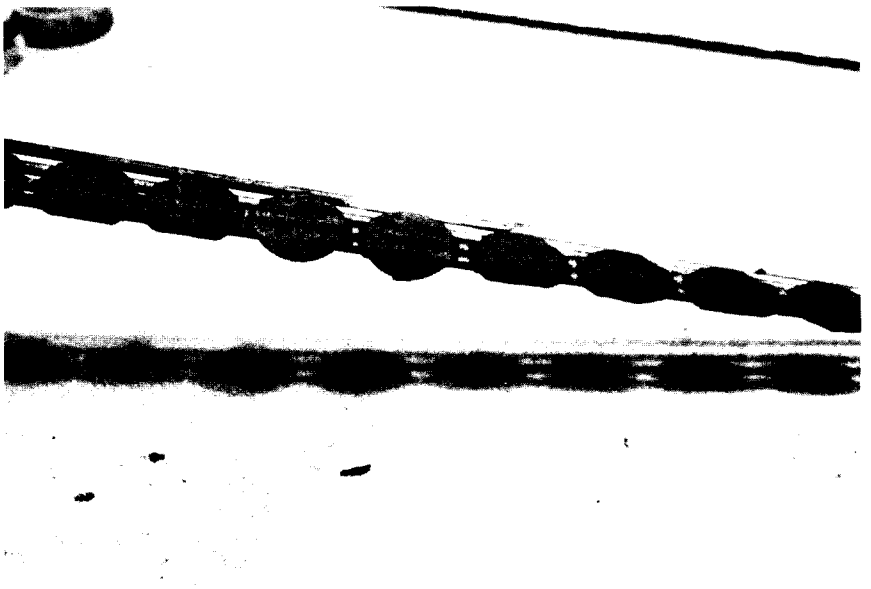


Figure 7. If superconductors are fired at too high a temperature, they droop and stick tenaciously to the ceramic support. Best results are obtained if they are fired just below this point--tricky near 1000 C.

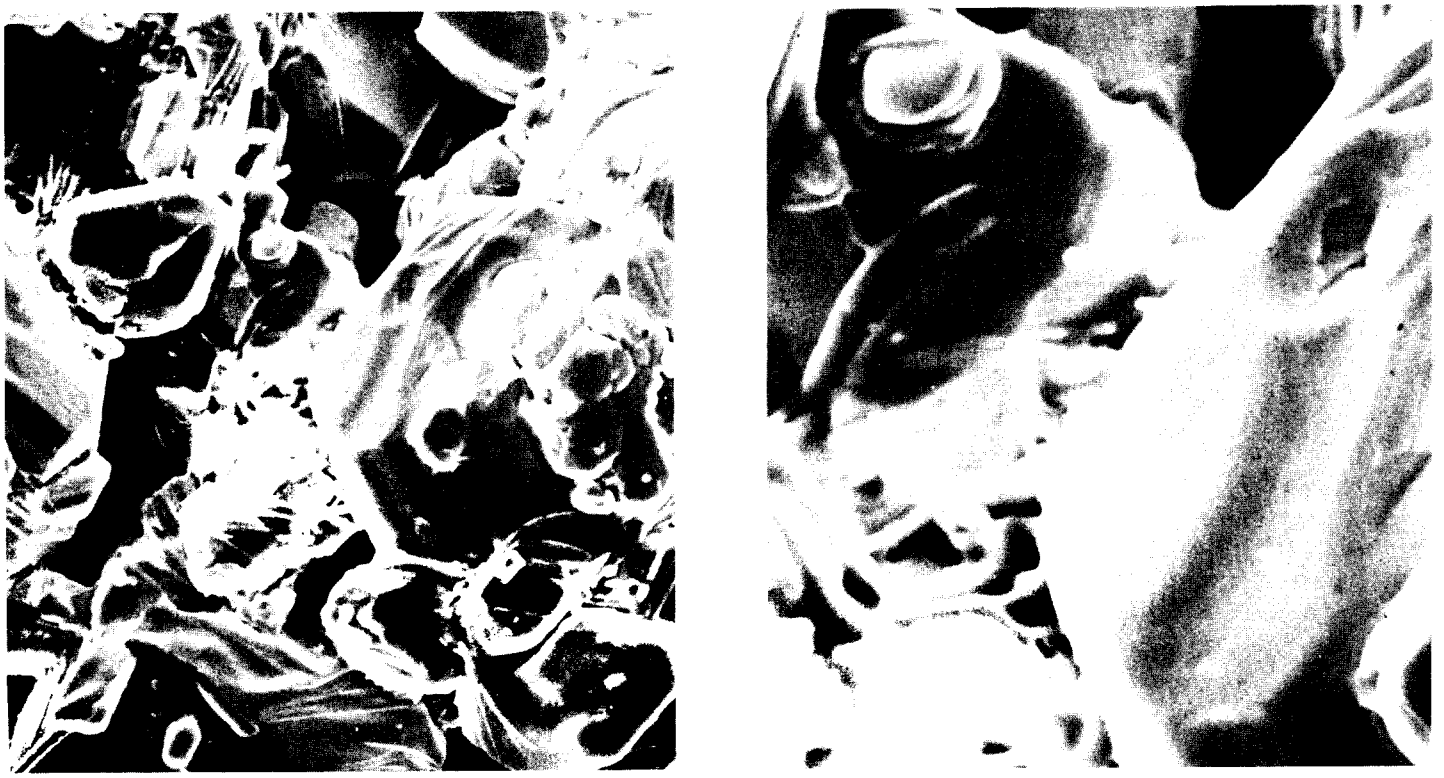


Figure 8. When superconductors were stacked for firing, the lower one showed glitter so we took a look at a) 500X SEM, and b) 1500X SEM. Note the planes within the crystals.

Reproduced From
Best Available Copy

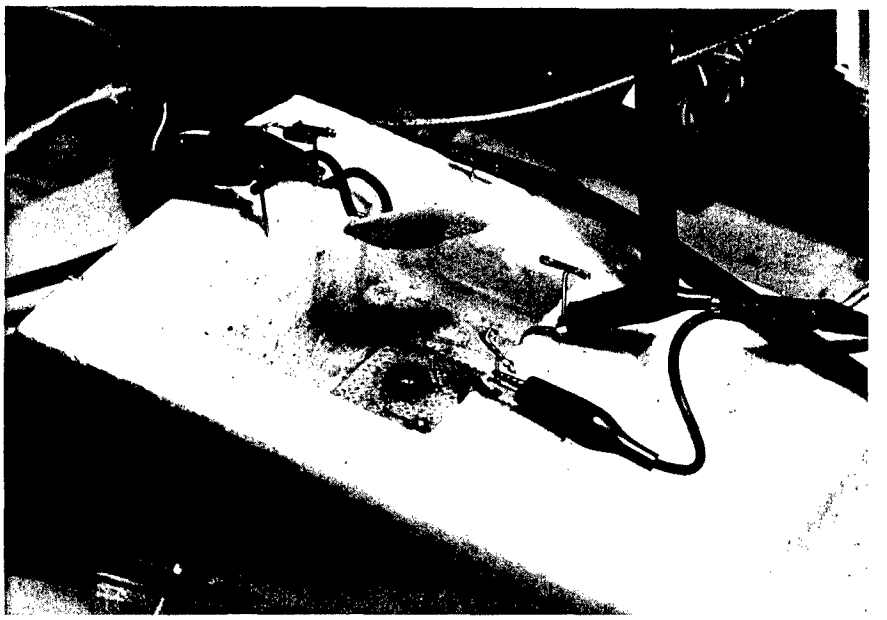


Figure 9. Two pancake coils are used to measure the magnetic susceptibility of superconductors. The AC signal is applied to one and measured with the other. When a superconductor placed between them passes Tc, the AC signal output vanishes.

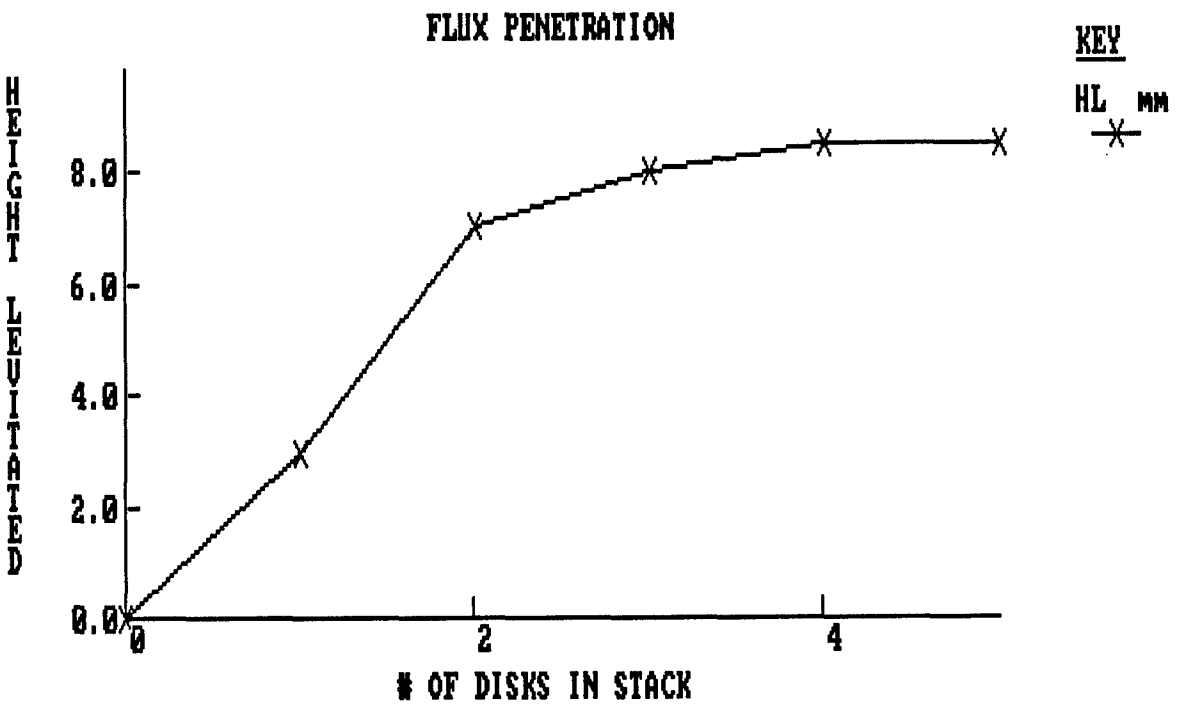


Figure 10. Flux penetration curve. With four disks in a stack the penetration depth for maximum levitation is about 8mm.

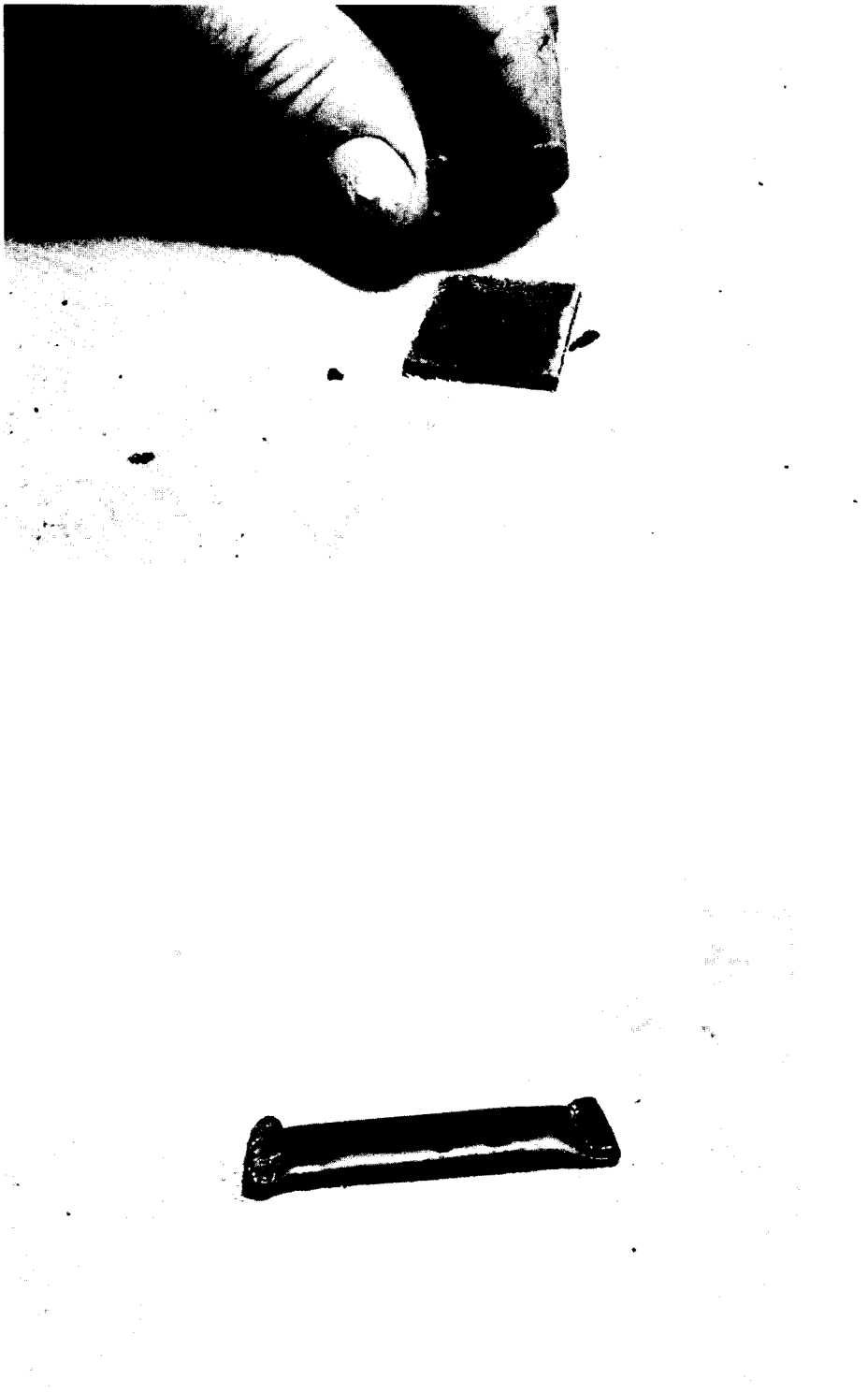


Figure 11. a) Silicone rubber used as a binder with a polyester non-woven fabric top and bottom gives a flexible superconductor; b) Granular superconductor compressed in copper tubing shows good Meissner effect when submerged in LN_2; and c) Very good superconductor bearings (above) can be machined from plastics using a high loading of particles passed through a 100-mesh sieve. Below, complex shapes can be molded.



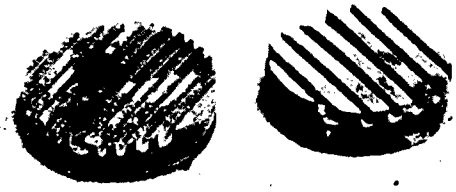




Figure 12. a) A fabric/wire mesh heap pipe used to cool plastic molded to its top; b) Percolation holes in the top of the plastic superconductor assist greatly in cooling; c) Magnet levitates above sample about 2 cm above a reservoir of LN_2.

Upcoming Planetary Missions and the Applicability of High Temperature Superconductor Bolometers

J. Brasunas, V. Kunde, H. Moseley
NASA/Goddard Space Flight Center, Greenbelt, MD 20771
B. Lakew
STX Corporation, Lanham, MD 20706

Abstract

A brief overview is given of planetary exploration to date, with a focus on outer planet missions, in particular the proposed 1996 Cassini mission to Saturn and Titan. A proposed infrared spectrometer, CIRS, for remote sensing of the atmospheres of Saturn and Titan from the Cassini orbiter is presented. The science return of CIRS would be significantly enhanced if a near phonon-noise limited 65-90K infrared detector could be developed. A description of the ongoing Goddard/NIST-Boulder effort to build a high sensitivity, high T_c bolometer is also presented.

Past and Present Planetary Exploration, and the 1996 Cassini Mission

A long line of Fourier Transform Spectrometers (FTS's) has made significant contributions to our understanding of planets and satellites, from the earth-observing FTS's of Nimbus 3 (1969) and Nimbus 4 (1970), through the Mars observing FTS of Mariner 9 (1971/1972) to the Voyager IRIS observations of Jupiter (1979), Saturn and Titan (1981), Uranus (1986), and Neptune (1989). These interferometers have returned substantial scientific benefits (see Figure 1), in spite of using relatively insensitive near-room-temperature thermal-type infrared detectors (detectivity $D^* \leq 10^9$ $cmHz^{1/2}/W$) as compared with the much more sensitive detectors ($D^* \geq 10^{14}$) available at liquid helium temperature. D^* is related to noise equivalent power (NEP) by the relationship $NEP = A_d^{1/2}/D^*$, where A_d is the detector area. A severely limited mass budget, and long lifetime in the case of outer planet missions, rule out the use of liquid helium. Radiative and mechanical coolers remain, for which the practical lower limit for the focal plane is 65-90K. There are no thermal detectors specifically optimized for these temperatures, and in fact no moderately-cooled thermal detector ($T \geq 65K$) offers substantial improvement in performance beyond the thermopile used on Voyager/IRIS ($D^* = 0.9 \times 10^9$).[1] To enhance the return from infrared remote sounding of the planets, planetary missions have a compelling need for sensitive 65-90K thermal-type detectors, a need that has not been met by detector development programs.

Preliminary investigations of the outer planets were performed by the Pioneer and Voyager spacecraft. Subsequent missions planned for in-depth exploration of Jupiter and Saturn from orbital spacecraft are Galileo and Cassini. Galileo, launched in 1989, is to acquire data while in Jupiter orbit. A probe will also be sent into Jupiter's atmosphere. A series of planetary missions utilizing a newly-designed

generic spacecraft, the Mariner Mark II, is now under development. The first two missions under the Mariner Mark II series will be the CRAF cometary encounter, and the Cassini mission to Saturn and Titan. The CRAF and Cassini missions are intended to provide information on the origin and evolution of the solar system.

The Cassini mission is a joint NASA/ESA enterprise. It will be launched in 1996 aboard a Titan/IV Centaur, with a Jupiter flyby in 2000, and Saturn arrival in 2002. At Saturn the ESA-supplied probe wil enter the atmosphere of Titan. Subsequently, the NASA-supplied orbiter will orbit Saturn about 60 times, making 35 close Titan flybys during 2002-2006. Figure 2 shows the outline of the Cassini orbiter and probe (To get a sense of scale, the high-gain antenna (HGA) has a diameter of 3.66 m). The orbiter has an allocation of 197 kg and about 200 watts for scientific instruments, and can return to earth about 1 to 2 millio bits per overpass of the deep-space network on earth.

CIRS is one of the baseline infrared experiments on the Cassini orbiter model science payload. CIRS will retrieve information on the atmospheres of Titan and Saturn with good vertical resolution, from dee in their tropospheres to high in their stratospheres, and into the uppe few centimeters of the regoliths of icy objects. The science addressed by CIRS includes: 1) determination of the global thermal structure to test theories of atmospheric dynamics and general circulation, 2) mapping and tracking the motion of thermal patterns to determine their role in dynamics, 3) determination of global gas composition (including isotope ratios), 4) mapping and tracking composition variations to determine effects of chemistry, photochemistry and dynamics, 5) studyin the synthesis of organic compounds, 6) determination of global information on clouds and hazes, 7) determination of information on non equilibrium processes in the upper stratosphere, and 8) determination o information on atmospheric transport and other processes obtained from simultaneous measurements of composition, temperature, and winds. The science addressed for satellites and rings includes the mapping of composition and thermal characteristics, to test theories of their origin and evolution.

CIRS will use a dual interferometer configuration with a common linear motor (figure 3). The far-infrared FTS (table 1) will cover 10-300 cm^{-1} with a single thermopile detector. The mid-infrared FTS will cover 200-1400 cm^{-1}, with a single thermopile detector from 200-650 cm^{-1}, a 1x20 photoconductive HgCdTe array from 600-1100 cm^{-1}, and a 1x20 photovoltaic HgCdTe array from 1100-1400 cm^{-1}. The choice of detectors is limited by the minimum achievable focal plane temperature, around 75 for the radiative cooler design in CIRS. The long-wavelength infrared detectors proposed for CIRS in focal planes 1 and 2 (table 1) are Schwarz-type thermopile detectors to be supplied by Karlsruhe Universit in Germany. The dc detectivity is 3 to $4x10^{9}$, with a time constant of 25 ms (Shimadzu of Japan makes a similar detector). By comparison, the thermodynamic limit (phonon-noise limit) at 80K is a D* of $5x10^{11}$. The area-solid angle product for CIRS dictates a minimum detector diameter of 1.1 mm for perfectly concentrating f/0.5 optics in vacuum.

Reproduced From
Best Available Copy

A rich array of molecular species on Saturn and Titan may be studied with the thermopile detectors currently baselined for CIRS. Nevertheless, a greater array of trace molecules over a wider range of altitudes could be observed, were more sensitive detectors to become available. Beyond Cassini, an improved thermal detector would benefit proposed missions to study the elemental composition, cloud structure, and meteorology of the planetary atmospheres of Uranus and Neptune.[2] Planetary observations from earth-orbiting telescopes (Plato) and on the Space Station would also benefit.

Possible Improvement with Long-Wavelength Detectors

Higher sensitivity with high temperature superconductor (HTS) detectors would greatly improve the determination of the presently detected hydrocarbons and nitriles in Titan's atmosphere, and will permit the detection of new nitriles. Knowledge of the altitude and spatial distribution of CO is central to the understanding of the chemistry of the oxygen-bearing molecules in Titan's atmosphere. A synthetic far-infrared limb spectrum has been calculated for Titan, a portion of which is shown in Figure 4. The emission lines are due to HCN and CO-- a strong CO line is evident at 42.2 cm^{-1}. Also shown are the error bars for the projected sensitivity of the CIRS thermopile detector, and for an HTS detector with an assumed D* of $3x10^{10}$. It is evident from the comparison that the increased sensitivity of the HTS detector is required for CIRS to map the altitude and spatial distribution of this key oxygen-bearing species.

The sharp change in magnetic and transport properties of high T_c superconductors at the transition opens the possibility of near-phonon-noise limited performance at or near 80K. Bolometric responses in granular and epitaxial HTS films have been demonstrated by a number of groups,[3,4,5] including a collaboration between Goddard and NIST/Boulder.[6] Another possibility for a sensitive detector is the kinetic inductance bolometer,[7] which has been demonstrated in low Tc materials but not yet in high Tc.

The initial Goddard/NIST effort was a transition-edge resistance bolometer in the composite geometry,[8] with independently fabricated radiation absorber, superconductor thermometer, and thermal isolator (figure 5). The superconductor thermometer is in the form of a meander line which is also suited to implementation as a kinetic inductance bolometer. A prototype device was fabricated in early 1989. The prototype suffered from a long time-constant, 30 seconds, due to the heat capacity of the underlying $SrTiO_3$ substrate, 500 microns thick.

Efforts since then have centered on reducing the heat capacity of the substrate. Attempts are underway at Goddard to etch $SrTiO_3$ to a thickness of 25 microns or so. Also under consideration is using a substrate with a lower specific heat. Work is being pursued under Goddard sponsorship at a number of locations to attempt HTS deposition on diamond, which has a volume specific heat 5 to 15 times lower that alternate substrates at 80K. The ATM corporation (Conn.) is being funded within the Small Business Innovation Research program, first under Phase I and now under Phase II, to grow HTS thin films (YBaCuO and

BiSCCO) via the MOCVD technique on artificially grown diamond films. Initial attempts without a buffer layer have failed; buffer layer development has begun and will be continued under Phase II. A small purchase order was awarded to CVC (New York) to attempt sputter deposition of YBaCuO on natural type IIa diamond. Deposition without a buffer layer resulted in poor adhesion. The initial attempt with a polycrystalline MgO buffer layer resulted in good adhesion. At Catholic University an attempt was made to deposit a thick film of YBaCuO on natural diamond -- this also resulted in poor adhesion. NIST/Boulder has implemented a laser ablation system and will attempt laser ablation deposition on diamond. NIST and Goddard will also be looking into a silicon based bolometer. Silicon as a substrate is a compromise choice -- while not having as low a specific heat as diamond, there is much more experience in working/thinning it, and various groups have already deposited HTS thin films on silicon.

In addition to the time constant, the low-frequency excess noise in HTS films needs to be controlled. It has been noted that minimization of the excess noise in YBaCuO films on $SrTiO_3$ requires c-axis alignment.[8,9,10] It is not known to what degree this is possible on diamond: Undoubtedly the choice of buffer layers will play a key role. As it has been noted that thallium films can have high critical currents even in unoriented form,[11] thallium films appear to have better intergranular contact and may be a candidate for low-noise, non-epitaxial films on diamond. Alternatively, a bolometer could be made with a silicon substrate and a $SrTiO_3$ buffer layer[12] or a $BaTiO_3/MgAl_2O_4$ buffer layer,[13] upon which epitaxial c-axis oriented YBaCuO has been grown.

Prospects for HTS Bolometers on Planetary Missions

Exciting data on the outer planets and their satellites have already been obtained with fairly insensitive, thermal-type infrared detectors. Future studies would benefit greatly from an improved sensitivity detector: In principle, HTS bolometers could provide this improved sensitivity. What needs to be demonstrated is superiority to Schwarz-type thermopiles, which are capable of a D* of 3 to 4×10^9 and a time constant of about 25 ms; for the CIRS detector diameter of 1.1 mm the NEP is about 3×10^{-11} W/Hz$^{1/2}$ over wavelength ranges of 16 to 50 microns and 30 to 1000 microns. To displace the thermopile detectors, the HTS bolometer would need either to improve the time constant to at least 10 ms, or improve the D* to at least 7×10^9. If improved sensitivity is demonstrated, certain environmental capabilities also need to be demonstrated. Below is a brief list of nominal requirements for the Cassini mission.

Lifetime/passivation (high vacuum):	12 years
Thermal cycling, 300K to 80K:	numerous times
Radiation hardness:	15 krads, total dose
Launch vibration:	~15 g's, ~ 3 minutes.

Reproduced From
Best Available Copy

This work was initially supported by the Director's Discretionary Fund at Goddard, and is currently being supported by the Planetary Instrument Definition and Development Program, and by OAST Code R, both at NASA Headquarters.

References

1. R. Hanel et al., "Infrared spectrometer for Voyager," Appl. Opt., 19, 1391, 1980.

2. A Strategy for Exploration of the Outer Planets: 1986:1996, National Academy Press, Washington, D.C., 1986.

3. M.G. Forrester et al., "Optical response of epitaxial films of $YBa_2Cu_3O_{7-d}$," Appl. Phys. Lett., 53, 1332, 1988.

4. M.G. Forrester et al., "Optical Response of Epitaxial and Granular FIlms of $YBa_2Cu_3O_{7-d}$ At Temperatures from 25K to 100K," IEEE Trans. Magn., **MAG-25**, 1327, 1989.

5. Y Enomoto et al., "Infrared Optical Detector Using Superconducting Oxide Thin Film," Physica C, **153-155**, 1592, 1988.

6. J.C. Brasunas et al., "Construction and performance of a high-temperature-superconductor composite bolometer," J. Appl. Phys., **66**, 4551, 1989.

7. C.A. Hamilton et al, "Standards and High-Speed Instrumentation," IEEE Proc., **77**, 1224, 1989.

8. P.L. Richards et al., "Feasibility of the high T_c superconducting bolometer," Appl. Phys. Lett., **54**, 283, 1989.

9. M.J. Ferrari et al., "Magnetic flux noise in thin-film rings of $YBa_2Cu_3O_{7-d}$," Appl. Phys. Lett., 53, 695, 1988.

10. R.D. Black et al., "Thermal fluctuations and 1/f noise in oriented and unoriented $Y_1Ba_2Cu_3O_{7-x}$ films," Appl. Phys. Lett., **55**, 2233, 1989.

11. S.H. Liou et al., "Highly oriented $Tl_2Ba_2Ca_2Cu_3O_{10}$ thin films by pulsed laser evaporation," Appl. Phys. Lett., **54**, 760, 1989.

12. H.J. Dietze et al., "High-T_c superconducting Bi-Sr-Ca-Cu-O thin films prepared by laser-induced plasma deposition," Z. Phys. B Condensed Matter, in press, 1990.

13. X.D. Wu et al., "High critical currents in epitaxial $YBa_2Cu_3O_{7-x}$ thin films on silicon with buffer layers," Appl. Phys. Lett., **54**, 754, 1989.

TABLE 1 CIRS INSTRUMENT PARAMETERS

TELESCOPE DIAMETER (CM):	50	
INTERFEROMETERS:	FAR-IR	MID-IR
TYPE:	Polarizing	Michelson
SPECTRAL RANGE (cm^{-1}):	10 - 300	200 - 1400
SPECTRAL RESOLUTION (cm^{-1}):	0.5 - 20	.05 - 20
INTEGRATION TIME (sec):	50	50

FOCAL PLANES:	FP1	FP2	FP3	FP4
SPECTRAL RANGE (cm^{-1}):	10-300	200-650	600-1100	1100-14
DETECTORS:	Thermopile (1)	Thermopile (1)	HgCdTe (1x20)	HgCdTe (1x20)
PIXEL F-O-V (mrad):	4.3	4.3	.2	.2
PIXEL AΩ (cm^2sr):	3×10^{-2}	3×10^{-2}	8×10^{-5}	8×10^{-5}
D* (cm Hz $^{1/2}$ W^{-1})	3×10^{9}	2×10^{9}	3×10^{10}	5×10^{11}
NEP ($WHz^{-1/2}$):	3×10^{-11}	5×10^{-11}	8×10^{-13}	5×10^{-1}
NESR (W cm^{-2} sr^{-1}/cm^{-1}):	4×10^{-9} ($0.5\ cm^{-1}$)	6×10^{-9} ($0.5\ cm^{-1}$)	4×10^{-10} ($5\ cm^{-1}$)	2×10^{-1} ($5\ cm^{-1}$)
DATABAND (Hz):	.4 - 12	8 - 26	24 - 44	44 - 56
TEMPERATURE (K):	170	170	80	80

INSTRUMENT TEMPERATURE (K):	170
DATA BIT RATE:	2000 Bits/sec
POWER:	21 W (Avg): 26 W (Peak)
WEIGHT: INSTRUMENT	19 Kg
ELECTRONICS/POWER SUPPLY	8 Kg
TOTAL	27 Kg

Reproduced From
Best Available Copy

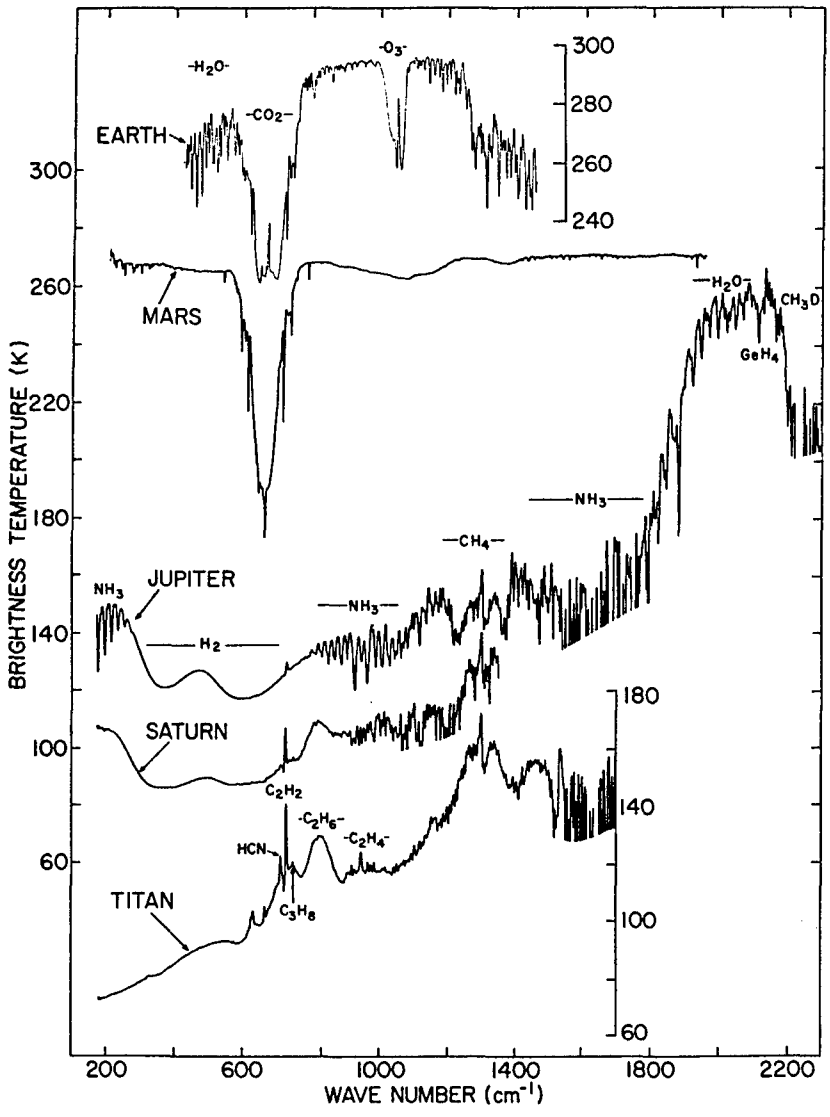


Fig. 1

The brightness temperatures of typical nadir emission spectra obtained by various spacecraft. The broad spectral coverage permitted unanticipated discoveries as well as the simultaneous retrieval of many atmospheric parameters including temperatures, gas abundances, and aerosol properties. CIRS will use limb sensing of Saturn's and Titan's stratospheres to obtain an altitude resolution < one scale height for temperature and composition studies.

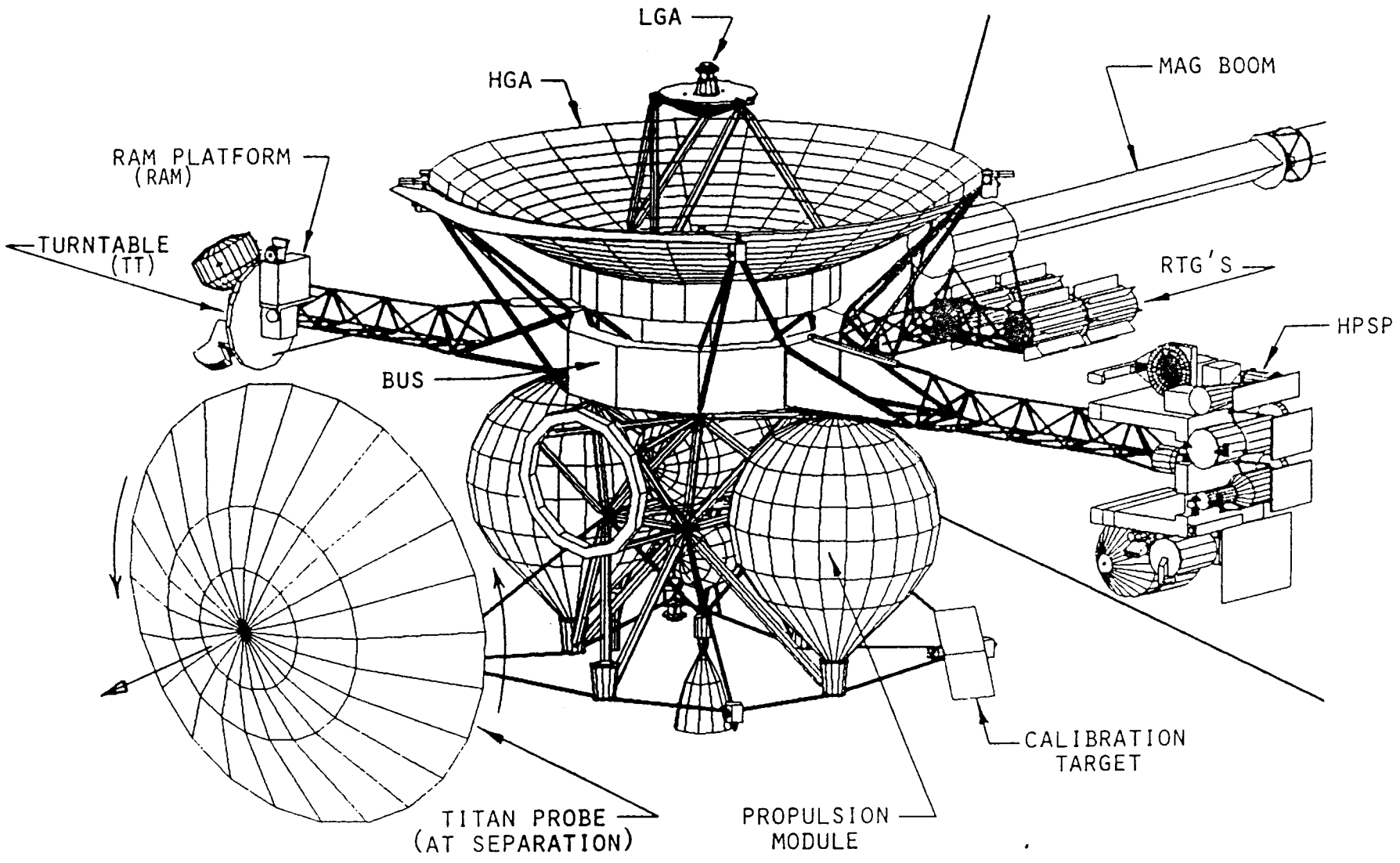


Fig. 2 CASSINI SPACECRAFT CRUISE CONFIGURATION -FRONT ISOMETRIC VIEW

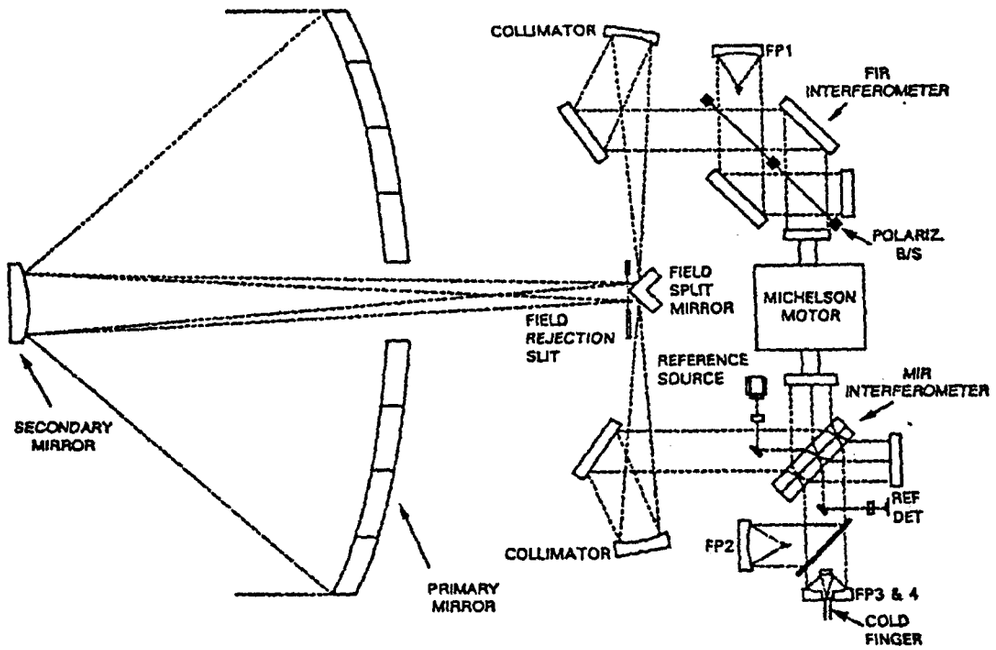


Fig. 3a Optical schematic of CIRS.

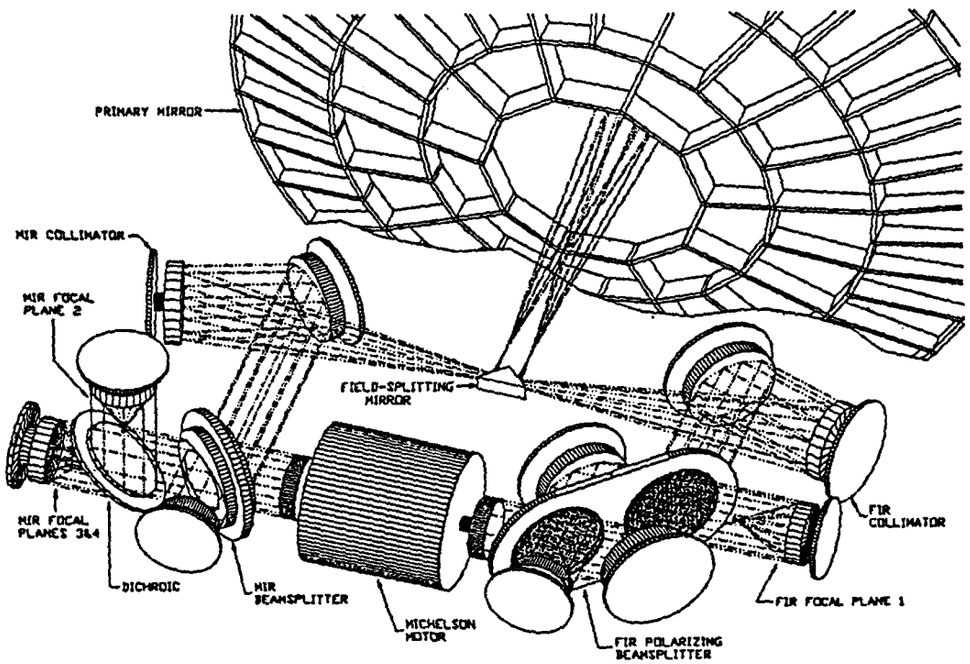


Fig. 3b Exploded view schematic of CIRS.

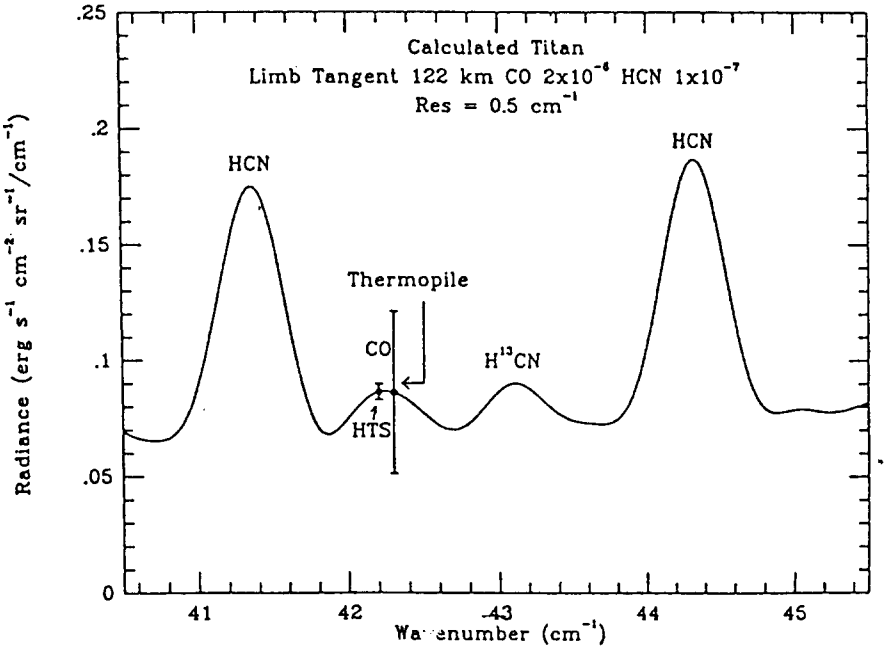


Fig. 4. Synthetic Titan limb tangent spectrum. The smaller 1σ error bars of the HTS detector will allow CO to be measured in the FIRS spectrum.

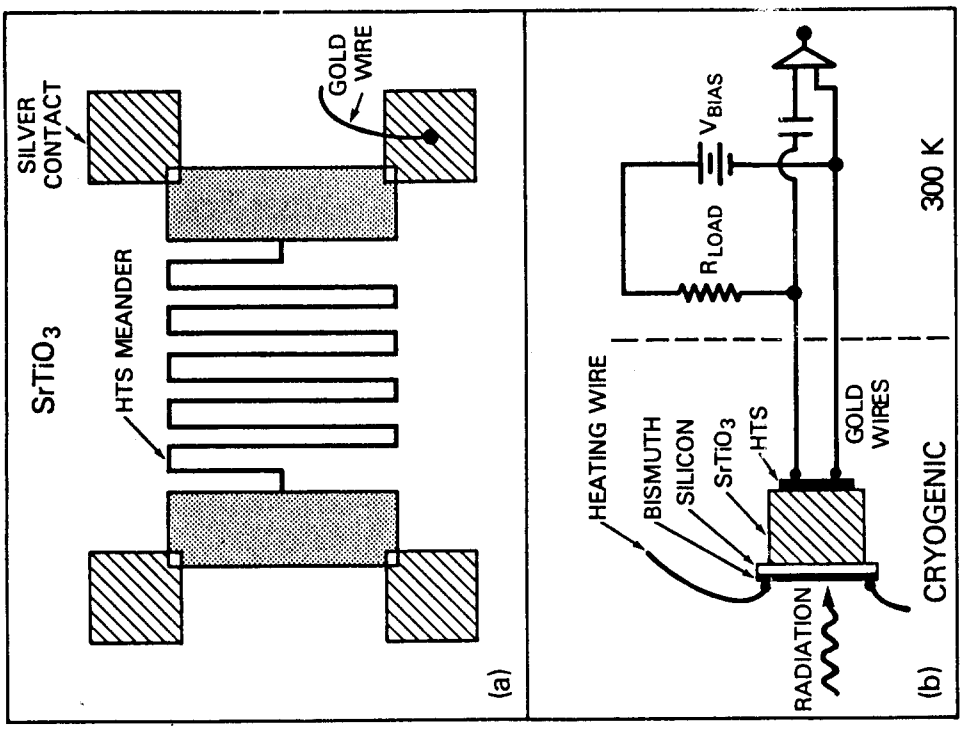


FIG. 5 a) 0.2-μm-thick $Y_1Ba_2Cu_3O_x$ film is patterned into a meander line with 20 μm width, filling an area of 1.5×1.5 mm with a total length of 76 mm; the 1.8×2.7 mm $SrTiO_3$ substrate is 500 μm thick. (b) 2.5×4.0 mm Si wafer, 25 μm thick, is coated on one side with 0.1 μm of bismuth and is bonded on the other side to the $SrTiO_3$ with epoxy.

THE EFFECT OF TEMPERATURE CYCLING TYPICAL OF LOW EARTH ORBIT SATELLITES ON THIN FILMS OF $YBa_2Cu_3O_{7-x}$

A. Mogro-Campero and L.G. Turner
GE Research and Development Center
Schenectady, NY 12301

A. Bogorad and R. Herschitz
GE Astro-Space Division
Princeton, NJ 08543-0800

ABSTRACT

Thin films of $YBa_2Cu_3O_{7-x}$ (YBCO) were temperature cycled to simulate conditions on a low earth orbit satellite. In one series of tests, epitaxial and polycrystalline YBCO films were cycled in temperature up to ± 80°C in vacuum and in nitrogen for hundreds of cycles. The room temperature resistance of an epitaxial YBCO film increased by about 10%, but the superconducting transition temperature was unchanged. The largest changes were for a polycrystalline YBCO film on oxidized silicon with a zirconia buffer layer, for which the transition temperature decreased by 3 K. An extended test was carried out for epitaxial films. After 3200 cycles (corresponding to about 230 days in space) transition temperatures and critical current densities remained unchanged.

INTRODUCTION

The refrigeration of superconductors in space poses a challenging problem. The problem could be less severe if superconducting materials were not cooled when not in use. Temperature cycling experiments of YBCO thin films were carried out in laboratory chambers to simulate temperature exposure in space missions.

Thermal cycling experiments were done to simulate a large number of eclipses of a low earth orbit satellite. Electrical measurements were performed to search for possible degradation in room temperature resistance, the zero resistance transition temperature, and the critical current density. The maximum number of cycles corresponds to more than half a year in space.

EXPERIMENTAL CONDITIONS

Thin films of YBCO were formed by coevaporation of Y, BaF_2, and Cu and furnace annealing in wet oxygen at 850°C for 3.5 h. The substrates used in this study were (100) $SrTiO_3$ and (100) $LaAlO_3$ for epitaxial films, and polycrystalline alumina and oxidized silicon with zirconia buffer layers for polycrystalline YBCO films. Processing, electrical, and microstructural studies of these types of films have been published [1-4].

Temperature cycling in vacuum is more relevant to space conditions, but cycling is relatively slow (10 cycles per day in the chamber used). For more extensive thermal cycling, a separate chamber with a nitrogen ambient was used, which allowed a cycling rate of 60 cycles per day.

Two groups of samples were used. The first consisted of an epitaxial YBCO film on (100) $SrTiO_3$, and polycrystalline YBCO films on a zirconia buffer layer on oxidized silicon and on polycrystalline alumina. These samples were unpatterned, and subjected to a few hundred cycles, as explained below. The second set of samples were patterned by photolithography and a weak nitric acid etch to produce a bridge 400 μm long and 20 μm wide. Silver contacts were evaporated on these samples and annealed at 550°C for 0.5 h to provide low resistance contacts for resistivity and critical current measurements. All samples were characterized by four probe electrical measurements by using pressure contacts. A 1 μV criterion for the determination of the critical current density was used for the patterned samples. The patterned samples were cycled in nitrogen for thousands of cycles, as explained in more detail in the next section.

RESULTS

Results for two samples are shown in Figures 1 and 2. Each sample had a cumulative exposure. The temperature cycling stages referred to in the figures are as follows (200 cycles corresponds to about 14 days in space):

1. Before temperature cycling
2. After 5 cycles at ± 50°C in vacuum
3. After an additional 200 cycles at ± 50°C in vacuum
4. After an additional 200 cycles at ± 60°C in nitrogen
5. After an additional 200 cycles at ± 80°C in nitrogen.

The zero resistance transition temperature (T_c) remains constant, the transition width is unchanged in Fig. 1 and increases by about one degree in Fig. 2, and the room temperature resistance normalized to that before temperature cycling (R_N) increases at first but seems to stabilize at increases of about 10% in Fig. 1 and about 20% in Fig. 2.

The largest changes were observed for a 0.9 μm thick YBCO film on oxidized silicon with a 0.5 μm zirconia buffer layer. This sample was subjected to 200 cycles at ± 80°C in nitrogen. The transition width increased from 3.1 to 3.6 K, T_c decreased from 86 to 83 K, and the room temperature resistance increased by a factor of 4.

An epitaxial YBCO film on (100) $LaAlO_3$ was subjected to extensive temperature cycling (3200 cycles at ± 80 °C in nitrogen). This sample and its control (which remained under nitrogen at room temperature) were 0.2 and 0.4 μm thick, respectively, and they were patterned so that critical current density (J_c) measurements could be performed. The T_c of 89 K, the J_c of 3-5 x 10^5 A cm^{-2} at 77 K, and the transition width of 1-2 K were unchanged for these samples after the period of testing. The normalized value of the room temperature resistance (R_N) was the only parameter which showed a change after taking

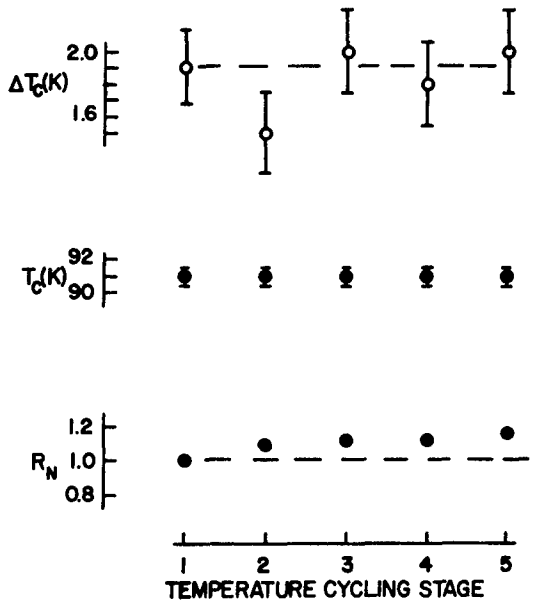


Fig. 1. Electrical parameters measured after each cycling stage (defined in the text) for a 0.5 μm thick YBCO film on (100) $SrTiO_3$. From top to bottom: the 10 to 90% transition width, the zero resistance transition temperature, and the room temperature resistance normalized to that before temperature cycling.

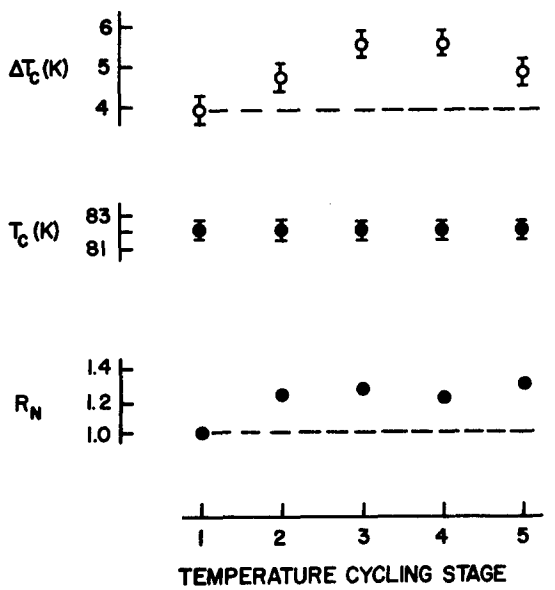


Fig. 2 Electrical parameters measured after each cycling stage (defined in the text) for a 0.7 μm thick YBCO film on polycrystalline alumina with a 0.5 μm zirconia buffer layer. The parameters are defined in the caption to Fig. 1.

into account measurement errors: an increase by 3% in the control sample and by 5% in the sample which underwent temperature cycling.

DISCUSSION

The temperature cycling experiments we have performed show that epitaxial YBCO films suffer only minor changes after temperature cycling, with somewhat greater changes found for polycrystalline YBCO films. Significant changes in electrical parameters of YBCO films have been reported after storage for a few days in nitrogen [5]. We believe that the relatively good performance of our films is related to the fact that BaF_2 was used as an evaporation source, leading to much more rugged films [6].

Even though the film annealing is performed in wet oxygen to remove the fluorine from the films, we have found by x-ray photoelectron spectroscopy that a clearly identified about 1 atomic % fluorine abundance remains in the surface region. We speculate that the fluorine improves the degradation performance of these films. As suggestive evidence we cite Tressaud et al. [7], who find for YBCO that a thin surface layer containing fluorine provides protection against hydrolysis and gas exchange, and Vasquez et al. [8], who report reduced reactivity to air for YBCO treated with HF.

CONCLUSION

The results of this study are encouraging for the use of epitaxial YBCO films in low earth orbit satellites from the viewpoint of temperature cycling, since the transition temperature and critical current density do not change after extensive temperature cycling. Thus, even with the lack of protective layers, the thin YBCO films do not necessarily have to be cooled when not in use.

REFERENCES

1. A. Mogro-Campero, L.G. Turner, E. L. Hall, and M.C. Burrell, " Characterization of thin films of Y-Ba-Cu-O on oxidized silicon with a zirconia buffer layer," Appl. Phys. Lett. 52 (24), 2068-2070, 1988.

2. A. Mogro-Campero, L.G. Turner, and G. Kendall," Thickness and annealing dependence of the superconducting transition temperature of $YBa_2Cu_3O_{7-x}$ thin films on oxidized silicon and polycrystalline alumina substrates," Appl. Phys. Lett. 53 (25), 2566-2568, 1988.

3. A. Mogro-Campero, L.G. Turner, and E.L. Hall," Large differences of critical current density in thin films of superconducting $YBa_2Cu_3O_{7-x}$," J. Appl. Phys. 65 (12), 4951-4954, 1989.

4. A. Mogro-Campero, L.G. Turner, E.L. Hall, M.F. Garbauskas, and N. Lewis, " Epitaxial growth and critical current density of thin films of $YBa_2Cu_3O_{7-x}$

on $LaAlO_3$ substrates," Appl. Phys. Lett. 54 (26), 2719-2721, 1989.

5. B.-Y. Tsaur, M.S. Dilorio, and A.J. Strauss, "Preparation of superconducting $YBa_2Cu_3O_x$ thin films by oxygen annealing of multilayer metal films," Appl. Phys. Lett. 51 (11), 858-860, 1987.

6. P.M. Mankiewich, J.H. Scofield, W.J. Skocpol, R.E. Howard, and A.H. Dayem, " Reproducible technique for fabrication of thin films of high transition temperature superconductors," Appl. Phys. Lett. 51 (21), 1753- 1755, 1987.

7. A. Tressaud, B. Chevalier, B. Lepine, J.M. Dance, L. Lozano, J. Grannec, J. Etourneau, R. Tournier, A. Sulpice, and P. Lejay," Passivation process of high T_c superconductors $YBa_2Cu_3O_{7-x}$ by fluorine gas treatment," Modern Phys. Lett. B_c 2 (10), 1183-1188, 1988.

8. R.P. Vasquez, B.D. Hunt, and M.C. Foote," Reduced reactivity to air on HF-treated $YBa_2Cu_3O_{7-x}$ surfaces," Appl. Phys. Lett. 54 (23), 2373-2375, 1989.

A YBCO RF-SQUID VARIABLE TEMPERATURE SUSCEPTOMETER AND ITS APPLICATIONS

Luwei Zhou, Jinwu Qiu, Xianfeng Zhang, Zhimin Tang, Yimin Cai, and Yongjia Qian
Department of Physics
Fudan University
Shanghai, 200433, China

ABSTRACT

The SQUID susceptibility using a high-temperature rf SQUID and a normal metal pick-up coil is employed in testing weak magnetization of the sample. The magnetic moment resolution of the device is $1x10^{-6}$ emu, and that of the susceptibility is $5x10^{-6}$ emu/cm^3.

1. INTRODUCTION

Since Colcough *et al.* (1) first revealed the existence of intrinsic rf SQUID effect in high-T_c superconducting Y-Ba-Cu-O, Zimmerman *et al.* (2) are the first who deviate from the applicable high temperature rf SQUID. Since then, many laboratories, including ours, have made rf SQUIDs with their own features (3-8). Before a liquid nitrogen superconducting flux transformer can be made, a pick-up coil made of normal metal is used in this device. The intention of this work is to substitute the low-temperature liquid helium device with the high-temperature SQUID while keeping the extraordinary features of a SQUID variable temperature susceptometer (VTS).

The temperature range of the VTS developed in this laboratory is from 77 K to 300 K, and the magnetic field range, 0-0.1T. The device has been used to characterize superconducting thin films.

2. EXPERIMENTAL SETUP AND OPERATIONS

The VTS includes the SQUID system, sample chamber, magnet, dewar, and a computerized data acquisition system. The SQUID system consists of the SQUID sensor, signal pick-up coil and correspondent electronics. The SQUID used here is a double-hole rf SQUID made of a YBCO bulk material working at 19 MHz. The flux resolution at 77 K is $5x10^{-4}\ \Phi_o/\sqrt{Hz}$ at the frequency range of 20-200 Hz, and $2x10^{-4}\ \Phi_o/\sqrt{Hz}$ near dc end.

Figure 1 gives the noise spectrum of the device at 77 K. The inset is its noise output characteristics near dc end. To reduce the external interferences, the SQUID is placed in a YBCO superconducting screening hollow cylinder. In this experiment, a pick-up coil made of normal metal is used to substitute the superconducting coil before a satisfactory superconducting flux transformer working in liquid nitrogen can be made. The inductances of the pick-up coil and the input coil do not have to be matched in the 77 K SQUID. When a signal is picked up with a normal metal coil, the amount of the signal depends not only on the moving speed of a sample, but also on its relative position. If a pick-up signal is calibrated with a standard sample in the same way that a sample is measured, then a normal metal pick-up coil can also generate a signal propor-

tional to magnetic moment. This idea is the mail feature of this apparatus, which bursts the idea that a superconducting flux transformer must be used in the application of a SQUID. Our recent test of a superconducting flux closed circuited in liquid nitrogen temperature using the SQUID

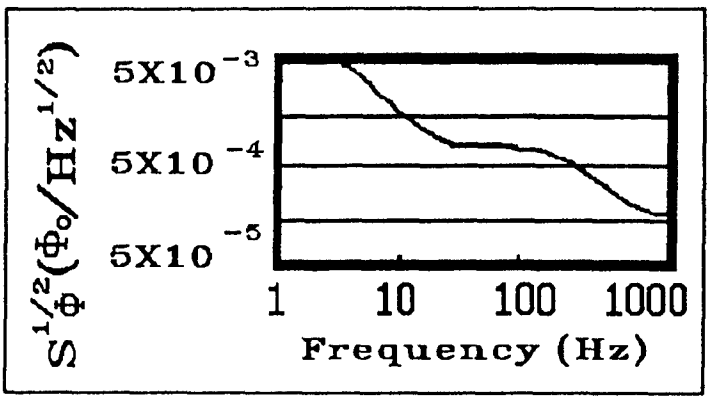


Figure 1. The noise spectrum of the device at 77 K.

shows that a closed flux transformer can be made (9), although it is not yet mature enough to be used in a susceptometer. The normal metal coils used in this experiment are a pair of counter-wound coils 100mm apart from each other and with the same number (N=60) of rings on each coil. The electronics employed here are those used in a usual liquid helium rf SQUID similar to the S.H.E. 330 SQUID system. Our sample chamber system consists of a thermostat, a temperature measuring and controlling part, and a sample transmission mechanism. The temperature difference between the sample space and the sample itself is corrected by the calibration.

A normal metal solenoid is used to supply the magnetic field for the system before a satisfactory high-T_c superconducting magnet can be made. The normal magnet used here supplies a center field as high as 0.1 T when the current is 2 A.

The vacuum adiabatic method is used to keep constant temperature. The temperature decrease is obtained with a phosphorous-copper ring mounted between the sample space and the liquid nitrogen chamber. The sample, which is suspended on a string, enters the sample space from the top of the dewar. When a heater is not turned on, the typical liquid nitrogen consumption is about 2 liters/day.

The procedures of sample measuring are similar to those for the liquid helium SQUID susceptometer. The difference in measuring with a superconducting flux transformer is that with a susceptometer, the amount of the signal has to be calibrated using a standard sample while maintaining the moving sample's orientation. The standard samples are annealed high-purity aluminum and gallium cylinders.

3. EXPERIMENTAL RESULTS

The experimental results demonstrate that the design of the normal metal coils does work, except the absolute value of the susceptibility has to be calibrated.

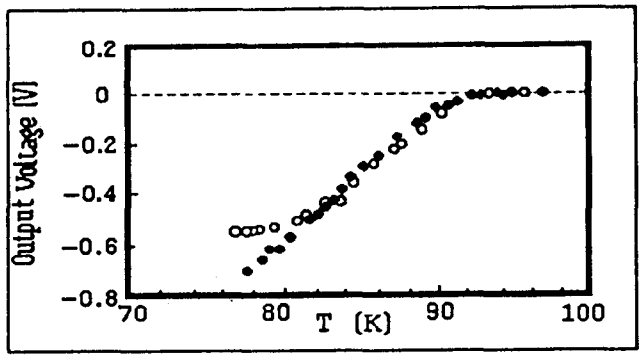


Figure 2. Meissner and screening effects of a small sample of YBCO.

Figure 2 displays the Meissner and magnetic screening effects of a small piece of Y-Ba-Cu-O sample (3 mg) detected by this device when the external field is 100 Oe. In measuring the magnetic screening effect, the magnetic field is lowered to zero first; the sample temperature is then dropped to 77 K from room temperature. After a certain magnetic field is applied, magnetic moment signal is measured at increasing temperatures. In measuring Meissner effect, the magnetic moment signals are measured at a given field while the sample temperature is lowering from a temperature well above T_c. The results in Figure 2 show that the Meissner signal is about 60 percent of that of screening effect, which gives useful information for improving the sample making technology.

Figure 3 gives a magnetic transition curve of a YBCO superconducting thin film detected by this apparatus. The film thickness is about 3000 to 5000 A, and the applied field is 3 Oe. The transition temperature determined by this VTS is 82.3 K which is very close to the value T_{co}, zero-resistance temperature found by the four-probe method. In the case when the SQUID is functioning as a sensor, the measured field is, in principle, a relative change, and a calibration has to be done to determine the absolute value of moment and susceptibility from a signal--even in a liquid helium SQUID susceptometer.

It is more important when normal metal pick-up coils are used in the liquid nitrogen device. A special moment calibrating coil is employed to supply a certain value of a magnetic moment. The moment, m, of the coils calculated as m=NSI, where N is the number of the circles of the coil, S is the average area of the coil, and I is the current through the coil. In this experiment, N=30, the average diameter of the coil is about 0.3 cm, and the moment resolution of the device is about 1×10^{-6} emu due to the signal size and the device resolution. Some metallic diamagnetic materials with high purity, such as aluminum and gallium are used to calibrate the susceptibility values.

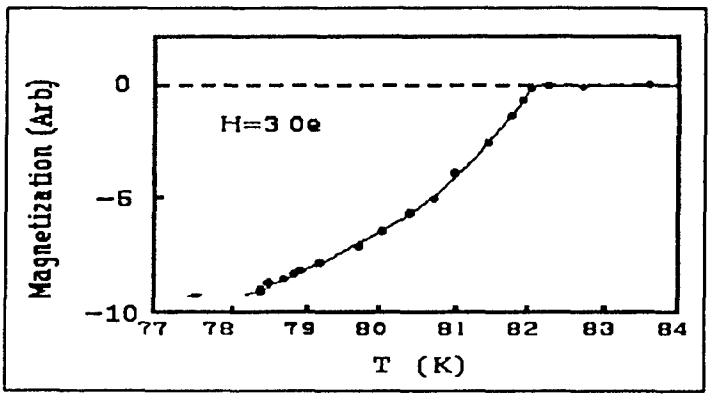


Figure 3. Magnetic transition curve of a YBCO thin film detected by the device.

The calibration shows that the susceptibility resolution of the device is consistent with that estimated from the measurement on a small sample of high-T_c superconductor, namely, about $5x10^{-6}$ emu/cm^3.

In summary, the SQUID susceptibility using a high-temperature rf SQUID and a normal metal pick-up coil can be employed in testing weak magnetization of a sample. The susceptibility transition curve of superconducting thin film and the calibrations of metallic diamagnetic samples show the feasibility of usage of the non-superconducting transformer on the SQUID. The magnetic moment resolution of the device is $1x10^{-6}$ emu, and that of the susceptibility is $5x10^{-6}$ emu/cm^3.

The work is supported by China National Center for Research and Development on Superconductivity, and Hong Kong's K.C. Wong Education Foundation.

REFERENCES

(1) Colcough, M.S. *et al.*, 1987, Nature, **323**, 47.

(2) Zimmerman, J.E. *et al*, 1987, Appl. Phys. Lett., **1**, 617.

(3) Pegrum, C.M. *et al.*, 1987, Appl. Phys. Lett., **51**, 1364.

(4) Harrop, S. *et al.*, 1988, Physica C, **153-5**, 1411.

(5) Harvey, I.K. *et al.*, 1988, Appl. Phys. Lett., **52**, 1634.

(6) Qiu, J.W. *et al.*, 1990, "Properties and Applications of YBCO RF-SQUID," Proceedings of BHTSC '89, ed. Z.Z. Gan, World Scientific Publishing Co., Singapore, in press.

(7) Chiao, W.C., 1990, "A YBaCuO Bulk RF-SQUID Operated at 77K and Its Application in Measurement of Weak Magnetic Field," Proceedings of BHTSC '89, ed. Z.Z. Gan, World Scientific Publishing Co., Singapore, in press.

(8) Xue, S.Q. *et al.*, "An RF-SQUID Operated in Liquid Nitrogen up to 85 K Made of High T_c YBCO Bulk," Proceedings of BHTSC '89, ed. Z.Z. Gan, World Scientific Publishing Co., Singapore, in press.

(9) To be reported elsewhere.

STATIC AND DYNAMICAL MEISSNER FORCE FIELDS*

B.R. Weinberger and L. Lynds
United Technologies Research Center
East Hartford, CT 06108

J.R. Hull and T.M. Mulcahy
Materials and Components Technology Division
Argonne National Laboratory
9700 South Cass Avenue
Argonne, IL 60439

The coupling between copper-based high temperature superconductors (HTS) and magnets can be represented by a force field. Zero-field cooled experiments were performed with several forms of superconductors: 1) cold-pressed sintered cylindrical disks, 2) small particles fixed in epoxy polymers, and 3) small particles suspended in hydrocarbon waxes. Using magnets with axial field symmetries, direct spatial force measurements in the range of 0.1 -10^4 dynes were performed with an analytical balance and force constants were obtained from mechanical vibrational resonances. Force constants increase dramatically with decreasing spatial displacement. The force field displays a strong temperature dependence between 20 K and 90 K and decreases exponentially with increasing distance of separation. Distinct slope changes suggest the presence of B-field and temperature-activated processes that define the forces. Hysteresis measurements indicated that the magnitude of force scales roughly with the volume fraction of HTS in composite structures. Thus, the net force resulting from the field interaction appears to arise from regions as small or smaller than the grain size and does not depend on contiguous electron transport over large areas. Results of these experiments will be discussed.

The practical implications are that machinable composite HTS structures with desirable strength, thermal and B-field properties can be produced. As an example, we will demonstrate a prototype magnetic rotor thrust bearing levitated over a modular composite HTS structure. Rotation is excited by a three phase square wave oscillator and the bearing can be operated at 20000 rpm.

* Work at the Argonne National Laboratory was performed under the auspices of the U.S. Department of Energy Superconductivity Pilot Center, Office of Energy Storage and Distribution, under Contract W-31-109-Eng-38.

Magnetic Forces in High-T_c Superconducting Bearings

F.C. Moon

Mechanical and Aerospace Engineering
Cornell University
Ithaca, New York 14853

In September 1987 researchers at Cornell levitated a small rotor on superconducting bearings at 10,000 RPM. In April 1989 a speed of 120,000 RPM was achieved in a passive bearing with no active control. The bearing material used was $YBa_2Cu_3O_7$. There is no evidence that the rotation speed has any significant effect on the lift force. We believe that the attainable rotation speeds in a vacuum will be over 300,000 RPM in the near future.

Magnetic force measurements between a permanent rare-earth magnet and high-T_c superconducting material versus vertical and lateral displacements have been made. A large hysteresis loop results for large displacements, while minor loops result for small displacements. These minor loops seem to give a slope proportional to the magnetic stiffness, and are probably indicative of flux pinning forces.

Experiments of rotary speed versus time show a linear decay in a vacuum. Measurements of magnetic drag forces of a magnetic dipole over a high-T_c superconducting disc of YBCO show that the drag force reaches a constant value, independent of the speed. Damping of lateral vibrations of levitated rotors have been measured which indicates that transverse flux motion in the superconductor will create dissipation.

As a result of these force measurements we have been able to design an optimum shape for the superconductor bearing pads which gives good lateral and axial stability. Recent force measurements on melt-quench processed superconductors indicate a substantial increase in levitation force and magnetic stiffness over free sintered materials. As a result, application of high-T_c supeconducting bearings are beginning to show great promise at this time.

F.C. Moon, M.M. Yanoviak, R. Ware, "Hysteretic Levitation Forces in Superconducting Ceramics," Appl. Phys. Lett., **52** (1988) 1534-1536.

SECTION 6:
SUPERCONDUCTIVITY
PROGRAMS

PROGRESS OF RESEARCH OF HIGH-Tc SUPERCONDUCTORS

Shoji Tanaka
Superconductivity Research Laboratory
ISTEC
10-13 Shononome 1-Chome, Koto-ku
Tokyo 135, Japan

ABSTRACT

The research of high-Tc superconductors has made big progress in these last few years. New materials were found and the systematic investigations of these materials must contribute to understanding the mechanism of high-Tc superconductivity.

The critical currents in thin films, bulks and tapes increased drastically, and the origin of flux pinning will be clarified in the near future.

These progressions give us a view of a bright future of high-Tc superconductivity in both the basic and application research areas.

Recent activities in research of high-Tc superconductivity and superconductors in Japan will be overviewed.

PROSPECTS AND PROGRESS OF HIGH Tc SUPERCONDUCTIVITY FOR SPACE APPLICATIONS

Robert R. Romanofsky and Marty M. Sokoloski
National Aeronautics and Space Administration
Washington, D.C. 20546

Abstract

It had been recognized from the onset that high temperature superconductivity held great promise for major advances across a broad range of NASA interests. The current effort is organized around four key areas: communications and data, sensors and cryogenics, propulsion and power, and space materials technology. Recently, laser ablated $YBa_2Cu_3O_{7-X}$ films on $LaAlO_3$ produced far superior RF characteristics when compared to metallic films on the same substrate. This achievement has enabled a number of unique microwave device applications, such as low insertion loss phase shifters and high-Q filters. Melt texturing and melt-quenched techniques are being used to produce bulk material with optimized magnetic properties. These yttrium-enriched materials possess enhanced flux pinning characteristics and could lead to prototype cryocooler bearings. Significant progress has also occurred in bolometer and current lead technology. Studies are being conducted to evaluate the effect of high temperature superconducting materials on the performance and life of high power magneto-plasma-dynamic thrusters. Extended studies have also been performed to evaluate the benefit of superconducting magnetic energy storage for LEO space station, lunar and Mars mission applications.

Introduction

NASA has sustained a significant effort in low temperature superconductivity research and development because of the unique applications to spaceborne science instrumentation. A current example is Gravity Probe B, an experiment being developed to confirm or refute certain tenets of Einstein's general theory of relativity. The experiment is designed to precisely measure an almost imperceptible gyroscope tilt which should result from the influence of a moving mass (the Earth) on space-time. SQUID magnetometers will be used to detect the London moment created by rotating niobium-coated quartz spheres. Additionally, superconducting lead sleeves will be used to attenuate the Earth's magnetic field and prevent interference with the sensitive instrumentation. Research efforts are also underway to develop superconducting/insulator/superconducting (SIS) tunnel junctions for submillimeter mixers to be used in heterodyne remote sensing systems. A 0.3 square micron NbN/MgO/NbN junction has been demonstrated at 205 GHz. Emphasis on applications of low temperature superconducting technology to sensor systems will continue.

The promise of revolutionary advancements in satellite and deep-space communications, astrophysics and Earth observation technology, and space-based magnetic energy storage and propulsion

inspired an intensive research effort. Preliminary activities concentrated on identifying applications which were peculiar to the NASA mission or of high priority interest. The ensuing application specific materials development has met with considerable success. Prototype thin film electronic devices promise to emerge first, although bulk materials technology for certain applications such as cryocooler current leads and magnetic bearings is evolving rapidly. Specific research and development efforts are described in subsequent sections.

Thin Film Applications

Thin film analog signal processing electronics was envisioned as the first practical application for high temperature superconductors. Development was not precluded by high current density or high critical magnetic field requirements. The major prerequisite for microwave communication devices and circuits was comparitively low RF surface resistance. Enthusiasm waned as tests on the new materials at microwave frequencies revealed fundamental limitations. Poor RF characteristics were attributed to grain boundaries and anisotropy. Recently; however, films deposited by laser ablation have produced excellent RF properties as high as 35 GHz [1]. Thin $YBa_2Cu_3O_{7-x}$ films were deposited on $LaAlO_3$, which was heated to 700 degrees Celsius in a 100 mtorr atmosphere. Samples were slowly cooled to room temperature at an oxygen pressure of one atmosphere. The best films had critical temperatures of approximately 90 K. Based on microstrip resonator techniques, the unloaded quality factor (Q) of the superconductor equalled that of a metalic (gold) film at approximately 60 K and exceeded the Q of the metalic film by 150 % at 25 K. Figure 1 shows typical measured resonator return loss data.

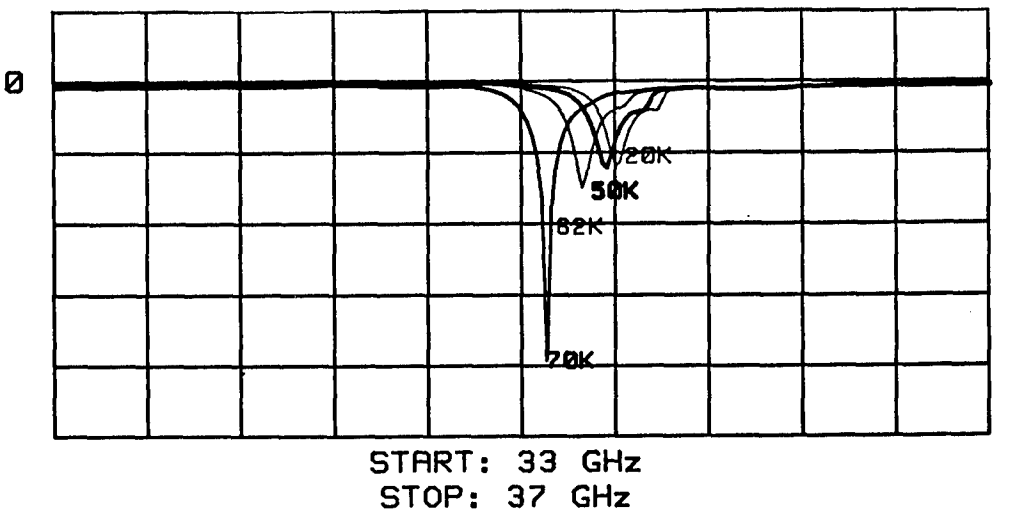


Figure 1. Resonator reflected power (10 dB/div)

Processing advantages of laser ablation such as exposure to relatively low temperatures are attractive for device applications. Such progress suggests the eventual possibility of hybrid superconducting/semiconducting circuits. Experiments based on transmission through $YBa_2Cu_3O_{7-x}$ films have also been performed

to assess additional microwave properties [2]. Table I summarizes important parameters derived from the data assuming Bardeen-Cooper-Schrieffer (BCS) behavior.

A number of devices are being developed including: filters, phase shifters, and antennas. A novel phase shifter has been designed which has theoretically symmetric insertion loss and is immune to bias line interactions [3]. High-Q bandpass microstrip filters, offering tremendous weight reduction compared to conventional waveguide implementations, are being fabricated. The new superconductors also enable practical electrically small antennas, normally shunned due to extremely poor efficiencies resulting from high ohmic loss (compared to radiation resistance). High gain, high directivity arrays are being investigated.

Table I
Thin film microwave properties including T=0 bandgap and magnetic penetration depth (conductivity units are S/m)

PARAMETER	MgO SE	LA	$LaAlO_3$	ZrO_2
σ_1 (70K, 35 GHz)	3.72×10^4	3.30×10^6	2.48×10^5	4.28×10^5
σ_2 (70K, 35 GHz)	3.47×10^4	8.51×10^6	4.75×10^6	9.23×10^5
σ_1 (40 K, 35 GHz)	4.46×10^3	3.52×10^5	2.64×10^4	4.57×10^4
σ_2 (40 K, 35 GHz)	1.22×10^5	3.32×10^7	6.44×10^6	1.10×10^7
$\frac{2\Delta}{KTc}$	4.19	4.35	4.32	4.31
λ (um)	3.33	0.40	0.69	1.23

NASA has unparalled requirements in science sensor technology because of unique and extensive astrophysics and Earth observation missions. The sensors thrust is focused on two major areas: detectors and cryogenic systems. NASA has a keen interest in applying the new materials to spectroscopy in the submillimeter to far-infrared spectrum, and in developing high sensitivity, high spectral resolution instruments. Assuming that existing theories are valid for the new class of superconductors, detection down to approximately 100 microns should be possible. Of equal importance is the need to develop reliable (long-life) cryogenic systems. Such systems could be enabling for prefatory interplanetary exploration leading to lunar and mars outposts. Existing options are limited to inefficient cryocoolers or stored cryogens. A number of potential benefits to these critical systems using high temperature superconductors have been identified. NASA has undertaken several major projects in these areas: bolometer detectors, superconducting tunnel junctions, cryocooler current leads, and passive magnetic bearings for cryocoolers.

Planetary missions rely on liquid helium cooled detectors or relatively poor performance >65K detectors. HgCdTe focal plane arrays are useful to approximately 20 microns; however, far infrared spectroscopy necessitates thermal sensors. The new oxide

superconductors enable an intermediate performance thermal detector capable of operating at 65 to 95 K. This is a temperature range potentially achievable through radiative cooling in space. The first approach was to use a transition-edge meander line bolometer [4]. Figure 2 shows a schematic of the composite bolometer assembly. In the bolometric mode, the film is held near its transition temperature, where the temperature derivative of resistance is maximum. Radiation is absorbed by a thin film of bismuth deposited on a silicon substrate in contact with the $YBa_2Cu_3O_{7-x}/SrTiO_3$ circuit. The DC responsivity was measured as 1900 V/W. Goals for this type of detector are a near DC detectivity of greater than 10^{10} cm$(Hz)^{0.5}$/W and a time constant of less than 300 mS. A near DC D^* of 1.1 X 10^8 and a time constant of 32 seconds was measured. Techniques to reduce the time constant, attributed primarily to the heat capacity of the $SrTiO_3$, include thinning the substrate or using a diamond substrate. A second approach is to build a kinetic inuctance bolometer. A superconducting meander line is configured as a wheatstone bridge and monitored by a SQUID galvanometer. Since the magnetic field penetration depth is temperature sensitive, the inductance will depend on temperature. This approach eliminates Johnson noise and is potentially more sensitive (higher D^*) than the transition-edge device.

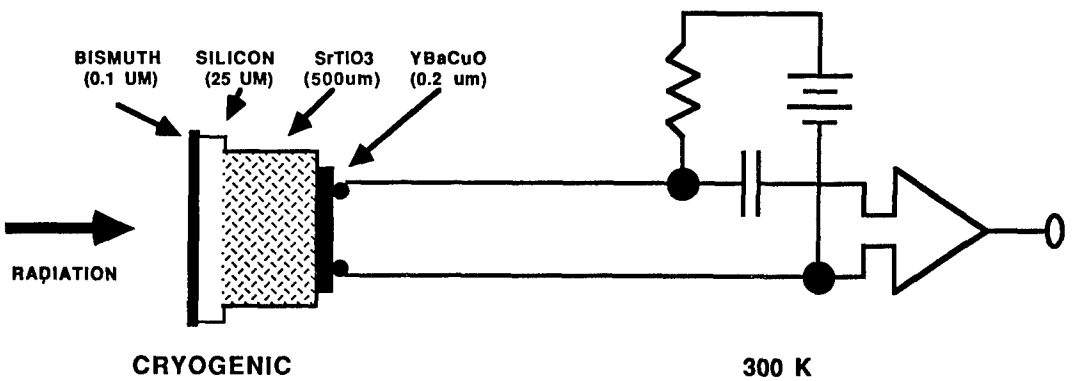


Figure 2. Composite transition-edge bolometer

The production of tunnel junctions and other microdevices requires high quality thin films with superconducting surfaces. To date; however, operation of high Tc junctions has been degraded by poor surface morphology and stoichiometry, and is further complicated by the extremely short coherence length of the new superconductors. Interaction at metal and substrate interfaces has also been detrimental. The elimination or prevention of non-superconducting surface layers is critical to eventual device fabrication. Significant improvements in the electrical properties of $YBa_2Cu_3O_{7-x}$ films have been demonstrated using a 1% Br by volume in ethanol etch [5]. Evidence suggests that the etch is effective in removing surface contamination layers without adversely affecting the stoichiometry. Table II lists properties of $YBa_2Cu_3O_{7-x}$/Au/Nb contacts. IcRn, which is proportional to the bandgap at the surface, increased by a factor of 10 to 20 for typical samples. Contact resistance decreased by approximately a factor of 10. Practical devices will also require surfaces which are insensitive to environmental effects. A promising passivation

technique using a post-anneal chemical treatment has been developed. Treatment with a nonaqueous HF solution has been shown to reduce the reactivity of the superconductor to air [6]. These, or similar, processing techniques are prerequisite to microdevice fabrication. The investigation of surface modification techniques is continuing. Short-term objectives include the fabrication of planar geometry tunnel junctions and the demonstration of high frequency local oscillators operating at 77 K using SNS microbridges.

Table II
Characteristics of 10 X 10 um^2 SNS contacts

	UNTREATED SAMPLE	30 SEC. Br ETCH
Jc (A/cm^2)	5	180
Rn (Ω)	10.5	2.8
IcRn	53 uV	0.5 mV
RnA(Ωcm^2)	1.05×10^{-5}	2.8×10^{-6}

Bulk Applications

Stored cryogens and closed cycle refrigerators play a vital role in numerous science and exploration missions. Astrophysics and Earth observation technology, in particular, demand cryogenically cooled high resolution sensor systems. Long duration science missions, prefatory to human exploration for example, require correspondingly long lifetime coolant systems. At the present time, both mechanical refrigerators and stored cryogen systems have significant drawbacks. Stored cryogen coolers have limited lifetimes because of parasitic heat loads, resulting in accelerated cryogen boil-off. Mechanical coolers require large power budgets, and have limited cooling capacity. High temperature superconductors have the potential to alleviate some of the major shortcomings. Specifically, High Tc current leads could reduce the parasitic heat load on stored cryogen coolers by as much as 50 %. Furthermore, High Tc passive magnetic bearings could reduce friction and heat leaks in mechanical coolers, improve stability, and significantly improve efficiency.

In typical stored cryogen cooler sensor systems, detectors at 4 K must interface with amplifiers at approximately 80 K. This interconnection is performed with copper or manganin wires, which represent substantial heat leaks. A unique characteristic of the ceramic superconductors is their ability to be excellent electrical conductors and poor thermal conductors simultaneously. Near liquid nitrogen temperatures, the thermal conductivities of copper and YBaCuO are approximately 400-500 W/mK and 5-10 W/mK respectively. Although key issues remain to be resolved, in this application the technology appears precocious. Current densities of 10^3 to 10^4 A/cm^2 in ambient fields of several hundred Gauss are obtainable. All High Tc materials are brittle ceramics and tend to

be unstable. TlCaBaCuO and BiCaSrCuO appear to offer better characteristics in terms of stability against oxygen diffusion. Silver/YBaCuO composites have greater flexibility but at the expense of thermal conductivity. Furthermore, clarification is required with regard to thermal cycling effects and radiation damage susceptibility. Despite these uncertainties, progress has been steady and indications suggest this could be one of the first practical bulk material applications. The potential to extend mission life by perhaps a factor of two simply using near optimal current leads is highly motivating. Protoype encapsulated current leads have already been developed. Rigid tape-cast leads, which are conformable in the green state, have undergone preliminary thermal and mechanical shock testing. Various techniques to produce continuous filaments and ribbons are being pursued.

Mechanical closed-loop refrigeration systems are being developed for long term missions. Such coolers have the potential to overcome the weight and lifetime penalties of stored cryogen systems. Conventional bearings for these coolers have several drawbacks, including: low reliability, excessive weight, large heat leaks, and active feedback control requirements. Passive High Tc magnetic bearings are inherently stable due to the Meissner effect. Potential benefits include considerable reductions in cryocooler input power, weight savings, and long-life, high reliability operation. Synthesis of suitable bulk High Tc materials, in terms of mechanical and magnetic properties, is the first priority. Synthesis of $YBa_2Cu_3O_{7-x}$ by crystallization from a melt has yielded encouraging results [7]. In general, microstructural defects act as flux pinning centers in type II superconductors and determine the character of the material. A balance between too few and too many defects produces material which exhibits optimum magnetic properties. Crystal orientation and the presence of voids also impacts the magnetic behavior. The partial melting technique fortuitously yields a 211 phase impurity which acts as a dopant. Evidence also suggests an optimal excess yttrium concentration to provide maximum magnetization. Experiments seeking to tailor the structure to produce maximum stiffness and levitation force for eventual use in passive magnetic bearings are underway. Critical current densities approaching 10^5 A/cm^2 at one Tesla have been deduced from magnetization data. A process to simultaneously exploit the advantages of melt quenched growth and controlled stoichiometry is undergoing further optimization. Melt quenched and partial melting techniques have produced favorable magnetic characteristics and have proven to be far superior to sintered material. Protoype cryocooler bearings with suitable force and stiffness characteristics are being developed for demonstration.

Alternate cooler embodiments, promising to benefit from High Tc superconductor technology, are also being explored. A flux compression magnetic refrigerator utilizing high Tc superconductors is being considered. Initial work has focused on conventional superconductor flux pump cooling. Calculations indicate that a 0.5 W refrigerator operating between 20 K and 2 K will require a six Tesla field. A superconducting cylinder approximately 15 cm in diameter and 10 cm long is necessary.

Research is motivated by the potential for this type of refrigerator to approach ideal Carnot performance.

Longer range applications include active (supercurrent) bearings for rocket engines. Liquid hydrogen turbopumps provide a natural environment for high Tc bearing insertion, and it is easy to speculate on tremendous improvements in terms of longevity and reliability. Although this application is still immature, progress leading to high current solenoids has been steady and encouraging.

Detailed system studies have been performed to evaluate potential benefits of High Tc superconductors to various space applications. Several candidate systems selected for emphasis include: magneto-plasma-dynamic (MPD) thrusters, superconducting magnetic energy storage (SMES), and power transmission.

An MPD system is a low thrust, high fuel efficiency alternative to conventional chemical propulsion promising pragmatic interplanetary travel. Unfortunately, state-of-the-art performance is inadequate due to limited thruster efficiency and electrode lifetime. A lunar based Mars cargo vehicle, for example, would require total impulse and electrode lifetime improvements approximately two orders of magnitude beyond demonstrated systems [8]. Figure 3 illustrates the thruster concept. The magnetic field forms a virtual nozzle which contains the applied arc currents generated between the cathode and anode. Acceleration is produced by the J X B forces on the plasma as well as the propellant pressure. High Tc superconducting magnets may have the potential to provide the necessary improvements in cathode lifetime and thruster efficiency. Mass and reliability enhancements are expected as well.

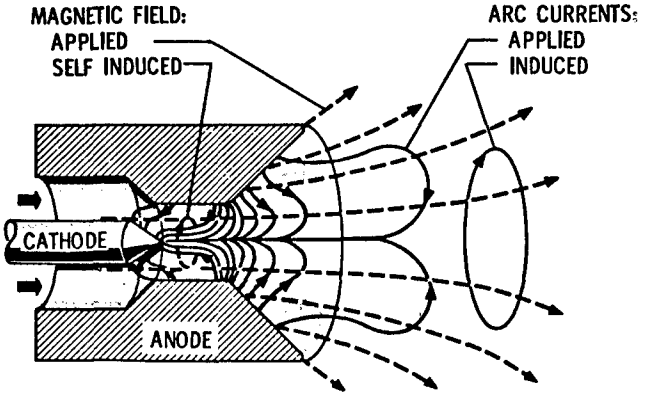


Figure 3. MPD thruster concept illustrating currents and fields

Energy storage is a crucial integral part of spacecraft operation, tending to be the most massive onboard system. Proven technologies, such as nickel-hydrogen cells, nickel-cadmium batteries, and regenerative fuel cells, often require careful trade-offs between cycling flexibility, weight, and lifetime. Principal advantages of SMES include high efficieny and insensitivity to demanding charge/discharge rates. SMES has the potential to equal the specific power of conventional systems and

should prove competitive in terms of the major relevant criteria.

The resurgence of interest in microwave-beam power transmission presents another opportunity for high Tc superconductors to provide enhancing, if not enabling, system contributions. A Mars satellite-to-rover power transmission scenario, for example, could alleviate numerous complications involved with surface power generation and transmission. High power submillimeter-wave transmission from synchronous orbit (17,000 Km) is feasible. High Tc superconductors could be utilized in at least two areas: high field solenoids for gyrotrons and SIS rectenna elements. In lieu of free-space power transmission, High Tc superconducting transmission lines could be used to distribute power from distant nuclear plants with high efficiency. In addition, with currently demonstrated current densities of 1000 A/cm^2, a one kilometer high Tc superconducting transmission line would be 500 % lighter than a high purity aluminum line [9].

Significant activities are also underway to develop innovative approaches for synthesizing bulk and thick film materials as well as to study the effects of processing on microstructure. For example, investigations to: explore the role of anisotropy, characterize susceptibility to radiation damage, and determine durability in an atomic oxygen environment have been initiated. A glass-ceramic approach based on bismuth compounds, which promises high density, pore-free fibers, is also being developed. Finally, composite materials, consisting of appropriate metallic or polymer matrices, are being explored and may eventually produce the necessary structural and environmental properties for space power and propulsion systems.

Figure 4 projects stages of development for various high Tc superconductor applications being pursued by NASA. The milestones represent ambitious but not overly optimistic goals. The chart reflects only a few examples from a myriad of applications under investigation by NASA, other government agencies, industry, and academia.

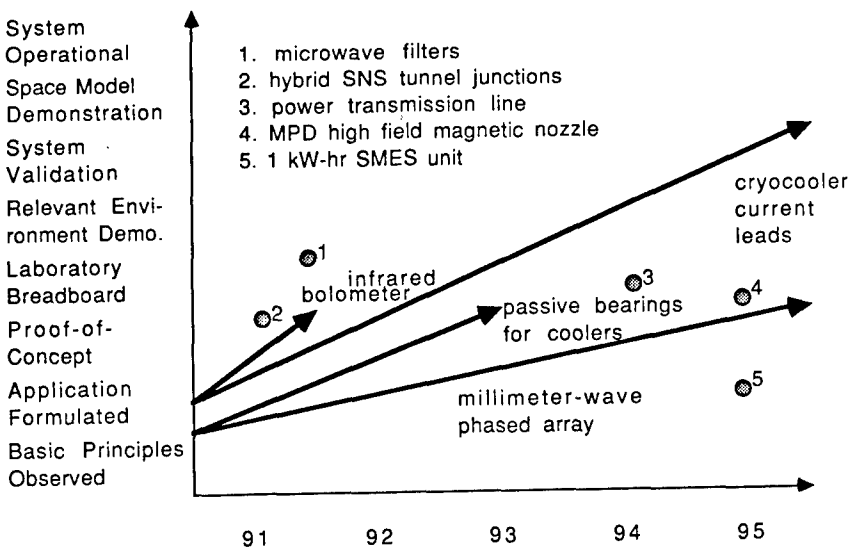


Figure 4. Projected maturity of several NASA high Tc superconductor applications

Conclusions

Many breakthroughs in processing technology have already occurred, and practical, near term applications have emerged for both thin film and bulk material. Amidst intermittent skepticism, tenacious researchers have continued to produce better and better materials. Current densities, critical fields (Hc_2), and film morphology have improved enough to satisfy requirements for many bulk and thin film devices, although implementation is still challenged by mechanical and structural limitations. Considering the brief history of high Tc technology; however, its evolutionary progress has been dramatic. The successful implementation of this burgeoning technology will require a concerted agency-wide and National effort to promote farsighted research and development.

Numerous near-term practical insertion opportunities as well as more speculative applications have been presented. Prototype cryocooler bearings, cryocooler current leads, superconductor-normal-superconductor microbridge oscillators, microwave filters and phase shifters, and infrared bolometers will likely evolve in very reasonable time frames. Capitalizing on recent developments for space and other applications will require unwavering committment to make the pivotal transition from materials research to prototype device development.

References

1. Bhasin, K.B.et al., "Performance and Modeling of Superconducting Ring Resonators at Millimeter-Wave Frequencies", 1990 IEEE MTT-S International Microwave Symposium, Dallas, Texas, May 8-10, 1990.

2. Miranda, F.A. et al., "Millimeter-Wave Transmission Studies of $YBa_2Cu_3O_{7-x}$ Thin Films in the 26.5 to 40.0 GHz Frequency Range", Third Annual Conference on Superconductivity and Applications, New York, September 19-21, 1989.

3. Romanofsky, R.R.et al., "Monolithic Millimeter-Wave Phase Shifter Using Optically Controlled High Tc Superconducting Switches", To Be Published.

4. Brasunas, J.C. et al., "Construction and Performance of a Thin-Film Transition-Edge, High Temperature Superconductor Composite Bolometer", NASA Goddard Space Flight Center Report, March, 1989.

5. Hunt, B.D. et al., "Electrical Contact Studies of Chemically Treated $YBa_2Cu_3O_{7-x}$ Surfaces", American Vacuum Society Proceedings, Boston, Ma., October 1989.

6. Vasquez, R.P., Hunt, B.D., and Foote, M.C., "Reduced Reactivity to Air on HF-Treated $YBa_2Cu_3O_{7-x}$ Surfaces", Appl. Phys. Lett., 54, June 1989, pp.2373-2375.

7. Hojaji, H. et al., "Yttrium Enrichment and Enhanced Flux Pinning in Partially Melted Y-Ba-Cu-O Materials", J. Mater. Res., 5, 1990.

8. Reed, C.B., and Sovey, J.S., "The Use of High Temperature Superconductors in Magnetoplasmadynamic Systems", Second Annual Conference on Superconductivity and Applications, New York, April, 1988.

9. Hull, J. and Myers, I., "High Temperature Superconductors for Space Power Transmission Lines", ASME, December, 1989.

US NAVY SUPERCONDUCTIVITY PROGRAM

Donald U. Gubser
Naval Research Laboratory
Washington DC 20375-5000

The U.S. NAVY has had a long running and sustained program dating back to 1946 supporting superconductivity and its technology. This is due to a recognition of the enormous military benefits that could be achieved if the unique properties of superconducting materials could be tapped in field operating systems. The present NAVY's program is broadly based with an emphasis on field operational systems. The NAVY is committed to developing a science and technology base for superconducting materials, both high temperature superconductors (HTS) and low temperature superconductors (LTS), and to undertaking key system tests leading to the eventual implementation of the technology. The program is well integrated throughout the NAVY with four organizations leading the way in specific areas. Those organizations are: 1) the Office of Naval Research (ONR) and the Office of Naval Technology (ONT) [responsible for contract funding in all areas of Naval interest], 2) the Naval Research Laboratory (NRL) [responsible for fundamental property studies, materials research and development, and electronic and space applications], 3) the Naval Coastal Systems Center (NCSC) [responsible for SQUID magnetometer systems development], and 4) the David Taylor Research Center (DTRC) [responsible for power applications of superconductivity and ship propulsion]. Other NAVY organizations participate in the total program and all are coordinated by the Naval Cónsortium for Superconductivity (NCS).

The NAVY's superconductivity program includes work in HTS and LTS and is divided into 5 main thrust areas. They are: 1) Fundamental properties and materials research (mostly HTS), 2) SQUID magnetometers and gradiometers (mostly LTS), 3) superconducting ship propulsion (exclusively LTS), 4) electronic applications including digital circuitry and IR sensors (50% LTS and 50% HTS) and 5) Space experiment (exclusively HTS). About 2/3 of a total NAVY's budget of $21M is split equally between fundamental properties/material research and the space experiment. SQUID research accounts for about 1/6 of the budget with the remaining going to power applications and electronic applications.

Almost half of the NAVY's program is focused on fundamental research and materials development. The NAVY believes this is essential if the technology is to meet its potential in Naval systems. The program is broad based with major efforts in theory, materials synthesis (primarily films), J_c and flux flow studies, surface resistance and noise studies, and radiation damage.

Superconducting electronics development in the NAVY began around 1966. Today the program is relatively broad based working on IR sensors (HTS), millimeter and micro wave devices (HTS and LTS), directional antennas (HTS), and digital circuit elements (LTS). Key to this program is assessments of the impact of the technology on specific systems performance vis a vis competing technologies. This program will develop, fabricate, and test device elements to certain their performance advantages and limitations. Close ties with industry and other DoD efforts in superconducting electronics gives the program an unusual breath.

The Space experiment at NRL began in 1988 and is designed to demonstrate the feasibility of millimeter wave and micro wave electronics for space use. The program includes material scientists, and electronic and spacecraft engineers. Various devices are being manufactured by over 15 different industries, made from a variety of HTS materials, and will be delivered to NRL by June 1990 for testing and evaluation. Devices which meet design criteria will be assembled into a space craft and launched into space sometime in the 1992 time frame. The tests are designed to demonstrate the virtues of superconducting electronics in space and to

space qualify the HTS devices. Space qualification means that the devices operate after the shock of space launch and exposure to space radiation environment.

The SQUID detection/surveillance systems development at NCSC began in 1969 and has focused on field operational demonstrations of the technology. Unanticipated problems associated with operation in motion while in the ambient earth's magnetic field had to be solved before the needed sensitivity levels could be reached. A gradiometer system designed to meet the requirements of Naval operation was built by Sperry Univac in 1985 and has been successfully demonstrated in field tests. This gradiometer is now being refurbished with newer sensors and electronics under a contract with IBM and will be used in subsequent tests. The original system as well as the refurbished system is based on bulk, niobium Nb technology. Advanced systems are now being designed which will use thin film technology, but still use Nb as the superconducting material. Thin film systems are expected to be smaller and less sensitive to certain types of system noise. Also under study is the eventual design as SQUID system based on HTS materials. Important issues of magnetic and thermal noise, flux motion, and hysteresis need to be improved before the HTS SQUID system becomes viable as a NAVY, field operational unit.

Superconducting ship propulsion systems development at DTRC began in 1969. This program has successfully demonstrated that industrially built (3000 Hp) superconducting motors can be installed in a small Naval vessel and operated at sea. NbTi wire was used in the magnet construction. The NAVY has been reluctant to take the next step to develop a larger scale demonstration on a mid sized Naval ship because 1) a reluctance to convert to a radically new drive system, 2) a reluctance to depend on a liquid helium technology, specifically in combat, and 3) cost of a mid sized Naval vessel demonstration would be large and particularly burdensome in times of budget austerity. Progress is being made, however, in that the NAVY has decided to make a major commitment to electric drive wherein superconductivity is seen as an advanced, but evolutionary concept. With this plan in mind, the NAVY has committed funds now to explore magnet stability for forces, strains, and vibrations anticipated in a Naval systems. The program will also explore advanced LTS conductor design (Aluminum stabilized matrix, and Nb_3Sn conductors) as well as improved refrigeration designs and test. HTS materials are not considered in this program at the present time.

NAVY scientists and managers are actively involved with other major DoD efforts in superconductivity. They serve as reviewers, advisors, and in some cases as agents in a number of programs. In this manner the NAVY's program is thoroughly integrated into the overall efforts of the nation as a whole toward the rapid development of superconducting products, military or commercial.

SECTION 7:
PANEL DISCUSSION
SUMMARIES

Structure-Property Relationships In HighTemperature Superconductors: Panel Discussion Summary

K. Moorjani,
The Johns Hopkins University - Applied Physics Laboratory
Laurel, MD. 20723, U. S. A.;
and
A. J. Berlinsky,
Institute for Materials Research, McMasters University
Hamilton, Ontario, L8S 4M1, Canada

The panel discussion on structure/property relationship in cuprate oxide superconductors focussed on three topics:

A. Structural and Compositional Disorder
B. Superconductivity and Magnetism
C. New Superconducting Materials

The bulk of the discussion was on topic A, essentially reflecting the thrust of the conference program. The major points dealt with the role of structural (e.g., defects and dislocations) and compositional (e.g., impurities and grain boundaries) disorder not only in bulk sintered samples but also in single crystals of cuprate oxide superconductors. Because of the small value of the coherence length in these materials, even small scale disorder of $\cong$10 Å leads to measurable effects, particularly in tunneling currents. Atomic level disorder can arise from impurities and/or incomplete oxygenation in La-Sr-Cu-O (214 phase) and Y-Ba-Cu-O (123 phase), the two systems discussed in some detail. The 214 phase is inherently inhomogeneous due to the inhomogeneous substitution of Sr for La which, as pointed out during the conference program, is also accompanied by a change in the position of the apical oxygen.

In spite of the availability of single crystal samples of both 214 and 123-phases, it was felt that the methods for assessing the quality of these samples are not easily available. Ideally, such methods must be capable of probing the entire sample, a difficult requirement given that the optical opacity of these materials rules out most spectroscopic approaches. The methods that do satisfy this requirement have various drawbacks. For example, x-ray and neutron diffraction methods are tedious and lack the sensitivity

required to detect small regions of inhomogeneity, while specific heat and other thermodynamic measurements are hard to interpret because of the limited theoretical understanding of the cuprate oxide superconductors.

The magnetically modulated resistance (MMR) methods, however, have played an important role in studying inhomogeneities in high temperature superconductors and have proved to be useful tools in assessing the quality of superconducting samples. The effect of inhomogeneities is revealed in the MMR data as the presence of multiple superconducting phases and/or features associated with tunneling arising from the presence of weak links caused by the separation of superconducting and non-superconducting phases on the atomic scale. The MMR methods can be implemented at zero or any finite frequency and, while experiments at microwave frequencies have provided information within the skin depth of the samples, conducting experiments at lower frequencies should probe larger dimensions of the samples due to the increased skin depth.

There was much discussion on impurity precipitation and segregation in grain boundaries, the types of defects in dislocations at the interfaces, but deriving useful conclusions was hampered by the lack of systematic experimental data.

One of the highlights of the conference was the recent availability of melt-processed, melt-growth (MPMG)bulk samples of the 123 phase from a number of laboratories. The samples essentially exhibit a single superconducting phase and carry the highest known critical currents (~ 2×10^4 A/cm^2 at 77 K) in bulk ceramic superconductors. It is, however, not clear whether the material is comprised of large aligned superconducting grains, and much remains to be learned about the nature and mechanism of pinning centers in this material.

Regarding topic B, it is clear that superconductivity and magnetism coexist not only in the doped (e.g., Fe substituting for Cu) 123-phase but possibly in the undoped 214-phase. The nature of the magnetic ordering is established to be akin to the spin glass phase. The questions during the panel discussion focussed on whether the spins that are responsible for magnetic ordering are the same that participate in the formation of the superconducting state. In the Fe-doped 123-phase, the answer is almost certainly negative in that it

is the Fe spins which freeze into the spin glass phase while Cu spins are responsible for the superconducting state. In the 214-phase, it could be that Cu spins are responsible for both phenomena, but, due to inhomogeneities, the Cu spins that freeze in the non-collinear magnetic structure belong to non-Sr-containing regions while superconductivity results from the Sr-containing regions. The interplay of the two and the role Cu spins in the dynamics of Fe spins need to be investigated further.

Concerning topic C, at least four new superconducting phases were added to the ever increasing list of cuprate oxide superconductors. But the maximum T_c of these new materials is less than 40 K, a value reported for $Bi_2Sr_5Cu_2O_y$. The new non-Cu containing superconducting materials were reported to have around 10 K.

Panel: Thin Films

Moderators: John C. Brasunas, NASA/Goddard, USA
Antonio Mogro-Campero, General Electric, USA

ABSTRACT

High Tc thin films promise to play an important role in low-power and electronics applications. This panel discussed film deposition techniques and various high Tc materials, looking for preferred approaches in either area. The panel also considered RF, IR sensor and SQUID applications, and environmental effects relevant to space applications.

Panel participants:

J. Dainer
R. Decher
R. Felten
P. Grant
V. Haubib
F. Miranda
K. Moorjani
P. Norris
D. Peterson
M. Velazquez

This discussion panel began with a presentation by Peter Norris of Emcore Corporation. He presented recent results on plasma enhanced MOCVD, which brought processing temperatures down from 800-900 C to 570 C. The resultant films are denser, scratch resistant, grow directly in the orthorhombic phase, and have a transition width of 1.5 K at 90 K. Further studies will show whether overall film quality is comparable to results obtained with higher processing temperatures.

Additional discussion considered the following areas.

Deposition Techniques

It was recognized that a variety of deposition techniques have led to high quality films, nevertheless special requirements may single out certain techniques. For instance, for large area films (>> 1 cm^2) evaporative and CVD techniques are likely choices. For applications requiring a low value of the surface resistance Rs, the panel was unable to reach agreement. One opinion held that in-situ techniques such as laser deposition (in spite of the presence of laser-induced debris) produced low Rs, whereas post-annealing techniques tended to produce high Rs even when Jc is high. Additionally, the surface roughness of post-annealed films could be a problem for some applications. An alternative opinion granted that more groups were using laser deposition, with the result that post-annealing techniques had not been optimized with the same level of effort. In fact, the Rs of some post-annealed films was claimed to be within a factor of two of the in-situ films.

Interestingly enough, a group at United Technologies Research Center is attempting to analyze the laser debris phenomenon by looking at a simpler material, gold. With laser-ablated gold they also see debris, including structures reminiscent of the well-known strobe photography shots of milk drops, taken many years ago. The universality of laser debris raises questions as to possible device yield implications.

High Tc Choice, Substrate Choice

It was noted that epitaxial 1-2-3 (YBaCuO) films can be grown without perfect lattice match to the substrate. Very high quality films can be grown on $LaAlO_3$ and $SrTiO_3$ with approximately a 1% mismatch. It is not known whether 1% is sufficient, or if even better films would result from a closer

ıtch, although certain properties such as critical currents are already approaching fundamental limits. SCCO and TBCCO films seem to be more forgiving of lattice mismatch, and yet the majority of thin-film 'orts for now appear to be directed to 1-2-3. Bulk applications, contrastingly, seem to be making a greater)ve towards BiSCCO and TBCCO. With respect to 1/f noise, although previously TBCCO films seemed have lower noise levels, recent results from Bellcore and IBM now show as low or lower noise levels th 1-2-3. Again, epitaxial films are necessary for the low noise levels.

)plications

The panel agreed that RF devices, at least passive RF devices, are likely to be the first area of practical plications since Rs is substantially superior to copper below about 30 GHz. No major roadblocks are)reseen. The same is not true for active devices which must deal with the very short coherence length.

For IR sensors, in particular high sensitivity thermal sensors, there is a challenge: To produce epitaxial films on a low heat capacity substrate. The best quality epitaxial films, necessary for low noise, need to be deposited on fairly high specific heat materials such as $SrTiO_3$ and $LaAlO_3$. It is not known how to thin these materials to 10 to 20 microns. For materials which can be thinned or have low specific heat, such as silicon, it is not known how to grow the highest quality epitaxial films. The development of buffer layers will play a key role.

For SQUIDS, there are serious questions of yield and reproducibility. Most high Tc SQUIDS to date have depended on the chance occurrence of intrinsic weak links. High quality SQUIDS usually require ngineered Josephson junctions, multilayer structures of superconductor-insulator-superconductor. The 'remely short coherence length of high Tc materials makes such junctions very challenging to fabricate. ı interesting alternative approach at IBM is a sort of engineered grain boundary: A grain boundary in the TiO_3 substrate creates a reproducible grain boundary in the high Tc film. Also promising is the provement in noise levels in high Tc films.

e Outer Space Environment

There appear to be promising signs for long-term reliability in outer space. Higher quality, epitaxial ns appear to be more stable against oxygen loss and may not require passivation. On the other hand, :cific environments such as low earth orbits present other challenges, for example atomic oxygen may d to film degradation. It was generally agreed that, unlike single crystals, for thin films radiation is likely be a negative influence, perhaps because films already have adequate pinning sites. It was noted that ns are edge-dominated, and that edges apparently are pinning sites.

Reproduced From
Best Available Copy

PANEL ON HTSC WIRES

Moderators: P. Arsenovic, NASA/GSFC, Greenbelt, Md, 20771.
I. Carlberg, NASA/LaRC, Hampton, Va, 23665.

Abstract: It is hoped that HTSC wires will play a key role in upcoming NASA missions that utilize cryogenic coolers in their payload. This panel discussed some methods of fabrication, the problem of brittleness in these wires, and some programs being started at NASA to examine this new technology in more detail.

The purpose of this discussion panel was to examine the current state of high temperature superconductor wires, to be used as ground straps or electrical leads. These would be beneficially utilized in future NASA payloads with sensitive instruments operating at cryogenic temperatures such as AXAF, SIRTF, Astromag, EOS, LDR, and SAFIRE. The use of HTSC electrical leads could greatly decrease the electrical noise of these instruments and increase the efficiency of the cryogenic cooling systems. This is due to the fact that these HTSC materials are excellent electrical conductors in the superconducting state, while their ceramic nature makes them good thermal insulators. Present day electrical leads can be resposible for as much as 50% of the parasitic heat load on cryogenic systems. A significant reduction of this load could be achieved with replacment of the present conventional materials, such as copper or manganin, with HTSC ceramic electrical leads.

Wires made from high temperature superconducting materials such as Yttrium-Barium-Copper-Oxide ($Y\text{-}Ba_2\text{-}Cu_3\text{-}O_7$)

are generally very brittle. Three possible configurations for these leads were discussed:

1) Find a way to make them reasonably flexible while keeping the desired electrical and thermal properties. The wires could then be used in any necessary configuration with regard to bending and routing in a cryogenic cooler.

2) Fabricate them into a preformed rigid condition - this would be appropriate for only one configuration at a time.

3) Fabricate the wires into preformed rigid sections, and link them together. It was pointed out that this could cause problems at the joints with regard to mechanical and thermal stability.

A test program is being set up at NASA-Goddard to examine the mechanical properties of these wires, such as strength, modulus, and flexibility, along with possible ways to improve on these factors; as well as looking into the electrical and thermal properties of these materials.

An additional program is beginning at NASA-Langley to study vacuum, radiation, magnetic, and thermal cycling effects on polymer bound, encapsulated superconductive leads. In this program, long term survivability of $Y\text{-}Ba_2\text{-}Cu_3\text{-}O_7$, Bismuth, and Thallium compounds will be determined in a simulated space environment.

Panel Discussion on Flux Pinning

Co-chairs: M. Murakami ISTEC, 1--13 Shinonome 1-chome
Koto-ku, Tokyo 135 JAPAN

L. Swartzendruber NIST, Gaithersburg, MD 20899

Introduction

In type II superconductors, when the external field exceeds the lower critical field, H_{c1}, magnetic flux can penetrate into the superconductor in the form of quantized fluxoids. This state is called the mixed state. When a current flows in the mixed state, a Lorentz force will acts on the fluxoids. If this force causes the fluxoids to move, energy will be dissipated and an electrical resistance will result. Therefore, we need to prevent the flux motion in order to obtain resistanceless current. Structural defects, such as grain boundaries or dislocations can interact with fluxoids and prevent them from moving. This phenomenon is known as flux pinning. The critical current density, J_c, in the mixed state is then determined by

$$\mathbf{F_p = J_c \times B}$$

where F_p is the bulk pinning force density due to structural defects and B is the magnetic induction. Therefore J_c can be strongly dependent on microstructure and is not an intrinsic material parameter.

High temperature superconductors are of type II and have relatively low values of H_{c1}. Therefore the introduction of pinning centers in required to achieve useable values for the critical current in these materials. In addition, even when the current is less than J_c, the fluxoids can escape from the pinning centers by a thermal activation process, leading to the phenomenon known as flux creep. In many high T_c superconductors, a combination of small pinning energy and large thermal energy is believed to cause "giant" flux creep. Most applications of high temperature superconductors are not feasible without overcoming the flux creep problem.

Discussion

In this panel discussion was focused on flux pinning and related problems in high temperature superconductors. A large fraction of the those attending the conference participated in the discussions. The following were among the topics introduced and discussed:

1) Is giant flux creep inherent to high T_c superconductors?

2) Is "flux melting" an intrinsic problem of the flux line lattice or a problem of flux pinning?

3) What are the pinning centers in high temperature superconductors?

After considerable discussion, the participants reached general agreement that, in addition to critical currents, both flux creep and flux melting are governed by the problem of flux pinning.

Considering "giant" flux creep, Murakami reminded the panel of some early results on flux creep measurements in conventional superconductors (Pb-Tl alloys, see Figure 1) which were reported by Beasley et al. in 1969 (Phys. Rev. 181, 682). Remarkably large ("giant") flux creep can be seen, indicating that giant flux creep is not peculiar to high temperature superconductors but is characteristic of superconductors with small pinning forces. Murakami also showed flux creep data for two YBCO crystals with and without non-superconducting particles . The crystal with non-superconducting particles showed a much slower rate of flux creep due to the larger flux pinning force. Prof. Wu also commented that the Ag doped samples showed narrower resistive transitions in a magnetic field than single crystals, presumably due to the improved flux pinning force. F.G. Reick commented that he has improved pinning using techniques which build a "spongy" structure.

A discussion comparing YBCO materials with high and low pinning forces was also given by Dr. Murakami. The temperature dependencies of the DC susceptibility in both field-cooled (fc) and zero-field-cooled (zfc) processes were compared. A reversible region in the fc and zfc processes can be observed down to fairly low temperature for material with low pinning force, such as some single crystals. This phenomenon has been ascribed to flux melting. However, the fact that the irreversibility temperature can be raised by the increased pinning forces in material containing non-superconducting particles indicates that the "flux melting" is not a problem of the flux line lattice but a problem of flux pinning. This was also discussed in a paper by Dr. Brandt at this conference.

Here we may conclude that both flux creep and flux melting are a problem of flux pinning. If so, the key issue is how to increase the flux pinning force. To do this we need to know what serves as pinning centers in high temperature superconductors.

It was pointed out that single crystals can show relatively large J_c values. Because of this and intrinsic pinning mechanism has been proposed by e.g. Takahashi and Tachiki. They believe a fluctuation in the order parameter can give rise to flux pinning because of the small coherence length along the c axis. Twins are also candidates for pinning centers in YBCO. Although results to date from several groups have definitely shown that twins can pin, the magnitude of their contribution is not yet clear. L.H. Bennett also pointed out that a small deficit in oxygen content might provide pinning centers since it is difficult to fabricate YBCO with an oxygen content of exactly 7.0.

Although the highest J_c values in YBCO, on the order of 10^7 A/cm^2, have been achieved in epitaxially grown thin films, the pinning mechanisms in such films are unclear. It should be noted that the thin films are grown on substrate materials and usually contain many structural defects.

In order to understand the pinning mechanism in thin films, we need to conduct much more microstructural observation.

According to results presented at this conference by Murakami, a direct summation model based on flux pinning due to 211 inclusions gives J_c proportional to V_f/d, where V_f is the volume fraction of 211 inclusions and d is their average size. He showed that a fine dispersion of 211 inclusions can help increase the flux pinning, and confirmed that J_c is proportional to V_f when d is constant. He noted that recent work by the Asahi glass group showed that J_c is proportional to 1/d when V_f is constant. These results serve to indicate that the 211 inclusion itself can contribute to flux pinning. Prof. Hojaji has also found that an increase in the volume fraction of 211 inclusions enlarges magnetic hysteresis. However, he stressed that we should not forget the possibility that the structural defects associated with the 211 inclusions may act as pinning centers. Further study will be needed to draw definite conclusions.

The possibility of flux pinning by other non-superconducting particles was also discussed. Prof. Wu pointed out that silver oxide may work as a pinning center in Ag doped YBCO since flux pinning behavior can be improved compared to single crystals. Murakami surmised that any non-superconducting particles, even voids, could contribute to flux pinning if the dispersion of those particles does not reduce the superconducting property of the matrix.

Although J_c values as high as 30,000 A/cm^2 at 77 K and 1 T have been attained for YBCO crystals with 211 inclusions, this may not be enough for many possible applications. Thus it is interesting to consider the Maximum J_c values that might be achieved by dispersion of non-superconducting particles. Murakami presented the data of AC measurements for YBCO crystals containing 211 inclusions which were taken by Prof. Matsuhita of Kyusyu university (Figure 2). He superimposed an AC field on a DC field. J_c was determined from flux changes during an increase in the AC field amplitude. The data indicate that there are two regions in the sample with different J_c values, 10^4 A/cm^2 and 10^6 A/cm^2. Microstructural observation revealed that the sample is not homogeneous and the density of 211 inclusions is different from place to place. A novel technique to observe flux distribution using magneto-optics developed by Gotoh and Dr. Koshizuka et al. of ISTEC made it clear that the sample consists of two regions with different pinning forces as shown in Figure 3. The region with black and white domains corresponds to a region with high pinning force where magnetic field cannot penetrate. This result suggests that it is possible to achieve 10^6 A/cm^2 even at 77 K in bulk materials.

Some results on the composition $Y_2Ba_2Cu_3O_{8+\delta}$ prepared by rapid thermal processing (RTP) were presented by Prof. R.G. Kulkarni. He found a sharp superconducting transition above 90 K and a wide hysteresis loop, indicating large pinning, in this material. He attributed the large pinning (corresponding to a magnetic J_c of about 2000 A/cm^2 at 77 K) to the extensive structural defects and grain boundaries introduced by the RTP technique.

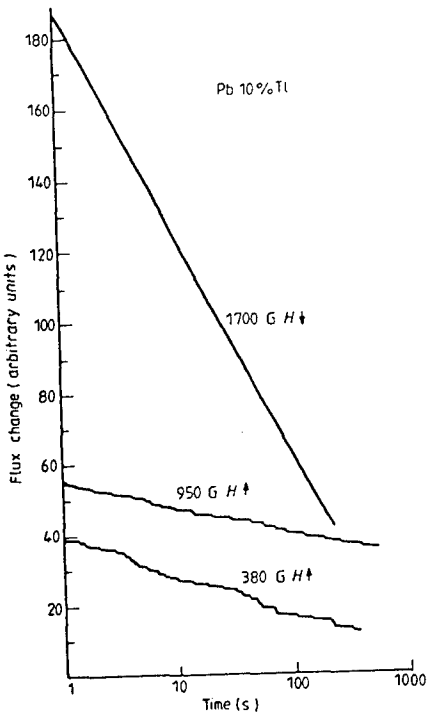


Fig. 1 Flux change versus ln t in a Pb-10 % Tl alloy for various applied magnetic fields (after Beasley et.al).

In conclusion, the exact nature of the pinning mechanisms in high temperature superconductors is still unclear. It does appear that pinning can be increased to high enough levels to overcome the problems of flux creep and flux melting, making many applications possible up to temperatures of 77 K. It is also true that the critical current density has been steadily improved by controlling the fabrication process and microstructure. There are indications, such as dramatic improvements in J_c obtained through neutron irradiation, that we have not yet reached the limit of what can be achieved in bulk materials through proper control of the microstructure.

The chairmen thank the participants for producing an interesting and lively session, in spite of the late hour at which it was held.

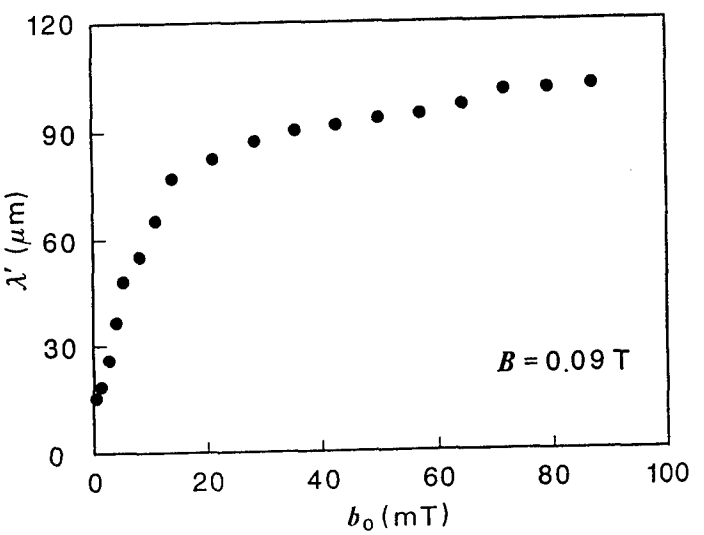


Fig. 2 AC susceptibility measurements as a function of AC field amplitude for a constant applied DC field of 0.09 T.

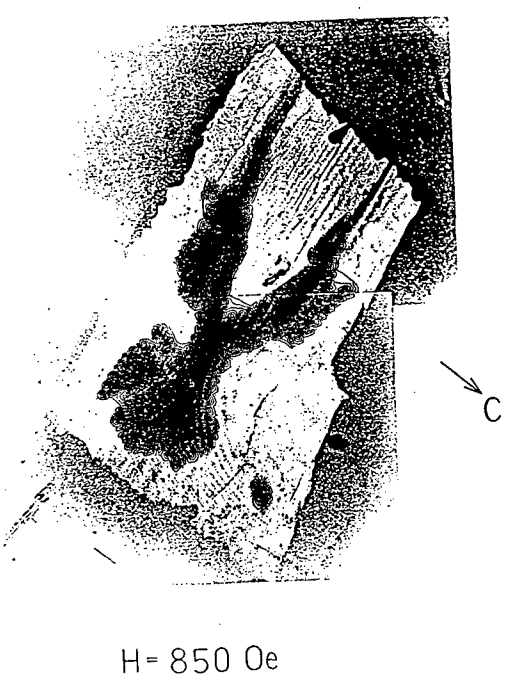


Fig. 3 Magneto-optical image of a YBCO crystal with 211 inclusions. Darker areas are areas with large pinning.

Summary of Panel Discussion
on High Temperature Superconducting Bearings
at AMSAHTS '90 Meeting
NASA Goddard Space Flight Center

April 1990

Francis C. Moon
Mechanical and Aerospace Engineering
Cornell University

The chairman of this discussion Dr. Y. Flom of NASA Goddard opened the session by raising the question of what are the most important material factors for improved passive magnetic bearings, such as critical currents and magnetization. Evidence was presented by Chiang of NIST and Weinberger of UTRC that samples made from composites produce levitation forces comparable to bulk materials. Weinberger concluded the intragranular currents were important and perhaps grain size. Moon from Cornell raised the question of magnetization and field gradients as essential components to calculating magnetic forces and that the relative size effect between permanent magnet and superconductor is important. He suggested that numerical methods be developed using magnetization curves. Bennett of NIST said that magnetization history was important, but that models to describe hysteresis in electromagnetic materials were wanting.

Murakami of ISTEC in Japan said he liked the Bean model and that it was useful to understand magnetization and levitation forces. Moon raised the question of the vector nature of magnetic forces whereas the Bean model was one dimensional and scalar. Brandt of Max Planck Institute, Stuttgart, believed that forces could be derived quite rigorously from a scalar function such as the dependence of critical current on magnetic field, provided one solved complex mathematical equations as outlined in his paper. This model would also incorporate flux creep effects.

Flom introduced the question of the Hellman/Bell Lab model for magnetic forces based on flux penetration into the superconductor. Moon and Brandt both criticized this model since it did not incorporate the excluded flux lines which were necessary for

repulsive levitation. Weinberger presented data for power law force behavior when the magnet-superconductor distance was large. However, Moon said that Argonne National Lab/Cornell experiments for small magnet-superconductor gaps showed an exponential force-distance relation which was not predicted by the Hellman model.

Flom then raised the final major question, namely, what is the best way to test materials for bearing/levitation applications. Weinberger and Moon both supported direct force measurements, although Weinberger suggested experimental evidence for a correlation between magnetization and levitation force. Bennett again pointed out that for a standard test one should know both magnetic field and field gradient. Moon favored a test with small test magnet and large cylindrical superconductor to get away from geometric effects. Moon also spoke of the importance of magnetic stiffness which applications engineers felt was of importance. Measurement of damping was also thought to be important.

The discussion ended with a demonstration of a superconducting motor with magnetic bearings by United Technology Research Center.

APPENDIX

CONFERENCE PARTICIPANTS

ADACHI, Hideaki	Matsushita Electric Indust. Co.
ADRIAN, Frank	The Johns Hopkins University
AGARWALA, Ashok	Eastman Kodak Company
AKBAR, Sheikh Ali	The Ohio State University
ALAUDDIN, Mohammad	Wagner College
ALLEN, Christine	NASA/Goddard Space Flight Center
ALTERESCU, Sidney	NASA/Goddard Space Flight Center
ANNETT, James	Pennsylvania State University
APRIGLIANO, Louis	David Taylor Research Center
ARORA, Om	David Taylor Research Center
BAYYA, Shyam	Alfred University
BENNETT, Larry	Nat'l. Institute of Standards and Technology
BERLINSKY, A.J.	McMaster University
BOONE, Bradley	The Johns Hopkins University
BOSE, Shyamalendu	Drexel University
BOURDILLON, Antony	SUNY at Stony Brook
BRAATEN, Ovar	University of Oslo
BRANDT, Ernst Helmut	Max-Planck-Institut
BRASUNAS, John	NASA/Goddard Space Flight Center
BUDNICK, Joseph	University of Connecticut
CARLBERG, Ingrid	NASA/Langley Research Center
CASE, Leslie	GLTron, Inc.
CHAKRAVERTY, Benoy Kumar	Centre Nationale Recherche Sci.
CHAUDHARI, Praveen	T.J. Watson Research Center
CHEN, Chung-Hsuan	Oak Ridge National Laboratory
CHIANG, C.K.	Nat'l. Institute of Standards and Technology
CURTIS, John	Ford Aerospace Corporation
DALAL, Nar	West Virginia University
DAS GUPTA, Amit	Department of Energy
DATTA, Timir	University of South Carolina
DELUCA, Robert	HiTc Superconco, Inc.
DECHER, Rudolf	NASA/Marshall Space Flight Center
ENDRES, Bill	U.S. Air Force
FELTON, Rainer	Battelle Europe
FIORANI, D.	ITSE-CNR
FLOM, Yury	NASA/Goddard Space Flight Center
GIESE, Luann	NASA/Goddard Space Flight Center
GOPALAKRISHNAN, Sudhakar	Alfred University
GRABOW, B.E.	The Johns Hopkins University

CONFERENCE PARTICIPANTS (continued)

GRANT, Peter	National Research Council
GREEN, Steven	University of Maryland
GREENE, R.L.	University of Maryland
GROSS, Fred	NASA/Goddard Space Flight Center
GRUDKOWSKI, Thomas	United Technologies Research
GUBSER, D.U.	Naval Research Laboratory
HALL, James	University of South Florida
HERR, Steven	Virginia Commonwealth University
HERSHITZ, Roman	General Electric Company
HICKMAN, Hugh	University of South Florida
HOFF, Henry	Naval Research Laboratory
HOJAJI, Hamid	Catholic University of America
KAISER, Debra	Nat'l. Institute of Standards and Technology
KAREN, Pavel	University of Oslo
KEEHN, Paul	EMCORE Corporation
KIM, Boris	The Johns Hopkins University
KOLLIE, Thomas	Oak Ridge National Laboratory
KOSTADINOV, Ivan Zahariev	University of Sofia
KRESIN, V.Z.	UCLA, Berkeley Laboratories
KULKARNI, R.G.	Saurashtra University
KURTZ, Robert	Nat'l. Institute of Standards and Technology
LAKEW, Brook	NASA/Goddard Space Flight Center
LAQUER, Henry	CryoPower Associates
LEROY, David	U.S. Patent and Trademark Office
LIEBENBERG, D.	Office of Naval Research
LITTLE, William	Stanford University
LOO, Boon	University of Alabama
LYNDS, Lahmer	UTRC
MACKEY, Terrance	U.S. Patent and Trademark Office
MARRIOTT, Richard	NASA/Goddard Space Flight Center
MCALLISTER, Gary	Bechtel Corporation
MCMULLEN, Thomas	Virginia Commonwealth University
MERLO, Vittorio	2nd Universita di Roma
MIRANDA, Felix	Case Western Reserve University
MIREBEAU, Isabelle	Laboratoire Leon Brillouin (CEA-CNRS)
MOGRO-CAMPERO, Antonio	General Electric
MOON, Francis	Cornell University
MOORJANI, Kishin	The Johns Hopkins University
MORISHITA, Masao	Tokyo Electric Power
MOTOWIDLO, Leseck	IGC Advanced Superconductors
MULCAHY, Thomas	Argonne National Laboratory
MURAKAMI, M.	Superconductivity Research Laboratory
MURR, L.E.	University of Texas

CONFERENCE PARTICIPANTS (continued)

NORRIS, Peter	EMCORE Corporation
PANDE, Chandra	U.S. Naval Research Laboratory
PETERSON, David Lee	
PICKETT, Warren	U.S. Naval Research Laboratory
PLOTKIN, Henry	NASA/Goddard Space Flight Center
POWERS, Charles	NASA/Goddard Space Flight Center
RASINES, I.	Instituto de Ciencia de Materiales (Spain)
REICK, Franklin	Fluoramics, Inc.
REILEY, Don	PTO/Mech/Gen Classification Gp
ROMANOFSKY, Robert	NASA Headquarters
ROYTBURD, A.	Nat'l. Institute of Standards and Technology
RUBINSTEIN, Mark	U.S. Naval Research Laboratory
RUSSO, Carl	American Superconductor Corporation
SAROHIA, V.	NASA/Jet Propulsion Laboratory
SCHRIEMPF, J.T.	Physical Sciences, Inc.
SHEAHEN, Thomas	Argonne National Laboratory
SHULL, Robert	Nat'l. Institute of Standards and Technology
SOKOLOSKI, M.M.	NASA Headquarters
SOVA, Ray	The Johns Hopkins University
STEINMUELLER, Peter	Embassy of the German Democratic Republic
SU, Sophia	GTE Laboratories, Inc.
SWARTZENDRUBER, Lyndon	Nat'l. Institute of Standards and Technology
TAKENAKA, Makoto	Cornell University
TAN, Ning Xia	SUNY at Stony Brook
TANAKA, Atsushi	Fugitsu Laboratories, Ltd.
TANAKA, Shoji	Superconductivity Research Laboratory
TESANOVIC, Zlatko	The Johns Hopkins University
TURCHINSKAYA, Marina	Nat'l. Institute of Standards and Technology
TYLER, Steven	ICD Group, Inc.
VAN SANT, Tim	NASA/Goddard Space Flight Center
VARMA, C.M.	AT&T Bell Laboratories
VELAZQUEZ, Marc	Electro-Science Laboratories
VENKATESAN, T.	Bellcore
VLASSE, Marcus	NASA/Marshall Space Flight Center
WALKER, J.C.	The Johns Hopkins University
WARNER, Joseph	NASA/Lewis Research Center
WEINBERGER, B.R.	United Technologies Research Center
WISE, Stephanie	Clemson University
WU, Maw Kuen	National Tsing-Hua University

CONFERENCE PARTICIPANTS (continued)

YAMAUCHI, Hisao	Int'l Superconductivity Research Center
YU, J.J.	Northwestern University
ZHAO, Jianmin	West Virginia State University
ZHAO, Jing	EMCORE Corporation
ZHOU, Lu-Wei	Fudan University
ZIA-UL-HAQ, Syed Mohammad	University of Karachi

AUTHOR INDEX

Adachi **281**
Adrian 89, 307
Agostinelli **189**
Akbar **107**
Alauddin 107
Aleksandrov **395**
Alterescu 19
Annett **375**
Antropov 385
Arsenovic **496**

Baldha 149
Barkatt 19
Bennett 127, 181, **213**, 249
Berlinsky 491
Bhalla 83
Bhasin **261**
Bogorad 423, 459
Bohandy 89, 307
Boone 307
Borsa **399**
Bose **331**
Botelho 107
Bowman 423
Braaten 117
Brandt **230**
Brasunas **449, 494**
Budnick **397**

Cai 464
Caignaert 61
Campa 45
Carlberg 496
Casais **45**
Chakraverty **341**
Chaudhari **333**
Chen, C.H. **271**
Chen, J.T. 3
Chen, M.F. 379
Chen, T.M. 145, 199
Chern 323
Chiang **127, 181**
Chorey 261
Chou 317
Cikmach **297**
Cook 127
Crain 319
Craver 379

Dalal **83**
Date 113
Datta **413**
Dekker 199
Dianoux 61
Diociaiuti 297
Drummer 107
Duran 165

Ebihara 261

Fain 37
Fair 107
Fernandez 165
Filipkowski 397
Fiorani 189
Fjellvag 117
Fontana 297
Freeman 365
Freiman 127
Fujimoto 241

Gallois 323
Gayle 249
Giovannella 297
Gluckler 397
Gopalakrishnan 173
Gordon 261
Gotoh 241
Grabow **307**
Green 307
Grosav **137**
Gubanov 385
Gubser 413, **487**
Gupta 113

Hall **145**
Han 43
Hayashi 281
Heinen 261
Hennion 61
Hermann 413
Herschitz **423**, 459

Hickman **199**
Hill 127
Hoff **97**
Hojaji **19**
Hsu 317
Hu 19
Huang 3
Hull 469
Hwang 127

Iannuzzi 297
Ichikawa 281
Ichinose 115
Ikegawa 115

Jasiolek **393**
Jeong 43
Joshi, H.H. **149**
Joshi, S.M. 149
Jotania 149

Kaiser 213, **249**
Kamehara 319
Kaneko 115
Karen **117**
Kasperczyk **389**
Kear 323
Khalil **69**
Khan **155**
Khokle 113
Khrustalev 395
Kim 89, 307
Kitazawa **257**
Kjekshus 117
Kohiki 281
Konopko 137
Koshizuka 241
Kostadinov **159**
Kresin **353**
Krivomazov 395
Kulkarni 149
Kumar 317
Kunde 449

Lakew 449
Lechter 97
Lee, S. 43
Leigh 37
Leporda 137
Li 323
Liechtenstein 385
Lim **43**
Little **337**
Longe 331
Lucchini 297
Lundy 213
Lynds 469

Mahl 83
Manka 377
Martin 375
Mateev 159
McCann 271
McMahan 375
Merlo 297
Messi 297
Michael 19
Michov 159
Millan 45
Miranda 261
Mirebeau **61**
Mogro-Campero 423, **459**,494
Mohan 149
Molak **377**
Moon **471, 491, 502**
Moorjani 61, **89**, 307
Moseley 449
Moure **165**
Mulcahy 469
Murakami **241, 498**
Murr **27**

Nagpal 113
Naqvi 155
Narayan 317
Niedermeyer 397
Niou 27
Niwa 319
Noh 323
Norris 323

Osofsky 97

Pachauri 113
Pande 97
Pandya, H.N. 149
Pandya, P.B. 149
Paoluzi 297

Park 43
Petrov 395
Phillips, R.C. 271
Phillips, T.E. 61
Polushkin **291**
Powers **417**
Pradhan-Advani 27

Qian 464
Qiu 464

Rakvin 83
Rasines 45
Recio 165
Recknagel 397
Reick **435**
Rigamonti 399
Ritter 213
Romanofsky 261, **477**
Roytburd **203**, 213

Schulze 173
Scopa 297
Seehra, M.S. 55
Seehra, S.S. 423
Setsune 281
Shapiro 127
Sheng 83
Shull 127, 181
Singh **317**
Sinha 317
Skumriev 159
Sololoski 477
Song 43
Sova 307
Sung 107
Swartzendruber 127, 181, 213, 249, 498

Taegashi 115
Tan 397
Tang 464
Tartaj 165
Tanaka, A. **319**
Tanaka, S. 115, 241, **475**
Tejada 189
Tesanovic 373
Testa 189
Thakur 317
Thorpe 19
Tripodi 297
Tsakin 159
Turchinskaya 181, 203 , 213
Turner 423, 459
Turshevski **385**

Uchaikin 291

Van Sant **429**
Varma **339**
Vasiliev 291
Vasilyev 395
Vaudin 127
Venkatesan **279**
Vezzoli **379**

Wada 115
Warner 261
Wasa 281
Weidinger 397
Weinberger **469**
Wise **37**
Wong 107
Wong-Ng 127
Wu **3**

Yamauchi **115**
Yu **365**

Zhang 464
Zhao, J. (WV) **55**
Zhao, J. (NJ) **323**
Zhou **464**
Zia-ul-Haq 155
Zwegintsev 395

NASA
National Aeronautics and Space Administration

Report Documentation Page

1. Report No.	2. Government Accession No.	3. Recipient's Catalog No.
NASA CP-3100		

4. Title and Subtitle	5. Report Date
AMSAHTS '90 Advances in Materials Science and Applications of High Temperature Superconductors	January 1991
	6. Performing Organization Code 313
7. Author(s) Larry H. Bennett, Yury Flom, and Kishin Moorjani, Editors	8. Performing Organization Report No. 90B00018
	10. Work Unit No.
9. Performing Organization Name and Address Goddard Space Flight Center Greenbelt, Maryland 20771	11. Contract or Grant No.
	13. Type of Report and Period Covered Conference Publication
12. Sponsoring Agency Name and Address National Aeronautics and Space Administration Washington, D.C. 20546-0001	14. Sponsoring Agency Code

15. Supplementary Notes

Larry H. Bennett: National Institute of Standards and Technology, Gaithersburg, MD.
Yury Flom: NASA Goddard Space Flight Center, Greenbelt, MD.
Kishin Moorjani: The Johns Hopkins University, Applied Physics Laboratory, Laurel, MD.

16. Abstract

This proceedings is comprised of both oral and poster presentations from AMSAHTS '90, held at Goddard Space Flight Center April 2-6, 1990. The 5-day conference focused on understanding high-temperature superconductivity with special emphases on materials issues and applications. AMSAHTS '90 highlighted the state of the art in the fundamental understanding of the nature of high-Tc superconductivity (HTSC) as well as the chemistry, structure, properties, processing, and stability of HTSC oxides. As a special feature of the conference, space applications of HTSC were discussed by NASA and Navy specialists.

17. Key Words (Suggested by Author(s))	18. Distribution Statement
High-Tc Superconductivity (HTSC), Flux Creep, Flux Pinning, Bulk HTSC, Thermodynamics, and Chemistry	Unclassified - Unlimited Subject Category 24

19. Security Classif. (of this report)	20. Security Classif. (of this page)	21. No. of pages	22. Price
Unclassified	Unclassified	520	A22

☆U.S. GOVERNMENT PRINTING OFFICE: 1991-528/333